20 February 2009 | $10

Science

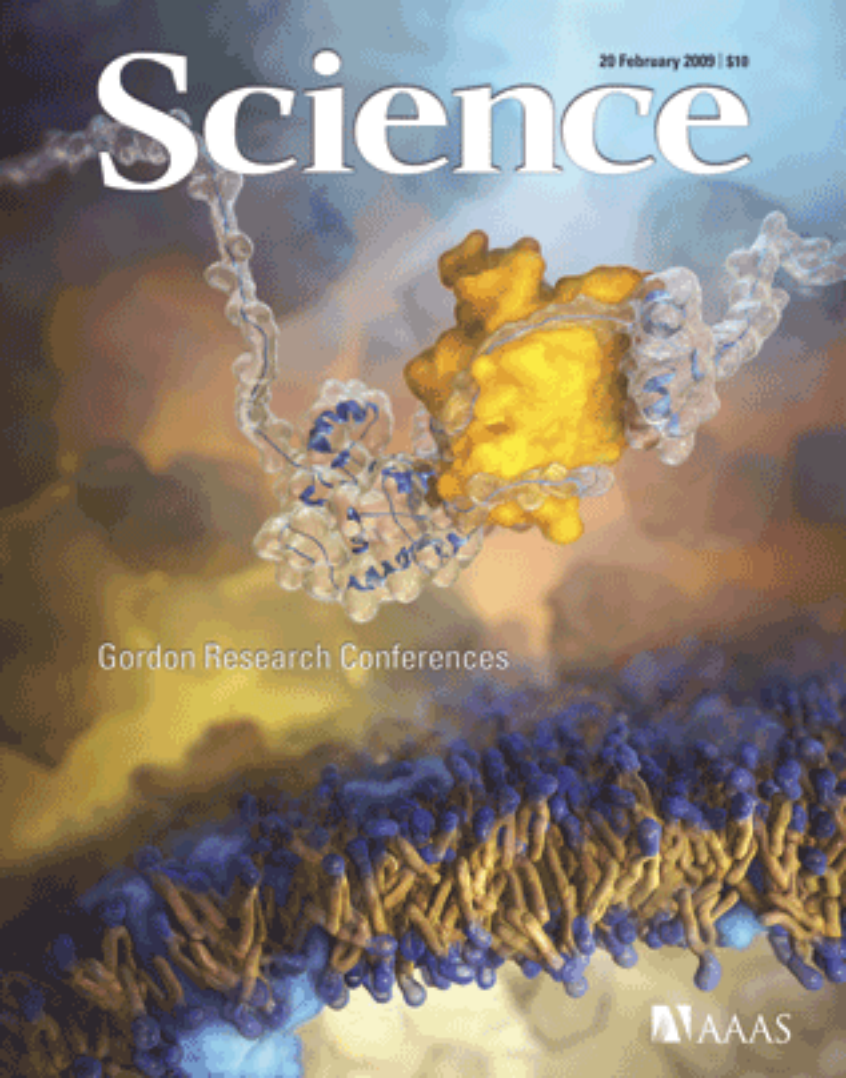

Gordon Research Conferences

AAAS

EDITORIAL

NEWS OF THE WEEK

NEWS FOCUS

LETTERS

BOOKS *ET AL.*

POLICY FORUM

PERSPECTIVES

BREVIA

CONTENTS continued **>>**

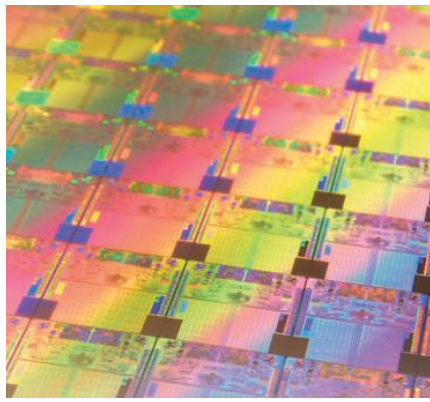

page 1000

page 1012

COVER

Maltose binding protein (translucent), shown suspended in its molten globule state with chaperone protein SecB (yellow), destined for transport across the cellular membrane. The Gordon Research Conference on Visualization in Science & Education will be held 26 to 31 July 2009 at Magdalen College, Oxford, UK. The schedules for the 2009 Gordon Research Conferences begin on page 1084.

Image: Graham Johnson/www.fivth.com and Scripps Research Institute; Sander Tans/AMOLF Institute

DEPARTMENTS

Published by AAAS

RESEARCH ARTICLE

REPORTS

CONTENTS continued **>>**

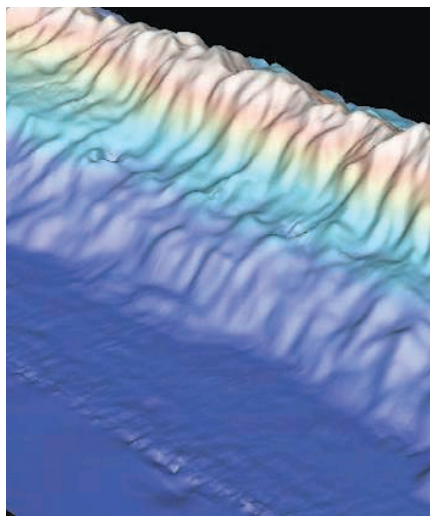

pages 1017 & 1048

page 1077

CREDIT (BOTTOM): BEN ARTHUR AND CHARLES WALCOTT/DEPARTMENT OF NEUROBIOLOGY/CORNELL UNIVERSITY

Published by AAAS

SCIENCEONLINE

SCIENCEXPRESS
www.sciencexpress.org

A Putative ABC Transporter Confers Durable Resistance to Multiple Fungal Pathogens in Wheat
S. G. Krattinger et al.
10.1126/science.1166453

A Kinase-START Gene Confers Temperature-Dependent Resistance to Wheat Stripe Rust
D. Fu et al.
10.1126/science.1166289
Several specific genes in wheat confer resistance to common fungal diseases.

Fermi Observations of High-Energy Gamma-Ray Emission from GRB 080916C
The Fermi LAT and Fermi GBM Collaborations
This highly luminous gamma-ray burst had the largest apparent energy release yet measured.
10.1126/science.1169101

Switchable Ferroelectric Diode and Photovoltaic Effect in $BiFeO_3$
T. Choi et al.
Single crystals of bismuth iron oxide contain a single ferroelectric domain that can be switched with an electric field.
10.1126/science.1168636

SCIENCENOW
www.sciencenow.org
Highlights From Our Daily News Coverage

The Whole Migration and Nothing But
Tiny geolocator backpacks let researchers follow every step of songbirds' journeys.

Ancient Virus Gave Wasps Their Sting
Find solves decades-old debate about mysterious toxins.

Horseshoes, Hand Grenades—and Slot Machines?
A near miss is almost as good as a win to gamblers' brains, keeping them playing.

SCIENCESIGNALING
www.sciencesignaling.org
The Signal Transduction Knowledge Environment

RESEARCH ARTICLE: The Precise Sequence of FGF Receptor Autophosphorylation Is Kinetically Driven and Is Disrupted by Oncogenic Mutations
E. D. Lew et al.
The order of FGFR1 tyrosine autophosphorylation is kinetically controlled and determined by primary and tertiary structures.

PERSPECTIVE: Von Gierke's Disease Adopts an Orphan (and Its Partner)
A. Cheng and A. R. Saltiel
The transcription of *glucose-6-phosphatase* is positively regulated by a nuclear receptor and coactivator.

PODCAST
T. Kino and A. M. VanHook
The guanine nucleotide exchange factor Brx is required in lymphocytes for the expression of *nfat5* in response to osmotic stress.

NETWATCH: The Cancer Genome Atlas
Clinical, cell biological, and genomic data from human tumors are available from the National Cancer Institute; in Bioinformatics Resources.

NETWATCH: CellBASE
Find online research and education resources for cell biologists at this site from the American Society for Cell Biology; in Technical Information.

SCIENCECAREERS
www.sciencecareers.org/career_magazine
Free Career Resources for Scientists

Perspective: Problem Finding and the Multidisciplinary Mind
L. Austin
Your choice of research problem may determine the course of your career as a physician-scientist.

Tooling Up: The Cold, Hard Truth About Finding a Job in 2009
D. Jensen
Finding a job now takes a plan, perseverance, and a positive attitude.

Faith and Science in Balance
E. Pain
Ph.D. student Imre Szilágyi strives to succeed in order to glorify God.

SCIENCEPODCAST
www.sciencemag.org/multimedia/podcast
Free Weekly Show
Download the 20 February *Science* Podcast to hear about open access and global participation in science, the role of water vapor in global warming, microchips sans silicon, and more.

ORIGINSBLOG
blogs.sciencemag.org/origins
A History of Beginnings

SCIENCEINSIDER
blogs.sciencemag.org/scienceinsider
Science Policy News and Analysis

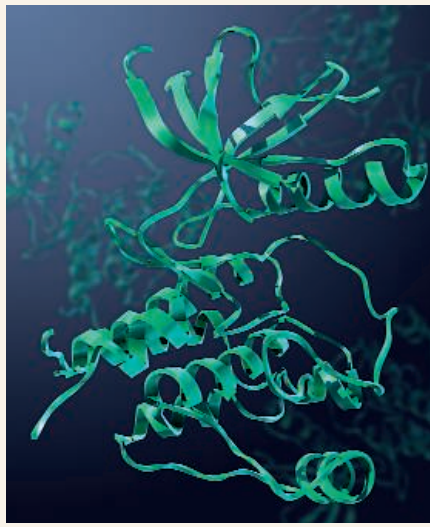

SCIENCESIGNALING
Tyrosine kinase domain of FGFR1.

SCIENCEONLINE FEATURE
www.sciencemag.org/sciext/gonzoscientist/

THE GONZO SCIENTIST: Gourmet Food, Served by Dogs
Starting with a dog-led truffle hunt and ending with a dog-food taste test, our reporter takes a real-world tour of hedonics (with audio slideshow).
>> News story p. 1006

CREDITS: (*SCIENCE SIGNALING*) CHRIS BICKEL; (*SCIENCE* ONLINE FEATURE) KATRIEN KOLENBERG

SCIENCE (ISSN 0036-8075) is published weekly on Friday, except the last week in December, by the American Association for the Advancement of Science, 1200 New York Avenue, NW, Washington, DC 20005. Periodicals Mail postage (publication No. 484460) paid at Washington, DC, and additional mailing offices. The title SCIENCE is a registered trademark of the AAAS. Domestic individual membership and subscription (51 issues): $146 ($74 allocated to subscription). Domestic institutional subscription (51 issues): $835; Foreign postage extra: Mexico, Caribbean (surface mail) $55; other countries (air assist delivery) $85. First class, airmail, student, and emeritus rates on request. Canadian rates with GST available upon request, GST #1254 88122. Publications Mail Agreement Number 1069624. **Printed in the U.S.A.**

Change of address: Allow 4 weeks, giving old and new addresses and 8-digit account number. **Postmaster:** Send change of address to AAAS, P.O. Box 96178, Washington, DC 20090–6178. **Single-copy sales:** $10.00 current issue, $15.00 back issue prepaid includes surface postage; bulk rates on request. **Authorization to photocopy** material for internal or personal use under circumstances not falling within the fair use provisions of the Copyright Act is granted by AAAS to libraries and other users registered with the Copyright Clearance Center (CCC) Transactional Reporting Service, provided that $20.00 per article is paid directly to CCC, 222 Rosewood Drive, Danvers, MA 01923. The identification code for *Science* is 0036-8075. *Science* is indexed in the *Reader's Guide to Periodical Literature* and in several specialized indexes.

AAAS
ADVANCING SCIENCE, SERVING SOCIETY

Elias A. Zerhouni is the immediate past director of the U.S. National Institutes of Health.

Beyond the Stimulus

THE AMERICAN PUBLIC UNDERSTANDS THAT INNOVATION IN SCIENCE AND TECHNOLOGY IS THE best guarantor of our economic future. National research budgets are not subsidies but strategic investments to be sustained even in the worst of times. Thanks to the relevant administration and congressional leaders, science has been well served in the stimulus package just signed by President Obama. The $21.5 billion for R&D projects over the next 2 years is the result of compromises based on a variety of opinions as to the proper levels of support for U.S. science. Take funding for the National Institutes of Health (NIH), for example. The House initially proposed that the NIH receive $3.5 billion, whereas the Senate, under the extraordinary leadership of Senator Arlen Specter, proposed $10 billion, the figure in the final bill. So what should the appropriate level of support be beyond the stimulus? Is there a quantifiable rationale beyond "more is always better?"

First, the timing and amount of this stimulus could not have been more opportune. Since 2003, U.S. science budgets have fallen, when compared to the rate of inflation. In good economic times, the impact of these federal budget shortfalls was lessened by increased support from philanthropic foundations, more generous private gifts, larger endowment proceeds, and other sources such as state funding or clinical revenues. But all of these nonfederal sources are now severely depleted. In 2007, the sum total of endowments for the top 75 U.S. universities amounted to about $300 billion. Today, a quarter to a third of that value, or $75 billion to $100 billion, has disappeared. Gift giving is also drastically down. Estimates of these combined losses range from $7 billion to $10 billion for 2009 alone. Many universities have announced deep cost reductions and freezes on new positions that will have particularly negative consequences for young scientists. I have testified in Congress that for every $1 billion shortfall in the NIH base budget, an estimated 6000 to 9000 scientific jobs are lost, with an equal number of jobs lost in indirect support activities. With increased layoffs in industry, one has to be deeply concerned about the human research capacity of the United States across all sciences, a key determinant of our future competitiveness.

The economic stimulus will lessen these risks in the short term. But it is only a partial answer. It will not stave off the loss of talented scientists unless it is coupled with a longer-term increase in the base budgets of the research agencies. This would avoid the detrimental and painful effects of a rapid rise followed by a fall in budgets, as has been experienced by the NIH in recent years. What should the level of long-term support be? The NIH lost 15% of its purchasing power, or $4 billion, between 2003 and 2009. At a time when research is characterized by an interdisciplinary convergence between the physical and biological sciences, the base federal support for the physical and engineering disciplines has decreased to an even greater degree; these critical research fields would require additional support variously estimated at about $6 billion per year to reach a better balance between biological and physical sciences. Thus, beyond the stimulus, the base science budgets of the relevant domestic agencies should increase by at least $10 billion per year, a minimum goal to strive for by fiscal year 2012.

A nation's most strategic resource is the strength of its scientific workforce. It is imperative that the entire scientific community coalesce around a quantifiable and shared rationale for rebalancing the base domestic federal research budget beyond the one-time stimulus package. This is a task that will be made more difficult by growing federal deficits, but it may well be attainable given the clear and welcome commitment to science just shown by the new U.S. administration and Congress.

– Elias A. Zerhouni

10.1126/science.1172425

Published by AAAS

www.sciencemag.org

Science

1200 New York Avenue, NW
Washington, DC 20005
Editorial: 202-326-6550, FAX 202-289-7562
News: 202-326-6581, FAX 202-371-9227
Bateman House, 82-88 Hills Road
Cambridge, UK CB2 1LQ
+44 (0) 1223 326500, FAX +44 (0) 1223 326501

Subscription Services For change of address, missing issues, new orders and renewals, and payment questions: 866-434-AAAS (2227) or 202-326-6417, FAX 202-842-1065. Mailing addresses: AAAS, P.O. Box 96178, Washington, DC 20090-6178 or AAAS Member Services, 1200 New York Avenue, NW, Washington, DC 20005

Institutional Site Licenses please call 202-326-6755 for any questions or information

Reprints: Author Inquiries 800-635-7181
Commercial Inquiries 803-359-4578

Permissions 202-326-7074, FAX 202-682-0816

Member Benefits AAAS/Barnes&Noble.com bookstore www.aaas.org/bn; AAAS Online Store www.apisource.com/aaas/ code MKB6; AAAS Travels: Betchart Expeditions 800-252-4910; Apple Store www.apple/eppstore/aaas; Bank of America MasterCard 1-800-833-6262 priority code FAA3YU; Cold Spring Harbor Laboratory Press Publications www.cshlpress.com/affiliates/aaas.htm; GEICO Auto Insurance www.geico.com/landingpage/go51.htm?logo=17624; Hertz 800-654-2200 CDP#343457; Office Depot https://bsd.officedepot.com/portalLogin.do; Seabury & Smith Life Insurance 800-424-9883; Subaru VIP Program 202-326-6417; VIP Moving Services www.vipmayflower.com/domestic/index.html; Other Benefits: AAAS Member Services 202-326-6417 or www.aaasmember.org.

science_editors@aaas.org	(for general editorial queries)
science_letters@aaas.org	(for queries about letters)
science_reviews@aaas.org	(for returning manuscript reviews)
science_bookrevs@aaas.org	(for book review queries)

Published by the American Association for the Advancement of Science (AAAS), *Science* serves its readers as a forum for the presentation and discussion of important issues related to the advancement of science, including the presentation of minority or conflicting points of view, rather than by publishing only material on which a consensus has been reached. Accordingly, all articles published in *Science*—including editorials, news and comment, and book reviews—are signed and reflect the individual views of the authors and not official points of view adopted by AAAS or the institutions with which the authors are affiliated.

AAAS was founded in 1848 and incorporated in 1874. Its mission is to advance science, engineering, and innovation throughout the world for the benefit of all people. The goals of the association are to: enhance communication among scientists, engineers, and the public; promote and defend the integrity of science and its use; strengthen support for the science and technology enterprise; provide a voice for science on societal issues; promote the responsible use of science in public policy; strengthen and diversify the science and technology workforce; foster education in science and technology for everyone; increase public engagement with science and technology; and advance international cooperation in science.

Information for Authors
See pages 807 and 808 of the 6 February 2009 issue or access www.sciencemag.org/about/authors

EDITOR-IN-CHIEF **Bruce Alberts**
EXECUTIVE EDITOR **Monica M. Bradford**
DEPUTY EDITORS **R. Brooks Hanson, Barbara R. Jasny, Katrina L. Kelner**
NEWS EDITOR **Colin Norman**

Editorial supervisory senior editor Phillip D. Szuromi; **senior editor/perspectives** Lisa D. Chong; **senior editors** Gilbert J. Chin, Pamela J. Hines, Paula A. Kiberstis (Boston), Marc S. Lavine (Toronto), Beverly A. Purnell, L. Bryan Ray, Guy Riddihough, H. Jesse Smith, Valda Vinson; **associate editors** Kristen L. Mueller, Jake S. Yeston, Laura M. Zahn; **online editor** Stewart Wills; **associate online editors** Robert Frederick, Tara S. Marathe; **web content developer** Martyn Green; **book review editor** Sherman J. Suter; **associate letters editor** Jennifer Sills; **editorial manager** Cara Tate; **senior copy editors** Jeffrey E. Cook, Cynthia Howe, Harry Jach, Barbara P. Ordway, Trista Wagoner; **copy editors** Chris Filiatreau, Lauren Kmec; **editorial coordinators** Carolyn Kyle, Beverly Shields; **publications assistants** Ramatoulaye Diop, Joi S. Granger, Jeffrey Hearn, Lisa Johnson, Scott Miller, Jerry Richardson, Jennifer A. Seibert, Brian White, Anita Wynn; **editorial assistants** Carlos L. Durham, Emily Guise, Patricia M. Moore; **executive assistant** Sylvia S. Kihara; **administrative support** Maryrose Madrid

News deputy news editors Robert Coontz, Eliot Marshall, Jeffrey Mervis, Leslie Roberts; **contributing editors** Elizabeth Culotta, Polly Shulman; **news writers** Yudhijit Bhattacharjee, Adrian Cho, Jennifer Couzin, David Grimm, Constance Holden, Jocelyn Kaiser, Richard A. Kerr, Eli Kintisch, Andrew Lawler (New England), Greg Miller, Elizabeth Pennisi, Robert F. Service (Pacific NW), Erik Stokstad; **intern** Jackie D. Grom; **contributing correspondents** Dan Charles, Jon Cohen (San Diego, CA), Daniel Ferber, Ann Gibbons, Robert Koenig, Mitch Leslie, Charles C. Mann, Virginia Morell, Evelyn Strauss, Gary Taubes; **copy editors** Linda B. Felaco, Melvin Gatling, Melissa Raimondi; **administrative support** Scherraine Mack, Fannie Groom; **bureaus** New England: 207-549-7755, San Diego, CA: 760-942-3252, FAX 760-942-4979, Pacific Northwest: 503-963-1940

Production director James Landry; **senior manager** Wendy K. Shank; **assistant manager** Rebecca Doshi; **senior specialists** Steve Forrester, Chris Redwood; **specialist** Anthony Rosen; **Preflight director** David M. Tompkins; **manager** Marcus Spiegler

Art director Yael Kats; **associate art director** Laura Creveling; **illustrators** Chris Bickel, Katharine Sutliff; **senior art associates** Holly Bishop, Preston Huey, Nayomi Kevitiyagala; **art associate** Jessica Newfield; **photo editor** Leslie Blizard

***Science* International**

Europe (science@science-int.co.uk) **editorial: international managing editor** Andrew M. Sugden; **senior editor/perspectives** Julia Fahrenkamp-Uppenbrink; **senior editors** Caroline Ash, Stella M. Hurtley, Ian S. Osborne, Peter Stern; **associate editor** Maria Cruz; **editorial support** Deborah Dennison, Rachel Roberts, Alice Whaley; **administrative support** John Cannell, Janet Clements; **news: Europe news editor** John Travis; **deputy news editor** Daniel Clery; **contributing correspondents** Michael Balter (Paris), John Bohannon (Vienna), Martin Enserink (Amsterdam and Paris), Gretchen Vogel (Berlin); **intern** Sara Coelho

Asia Japan Office: Asca Corporation, Eiko Ishioka, Fusako Tamura, 1-8-13, Hirano-cho, Chuo-ku, Osaka-shi, Osaka, 541-0046 Japan; +81 (0) 6 6202 6272, FAX +81 (0) 6 6202 6271; asca@os.gulf.or.jp; **asia news editor** Richard Stone (Beijing: rstone@aaas.org); **contributing correspondents** Dennis Normile (Japan: +81 (0) 3 3391 0630, FAX +81 (0) 3 5936 3531; dnormile@gol.com); Hao Xin (China: +86 (0) 10 6307 4439 or 6307 3676, FAX +86 (0) 10 6307 4358; cindyhao@gmail.com); Pallava Bagla (South Asia: +91 (0) 11 2271 2896; pbagla@vsnl.com)

EXECUTIVE PUBLISHER **Alan I. Leshner**
PUBLISHER **Beth Rosner**

Fulfillment Systems and Operations (membership@aaas.org); **director** Waylon Butler; **senior systems analyst** Jonny Blaker; **customer service supervisor** Pat Butler; **specialists** Latoya Casteel, LaVonda Crawford, Vicki Linton, April Marshall; **data entry supervisor** Cynthia Johnson; **specialists** Eintou Bowden, Tarrika Hill, William Jones

Business Operations and Administration director Deborah Rivera-Wienhold; **assistant director, business operations** Randy Yi; **manager, business analysis** Michael LoBue; **manager, business operations** Jessica Tierney; **financial analysts** Priti Pamnani, Celeste Troxler; **rights and permissions: administrator** Emilie David; **associate** Elizabeth Sandler; **marketing director** Ian King; **marketing manager** Allison Pritchard; **marketing associates** Aimee Aponte, Alison Chandler, Mary Ellen Crowley, Julianne Wielga, Wendy Wise; **marketing executive** Jennifer Reeves; **marketing/member services executive** Linda Rusk; **director, site licensing** Tom Ryan; **director, corporate relations** Eileen Bernadette Moran; **publisher relations, eResources specialist** Kiki Forsythe; **senior publisher relations specialist** Catherine Holland; **publisher relations, east coast** Phillip Smith; **publisher relations, west coast** Philip Tsolakidis; **fulfillment supervisor** Iquo Edim; **fulfillment coordinator** Laura Clemens; **electronic media: manager** Lizabeth Harman; **project manager** Trista Snyder; **assistant manager** Lisa Stanford; **senior production specialists** Christopher Coleman, Walter Jones; **production specialists** Nichele Johnston, Kimberly Oster

Advertising director, worldwide ad sales Bill Moran

Product (science_advertising@aaas.org); **midwest/west coast/w. canada** Rick Bongiovanni: 330-405-7080, FAX 330-405-7081; **east coast/e. canada** Laurie Faraday: 508-747-9395, FAX 617-507-8189; **uk/europe/asia** Roger Goncalves: TEL/FAX +41 43 243 1358; **japan** Mashy Yoshikawa: +81 (0) 3 3235 5961, FAX +81 (0) 3 3235 5852; **senior traffic associate** Deiandra Simms

Commercial Editor Sean Sanders: 202-326-6430

Project Director, Outreach Brianna Blaser

Classified (advertise@sciencecareers.org); **inside sales manager: midwest/canada** Daryl Anderson: 202-326-6543; **inside sales representative** Karen Foote: 202-326-6740; **key account manager** Joribah Able; **northeast** Alexis Fleming: 202-326-6578; **southeast** Tina Burks: 202-326-6577; **west** Nicholas Hintibidze: 202-326-6533; **sales coordinators** Rohan Edmonson, Shirley Young; **international: sales manager** Tracy Holmes: +44 (0) 1223 326525, FAX +44 (0) 1223 326532; **sales** Susanne Kharraz, Dan Pennington, Alex Palmer; **sales assistant** Louise Moore; **japan** Mashy Yoshikawa: +81 (0) 3 3235 5961, FAX +81 (0) 3 3235 5852; **advertising production operations manager** Deborah Tompkins; **senior production specialist/graphic designer** Amy Hardcastle; **senior production specialist** Robert Buck; **senior traffic associate** Christine Hall; **publications assistant** Mary Lagnaoui

AAAS Board of Directors retiring president, chair James J. McCarthy; **president** Peter C. Agre; **president-elect** Alice Huang; **treasurer** David E. Shaw; **chief executive officer** Alan I. Leshner; **board** Alice Gast, Linda P. B. Katehi, Nancy Knowlton, Cherry A. Murray, Julia M. Phillips, Thomas D. Pollard, David S. Sabatini, Thomas A. Woolsey

AAAS
ADVANCING SCIENCE, SERVING SOCIETY

New teammates
995

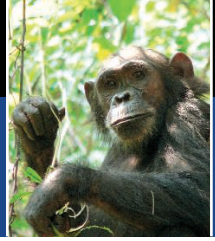

AIDS and wild chimps
996

U.S. BUDGET

Science Wins $21 Billion Boost as Stimulus Package Becomes Law

The scene: a jittery Washington, D.C., amid the worst global economic crisis in decades. The main character: a young president who has promised to "restore science to its rightful place." The supporting cast: a Congress dominated by Democrats heeding President Barack Obama's call not only to "create new jobs but to lay a new foundation for growth."

This week, those elements culminated in a historic $787 billion economic stimulus package that provides more than $21 billion for research and scientific infrastructure. Having a role in the biggest one-time federal outlay since the New Deal has been a surprise for scientists, on whom the Obama plan lavished a variety of cash investments. These include $10 billion for the National Institutes of Health (NIH), $3 billion for the National Science Foundation (NSF), and $1.6 billion for the Department of Energy's (DOE's) Office of Science.

Scientists are euphoric. "It's incredible; more than we've seen in a long time," said Francis DiSalvo, a materials chemist at Cornell University. The infusion comes after a series of annual appropriations bills that doled out relatively flat budgets for many federal science agencies. Some research policy experts are wary of the audacious lump-sum approach. "It's an incredibly rapid infusion of an unprecedented amount of money for scientific research to be spent in an extremely short amount of time," said Daniel Sarewitz of Arizona State University, Tempe.

U.S. science lobbyists first realized that they might be in for a piece of the stimulus pie soon after Obama was elected. As talk spread of combating the deteriorating economy with aggressive spending and tax breaks, the initial focus was on scientific construction projects, says Michael Lubell of the American Physical Society. But Obama's transition team and congressional staffers soon broadened their requests to include proposed investment in research, arguing that putting people to work on innovative ideas could generate even more well-paying jobs down the road (*Science*, 16 January, p. 318).

House Speaker Nancy Pelosi (D–CA) led the way by declaring that "science, science, science" was central to the Democratic agenda. In turn, the House version of the stimulus bill included the large boosts for DOE, NSF, and NASA that ended up in the final bill. Those increases mirrored levels Congress proposed as part of the 2007 America COMPETES Act, which authorizes spending that has never materialized.

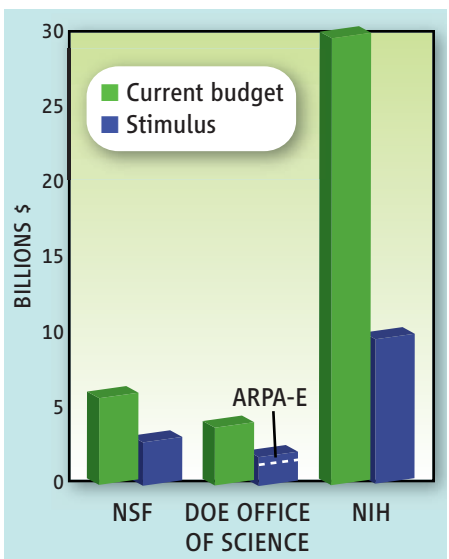

Much more. The stimulus adds a significant fraction to what these three science agencies now spend.

Senate Majority Leader Harry Reid (D–NV) had a tougher political job. Two votes shy of a filibuster-proof majority, he had to woo a few Republicans, who generally wanted less spending and more tax cuts. Maine's two moderate Republicans, senators Susan Collins and Olympia Snowe, teamed up with Senator Ben Nelson (D–NE) to craft a compromise bill that lopped off $100 billion from what was then before the Senate.

The science community was aghast when the first version of the compromise proposed dropping NSF from the package entirely. They enlisted heavyweights from academia and industry to make the case for the agency's role as an economic driver. At the same time Senator Arlen Specter (R–PA), a longtime supporter of biomedical research, successfully added $6.5 billion to the $3.5 billion that NIH had been allocated and made it clear that his support for the overall package was contingent on retaining a boost of that magnitude. "The cost-of-living adjustments have not been made," Specter said during floor debate on the bill. "There has been an actual decline of some $5.2 billion of NIH funding in the last 7 years."

The compromise Senate bill still provided generally lower levels for most science agencies, however, and lobbyists credit Pelosi as well as the White House for restoring the House levels in a conference between the two bodies. "She deserves great credit, as does the Obama Administration," says Toby Smith of the Association of American Universities in Washington, D.C.

In the end, NIH received the biggest bounty. The $30-billion-a-year agency receives an additional $8.2 billion for research, spread out over the current and next fiscal years, as well as $500 million for construction and renovation of NIH's intramural labs and $1.3 billion for research facilities and instrumentation elsewhere. NASA will get $1 billion on top of its yearly $17 billion budget, with lawmakers targeting Democratic favorites such as supercomputing and earth science ($400 million), aeronautics ($150 million), and a new launcher ($400 million). DOE's $4 billion Office of Science receives an extra $1.6 billion, with no strings attached. The need is great, say scientists. "Most buildings here are very old," says physicist Michael Norman of DOE's Argonne National Laboratory in Illinois, which is hoping for a new interdisciplinary center for energy research.

Congress also added another $400 million for a new entity called the Advanced Research Projects Agency for Energy. The idea is to emulate the long-standing Defense Advanced Research Projects Agency (DARPA), credited with giving birth to the Internet and other important commercial technologies. Jane "Xan" Alexander, former deputy director of DARPA, says the new agency will help technologies avoid the so-called Valley of Death that separates basic and applied research at DOE.

SOURCE: U.S. CONGRESS

Published by AAAS

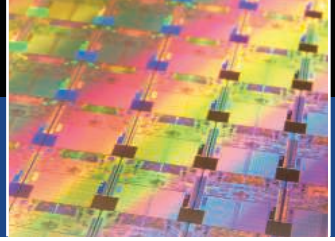

Chipping away at silicon 1000

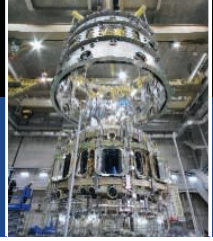

A STAR in Korea 1003

But it's arguably NSF that will see the biggest impact from the stimulus bill. Steven Beering, chair of its oversight body, the National Science Board, says the $3 billion spending boost for the $6-billion-a-year agency "is phenomenal. … It'll enfranchise many people who wouldn't otherwise have been funded and allow NSF to fund more high-risk, transformational research." Some $2 billion will be spent on research grants and $100 million for education programs. It also contains $900 million for various infrastructure projects, including $200 million to revive an academic facilities program. The board will take up how the influx affects NSF's priorities at its meeting next week, Beering adds.

Although Sarewitz says that funding science may be a worthy cause, he sees potential harm from its inclusion in the stimulus package. "If this spending is for [economic] stimulus, then it's not at all clear that R&D is a good way to get money into the economy quickly," he says. "If, on the other hand, it's long-term investment, then there's no reason to ram it into the system so quickly."

But such doubts are hard to find among a science establishment grown accustomed to flat budgets. Richard Marchase, president of the Federation of American Societies for Experimental Biology, admits to some worries of a poststimulus letdown. But for right now, he says, "we're very, very appreciative."

–ELI KINTISCH

With reporting by Dan Charles, Lila Guterman, Andrew Lawler, and Jeffrey Mervis.

PARTICLE PHYSICS

LHC Delays Give Tevatron a Shot at Higgs Boson

One lab's setback can be another lab's opportunity. Last week, officials at the European particle physics laboratory, CERN, near Geneva, Switzerland, announced that it will take longer than previously estimated to fix the world's highest energy particle smasher, the Large Hadron Collider (LHC), which suffered a catastrophic malfunction last year before ever taking data (*Science*, 26 September 2008, p. 1753). The LHC will not start up again before late September, 2 months later than previously announced. Meanwhile, the older Tevatron collider at Fermi National Accelerator Laboratory (Fermilab) in Batavia, Illinois, may be gaining the edge in the race to spot the Higgs boson, the last missing piece in the standard model of fundamental particles.

"Three years ago, nobody would have bet a lot that the Tevatron would be competitive [with the LHC] in the Higgs search. Now I think the tables are almost turned," says Tommaso Dorigo, a physicist from the University of Padua in Italy who works with the CDF particle detector fed by the Tevatron and the CMS particle detector fed by the LHC.

Given the continuing delays with the LHC, Fermilab physicists are hoping for the chance to continue running their 26-year-old collider through 2011. Officials at the Department of Energy, which owns Fermilab, declined to comment because they are still formulating their budget for the next fiscal year, which starts on 1 October. But they would likely have to make that decision before the LHC comes back on.

Fermilab scientists say it's only prudent to keep the Tevatron running. "We don't think that a running accelerator complex should be shut off until it's displaced by another running accelerator complex that's producing physics," says Fermilab's Rob Roser, co-spokesperson for the 602-member CDF team. But some say the call should not be made on the assumption that the LHC will have more problems. "You should look at your own program and assume the other guy will succeed," says Sheldon Stone of Syracuse University in New York state.

Chances are. The projected probability that the Fermilab experiments will glimpse the Higgs boson depends on the particle's mass.

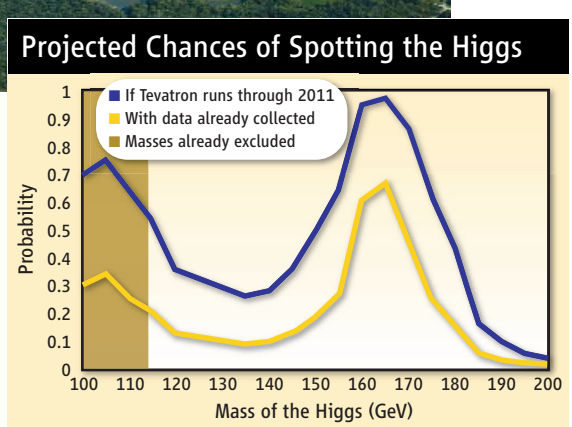

CREDIT: REIDAR HAHN/FERMILAB; SOURCE: CDF COLLABORATION

The numbers show that the Tevatron is performing superbly. Physicists measure the amount of data produced in units of "inverse femtobarns." From the beginning of the current run in 2001 until the end of September, the Tevatron produced 5 inverse femtobarns. It is now on pace to nearly double that amount by the end of 2010, and it could rack up 12 inverse femtobarns by the end of 2011.

That should be enough data to give researchers with CDF and the neighboring D0 particle detector a chance to see evidence of the Higgs boson—if it's there. "Evidence" is jargon for a signal that's stronger than a certain level but not strong enough to claim a definite discovery. The probability of seeing such a signal depends on what the Higgs might weigh. Researchers with CDF estimate that if the Higgs weighs between about 120 and 195 times as much as a proton—that's 114 and 182 giga–electron volts (GeV) in the units physicists prefer—then CDF and D0 working together should have at least a 25% chance of seeing it if the Tevatron runs through 2011 (see figure).

Scientists at the Tevatron seem to like their chances. More people are sticking around than a 2004 survey had projected, says Fermilab's Dmitri Denisov, co-spokesperson for the 530-member D0 collaboration. "We expected that we would lose between 10% and 15% of our people per year, but between a year ago and now, we're down about 5%," Denisov says. CDF's losses are also lighter ▶

Published by AAAS

than expected, Roser says.

Ultimately, whether the Tevatron runs in 2010 or 2011 depends on Fermilab's budget. In preparing for life after the Tevatron, Fermilab is planning to build a proton accelerator to power neutrino beams and other experiments (*Science*, 31 August 2007, p. 1155). If there isn't enough money, says Fermilab Director Pier Oddone, "then we will stop the Tevatron to get the resources to develop the future of the lab."

Across the Atlantic, CERN officials have laid out a timeline for repairing the LHC and making modifications to prevent a repeat of the 19 September failure. The problem began when a splice in a superconducting electrical line melted, triggering a leak of boiling liquid helium and a concomitant pressure wave that damaged 53 of the machine's more than 1600 superconducting magnets. Workers need an additional 6 weeks to make those fixes, says CERN spokesperson James Gillies. To make up for lost time, Gillies says, CERN will run the LHC through next winter despite the higher cost of electricity, which normally dictates a halt in operations.

Still, CERN officials can't guarantee that the LHC won't run into some new sort of problem that will cause further delays. Meanwhile, Fermilab researchers see a more predictable path to their shot at glory. **–ADRIAN CHO**

Teammates. John Holdren and Jane Lubchenco after their Senate testimony last week.

CREDIT: SAM KITTNER

OBAMA ADMINISTRATION

No News Is Good News for Holdren, Lubchenco at Confirmation Hearing

Senate confirmation hearings generate news only if a presidential nominee unintentionally gets ahead of the boss in announcing some new policy or falls into a trap set by a legislator from the opposing party. But sometimes, if the committee is genuinely interested in the business of governing, the hearing can give consensus nominees a chance to discuss issues at the agencies they've been asked to lead even without making news.

That's what happened last week when John Holdren and Jane Lubchenco appeared before the Senate Committee on Commerce, Science, and Transportation. President Barack Obama has nominated Holdren, a physicist, to lead the White House Office of Science and Technology Policy and Lubchenco, a marine ecologist, to head the National Oceanic and Atmospheric Administration (NOAA).

The committee was more than gracious: "My hope is to move your nominations [through the Senate] as quickly as possible," chair Senator Jay Rockefeller (D–WV) explained at the start and end of the 2-hour hearing. Senator David Vitter (R–LA) was the only committee member who challenged Holdren, grilling him over a series of papers the Harvard physicist had written or co-written, dating back to 1971, that discussed the possible dire consequences of several disturbing political, environmental, and cultural trends. Holdren, unruffled, parried the attack by saying that he was simply calling attention to mounting ecological worries or that accumulating scientific evidence now points in a different direction.

Not surprisingly, environmental issues dominated the discussion. But the tone was conversational rather than confrontational. Asked by Rockefeller how she deals with disagreement among scientists on climate change, Lubchenco explained that "science doesn't tell us what to do. It's one of many factors." Holdren's answer was more assertive: "It's real, it's accelerating, it's caused in large part by human activity, it's dangerous, and it's getting worse." But Holdren also used the question to offer advice on how policymakers might approach any science-based issue. "Policymakers should look at the range of scientific opinion, the center of gravity, and what most expert bodies have said [about an issue]," Holdren said. "If I were betting the public's money, I'd go with the mainstream."

Holdren painted an expansive picture of his office, telling Rockefeller that "it is my responsibility to look at any place where science and technology is not being put to its best use." Few of his predecessors have been given such a broad portfolio, and it remains to be seen whether Holdren will fare any better in the rough-and-tumble of White House politics. But he's going to try. Noting that an interagency coordinating body called the National Science and Technology Council had "languished" under the Bush Administration, Holdren promised it would have a voice on everything from Arctic exploration policy to water allocations during droughts. He also reiterated Obama's promise to create a National Space Council to coordinate federal policy.

Lubchenco endorsed a proposal from her predecessor, former Navy Vice Admiral Conrad Lautenbacher, to create a National Climate Service within NOAA that would "do the same thing for climate as the National Weather Service does for weather … coordinating a wealth of data from other agencies to model how the climate system works." At the same time, she criticized NOAA's partnership with two other federal agencies in developing a multibillion-dollar system of Earth-monitoring satellites, calling the current collaboration an "embarrassment that needs to be fixed." **–JEFFREY MERVIS**

RETROVIRUS MEETING

HIV/AIDS Researchers Reach for High-Hanging Fruit

MONTREAL, CANADA—As Ringo Starr once sang, "It don't come easy." That was the unofficial refrain at the HIV/AIDS meeting held here last week, the largest annual gathering for the field in North America.

The 4200 researchers who attended the 16th Conference on Retroviruses and Opportunistic Infections heard about steady progress on several fronts, but unlike in years past, there was hardly a peep about new anti-HIV drugs and no major surprises surfaced about existing treatment or prevention strategies. "There's nothing that knocks my socks off," said Mario Stevenson, a virologist at the University of Massachusetts, Worcester, who helped organize the meeting. "We're in an era of just hammering away at AIDS. We're not going to have breakthroughs and eureka moments at every meeting." Yet the presentations here did offer many unexpected findings on a wide range of topics, including microbicides, the search for a cure, "elite controllers," and even chimpanzees.

Harm's way. New evidence from chimpanzees in Gombe suggests that SIVcpz, contrary to common wisdom, can outwit their immune systems and cause AIDS.

The most talked about prevention study starkly illustrated that "success" now often comes with a long list of provisos. Trials of microbicide gels to protect women against HIV infection have a perfect record: Not one has worked, and some were even harmful. Now, however, a large international study of a vaginal microbicide called PRO 2000 may have finally ended that curse, although the gel's benefits appear to be modest and require confirmation.

Epidemiologist Salim Abdool Karim of the Centre for the AIDS Programme of Research in Durban, South Africa, reported that PRO 2000 reduced the risk of HIV infection by 30% during the 3-year, $90 million study, which involved 3000 sexually active women in four sub-Saharan African countries and the United States. Before intercourse, the women used PRO 2000, another experimental microbicide called BufferGel, an inert placebo gel, or nothing at all. The 750 women in the PRO 2000 arm of the study had 36 HIV infections, whereas the other groups had between 51 and 54 infections each.

Although this was a low level of protection and the finding did not reach statistical significance, Karim emphasized that women in much of sub-Saharan Africa often do not have the option of using condoms. "In that population, 30% protection to me is a big difference," said Karim. "Finally, there's been a signal in the microbicide field, and that's a thrilling event," said epidemiologist Sten Vermund of Vanderbilt University in Nashville, Tennessee.

The study lends support to an all-but-rejected prevention approach, a microbicide gel with a so-called nonspecific mechanism. PRO 2000 has a negative charge that theoretically can bind to positively charged HIV surface proteins, blocking the virus's ability to infect cells. Several failures of such nonspecific approaches have led many investigators to place their bets on products that incorporate anti-HIV drugs. A larger study of PRO 2000 is under way and should determine whether it works later this year, but even the cautious are hopeful. "It's exciting to find a positive trend," said a skeptic of nonspecific approaches, virologist Robert Grant of the University of California, San Francisco (UCSF).

For the HIV-infected, the most pressing question is whether treatments can eliminate the virus altogether—a cure. Anti-HIV drugs can powerfully suppress the virus, but ultrasensitive assays have shown that no one has eliminated it. How the residual virus persists in blood and tissues is not clear.

One camp holds that drugs do not stop all replication, allowing the virus to constantly infect new cells and copy itself at low levels. This, in turn, replenishes a reservoir of infected, long-lived cells that otherwise would die off in a few years. If so, then intensifying treatment with more potent drug cocktails could knock out the virus entirely.

Virologist Robert Siliciano of Johns Hopkins University in Baltimore, Maryland, and colleagues tested that hypothesis by adding powerful anti-HIV drugs to the cocktails people with undetectable levels of virus were already taking. "What happens is that nothing happens," said Siliciano. "Intensification has no effect on residual viremia."

This finding, he says, lends credence to another theory for HIV persistence: that the infected reservoir is made up of cells that provide immunologic memory for decades and thus is stable and does not need to be replenished. If so, drugs that target viral replication can never eradicate the reservoirs, he said, and a cure will require a different strategy.

Researchers have long hoped that "elite controllers," the small percentage of infected people in whom the virus remains undetectable for many years on the standard test *without* taking anti-HIV drugs, may have effective immune responses that hold clues for vaccine makers. Steven Deeks of UCSF, however, had dispiriting news about these lucky few.

Deeks's studies suggest that in the majority of these controllers, the immune system works overtime to thwart the virus—with deleterious effects. These elite controllers have high levels of "activation," an inflammatory state caused by the immune system laboring to control HIV. That activation depletes critical CD4 white blood cells, the hallmark of AIDS; it also causes systemic inflammation that contributes to atherosclerosis and other complications. Indeed, four of 58 elite controllers he studied progressed to AIDS despite having only residual viremia. "If I were an elite controller, I'd seriously think about going on treatment," he said.

CREDIT: MICHAEL WILSON

In 40% of elite controllers, another immune mechanism seems to control HIV, but Deeks says he has no idea what that is. These controllers do not have high levels of activation, nor do they have much T-cell immunity—which many believe is a key immune response to battle HIV.

Both of these findings throw a curve ball to vaccine makers. Researchers assume that even if an AIDS vaccine does not stop an infection, it will bolster immune systems so people who do become infected effectively become elite controllers. But if most elite controllers suffer from immune activation, this becomes a far-from-ideal outcome. The second group of controllers who do not have an activation problem further confound the vaccine search, as T-cell immunity is a cornerstone of most products under development. Is there another critical immune response that vaccine makers need to target?

One of the biggest surprises at the meeting came from studies of wild chimpanzees. Researchers have long assumed that SIVcpz, the chimpanzee virus that infected humans and triggered the AIDS epidemic, caused no harm to apes. But new data reveal that wild chimps infected with SIVcpz are more likely to die than are uninfected chimps. The animals also show AIDS-like damage to their immune systems. The finding raises the possibility that some chimp populations are suffering from AIDS epidemics.

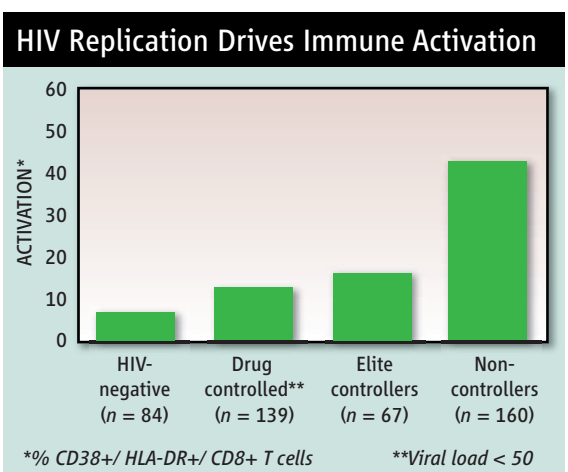

Control issues. Untreated HIV-infected "elites" have higher levels of immune activation than do people who suppress their virus with drugs.

SOURCE: STEVEN DEEKS/UCSF

Evidence suggests that SIVcpz, discovered in 1989, is most closely related to HIV-1 and predates it. Captive chimps experimentally infected with HIV-1 typically suffer no harm, which led several researchers to propose that chimps had lived with SIVcpz for centuries and that their immune systems had evolved to coexist with the virus. But few SIVcpz-infected chimps in the wild were identified until about a decade ago, when researchers led by Beatrice Hahn of the University of Alabama, Birmingham, developed a way to routinely test fecal samples for evidence of the virus. Although SIVcpz has not been found in several chimp communities studied, some have a prevalence as high as 35%.

Rebecca Rudicell, a graduate student in Hahn's lab, reported that she and her colleagues analyzed 1099 fecal samples collected between 2000 and 2008 from chimpanzees living in Gombe Stream National Park in Tanzania. They found evidence of SIVcpz infection in 18 chimps. Seven of the 18 infected chimps died during the study period, compared with 10 of 76 uninfected animals, said Rudicell. When they corrected for age and other variables, the scientists found that the SIVcpz-infected chimps had a 15-fold higher risk of death than did virus-free apes, meaning that SIVcpz poses nearly as great a risk as HIV-1 does to humans. Studies of lymph nodes from two of the infected chimps that died also showed the type of immunologic destruction seen in HIV-infected humans. And these chimps had low levels of CD4 cells, the lymphocytes that are the main targets of SIVcpz and HIV-1. "We were shocked at the initial discovery of SIVcpz in the Gombe chimps and even more dismayed when we established that it seems to be pathogenic," said behavioral ecologist Anne Pusey, who runs the Jane Goodall Institute's Center for Primate Studies at the University of Minnesota, Twin Cities, and collaborates with Hahn. "It must be the case that some of the [chimp] mortality over the last decades has been due to SIV." During their study period, the prevalence ranged from 9% to 18%, which mirrors the devastating levels of infections seen in human populations in the hardest hit countries in sub-Saharan Africa.

The finding raises provocative questions about the relationship between HIV-1 and SIVcpz. For instance, why does SIVcpz harm chimp immune systems when HIV-1 doesn't? The work might offer clues to vaccine makers, too, about which immune responses to target. Also unknown is whether SIVcpz has contributed to the alarming chimp decline seen elsewhere. But once again, the answers to those questions surely won't come easy. **–JON COHEN**

*Science*Insider

From the *Science* Policy Blog

Lifestyles of the rich and famous. That's one way to describe the world of science this week. Here are some highlights from our science policy blog, *Science*Insider.

First the **rich**. Science agencies continued to rack up billions, as Congress finally completed work last week on a $787 billion economic stimulus package. The biggest winner is the National Institutes of Health, which would receive $10 billion for research and facilities. Also seeing green is the Advanced Research Projects Agency for Energy, established by Congress 2 years ago to inspire risky energy and climate-related research. The concept hadn't gotten a dime in the regular appropriations, but lawmakers threw $400 million at it as part of the stimulus.

Now for the **famous**, and it doesn't get any more famous than Tom Hanks. This week, the movie star stopped by CERN near Geneva, Switzerland, to chat about Illuminati and antimatter. So what does he think of the world's largest particle physics laboratory? "I love seeing science fiction become science fact," he told one of our reporters on the scene. Speaking of CERN, its Large Hadron Collider should be back in business by late September.

In **Washington**, John Holdren and Jane Lubchenco sailed through a joint Senate confirmation hearing, while the House of Representatives passed legislation to overhaul environmental and safety research related to nanotechnology. If the Senate follows suit, the new law will set up a nano czar in the White House and require a research plan.

Finally, what do you get when you cross a vacuum cleaner with a tree? A potential **geoengineering** solution called air capture, which aims to lower atmospheric CO_2 levels by literally sucking the greenhouse gas out of the sky. We smell a sci-fi movie. Someone get Tom Hanks.

For the full postings and more, go to **blogs.sciencemag.org/scienceinsider**.

Published by AAAS

Al Gore to Scientists: 'We Need You'

At a meeting full of scientific celebrities, a former politician proved to be the greatest draw. Of course, Al Gore is no ordinary politician, especially to any scientist interested in climate change. One might say he's a politician turned scientist, and as an invited speaker on the second night of the meeting, the former vice president sought to reverse the equation: He asked all the scientists in the audience to get involved in politics. Gore began by saying that the economic crisis is intertwined with the climate crisis. Both, he said, have their roots in our dependence on carbon-based fuels. He even went as far as to compare climate change with the mortgage meltdown. "We now have $7 trillion worth of subprime carbon assets whose value is based on the assumption that it is perfectly all right to put 70 million tons of global warming pollution into the thin shell of atmosphere surrounding our planet," he said.

Then it was on to *An Inconvenient Truth* territory, with Gore updating the doomsday scenarios he laid out in his book and 2006 movie: The Arctic ice is melting faster than we anticipated, the Maldives is trying to buy itself a country that won't be under water, and no one seems to notice anymore when 1 million people are evacuated from New Orleans. "Is this the new normal?" Gore asked.

So what can scientists do?

Educate the public, for one. These days, Gore's number-one enemy is "clean coal." He says the coal industry is spending half a billion dollars to mislead society about the dangers of fossil fuels—much like the tobacco companies whose ads touted the health benefits of cigarettes in the mid-1900s. "When they spend $500 million putting their version of this story in the minds of the American people, it increases the importance of you being willing to speak out," Gore said.

But Gore wants scientists to do more than talk. He wants them to get involved. Science and politics have been separated for too long, he said. "Now that the survival of our civilization is at risk, and now that the solution to this crisis depends on the rapid spread of understanding from the world of science into the world of policy, … scientists can no longer in good conscience accept this division between the work you do and the civilization in which you live."

Some scientists have already joined the fray, Gore noted, referring to John Holdren, Jane Lubchenco, and other researchers who will advise President Barack Obama. "The policymakers are *of* you," Gore said. "Keep your connections to them. Become a part of this struggle. We need you."

Judging from the standing ovation, Gore might have won a few recruits. **–DAVID GRIMM**

Will Many Endangered Species Recover?

In the past 35 years, only the peregrine falcon and a handful of other species have recovered enough to be taken off the U.S. government's list of threatened and endangered species. Others, such as the California condor, require constant help from humans to survive the threats they face. In fact, the vast majority of these species are "conservation reliant," said John Wiens of PRBO Conservation Science in Petaluma, California. And they may never be taken off the list.

Wiens and Michael Scott of the U.S. Geological Survey in Idaho wanted to know how many of the 1300 listed species will require constant conservation to endure. They examined recovery plans issued for 1100 species and checked whether they will need continual help. More than 80% are conservation reliant and will need to remain on the list, they found. "We thought it would be lower," Wiens said. "We were quite astounded."

The situation is likely to get worse. Because habitat destruction and other threats are increasing, more species will probably need to be listed—adding to costs of keeping

FINDINGS
The Science Magazine News Blog

Time Traveling at AAAS

Here are some of the highlights of other stories filed by Science *reporters at the AAAS meeting.* For more complete coverage of the meeting, go to **blogs.sciencemag.org/newsblog/**.

Considering the theme of this year's meeting, "Our Planet and Its Life: Origins and Futures," it's no surprise that many of the talks traveled through time. First, it was off to the future with a sober assessment of what lies ahead for our planet. Perhaps the most frightening news is that the worst case scenarios analyzed by the Intergovernmental Panel on Climate Change (IPCC) may not have been dire enough. Humans have recently been pumping out climate-warming gases faster than the IPCC anticipated. These changes spell bad news for humans, as coastal cities flood and diseases like malaria spread to new areas.

Another series of talks focused on the "Origins" theme of the meeting by peering into humanity's past. Particle accelerators are allowing scientists to view our history like never before, as beams a billion times brighter than a hospital x-ray bring ancient manuscripts and statues to life. Scientists are also learning more about our distant relatives. Neandertals at one site rarely knew their grandparents, for example, as most died before the age of 30. And what of those Indonesian "hobbits" that have confounded scientists since their discovery in 2004? Researchers presented additional evidence at the meeting that they are not deformed *Homo sapiens* but rather represent a small species of human.

Speaking of small, scientists reported a genetic mutation that explains why little dogs, such as dachshunds and Scottish terriers, have such stumpy legs. Other researchers, perhaps seizing on the fact that Valentine's Day fell during the meeting, probed the evolutionary importance of kissing. And if you ever wanted to fold a piece of paper into a three-dimensional rabbit, scientists are working on a computer program called an origamizer to help you out.

species on life support. That means more thinking will be needed about how to prioritize funds spent on endangered species.

–ERIK STOKSTAD

First Globetrotters Had Primitive Toolkits

Ever since researchers found fossils of *Homo erectus* beneath a medieval castle in Dmanisi, Georgia, they have been chipping away at the image of this venerable human ancestor. At 1.8 million years old, the fossils are the earliest members of the human family known outside Africa. Now, it turns out that they managed to trek all the way across Africa and the Middle East with the most primitive kind of stone tools known rather than with more sophisticated stone hand axes that were thought to be essential for intercontinental travel.

The textbook vision of the first world traveler has changed, says paleoanthropologist David Lordkipanidze of the Georgian National Museum in Tbilisi. This is the third time Lordkipanidze's team has revised the textbook view of early *H. erectus*, suggesting that it was more primitive than expected. First, his group published the brain size of the fossils at Dmanisi, which had a volume of just 650 cubic centimeters—not much larger than an australopithecine's brain volume of 450 cc. Then, the team found leg bones and announced that the Dmanisi people were short. Now, they have found Oldowan, Mode 1 stone tools at Dmanisi (see picture), not the retouched Acheulean hand axes that were a kind of Swiss Army knife for *H. erectus* in Africa.

"I'm not at all surprised," says paleoanthropologist Robert Blumenschine of Rutgers University in New Brunswick, New Jersey. He says it's not uncommon to find evidence of both types of technologies in the same fossil locality. "The Oldowan tools were still good tools—they used them for different things," says Blumenschine. There was no such thing as technological obsolescence—yet.

–ANN GIBBONS

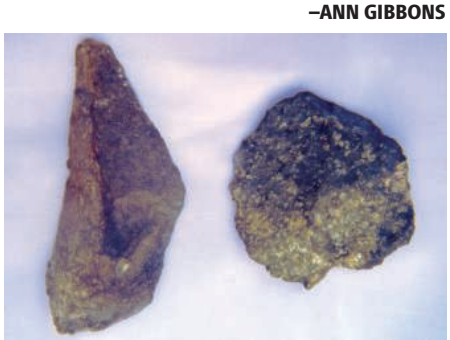

CREDITS (TOP TO BOTTOM): COURTESY OF KEVIN J. ANCHUKAITIS/COLUMBIA UNIVERSITY; COURTESY OF DAVID LORDKIPANIDZE

ECOLOGY

Tree Rings Tell of Angkor's Dying Days

Archaeologists have long puzzled over the collapse of the mighty medieval Khmer kingdom in Southeast Asia best known for its resplendent capital, Angkor. New findings suggest that a decades-long drought at about the time the kingdom began fading away in the 14th century may have been a major culprit.

Evidence for a megadrought comes from centuries-old conifers that survived the Angkor era. At a conference* earlier this week in Dalat, Vietnam, tree-ring scientist Brendan Buckley of Columbia University's Lamont-Doherty Earth Observatory in Palisades, New York, described how the annual growth rings of conifers in Vietnam reveal a sharp weakening of Asia's summer monsoon from 1362 to 1392 C.E. and again from 1415 to 1440 C.E., just as the Little Ice Age was setting in and right when the Khmer kingdom was reeling. The tree-ring chronologies "represent a major breakthrough in tropical dendrochronology," says David Stahle, a tree-ring expert at the University of Arkansas in Fayetteville.

Finding this new trove of data wasn't easy. Many tree species in Southeast Asia lack growth rings or have ones that cannot be used to reveal annual patterns, says Buckley. But in the past 5 years, he and others have validated several species in the region with annual growth rings. The evidence presented in Dalat comes from a rare conifer, the po mu (*Fokienia hodginsii*), spanning 7 centuries.

Its drought-revealing tree rings corroborate similar climate data from coral reefs and, most recently, stalagmites and stalactites that peg monsoon changes to the fall of other Asian societies (*Science*, 7 November 2008, p. 837). "The evidence for pronounced weakening of the monsoon is indisputable," says Daniel Penny, co-director of the Greater Angkor Project (GAP) at the University of Sydney in Australia.

The Khmer kingdom, which encompassed much of modern-day Cambodia, central Thailand, and southern Vietnam, would not be the first civilization to literally bite the dust. A series of droughts devastated the Maya city-states of the Yucatán Peninsula between 800 and 900 C.E., around the time Angkor was rising. It's still unclear whether prolonged drought several centuries later brought a vibrant Khmer kingdom to its knees or was a coup de grâce to a staggering society. Nevertheless, the medieval tree rings may offer a lesson for the modern world: Harsh weather events, predicted to grow more frequent with global warming, may imperil communities on the knife edge of sustainability.

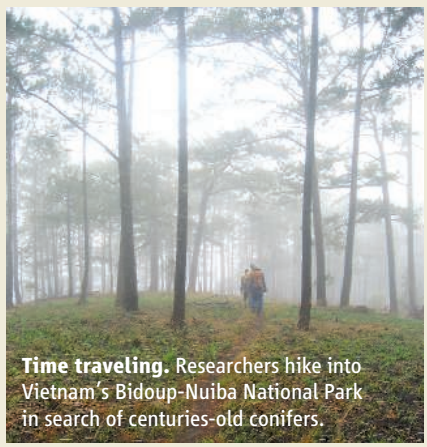

Time traveling. Researchers hike into Vietnam's Bidoup-Nuiba National Park in search of centuries-old conifers.

Angkor's rulers, on the backs of a huge corvée labor force, built hundreds of temple complexes—including Angkor Wat, humanity's largest religious monument—and carved hundreds of kilometers of canals and massive reservoirs that appear to have been used both for irrigation and for religious ceremonies. Then, in one of archaeology's enduring mysteries, Angkor was largely abandoned by the 16th century.

Theories abound for how the wealthy kingdom fell, with one of the latest ideas being that Angkor's vaunted waterworks grew too complex to maintain (*Science*, 10 March 2006, p. 1364). Recent archaeological and pollen findings from GAP indicate that Angkor's great reservoirs and storage ponds began operating at sharply reduced capacity several decades before the back-to-back droughts. That evidence suggests Angkor was in trouble long before drought set in, says GAP co-director and Sydney archaeologist Roland Fletcher. "Climate instability would have been a severe problem for a massive and inflexible water network to manage," he says.

"I'm very concerned that the story will end with, there was a drought and Angkor collapsed," adds Penny. "It's not as simple as that—and [it's] far more interesting."

–RICHARD STONE

*Climate Variability in the Great Mekong River Basin, 16–18 February.

Published by AAAS

Is Silicon's Reign Nearing Its End?

Silicon is almost synonymous with computer chips. But as the semiconductor struggles at the minute scales of today's devices, chipmakers are being forced to consider other materials

If you want to see real nanotechnology in action, check out Intel's Penryn computer chip. It contains some 820 million transistors, each with features just a few tens of nanometers across. These transistors are so small that more than 2 million can fit on the period at the end of this sentence. A device inside each one flips an electrical switch on and off as many as 300 billion times a second. In the time it takes for one such flip, light travels less than half a centimeter.

Amazing—but not good enough. Late this year or early next, Intel plans to introduce a new line of chips that shrinks the components even smaller. For the past half-century, this perpetual contraction has been at the heart of the industry's favorite trend: Moore's Law, which holds that the number of transistors on chips will double about every 2 years. For most of that history, this downsizing, known as scaling, came about as engineers developed ever sharper chip-patterning techniques. But the past few years have brought a quiet revolution to chipmaking. Because conventional materials have started misbehaving at such small scales, engineers have had to call in reinforcements. Since the 1990s, chipmakers have gone from making their devices out of about 15 chemical elements to making them out of more than 50, in hope that the new additions will help them keep shrinking the devices.

Few doubt that Moore's Law will hold for a couple more generations of chips, and perhaps even longer. But continuing this trend will not be a straightforward enterprise. Researchers are looking at redesigning the way they make transistors, incorporating new insulators, and even replacing silicon as the semiconductor through which electrical charges flow in their circuitry. "There are very serious challenges ahead," says electrical engineer Jesús del Alamo of the Massachusetts Institute of Technology (MIT) in Cambridge. Adds electrical engineer Mark Rodwell of the University of California, Santa Barbara, "Regardless of which [technology] wins, there's a real sense that there aren't too many years left to play this game."

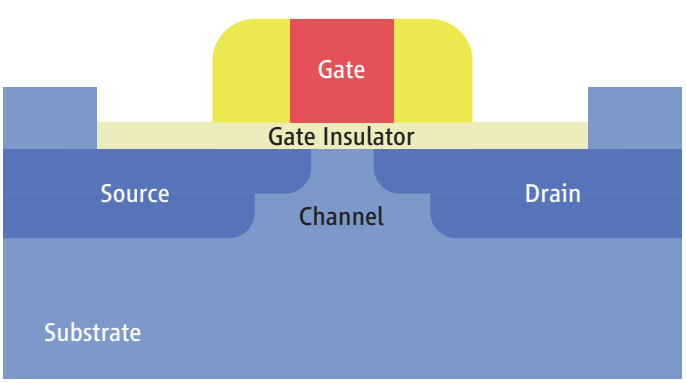

Logical. Conventional transistors, known as MOSFETs, keep getting smaller and better. Today, more than 30 million can fit on the head of a pin.

CREDITS (TOP TO BOTTOM): COURTESY OF INTEL CORPORATION; J. NEWFIELD/*SCIENCE*

Matchmaker, matchmaker

At the center of this game are transistors, or more precisely, metal-oxide-semiconductor field-effect transistors (MOSFETs). They work by sending a pulse of electricity to a central electrode called the gate (see figure, below). The charge on this gate causes a spike in the electrical conductivity of a semiconducting channel that sits below it. This opens an electrical doorway in the channel, allowing an electric current to flow between two other electrodes—known as the source and the drain—that sit at opposite ends of the channel. The high electrical output at the drain is a "1" in the on/off digital world. If you turn off the charge on the gate, the channel door closes and the current flow to the drain shuts off, giving you a digital "0."

Silicon MOSFETs have worked wonders in recent decades, thanks in large part to a unique marriage in the material world. In a MOSFET, the gate electrode and the conducting channel beneath it must be insulated from each other, so that when the gate is closed, any excess charges in the gate aren't able to open the channel and let current flow between the source and the drain. In traditional logic chips that are the brains of desktop computers and servers, that insulating layer has been provided by silicon dioxide (SiO_2).

Silicon and silicon dioxide's

storybook marriage has thrived for decades because where they meet, they form a near-perfect union. At these interfaces, each silicon atom binds readily to four oxygen atoms. That's good, because it ties up unfilled bonds at the silicon channel's edge that can trap electrical charges in place and disrupt the transistor's ability to switch when prodded. Whenever defects occur, engineers can easily neutralize them by piping in hydrogen to latch onto any free bonds. The result has been that although other semiconductors are faster and stronger, the near-perfect union between silicon and silicon dioxide has made it possible to continually improve transistors.

Online
sciencemag.org
Podcast interview with author Robert F. Service

Recently, however, the stress of relentless scaling has proved too great for SiO_2, which is only a moderately effective insulator. As transistors continued to shrink, engineers were forced to make their SiO_2 layer as thin as 1 nanometer, or about three atomic layers thick. That was so thin that it started to leak. "We were just running out of atoms," says Suman Datta, an electrical engineer and Intel veteran, who now works at Pennsylvania State University, University Park.

In the mid- to late 1990s, researchers at Intel, IBM, and elsewhere realized the days for silicon dioxide were just about up and that they needed to ditch silicon's devoted partner for a new trophy wife. Their goal was to find a material with a higher insulating value, known as its dielectric constant and denoted by the Greek letter kappa (κ). Researchers tested dozens of "high-k" alternatives, finally settling on a new bride called hafnium dioxide (HfO_2).

"It started off innocently, saying we'll just swap out the SiO_2 with a high dielectric constant [material] and be on our way," says Supratik Guha, a materials scientist and senior manager at IBM in Yorktown Heights, New York. Unfortunately, the change wasn't so simple. Among many other problems, the new insulator didn't form a clean interface with the gate above it, which was made from polycrystalline silicon. So engineers were forced to replace the polysilicon gate with titanium-based alloys that performed better. That change raised new problems, because the metal alloys couldn't handle the high temperatures used in manufacturing some of the other components. Ultimately, Intel worked out a manufacturing strategy, and last year the company began shipping chips made with the new metal gates and HfO_2 insulator. At the time, Gordon Moore, co-founder of Intel and eponymous drafter of the law, called the switch "the biggest change in transistor technology since … the late 1960s."

What is sobering is that this relatively straightforward change took the industry a good 10 years to accomplish, and the challenges ahead appear to be far greater. "The complexity of the problems is only going to grow," Datta says. For starters, as Intel and other chip companies prepare to contract from the 45 nanometer scale to 32 nanometers (the numbers refer to half the distance between adjacent lines of memory cells), it appears that silicon dioxide is set to cause a new round of trouble. Even though SiO_2 was supposedly replaced as the gate insulator, a little bit has remained behind because it is nearly impossible to eliminate. When silicon is placed next to hafnium dioxide, Datta explains, some oxygen atoms at the interface invariably break their bonds to hafnium and hook up with silicon. This isn't all bad, he says, because the clean interface with that ultrathin layer of SiO_2 seems to improve the conduction of electric charges through the semiconductor channel. But with all the device components set to shrink again, the SiO_2 layer must also get thinner—and that could disrupt the flow of charges in the silicon. "It's a very tough problem," Datta says.

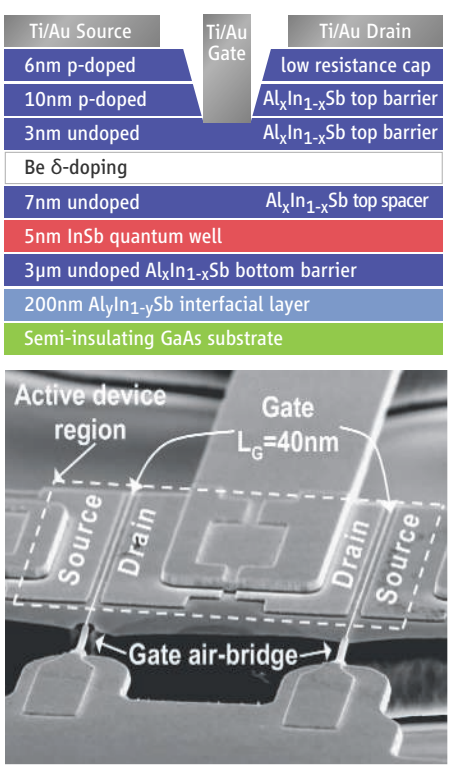

Speed boost. Novel high-speed transistors (*above*) from Intel push positive charges through a thin layer of InSb (*top*, red).

CREDITS (TOP TO BOTTOM): RADOSAVLJEVIC *ET AL.*, *IEEE* APRIL 2008, P. 728; RADOSAVLJEVIC *ET AL.*, *IEEE* APRIL 2008, P. 729

At the International Electron Devices Meeting (IEDM) in San Francisco in December 2008, Intel researchers reported that they had solved this problem and many others. The company announced that it had completed the development phase of its 32-nanometer–manufacturing process and would begin turning out the new chips by the end of 2009. Intel researchers haven't revealed their latest tricks, but Datta calls the performance data they have presented "excellent." Datta says he expects Intel to stick with HfO_2 for now, because it was so expensive to make the switch in the first place.

A new look

So if the next step in shrinking silicon electronics is on track, what's next? After 32 nanometers, the next step down is 22 nanometers. "This is where things get very interesting," Datta says. At this dimension, it's likely that HfO_2 will also begin to fail to contain current within its walls. If that happens, one option is to change to a material with an even higher dielectric constant, says Darrell Schlom, a high-k expert at Cornell University. Schlom's group has tested more than a dozen. Among the best, he says, is crystalline lanthanum lutetium oxide, which has a dielectric constant of 40, more than 10 times that of SiO_2 and nearly double that of HfO_2. A big challenge, however, is that the more elements make up the insulating material, the harder it is to keep the perfect order of the material at the interfaces.

Another option at this scale is to redesign the architecture of transistors altogether. One alternative, considered most likely for 22-nanometer scale devices, is to move away from layered, sandwichlike devices and stand the silicon channel on its side. Such devices, known as FinFETs (because the vertical silicon channel looks a bit like a fish fin), in principle would allow engineers to surround the channel on three sides with dielectrics and gate materials. Then using several gates in concert to trigger the flow of current in the channel could make it easier for engineers to control when the devices flip on and off and how much current they put out when they do.

Academic researchers have been turning out FinFETs and other exotic-shaped devices for years. Now, however, even the big chip players are looking at exotic designs. At IEDM, for example, a consortium of researchers from Toshiba, IBM, and Advanced Micro Devices reported making

Published by AAAS

the world's smallest FinFET transistors with high-k dielectrics and metal gates. The new transistors were only half the size of previous FinFET record holders, and studies revealed that their geometry made them more reliable than planar versions, according to company press materials. But, at least for now, the new devices suffer from poor electrical contacts between the source and drain electrodes, Datta says.

	Speed of Charges in Different Materials ($cm^2/V·s$)				
Charges	Si	GaAs	$In_{0.53}Ga_{0.47}As$	InAs	InSb
Electrons*	300	7000	10,000	15,000	30,000
Holes*	450	400	200	460	1250

*Electron carrier mobilities measured in transistor channels with electron concentration of $1x10^{12}$ cm^{-2}. Hole mobilities in bulk.

Racing form. Engineers can speed up transistors by using higher-speed materials. But although negatively charged electrons move quickly in most III-V materials, positively charged "holes" typically do not.

Beyond silicon

Even that switch, however, looks simple compared with the changes further ahead. After the 22-nanometer scale comes 15 nanometers, and it appears—at least for now—that improvements in transistor speed and performance will have to come from new materials rather than from scaling silicon further. "Now that you've gotten rid of the SiO_2, why not have the high-mobility channel and high-k materials to put on top of it?" Schlom asks. In other words, why not replace the silicon with a better semiconductor?

Top candidates for this switch are semiconductor alloys know as III-Vs, due to the position of their elements in the periodic table. Examples include gallium arsenide, indium gallium arsenide (InGaAs), and indium antimonide (InSb), all of which can ferry electrical charges much faster than silicon can (see table, above).

But there are lots of problems in marrying III-Vs with modern logic-chip technology. For starters, it is not currently possible to make large-scale III-V wafers on which to construct the devices from the ground up. That means engineers need to integrate III-V materials on the silicon wafers that are the industry standard. That's no easy task, because the atomic spacing in III-Vs is significantly different from silicon. Try to grow InGaAs, for example, directly on silicon and you get an interface riddled with free atomic bonds that drastically slow the flow of charges in the device. If the interface between a III-V semiconductor and the silicon wafer beneath it is a problem, equally difficult is the interface to a high-k dielectric above it. And so far, efforts to neutralize defects have proven underwhelming. Unlike silicon and SiO_2's perfect marriage, "there's no wonderful interface with the III-Vs," Schlom says.

Another challenge is making transistors that conduct positive charges, called holes. That's important for chip designers, as it allows them to alternate transistors that carry negative charges (n-type) and positive charges (p-type), which, when working together, give clearer electronic readouts and use less power. Silicon ferries holes nearly as well as it does electrons. But most III-Vs are far better at conducting electrons than holes. "There are a lot of problems that may seem insurmountable," Schlom says, "but I'm cautiously optimistic that they can be solved."

Some steps toward those solutions are already evident. In 2007, for example, researchers at Intel led by Robert Chau reported growing InGaAs transistors atop a thin buffer layer sitting on a silicon wafer. The buffer allowed the two dissimilar materials to sit next to each other with relatively few problems. Researchers elsewhere have also had success with InGaAs. In one example, researchers led by Peide "Peter" Ye of Purdue University in West Lafayette, Indiana, reported in the April 2008 issue of *IEEE Electron Device Letters* that they had made high-speed InGaAs n-type transistors that had a large output current when switched on, an important hurdle for the field.

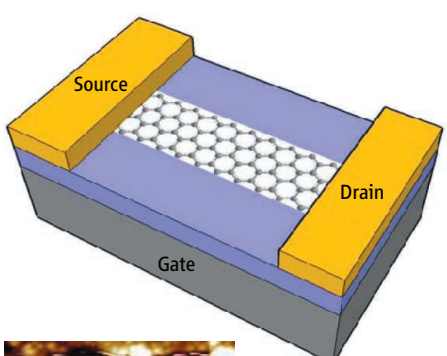

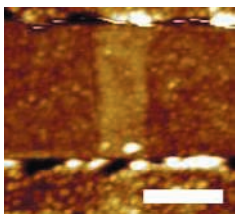

New kid. Transistors made from graphene nanoribbons could be blinding fast. But can they perform on an industrial scale?

Still, Ye and others acknowledge that III-Vs aren't there yet. Ye's InGaAs devices, for example, work splendidly when switched on, says materials scientist Paul McIntyre of Stanford University in Palo Alto, California; but try to switch one off and current still leaks through, like water overtopping a levee. In addition, neither Ye's group nor any other has had much luck in making high-quality p-type transistors from InGaAs. At IEDM, Chau and colleagues at Intel did report novel InSb p-type transistors that are the fastest to date. But, for now, they too remain leaky when switched off.

There might be a workaround. Researchers at IBM and elsewhere have also had some success with making high-speed p-type transistors using germanium (Ge). And though Ge isn't itself a III-V compound, it seems to integrate fairly well with them. One hope, Ye and others say, is that researchers will be able to make integrated circuitry using InGaAs n-type transistors next to Ge or InSb p-type transistors. Even if they succeed, however, the circuits could be prohibitively expensive to manufacture, as they require patterning very different materials in the same layer of the chips. Still, despite these challenges, Ye remains optimistic. "I think the future is still bright because there is no other choice," he says.

That's not entirely true. If III-Vs don't pan out, or perhaps even if they do and last only a generation or two, there are plenty of far-out ideas for reinventing microelectronics. Among them: transistors made with single-layer carbon sheets called graphene, carbon nanotubes, or III-V nanowires. But for now, these upstarts still need plenty of work to have a shot at dethroning more-conventional approaches.

In any case, it's clear that this work needs to happen soon, or the steady progress of Moore's Law will begin to slow if not stop. "My own view is that we will not see another decade of scaling," McIntyre says. Perhaps not. But MIT's del Alamo and others point out that the $260-billion-a-year chip industry has been jumping over roadblocks for years. "The potential payoff is gigantic," del Alamo says. Adds Datta: "One thing I've learned is, don't predict the end of Moore's Law."

–ROBERT F. SERVICE

CREDITS (TOP TO BOTTOM): DEL ALAMO, KIM AND WALDRON/MICROSYSTEMS TECHNOLOGY LABORATORIES/MIT; DAI *ET AL.*, *PHYSICAL REVIEW LETTERS* 23 MAY 2008, VOL 100 ISSUE 20

Published by AAAS

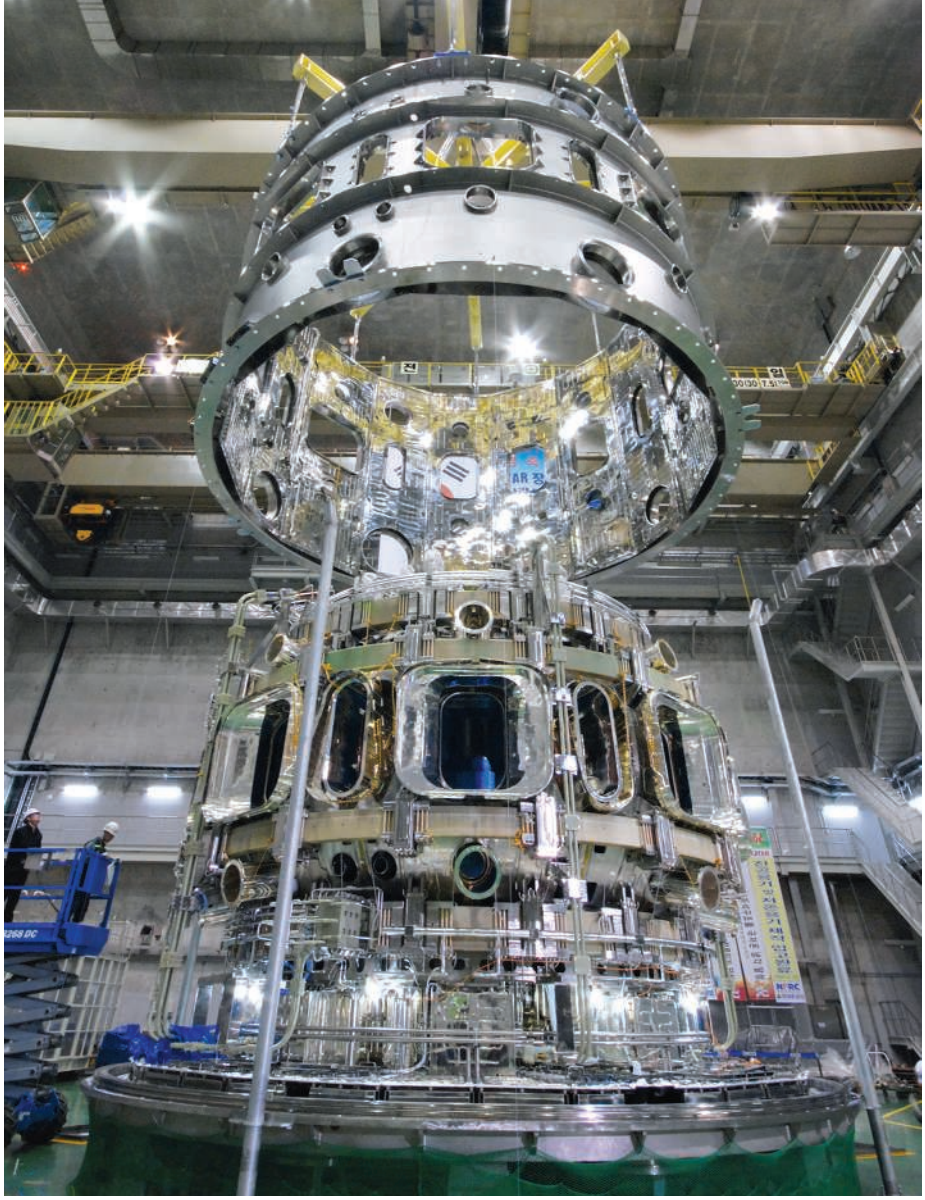

CREDIT: NATIONAL FUSION RESEARCH INSTITUTE

All fired up. KSTAR research will start this fall.

APPLIED PHYSICS

New Facility Propels Korea to the Fusion Forefront

Using innovative magnets that should confine plasmas for minutes rather than seconds, KSTAR is poised to become a premier testbed for fusion research

DAEJEON, SOUTH KOREA—At first glance, the fist-size bundle of wires on a conference table at the National Fusion Research Institute (NFRI) here looks like scrap metal doubling as a paperweight. But then NFRI President Gyung-Su Lee points to it as evidence of the engineering prowess that has thrust Korea to the fusion frontier: The wires are a sample of superconductive cable that's wound into magnets at the heart of the world's most advanced fusion research facility, the Korean Superconducting Tokamak Reactor (KSTAR).

The ability to fashion high-performance superconducting magnets from a niobium-tin alloy was a key technology that NFRI's industrial partners mastered while building a machine that fired up its first plasma a few months ago. Engineers are now installing control and diagnostic equipment that will allow research to begin in earnest this fall. KSTAR's explorations will reverberate all the way to Cadarache, France, where a consortium is assembling the most important fusion experiment ever, the International Thermonuclear Experimental Reactor (ITER), expected to come online in 2016.

"We definitely [wanted to] make KSTAR a really useful device for ITER preparation," says Lee. Fusion physicists say the Koreans have succeeded. "KSTAR has a very important role to play [in providing data] that will be used to design operating scenarios for ITER," says Hutch Nielson, a plasma physicist at the Princeton Plasma Physics Laboratory.

ITER will tackle a decades-old question: whether the fusion process that powers stars can be harnessed to produce electricity (*Science*, 13 October 2006, p. 238). It will use powerful magnets to confine a plasma within a doughnut-shaped high-vacuum vessel called a tokamak. At about 1 million degrees Celsius, the plasma's charged particles fuse, releasing energy. ITER will be several times larger and, at $6 billion, far more expensive than any existing tokamak.

Because ITER could cost more than $1 million a day to run, "you're going to have to operate as efficiently as possible," says David Campbell, ITER assistant deputy director general for fusion science and technology. Before ITER comes online, he says, researchers will be learning to control plasmas using the world's existing half-dozen major tokamaks. KSTAR, ⅕ of ITER's size, is the youngest in this cohort and will cost about $800 million after upgrades planned over the next several years. KSTAR's biggest advantage is its superconducting coils, which will enable it to confine plasmas for up to 300 seconds, compared with the 20 or so seconds of older tokamaks.

Catching up

Soviet Premier Mikhail Gorbachev proposed building what became known as ITER to U.S. President Ronald Reagan in 1985. The original four partners represented all those nations with a serious investment in fusion research—the Soviet Union, the United States, the European Union, and Japan. Twenty years later, as ITER was moving from design to construction, three Asian nations wanted in. China and Korea joined the project in 2003, and India joined in 2005.

The newcomers were intent on showing that they could bring expertise as well as cash to the table. India embarked on its Steady State Superconducting Tokamak in 1994; technical problems have delayed commissioning. Korea initiated KSTAR in 1995, although it was put on hold for 2 years because of the 1997 Asian financial crisis. China completed its Experimental Advanced Superconducting Tokamak in 2006 (*Science*, 19 May 2006, p. 992). The three countries "are much more significant players in fusion than they were a decade ago," says Nielson.

Of the new facilities, experts say

Published by AAAS

Fusion star. Gyung-Su Lee of Korea.

KSTAR is particularly outstanding given Korea's limited experience in fusion research. Before KSTAR, Korea had a handful of fusion researchers working with pint-sized tokamaks. Building the most advanced tokamak to date "was courageous and visionary," says Nielson, who consulted on KSTAR's design. He and others credit Korea's success to Lee. The physicist, like his colleagues in China and India, drummed up support for fusion research and for joining ITER by raising the alarm over future energy supplies. Korea is totally dependent on imported energy. "Because of the energy crisis and global warming, someday [fusion energy] had to get going, but Korea was not prepared," Lee explains.

Lee first won backing from Korea's industrial titans by convincing them to get in on the ground floor or risk having to license fusion reactor technology from others. He then got the government to put up "a huge magnitude of money" by persuading bureaucrats that investing in a future energy source was like buying insurance.

Paving the way

As planned for ITER, KSTAR uses superconducting magnets for both the toroidal field, which vertically rings the vacuum chamber, and the poloidal field, which follows the curve of the torus horizontally. Only one other tokamak—China's—features fully superconducting coils and can confine plasmas for 300 seconds or more. Older tokamaks use copper magnets that operate in pulses of up to only 20 seconds or so before overheating. "The significance of KSTAR and [China's tokamak] is that they can run long pulses and explore how to operate for a long duration and also what kind of physics you're going to encounter in that long duration," says David Humphreys, a plasma physicist at General Atomics in San Diego, California. ITER is expected to initially operate in 300- to 500-second pulses before ramping up to 3000 seconds.

KSTAR will also manipulate the plasma in ways particularly relevant to ITER, says Campbell. Some older tokamaks form plasma into a circular cross section. But ITER and KSTAR will aim for a sharply angled "D," which is more effective for confining the plasma and reducing instabilities that can leak energy and damage the vessel. Scientists hope to refine the "D" in Daejeon. "The KSTAR magnets were designed to allow strong plasma shaping control research," says Yeong-Kook Oh, head of experiments and operations for KSTAR.

Also paving the way for ITER, KSTAR uses the same systems to heat plasma and boost plasma current. These include injecting neutral particles and zapping the plasma with radio waves. KSTAR will also test exotic methods of taming instabilities, such as firing pellets of frozen deuterium into the plasma to release pockets of pent-up energy that otherwise cause turbulence.

The KSTAR tokamak will initially be lined with carbon-based tiles, but it might be modified later to test tungsten-based materials favored for ITER, says Oh. Already, KSTAR has proven the feasibility of working with the finicky niobium-tin alloy that ITER intends for its magnets.

No existing tokamak, KSTAR included, can achieve a burning plasma, in which at least half the energy necessary for fusion is generated internally. ITER is designed to produce more energy than it consumes. It will achieve that goal in part by relying on a fuel mix of deuterium and tritium, which fuses at a lower temperature than other gases, including deuterium alone, which is what fuels KSTAR and most other tokamaks.

KSTAR can't prove fusion is the energy of the future. But until ITER is fired up, this Asian upstart will be the hottest testbed in the world for fusion research. **–DENNIS NORMILE**

PROFILE: RICHARD RICHARDS

Making Every Drop Count in the Buildup to a Blue Revolution

Richard Richards is breeding wheat varieties that can tough out prolonged droughts—and keep people fed

LEETON, AUSTRALIA—Kneeling in verdant young wheat at Leeton Field Station, Richard Richards uproots seedlings of two varieties and splays them out for inspection. Looking on are several stern farmers and scientists from the Grains Research and Development Corp., which funds his work. They're a tough bunch to impress—but Richards has them spellbound. One seedling, "Vigour X-25," has a coleoptile, or seed sprout, that's twice as long as the other's. To this audience, the meaning is clear. In drought, when the top few centimeters of soil dry out, seeds that grow longer coleoptiles can be sown deeper, in moist soil needed for germination.

In the 1950s, wheat breeder Norman Borlaug launched the Green Revolution by dwarfing wheat varieties, which diverts plant energy from stalk to grain and boosts yields several-fold. Today, a golden dwarf sea stretches from the U.S. Great Plains to southern Australia's Wimmera Plains. But dwarfs have a major shortcoming: short coleoptiles. That's a serious problem in many regions, where water availability is a key constraint for crop yields. With a rallying cry of "more crop per drop," Borlaug exhorted fellow breeders to foment a Blue Revolution.

After 3 decades of dogged effort, Richards, a soft-spoken geneticist at CSIRO Plant Industry in Canberra, has nudged wheat to the brink of a Blue Revolution. "Richards uses a surgeon's scalpel" to tweak just the right physiological processes, says Brett Carver, a wheat breeder at Oklahoma State University, Stillwater. As a result, although most breeders these days content themselves with wheat yield gains of about 0.5%, Vigour X-25 and another Richards creation, Drysdale, are yielding 10% to 20% gains in arid conditions.

Hailing his achievements, the American Society of Agronomy last October awarded Richards its Martin and Ruth Massengale Medal for "significant contributions to new and innovative research in crop physiology and metabolism." He's not resting on his laurels. Using DNA tags that track genes conferring more efficient transpiration and long

Sow moist. The longer coleoptile of Vigour X-25 (*left*) helps it tough out drought.

CREDITS (TOP TO BOTTOM): D. NORMILE/*SCIENCE*; E. FINKEL/*SCIENCE*

Published by AAAS

coleoptiles, Richards is combining the best of Drysdale and Vigour X-25 in a variety that should be ready for commercialization next year.

The long and short of it

Australia's southern wheat belt has a Mediterranean-like climate, in which much of the annual rainfall comes during a mild winter. In the early 1980s, Richards's CSIRO team pondered how it could help farmers make the most of that precipitation pattern.

One day in 1985, a farmer sowed an idea in Richards's mind. "Wheat's slow off the mark, not like barley," he recalls the farmer saying. Richards knew that barley is prized for its ability to thrive during drought. He speculated that barley's vigorous leafy growth acts as a shade to prevent evaporation from the soil. When wheat and barley are planted side by side, one obvious difference is that barley seedlings roll out wide leaves whereas wheat foliage looks spindly. A second difference lay nestled in the seed: Barley's embryo is nearly twice as big as a wheat embryo, giving it a substantial head start.

Guided by these clues, Richards scoured seed banks for wheat with larger embryos and wider leaves. Jinghong, a Chinese variety, has embryos that are 50% bigger, on average, than those of other wheats. And Kharchia from India has wide leaves. After crossing, the hybrids were even more vigorous than barley and cut evaporation from a field by 30%.

To Richards's surprise, the hybrids also had long coleoptiles. Those of Green Revolution varieties are 5 to 7 centimeters—short enough to lead to crop failure in parched conditions. "It's the baggage of the Green Revolution," Richards says. The new varieties had another advantage: more highly branched roots, which double nitrogen uptake from soil. To add the benefits of dwarfing, Richards began crossing the hybrids with varieties of dwarf wheat with long coleoptiles. His newly developed Vigour X-25 is the result of a cross between an Italian dwarf and the Chinese-Indian hybrids.

U.S. farmers could benefit from this advance, says Carver. Great Plains wheat is sown in late summer to take advantage of sporadic summer rain, but because local varieties have short coleoptiles, farmers can lose up to one in 10 fields in dry summers and must resow. "We really need to incorporate [long coleoptiles] in the Great Plains," says Carver, who has begun breeding Richards's varieties with local wheat.

Slow but steady

Breeding for drought tolerance is notoriously difficult. Some breeders have selected varieties based on an ability to survive drought, but the result tends to be cactuslike plants that grow slowly and produce little grain. Breeders have also zeroed in on traits such as leaf curling to reduce evaporation, but these often vanish when bred into other varieties or when environmental conditions are altered.

Buoyed by the success of transgenic crops resistant to insects and to viruses, efforts are under way to design drought-tolerant crops (*Science*, 11 April 2008, p. 171). It's a big challenge, as many genes are involved. "To think gene transfer replaces conventional breeding for drought is unrealistic," says Matthew Reynolds of CIMMYT, the International Maize and Wheat Improvement Center in El Batan, Mexico. "We don't yet understand the gene interactions well enough."

Although many colleagues have embraced transgenic techniques, Richards is old school, patiently crossing varieties. He credits high school friend Graham Farquhar, a biophysicist at Australian National University in Canberra, for the inspiration that seeded Drysdale, his most successful cultivar. In the early 1980s, Farquhar, like Richards, was exploring how to alter plant physiology to resist drought. He targeted RuBisCO, an enzyme complex that captures CO_2 and converts it into sugars. RuBisCO prefers CO_2 with the carbon-12 isotope rather than heavier carbon-13. (About 1.1% of carbon in the atmosphere is carbon-13.)

Farquhar expected that the isotope ratio in plant tissue might shed light on plant breathing habits. Plants take in CO_2 through stomata, which open and close like mouths. Farquhar imagined that some plants are like sponge divers, taking big gulps of air, then holding their breath for minutes. Other plants are like swimmers taking frequent sips of breath. With fresh CO_2 every few seconds, swimmers have the luxury of picking out lighter carbon. Divers consume most CO_2 in each gulp, including carbon-13. Compared with swimmers, the isotope ratio in divers should be closer to that of air. Crucially, because divers keep their stomata closed longer, they should lose less water.

Testing Farquhar's hypothesis, Richards confirmed that the most water-efficient wheat varieties had the highest carbon-13 to carbon-12 ratios. "That was a eureka moment," says T. J. Higgins, deputy chief of CSIRO Plant Industry. At last, Richards had a solid physiological trait to select for drought tolerance. With that tool, he bred Drysdale, a variety that's more like a gulper than a sipper. Richards's isotope-discrimination technique, "Delta," has revolutionized breeding for drought tolerance, says CIMMYT's José Luis Araus, who is applying it to breed drought-tolerant maize in sub-Saharan Africa.

As Australia's summers get hotter and drier, a new challenge is to breed wheat that matures faster and can be harvested before the grain withers. Again, Richards is eyeing barley: "It's got this magical property of producing a large amount of grain in a short period of time. If we can do that with wheat, it will be a massive breakthrough." With his dedication to the Blue Revolution, that should only be a matter of time.

Eureka moment. When he confirmed that water-efficient wheats have higher carbon-13 to carbon-12 ratios, Richards had a solid trait to select for drought tolerance.

CREDIT: BRAD COLLIS/CORETEXT

–ELIZABETH FINKEL

Elizabeth Finkel is a writer in Melbourne, Australia.

Black gold. The genome of the black truffle has now been sequenced.

GENETICS

Rooting Around the Truffle Genome

A favorite of gourmets, truffles are revealing their delicious secrets to the biologists studying the mysterious fungi

ALBA, ITALY—Upon first glance, it's hard to believe that this is one of the most prized and expensive foods in the world. The muddy clods laid out in the display case bear a striking resemblance to animal droppings. But their true identity is revealed the moment the seller, Stelvio Casetta, lifts the glass lid. The aroma—a potent, earthy cocktail of sulfurous chemicals—is unmistakable. Then you see the price tags, ranging from $100 to $400 for a lump of fungus smaller than Brussels sprouts. These are *tartufi* or, as the many English-speaking tourists here call them, truffles.

Casetta plucks out a $300 creamy, golden nugget with the same enormous hand with which he unearthed it just days ago at his secret location in a nearby forest. (You can join *Science* on a truffle hunt and an unusual taste test at www.gonzoscientist.org.) "You can't know a truffle just using your eyes," he tells potential buyers before handing it to a nearby woman, who takes it to her nose, inhales deeply, and smiles at the recognizable odor.

Paola Bonfante, a microbiologist at the nearby University of Turin, knows her truffles, in some ways better than Casetta does. She is part of a Franco-Italian team exploring in intimate detail the prized fungi that make up the truffle genus. At a meeting in November,* the group gave a preview of the first full genome sequence of the black truffle (*Tuber melanosporum*), just the second symbiotic soil fungus to be so deciphered, and the genome sequence of the white truffle (*T. magnatum*) is expected by summer. Already, the European investigators have dug up several surprises among the fungal DNA sequence, including one that may help stem the truffle black market and another that rewrites the sex life of these subterranean organisms.

The truffle is the latest in a series of gourmet genome projects pursued by European researchers. French and Italian scientists clinked glasses last year after sequencing the genome of the grape used for wine production (*Science*, 25 April 2008, p. 475). French scientists are now sequencing the genomes of the microbes responsible for Camembert and Roquefort cheeses. "It is natural that these should be French and Italian projects, … food is so important to our culture" says Francis Martin, a plant and fungal physiologist at the French National Institute for Agricultural Research (INRA) in Nancy who led the black truffle genome project.

Precious fungus. White truffles have resisted domestication and command the highest prices.

Truffle trouble

For commodities such as gold and silver, the market value is the same regardless of where they are mined. But the price of a truffle is strongly determined by its geographic origin. The most highly regarded black truffle is *la truffe noire du Périgord*, harvested for centuries beneath oak trees in southwestern France. French researchers discovered how to reliably cultivate black truffles in orchards in the early 19th century and continue to do so to this day. But the white truffle has resisted domestication and thus commands far more money. The fungi can be found—with the help of pigs or trained dogs—only in a narrow swath of forests between the Istrian peninsula of Croatia and central Italy. And here at the Alba market, *tartufo bianco d'Alba*—the locally grown white truffle—is the undisputed king, routinely selling for $4000 per kilogram.

But a major problem for truffle buyers is "counterfeiting." Black truffles bearing the prestige and price of the name Périgord sometimes originate from less famous regions. White truffles harvested in Croatia are brought to Italy and sold with "d'Alba" labels. Sometimes similar looking species, such as the plentiful but less aromatic Chinese truffles (*T. indicum*), which resemble black truffles, "are sold with a small amount of black truffle included to provide the right smell," says Francesco Paolocci, a fungus researcher at the Institute of Plant Genetics (IGV) in Perugia, Italy.

So the truffle industry is turning to molecular biology for help. Researchers have "assumed for decades that truffles are almost clonal," says Martin, with hardly any genetic differences between the fungi growing in different regions. Any distinct flavors, aromas, or appearances are chalked up to variations in the environment. Sampling the genomes of black truffles from around Europe has turned this view on its head, however.

The newly completed black truffle genome revealed areas with highly variable amounts of repetitive DNA. A team of Italian and French geneticists led by Paolocci, Andrea Rubini, and Sergio Arcioni at IGV and Claude Murat at INRA used these markers to take DNA fingerprints of more than 200 black truffles from 13 regions across southern Europe. Far from being a monoculture, black truffles form local varieties that are genetically distinct, the researchers reported at the November meeting. Paolocci's group has also fingerprinted more than 300 white truffles from 26 different areas across

*3rd International Truffle Congress, Spoleto, Italy, 24–28 November 2008

CREDITS: KATRIEN KOLENBERG

Published by AAAS

its range, and early results indicate that it may also form distinct regional populations. "Now that we have the global picture," says Martin, "you see that the Tuber genome is like a mosaic," with "islands" of stable genes separated by "an ocean of repeating DNA" that change rapidly over the centuries.

DNA analysis has already caught imposter species, such as the Chinese truffle, says Bonfante. The next step will be to refine the genetic fingerprinting to determine if truffles of the same species but different regions can be distinguished. "This will become important," she says, if governments adopt the wine industry's "controlled geographical origin" system. The European Union will then require authentication of a truffle's birthplace.

Beyond fighting counterfeit fungi, the genetic data is filling out the truffle's evolutionary story. Using the new map of black and white truffle diversity, Martin and Murat recently modeled the spread of truffles going back 12,000 years to the last Ice Age. By the time that Europe was thawing, only two small populations of black truffles existed, in southern Italy and Spain, and white truffles were restricted to central Italy. Black truffles then spread over the Alps and across Europe, but white truffles never did. What held the white truffles back is a mystery. Considering changing climates, the question is of more than academic interest. "It is expected that the black truffle will be able to adapt to global warming by moving northward," says Martin, but the white truffle, blocked by the Alps, could become extinct.

Sex in the soil

Everyone in Alba seems willing to testify that truffles are an aphrodisiac. The origin of this legend may be that, among the hundreds of volatile compounds that truffles emit, there is indeed a close mimic of androstenol, a mating pheromone secreted in boar saliva. This may explain the frenzied enthusiasm of sows when they locate truffles beneath leaf litter, says Bonfante. Evidence of any such behavioral effect on humans is lacking, but the question of the truffle's own sexual behavior has now been answered, thanks to the new genome data.

The only part of the fungus that ends up on dinner tables is the fruiting body, a temporary reproductive organ created at specific times of the year—between November and December for white truffles, December and February for black. The rest of the organism exists year-round as a fine web of hairlike cells, the hyphae, that sheath the roots of a tree, providing minerals in exchange for food. The spores packed into the fruiting body each contain two copies of the truffle's chromosome complement, whereas the hyphae cells only contain a single set. The elusive question has been what sexual acts hyphae get up to when producing spores.

According to the prevailing model, truffles do not have sex with strangers. Instead, they self-mate, with two hyphae of a single fungus fusing. The resulting cell, which would have two identical sets of the genome, then divides rapidly to form the spores of the fruiting body, surrounded by a matrix of cells, called the gleba, each containing single-copy genomes.

With the highly variable markers from the fully-sequenced truffle genome in hand, the IGV group has now tested whether the fungi are really so chaste. The investigators compared the DNA of gleba cells and spores in dissected black and white truffles. Like catching an adulterer in the act, they found different genetic fingerprints in the two cell types of both truffles. The gleba cells contained one set of DNA markers, and the spores carried those same markers plus a foreign set, the team reported at the meeting. In one stroke, says Paolocci, this work showed not only that the fruiting bodies were the result of a sexual encounter between two different fungi but also that gleba and spores have different cellular origins. Like a mother's womb, all of the fruiting body's gleba cells have just the "maternal" genotype, whereas the spores carry both, like a fertilized egg.

Confirming this, the researchers inoculated the roots of potted tree seedlings in the laboratory with black truffle spores. In each case, the hyphae cells that grew contained a Mendelian assortment of genotypes, exactly as predicted for sexual reproduction.

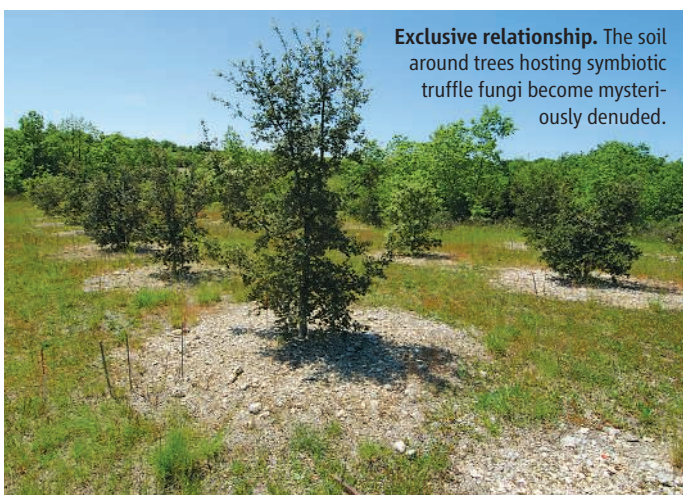

Exclusive relationship. The soil around trees hosting symbiotic truffle fungi become mysteriously denuded.

CREDIT: ANTONIETTA MELLO

The discovery has "major implications" for the truffle industry, says Charles Lefevre, a mycologist based in Eugene, Oregon, who is considered one of the world's experts on the delicacy. Companies that sell tree seedlings colonized by black truffle fungi "have benefited from low or nonexistent seedling quality standards," he says. Now sellers may have to prove that their trees are colonized by multiple truffle mating types that can produce the edible fruiting bodies.

What's that smell?

The sex life of truffles is only one of their secrets, says Martin. "We really don't understand truffle ecology." For one thing, the nature of the chemical crosstalk between the hyphae and roots is still "a black box," he says. And then there are the countless interactions with all the other residents of the soil. One clue to this ecosystem may literally be under our noses. "All those volatile chemicals that make truffles smell delicious to us may serve other purposes," says Bonfante. When truffle fungi colonize a tree, a denuded zone, or brulé, that looks as though the ground has been scorched often develops around the trunk. Bonfante's group has shown that the microbial community structure in brulé soils is dramatically different when compared with soil around neighboring trees. "Truffles seem to trigger these changes with chemical signals," possibly with the help of the tree, says Bonfante, "but we don't know how it works."

Martin and his Italian colleagues plan to take a crack at the problem by creating a "volatile map" of truffle aroma in the field. "The idea is to capture the gases released by truffles at various stages of maturation and freeze samples of the tissue immediately," Martin explains. Back in the lab, gene-expression patterns in the fruiting body and other tissues will be correlated with changes in the cocktail of chemicals released. The ultimate aim is to find the genes responsible for fruiting body development and for the symbiosis between tree and fungus.

Of course, learning the delicious secrets of truffle biochemistry could make it possible to genetically engineer truffle aroma into more easily cultivated organisms, such as mushrooms. But would Europeans accept genetically modified portabellos with the whiff of *tartufo bianco d'Alba*? "Absolutely not!" says Martin.

–JOHN BOHANNON

Published by AAAS

LETTERS

edited by Jennifer Sills

For Teachers, All the Classroom's a Stage

IN HIS PERSPECTIVE "FAREWELL, LECTURE?" (2 JANUARY, P. 50), E. MAZUR CRITICIZES TRADITIONAL lectures while praising the virtues of a new interactive electronic approach. While the new approach may enhance student learning, the traditional lecture approach can be very effective if conducted with a passion for teaching, respect for the students, strong knowledge of the subject area, easy accessibility in and out of the classroom (getting to know the student), and, above all, theatrical performance.

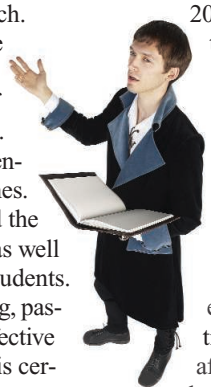

A teacher is similar to an actor, whose sole goal is to capture the audience's attention for the duration of the performance, while at the same time delivering the lines. Teaching is indeed a form of acting, with all of its intricacies: movement around the classroom, voice inflections, display of emotions, and intense physical gestures, as well as visual, verbal (questions and answers), and even physical interactions with students. Capturing and holding the attention of each student with an intense, strong, exciting, passionate, and memorable acting (teaching) performance is indeed a worthy and effective approach that enhances the traditional lecture experience and overall learning. It is certainly one that is ultimately deeply appreciated and amply rewarded by the students.

MICHAEL HADJIARGYROU

Department of Biomedical Engineering, State University of New York at Stony Brook, Stony Brook, NY 11794, USA. E-mail: michael.hadjiargyrou@sunysb.edu

Earlier Treatment May Explain Diabetes Data

IN THE NEWS FOCUS STORY "PARADOXICAL effects of tightly controlled blood sugar" (17 October 2008, p. 365), G. Taubes reported that tight glucose control in the Action to Control Cardiovascular Risk in Diabetes (ACCORD), ADVANCE, and Veterans Affairs Diabetes Trial (VADT) trials failed to reduce macrovascular disease, whereas the United Kingdom Prospective Diabetes Study (UKPDS) follow-up trial showed the opposite result. It was suggested that these discordant conclusions may have occurred because the former studies were not "run long enough" to see a benefit.

As reported by authors of the UKPDS follow-up studies, ACCORD and ADVANCE patients were younger (by 8 and 12 years, respectively), had more advanced diabetes (having been treated for 8 to 10 years, compared with newly diagnosed diabetics in UKPDS), and had more macrovascular disease (one out of three, compared with 7.5% in UKPDS) (*1*). These demographic differences may explain the different outcomes of these studies.

For the younger patients with recent diagnoses of diabetes, enrolling in the UKPDS trial meant that their glycemic control was initiated earlier, possibly before the onset of macrovascular disease. In contrast, the other three trials were specifically designed to include patients who were already at risk for macrovascular disease. Endothelial changes had likely started in the majority of these patients by the time glycemic control had been achieved.

Treating patients 10 years earlier (resulting in demographics similar to UKPDS) may be the key to decreasing the incidence of stroke and cardiovascular disease.

DAVID M. ABBEY

School of Medicine, University of Colorado Denver, Poudre Valley Health System, Ft. Collins, CO 80525, USA. E-mail: history3345@comcast.net

Reference

1. R. R. Holman *et al.*, *N. Engl. J. Med.* **359**, 1577 (2008).

The Vital Role of ORWH

WE WOULD LIKE TO ADDRESS MISCONCEPTIONS created by the News story "Women abound in NIH trials" (Special Section on Clinical Trials and Tribulations, 10 October 2008, p. 219), in which C. Holden questions whether the Office of Research on Women's Health (ORWH) is still needed at NIH. The importance of ORWH extends well beyond ensuring that women are included in clinical trials. It also plays a unique role in promoting and funding science and career development in women's health and gender biology.

ORWH initiatives (*1*) strengthen and enhance interdisciplinary and translational research related to conditions that affect women and men, and they support the recruitment, retention, reentry, and advancement of women in biomedical careers. ORWH funds or co-funds research and career development grants through the NIH institutes and centers, and it advances research on women's health and related sex/gender factors. In addition, ORWH pioneered a K–12 mentored career development program to support the training of junior faculty researchers in women's health research. This innovative program has served as a model for career development awards throughout the NIH.

SCOTT HULTGREN,[1]* JILL M. GOLDSTEIN,[2] JOHN O. L. DELANCEY,[3] EMMALEE S. BANDSTRA,[4] KATHLEEN T. BRADY,[5] JEANETTE S. BROWN,[6] HONG-WEN DENG,[7] ANDREA DUNAIF,[8] DAVID A. EHRMANN,[9] EMERAN A. MAYER,[10] RAJITA SINHA,[11] STUART TOBET,[12] JON E. LEVINE[13]

[1]Department of Molecular Microbiology and Center for Women's Infectious Disease Research, Washington University School of Medicine, St. Louis, MO 63110, USA. [2]Department of Psychiatry and Medicine, Harvard Medical School and Connors Center for Women's Health and Gender Biology, Brigham and Women's Hospital, Boston, MA 02115, USA. [3]Department of Obstetrics and Gynecology, University of Michigan, Ann Arbor, MI 48109, USA. [4]Department of Pediatrics and Obstetrics and Gynecology, Miller School of Medicine, University of Miami, Miami, FL 33101, USA. [5]Department of Psychiatry, Medical University of South Carolina, Charleston, SC 29425–1950, USA. [6]Department of Obstetrics, Gynecology, and Reproductive Sciences and Women's Health Clinical Research Center, University of California, San Francisco, San Francisco, CA

Published by AAAS

94155, USA. [7]Franklin D. Dickson/Missouri Endowed Chair, Human Genetics/Genomics Center, and Orthopedic Research, Departments of Orthopedic Surgery and Basic Medical Sciences, University of Missouri, Kansas City, Kansas City, MO, 64108–2792, USA. [8]Department of Medicine, Feinberg School of Medicine, Northwestern University, Chicago, IL 60611, USA. [9]Department of Medicine, University of Chicago, Chicago, IL 60637, USA. [10]Department of Medicine, Physiology, Psychiatry, and Biobehavioral Sciences and UCLA Division of Digestive Diseases, University of California, Los Angeles, Los Angeles, CA 90073, USA. [11]Yale Stress Center, Yale University, New Haven, CT 06519, USA. [12]Department of Biomedical Sciences, Colorado State University, Fort Collins, CO 80523, USA. [13]Department of Neurobiology and Physiology, Northwestern University, Evanston, IL 60208, USA.

*To whom correspondence should be addressed. E-mail: hultgren@borcim.wustl.edu

Letters to the Editor

Letters (~300 words) discuss material published in *Science* in the previous 3 months or issues of general interest. They can be submitted through the Web (www.submit2science.org) or by regular mail (1200 New York Ave., NW, Washington, DC 20005, USA). Letters are not acknowledged upon receipt, nor are authors generally consulted before publication. Whether published in full or in part, letters are subject to editing for clarity and space.

References and Notes

1. Office of Research on Women's Health (http://orwh.od.nih.gov/index.html).
2. The authors are all directors or co-directors of NIH/ORWH Specialized Centers of Research on Sex and Gender Factors Affecting Women's Health (SCORs) funded by ORWH and sponsoring NIH institutes.

The Nonscientist Science Adviser

E. KINTISCH'S NEWS FOCUS STORY ("BENDING the president's ear," 2 January, p. 28) on the role of the science adviser to the president contains an important historical error: The first science adviser, James Killian, was not an electrical engineer. In fact, Killian was not a scientist or engineer at all. His academic training was in management and administration, and his experience included serving as the president of the Massachusetts Institute of Technology and on a number of government advisory committees (*1*). That the first science adviser was not a scientist is not widely appreciated, and it is not widely advertised in the science community that Killian did not earn a doctorate. Killian had been awarded an honorary doctorate from Middlebury College in 1945 (*2*), and he was later awarded honorary degrees from Union College, Drexel Institute of Technology, and the College of William and Mary (*3*). That the first science adviser—often held up as the exemplar of the role—was a management expert should not be overlooked (*1*).

ROGER A. PIELKE

Center for Science and Technology Policy Research, University of Colorado/CIRES Boulder, CO 80309, USA. E-mail: pielke@colorado.edu

References

1. R. Pielke Jr., R. Klein, *Minerva* **47**, 5 (2009).
2. Anonymous, *The Tech* **65**, 4 (13 July 1945).
3. Anonymous, *The Tech* **77**, 1 (26 April 1957).

The Enduring Spoken Word

IN HIS PERSPECTIVE ("UNLOCKING THE potential of the spoken word," 26 September 2008, p. 1787), D. W. Oard describes how writing caused a landslide in humanity's cultural landscape, in large part because it was a findable, permanent record. He suggests that today's speech recognition and recording technologies may mean that the comeback of the spoken word is upon us. However, Oard's argument suggests a radical turn where there is none,

for the simple reason that speech has never left our side.

The invention of writing allowed information to be stored reliably in a medium other than human memory. Speech processing technology is just a variation on that theme. Oard highlights the potential of the spoken word for information retrieval purposes. In no sense does this bring us to "the threshold of a new era"; it merely dusts off the worn-out view of the spoken word as mere vehicle for transporting ideas (*1*).

The full potential of the spoken word has always been more complex than the words themselves; the speaker and listener jointly construct meaning guided by common ground, social relationships, gestures, body language, and facial expressions as much as by the auditory signal (*2*–*5*).

Discourse over the past 50,000 years has encompassed a lot more than neat text ready to be data-mined. Unlocking its full potential requires a richer and more dynamic view of language than that espoused by Oard.

MARK DINGEMANSE

Max Planck Institute for Psycholinguistics, Nijmegen, Netherlands. E-mail: mark.dingemanse@mpi.nl

References

1. M. J. Reddy, in *Metaphor and Thought*, A. Ortony, Ed. (Cambridge Univ. Press, Cambridge, 1979), pp. 284–297.
2. D. Tedlock, B. Mannheim, *The Dialogic Emergence of Culture* (Univ. of Illinois Press, Champaign, IL, 1995).
3. D. Tannen, *Talking Voices: Repetition, Dialogue, and Imagery in Conversational Discourse* (Cambridge Univ. Press, Cambridge, ed. 2, 2007).
4. H. H. Clark, *Using Language* (Cambridge Univ. Press, Cambridge, 1996).
5. N. J. Enfield, S. C. Levinson, *Roots of Human Sociality: Culture, Cognition, and Human Interaction* (Berg, Oxford, 2006).

Response

RATHER THAN ARGUING THAT SPEECH WOULD overcome writing in another radical cultural shift, my intent was to suggest that speech would reemerge to stand side by side with writing as a conduit for transporting ideas with permanence and findability. As M. Dingemanse observes, speech can be so much more than a mere conduit, and I would agree that we are far from being able to build machines that can reasonably model the full richness of human expression, whether spoken or written. Many of our most widely used machines for processing language (such as search engines and translation systems) rely on fairly shallow representations of meaning, and predicting fundamental changes in that situation would seem to me highly speculative. Machines are merely tools, however—it is we, not our machines, who must ultimately make sense of what we see, hear, and read. But we should not underestimate the importance of having machines that can help us to find what we need. Dingemanse's critique reminds us that change and continuity coexist, and that although permanence and findability can help us to use speech in new ways, many of the ways speech presently pervades our lives will surely also remain with us.

DOUGLAS W. OARD

College of Information Studies, University of Maryland, College Park, MD 20742–4345, USA. E-mail: oard@umd.edu

CORRECTIONS AND CLARIFICATIONS

News Focus: "Astronomy hits the big time" by A. Cho and D. Clery (16 January, p. 332). The first observation of a very high-energy gamma-ray source was not the work of the H.E.S.S. telescopes in 2004, as stated, but was made some 20 years earlier by a collaboration using the Whipple Observatory's 10-meter optical reflector in southern Arizona. More than 10 sources had been established before 2004, including a number of extragalactic sources.

Published by AAAS

HISTORY OF SCIENCE

What Scientists Caught from Kuru

M. Susan Lindee

The Collectors of Lost Souls
Turning Kuru Scientists into Whitemen

by Warwick Anderson

Johns Hopkins University Press, Baltimore, 2008. 328 pp. $24.95. ISBN 9780801890406.

In this magisterial account, Warwick Anderson reconstructs the world of kuru and its diverse stakeholders. The disease was gruesome, some of those who worked on it were thoroughly unappealing, and the story involved cannibalism, pedophilia, sorcery, ugly rivalries, and slow, painful death. Yet in *The Collectors of Lost Souls*, Anderson provides a rich, sensitive perspective on this messy confluence of tragedy and knowledge. He sees science as a point of contact between isolated people like the Fore of New Guinea and the "whitemen" who came to them longing for knowledge and adventure. Scientific interests brought the Fore into technocratic order, systems of material exchange, and global relationships. At the same time, the Fore brought their scientific visitors into social relations that were eventually crucial to their ability to interpret a baffling disease. The disease scientists caught from kuru, in Anderson's characterization, was a lust for brains, blood, and genealogies that reflected both the practical problems of understanding the disease and the baroque sensibilities of leading kuru scientists like Vin Zigas, D. Carleton Gajdusek, and Stanley Prusiner.

Kuru was a new disease in the 1950s when it came to scientific attention. It had appeared only about two generations earlier among the Fore, a group living in the eastern highlands of New Guinea. Briefly known as "laughing death," it produced a staggering gait, tremors, dancelike movements, wandering eyes, and eventually silence, passivity, and death. The odd new disease attracted scientific attention and became the subject of international rivalry. Scientific theories of causation for kuru at various times included heredity, a virus or bacteria, and psychogenesis, a technical way of characterizing the Fore perspective that kuru was caused by sorcery.

Anderson's story tracks the earliest accounts of interactions with the Fore in the late 1940s, through the 1950s and 1960s, and then the identification and elucidation of kuru's causative agent as a prion in the 1980s. In the 1990s, the epidemiology of kuru became a model for the possible future impact of "mad cow" disease in European populations. Gajdusek shared the Nobel Prize in Physiology or Medicine in 1976 for his discovery that kuru was caused by a transmissible agent that took years to affect the brain, the first human "slow virus." Prusiner won the same prize in 1997 for his work on infectious proteins, prions—entities that seemed incredible even as the prize was awarded. Kuru became one of a family of transmissible spongiform encephalopathies that now include Creutzfeldt-Jakob disease, scrapie in sheep, and bovine spongiform encephalopathy. The evidence that kuru was caused by oral transmission, acquired during mortuary feasts, when Fore family members consumed their dead loved ones as a sign of respect, explained the epidemiology in New Guinea.

Anderson takes seriously the roles of all participants, including Fore informants and assistants, patrol officers who marked the boundaries of the managed world, and field workers who found New Guinea intolerable (there were many). The portrait of the unappealing Gajdusek is particularly complex and well managed. Gajdusek desired both young boys and adventure and found scientific subjects that helped him to fulfill his desires, in regions that were among the most isolated places on the globe. The huge populations living in the highlands of New Guinea were unknown to European visitors well into the 1920s, coming to the general attention of missionaries, scientists, and colonial authorities only in the 1950s. When Gajdusek and other kuru scientists began to study them, the Fore were in a period of rapid social change, responding to the new possibilities of interactions with the broader world. Quick to understand the opportunities, and quick to adapt to the promises of medical tourism, they were active participants in the struggle to understand kuru.

The book closes with two final portraits. The first is of the Fore in 2003 when Anderson visited them himself. He presents his field adventures as an intrepid historian-ethnographer who worried about tropical ulcers and lice and posed in the market with Masasa, one of Gajdusek's former "boys." The second chronicles the arrest and imprisonment of Gajdusek, whose informally adopted families of Melanesian and Micronesian boys (sometimes nine or ten at a time) attracted the attention of child welfare authorities, leading to his conviction for pedophilia in 1996. Having served his time, Gajdusek left the United States. He died last December, an expatriate, in Norway.

Anderson, both a medical doctor and a Ph.D. historian of medicine, holds professo-

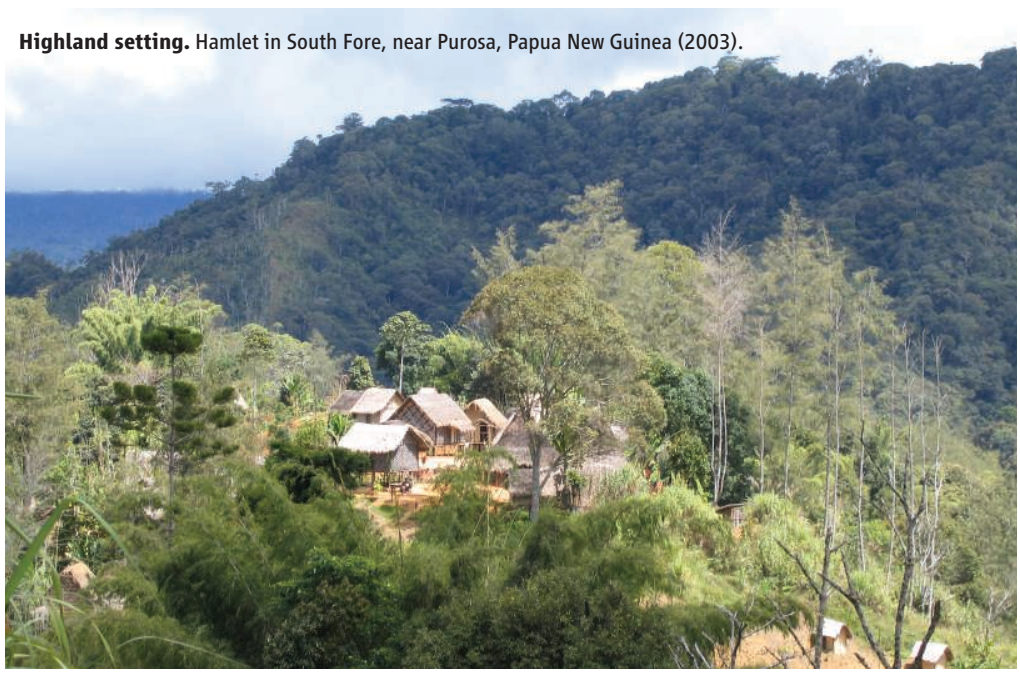

Highland setting. Hamlet in South Fore, near Purosa, Papua New Guinea (2003).

CREDIT: WARWICK ANDERSON

The reviewer is at the Department of History and Sociology of Science, 365 Logan Hall, University of Pennsylvania, 249 South 36th Street, Philadelphia, PA 19104–6304, USA. E-mail: mlindee@sas.upenn.edu

rial positions in both fields at the University of Sydney. He is able to comfortably bring together the technical and social elements in the kuru story. Drawing on a wide range of sources—including the ethnographic literature, interviews, colonial records, correspondence, diaries, and field notes—he is able to reconstruct interactions between participants in telling detail. The writing style is clear and straightforward (the book sometimes reads almost like a murder mystery). But underlying the narrative are sophisticated theoretical perspectives on science, knowledge, and colonialism that have clearly informed Anderson's thinking at every stage in the long process of writing this book (he describes a 20-year trajectory). He has deployed all these resources to good effect. Many individual patients, from whom kuru brains were taken and distributed and traded after they died, come vividly alive in these pages, as does the rapacious Gajdusek: hungry for everything, blithe and self-absorbed, and generating enemies and admirers while producing a remarkable set of records, ideas, and biological materials.

When all the details of the history of kuru are considered together, the story seems almost implausible. Anderson's compelling study captures the texture of 20th-century medical fieldwork and provides insight into the social dynamics and ethical realities of globalized science and medicine. *The Collector of Lost Souls* persuades us that these things really happened and shows us why they matter.

10.1126/science.1168944

EDUCATION

A Foundation, But Can We Use It?

James V. Wertsch

One of the hallmarks of our anxieties about the future is confusion over how to prepare young people for it. What is it that we are supposed to be educating students for? We know that today's young people will, during their lifetimes, face multiple changes in jobs if not professions, and we assume that their futures will be shaped by technologies that we cannot yet imagine. But when we try to translate these observations into what elementary and secondary schools should be doing, the result is usually a rehash of tired old complaints.

If we are ever to break out of this cycle, we are going to need some very big ideas presented in some very accessible ways, and these are what Kieran Egan provides in his slim but ambitious volume, *The Future of Education*. Egan (a professor of education at Simon Fraser University) recognizes the temptation to place blame for schools' failures on incompetent teachers, malicious and simple-minded politicians, and others, but he wants a deeper and more useful explanation. The key to obtaining this lies in addressing the problematic yet unchallenged assumptions that trap today's debate in an endless cycle of frustration.

Drawing on evolutionary psychology and cognitive science as well as history and philosophy, Egan outlines three widely accepted schools of thought about the goals of education. The first takes education to be a matter of socializing humans into the membership of nations and other collectives. "Governments are in the business of schooling" for this reason, but socialization is pursued at a cost because "homogenizing requirements will always be at odds with the ambitions of our imaginations." Indeed, if the goal of socialization is pursued too assiduously, we call it indoctrination—at least when others do it.

The Future of Education
Reimagining Our Schools from the Ground Up

by Kieran Egan

Yale University Press, New Haven, CT, 2008. 203 pp. $30. ISBN 9780300110463.

With the emergence of literacy in human history came a second big goal for education: Plato's academic ideal. Mastering the new forms of coded knowledge that came with literacy has become the purpose of much of contemporary education and, for better or for worse, underlies much of the testing that now shapes it.

Egan traces the third lens through which we see education back to figures such as John Locke and Jean-Jacques Rousseau, and more recently John Dewey and Jean Piaget. This is the "developmental" idea, through which education is viewed as "supporting the fullest achievement of the natural process of mental development."

Like the blind men who encounter an elephant, these ideas bring limited perspectives to the discussion. Worse yet, they bring views that often stand in direct contradiction to one another. Egan's goal is to transcend this stalemate. He does so by arguing that we must view education as a process of mastering the "cognitive tools" provided by society. The author emphasizes the massive transformation of knowledge that occurs because of our dependence on external symbol systems and technical means (what he calls a "tool kit for the brain"), but he rightfully insists that this does not mean that knowledge is somehow out there in libraries or computers. As he puts it: "There is no mind in the brain until the brain interacts with the external symbolic store of culture." And in such interaction, the possibilities for innovation reside as well.

Drawing on the ideas of the Russian psychologist and educator Lev Vygotsky, Egan maintains his focus on the dynamics between brain and external symbolic material, refusing to fall prey to the temptation to take one side or the other of this opposition as the bedrock of the enterprise. This is harder than first appears due to the reductionist tendencies of academic disciplines. Egan recognizes the importance of neuroscience discoveries in formulating new educational practices. At the same time, however, he understands the task of neuroscience in the context of the historical forces that shape a constantly changing environment of cognitive tools. The result is a complex but productive approach.

It is difficult enough to keep the tension between brain and external symbolic material at the center of a line of intellectual inquiry, but it is much harder to build a public campaign for change around it. That, however, is precisely what Egan sees as the key to reimagining our schools from the ground up. In the book's second half, he presents a series of vignettes that form an imaginary account of education reform between 2010 and 2060. These come from students, student teachers, educational researchers, and others as they struggle to understand and institute a new curriculum based on cognitive tools. His account is sufficiently honest that it includes reminders of the powerful political forces that resist such undertakings, and as a consequence it is sometimes hard to see why Egan thinks his new approach has any better chance at education reform than others.

In the end, Egan provides a brilliant conceptual foundation for the future of education, but he is less convincing when it comes to how this would lead to a serious transformation of education. As we move further into a new century, there is greater need than ever to bring bright ideas to the table to deal with the challenges and opportunities for educating thoughtful, humane, and innovative citizens. Egan's account in *The Future of Education* is an ingenious attempt to do this.

10.1126/science.1168116

The reviewer is at the McDonnell International Scholars Academy, Washington University, Campus Box 1173, 1 Brookings Drive, St. Louis, MO 63130–4899, USA. E-mail: jwertsch@wustl.edu

ECOLOGY

Controlling Eutrophication: Nitrogen and Phosphorus

Improvements in the water quality of many freshwater and most coastal marine ecosystems requires reductions in both nitrogen and phosphorus inputs.

Daniel J. Conley,[1]* Hans W. Paerl,[2] Robert W. Howarth,[3] Donald F. Boesch,[4] Sybil P. Seitzinger,[5] Karl E. Havens,[6] Christiane Lancelot,[7] Gene E. Likens[8]

The need to reduce anthropogenic nutrient inputs to aquatic ecosystems in order to protect drinking-water supplies and to reduce eutrophication, including the proliferation of harmful algal blooms (*1*) and "dead zones" in coastal marine ecosystems (*2*) has been widely recognized. However, the costs of doing this are substantial; hence, developing the appropriate nutrient management strategy is very important. Nitrogen (N), needed for protein synthesis, and phosphorus (P), needed for DNA, RNA, and energy transfer, are both required to support aquatic plant growth and are the key limiting nutrients in most aquatic and terrestrial ecosystems. However, a cascading set of consequences has been set in motion, arising from massive increases in fixed N additions to the biosphere, largely through the production of fertilizers and increases in fossil fuel emissions (*3*). P levels have also significantly increased because of fertilizer use, as well as from municipal and industrial wastewater. Here, we explore the rationale for dual–nutrient reduction strategies for aquatic ecosystems, especially in estuarine and coastal marine regions.

The question of whether one or both nutrients should be controlled to reverse the detrimental effects of eutrophication of lakes was thought to be solved in the early 1970s by Schindler (*4*), who established that P was the primary limiting nutrient in remarkable long-term experimental manipulations at Lake 227 in the Experimental Lakes Area, Canada (*5*). These and other results (*6*) led to widespread reductions in P loading to North American and European lakes and consequent improvements in water quality (*7*). On the basis of lake examples, P controls were prescribed by environmental regulatory agencies for estuarine and coastal marine ecosystems as well (*8*). P-reduction programs improved water quality in many lakes, but broader water- and environmental-quality goals were not achieved, particularly in estuaries and coastal marine ecosystems. This led to the general recognition of the need to control N input to coastal waters (*9*).

Too much algae. (Top) Removing macroalgal blooms at the Olympic Sailing venue, China. **(Middle)** Seagrasses covered with attached algae in a Danish estuary. **(Bottom)** Non–N2-fixing cyanobacteria blooms in Lake Okeechobee, Florida, U.S.A.

In lakes, the key symptom of eutrophication is cyanobacterial blooms (see figure, left). Planktonic N_2-fixing cyanobacteria bloom in fresh waters when P is replete and N availability is low. Such blooms are undesirable because cyanobacteria can be toxic, cause hypoxia, and disrupt food webs (*1*, *10*). N_2 fixation by cyanobacteria also can help to alleviate N shortages and hence maintain a lake in a P-limited condition (*5*).

N_2 fixation by planktonic cyanobacteria is much less likely in estuaries and coastal seas than in lakes. Significant coastal planktonic N_2 fixation has not been observed at salinities greater than 8 to 10 (ocean salinity is ~35), even in estuaries that are strongly N-limited, except in rare cases (*11*). If N limitation were the only factor governing blooms of N_2-fixing cyanobacteria, then their blooms would be widespread in estuarine and coastal marine ecosystems around the world, and they are not. Thus, reducing N loads to the saline waters of estuaries should not cause blooms of N_2-fixing cyanobacteria (*5*). Furthermore, estuarine and coastal marine ecosystem eutrophication results in loss of seagrasses and hypoxia (*2*), which are more serious recurrent problems than cyanobacterial blooms (see the figure).

Why is N_2 fixation in the saline waters of estuaries and coastal marine ecosystems so much less than that in lakes, and why is this process unresponsive to reduced N loads in estuaries? Numerous hypotheses have been put forward (*10*, *12*). Most researchers have concluded that no single factor is responsible, but rather interactions between two or more factors control the rates (*13*, *14*). Mesocosm experiments in Narragansett Bay (*12*) have indicated that the combination of slow growth rate from sulfate inhibition of molybdenum uptake and zooplankton grazing limited the accumulation of N_2-fixing cyanobacteria. Globally, significant N_2 fixation, particularly by the cyanobacterium *Trichodesmium*, does occur in the tropical and subtropical ocean,

[1]GeoBiosphere Science Centre, Department of Geology, Lund University, Sölvegatan 12, SE-223 62 Lund, Sweden. E-mail: daniel.conley@geol.lu.se. [2]Institute of Marine Sciences, University of North Carolina at Chapel Hill, 3431 Arendell Street, Morehead City, NC 28557, USA. E-mail: hpaerl@email.unc.edu. [3]Department of Ecology and Evolutionary Biology, Cornell University, Ithaca, NY, 14873, USA. E-mail: rwh2@cornell.edu. [4]University of Maryland Center for Environmental Science, Post Office Box 775, Cambridge, MD 21613, USA. E-mail: boesch@umces.edu. [5]International Geosphere-Biosphere Programme, Royal Swedish Academy of Sciences, Box 50005, SE-104 05 Stockholm, Sweden. E-mail: sybil.seitzinger@igpb.kva.se. [6]Florida Sea Grant, University of Florida, Gainesville, FL 32611, USA. E-mail: khavens@ufl.edu. [7]Ecologie des Systèmes Aquatiques, Université Libre de Bruxelles, Campus Plaine CP 221, B1050 Brussels, Belgium. E-mail: lancelot@ulb.ac.be. [8]Cary Institute of Ecosystem Studies, Box AB, Millbrook, NY, 12545, USA. E-mail: likensg@ecostudies.org

*Author for correspondence.

where denitrification depletes the available N and can be limited by P and Fe (*15*), but is not found in the more productive waters of estuaries and coastal seas.

P-only reduction strategies are likely to fail in Lakes Apopka, George, and Okeechobee, USA; Lakes Taihu and Donghu in China; and Lake Kasumigaura in Japan (*16*). In these lakes, P is rapidly recycled between sediments and water, and phytoplankton is dominated by non–N_2-fixing cyanobacteria, such as *Planktolyngbya*, *Oscillatoria*, and toxic *Microcystis*. *Microcystis* can vertically migrate, consume excess phosphorus at the sediment-water interface, and then rise to the water surface to form blooms (*10*). Careful simultaneous control of both P and N is required in such lakes to effectively control *Microcystis* and N_2 fixers.

Estuaries and coastal marine ecosystems that have been heavily loaded with nutrients can display P limitation, N limitation, and co-limitation (*17*), and what nutrient is most limiting can change both seasonally and spatially (*18*). At the transition between fresh and saline water, P can often be the limiting nutrient (*17*, *19*). P and dissolved silicate are also often limiting during the spring, with N limitation commonly occurring during summer months (*18*). Algal production during summer is supported by rapidly recycled P within the water column or released from sediments. This condition is particularly true for coastal ecosystems, where the elevated salinity provides sulfate for microbial reduction in bottom sediments, which results in the release of large quantities of P (*19*). Also, although much of the P in freshwater systems is not biologically available because it is adsorbed by clay and other particles, a considerable fraction of the P desorbs as readily available, dissolved phosphate under saline conditions (*13*). Thus, as the summer progresses, available P increases as N declines and is not effectively compensated by N_2 fixation.

Pristine lakes are sufficiently different from estuarine and coastal marine ecosystems that they may be poor analogs (*5*). For example, the low-salinity conditions of the Baltic Sea present a complex situation where N_2 fixation does play an important role. The Baltic exhibits permanent bottom-water hypoxia (*20*), which increases N loss due to denitrification and anaerobic ammonium oxidation (annamox) at the interface between oxygenated and deoxygenated waters. The hypoxic conditions also result in injection of large amounts of P back into surface waters during deep winter mixing (*21*). The annual variation in sediment releases of P due to hypoxia is nearly an order of magnitude greater than the controllable P loads (*20*). Nitrogen has clearly been established as the nutrient limiting spring phytoplankton production; it is the sinking spring bloom that sends organic matter to bottom waters, which partly sustains hypoxia. The excess P in the water column leads to summer blooms of cyanobacteria, some of which are N_2 fixers that increase N concentrations in surface waters when they are abundant. This new N helps to sustain the springtime production and produces a "vicious circle" of eutrophication (*21*). Models suggest that, here, too, reductions in the inputs of both P and N are required for significant improvements in dissolved oxygen concentrations, transparency, and other water-quality conditions in the Baltic Sea (*22*).

Controlling only P inputs to freshwaters and ignoring the large anthropogenic inputs of N can reduce algal uptake of N and thus allow more N to be transported downstream where it can exacerbate eutrophication problems in estuarine and coastal marine ecosystems (*13*). For example, reductions in P loadings by improved wastewater treatment and banning the use of P-based detergents succeeded in arresting algal blooms in freshwater portions of the Neuse River estuary, North Carolina, USA, but increased eutrophication and hypoxia downstream in the estuary, where P is more rapidly recycled (*11*). Similarly, dramatic reductions in P loading from the Rhine River and other rivers draining into the North Sea before concomitant N reductions resulted in strong P limitation in the river plume, but greater N export, exacerbating eutrophication in waters of the Wadden Sea (*23*) and as far away as the Norwegian coast of the Skagerrak (*24*). Reductions in P loading have also been suggested to limit phytoplankton growth in the plume of the Mississippi River in the northern Gulf of Mexico, which was previously more strongly limited by N. However, the increasing and excessive loading of N, relative to P, from agriculture has driven the plume of the Mississippi River to periodic P limitation, especially during the spring bloom period (*25*). Implementing only P reductions without reducing N loads could displace the dead zone westward and increase its size (*26*).

It is prudent, and in most cases essential, to implement a dual–nutrient-reduction strategy when developing measures to control eutrophication. A focus on only P or N reduction should not be considered unless there is clear evidence or strong reasoning that a focus on only one nutrient is justified in that ecosystem and will not harm downstream ecosystems. Just as care should be taken to avoid reducing N inputs in a way that will increase compensating N_2 fixation, attention should also be given to avoid displacing the effects of eutrophication downstream by concentrating only on P in freshwater systems and avoiding watershed N reductions that can be very important for coastal marine ecosystems. Although some would suggest that management strategies that control one nutrient, such as the reduced use of fertilizers, handling of manure, soil conservation practices, and restoring wetlands and riparian buffers, would also control the other, this is not always the case (*27*). For example, the technologies for wastewater treatment to reduce P versus N differ markedly, and reducing atmospheric N deposition does not affect P inputs to aquatic ecosystems. Alleviation of eutrophication in aquatic ecosystems along the land-ocean continuum requires a balanced and strategic approach to control both nutrients appropriately.

References and Notes

1. J. Huisman, H. C. P. Matthijs, P. M. Visser, *Harmful Cyanobacteria* (Springer Aquatic Ecology Series 3, Springer, Dordrecht, 2005).
2. R. J. Diaz, R. Rosenberg, *Science* **321**, 926 (2008).
3. J. N. Galloway *et al*., *Science* **320**, 889 (2008).
4. D. W. Schindler *et al*., *Proc. Natl. Acad. Sci. U.S.A.* **105**, 11254 (2008).
5. D. W. Schindler, *Science* **184**, 897 (1974).
6. G. E. Likens, *Limnol. Oceanogr. Spec. Symp.* **1,** 328 (1972).
7. National Research Council, *Restoration of Aquatic Ecosystems* (National Academies Press, Washington, DC, 1992).
8. J. H. Ryther, W. N. Dunstan, *Science* **171**, 1008 (1971).
9. R. W. Howarth, R. Marino, *Limnol. Oceanogr.* **51**, 364 (2006).
10. H. W. Paerl, R. S. Fulton III, in *Ecology of Harmful Marine Algae*, E. Graneli, J. Turner, Eds. (Springer, Berlin, 2006), pp. 95–107.
11. H. W. Paerl, L. M. Valdes, A. R. Joyner, M. F. Piehler, *Environ. Sci. Technol.* **38**, 3068 (2004).
12. R. Marino, F. Chan, R. W. Howarth, M. L. Pace, G. E. Likens, *Mar. Ecol. Prog. Ser.* **309**, 25 (2006).
13. National Research Council, *Clean Coastal Waters* (National Academies Press, Washington, DC, 2000).
14. P. M. Vitousek *et al*., *Biogeochemistry* **57/58**, 1 (2002).
15. K. R. Arrigo, *Nature* **437**, 349 (2005).
16. K. E. Havens *et al*., *Environ. Pollut.* **111**, 263 (2001).
17. D. J. Conley, *Hydrobiologia* **410**, 87 (1999).
18. T. C. Malone *et al*., *Estuaries* **19**, 371 (1996).
19. S. Blomqvist, A. Gunnars, R. Elmgren, *Limnol. Oceanogr.* **49**, 2236 (2004).
20. D. J. Conley, C. Humborg, L. Rahm, O. P. Savchuk, F. Wulff, *Environ. Sci. Technol.* **36**, 5315 (2002).
21. E. Vahtera *et al*., *Ambio* **36**, 186 (2007).
22. F. Wulff, O. P. Savchuk, A. Sokolov, C. Humborg, C.-M. Mörth, *Ambio* **36**, 243 (2007).
23. J. E. E. van Beusekom, *Helgol. Mar. Res.* **59**, 45 (2005).
24. M. D. Skogen, H. Søiland, E. Svendsen, *J. Mar. Syst.* **46**, 23 (2004).
25. J. B. Sylvan, A. Quigg, S. Tozzi, J. W. Ammerman, *Limnol. Oceanogr.* **52**, 2679 (2007).
26. D. Scavia, K. A. Donnelly, *Environ. Sci. Technol.* **41**, 8111 (2007).
27. R. W. Howarth *et al*., in *Millennium Ecosystem Assessment* (Island Press, Washington, DC, 2005), pp. 295–311.

28. We thank the European Union (EU), the U.S. NSF Program, and the Environmental Protection Agency for funding. D.J.C. was supported by an EU Marie Curie Chair (MEXC-CT-2006-042718).

10.1126/science.1167755

SYSTEMS BIOLOGY

Attractors and Democratic Dynamics

Cellular transcription networks are conceptualized as distributed control systems that regulate gene expression.

Yaneer Bar-Yam,[1] Dion Harmon,[1] Benjamin de Bivort[1,2]

The functional identity of a cell is largely determined by the regulated expression (transcription) of thousands of genes, so how it maintains a particular transcriptional state is of critical importance. Developmental biologists study how embryonic cells navigate a series of intermediate transcriptional states before settling into a final adult state; microbiologists identify the mechanisms by which transcription is altered by environmental perturbation; and oncologists seek to identify how cells switch from benign to cancerous. Consider two concepts of transcriptional regulation. In a "molecular autocracy," master genes respond to environmental or developmental stimuli by regulating thousands of genes, either directly or through other transcription factors. In a "molecular democracy," all genes exert a regulatory influence on all other genes, and phenotypic change (altered cell behavior) is brought about through the concerted action of thousands of genes. These scenarios are extreme and cells operate under a condition that is somewhere intermediate (see the figure) (*1*). But the choice of concept affects how regulation is studied.

The autocratic framework can be directly investigated by studies of individual molecular mechanisms and has been the starting point for discussions of biological processes. But a broader understanding of regulatory mechanisms is needed that incorporates essential features of both extreme views. The democratic framework relies on mutual regulation, which tends toward a self-consistent gene expression state that is stable in the face of fluctuations. In other words, this view has its roots in the conceptual understanding of stability and homeostasis of cell types (*2*, *3*). The democratic view has only recently gained empirical support, perhaps because its characterization involves studies of genome-wide dynamical processes.

A dynamic system with extensive mutual regulation tends to transition toward particular states, known as attractors, over time (often envisioned as valleys in a landscape). Background "noise" causes deviation in one cell over time, and among cells at one instant, but they recover. That there is an attractor state in the space of transcriptional states (*4*, *5*) supports the prediction of a democratic system. Chang *et al*. (*6*) recently identified transcriptional variability in clonally related mouse hematopoietic precursor cells, and separated the cells into several groups with expression differences in thousands (but still a minority) of genes. Over days, these cell group lineages converged to the same transcriptional state distribution. That is, the cell groups became indistinguishable, having the same average gene expression, as well as noise-induced variation, among individual cells. Such convergence is the signature of an attractor, in which many individual differences in transcription are insufficient to change the overall cell phenotype (a "controlling" majority of transcribed genes does not change) and mutual interactions among the genes cause trends toward specific mutually reinforcing states.

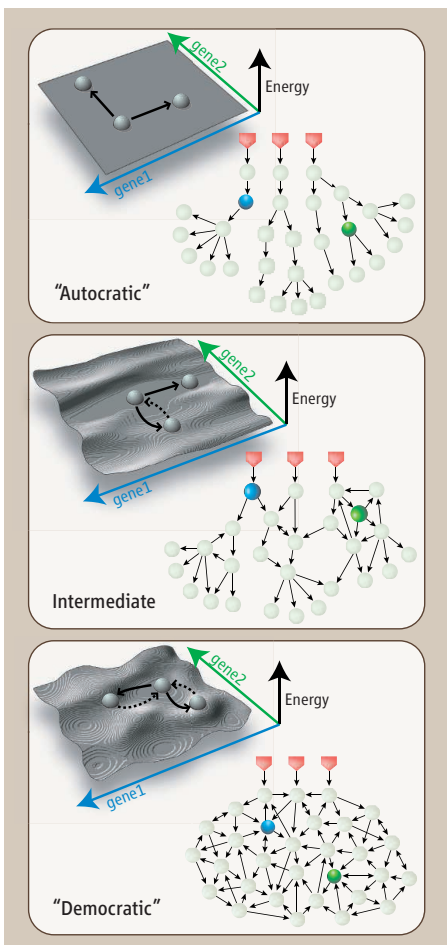

Transcription regulatory architecture. In autocratic regulatory networks (**top**), individual master regulator genes (pointed squares) are stimulated by external signals and control many other genes (circles). As shown by the energy landscape, the transcriptional states (spheres) may have no preferences (black arrows represent changes in expression of genes 1 and 2). In democratic networks (**bottom**), all genes act as mutual regulators. A few specific gene expression patterns become stable, shown as basins of attraction (cell types) in the landscape. Once a cell reaches one of these states, changing the expression of one gene is unlikely to switch the cell type (black arrows). Intermediate networks (**middle**) have mutual regulation, but certain genes (blue circle) are major controllers.

The attractor paradigm has practical implications: If distinct cell types (such as a precursor cell and a fully differentiated cell) correspond to distinct attractors, then there are multiple parallel ways to shift the transcriptional state from one attractor to another. Such families of trajectories are expected to engage multiple interconnected signaling pathways whose collective behavior (and outcome) is simple. In a limited way, this has been observed in the differentiation of immune cells (*4*) and stem cells (*7*). If the attractor picture is generically valid, it should be possible to create cocktails of large numbers of gene products that switch cells between different types. Any sufficiently large subset of gene products should be sufficient to cause the switch. Consider the number of gene expression levels that are needed to robustly characterize distinct cell types. An analysis (see fig. S1) of the transcriptional profiles of 79 human tissues and tumor cell types (*8*) reveals that about 200 highly variable gene expression values are sufficient to capture the relationships among the tissues and tumor cells, whereas fewer than 80 are not. By this measure, cocktails with a couple of hundred gene products chosen to mimic the differences between two cell types should generically cause transitions between them.

Still, paradoxically, Chang *et al*. (*6*) segregated cells according to the expression of a single gene, and showed that specific genes can

[1]New England Complex Systems Institute, 24 Mt. Auburn Street, Cambridge, MA 02138, USA. [2]Roland Institute at Harvard University, 100 Edwin Land Boulevard, Cambridge, MA 02139, USA. E-mail: yaneer@necsi.edu

CREDIT: N. KEVITIYAGALA/*SCIENCE*

Published by AAAS

control the overall cell state (and cell fate). This has also been observed in developing cells that are highly sensitive to external signaling molecules (*9*), but attain a highly stable differentiated state (*4*). More generally, cells are robust to noise and small perturbations in transcription (*10*), but sensitive to small changes in specific external (*11*) and internal (*12*) cues. Indeed, whereas regulatory networks have been characterized as robust to random failure and vulnerable to targeted attack (*13*), from a regulatory perspective, generic stability with sensitivity to specific perturbations is a positive property rather than a negative one (*14*). What is missing is a framework in which individual genes and collective states can be considered together.

What framework should be used to study collective state control? The difficulty is that for individual gene effects, individual transcription levels are important. For attractors, collective dynamics of the transcriptome within a cell type, rather than specific gene expression signatures, characterize cell behavior (not just cell type differences). What is needed are control coefficients that measure change in collective states relative to archetypes (see supporting text), and in relation to individual gene transcription level changes. Relating the variation of small sets of gene expression values to deviation or conformity to archetypes can provide a framework to study the interplay of attractors and master regulators. Such observations, best taken from unaveraged data, should identify the dispersal and convergence of cells near an attractor, and the mechanisms of homeostatic control. Using multiple archetypes also should enable the study of cell fate trajectories.

References

1. E. H. Davidson *et al.*, *Science* **295**, 1669 (2002).
2. C. H. Waddington, *Principles of Embryology* (Allen and Unwin, London, 1956).
3. S. A. Kauffman, *J. Theor. Biol.* **22**, 437 (1969).
4. S. Huang *et al.*, *Phys. Rev. Lett.* **94**, 128701 (2005).
5. P. Ao *et al.*, *Med. Hypotheses* **70**, 678 (2008).
6. H. H. Chang *et al.*, *Nature* **453**, 544 (2008).
7. A. G. Bang, M. K. Carpenter, *Science* **320**, 58 (2008).
8. A. I. Su *et al.*, *Proc. Natl. Acad. Sci. U.S.A.* **101**, 6062 (2004).
9. K. L. Medina *et al.*, *Dev. Cell* **7**, 607 (2004).
10. J. A. de Visser *et al.*, *Evolution* **57**, 1959 (2003).
11. G. Balazsi *et al.*, *Proc. Natl. Acad. Sci. U.S.A.* **102**, 7841 (2005).
12. R. Losick, C. Desplan, *Science* **320**, 65 (2008).
13. R. Dobrin *et al.*, *BMC Bioinformatics* **5**, 10 (2004).
14. Y. Bar-Yam, I. R. Epstein, *Proc. Natl. Acad. Sci. U.S.A.* **101**, 4341 (2004).

Supporting Online Material

www.sciencemag.org/cgi/content/full/323/5917/1016/DC1
SOM Text
Figs. S1 and S2

10.1126/science.1163225

GEOCHEMISTRY

Making a Crust

Dating zircons from the mid-Atlantic ridge provides clues about how the oceanic crust is formed.

Peter J. Michael[1] and Michael J. Cheadle[2]

The discovery of seafloor spreading in the 1960s enabled the formulation of the theory of plate tectonics. Modern geology textbook wisdom provides an image of magnetic stripes being made neatly on the seafloor when new oceanic crust is produced at a very narrow mid-ocean ridge axis, and subsequently moves outward. But how is the 6-km-thick crust actually produced at the ridge axis? On page 1048 of this issue, Lissenberg *et al.* (*1*) address this and other questions of ocean crust formation by applying state-of-the-art dating techniques to date samples from the mid-Atlantic ridge. They report that the tiny zircon crystals that are relatively abundant in the oceanic crust make it easy to date the crust, thereby providing a clearer picture of the formation processes involved.

Marine geologists have a good understanding of the different rock layers that are present in ocean crust. A kilometer-thick basalt layer at the seafloor is produced by magma that is fed through sheet-like intrusions called dikes. The deepest 4 km of the crust is formed from basaltic magma that crystallizes to form intrusive gabbro rock. Numerous studies have elucidated how long it takes to form the basaltic and dike layers (*2*). Much less is known about how the gabbroic lower crust accretes, because it is less accessible, buried beneath the basalts and dikes. Does it grow from the top down, or randomly? Is the width of accretion the same as the width of the axial valley (~10 to 12 km)? Or does some of it accrete farther off axis? How deep do gabbros crystallize? Are they confined to the crust, or can they crystallize in the uppermost mantle? How quickly does the lower crust cool and become rigid after it crystallizes?

The best exposures of gabbroic crust are found at slow-spreading ridges, where faulting accounts for some of the plate spreading. Earlier work (*3*–*5*) used an ion microprobe technique to date zircons and concentrated on oceanic core complexes that expose large sections of gabbroic crust by detachment faulting (*6*). Although the zircon crystallization ages were consistent with the magnetic spreading ages, about 10% of their analyses showed anomalous old ages. These results suggested that some gabbro crystallization had occurred at depth in the upwelling mantle before being transported to shallower levels in the crust.

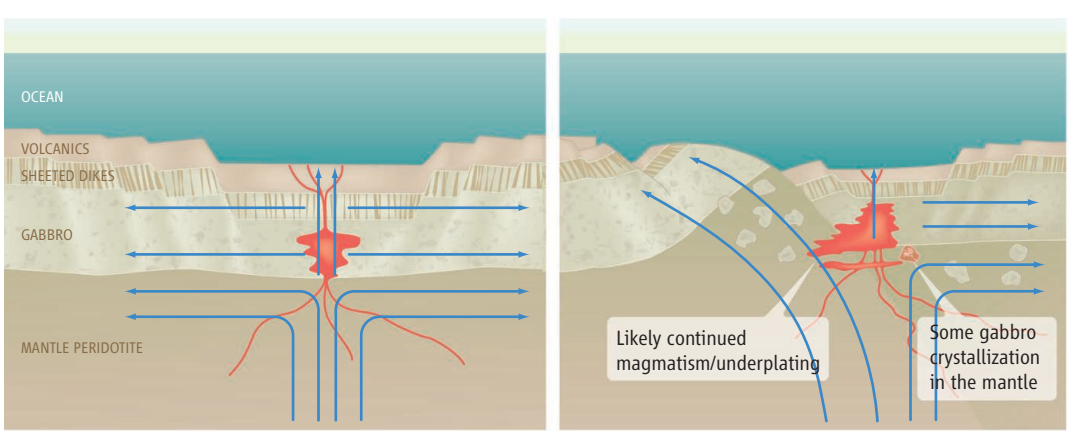

Crustal formation. (**Left**) Traditional model for construction of oceanic crust where there is no detachment faulting, similar to where Vema lithospheric section may have been produced as suggested by (*1*). (**Right**) Model for more complicated ridges, with some gabbro crystallization in the uppermost mantle and detachment faulting exposing crustal sections at core complexes, as advocated by (*3*).

[1]Department of Geosciences, University of Tulsa, Tulsa, OK 74104, USA. [2]Department of Geology and Geophysics, University of Wyoming, Laramie, WY 82071, USA. E-mail: pjm@utulsa.edu; cheadle@uwyo.edu

Lissenberg *et al*. used the more precise, but time-consuming, chemical abrasion–thermal ionization mass spectrometry (CA-TIMS) method. They studied gabbros that were formed at a mid-oceanic ridge that had a simpler constructional history. The gabbro is exposed on the fault scarp of a fracture zone that offsets the mid-Atlantic ridge. Although their zircon ages match the seafloor spreading ages, they find no anomalous old ages. At first glance, the results appear to contrast with the earlier studies suggesting that there may be different styles of gabbroic emplacement (see the figure) at slow-spreading ridges. The disadvantage of the new technique, however, is the small number of analyses that are feasible. It is possible that anomalously old zircons were simply not encountered. At this point, then, it is not clear how different the new results are. However, it is clear that this exciting methodology will ultimately help us decipher the different styles of gabbroic accretion at slow-spreading ridges.

Thermochronologists estimate cooling rates of rocks by measuring ages for different mineral "clocks" that start recording age information at different temperatures. John *et al.* (*7*) examined the temperature range of 800° to 100°C by means of U-Pb dating of zircon, argon in biotite, and fission track density in zircon and apatite, using average ages and temperatures for each mineral system. Coogan *et al.* (*8*) used the technique of olivine speedometry to examine cooling rates over the 1000° to 600°C temperature range.

Lissenberg *et al.* now estimate cooling rates for oceanic crust by using each zircon crystal as a separate clock. They take advantage of the very high age resolution of their data to suggest that zircon crystallized over a period of 90,000 to 235,000 years in individual samples. They then use the new titanium-in-zircon mineral geothermometer (*9*), in combination with published Ti data (*5*, *10*, *11*), that show that zircon crystallizes over a temperature interval of 60° to 120°C in oceanic gabbros and hence derive cooling rates for the 950° to 750°C temperature range. The slowest cooling rates, which they suggest might indicate partially molten gabbro up to 8 km from the axis, are surprisingly slow relative to the earlier studies (*7*), given that the study area is located at the end of a ridge segment where it abuts a fracture zone and where the crust and the gabbro layer are thin. But these rates are also compatible with more complicated scenarios of crustal growth. These intriguing results certainly bear further investigation.

Some of the next advances with the technique introduced by Lissenberg *et al.* will be made when the ion microprobe and CA-TIMS methods are used together to study the same zircons. The ion microprobe measurements can be used to examine large numbers of zircons in many samples to carefully ascertain whether there are any anomalous old ages. The temperatures would be determined directly from the Ti contents of the zircons, whose ages would then be determined by CA-TIMS. A larger sample density will enable the zircon and spreading ages to be compared with a greater degree of confidence, allowing geologists to rigorously assess different styles of crustal accretion. The finding of a positive correlation between the U-Pb ages and Ti temperatures within samples would instill confidence that the approach is valid for estimating cooling rates. Accurate cooling rates will place constraints on how oceanic crust grows and may even help to constrain how deep hydrothermal circulation might go.

References

1. C. J. Lissenberg *et al.*, *Science* **323**, 1048 (2009); published online 29 January 2009 (10.1126/science.1167330).
2. E. E. E. Hooft *et al.*, *Earth Planet. Sci. Lett.* **142**, 289 (1996).
3. J. J. Schwartz *et al.*, *Science* **310**, 654 (2005).
4. A. G. Baines *et al.*, *Earth Planet. Sci. Lett.* **273**, 105 (2008).
5. C. B. Grimes *et al.*, *Geology* **35**, 643 (2007).
6. J. R. Cann *et al.*, *Nature* **385**, 329 (1997).
7. B. E. John *et al.*, *Earth Planet. Sci. Lett.* **222**, 145 (2004).
8. L. A. Coogan *et al.*, *J. Petrol.* **48**, 2211 (2007).
9. J. M. Ferry, E. B. Watson, *Contrib. Mineral. Petrol.* **154**, 429 (2007).
10. L. A. Coogan, R. W. Hinton, *Geology* **34**, 633 (2006).
11. B. Fu *et al.*, *Contrib. Mineral. Petrol.* **156**, 197 (2008).

10.1126/science.1169556

MATERIALS SCIENCE

Atomically Engineered Oxide Interfaces

New solid-state phenomena emerge when interfaces between different oxides are created with atomic-scale precision.

J. W. Reiner, F. J. Walker, C. H. Ahn

Crystalline oxides can exhibit nearly every possible effect seen in solid-state physics, including magnetism and superconductivity. An even richer spectrum of possibilities becomes available if thin films of different crystalline oxides are combined layer by layer to create artificially structured, heterogeneous materials. The study of these engineered materials is just beginning, but an emerging theme is that the interface between different oxide layers plays a crucial role because it provides an avenue for the study and control of solid-state phenomena at the nanoscale (see the figure, panel A). The interface can control intrinsic properties of the bulk materials so that, for example, magnetism can be switched on and off reversibly (*1*), or it can have properties entirely different from both constituents, such as a metallic layer forming at the interface between two insulators (*2*). An example of controlling this metallic response is reported by Cen *et al.* (*3*) on page 1026 of this issue.

These developments are the result of the intrinsic ability of oxides to form heterostructures, coupled with methods for fabricating and characterizing these structures with atomic-layer sensitivity and control. Epitaxial growth—growing a single crystal on top of another—requires a close match of the sizes of the crystal lattices. Heterogeneous crystalline oxide films lend themselves to epitaxial growth because, despite having different cations, they often share a common sublattice of oxygen atoms.

The development of sophisticated tools for growing complex oxides as thin films was driven by the discovery of the high-temperature superconducting oxides, which have complex crystal structures and compositions. The growth of complex oxides demanded improved control over the vapor pressure of the cation sources, highly reactive sources of oxygen, and the development of corrosion-resistant equipment that could survive strong oxidizing conditions. Structural tools and spectroscopic methods with exquisite spatial and energy resolution were also needed to assess the quality of the layers and interfaces that were grown and to determine the chemistry and valence states of the oxides and their interfaces (*4*, *5*). The degree of crystalline per-

Department of Applied Physics and Center for Research on Interface Phenomena and Structures, New Haven, CT 06520–8284, USA. E-mail: james.reiner@yale.edu; fred.walker@yale.edu; charles.ahn@yale.edu

fection now possible in oxide film synthesis rivals that attained in semiconducting systems. For example, the observation of the quantum Hall effect, which requires precise interfacial engineering in semiconducting materials, was recently reported for an oxide interface (*6*).

The properties of an interface region between one oxide building block and the next are determined by how the individual properties of each oxide couple together. For example, by layering ferroelectrics (materials with enormous, built-in, switchable electric dipoles) with superconductors, a superconducting switch controlled by the direction of the electric dipoles has been made (*7*). Superconductivity can be turned on and off in different regions of the interface on a nanometer scale (*8*) (see the figure, panel B). Analogous magnetic switching has been achieved by integrating ferromagnetic and ferroelectric oxides in a "multiferroic" composite structure, which allows the control of magnetism in the solid state by applying an electric field (*1*, *9*). Although these effects occur in an interfacial region only a single nanometer across, oxide superlattices, in which the growth of different layers is repeated in a regular fashion, can extend this coupling across the entire structure (*10*).

Researchers are using composite oxide materials structures to address numerous applications, including environmental energy harvesting, thermoelectric energy conversion, nonvolatile memory devices, chemical sensors, and more densely integrated logic circuits. Many of the electronics applications will benefit greatly from creating complex crystalline oxide structures directly on silicon (*11*) (see the figure, panel A), making it possible to combine all these applications on a single silicon-based chip. Silicon is chemically and structurally different from the crystal oxide building blocks, so this stacking is far more difficult to achieve. By paying careful attention to the thermodynamic requirements of each atomic layer, however, a handful of crystal oxides have been successfully sandwiched directly on the silicon surface.

Some potential technology applications exploit effects that are well understood, but unexpected phenomena have also emerged at materials interfaces. One striking example is the recently developed interface between lanthanum aluminate ($LaAlO_3$) and strontium titanate ($SrTiO_3$). Both $LaAlO_3$ and $SrTiO_3$ are ordinary band insulators in which large energy gaps prevent electrons from populating conduction bands. However, if these materials are layered together with a precise number of $LaAlO_3$ atomic planes, a metallic state forms at the nanoscale interface between the nonconducting constituents (*2*). Moreover, at very low temperatures, the interface is superconducting and possibly magnetic (*12*, *13*).

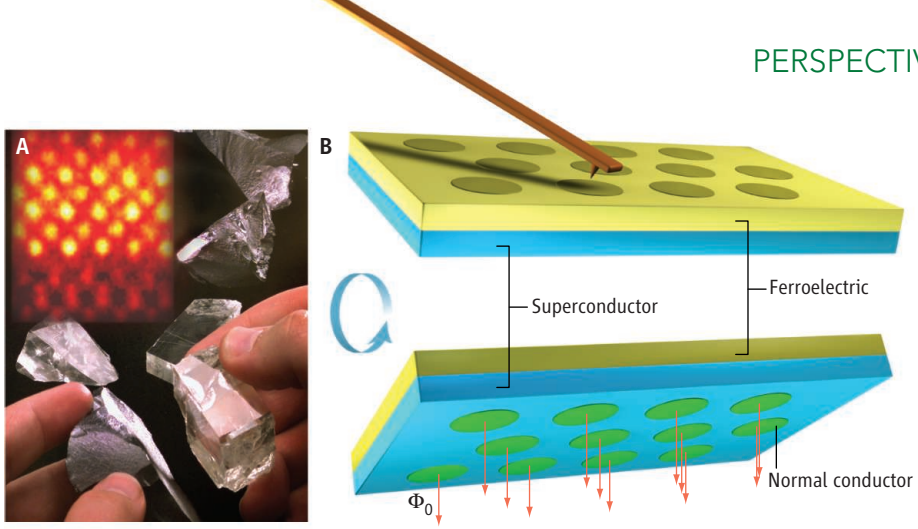

Really thin sandwiches. (**A**) In the nascent days of the electronics industry, researchers would glue materials together by hand to develop new device structures. Today, it is possible to sandwich oxide materials together with atomic-scale precision, leading to the observation of novel interfacial phenomena at the single-nanometer scale. The background shows an atomic-resolution electron micrograph (cross-sectional view) of an oxide-semiconductor ($SrTiO_3$-Si) sandwich structure (*11*). (**B**) Creating patterns in a superconducting Nb-$SrTiO_3$ layer (light blue, Nb, niobium) beneath a ferroelectric Pb(Zr,Ti)O_3/layer (yellow; Pb, lead, and Zr, zirconium). By switching the ferroelectric polarization locally with a voltage pulse delivered by an atomic force microscope tip, regions in the Nb-$SrTiO_3$ layer about 100 nanometer in diameter (green) become normal conductors and an array of magnetic pinning centers can be created in the superconducting film (*8*).

This metallic behavior can be turned on and off in specific regions of the interface by applying a voltage to the oxide structure. When this voltage is applied with an atomic force microscope tip, devices such as field-effect transistors can be created out of the metallic and insulating regions (*3*). The resulting circuits are reconfigurable, because new devices can be created out of the same material just by applying a new pattern of voltages (*14*).

The physical origin of these properties of the $LaAlO_3/SrTiO_3$ interface is still under study, but one model for the source of the charge carriers responsible for the observed behavior involves a phenomenon called the polar catastrophe, in which the polar nature of $LaAlO_3$ drives electrons to accumulate in the nonpolar $SrTiO_3$, resulting in a two-dimensional, high-mobility electron gas at the interface. More recently, the use of similar atomic layering approaches has led to the observation of superconductivity at the interface between two nonsuperconducting oxides (*15*).

The number of potential interfaces that can be made is essentially limitless, so experimentalists will continue to look to theoretical predictions for guidance. First-principles electronic structure calculations can now predict electronic ground states of complex oxide materials with remarkable quantitative accuracy (*16*), and this capability has paid enormous dividends in the study of ferroelectrics (*17*). Theorists have motivated experimentalists to use strain, composition, and other tunable external control parameters to optimize and control ferroelectricity in novel oxide systems (*18*) and have already begun to make predictions for novel interfacial properties in select oxide heterostructures (*9*). One outstanding challenge for theorists, however, will be to predict how some of the more complicated interactions, such as strong electronic correlations that arise from the Coulombic forces between electrons, lead to novel ground states, including superconductivity and magnetism.

Initial applications of these materials are likely to be in areas such as sensors and energy harvesting, where the interactions are simpler. As the relation between structure and behavior is understood for more complicated materials systems, the number of potential applications will increase dramatically.

References

1. Y. H. Chu *et al.*, *Nat. Mater.* **7**, 478 (2008).
2. A. Ohtomo, H. Y. Hwang, *Nature* **427**, 423 (2004).
3. C. Cen *et al.*, *Science* **323**, 1026 (2009).
4. D. D. Fong *et al.*, *Science* **304**, 1650 (2004).
5. A. Ohtomo *et al.*, *Nature* **419**, 378 (2002).
6. A. Tsukazaki *et al.*, *Science* **315**, 1388 (2007).
7. C. H. Ahn *et al.*, *Science* **284**, 1152 (1999).
8. K. S. Takahashi *et al.*, *Nature* **441**, 195 (2006).
9. N. A. Spaldin, M. Fiebig, *Science* **309**, 391 (2005).
10. D. G. Schlom *et al.*, *Mater. Sci. Eng. B* **87**, 282 (2001).
11. R. A. McKee *et al.*, *Phys. Rev. Lett.* **81**, 3014 (1998).
12. N. Reyren *et al.*, *Science* **317**, 1196 (2007).
13. A. Brinkman *et al.*, *Nat. Mater.* **6**, 493 (2007).
14. C. H. Ahn *et al.*, *Science* **276**, 1100 (1997).
15. A. Gozar *et al.*, *Nature* **455**, 782 (2008).
16. W. Zhong *et al.*, *Phys. Rev. Lett.* **73**, 1861 (1994).
17. C. H. Ahn *et al.*, *Science* **303**, 488 (2004).
18. K. J. Choi *et al.*, *Science* **306**, 1005 (2004).

10.1126/science.1169058

CREDIT: (A) Z-CONTRAST MICROGRAPH, M. F. CHISHOLM, R. A. MCKEE/OAK RIDGE NATIONAL LABORATORY; (B) ADAPTED FROM K. S. TAKAHASHI, J.-M. TRISCONE/UNIV. OF GENEVA

ATMOSPHERIC SCIENCE

A Matter of Humidity

How strong a part does water vapor play in global warming?

Andrew E. Dessler[1] and Steven C. Sherwood[2]

The water vapor feedback is the process whereby an initial warming of the planet, caused, for example, by an increase in atmospheric carbon dioxide, leads to an increase in the humidity of the atmosphere. Because water vapor is itself a greenhouse gas, this increase in humidity causes additional warming. The water vapor feedback has long been expected to strongly amplify climate changes because of the expectation that the atmosphere's relative humidity would remain roughly constant—meaning that the specific humidity would increase at the rate of the equilibrium vapor pressure, which rises rapidly with temperature. However, observational evidence has been harder to come by, and the effect has been controversial. Much of that controversy can now be laid to rest, thanks to new observations and better theoretical understanding.

In the 1990s, there was little observational or theoretical understanding of atmospheric humidity and how it varied with global climate. As a result, debate raged over whether the water vapor feedback would really occur, with some very influential proposals that it would not (*1*). In particular, many believed that atmospheric humidity and the water vapor feedback were controlled by processes—such as the details of cloud dynamics and microphysical processes—that are not sufficiently well understood and inadequately represented in climate models.

Successive reports from the Intergovernmental Panel on Climate Change (IPCC) have suggested increasing confidence in our understanding of the water vapor feedback, but they have remained cautious in defending its magnitude. However, recent advances have placed the traditional view of the water vapor feedback on a stronger footing than is widely appreciated.

The water vapor feedback mainly results from changes in humidity in the tropical upper troposphere (*2*), where temperatures are far below that of the surface and the vapor is above most of the cloud cover. The distribution of humidity in this region is well reproduced by "large-scale control" models, in which air leaves stormy regions in a saturated condition, but with negligible ice or liquid content. Water vapor is thereafter transported by the large-scale circulation, which conserves the specific humidity (the ratio of the mass of water vapor to the total mass in a unit volume of air), except during subsequent saturation events, when loss of water occurs instantaneously to prevent supersaturation. Despite the simplicity of this idea, which entirely neglects detailed microphysics and other small-scale processes, such models accurately reproduce the observed water vapor distribution for the mid and upper troposphere (*3*, *4*). One recent study (*5*) estimated the uncertainty in the water vapor feedback associated with microscale process behavior at less than 5%, as a result of the overwhelming control of humidity by the large-scale wind field.

Thus, the water vapor feedback is essentially controlled by the large-scale dynamics and the saturation specific humidity in the outflow of the tropical deep convective systems. Convective outflow temperature should, on average, warm along with the mean atmosphere, thus producing the feedback (*6*, *7*).

Given these considerations, there are good reasons to expect global climate models to accurately simulate the water vapor feedback: The large-scale wind and temperature fields that mainly control the humidity are explicitly calculated from the basic fluid equations, unlike small-scale processes that must be represented by crude parameterizations.

Although the water vapor feedback is strong in all global climate models, its magnitude varies somewhat due to differences among the models in the amount of upper tropospheric warming (and hence the increase in specific humidity) per unit of surface warming. The spread among models in the water vapor feedback is, however, largely compensated by an opposite spread in the "lapse-rate feedback," a negative feedback that occurs because a warmer atmosphere radiates more power to space, thereby reducing net surface warming. As a result, the sum of the two feedbacks is insensitive to errors in predicted warming of the upper troposphere, and to quantify the sum accurately, one only needs to know how relative humidity (the ratio of specific humidity to that in a saturated condition) changes as the climate warms. The sum of the feedbacks is also smaller than the water vapor feedback—about half the magnitude—and more consistent among climate models (*8*), because no model predicts substantial and systematic changes in relative humidity.

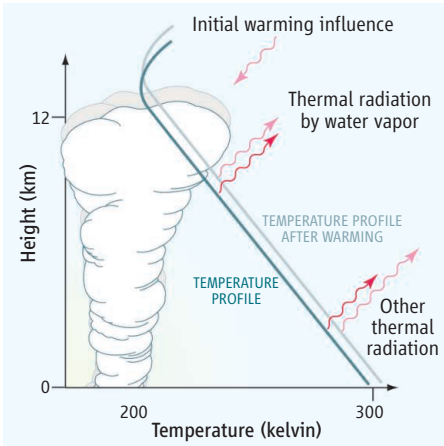

Schematic of the water vapor feedback. Because thermal emission to space by water vapor does not increase, more warming is needed to balance a given energy input.

Despite these advances, observational evidence is crucial to determine whether models really capture the important aspects of the water vapor feedback. Such evidence is now available from satellite observations of the response of atmospheric humidity (and its impacts on planetary radiation) to a number of climate variations. Observations during the seasonal cycle, the El Niño cycle, the sudden cooling after the 1991 eruption of Mount Pinatubo, and the gradual warming over recent decades all show atmospheric humidity changing in ways consistent with those predicted by global climate models, implying a strong and positive water vapor feedback (*9*–*13*). A strong and positive water vapor feedback is also necessary for models to explain the magnitude of past natural climate variations (*14*).

Both observations and models suggest that the magnitude of the water vapor feedback is similar to that obtained if the atmosphere held relative humidity constant everywhere. This should not be taken to mean that relative humidity will remain exactly the same everywhere. Regional variations of relative humidity are seen in all observed climate variations and in model simulations of future climate, but have a negligible net impact on the global feedback (*12*).

[1]Texas A&M University, College Station, TX 77843, USA. E-mail: adessler@tamu.edu. Climate Change Research Centre, University of New South Wales, Sydney, Australia. E-mail: s.sherwood@unsw.edu.au

Published by AAAS

Thus, although there continues to be some uncertainty about its exact magnitude, the water vapor feedback is virtually certain to be strongly positive, with most evidence supporting a magnitude of 1.5 to 2.0 W/m^2/K, sufficient to roughly double the warming that would otherwise occur. To date, observational records are too short to pin down the exact size of the water vapor feedback in response to long-term warming from anthropogenic greenhouse gases. However, it seems unlikely that the water vapor feedback in response to long-term warming would behave differently from that observed in response to shorter-time scale climate variations. There remain many uncertainties in our simulations of the climate, but evidence for the water vapor feedback—and the large future climate warming it implies—is now strong.

References

1. R. S. Lindzen, *Bull. Am. Meteor. Soc.* **71**, 288 (1990).
2. I. M. Held, B. J. Soden, *Ann. Rev. Energy Environ.* **25**, 441 (2000).
3. R. T. Pierrehumbert, H. Brogniez, R. Roca, in *The Global Circulation of the Atmosphere*, T. Schneider, A. H. Sobel, Eds. (Princeton Univ. Press, Princeton, 2007), pp. 143–218.
4. I. Folkins, K. K. Kelly, E. M. Weinstock, *J. Geophys. Res.* **107**, 4736 (2002).
5. S. C. Sherwood, C. L. Meyer, *J. Climate* **19**, 6278 (2006).
6. D. L. Hartmann, K. Larson, *Geophys. Res. Lett.* **29**, 1951 (2002).
7. K. Minschwaner, A. E. Dessler, *J. Climate* **17**, 1272 (2004).
8. B. J. Soden, I. M. Held, *J. Climate* **19**, 3354 (2006).
9. B. J. Soden, R. T. Wetherald, G. L. Stenchikov, A. Robok, *Science* **296**, 727 (2002).
10. P. M. D. Forster, M. Collins, *Climate Dyn.* **23**, 207 (2004).
11. B. J. Soden, D. L. Jackson, V. Ramaswamy, M. D. Schwarzkopf, X. Huang, *Science* **310**, 841 (2005).
12. A. E. Dessler, P. Yang, Z. Zhang, *Geophys. Res. Lett.* **35**, L20704 (2008).
13. A. K. Inamdar, V. Ramanathan, *J. Geophys. Res.* **103**, 32177 (1998).
14. A. Hall, S. Manabe, *J. Climate* **12**, 2327 (1999).

15. We thank T. Schneider, P. O'Gorman, and P. Forster for their comments on this perspective. This work was supported by NASA grant NNX08AR27G to Texas A&M University.

10.1126/science.1171264

CELL BIOLOGY

Stress Response and Aging

Transcriptional regulators that respond to stress also influence life span.

Laura R. Saunders and Eric Verdin

Exposure to a variety of mild stressors, including calorie restriction, thermal stress, or hyperbaric oxygen, induces an adaptive biological response that increases eukaryotic life span (*1*). There are also a variety of mutations associated with both increased resistance to stress and increased longevity, such as those associated with altered insulin/IGF1 (insulin-like growth factor 1) signaling in the nematode *Caenorhabditis elegans* (*2*). Adaptive responses to stressors are mediated by transcription factors that regulate both stress response and life span. On page 1063 of this issue, Westerheide *et al.* (*3*) connect two additional transcriptional regulators to stress responses and longevity. The results support the idea that low levels of stressors influence life span and provide additional potential molecular targets that can be further manipulated experimentally or therapeutically.

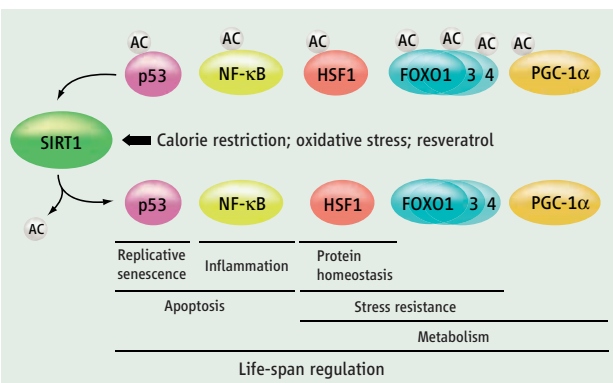

Handling stress. SIRT1 is a deacetylase that is activated by a variety of stressors and targets transcriptional regulators including p53, NF-κB, HSF1, FOXO1, 3, and 4, and PGC-1α. These factors then control adaptive responses that modulate life span. AC, acetyl group.

Westerheide *et al.* demonstrate that the activity of a transcription factor called heat shock factor 1 (HSF1) is regulated by the enzyme sirtuin 1 (SIRT1). HSF1 exists as a monomer in unstressed mammalian cells. In response to a variety of stresses—including heat shock, hypoxia, misfolded proteins, free radicals, and adenosine triphosphate depletion—HSF1 trimerizes, translocates to the nucleus, becomes phosphorylated, and binds to regulatory elements (promoters) of genes that encode heat shock proteins (*4*). Heat shock proteins such as Hsp70 serve as chaperones and proteases that resolve damaged, misfolded, and aggregated proteins.

SIRT1, a mammalian ortholog of the yeast transcriptional regulator Sir2, is a stress-activated nicotinamide adenine dinucleotide (NAD^+)–dependent protein deacetylase that regulates cell survival, replicative senescence, inflammation, and metabolism through the deacetylation of histones (the major protein components of chromatin) and other cellular factors including the transcription factors p53, NF-κB, and FOXO1, 3, and 4, and the transcriptional regulator PGC-1α (*5*) (see the figure). Calorie restriction extends life span in part by increasing SIRT1 expression, and in yeast, worms, and fruit flies, the lack of Sir2 abrogates the effects of calorie restriction on life span (*6*). Similarly, mice lacking SIRT1 do not show some of the beneficial effects of calorie restriction related to longevity (*7*, *8*). The enzymatic activity of SIRT1 is activated by resveratrol, a polyphenol produced by plants under stress. Resveratrol extends the life-span of yeast, worms, and flies only when Sir2 is present (*9*).

Westerheide *et al.* show that in mammalian cells, SIRT1 directly deacetylates HSF1 and thereby regulates the heat shock response. The effect of SIRT1 on HSF1 appears to be dynamically regulated. In response to stresses, including heat shock, HSF1 is acetylated by the histone acetyltransferase p300, a modification that is thought to function as an "off" signal by triggering the dissociation of HSF1 from its target gene. Inhibiting SIRT1 expression via small interfering RNA prevents HSF1 from binding to the *hsp70* promoter and suppresses transcription of the gene when cells are exposed to heat shock. Conversely, Westerheide *et al.* observed that SIRT1 activation by resveratrol or SIRT1 overexpression in cells decreases HSF1 acetylation, prolongs HSF1 binding to target promoters, and enhances the heat shock response.

HSF1 is acetylated on at least nine lysine residues. One acetylated residue, Lys^{80}, controls HSF binding to DNA. Thus, acetylation of HSF1 at Lys^{80} may cause the release of

Gladstone Institute of Virology and Immunology, 1650 Owens Street, San Francisco, CA 94158, USA, and University of California, San Francisco, CA 94158, USA. E-mail: everdin@gladstone.ucsf.edu

HSF1 from DNA and represents a negative regulatory step during the heat shock response. The authors also found that SIRT1 overexpression enhances the ability of cultured cells to survive prolonged exposure to lethal heat shock temperatures. SIRT1 therefore functions as a positive cofactor of HSF1 and enhances the heat shock response.

Aging and cellular senescence reduce an organism's ability to respond to stress and maintain homeostasis (*10*). During aging, a decrease in HSF1 binding to DNA reduces the expression of heat shock proteins (*11*). Whereas HSF1 protein concentration increases with age, the amount of SIRT1 protein decreases with age (*11*, *12*). Accordingly, Westerheide *et al.* observed in an in vitro model of aging and senescence (early and late passage of cultured human fibroblasts) that concomitantly with a decrease in SIRT1 protein expression, HSF1 DNA binding and expression of heat shock proteins decrease.

Expression of SIRT1 is controlled by the transcription factors p53, FOXO3a, and E2F1, and at the posttranscriptional level by the protein HuR, which stabilizes SIRT1-encoding mRNA. At the functional protein level, it is controlled by the cellular concentration of NAD^+ and the proteins AROS and DBC1, which interact with SIRT1 (*13*). SIRT1 enzymatic activity can also be allosterically enhanced by small molecules, including resveratrol (*14*, *15*). Thus, regulators of SIRT1 expression and enzymatic activity are likely to modulate HSF1 acetylation and therefore affect its DNA binding activity and the extent of the heat shock response.

These observations also provide insights into the mechanism of action of Sir2 and SIRT1 on stress responses and life span, and suggest that HSF1 might be one of the critical effectors of SIRT1. Calorie restriction is of particular interest because it is one of the stressors that induce life span extension in all organisms in which it has been tested. Calorie restriction is associated with increased SIRT1 expression and with an increased ratio of NAD^+ to its reduced form, NADH (*16*). The age-related decline in HSF1 DNA binding and heat shock response is partially reversed by calorie restriction, which may be explained by the induced expression of SIRT1 (*6*, *17*). Overexpression of the HSF1 ortholog in *C. elegans* extends life span (*18*). It remains to be determined whether the *C. elegans* HSF1 ortholog is necessary for Sir2 to enhance life span in this model system, or whether HSF1 is necessary for the beneficial effects of calorie restriction in higher organisms.

These observations indicate that SIRT1 and HSF1 function together to protect cells from various stresses, promote survival, and extend life span. However, too much of a good thing can be detrimental. Indeed, increased resistance to stress induced by HSF1 may also promote cancer development by helping cancer cells to deal with stress (*19*). HSF1 supports malignant transformation by orchestrating a network of core cellular functions, such as cell proliferation, survival, protein synthesis, and glucose metabolism. Human cancer cell lines of diverse origins show much greater dependence on HSF1 function to maintain proliferation and survival than do their nontransformed counterparts (*19*). Likewise, SIRT1 may contribute to tumorigenic potential; it is overexpressed in many cancers, and inhibition of its enzymatic activity by small molecules kills tumor cells (*5*). Determining the relative contributions of distinct SIRT1 targets (including NF-κB, p53, PGC-1α, HSF1, and FOXO1, 3, and 4) toward its effects on age-related diseases such as neurodegeneration, cardiovascular disease, and diabetes may point to possible therapeutic approaches.

References

1. D. Gems, L. Partridge, *Cell Metab.* **7**, 200 (2008).
2. G. J. Lithgow, G. A. Walker, *Mech. Ageing Dev.* **123**, 765 (2002).
3. S. D. Westerheide, J. Anckar, S. M. Stevens Jr., L. Sistonen, R. I. Morimoto, *Science* **323**, 1063 (2009).
4. L. Pirkkala, P. Nykanen, L. Sistonen, *FASEB J.* **15**, 1118 (2001).
5. L. R. Saunders, E. Verdin, *Oncogene* **26**, 5489 (2007).
6. M. C. Haigis, L. P. Guarente, *Genes Dev.* **20**, 2913 (2006).
7. H. Y. Cohen *et al.*, *Science* **305**, 390 (2004); published online 17 June 2004 (10.1126/science.1099196).
8. G. Boily *et al.*, *PLoS ONE* **3**, e1759 (2008).
9. J. A. Baur, D. A. Sinclair, *Nat. Rev. Drug Discov.* **5**, 493 (2006).
10. M. A. Bonelli *et al.*, *Exp. Cell Res.* **252**, 20 (1999).
11. A. R. Heydari *et al.*, *Exp. Cell Res.* **256**, 83 (2000).
12. E. Michishita, J. Y. Park, J. M. Burneskis, J. C. Barrett, I. Horikawa, *Mol. Biol. Cell* **16**, 4623 (2005).
13. H. S. Kwon, M. Ott, *Trends Biochem. Sci.* **33**, 517 (2008).
14. J. A. Baur *et al.*, *Nature* **444**, 337 (2006).
15. J. C. Milne *et al.*, *Nature* **450**, 712 (2007).
16. S. J. Lin *et al.*, *Genes Dev.* **18**, 12 (2004).
17. A. R. Heydari *et al.*, *Dev. Genet.* **18**, 114 (1996).
18. A.-L. Hsu, C. T. Murphy, C. Kenyon, *Science* **300**, 1142 (2003).
19. C. Dai, L. Whitesell, A. B. Rogers, S. Lindquist, *Cell* **130**, 1005 (2007).

10.1126/science.1170007

ECOLOGY

Peter Principle Packs a Peck of Phytoplankton

Daniel Grünbaum

Biomechanical interactions between motile cells and environmental flows may cause the rapid formation of ecologically important phytoplankton patches.

Almost 50 years ago, Hutchinson noted the "paradox of the plankton" (*1*): the fact that the large number of phytoplankton species is difficult to explain by competition for relatively few limiting nutrients. This paradox reflects a more general truth in ecology. The mechanisms that create and maintain biological diversity are not well understood, in the oceans or elsewhere. Among the least-understood aspects of diverse ecosystems is the role of small-scale spatial and temporal heterogeneity—patchiness—that exists, often unseen, in almost every environment. On page 1067 of this issue, Durham *et al.* (*2*) describe a new mechanism through which this patchiness is generated and maintained.

Patchiness not only implies a greater variety of microenvironments than meets the eye; it also opens up a universe of possible specializations in locomotion, sensing, and behavior for organisms that move between microenvironments. Opportunities for specialization promote coexistence and diversity, but understanding the long-term ecological and evolutionary consequences of patchiness requires knowledge of its characteristics and causal mechanisms. Durham *et al.* identify one such mechanism, gyrotactic trapping, through which velocity gradients in the upper ocean can cause intense, highly localized, and ecologically important patches of phytoplankton in specific, predictable positions in the water column.

Phytoplankton—the microscopic photosynthetic organisms at the base of oceanic food webs—play a key role in the ecology of our planet. Unlike terrestrial plants, marine photosynthesizers are mostly unicellular, and many are active, effective swimmers. For example, 29 of the 33 species known to cause harmful algal blooms off the west coast of

School of Oceanography, University of Washington, Seattle, WA 98195–7940, USA. E-mail: grunbaum@ocean.washington.edu

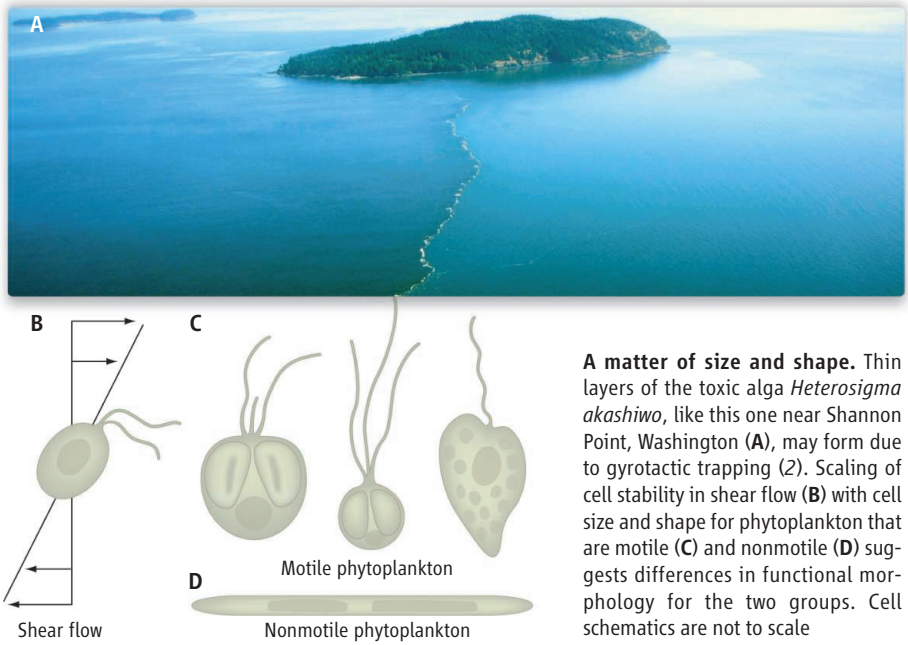

A matter of size and shape. Thin layers of the toxic alga *Heterosigma akashiwo*, like this one near Shannon Point, Washington (**A**), may form due to gyrotactic trapping (*2*). Scaling of cell stability in shear flow (**B**) with cell size and shape for phytoplankton that are motile (**C**) and nonmotile (**D**) suggests differences in functional morphology for the two groups. Cell schematics are not to scale

CREDITS: PHOTO IN PANEL A: K. FREDRICKSON/WESTERN WASHINGTON UNIVERSITY; PHYTOPLANKTON CELL SCHEMATICS: ADAPTED FROM D. MONTAGNES, HARMFUL PLANKTON PROJECT/UNIVERSITY OF LIVERPOOL

North America are motile (*3*). Nutrients are often quickly depleted in well-lit surface waters but remain available at depth; motile phytoplankton can access both light and nutrients by migrating between deeper and shallower water—a potentially important advantage over nonmotile competitors.

Durham *et al*. link phytoplankton motility to "thin layers," strata spanning a meter or less vertically but kilometers horizontally, in which plankton and detritus concentrate (*4*–*6*). They focus on thin layers in strata with strong hydrodynamic shear (that is, where ambient horizontal current velocities vary rapidly with depth). Strong shear can overcome the orientation mechanisms used by motile cells for directed swimming.

The authors demonstrate a sort of Peter principle (*7*) for algae migrating in shear: Cells swim up until they reach their level of instability. At this critical shear level, cells can swim in, but they cannot swim out. The resulting aggregation, in what is arguably an unfavorable microenvironment, may have widespread consequences, as harmful blooms of toxic algae often take the form of thin layers (see the figure, panel A).

Phytoplankton cell orientation is usually attributed to three main mechanisms, each implying biomechanical limits to cell stability (*8*). First, cells may actively steer toward or away from gravity or light. Second, cells can be bottom-heavy so that if they are tilted, the offset between the centers of buoyancy and gravity induces a corrective torque back toward the vertical. Third, cells, which are typically denser than the surrounding water, can have morphological features that act as vanes to orient them as they sink (*9*).

This last mechanism can act in counterintuitive ways. For example, a uniformly dense spherical cell with inactive flagella sinks with flagella trailing upward. If the cell becomes buoyant, it rises flagella-downward. But if the cell stays heavy and activates its flagella, it swims upward with flagella pointing up. In effect, it is sinking and rising at the same time: The sinking movement orients the cell and drags the surrounding water downward, while the flagella pull the cell upward through the descending water. Many motile phytoplankton species seem to take advantage of this stabilizing hydrodynamic effect by adopting a flagella-up swimming posture.

These cell orientation mechanisms can be summarized by a reorientation time scale, which indicates how quickly perturbed cells can right themselves in still water (*2*). Cells in shear experience a torque, proportional to differences in flow on their various surfaces, that tilts them off their vertical orientation (see the figure, panel B). In weak shear, this perturbation is small, and cells still move upward. Durham *et al.* now show that when the shear exceeds a critical value, the cells' orientation machinery fails and they spin continuously: They are gyrotactically trapped. This process is highly selective, because morphologies and behaviors (and hence reorientation time scales) vary strongly between and even within phytoplankton species. Each cell is segregated at its own particular critical shear along with others of its kind—a gift to predators and pathogens.

Durham *et al.*'s analysis suggests new questions about the evolution of cell size, shapes, and motility. Are phytoplankton cells as stable as biomechanically possible? If so, how does this constraint influence cell size and shape? If not, which behavioral or physiological requirements would be compromised if cells became more stable? And what does a migration-based nutrient-acquisition strategy, rather than a nonmotile diffusion-only strategy, imply for phytoplankton morphology?

Scaling relationships suggest that stability requirements may spur very different morphologies for motile and nonmotile phytoplankton (see the figure, panels C and D). Motile phytoplankton may be better able to acquire nutrients using a migratory strategy if they are large and have small length/width ratios that enable them to maintain vertical orientations; in contrast, nonmotile phytoplankton may better maintain depth and acquire resources through diffusion if they are small and have large length/width ratios, which may cause them to adopt mainly horizontal orientations in shear (*9*–*14*).

Beyond cell-level function, understanding how gyrotactic trapping propagates physical flows into biological patches may improve estimates of phytoplankton diversity, abundance, and productivity at large spatial and temporal scales. Such estimates are badly needed. The models currently used to address urgent problems such as harmful algal blooms, damaged fisheries, and ocean acidification simulate only a fraction of the diverse species and mechanisms that drive marine ecosystems. Insights that enable more accurate approximations of complex dynamics with simpler ones are major steps toward more useful ecosystem models.

References and Notes

1. G. E. Hutchinson, *Am. Nat.* **95**, 137 (1961).
2. W. M. Durham, J. O. Kessler, R. Stocker, *Science* **323**, 1067 (2009).
3. R. A. Horner, D. L. Garrison, F. G. Plumley, *Limnol. Oceanogr.* **42**, 1076 (1997).
4. M. M. Dekshenieks *et al.*, *Mar. Ecol. Prog. Ser.* **223**, 61 (2001).
5. M. T. Stacey, M. A. McManus, J. V. Steinbuck, *Limnol. Oceanogr.* **52**, 1523 (2007).
6. D. A. Birch, W. R. Young, P. J. S. Franks, *Deep-Sea Res. I* **55**, 277 (2008).
7. L. J. Peter, R. Hull, *The Peter Principle: Why Things Always Go Wrong* (Morrow, New York, 1968).
8. A. M. Roberts, *Biol. Bull.* **210**, 78 (2006).
9. A. M. Roberts, F. M. Deacon, *J. Fluid Mech.* **452**, 405 (2002).
10. L. Karp-Boss, E. Boss, P. A. Jumars, *Oceanogr. Mar. Biol. Annu. Rev.* **34**, 71 (1996).
11. Z. V. Finkel *et al.*, *Proc. Natl. Acad. Sci. U.S.A.* **104**, 20416 (2007).
12. D. Kamykowski *et al.*, *Mar. Biol.* **113**, 319 (1992).
13. L. Karp-Boss, P. A. Jumars, *Limnol. Oceanogr.* **43**, 1767 (1998).
14. M. Pahlow *et al.*, *Limnol. Oceanogr.* **42**, 1660 (1997).
15. I thank the Office of Naval Research (grant N00014-05-1-0026) and National Oceanic and Atmospheric Administration Washington State Sea Grant (number NA040AR170032) for support, and M. Groom, M. Grünbaum, P. A. Jumars, and S. Menden-Deuer for insightful comments and suggestions.

10.1126/science.1170662

Open Access and Global Participation in Science

James A. Evans[1]* and Jacob Reimer[2]

The issue of open access (OA), free and unrestricted online access to scientific publications, has stirred debate among scientists, policymakers, and editors in recent years. Most previous research claimed that OA articles are cited about 100% more (*1*), although these studies have been limited to a single journal or lacked analysis of commercial electronic availability or changes over time (*2*–*4*). In contrast, recent experiments suggested that OA may have no effect on journal citations or even a negative impact (*5*–*7*). We used more extensive citation data than those of previous studies to show the influence of OA on research attention and highlight its greatest impact: developing world participation in global science.

Citation data were from Thomson Scientific's Science, Social Science, and Humanities Citation Indexes (CI), including articles and associated citations from the 8253 most highly cited journals going back to 1945. We linked this with online availability of journals by means of Information Today, Incorporated's Fulltext Sources Online. Merged, this data set comprises 26,002,796 articles whose journals came online by 2006, 88% of which are published in English. For CI articles, 77% showed author institutions, which we coded and linked to World Bank and United Nations Educational, Scientific, and Cultural Organization data on per capita gross national income (GNI) (*8*).

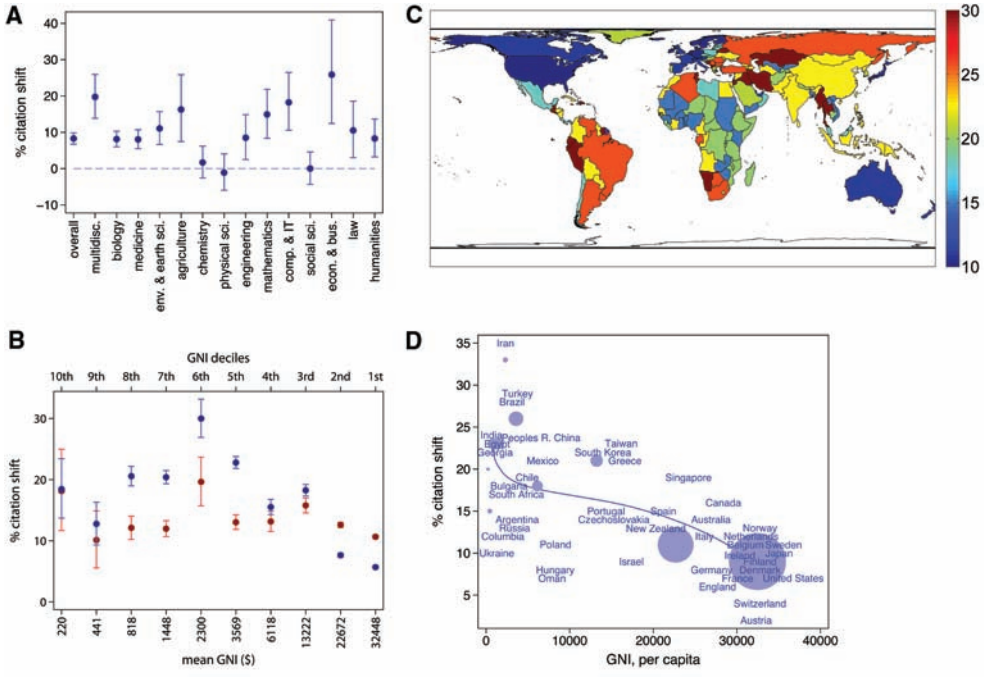

Fig. 1. (**A**) Percentage increase in citations for subfields after free online availability, 1998–2005. Online availability is measured in the previous year. Error bars indicate 95% confidence intervals. (**B**) Percentage increase in citations after free (blue) and commercial (red) online access for GNI country deciles of the richest country hosting a citing author. (**C**) Global projection of percentage increase in citations for GNI country deciles of the poorest country hosting a citing author after free online availability. (**D**) Percentage increase in citations after free online access for the poorest individual countries and GNI deciles (blue circles, sized proportional to the total number of citations they generate). The downward sloping line is a prediction of the OA citation shift for GNI deciles based on estimation of a fractional polynomial of GNI. All countries represented in deciles, but only 44 individually because some have very few citations in the CI.

Within the natural sciences, OA influence was strongest for multidisciplinary journals (Fig. 1A). In three areas, OA confers no additional attention, including physics, where preprint and publication databases already provide nearly complete access, and the social sciences, where personal preprint archiving and lengthy review times are common. Across subfields, the impact of commercial online availability was positive, statistically significant, and on average 40% larger than the OA effect, suggesting that most researchers rely on institutional subscriptions.

We tested the influence of OA on dissemination of science to poor countries by first calculating the per capita GNI for the poorest country hosting an author on every paper that cites an article in our data set (*9*). Although commercial availability had double the effect of OA for countries in the top two deciles, OA had greater influence in all lower deciles (Fig. 1B). Online OA had the greatest effect in the developing Southern Hemisphere rather than the wealthy Northern and Western (Fig. 1C). The influence of OA was more than twice as strong in the developing world but was less apparent in the very poorest countries where electronic access is limited (Fig. 1D).

Lastly, we regressed average per capita GNI for the poorest countries hosting citing papers on Internet availability the prior year. OA had a strong, negative effect even while controlling for commercial access. After the average journal volume became OA, the average per capita GNI of the poorest countries hosting scientists that cited it dropped by $804 ± 26 (SEM). After adding the effect of commercial availability, the GNI lowered by $1705 ± 42 (SEM), equivalent to extending access from scientists in Russia to those in Western Sahara.

The influence of OA is more modest than many have proposed, at ~8% for recently published research, but our work provides clear support for its ability to widen the global circle of those who can participate in science and benefit from it.

References and Notes

1. M. J. Kurtz *et al.*, *Inform. Process. Manag.* **41**, 1395 (2005).
2. E. A. Henneken *et al.*, http://arxiv.org/abs/cs/0604061 (2006).
3. S. Lawrence, *Nature* **411**, 521 (2001).
4. G. Eysenbach, *PLoS Biol.* **4**, e157 (2006).
5. P. M. Davis, M. J. Fromerth, *Scientometrics* **71**, 203 (2007).
6. E. R. Maher, *J. Med. Genet.* **42**, 97 (2005).
7. P. Davis *et al.*, *Br. Med. J.* **337**, a568 (2008).
8. GNI is used instead of gross domestic product (GDP) because it more precisely captures average, realized income. We first used fixed effects Poisson regression models with robust standard errors to compare citations to journal volumes in periods when their articles were not available electronically to periods in which they were, commercially and for free. To control for the number of citations that would have been received without a change in online access, we used a log-normal curve fit to the empirical distribution of citations (*10*). All models control for the online commercial availability of research and are estimated for those articles published in years 1998–2005, after published research began to become available online and the influence of online access on subsequent citations became consistently positive (*9*, *11*). Exponentiated Poisson coefficients represent incidence ratios: the ratio of citations in years with OA to those in years without. Reduced by one and multiplied by 100, these become percentage shifts in citation after free availability.
9. Materials and methods are available as supporting material on *Science* Online.
10. M. J. Stringer, M. Sales-Pardo, L. A. N. Amaral, *PLoS One* **3**, e1683 (2008).
11. J. A. Evans, *Science* **321**, 395 (2008).
12. Supported by NSF grant 0242971. We thank Thomson Reuters, Incorporated, for use of its SCI data.

Supporting Online Material

www.sciencemag.org/cgi/content/full/323/5917/1025/DC1
Materials and Methods
Fig. S1
References

21 December 2007; accepted 12 December 2008
10.1126/science.1154562

[1]Department of Sociology, University of Chicago, Chicago, IL 60637, USA. [2]Department of Neurobiology, University of Chicago, Chicago, IL 60637, USA.

*To whom correspondence should be addressed. E-mail: jevans@uchicago.edu

Oxide Nanoelectronics on Demand

Cheng Cen,[1] Stefan Thiel,[2] Jochen Mannhart,[2] Jeremy Levy[1]*

Electronic confinement at nanoscale dimensions remains a central means of science and technology. We demonstrate nanoscale lateral confinement of a quasi–two-dimensional electron gas at a lanthanum aluminate–strontium titanate interface. Control of this confinement using an atomic force microscope lithography technique enabled us to create tunnel junctions and field-effect transistors with characteristic dimensions as small as 2 nanometers. These electronic devices can be modified or erased without the need for complex lithographic procedures. Our on-demand nanoelectronics fabrication platform has the potential for widespread technological application.

Controlling electronic confinement in the solid state is increasingly challenging as the dimensionality and size scale are reduced. Bottom-up approaches to nanoelectronics use self-assembly and templated synthesis; examples include junctions between self-assembled molecule layers (*1*, *2*), metallic and semiconducting quantum dots, carbon nanotubes (*3*–*6*), nanowires, and nanocrystals (*7*, *8*). Top-down approaches retain the lithographic design motif used extensively at micrometer and submicrometer scales and make use of tools such as electron-beam lithography, atomic force microscopy (AFM) (*9*), nanoimprint lithography (*10*), dip-pen nanolithography (*11*), and scanning tunneling microscopy (*12*). Among the top-down approaches, those that begin from modulation-doped semiconductor heterostructures have led to profound scientific discoveries (*13*, *14*).

The interface between polar and nonpolar semiconducting oxides displays remarkable properties reminiscent of modulation-doped semiconductors (*15*–*21*). When the thickness of the polar insulator (e.g., $LaAlO_3$) exceeds a critical value (d_c = 3 unit cell), because of the polarization discontinuity at the interface, the potential difference across $LaAlO_3$ will generate a "polarization catastrophe" and induce the formation of a quasi–two-dimensional electron gas (q-2DEG) at the interface joining the two insulators (*17*). In addition to the key role played by the polar discontinuity, there is evidence that, when present, oxygen vacancies in the $SrTiO_3$ also contribute to the formation of the electron gas (*22*, *23*).

We focus on $LaAlO_3$-$SrTiO_3$ heterostructures. Because of the large conduction-band offset between $LaAlO_3$ and $SrTiO_3$, the q-2DEG is confined largely within the first few unit cells of $SrTiO_3$ (*22*, *24*), with very little penetration into the $LaAlO_3$ layer (*25*). Electric fields have been used to control the metal-insulator transition at room temperature (*17*) and the superconductor-insulator transition at cryogenic temperatures (*21*). Further in-plane confinement of the q-2DEG has been achieved by lithographically modulating the thickness of the crystalline $LaAlO_3$ layer (*26*). Control over the metal-insulator transition at scales of <4 nm was demonstrated by means of a conducting AFM probe (*24*). This latter method forms the basis for the results reported below.

[1]Department of Physics and Astronomy, University of Pittsburgh, Pittsburgh, PA 15260, USA. [2]Experimental Physics VI, Center for Electronic Correlations and Magnetism, Institute of Physics, University of Augsburg, D-86135 Augsburg, Germany.

*To whom correspondence should be addressed. E-mail: jlevy@pitt.edu

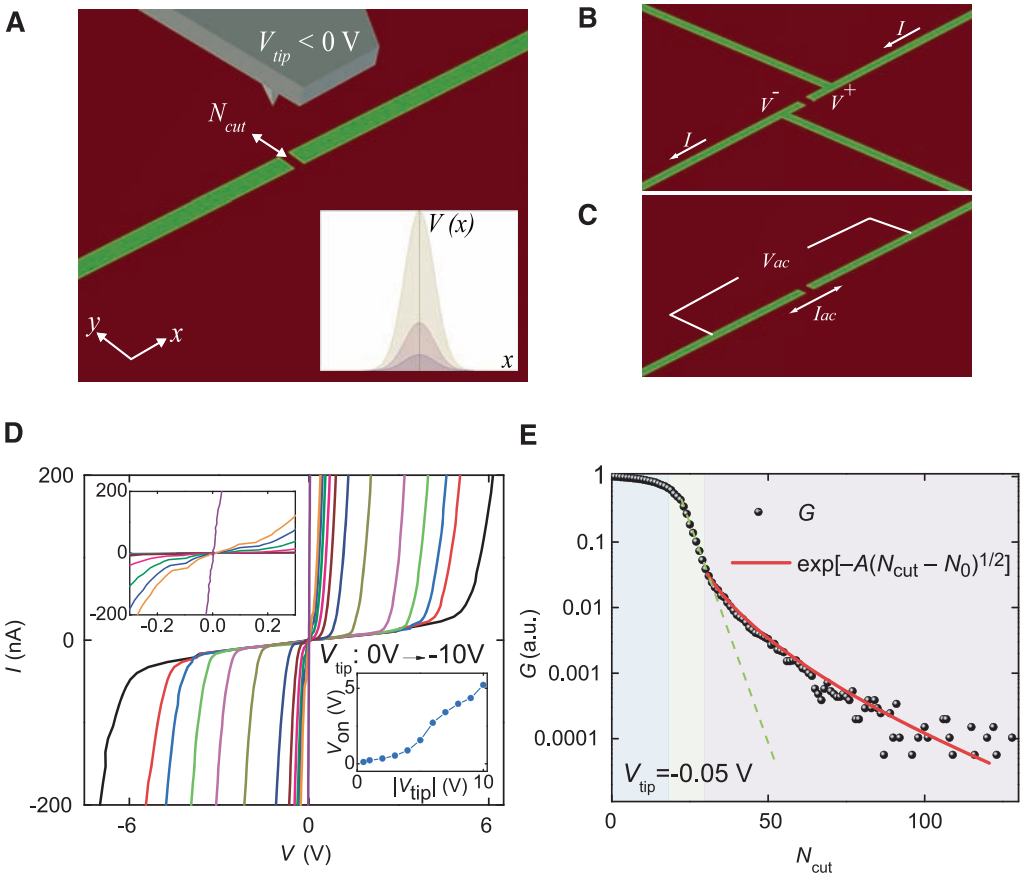

Fig. 1. Creation of nanoscale tunnel barriers. (**A**) Sketch illustrating how a potential barrier is created by scanning a negatively biased AFM probe. Inset: Sketch of the barrier potential. Either increasing the magnitude of negative tip bias (V_{tip}) or scanning across the wire for a greater number of cuts (N_{cut}) with the same tip bias will increase the height of the barrier potential $V(x)$. (**B**) Illustration of structure used for four-probe measurement (**C**) Sketch of two-probe ac measurement scheme. (**D**) *I-V* characteristics of an uncut wire section 2 μm long and 12 nm wide (V_{tip} = 0 V), and the same section with various potential barriers in the middle created with different negative tip bias (V_{tip} = –0.5 V, –1 V, –2 V, …, –10 V). The upper inset shows the conductance of the uncut wire (slope of the *I-V* curve) to be 6.8 μS. The lower inset shows the turn-on voltage of the nanowire section with a potential barrier as a function of the V_{tip} that is used to create the barrier. (**E**) Conductance of a wire 12 nm wide, with a potential barrier at the middle written with V_{tip} = –0.05 V, measured as the number of cuts N_{cut} increases (i.e., barrier height increases). The green dashed line shows an exponentially decaying conductance G as a function of barrier height, $G \propto \exp[-A'N_{cut}]$, which is typical for thermal activated hopping. The red solid line shows a reference curve following behavior, $G \propto \exp[-A(N_{cut} - N_0)^{1/2}]$ as expected by us for tunneling, with best-fit parameters A = 0.99, N_0 = 17.2.

Writing and erasing. On the basis of the experimental finding that nanoscale conducting regions can be created and erased using voltages applied by a conducting AFM probe (*24*), various multiterminal devices have been constructed. The structure investigated here consists of nominally 3.3 unit cell thick $LaAlO_3$ films grown on $SrTiO_3$ [see (*27*) for fabrication and measurement details]. A conducting AFM tip is scanned along a programmed trajectory $x(t)$, $y(t)$ with a voltage $V_{tip}(t)$ applied to the tip. Positive tip voltages above a threshold $V_{tip} > V_t \sim 2$ to 3 V produce conducting regions at the $LaAlO_3$-$SrTiO_3$ interface directly below the area of contact. The lateral size δx of this conducting nanoregion increases monotonically with tip bias. Typical values are $\delta x = 2.1$ nm and 12 nm at $V_{tip} = +3$ V and +10 V, respectively (fig. S2, A and B). Subsequent erasure of the structures can be induced by scanning with a negative voltage or by illuminating with light of photon energy $E > E_g$ (band gap of $SrTiO_3 \sim 3.2$ eV) (*17*, *18*). Structures can be written and erased hundreds of times without observable degradation (fig. S2C). All of the structures described here are written within the same working area; similar structures have been created and measured for other electrode sets, with consistent results.

Designer potential barriers. The writing and erasing process allows for a remarkable versatility in producing quantum mechanical tunneling barriers (Fig. 1A). The transport properties of these tunnel barriers are investigated in two different experiments. Both begin with nanowires (width $w \sim 12$ nm) written with a positive tip voltage $V_{tip} = +10$ V. In the first study, a four-terminal transport measurement is performed. A current (I) is sourced from two leads, while a second pair of sense leads is used to measure the voltage (V) across a section $L = 2$ μm at the middle of the nanowire (Fig. 1B). As prepared, the nanowire is well-conducting (resistance $R_0 = 147$ kilohms, corresponding to a conductivity $\sigma = 6.8$ μS) (Fig. 1D, upper inset). This conductivity together with the nanowire's aspect ratio (length/width = 160) yield a sheet conductance $\sigma_S = 1.1 \times 10^{-3}$ S, which is ~200 times that of the unstructured sample with $LaAlO_3$ film thickness exceeding d_c [$\sigma_S^{film} \approx 2 \times 10^{-5}$ S (*17*)].

A negatively biased tip ($V_{tip} < 0$ V) is then scanned across the wire. *I-V* curves are acquired after each pass of the tip. Scanning with a negative bias restores the insulating state, presumably by shifting the local density of states in the $SrTiO_3$ upward in energy (*24*), thus providing a barrier to conduction (Fig. 1A, inset). The tip bias starts at $V_{tip} = -0.5$ V and then increases linearly in absolute numbers (–1 V, –2 V, –3 V, …, –10 V). All these *I-V* characteristics are highly nonlinear (Fig. 1D), showing vanishing conductance at zero bias, and a turn-on voltage V_{on} (defined as the voltage for which the current exceeds 10 nA) that increases monotonically with tip voltage (Fig. 1D, lower inset). A small residual conductance (4.1 nS) is observed, which is independent of V_{tip} and hence is associated not with the nanowire and tunnel barrier but with an overall parallel background conductance of the heterostructure.

In the second study, an AFM tip is scanned repeatedly across a nanowire with relatively small fixed bias $V_{tip} = -50$ mV (Fig. 1A). An alternating voltage ($V_{ac} = 1$ mV) is applied across the nanowire (Fig. 1C) and the resulting in-phase ac current I_{ac} is detected with a lock-in amplifier. With each pass of the AFM tip, conductance $G = I_{ac}/V_{ac}$ decreases monotonically, exhibiting three qualitatively distinct regimes (Fig. 1E). For $N_{cut} < 10$, we observe that the conductance reduces only slightly with each pass. For $10 < N_{cut} < 25$, the behavior transitions to one in which the conductance decays approximately exponentially with N_{cut}. For $N_{cut} > 25$, we observe a clear deviation from this straight exponential fall-off. We propose that the AFM probe is gradually increasing the potential barrier between the nanowire leads (*24*). Although this process must eventually saturate for large N_{cut}, for the regime explored the potential appears to scale linearly with N_{cut}, as suggested by the observed dependence of the conductance with N_{cut} over many experiments (Fig. 1E). Along the center of the wire, the induced potential after N_{cut} passes is therefore described by an effective potential: $V_N(x) = V_0 + N_{cut}V_b(x)$, where $V_b(x)$ is a sharply peaked (~2 nm wide) function of position. The conductance of the nanowire measured as a function of N_{cut} (Fig. 1E) shows evidence for a crossover from a highly conducting regime ($N_{cut} < 10$) to an exponential thermal hopping regime ($10 < N_{cut} < 25$) to one dominated by quantum mechanical tunneling through the barrier ($N_{cut} > 25$). The latter nonexponential form is consistent with a tunneling probability $t \propto \exp[-A'(V - E_F)^{1/2}]$ (where A' is a material-dependent constant, and E_F is the Fermi energy), as can be seen by a comparison with the functional dependence $G \propto \exp[-A(N_{cut} - N_0)^{1/2}]$ (where G is the conductance across the barrier, and A and N_0 are dimensionless fitting parameters). We conclude that the barrier written by the AFM tip acts as a tunnel junction that interrupts the written nanowires.

SketchFET. The ability to produce ultrathin potential barriers in nanowires enables the creation of field-effect devices with strongly nonlinear characteristics. We demonstrate two families of such devices. Both begin with a "T-junction" of nanowire leads written with $V_{tip} = 10$ V ($w \sim 12$ nm)

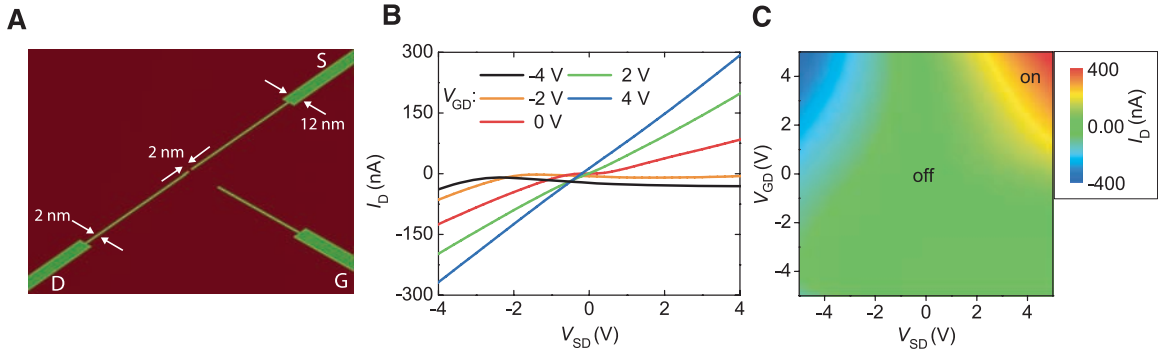

Fig. 2. SketchFET device. (**A**) Schematic diagram of SketchFET structure. S, source electrode; D, drain electrode; G, gate electrode. (**B**) *I-V* characteristic between source and drain for different gate biases $V_{GD} = -4$ V, –2 V, 0 V, 2 V, and 4 V. (**C**) Intensity plot of I_D (V_{SD}, V_{GD}).

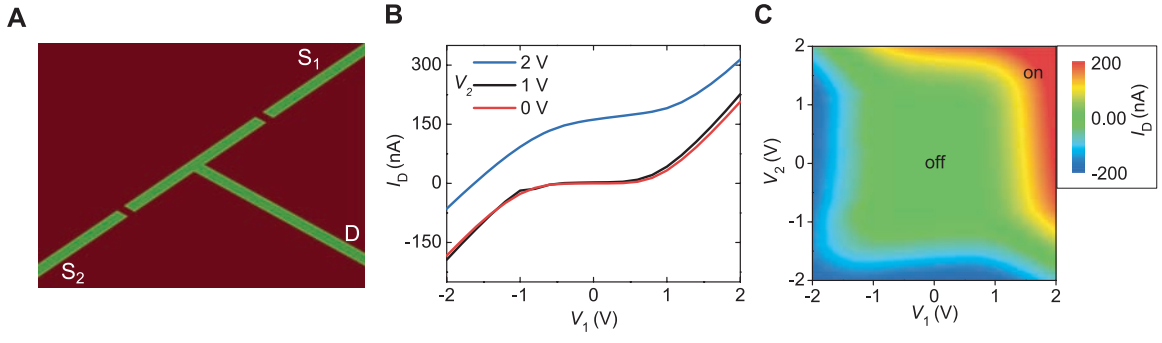

Fig. 3. Double-junction device. (**A**) Schematic of a double-junction structure. (**B**) *I-V* characteristic between source 1 and drain for different source biases $V_2 = 0$ V, 1 V, and 2 V. (**C**) Intensity plot of $I_D(V_1, V_2)$.

(fig. S3A). As constructed, the T-junction behaves as a simple resistive network (fig. S3B).

The creation of the first device (Fig. 2A) begins with erasing the central region (within 1 μm from the center) of a T-junction of source, gate, and drain electrodes and then reconnecting the channels with V_{tip} = 3 V (w ~ 2 nm), followed by a subtractive step in which the AFM probe is scanned under negative bias (V_{tip} = –3 V), starting from the center of the junction across the source-drain channel and moving a gap distance g_2 = 50 nm along the direction of the gate electrode. This step also creates a barrier g_1 = 2 nm between source and drain. The asymmetry in the two gaps (fig. S4A) enables the gate electrode to modulate the source-drain conductance with minimal gate leakage current. We refer to this device as a SketchFET (sketch-defined electronic transport within a complex-oxide heterostructure field-effect transistor).

Transport measurements of this SketchFET are performed by monitoring the drain current I_D as a function of the source and gate voltages (V_{SD} and V_{GD}, respectively). Both V_{SD} and V_{GD} are referenced to the drain, which is held at virtual ground. At zero gate bias, the I-V characteristic between source and drain is highly nonlinear and nonconducting at small $|V_{SD}|$ (Fig. 2B). A positive gate bias $V_{GD} > 0$ lowers the potential barrier for electrons in the source and gate leads. With V_{GD} large enough (≥4 V in this specific device), the barrier eventually disappears. In this regime, ohmic behavior between source and drain is observed. The field effect in this case is nonhysteretic, in contrast to field effects induced by the AFM probe (*24*). At negative gate biases the nonlinearity is enhanced, and a gate-tunable negative-differential resistance (NDR) is observed for $V_{SD} > -2.5$ V. When a sufficiently large gate bias is applied, a small gate leakage current I_{GD} also contributes to the total drain current I_D (fig. S4A). The NDR regime is associated with this gate leakage current (see below).

By increasing the source-drain gap (g_1 = 12 nm) of the SketchFET (fig. S5), the source-drain characteristic becomes more symmetric. This structure requires a larger positive gate bias to switch the channel on. Tunneling through such a wide barrier width is highly unusual, but it is assisted by the triangular nature of the tunneling barrier under large applied fields (on the order of MV/cm), and the barrier width is renormalized by the large dielectric constant of $SrTiO_3$ (ε ~ 300 at room temperature).

One of the most important technological applications of FETs is making logic elements. The applied values of V_{SD} and V_{GD} can be interpreted as "on" (>4 V) or "off" (<4 V) input states of a logic device; the measured values of I_D can be understood as "on" (>200 nA) or "off" (<200 nA) output states. A full exploration of $I_D(V_{SD}, V_{GD})$ reveals an "AND" functionality (e.g., output is "on" only when both inputs are "on") (Fig. 2C). Because of the nonlinear character of the junction, the resultant drain current when both V_{SD} and V_{GD} are "on" is ~3 times the sum of the individual contributions when only one input is "on": I_D(4 V, 4 V) ~ 3[I_D(4 V, 0 V) + I_D(0 V, 4 V)], which yields a promising on-off current ratio.

Frequency response. One gauge of the performance of a transistor is its ability to modulate or amplify signals at high frequencies, as quantified by the cutoff frequency f_T. We characterized the frequency dependence of the SketchFET described in Fig. 2 using a heterodyne circuit that incorporates the SketchFET as a frequency mixer. The experimental arrangement is shown schematically in fig. S6A.

The results of this heterodyne measurement over a frequency range 3 kHz to 15 MHz show that the SketchFET operates at frequencies in excess of 5 MHz. In the measurement setup used, this frequency is most likely limited by the large (~megohm) resistance of the three leads connecting to the device. The high mobility of the channel and the fact that the I-V characteristics are far from saturation

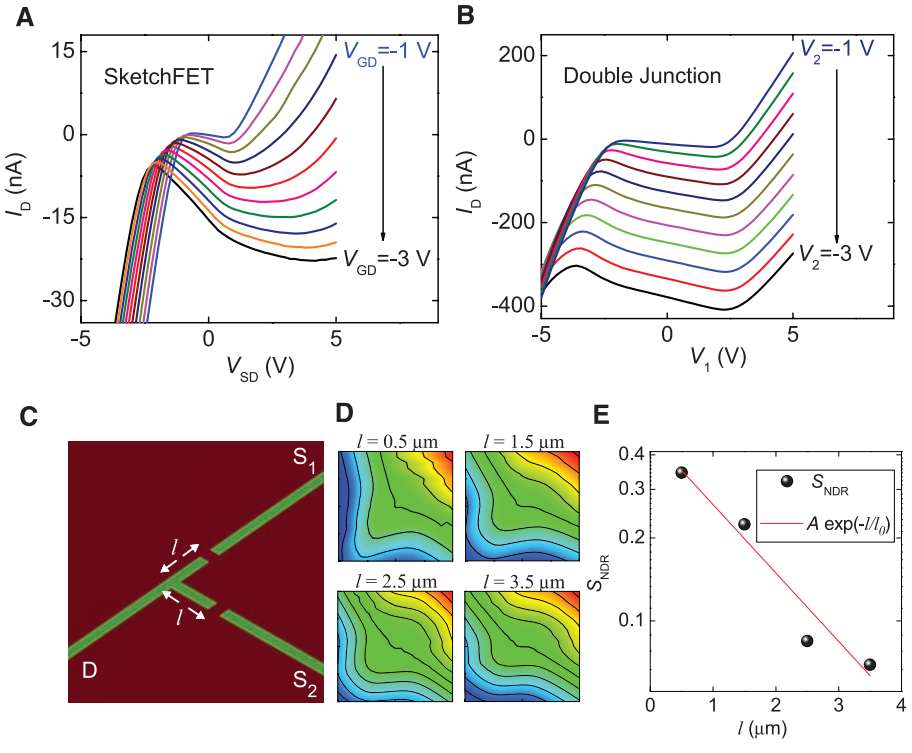

Fig. 4. Negative differential resistance (NDR). (**A**) NDR observed in SketchFET structure. Gate bias V_{GD} ranges from –1 V to –3 V with steps of –0.2 V. (**B**) NDR observed in double-junction structure with a junction separation of 5 μm. Source bias V_2 ranges from –1 V to –3 V with steps of –0.2 V. (**C**) Schematic of a structure of two perpendicular junctions with a distance l from the junction center. (**D**) For structures with l = 0.5 μm, 1.5 μm, 2.5 μm, and 3.5 μm, drain current I_D is plotted as V_1 and V_2 is varied from –2 V to 2 V. Contours are spaced 100 nA apart. (**E**) Coupling strength S_{NDR} = max[$-(\partial I_D/dV_1)/(\partial I_D/dV_2)$], equivalent to largest contour line slope, plotted as a function of l (black dots) fitted with exponential decay function A exp($-l/l_0$), with best-fit parameters A = 0.47, l_0 = 1.75 μm.

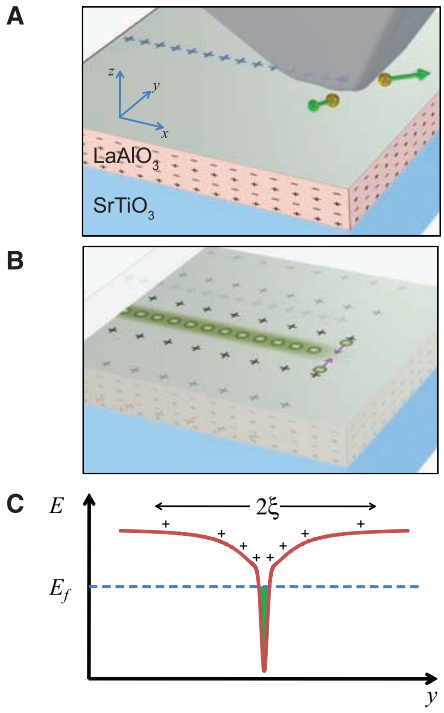

Fig. 5. Lateral modulation doping of nanowires. (**A**) AFM tip moving left to right above $LaAlO_3$-$SrTiO_3$ heterostructure, removing oxygen-containing ions and locally changing the charge state of the surface. (**B**) View of same structure revealing the conducting nanowire formed at the interface. Electrons screen the surface charges by ionizing nearby states in the $SrTiO_3$ (lateral modulation doping) as well as from the top surface. (**C**) Illustration of potential profile across the nanowire. Modulation doping occurs over a screening length ξ on the order of micrometers; E_f describes the Fermi energy.

in the conducting regime suggest that f_T of the SketchFET, without the large lead resistances, could extend into the gigahertz regime.

Double junction. The fabrication of a second family of structures begins by patterning the T-junction, followed by two erasure steps in which a negatively biased AFM probe (V_{tip} = –10 V) scans across two of the leads (Fig. 3A). The result is a device with two comparable tunneling gaps separated by a distance l from the intersection. The *I-V* characteristic of each junction is shown in fig. S4B. The electrodes connected by these two sections are labeled S_1 and S_2; the third electrode is labeled as "drain" (D). Transport experiments to measure the drain current as a function of the voltages V_1 and V_2 applied to S_1 and S_2, respectively [$I_D(V_1, V_2)$]. performed using the methods described above. Positive values of V_2 have little effect on the *I-V* characteristic between S_1 and D (Fig. 3B), and vice versa. Negative values of V_2 can induce NDR in the channel between S_1 and D. A full exploration of $I_D(V_1, V_2)$ reveals an "OR" functionality (e.g., drain output is "on" when either one of the source inputs is on) (Fig. 3C), which is not surprising given the topology of the junctions. We refer to this structure as a double junction.

Negative differential resistance. A qualitative explanation of the SketchFET NDR (Fig. 4A) originates from the fact that for a three-terminal junction each nanowire exhibits a field effect on the other two. When $|V_{SD}|$ is small, conductivity between source and drain is greatly suppressed; I_D is mainly composed of current from the negatively biased gate. Increasing V_{SD} will improve the conductivity between gate and drain and will drive more negative gate current to the drain, which manifests itself as NDR. When $|V_{SD}|$ is large enough, the drain current I_D is dominated by current flowing from the source, and the NDR vanishes.

For the double-junction structure, the origin of the NDR (Fig. 4B) is less straightforward. To study the nature of the coupling, we created a family of double-junction structures and characterized them for various distances l between the junctions and the center of the T-intersection (Fig. 4C). The normalized magnitude of NDR is quantified as $-(\partial I_D/dV_1)/(\partial I_D/dV_2)$, which can be visualized as the slope of contour lines in a two-dimensional plot of $I_D(V_1, V_2)$. Smaller values of l resulted in stronger coupling between the two junctions (Fig. 4D), manifested as a larger NDR effect. The coupling strength—given by the maximum NDR observed, $S_{NDR} = \max[-(\partial I_D/dV_1)/(\partial I_D/dV_2)]$—is calculated as a function of junction separation (Fig. 4E). An approximately exponential decay of this coupling strength is observed, with a fitted decay length l_0 = 1.75 μm.

The long-range coupling of tunnel junctions is consistent with the observation that the sheet conductance of the nanowires is two orders of magnitude larger than for unpatterned interfaces. A possible explanation of where these extra electrons come from, consistent with both observations, is sketched in Fig. 5. The writing process is assumed to create positively charged regions (e.g., oxygen vacancies) on the top $LaAlO_3$ surface (Fig. 5A) (*24*). Directly below, at the $LaAlO_3$-$SrTiO_3$ interface, electrons screen this positive charge (Fig. 5B). These electrons can come from two sources: either from the top $LaAlO_3$ surface, or from weakly bound donor states (associated with defects in the $SrTiO_3$) that become ionized over a length scale ξ in the range of several micrometers (Fig. 5C). This screening is a type of lateral modulation doping that can produce a considerably higher electron density relative to planar unpatterned q-2DEG as well as a lateral potential profile much wider than the real conductive nanowire region. Experiments in which many parallel wires are connected show saturation of the net conductance toward the unpatterned q-2DEG value, again consistent with this picture of lateral modulation doping.

The high conductance of the 12-nm wires, produced by the large (~100 MV/cm) transient electric field of the AFM probe, is metastable and prone to partial relaxation toward the unpatterned q-2DEG value on a time scale that depends on the ambient environmental conditions. Experiments performed on a SketchFET stored under vacuum conditions (fig. S8) show a nonexponential decay of the overall conductance (dominated by that of the 12-nm leads) toward a steady-state value that is comparable to the sheet conductance of the unpatterned film. No discernible degradation in the SketchFET switching performance was observed over a 9-day period. The extreme sensitivity of electron tunneling to barrier thickness demonstrates that the SketchFET and related structures are stable at length scales that are small relative to their feature size (e.g., 2-nm gap) and at time scales considerably longer than the observation period.

Concluding remarks and outlook. The nanoscale structures patterned above are representative of a versatile family of nanoelectronic devices operating at the interface between a polar and a nonpolar oxide insulator. The conducting nanostructures have dimensions comparable to those of single-walled carbon nanotubes, yet they can be freely patterned and repeatedly modified. Their ultimate suitability for logic and memory applications will depend on a variety of factors, such as the mobilities of the charge carriers, how effectively power dissipation can be minimized, and whether this system can be integrated with silicon. The devices demonstrated here suggest many other possible applications and research directions.

With sufficient control it may be possible to demonstrate single-electron effects such as Coulomb blockade, resonant tunneling, or single-electron transistor behavior, possibly at room temperature. At low temperatures, strongly correlated electron behavior associated with low dimensionality (i.e., Luttinger liquid behavior) may also be accessible. The discovery and control of superconductivity at the $LaAlO_3$-$SrTiO_3$ interface (*20*, *21*) provides a possible avenue for exploration of mesoscopic superconducting phenomena.

A 2-nm nanowire carrying 100 nA of current will produce an in-plane magnetic field $B \sim 10$ G at the top surface of the $LaAlO_3$. These magnetic fields are large enough to excite and detect spin waves in nearby magnetic nanostructures, and if the frequency response can be improved, it may be possible to sketch current loops around nanoscale samples for nuclear magnetic resonance or electron spin resonance experiments. On-site amplification of these small signals might be possible with SketchFET-based preamplifiers.

The tunnel junctions at the center of the SketchFETs may be optimized to be sensitive to the charge or oxidation state of the $LaAlO_3$ surface above. The active area is <5 nm^2, allowing for high spatial selectivity for a variety of biological and chemical sensing applications.

The $LaAlO_3$-$SrTiO_3$ system is sufficiently versatile to allow basic materials physics questions to be addressed. Previously we showed (*24*) that the measured width of written nanowires places a strong constraint on the thickness of the q-2DEG layer. Four-terminal resistance measurements were performed on nanowires by creating nanowire sense leads. The experiments with double junctions provide new quantitative evidence for in-plane modulation doping. Such self-referential measurements will continue to be useful in learning more about this fascinating material system.

References and Notes

1. G. M. Whitesides, J. P. Mathias, C. T. Seto, *Science* **254**, 1312 (1991).
2. M. A. Reed, C. Zhou, C. J. Muller, T. P. Burgin, J. M. Tour, *Science* **278**, 252 (1997).
3. R. P. Andres *et al.*, *Science* **273**, 1690 (1996).
4. D. Leonard, M. Krishnamurthy, C. M. Reaves, S. P. Denbaars, P. M. Petroff, *Appl. Phys. Lett.* **63**, 3203 (1993).
5. P. G. Collins, A. Zettl, H. Bando, A. Thess, R. E. Smalley, *Science* **278**, 100 (1997).
6. A. Bachtold, P. Hadley, T. Nakanishi, C. Dekker, *Science* **294**, 1317 (2001); published online 4 October 2001 (10.1126/science.1065824).
7. X. Duan, Y. Huang, Y. Cui, J. F. Wang, C. M. Lieber, *Nature* **409**, 66 (2001).
8. D. L. Klein, R. Roth, A. K. L. Lim, A. P. Alivisatos, P. L. McEuen, *Nature* **389**, 699 (1997).
9. E. S. Snow, P. M. Campbell, *Appl. Phys. Lett.* **64**, 1932 (1994).
10. S. Y. Chou, P. R. Krauss, P. J. Renstrom, *J. Vac. Sci. Technol. B* **14**, 4129 (1996).
11. R. D. Piner, J. Zhu, F. Xu, S. Hong, C. A. Mirkin, *Science* **283**, 661 (1999).
12. A. J. Heinrich, C. P. Lutz, J. A. Gupta, D. M. Eigler, *Science* **298**, 1381 (2002); published online 24 October 2002 (10.1126/science.1076768).
13. A. R. Dingle, A. H. L. Stormer, A. A. C. Gossard, A. W. Wiegmann, *Appl. Phys. Lett.* **33**, 665 (1978).
14. D. C. Tsui, H. L. Stormer, A. C. Gossard, *Phys. Rev. Lett.* **48**, 1559 (1982).
15. A. Ohtomo, D. A. Muller, J. L. Grazul, H. Y. Hwang, *Nature* **419**, 378 (2002).
16. A. Ohtomo, H. Y. Hwang, *Nature* **427**, 423 (2004), corr. Nature **441**, 120 (2006).
17. S. Thiel, G. Hammerl, A. Schmehl, C. W. Schneider, J. Mannhart, *Science* **313**, 1942 (2006); published online 23 August 2006 (10.1126/science.1131091).
18. M. Huijben *et al.*, *Nat. Mater.* **5**, 556 (2006).
19. A. Kalabukhov *et al.*, *Phys. Rev. B* **75**, 121404 (2007).
20. N. Reyren *et al.*, *Science* **317**, 1196 (2007); published online 1 August 2007 (10.1126/science.1146006).

21. A. Caviglia *et al.*, *Nature* **456**, 624 (2008).
22. M. Basletic *et al.*, *Nat. Mater.* **7**, 621 (2008).
23. W. Siemons *et al.*, *Phys. Rev. Lett.* **98**, 196802 (2007).
24. C. Cen *et al.*, *Nat. Mater.* **7**, 298 (2008).
25. J. M. Albina, M. Mrovec, B. Meyer, C. Elsasser, *Phys. Rev. B* **76**, 165103 (2007).
26. C. W. Schneider, S. Thiel, G. Hammerl, C. Richter, J. Mannhart, *Appl. Phys. Lett.* **89**, 122101 (2006).
27. See supporting material on *Science* Online.
28. Supported by NSF grant 0704022, Deutsche Forschungsgemeinschaft grant SFB 484, and the European Community NANOXIDE project.

Supporting Online Material
www.sciencemag.org/cgi/content/full/323/5917/1026/DC1
Figs. S1 to S8

10 November 2008; accepted 2 January 2009
10.1126/science.1168294

REPORTS

Macroscopic 10-Terabit–per–Square-Inch Arrays from Block Copolymers with Lateral Order

Soojin Park,[1]* Dong Hyun Lee,[1] Ji Xu,[1] Bokyung Kim,[1] Sung Woo Hong,[1] Unyong Jeong,[2] Ting Xu,[3]† Thomas P. Russell[1]†

Generating laterally ordered, ultradense, macroscopic arrays of nanoscopic elements will revolutionize the microelectronic and storage industries. We used faceted surfaces of commercially available sapphire wafers to guide the self-assembly of block copolymer microdomains into oriented arrays with quasi–long-range crystalline order over arbitrarily large wafer surfaces. Ordered arrays of cylindrical microdomains 3 nanometers in diameter, with areal densities in excess of 10 terabits per square inch, were produced. The sawtoothed substrate topography provides directional guidance to the self-assembly of the block copolymer, which is tolerant of surface defects, such as dislocations. The lateral ordering and lattice orientation of the single-grain arrays of microdomains are maintained over the entire surface. The approach described is parallel, applicable to different substrates and block copolymers, and opens a versatile route toward ultrahigh-density systems.

Producing a surface with an ultradense array of addressable nanoscopic elements that is perfectly ordered over macroscopic length scales is a formidable challenge. The self-assembly of block copolymers (BCPs), two chemically dissimilar polymers joined together, is emerging as a promising route to generate templates and scaffolds for the fabrication of nanostructured materials and offers a potential solution to this challenge (*1*–*3*). Despite the substantial advances that have been made to enhance the lateral ordering of the BCP microdomains in thin films, achieving perfect order over macroscopic length scales has not been possible (*4*–*7*). In thin films, BCPs self-assemble into grains, tens of microns in size, of laterally ordered nanoscopic microdomains. Electron beam (e-beam) lithography is a serial writing process, and although slow, has been successfully used to produce nanoscopic chemical or topographic surface patterns that can be used to guide the self-assembly of BCPs (*4*, *5*, *8*, *9*). However, even though the self-assembly of BCPs can correct errors in the patterns, perfect ordering over large areas has not yet been achieved. Nanoimprint lithography (*10*, *11*), on the other hand, is a parallel patterning process but requires a perfect master to replicate. We show that most of these limitations can be overcome by capitalizing on a well-established surface reconstruction of commercially available single-crystalline wafers to generate nanoscopic surface facets that can guide the self-assembly of BCPs into a highly ordered, single-grain array of nanoscopic elements with a well-defined orientation over large areas.

Large, defect-free single-crystalline wafers, such as silicon or sapphire, with a well-defined orientation of the crystal lattice are commercially available (*12*–*14*). By the cutting of single crystals along specific crystallographic planes, unstable surfaces can be produced that, upon heating, reconstruct, generating crystal facets that form a sawtooth topography, where the orientation of the ridges formed by the sawtooth persists over the entire surface (*13*, *14*). Sapphire (α-Al_2O_3), cut along the $(10\bar{1}0)$ or M plane, is used as an example, although the concept applies to other single-crystalline materials. The surface reconstruction is shown schematically in Fig. 1 along with atomic force microscopy (AFM) images of a freshly cut and a faceted sapphire surface (*13*, *14*). Initially the surface is featureless. Upon annealing, the surface reconstructs and crystalline facets form a sawtooth pattern on the surface. With the sapphire substrates used in this study, the pitch of the sawtooth was varied from 160 to 24 nm, with peak-to-valley heights or amplitudes ranging from 20 to 3 nm by being annealed in air at temperatures from 1300° to 1500°C for 24 hours [supporting online material (SOM), section S1]. Crystallographic registry of the facets over macroscopic distances is ensured, because the sapphire is a single crystal (*14*). There are, though, dislocations and an ~26% variation in the pitch, randomly located across the surface.

Five different polystyrene-*block*-poly(ethylene oxides) (PS-*b*-PEOs), with number-average molecular weights (M_n) from 7 to 43.0 kg/mol, polystyrene-*block*-poly(2-vinylpyridine) (PS-*b*-P2VP) (M_n = 19.5 kg/mol), and PS-*b*-P4VP (M_n = 19 kg/mol), all with narrow molecular weight distributions and minor volume fractions of ~0.3, were used (SOM, section S1). In the bulk, these BCPs microphase-separate into hexagonal arrays of cylindrical microdomains of PEO, P2VP or P4VP in a PS matrix. Thin films of the BCPs were spin-coated onto the faceted surfaces, which were cleaned with oxygen plasma (SOM, section S1).

Shown in Fig. 1E is a solvent-annealed, 24-nm-thick (as measured on a flat surface) film of PS-*b*-PEO (M_n = 43.0 kg/mol) on a sapphire surface, with facets having an average pitch of 130 nm and amplitude of 14 nm. Upon solvent annealing, the film is sufficiently thin that the copolymer is entrained into and confined within the regions between the facets. The solvent annealing process orients and orders the PS-*b*-PEO (*15*), but the average period is 23 nm, much less than the 29.5-nm period seen for this copolymer solvent annealed on a smooth surface. Consequently, the confinement causes a reduction in the fundamental period of the copolymer, as seen in studies of copolymers confined between planar surfaces (*16*–*18*) or within lithographically generated surface patterns (*19*). The facets essentially isolate strips of the copolymer across the surface.

With increasing film thickness, the amount of copolymer within each sawtooth increases, effectively reducing the amount of lateral confinement, which gives rise to the observed increase in the repeat period of the copolymer (SOM, section S2). When the film is sufficiently thick, as shown in Fig. 1F for a 34-nm-thick film of the same copolymer on a surface with facets having a pitch of 100 nm and amplitude of 10 nm, solvent annealing generates a single hexagonal array of cylindrical microdomains oriented normal to the film surface, with an average period of

[1]Department of Polymer Science and Engineering, University of Massachusetts, Amherst, MA 01003, USA. [2]Department of Materials Science and Engineering, Yonsei University, Seoul 120-749, Korea. [3]Department of Materials Science and Engineering, Department of Chemistry, University of Berkeley, and Material Sciences Division, Lawrence Berkeley National Laboratory, Berkeley, CA 94720, USA.

*Present address: School of Nano Bio Chemical Engineering, Ulsan National Institute of Science and Technology, BanYeon-Ri 194, Ulsan 689-805, Korea.

†To whom correspondence should be addressed. E-mail: russell@mail.pse.umass.edu (T.P.R.); tingxu@berkeley.edu (T.X.)

29.5 nm, equal to that of the copolymer solvent annealed on a planar surface. A single array covers the entire surface, where the (10) planes of the hexagonal array run parallel to the edges of the facets, which preferentially divide two adjacent (10) planes. This orientation of the hexagonal array minimizes perturbations of the lateral packing of the BCP chains and the deformation of the chains at the substrate (SOM, section S2). Because the BCP film is continuous across the edges, the lateral ordering, as opposed to the substrate topography, determines the exact placement of the microdomains, because the entropic penalty is less than that if the BCP were to follow the substrate topography exactly. Consequently, defects in the lateral packing of the microdomains that arise from the substrate topography are healed by the lateral assembly. Thus, a single copolymer array with a high degree of lateral order is produced, in which the orientation of the lattice is guided by the substrate topography. Consequently, the period of the copolymer, L, and the pitch of the substrate topography, L_S, must not be equal. We used L_S/L ratios of up to 3 without degrading the lateral ordering. If the thickness of the film relative to the amplitude of the facets is too large, the substrate no longer guides the lateral ordering, and results similar to those of films generated on a planar surface are found (SOM, section S2).

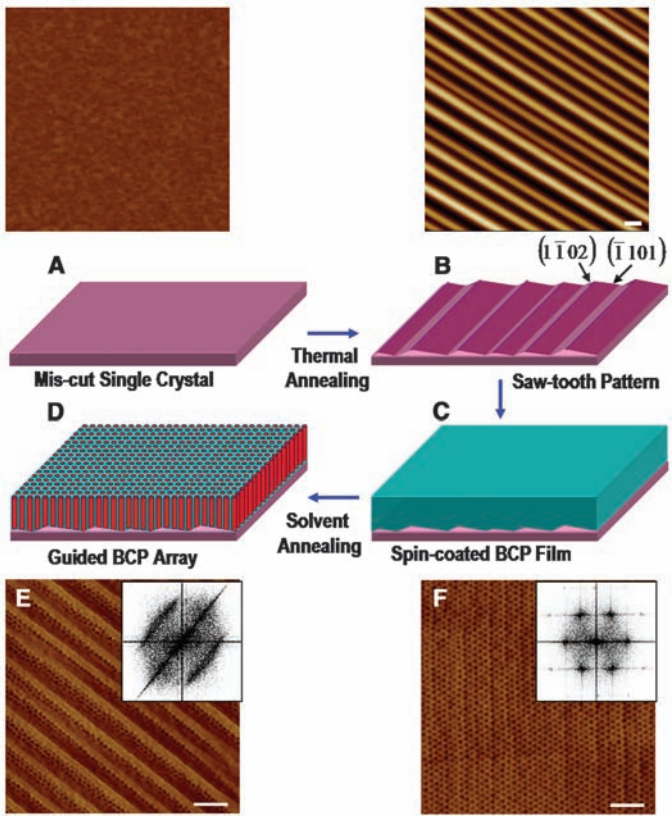

Fig. 1. Schematic illustration of the strategy used for generating BCP cylindrical microdomains on highly oriented crystalline facets on a single-crystal surface. Here, the M-plane sapphire (**A**) was annealed in air at 1300° to 1500°C for 24 hours to form sawtooth patterns. (**B**) Upon thermal annealing, the flat surface of the M-plane sapphire reconstructs into facets with the $(\bar{1}101)$ and $(1\bar{1}02)$ planes on opposite edges. (**C**) Smooth PS-*b*-PEO (M_n = 43.0 kg/mol) thin films were spin-coated onto these surfaces that, upon annealing in o-xylene vapors (**D**), produced highly ordered cylindrical microdomains oriented normal to the film surface. AFM height images of the substrate at each step are shown at the top. (**E** and **F**) AFM phase images of solvent-annealed PS-*b*-PEO (M_n = 43.0 kg/mol) films with thicknesses of (E) 24 nm and (F) 34 nm on a surfaces with facets having pitches of 130 and 100 nm with amplitudes of 14 and 10 nm. Scale bars, 200 nm.

Figure 2, A and D, show AFM images of two faceted sapphire surfaces along with thin films of four different PS-*b*-PEOs. These are M-plane sapphire surfaces annealed at 1400° and 1500°C in air for 24 hours with facet pitches of ~48 and ~24 nm and amplitudes of ~6 and ~3 nm, respectively. Figure 2, B and C, show AFM height images of ~43.5- and ~41.2-nm-thick films of PS-*b*-PEO (M_n = 26.5 kg/mol and M_n = 25.4 kg/mol, respectively), that were spin-coated and solvent-annealed in o-xylene on the surface shown in Fig. 2A, whereas Fig. 2, E and F, show AFM height images of ~30.6- and ~20.0-nm-thick films of PS-*b*-PEO (M_n = 21.0 kg/mol) and Au salt-complexed PS-*b*-PEO (M_n = 7.0 kg/mol) that were prepared on the surface in Fig. 2D. Au complexation was used to induce the microphase separation of the PS-*b*-PEO (M_n = 7.0 kg/mol), which is otherwise phase-mixed in the bulk (SOM, section S1). In all cases, regardless of the position on a 1.5 × 1.5 cm^2 sapphire wafer, the solvent-annealed films show lateral ordering of the hexagonally packed cylindrical microdomains over the entire area scanned (2 × 2 μm). The facets on the substrate do not confine the BCP laterally or influence its period. The Fourier transform of the AFM images in Fig. 2, B and C, show multiple higher-order interferences characteristic of the long-range ordering of the cylindrical microdomain arrays that are aligned with the facets on the substrate. Moiré patterns (*20*), which are interference patterns produced by overlaying a reference grating on the AFM image, show a single grain of the cylindrical microdomains over 25 × 25 μm^2 areas for PS-*b*-PEO on the faceted sapphire surface in Fig. 2D (SOM, fig. S4). From the AFM image, an orientational order parameter (SOM, section S4) of 0.93 is found that does not decay. An algebraically decaying correlation function of the translational order with an exponent of 0.32 (SOM, section S5) is found,

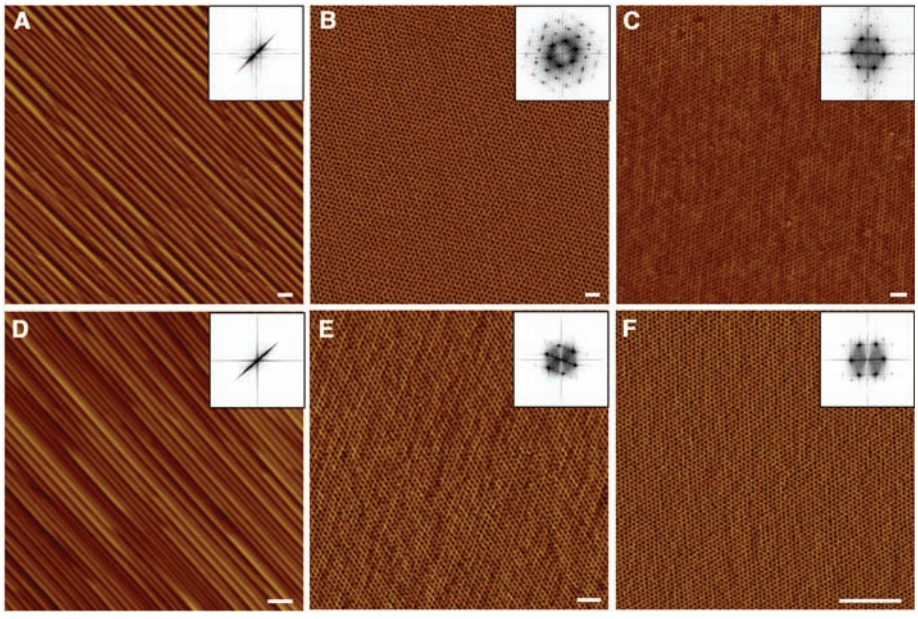

Fig. 2. AFM height images of sawtooth patterns and phase images of solvent-annealed PS-*b*-PEO thin films. (**A** and **D**) When M-plane sapphire was annealed at 1400° and 1500°C, a pitch of ~48 and ~24 nm and a peak-to-valley depth of ~6 and ~3 nm were obtained, respectively. Highly ordered PEO cylindrical microdomains having areal densities of 0.74 to 10.5 terabit/$inch^2$ from PS-*b*-PEO (M_n = 26.5 kg/mol) (**B**), PS-*b*-PEO (M_n = 25.4 kg/mol) (**C**), PS-*b*-PEO (M_n = 21.0 kg/mol) (**E**), and PS-*b*-PEO (M_n = 7.0 kg/mol) (**F**) BCP thin films annealed in o-xylene vapor were obtained. Scale bars, 100 nm.

characteristic of quasi–long-range crystalline order (*21*). Feature sizes ranging from 13 to 3 nm, with lattice spacings from 30.2 to 6.9 nm, respectively, are shown in Fig. 2 that correspond to areal densities of the microdomains from 0.74 to 10.5 terabit/inch^2. With decreasing size and period of the BCP microdomains, the orientational order and translational order were found to be improved. Similar results were also obtained with PS-*b*-P2VP and PS-*b*-P4VP, underscoring the generality of this approach (SOM, fig. S9, A and B).

Although AFM characterizes the local ordering of the microdomains (typically 20 × 20 μm), characterization of the ordering on the nanoscopic level over macroscopic length scales is required. Grazing incidence small-angle x-ray scattering (GISAXS) (SOM, section S6), in which x-rays impinge on the surface of the film at very small angles, was used to characterize the nanoscopic ordering of the BCP thin films over macroscopic distances, because the footprint of the x-ray beam is ~2 cm in length across the surface (*22*, *23*). At incidence angles above the critical angle of the polymer (~0.16°) but below the critical angle of sapphire (~0.28°), the x-rays penetrate into the polymer film and are totally reflected at the sapphire interface. When PS-*b*-PEO (M_n = 26.5 kg/mol) was solvent-annealed in a benzene and water environment, the sizes and separation distances of the cylindrical microdomains were larger than those seen in the bulk, because solvent annealing leaves the BCP film in a nonequilibrium (though highly reproducible) state (*15*, *24*). PS-*b*-PEO (M_n = 26.5 kg/mol) shows an average center-to-center distance between the cylindrical microdomains of 63.5 nm, whereas the center-to-center distance in the bulk is 36.5 nm. By rotating the film about the surface normal, discrete directions were found that corresponded to specific lattice lines of a two-dimensional (2D) hexagonal array. The sample was aligned so that the direction of the x-ray beam coincided with the (10) plane of the hexagonal array (schematically shown in the insets of Fig. 3) to collect the GISAXS pattern in Fig. 3A. Bragg rods (reflections along the horizon that are extended in the vertical) are seen at scattering vectors characteristic of the (*h*,0) planes, where *h* is an integer, of a hexagonal array of cylindrical microdomains oriented normal to the surface that are truncated at the surface (*25*). A line scan along the horizon is shown in the inset. No evidence of (*hk*) reflections, where *k* is nonzero, is observed, indicating that there is no misorientation of the lattice over the area sampled by the beam (that is, the BCP array consists of a single grain). When the sample is rotated 30° (schematically shown in the inset of Fig. 3B), Bragg rods are seen at scattering vectors corresponding to the (10), (11), (20), (21), (30), etc. planes characteristic of a hexagonal array of cylinders oriented normal to the film surface (Fig. 3B). A line scan along the horizon is shown in the inset. When the sample is rotated 30° further (Fig. 3C), only (*h*,0) reflections are seen and another 30° rotation (Fig. 3D) shows an orientation identical to that in Fig. 3B. Because only (*h*,0) reflections at three views separated by 60° from a known hexagonal array, we conclude that the film contains a single hexagonal array with no grains or misorientations of the lattice over macroscopic length scales; that is, the in-plane orientational ordering is perfect over the entire surface (~4 cm^2 of area).

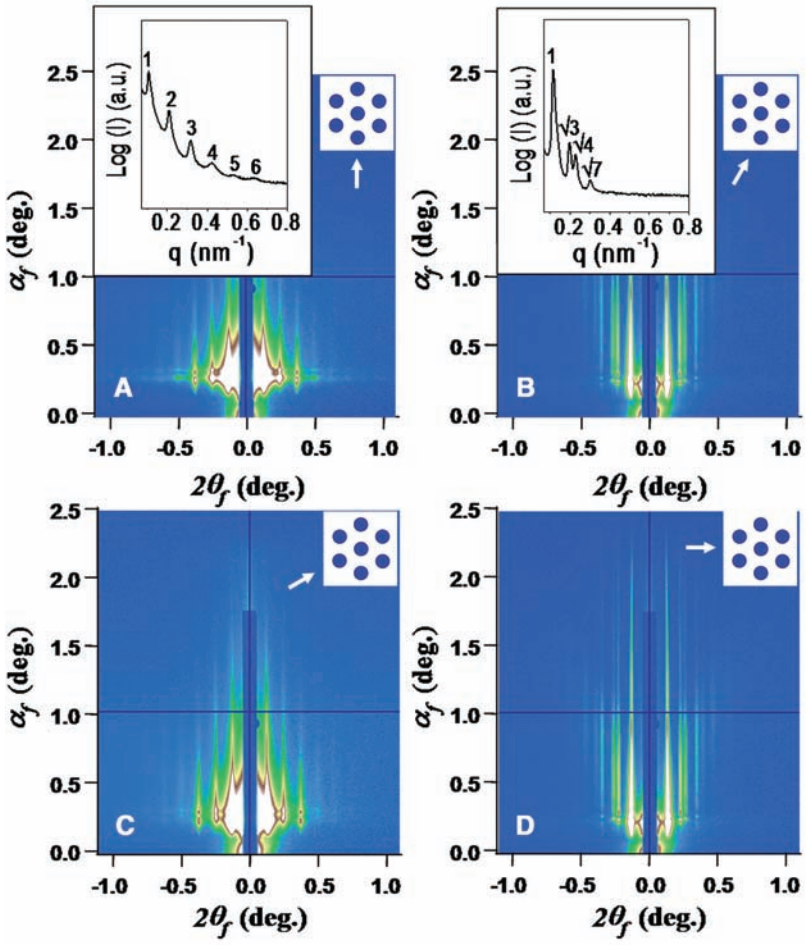

Fig. 3. Schematic 2D hexagonal lattices (insets at right) and the GISAXS patterns of PS-*b*-PEO thin films annealed in benzene and water vapors. (**A** and **C**) Integer-order diffraction peaks are shown from GISAXS patterns of cylindrical microdomains, when the x-ray beam follows the (10) lattice line (0° or 60°). (**B** and **D**) When the sample stage is rotated to 30° or 90° from this position (schematic in insets), diffraction peaks from (11) and (21) lattice lines are seen. Line profiles of the scattering as a function of the scattering vector are shown in the insets at left in (A) and (B). θ_f, in-plane scattering angle; *q*, in-plane scattering vector; a.u., arbitrary units.

The reconstruction of BCP thin films by immersion in a good solvent for the minor component but a nonsolvent for the matrix was used to convert the BCP films into nanoporous films in which the diameter of the pores is commensurate with the original diameter of the cylindrical microdomains (*25*, *26*). For films of PS-based BCPs with PEO, P2VP, and P4VP cylindrical microdomains, if the film's thickness corresponds to one period, then immersion in ethanol produces ultrahigh-density nanoporous films (SOM, fig. S9, A and B) that are ideal templates and scaffolds for the fabrication of ordered nanoscopic arrays of inorganic materials suitable for device applications (*25*, *27*).

On any single-crystalline substrate, there will be defects such as dislocations in the facets on the reconstructed surface. These defects are not seen in the BCP microdomain arrays. Shown in Fig. 4A is a 40-nm-thick film of PS-*b*-PEO (M_n = 26.5 kg/mol) with a highly ordered hexagonal array of cylinders oriented normal to the surface. The image of Fig. 4B was taken by translating the sample by ~2 μm. A piece of the film was removed from the surface, revealing the underlying substrate. One dislocation (indicated by an arrow in Fig. 4A) was located on the uncovered area that served as a marker. Subsequently, the entire PS-*b*-PEO film was removed by thoroughly rinsing the substrate with benzene. AFM images of the cleaned sapphire surface are shown in Fig. 4D and, with the sample translated by ~2 μm, in Fig. 4E. The marker dislocation was identified (indicated by an arrow in Fig. 4D) and, even though the sapphire surface shown in Fig. 4, D and E, contained many dislocations (circled in Fig. 4F, the black and white image of Fig. 4E), the ordering of the copolymer film shown in Fig. 4B, taken over the same area as in Fig. 4D, was unperturbed. A Voronoi diagram (*21*) of the data in Fig. 4B is shown in Fig. 4C, where only a single bound pair of defects is seen (SOM,

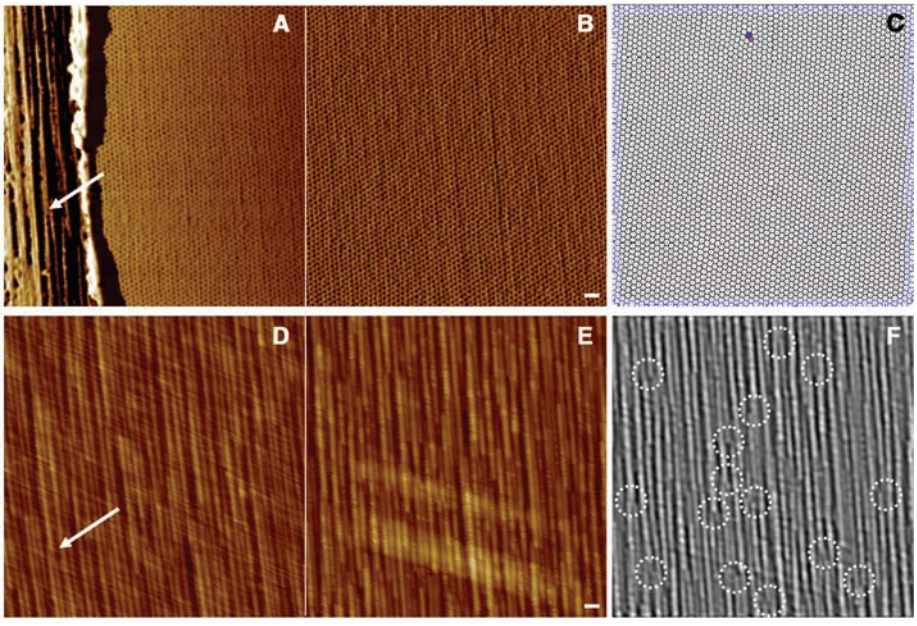

Fig. 4. (**A**) AFM height images of solvent-annealed PS-*b*-PEO (M_n = 26.5 kg/mol) thin films. To reveal the underlying substrates, a strip of the film was scratched from the surface and a dislocation (indicated by an arrow) was identified. (**B**) AFM image of a region shifted by ~2 μm from the image in (A). (**C**) The corresponding Voronoi construction of (B). (**D** and **E**) AFM images of the substrate surface after removal of the BCP film with the same dislocation in (A) indicated by the arrow in (D). (**F**) AFM image of the substrate underneath the BCP film from which the Voronoi diagram was constructed, with dotted circles indicating some of the dislocations. Scale bars, 100 nm.

section S8). This pair of defects is not associated with any defect on the underlying substrate but originates from the BCP self-assembly. These results show that the BCP self-assembly does not follow the substrate defects and that the BCP self-assembly overrides these defects.

We have demonstrated a very simple, general route to obtain highly ordered ultradense arrays in BCP films over macroscopic distances using faceted surfaces of commercially available single-crystal sapphire substrates. Despite defects in the surface topography, such as dislocations and a distribution of pitches, the BCPs self-assemble into hexagonal arrays of cylindrical microdomains oriented normal to the film surface with essentially perfect orientational order and a quasi–long-range crystalline order. The self-assembly overrides substrate defects and uses the topography only as a guide to the orientation of the arrays. Arrays of 3-nm-diameter cylindrical microdomains oriented normal to the film surface with a center-to-center distance of 6.9 nm (that is, having areal densities in excess of 10 terabit/inch^2), which is at least an order of magnitude over current capabilities, have been produced. These BCP films are promising candidates for the generation of ultrahigh-density media that have the potential of being addressable.

References and Notes

1. G. H. Fredrickson, F. S. Bates, *Annu. Rev. Mater. Sci.* **26**, 501 (1996).
2. F. S. Bates, G. H. Fredrickson, *Phys. Today* **52**, 32 (1999).
3. C. J. Hawker, T. P. Russell, *MRS Bull.* **30**, 952 (2005).
4. R. Ruiz *et al.*, *Science* **321**, 936 (2008).
5. I. Bita *et al.*, *Science* **321**, 939 (2008).
6. C. Tang *et al.*, *Science* **322**, 429 (2008).
7. M. Lazzari, G. Liu, S. Lecommandoux, *Block Copolymers in Nanoscience* (Wiley-VCH, Weinheim, Germany, 2006), chap. 9.
8. R. A. Segalman, H. Yokoyama, E. J. Kramer, *Adv. Mater.* **13**, 1152 (2001).
9. J. Y. Cheng, A. M. Mayes, C. A. Ross, *Nat. Mater.* **3**, 823 (2004).
10. H.-W. Li, W. T. S. Huck, *Nano Lett.* **4**, 1633 (2004).
11. C. L. Soles, Y. Ding, *Science* **322**, 689 (2008).
12. L. Rockford *et al.*, *Phys. Rev. Lett.* **82**, 2602 (1999).
13. M. Huth *et al.*, *Adv. Funct. Mater.* **12**, 333 (2002).
14. R. Gabai, A. Ismach, E. Joselevich, *Adv. Mater.* **19**, 1325 (2007).
15. S. H. Kim, M. J. Misner, T. Xu, M. Kimura, T. P. Russell, *Adv. Mater.* **16**, 226 (2004).
16. D. G. Walton *et al.*, *Macromolecules* **27**, 6225 (1994).
17. M. J. Fasolka *et al.*, *Phys. Rev. Lett.* **79**, 3018 (1997).
18. P. Lambooy *et al.*, *Phys. Rev. Lett.* **72**, 2899 (1994).
19. J. Y. Cheng, A. M. Mayes, C. A. Ross, *Nat. Mater.* **3**, 823 (2004).
20. A. Hexemer, G. E. Stein, E. J. Kramer, S. Magonov, *Macromolecules* **38**, 7083 (2005).
21. R. A. Segalman, A. Hexemer, R. C. Hayward, E. J. Kramer, *Macromolecules* **36**, 3272 (2003).
22. B. Lee *et al.*, *Macromolecules* **38**, 4311 (2005).
23. G. E. Stein, E. J. Kramer, X. Li, J. Wang, *Phys. Rev. Lett.* **98**, 086101 (2007).
24. S. Park, J.-Y. Wang, B. Kim, J. Xu, T. P. Russell, *ACS Nano* **2**, 766 (2008).
25. S. Park, J.-Y. Wang, B. Kim, T. P. Russell, *Nano Lett.* **8**, 1667 (2008).
26. T. Xu *et al.*, *Adv. Funct. Mater.* **13**, 698 (2003).
27. S. Park, B. Kim, J.-Y. Wang, T. P. Russell, *Adv. Mater.* **20**, 681 (2008).
28. This work was supported by the U.S. Department of Energy (DOE) under contracts DE-FG-0296ER45612 (to T.P.R., S.P., and S.H.), DE-FG-0296ER42126 (T.P.R.), and DE-AC02-05CH11231 (T.X.); by the NSF-supported Materials Research Science and Engineering Center [DMR-0820506 (J.X. and B.K.); and by the Nanoscale Science and Engineering Center (DMI-0531171 (D.L.)] at the University of Massachusetts, Amherst. Use of the Advanced Light Source, Berkeley National Laboratory, was supported by the DOE, Office of Science, Office of Basic Energy Sciences under contract DE-AC02-05CH11231. U.J. acknowledges the support of the Korea Science and Engineering Foundation through grant R11-2007-050-02004-0. The authors are also most indebted to the insightful comments of one referee whose persistence substantially enhanced our arguments.

Supporting Online Material

www.sciencemag.org/cgi/content/full/323/5917/1030/DC1
SOM Text
Figs. S1 to S9
Table S1
References

5 November 2008; accepted 15 January 2009
10.1126/science.1168108

The Formation of Warm Dense Matter: Experimental Evidence for Electronic Bond Hardening in Gold

Ralph Ernstorfer,* Maher Harb, Christoph T. Hebeisen, Germán Sciaini, Thibault Dartigalongue, R. J. Dwayne Miller†

Under strong optical excitation conditions, it is possible to create highly nonequilibrium states of matter. The nuclear response is determined by the rate of energy transfer from the excited electrons to the nuclei and the instantaneous effect of change in electron distribution on the interatomic potential energy landscape. We used femtosecond electron diffraction to follow the structural evolution of strongly excited gold under these transient electronic conditions. Generally, materials become softer with excitation. In contrast, the rate of disordering of the gold lattice is found to be retarded at excitation levels up to 2.85 megajoules per kilogram with respect to the degree of lattice heating, which is indicative of increased lattice stability at high effective electronic temperatures, a predicted effect that illustrates the strong correlation between electronic structure and lattice bonding.

Photo-induced structural dynamics of crystals have been extensively studied with the use of femtosecond spectroscopic methods based on all-optical pump-probe techniques. Although this approach can probe the electronic response of metals and semiconductors to optical excitation with high time and energy resolution, it only provides indirect information on the nu-

clear response of a system. In contrast, the more recently developed techniques of femtosecond electron (*1*) and x-ray (*2*, *3*) diffraction combine atomic-scale spatial and femtosecond temporal resolution.

Modern laser technology allows the creation of highly excited, rarified states of matter. As visible and near-infrared laser light is absorbed by the electrons, intense short-pulsed optical excitation initially forms highly nonequilibrium conditions (that is, very hot electrons within a cool lattice). There has been considerable theoretical interest in this transient state of matter (*4*, *5*), which is the precursor in the formation of high-density plasmas, also referred to as warm dense matter. Time-resolved diffraction experiments enable us to follow the evolution of the atomic structure under these conditions, which is governed by the instantaneous electronically induced change of the lattice potential, as well as the strength of the electron-phonon coupling. In particular, the dynamics of the subsequent order-to-disorder structural transition directly reflect the lattice stability under metastable conditions.

In the case of canonical free-electron metals like aluminum, the lattice stability appears to be mostly unaffected by electronic excitation (*4*). Subsequent to the optical excitation, electron-phonon scattering heats the lattice and results in thermal melting on the picosecond time scale (*1*, *6*).

In contrast, the excitation of semiconductors weakens the covalent bonding, softens the lattice, and, at the excitation level of ~10% of the valence electrons, leads to the collapse of the transverse acoustic phonon branch (*4*, *7*, *8*), resulting in electronically driven disordering of the lattice. With the use of time-resolved diffraction techniques, this order-to-disorder transition has been experimentally observed for various systems like Si (*9*) and InSb (*2*, *3*).

In this context, Peierls-distorted crystals like bismuth (i.e., lattices with reduced symmetry stabilized by the ground state electronic structure) can be considered a third class of systems. Impulsive electronic excitation of those crystals shifts the minimum of the potential energy surface and launches coherent, large-amplitude optical phonons (*10*), equivalent to excited-state wave packet motion in a molecular system. For excitation below the melting threshold, a softening of the interatomic potential with increasing carrier density has been observed (*11*).

For all of the systems mentioned, electronic excitation either softens or does not substantially affect the interatomic potential. In the case of gold, however, the opposite effect has been predicted in recent theoretical studies based on electronic structure calculations (*4*, *5*): Strong electronic excitation reduces the screening of the attractive internuclear potential, resulting in a steepening of the phonon dispersion and a hardening of the lattice. Observing this effect requires probing the lattice stability on extremely short time scales, faster than equilibration between the excited electrons and the underlying lattice that occurs on picosecond-to-subpicosecond time scales.

Laser-induced melting of gold has also been studied by molecular dynamics simulations, but only for lower excitation levels where electronic effects on lattice stability are not expected (*12*). Experimental studies on strongly excited gold films mostly employed all-optical pump-probe spectroscopy. Gou and Taylor concluded from time-resolved reflectivity and surface second-harmonic generation experiments that there is an electronic (nonthermal) contribution to the driving force of the solid/liquid phase transition (*13*). Ng *et al*. observed a quasi–steady state in the optical response of warm dense gold films that has been attributed to the existence of a nonequilibrium liquid state formed by nonthermal melting (*14*, *15*). In contrast, on the basis of ab-initio simulations, Mazevet *et al*. attributed the experimentally observed optical response to a superheated state of ordered, electronically stabilized warm dense gold (*16*); however, this finding has been disputed (*17*). Hitherto, the structural response of gold has been studied with lower excitation (*18*) and for nanoparticles by electron diffraction under reversible excitation conditions (*19*) and by synchrotron-based x-ray diffraction with a time resolution of 100 ps (*20*).

In the present work, we studied the structural evolution of 20-nm-thick free-standing 111-oriented polycrystalline gold films upon 387-nm laser excitation up to 2.85-MJ/kg excitation levels, using synchronously timed femtosecond electron pulses in diffraction mode to provide atomic resolution of the nuclear response. Solid-density matter with such energy density is often referred to as dense plasma or warm dense matter. The highest excitation level employed corresponds to ~14 times the energy required to melt the sample starting from room temperature. Under such irreversible conditions, the sample must be moved to a new position for each laser shot. This puts severe constraints on the electron gun design. The experiment requires high time resolution to access the ultrashort time scale under which a nonequilibrium electron distribution persists and sufficient electron number density to provide near single shot structure determinations to record a full time sequence of events within a limited sample area. Our latest femtosecond electron diffraction (FED) setup (Fig. 1) was designed to achieve these conditions by minimizing the propagation time to the sample and thereby reduce the time for coulombic repulsion between electrons to broaden the electron pulses. The electron pulse duration under the experimental conditions (areal density = 4×10^7 cm^{-2}) was directly determined at the sample position to be 400-fs full width at half maximum using grating-enhanced laser pondermotive scattering (*21*). Another critical element to FED experiments under high excitation conditions is the suppression of strong background

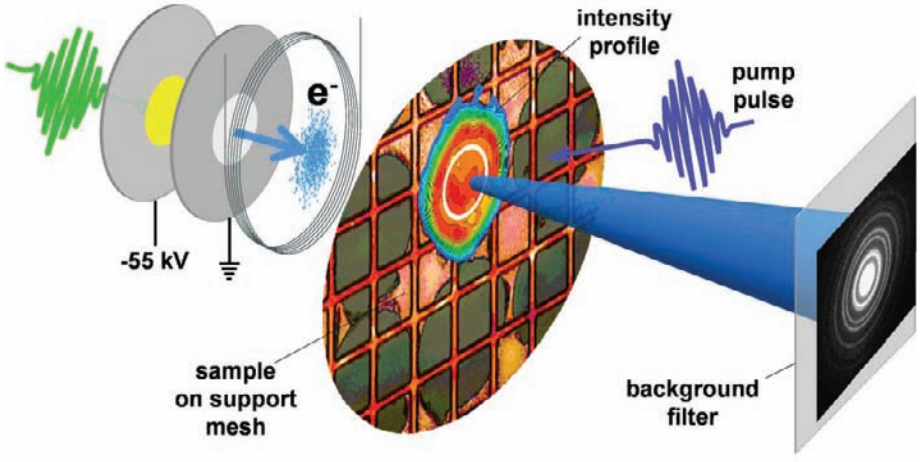

Fig. 1. Schematic depiction of the FED setup. Photoelectrons are emitted via two-photon photoemission from a Au photocathode through back-illumination with a 40-fs visible pulse. The electrons are accelerated over a distance of 6 mm by a static electric field over a potential difference of 55 kV and subsequently collimated by a magnetic lens before arriving at the sample that is placed less than 30 mm from the photocathode. The sample (depicted by a photograph taken after the experiment) is excited by a counter-propagating (angle = 10°) optical pulse (λ_c = 387 nm, 200 fs) with either flat top–like or Gaussian intensity profile. The flat-top pump profile (diameter = 265 μm) is shown in the image and is obtained by 1:1 imaging of an aperture outside the vacuum chamber by a single lens in 4f configuration. The root mean square intensity variation within the probed area (indicated by a white circle) is below 4%, ensuring homogeneous excitation conditions while minimizing the sample area exposed to a single pump pulse. The two-dimensional diffraction pattern is detected by a pair of multichannel plates and a phosphor screen, and the signal of each electron pulse is captured individually by a charge-coupled device camera. In addition to the actual time-resolved diffraction image taken with pump and probe pulses at given time delay, the static diffraction patterns at every sample position before and after irradiation with the pump pulse are recorded. Between 5 and 60 images were recorded and averaged per time point.

Institute for Optical Sciences and Departments of Chemistry and Physics, 80 Saint George Street, University of Toronto, Toronto, ON M5S 3H6, Canada.

*Present address: Physik Department E11, Technische Universität München, D-85747 Garching, Germany.

†To whom correspondence should be addressed. E-mail: dmiller@lphys.chem.utoronto.ca

signals originating from photoelectrons and ions emitted from the sample, as well as stray pump light. We achieved this by using a thin mesh-supported film of amorphous carbon placed directly in front of the detector as a filter.

Although the skin depth of 387-nm light in gold is below 10 nm, the range of ballistic electron transport is on the order of 100 nm (*22*), resulting in a homogeneous, isochoric excitation of the gold films within the duration of the optical pump pulse. Figure 2A shows raw data [radially averaged scattering intensity, $I(s)$; s, scattering vector] of the oriented Au(111) film excited with 470 J/m^2 (absorbed fluence) for selected time points. Because of the normal incidence of the electron pulses and the 111-morphology of the sample, several Bragg peaks—particularly the (111) peak—are strongly suppressed compared with the pattern formed by an isotropic polycrystalline sample. This feature was deliberately exploited so that the (111) order, in particular, would not obscure the onset of lattice disordering that is most pronounced near this scattering direction (vide infra). The static diffraction patterns show a substantial background, arising from inelastic (e.g., phonons, single-electron excitations, collective electronic excitations) and multiple elastic scattering. In the case of a high–atomic number material like gold, thermal diffuse scattering (DS) is expected to dominate the inelastically scattered intensity (*23*). Upon photoexcitation, this background and the intensity of the unscattered electrons (center of the diffraction image) show a dynamic increase and decrease, respectively. The decrease of the zero-order peak reflects the reduction of the inelastic mean free path of the probe electrons. For polycrystalline gold excited modestly above the melting temperature (T_m), we indeed found that the diffraction intensity between the Bragg peaks as well as the zero-order diffraction intensity show the same dynamics compared to the evolution of the lattice temperature as extracted from the Debye-Waller effect. The diffraction pattern of liquid gold (Fig. 2A) exhibits increased DS background over the whole detected scattering range and one single broad diffraction peak near 0.43 Å^{-1}, corresponding to the liquid structure factor. By using 111-oriented gold, this peak (the signature of the product state of the phase transition) arises within a range of the scattering vector s that is essentially free of Bragg peaks in the crystalline state. This allows us to distinguish heating and disordering of the lattice directly from the data obtained in reciprocal space, rather than from real-space data obtained by Fourier transformation (*18*). For unoriented polycrystalline gold under strong optical excitation, the distinction between a strongly superheated lattice and a disordered state based on the real-space reduced density function is less definitive, especially in the presence of a time-dependent scattering background.

Figure 2B shows the temporal evolution of the diffraction pattern after excitation with 470 J/m^2 plotted as relative diffraction intensity $I(s,t)/I(s,t<0)$, where $I(s,t<0)$ denotes the diffraction signal averaged over all negative delay points. In the range from 0.3 to 1.1 Å^{-1}, there are three distinct effects: (i) the increase in DS, which spans the whole displayed range but that is most obvious in the Bragg

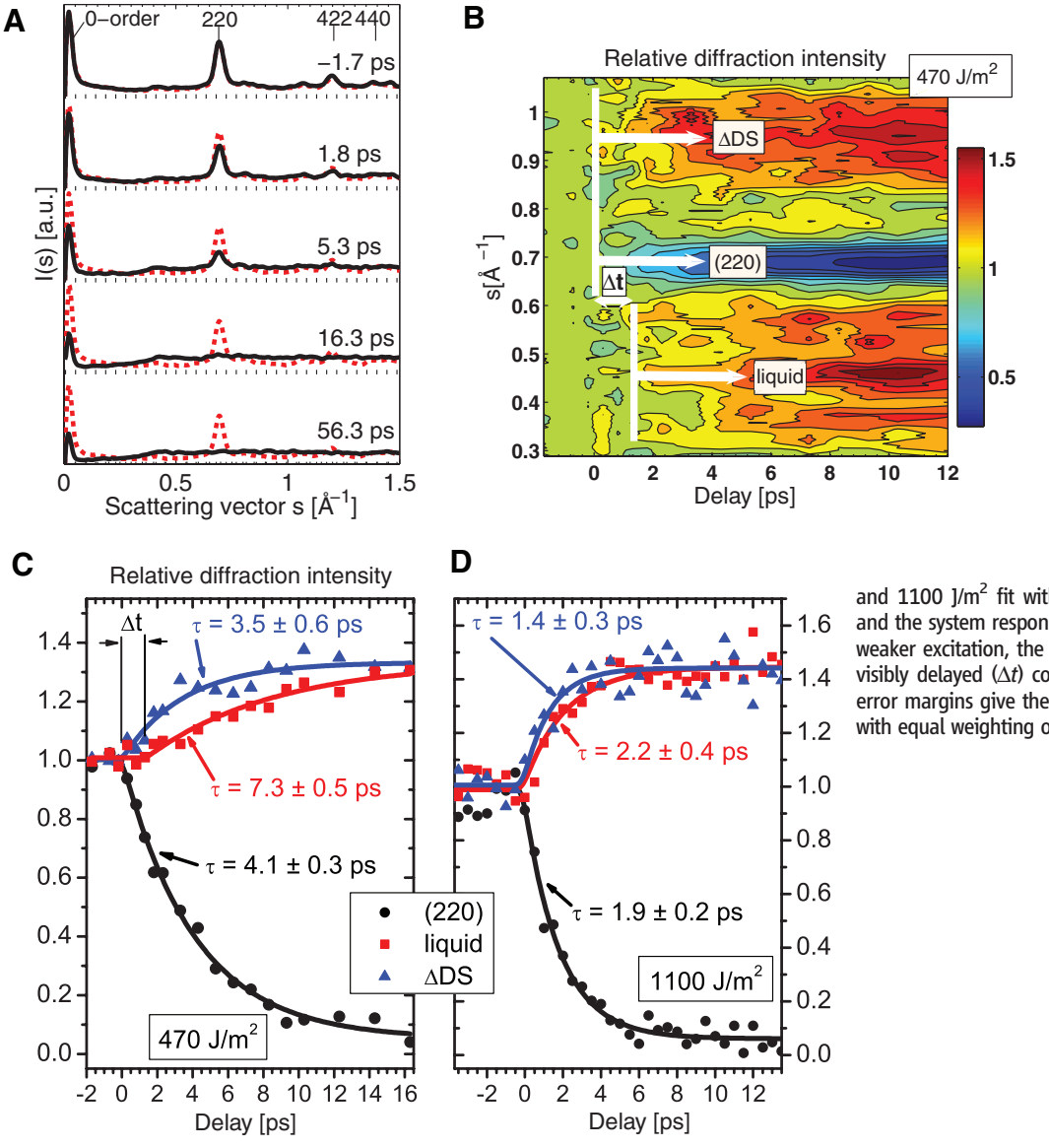

Fig. 2. Temporal evolution of the diffraction signal. (**A**) Raw radially averaged diffraction pattern of 111-oriented gold excited with an absorbed fluence of 470 J/m^2 at selected time points (solid black lines), the equivalent diffraction signals without excitation (dashed red lines), and the vertically shifted baselines (dotted black lines). a.u., arbitrary units. (**B**) Temporal evolution of the diffraction signal shows three distinct features in the scattering range from 0.3 to 1.1 Å^{-1}: (i) the rise of the diffraction peak characteristic for a liquid, (ii) the decay of the (220) Bragg peak, and (iii) an overall rise in diffuse background. (**C** and **D**) Time traces of the rise of the liquid peak (red squares), the decay of (220) (black circles), and the rise of DS (blue triangles) for absorbed excitation fluences of 470 and 1100 J/m^2 fit with convolutions of single exponentials and the system response function (solid lines). In case of the weaker excitation, the onset of the rise of the liquid peak is visibly delayed (Δt) compared with the heating effects. The error margins give the standard error obtained from the fits with equal weighting of the data points.

peak-free region between 0.9 and 1.05 Å^{-1}, (ii) the decay of the (220) Bragg peak, and (iii) the rise of the liquid structure factor at ≈0.43 Å^{-1}, which dominates over the DS rise in this range. The temporal evolutions of these three features differ significantly, as shown in Fig. 2, C and D, for two excitation levels. Lacking a reliable model to describe the various effects contributing to the transient signals, we performed monoexponential fits to quantify the dynamics. The increase in DS shows the fastest dynamics. In comparison, the decay of the Bragg peak, being a probe for lattice heating as well as disordering, is slightly but consistently slower. For an absorbed excitation fluence of 470 J/m^2 (Fig. 2B), the rise of the liquid structure factor is delayed by 1.4 ± 0.3 ps compared with the DS and (220) dynamics. This retardation of the onset reflects the time required to heat the lattice above T_m, which is an indication of a thermal melting process. Employing a two-temperature model (TTM) that takes the electronic structure of gold specifically into account (*24*)—in particular, the dependence of the electron heat capacity $C_e(T_e)$ and the electron-phonon coupling $G(T_e)$ on the electron temperature T_e—the lattice temperature T_l is expected to reach the lattice melting temperature T_m within 1 ps at this excitation level. Subsequently, the lattice is expected to rapidly superheat and melt homogeneously on the time scale of ~1 ps (*25*); i.e., for $T_l \geq 1.4\ T_m$, the lattice disorders within a few vibrational periods. In the case of aluminum, this mechanism has been experimentally observed (*1*, *6*, *26*). In contrast, the rise time of the liquid peak in gold excited with 470 J/m^2 (corresponding to an absorbed energy density of ~1.2 MJ/kg) is 7 ps, clearly separated from the other two time constants that mostly reflect lattice heating. This behavior is also in contrast to that of InSb excited above the ablation threshold, where the decay of the (111) Bragg peak and the rise of DS were found to be synchronous (*27*). We would like to emphasize that the appearance of the liquid structure factor in our data reflects the transition from an anisotropic polycrystalline state to a fully isotropic disordered state.

With increasing excitation up to 2.85 MJ/kg, the overall dynamics accelerate, whereas the different time constants remain in their relative order (Fig. 3A), and the retardation Δt of the liquid structure factor drops to 0.3 ps (close to the experimental time resolution). Figure 3A also shows the time $t(T_l = 1.4T_m)$ (gray circles) when T_l reaches $1.4T_m$, according to the decay of the (220) peak. The significant difference between these points in time when ultrafast melting is expected ($t_T = 1.4T_m$) and the time constant τ_{liquid} indicates enormous superheating that cannot be explained by classical nucleation theory (*12*, *25*). Recent ab initio calculations predict a hardening of the phonon modes in gold due to increased T_e, resulting in an increase of T_m (*4*, *5*, *16*). This effect has been qualitatively explained by increased electronic delocalization and decreased screening of the attractive nuclear potential (*4*, *5*). The highest excitation conditions employed in this work correspond to an initial T_e of ~4 eV, which instantaneously increases T_m from 1340 to 2400 K (or, equivalently, the Debye temperature θ_D from 180 to 250 K), according to ab initio calculations (*4*). Alternatively, the effect of electronic excitation has been discussed in terms of electronically induced pressure, resulting in a reduction of the concentration of monovacancies (seeds for homogeneous nucleation) (*5*).

In general, the temporal evolution of T_l before melting can be estimated from the decay of the Bragg peaks. By describing electronic lattice hardening by a T_e-dependent Debye temperature, however, the Debye-Waller factor (DWF) becomes a function of T_e as well [see supporting online material (SOM)]. Figure 3B shows comparisons of the decay of the (220) peak for all employed excitation levels with the simulated decay according to two different models: DWF$\{T_l(t)$, $\theta_D[T_e(t)]\}$ takes the effect of bond hardening through $\theta_D[T_e(t)]$ explicitly into account, whereas DWF$[T_l(t)$, θ_D = constant] ignores the effect of bond hardening. We apply an advanced TTM based on a nonlinear electron heat capacity $C_e(T_e)$ and a T_e-dependent electron-phonon coupling $G(T_e)$ (*24*), which we solve for $T_l(t)$ and $T_e(t)$. The simulations account for the experimental temporal resolution. Although both models are free of any adjustable parameter, the model taking electronic bond hardening into account shows significantly better agreement with the experimental data.

The good agreement between the simulation and the experimental results justifies estimating $T_l(t)$ according to the relation between DWF(T_l,T_e) and $T_l(t)$ obtained from the model. At the points in time, when the DWFs drop to 1/*e* of the room temperature value, the lattice temperatures reach ~3000, 3600, and 4100 K for the three employed excitation levels, respectively, indicative of strong superheating of the face-centered cubic lattice (see also SOM). The smooth decay of (220) within the first picoseconds, which is temporally well resolved in our experiments, supports the conclusion of a substantial superheating of the crystal. In this stage, isochoric heating of the lattice can be expected to further increase the stabilization of the crystal structure (Clapeyron effect) (*28*).

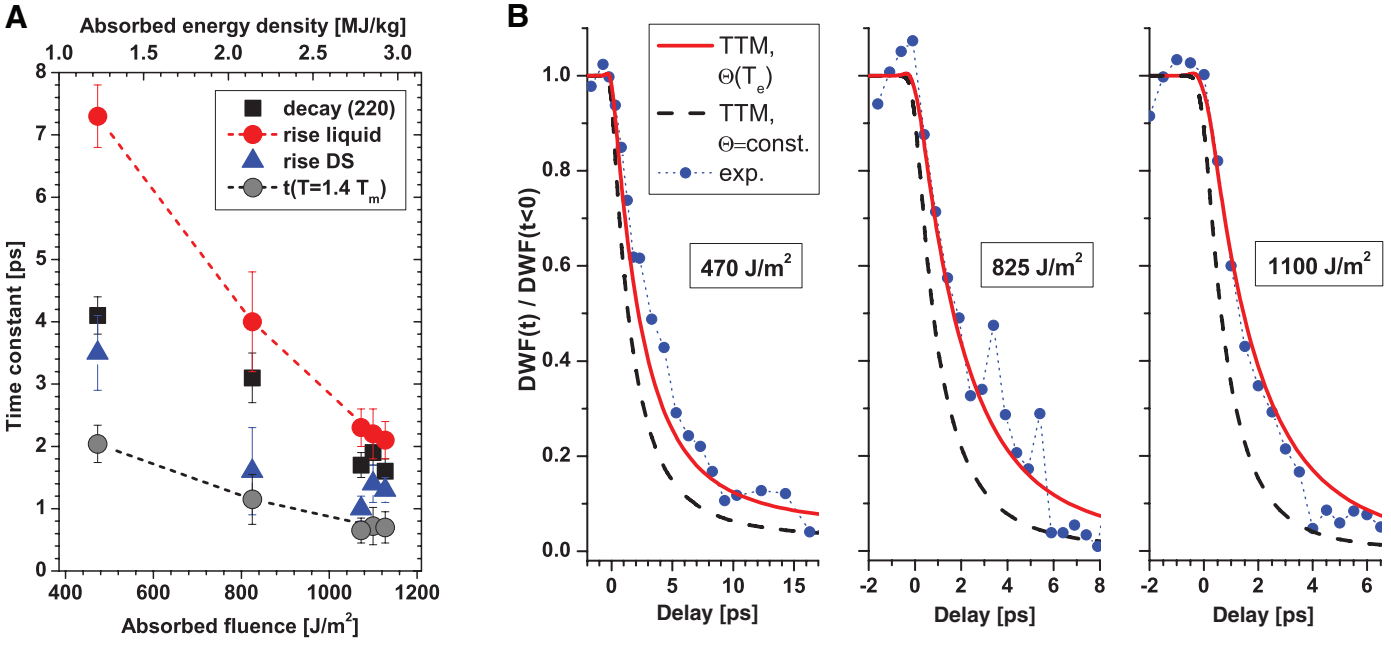

Fig. 3. Fluence-dependence of heating and disordering. (**A**) Summary of the time constants shown in Fig. 2 for five different data sets. The gray circles indicate the times when the lattice temperature reaches $1.4T_m$. Error bars indicate the standard error. (**B**) Experimental data of the (220) decay (solid blue circles) compared with two different models for the DWF—DWF$[\theta_D(T_e)]$ (solid red lines) and DWF(θ_D = constant) (dashed black lines)—for different excitation levels. T_e and T_l are obtained from a TTM. See text and SOM for details.

The above experiments and SOM provide an atomic-level perspective on the formation of warm dense matter. The observations demonstrate that warm dense gold is formed in a purely thermal process. Previously observed quasi–steady state signatures in the optical response cannot be assigned to instantaneous, nonthermal formation of a liquid-like state. The difference in the rate of substantial superheating and lattice disordering, at the predicted electronic temperatures for increased lattice stability, supports a photo-induced bond hardening mechanism and the concept of a T_e-dependent melting temperature. The increased lattice stability will also increase the barrier to nucleation as the electron distribution and nuclear configurations are strongly coupled. Full-scale ab initio molecular dynamics calculations are now needed to understand this phenomenon to which the experiment provides rigorous benchmarks for comparison.

References and Notes

1. B. J. Siwick, J. R. Dwyer, R. E. Jordan, R. J. D. Miller, *Science* **302**, 1382 (2003).
2. A. Rousse *et al.*, *Nature* **410**, 65 (2001).
3. A. M. Lindenberg *et al.*, *Science* **308**, 392 (2005).
4. V. Recoules, J. Clérouin, G. Zérah, P. M. Anglade, S. Mazevet, *Phys. Rev. Lett.* **96**, 055503 (2006).
5. F. Bottin, G. Zérah, *Phys. Rev. B* **75**, 174114 (2007).
6. M. Kandyla, T. Shih, E. Mazur, *Phys. Rev. B* **75**, 214107 (2007).
7. R. Biswas, V. Ambegaokar, *Phys. Rev. B* **26**, 1980 (1982).
8. E. S. Zijlstra, J. Walkenhorst, M. E. Garcia, *Phys. Rev. Lett.* **101**, 135701 (2008).
9. M. Harb *et al.*, *Phys. Rev. Lett.* **100**, 155504 (2008).
10. K. Sokolowski-Tinten *et al.*, *Nature* **422**, 287 (2003).
11. D. M. Fritz *et al.*, *Science* **315**, 633 (2007).
12. Z. Lin, L. V. Zhigilei, *Phys. Rev. B* **73**, 184113 (2006).
13. C. Guo, A. J. Taylor, *Phys. Rev. B* **62**, R11921 (2000).
14. K. Widmann *et al.*, *Phys. Rev. Lett.* **92**, 125002 (2004).
15. T. Ao *et al.*, *Phys. Rev. Lett.* **96**, 055001 (2006).
16. S. Mazevet, J. Clérouin, V. Recoules, P. M. Anglade, G. Zérah, *Phys. Rev. Lett.* **95**, 085002 (2005).
17. Y. Ping *et al.*, *Phys. Rev. Lett.* **96**, 255003 (2006).
18. J. R. Dwyer *et al.*, *Philos. Trans. R. Soc. London. Ser. A* **364**, 741 (2006).
19. C.-Y. Ruan, Y. Murooka, R. K. Raman, R. A. Murdick, *Nano Lett.* **7**, 1290 (2007).
20. A. Plech, V. Kotaidis, S. Gresillon, C. Dahmen, G. von Plessen, *Phys. Rev. B* **70**, 195423 (2004).
21. C. T. Hebeisen *et al.*, *Opt. Express* **16**, 3334 (2008).
22. J. Hohlfeld *et al.*, *Chem. Phys.* **251**, 237 (2000).
23. G. Radi, *Acta Crystallogr. A* **26**, 41 (1970).
24. Z. Lin, L. V. Zhigilei, V. Celli, *Phys. Rev. B* **77**, 075133 (2008).
25. B. Rethfeld, K. Sokolowski-Tinten, D. von der Linde, S. I. Anisimov, *Phys. Rev. B* **65**, 092103 (2002).
26. B. J. Siwick, J. R. Dwyer, R. E. Jordan, R. J. D. Miller, *Chem. Phys.* **299**, 285 (2004).
27. A. M. Lindenberg *et al.*, *Phys. Rev. Lett.* **100**, 135502 (2008).
28. D. S. Ivanov, L. V. Zhigilei, *Phys. Rev. B* **68**, 064114 (2003).

29. We thank A.-A. Dhirani and the Emerging Communications Technology Institute at the University of Toronto for the usage of their deposition chambers and L. Zhigilei, Z. Lin, and S. Mazevet for helpful discussions. We also thank A. Ng for initial discussions that led to this study. Funding was provided by the Natural Science and Engineering Research Council. R.E. thanks the Alexander von Humboldt Foundation for financial support.

Supporting Online Material

www.sciencemag.org/cgi/content/full/1162697/DC1
SOM Text
Figs. S1 and S2
References

3 July 2008; accepted 8 January 2009
Published online 22 January 2009;
10.1126/science.1162697
Include this information when citing this paper.

Switching Off Hydrogen Peroxide Hydrogenation in the Direct Synthesis Process

Jennifer K. Edwards,[1] Benjamin Solsona,[1] Edwin Ntainjua N,[1] Albert F. Carley,[1] Andrew A. Herzing,[2,3] Christopher J. Kiely,[3] Graham J. Hutchings[1]*

Hydrogen peroxide (H_2O_2) is an important disinfectant and bleach and is currently manufactured from an indirect process involving sequential hydrogenation/oxidation of anthaquinones. However, a direct process in which H_2 and O_2 are reacted would be preferable. Unfortunately, catalysts for the direct synthesis of H_2O_2 are also effective for its subsequent decomposition, and this has limited their development. We show that acid pretreatment of a carbon support for gold-palladium alloy catalysts switches off the decomposition of H_2O_2. This treatment decreases the size of the alloy nanoparticles, and these smaller nanoparticles presumably decorate and inhibit the sites for the decomposition reaction. Hence, when used in the direct synthesis of H_2O_2, the acid-pretreated catalysts give high yields of H_2O_2 with hydrogen selectivities greater than 95%.

Hydrogen peroxide (H_2O_2) is an important commodity chemical used primarily for disinfection and bleaching (*1*) and will be used in the future for the manufacture of propylene oxide using the titanium silicalite TS-1 as a catalyst (*2*). It is currently produced by an indirect process in which H_2 and O_2 are kept apart using the sequential hydrogenation and oxidation of an anthraquinone (*2*). For economic reasons, the indirect process is carried out on a large scale and produces concentrated H_2O_2, although most applications require very dilute solutions. Direct processes that oxidize H_2 have been investigated, and supported palladium catalysts are known to be effective (*3*–*5*). However, as in any redox process where a reactive intermediate is required as the final product, the key problem is stabilizing the resulting H_2O_2 so that it does not decompose and form water. Indeed, all catalysts so far identified for direct H_2O_2 synthesis are equally effective for its sequential hydrogenation or decomposition to water (*6*–*12*) (Scheme 1), and acid and halides must be added to ensure that some H_2O_2 is retained (*6*, *9*–*12*).

To date, the best H_2 selectivity reported for the direct synthesis process using Pd is ~80% (*3*). We have shown (*8*, *13*–*16*) that alloying gold with palladium markedly enhances the catalyst activity and selectivity, with a selectivity of 80% being achieved even in the absence of halide and acid promoters (*17*). For commercial competitiveness with the indirect process, it is essential that H_2 selectivity is increased to >95%. We have now addressed this problem and show that acid pretreatment of carbon support materials can switch off the sequential hydrogenation and decomposition of H_2O_2, thereby achieving the target selectivities and producing high rates of H_2O_2 synthesis under intrinsically safe conditions.

We have previously investigated a variety of support materials for Au-Pd catalysts (*8*, *13*, *14*, *16*) and, specifically, the selectivities for H_2 utilization under our standard reaction conditions (*18*) are carbon (80%) ~ SiO_2 (80%) > TiO_2 (70%) > Al_2O_3 (14%) (*17*). To understand these selectivity differences, we investigated the hydrogenation and decomposition of H_2O_2 over these catalysts and supports (Table 1). The oxide supports showed no activity in the absence of the metals, but the carbon support did show some reactivity, as noted previously (*15*). When the metals are added, all show appreciable activity for these nonselective reactions with the order of activity being broadly in line with the observed H_2 selectivities in the synthesis reaction. Because these catalysts are prepared by wet impregnation of an acidic solution of the metal salts onto the support (*18*), we investigated the effect of an initial acid pretreatment step in which the support

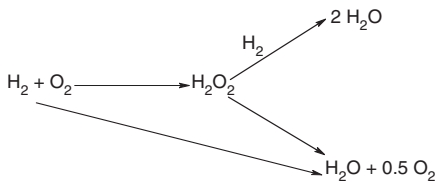

Scheme 1.

[1]School of Chemistry, Cardiff University, Main Building, Park Place, Cardiff CF10 3AT, UK. [2]National Institute of Standards and Technology, Surface and Microanalysis Science Division, 100 Bureau Drive, Mailstop 8371, Gaithersburg, MD 20899–8371, USA. [3]Center for Advanced Materials and Nanotechnology, Lehigh University, 5 East Packer Avenue, Bethlehem, PA 18015—3195, USA.

*To whom correspondence should be addressed. E-mail: hutch@cardiff.ac.uk

was treated with 2% aqueous HNO_3 and dried before addition of the metals (*18*). For the Au-Pd catalysts on oxide supports, this step led to a decrease in combined hydrogenation and decomposition, but for the carbon support, the Au-Pd catalysts showed no such activity when reacting a 4 weight percent (wt %) H_2O_2 solution (Table 1).

To investigate this effect, we examined the stability of higher concentration solutions of H_2O_2 using the carbon-supported materials. Solutions of H_2O_2 were stirred with high pressure H_2 (5% H_2/CO_2, 3 MPa) in the presence of the support or the catalyst (10 mg) for 30 min at 2°C (i.e., standard reaction conditions without the addition of O_2); representative data are shown in Fig. 1. Pd and Au-Pd catalysts on untreated carbon, as well as the bare support itself, react in a similar manner and give sequential hydrogenation. These results show that the support plays a crucial role in the performance of catalysts for the direct reaction because it controls the manner in which the active components are dispersed, as well as providing the sites on which H_2O_2 hydrogenation-decomposition, and hence product loss, occurs. However, the acid-pretreated carbon support shows some reduction in H_2O_2 hydrogenation activity relative to the nontreated material, but when it is loaded with Pd the rate of hydrogenation of H_2O_2 becomes identical to that of the corresponding nontreated Pd/C catalyst, showing that the nonselective hydrogenation sites have been restored (Fig. 1A). In stark contrast, the acid-pretreated Au-Pd alloy catalyst shows no substantial activity for the sequential hydrogenation of H_2O_2, up to 14 wt % H_2O_2, and only at a concentration of 17.5 wt % does some sequential hydrogenation begin to occur.

We then investigated the carbon-supported Au-Pd catalysts at 2°C using nonexplosive dilute H_2/O_2 mixtures [(H_2 < 4 volume percent (vol %)] with CO_2 as a diluent and using methanol/water as a solvent; under these conditions, we observed a marked increase in the yield of H_2O_2 and the selectivity of H_2 utilization (Table 2, experiments 1 to 3). No enhancement was observed for similarly pretreated Pd-only catalysts (Table 2, experiments 4 to 6), whereas a slight positive effect is still observed for pretreated Au catalysts (Table 2, experiments 7 to 9). An enhancement was always observed with the Au-Pd alloy catalysts when the acid pretreatment was conducted before metal addition (Table 2, experiments 1 to 3). Nitric and acetic acids were the most effective acids tested to date (Table 2, experiments 9 to 12), whereas base pretreatment with ammonium hydroxide invariably led to a decrease in yield (Table 2, experiment 13). Treatment with water alone, or ammonium, sodium, or potassium nitrates had no effect (Table 2, experiments 2, 14 to 16), confirming that it is the exposure to acid that is important. The materials prepared using acid-pretreated supports combined with a calcination at 400°C were found to give catalysts that could be reused several times (Fig. 1B) without any loss of performance. For each use, the acid-pretreated catalyst gave an initial rate of 640 mol H_2O_2 $kg_{cat}^{-1}.h^{-1}$ determined at 2 min reaction time, and 160 mol H_2O_2 $kg_{cat}^{-1}.h^{-1}$ determined at 30 min reaction time, with 40% hydrogen conversion. The addition of nitric acid to the reaction mixture before H_2O_2 synthesis—which is an established procedure for stabilizing H_2O_2 (*1*, *2*, *10*–*12*) because H_2O_2 decomposition is known to be a base catalyzed process—also led to an enhancement in the yield of H_2O_2, but the effect was not sustained upon subsequent catalyst reuse (Fig. 1B). Treatment of any of the supports after metal deposition did not enhance catalyst performance, and addition of nitric or hydrochloric acid during the metal impregnation step did not lead to any enhancement (Table 2, experiments 17,18); indeed, the addition of hydrochloric acid was deleterious. These results demonstrate the importance of the precise manner in which the acid pretreatment is carried out. However, neither the acid concentration nor the duration of the acid pretreatment are critical; the effect can be observed even when quite dilute acid solutions (2 vol %) are used.

Interestingly, both the untreated and the acid-pretreated Au catalyst also show no activity for sequential hydrogenation (Fig. 1A); unfortunately, both these catalysts also show remarkably little activity for H_2O_2 synthesis (Table 2, experiments 7 to 9). However, these results do show that the adsorption of Au onto the surface of the carbon support blocks the sites responsible for loss of H_2O_2 because the catalyst has no activity for the decomposition reaction. Hence, we consider that it is the interaction of Au with the pretreated C support that is crucial for observing this new effect of switching off H_2O_2 hydrogenation/decomposition. The switch-off phenomenon was also observed after the acid-pretreated Au-Pd/C catalysts had been used for the direct synthesis reaction, and, indeed, this effect was sustained after several

Table 1. Effect of acid pretreatment of the support on the hydrogenation and decomposition of H_2O_2.

Support	Support only				Au-Pd catalyst*			
	Untreated		Pretreated†		Untreated		Pretreated†	
	Hydrog‡	Decomp§	Hydrog‡	Decomp§	Hydrog‡	Decomp§	Hydrog‡	Decomp§
Al_2O_3	0	0	0	0	24	3	16	8
TiO_2	0	0	0	0	12	6	13	4
SiO_2	0	0	0	0	15	8	12	1
Carbon	4	1	3	1	5	2	0	0

*Catalysts contain 2.5 wt % Au–2.5 wt % Pd co-impregnated onto the support (wt % = mass fraction). †Treated with 2% HNO_3 in aqueous solution (volume fraction = 2% HNO_3). ‡H_2O_2 hydrogenation conditions: catalyst (10 mg), 2.9 MPa H_2 (volume fraction 5%)/CO_2, 2°C, 0.5 hours, methanol/water as solvent, stirring rate 1200 rpm (126 rad/s). §H_2O_2 decomposition conditions: catalyst (10 mg), air, atmospheric pressure, 2°C, 0.5 hours, methanol/water as solvent, stirring rate 1200 rpm.

Table 2. Activity and selectivity of pretreated and untreated carbon-supported catalysts for H_2O_2 synthesis at 2°C. All catalysts calcined in air 400°C for 3 hours. Reaction conditions: 10 mg catalyst using carbon as support, 2.9 MPa H_2 (5% volume fraction)/CO_2 1.1 MPa O_2 (25% volume fraction)/CO_2, 2°C, 0.5 hours, methanol/water as solvent, pretreated as indicated for 30 min.

Experiment number	Catalyst*	Pretreatment†	H_2O_2 selectivity (%)	Productivity (mol kg_{cat}^{-1} h^{-1})
1	2.5% Au–2.5% Pd/carbon	None	80	110
2	2.5% Au–2.5% Pd/carbon	Water	80	112
3	2.5% Au–2.5% Pd/carbon	2% HNO_3	>98	160
4	5% Pd/carbon	None	42	50
5	5% Pd/carbon	Water	42	50
6	5% Pd/carbon	2% HNO_3	42	52
7	5% Au/carbon	None	nd‡	0.4
8	5% Au/carbon	Water	nd‡	0.4
9	5% Au/carbon	2% HNO_3	nd‡	0.5
10	2.5% Au–2.5% Pd/carbon	2% CH_3COOH	>98	175
11	2.5% Au–2.5% Pd/carbon	2% H_3PO_4	30	120
12	2.5% Au–2.5% Pd/carbon	2% HCl	15	130
13	2.5% Au–2.5% Pd/carbon	2% NH_4OH	24	70
14	2.5% Au–2.5% Pd/carbon	2% NH_4NO_3	80	100
15	2.5% Au–2.5% Pd/carbon	2% KNO_3	80	120
16	2.5% Au–2.5% Pd/carbon	2% $NaNO_3$	80	122
17	2.5% Au–2.5% Pd/carbon	HCl§‖	5	20
18	2.5% Au–2.5% Pd/carbon	HNO_3§‖	35	98

*Metal loadings denoted as mass fractions. †Acid concentration expressed in terms of volume fraction. ‡Not determined due to yields being very low. §Added to slurry during catalyst preparation. ‖Concentration 1 kmol/m^3 in aqueous solution.

uses. Hence, the catalysts can be used multiple times without loss of activity for the direct H_2O_2 formation reaction or gaining activity for H_2O_2 hydrogenation/decomposition.

We carried out a direct synthesis reaction with the pretreated AuPd/C catalyst in the presence of H_2O_2 (4.3 wt %), and after 30 min of reaction additional H_2O_2 is produced (0.1 wt %), whereas with the untreated catalyst only decomposition/hydrogenation is observed (*18*). The opposing reactivity of this pair of catalysts directly shows that the acid pretreatment has switched off the sequential hydrogenation of H_2O_2 for the Au-Pd catalyst, thus leading to the observed enhanced activities and selectivities. In our synthesis experiments, we used a stirred autoclave and can only synthesize relatively dilute H_2O_2 solutions. However, the acid-pretreated Au-Pd/C catalysts could be used in a set of sequential experiments in which the gases were repeatedly replenished at 30-min intervals (Fig. 1C). Acid-pretreated Au-Pd catalysts steadily increased the H_2O_2 concentration, whereas untreated Pd and Au-Pd catalysts exhibited markedly inferior performance because of enhanced H_2O_2 hydrogenation/decomposition.

Bulk and surface analysis of the acid pretreated supported catalysts revealed no marked distinguishing characteristics (figs. S1 to S3) (*18*), but our previous scanning transmission electron microscopy (STEM) annular dark field (ADF) analysis of the untreated Au-Pd/C sample revealed a trimodal particle size distribution (*19*). The smallest particles fell in the range of 2 to 5 nm, intermediate size particles were ~10 to 50 nm in size, and occasional particles were observed exceeding 70 nm. X-ray energy dispersive spectroscopy (STEM-XEDS) spectrum images also showed that the composition of the metal nanoparticles varied with size in a systematic manner (*19*), such that the smallest particles tended to be Pd-rich whereas the largest particles were highly Au-rich.

However, as shown in the STEM-XEDS spectrum image data presented in Fig. 2, A to F, and fig. S4 (*18*), no surface segregation of Pd or Au was detected in either the untreated or acid pretreated catalysts, and this was confirmed by x-ray photoemission spectroscopy (XPS) (figs. S2 and S3) (*18*). Instead, all of the particles were homogeneous Au-Pd alloys, in contrast to the core-shell structure observed previously in similar Au-Pd particles on oxide supports. Finally, the STEM-XEDS data indicates that the acid pretreatment does not appear to alter the trend in the particle-size/composition dependence, and, thus, the switching off of H_2O_2 hydrogenation/decomposition and enhancement in activity observed with acid pretreatment is not caused by the specific morphology changes of the Au-Pd alloy particles.

A major difference between the acid-treated and untreated Au-Pd/C samples was found in the alloy particle size distribution (see the histogram in Fig. 2G). Acid pretreatment of the support improved nanoparticle nucleation and favored the formation of a greater number fraction of the smallest (Pd-rich alloy) particles at the expense of the intermediate (similar Au-Pd content) and large (Au-rich) particles, which is consistent with the increased surface Au content determined from XPS (figs. S2 and S3) (*18*). The acid-pretreated Au-Pd/C sample exhibited only the small (2 to 5 nm) and intermediate (10 to 50 nm) Au-Pd homogeneous alloy particles of similar composition to their counterparts observed in the untreated sample. Furthermore, no Au-Pd particles >50 nm were found in the acid-pretreated catalyst, whereas very large Au-rich particles were readily observed on the untreated carbon support. Thus, the beneficial effect of acid pretreatment is to enhance the gold dispersion in the bimetallic alloy particles by generating smaller Au-Pd nanoparticles, and these presumably decorate sites on the support that are otherwise active for the hydrogenation/decomposition of H_2O_2. The increase in activity for the direct synthesis of H_2O_2 is therefore due to the formation of smaller active alloy nanoparticles, and the enhancement in selectivity toward H_2O_2 is caused by these small particles switching off the active sites for H_2O_2 decomposition. The observation that small nanoparticles are required for high activity is consistent with recent observations for Au and Pd catalysts (*20*–*22*).

We find similar effects for pure Au/C catalysts where the acid pretreatment decreases the average Au particle size (Fig. 2H). Interestingly, no such effect is observed for the dispersion of pure Pd/C (Fig. 2I), which is consistent with the concomitant lack of enhancement in the catalytic

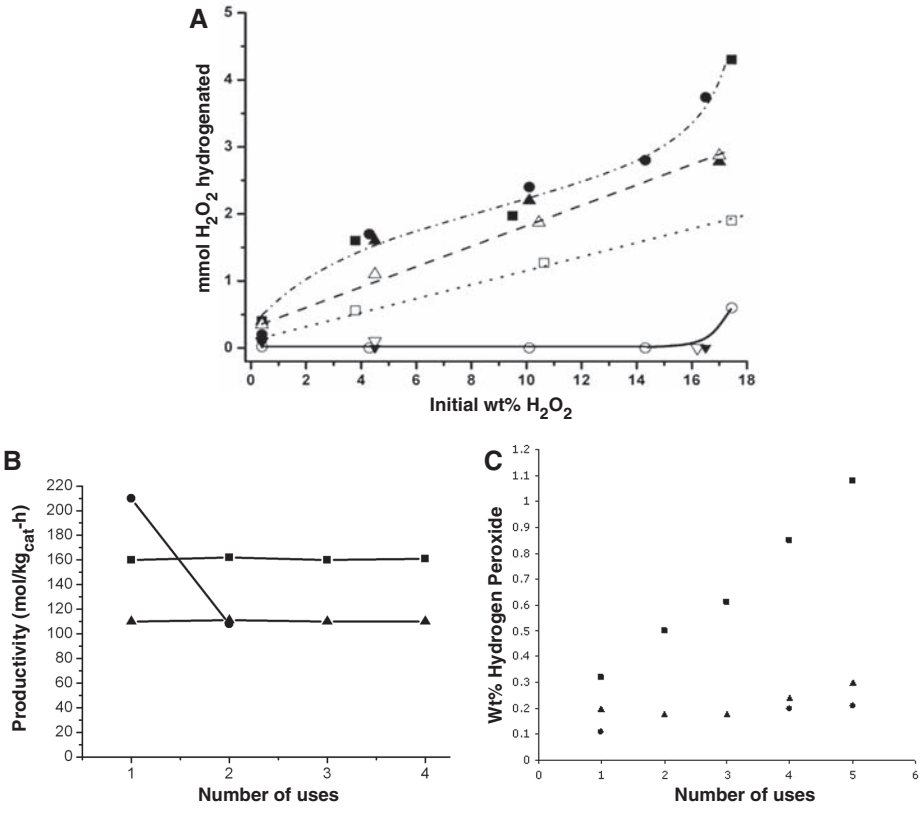

Fig. 1. (**A**) Performance of acid-pretreated carbon-supported catalysts compared with nontreated catalysts for the hydrogenation of H_2O_2. Dashed-dotted line: filled squares, untreated 2.5% Au–2.5% Pd/C; filled circles, untreated carbon support. Dashed line: filled triangles, untreated 5% Pd/C; open triangles, pretreated 5% Pd/C. Dotted line: open squares, pretreated support. Solid line: open circles, pretreated 2.5% Au–2.5% Pd/C; inverted open triangles, pretreated 5% Au /C; inverted filled triangles, untreated 5% Au /C. Reactions were carried out with H_2O_2 in solvent [methanol (5.6 g) and water (2.9 g)] at 2°C with 1200 rpm, stirring for 30 min under 420 psig (2.90×10^6 Pa) 5% H_2/CO_2. The data show that for the pretreated Au-Pd and Au catalysts the hydrogenation and decomposition of H_2O_2 is switched off, whereas extensive hydrogenation/decomposition is observed with nontreated AuPd and Pd catalysts; results are shown for the extent of hydrogenation/decomposition (wt % = mass fraction). (**B**) Performance of acid-pretreated catalysts compared with nontreated catalysts for the synthesis of H_2O_2. The untreated (triangles) and 2% HNO_3 treated (squares) catalysts are stable over four uses, with the latter showing a higher activity. The addition of 2% HNO_3 in the autoclave with the untreated catalyst (circles) shows a higher initial activity that is lost on subsequent reuse (it remains at the same level as the untreated catalyst in subsequent reuses). (**C**) The effect of sequential experiments using gas top-up on hydrogen peroxide concentration. The acid-treated Au-Pd/carbon (squares) catalyst shows increasing hydrogen peroxide concentration as reactant gases are refreshed (*18*). In contrast, the untreated Au-Pd/carbon (triangles) catalyst and 5% Pd/carbon (circles) catalyst show no increase in hydrogen peroxide concentration as the gases are refreshed, due to enhanced hydrogen peroxide hydrogenation/decomposition for the nontreated catalysts.

performance due to acid pretreatment (Table 2, experiments 4 to 6). Apparently, to observe this particle size redistribution, Pd has to be alloyed with Au. Hence, we conclude that the acid pretreatment of the carbon support, by itself, leads to a partial decrease in the active sites for nonselective hydrogenation, which gives rise to a subsequent improvement in the dispersion of the Au-Pd alloy particles and leads to a complete switching off of the sites for sequential hydrogenation. This effect is probably achieved by Au altering the physical or electronic structure of Pd sufficiently to inhibit its hydrogenation ability. This inhibition is analogous to the observation by Goodman and co-workers (*23*) for Au-Pd model catalysts for the synthesis of vinyl chloride monomer (VCM), where Au promoted the reaction through a slight alteration of the atomic spacing of Pd, which did not affect VCM synthesis but did inhibit its decomposition.

The results above are based on small-scale experiments in a stirred autoclave for short reaction periods (30 min). In a further set of experiments designed to examine the stability of these catalysts, we stirred the pretreated catalyst (100 mg) in the reaction medium (5.6 g MeOH and 2.9 g H_2O) in the presence of the reaction gases (5% H_2/CO_2 and 25% O_2/CO_2 mixed to give a H_2/O_2 mol ratio = 1:2, 3.7 MPa) at 2°C for 98 hours. We then recovered the catalyst that had been aged in this way and carried out the synthesis of H_2O_2 under standard reaction conditions and found that the reactivity and selectivity were identical to that of a fresh catalyst. In addition, the key effect had been retained because the decomposition of H_2O_2 remained switched off in the aged catalyst. We also note from high-angle ADF (HAADF)

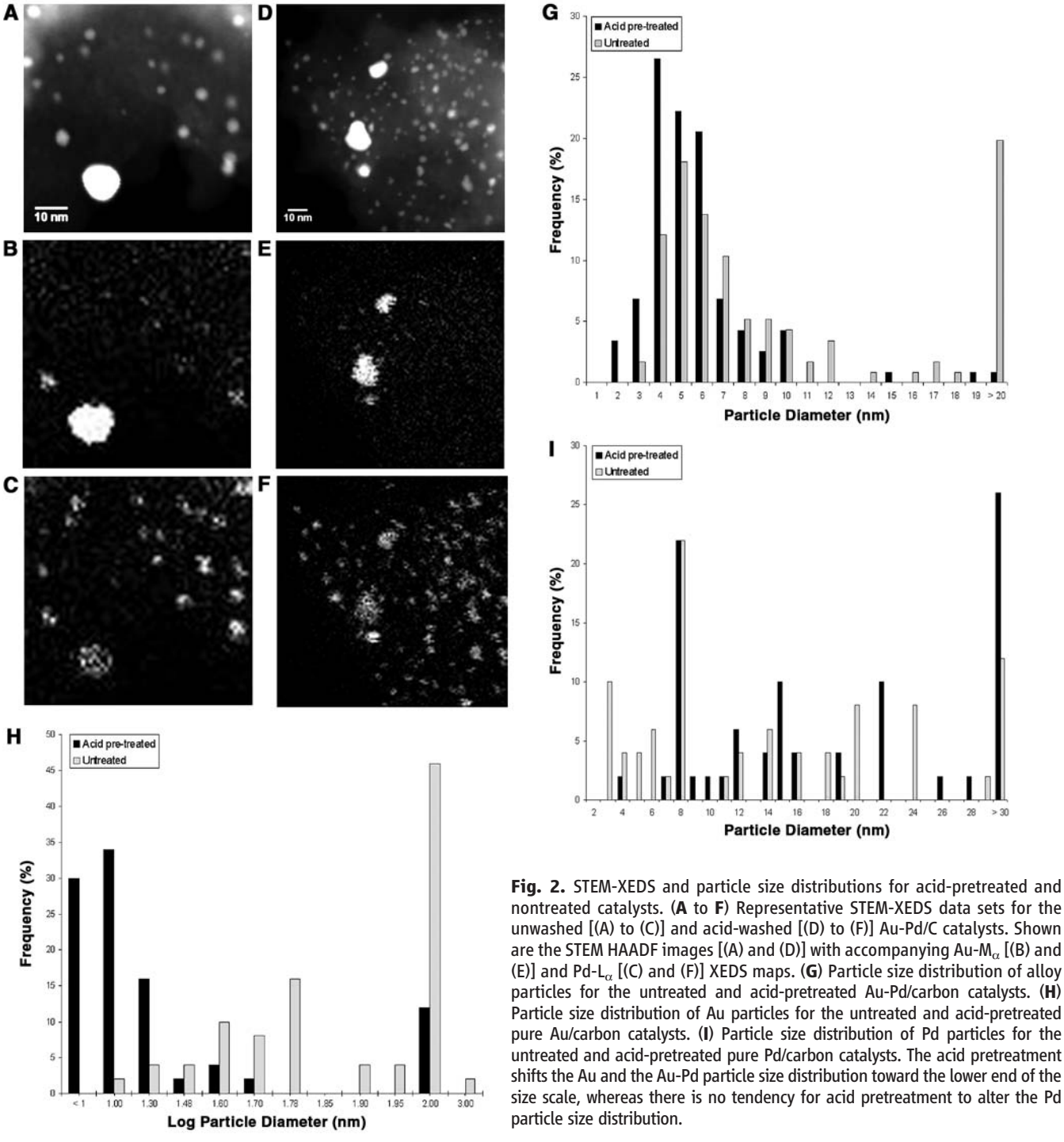

Fig. 2. STEM-XEDS and particle size distributions for acid-pretreated and nontreated catalysts. (**A** to **F**) Representative STEM-XEDS data sets for the unwashed [(A) to (C)] and acid-washed [(D) to (F)] Au-Pd/C catalysts. Shown are the STEM HAADF images [(A) and (D)] with accompanying Au-M_α [(B) and (E)] and Pd-L_α [(C) and (F)] XEDS maps. (**G**) Particle size distribution of alloy particles for the untreated and acid-pretreated Au-Pd/carbon catalysts. (**H**) Particle size distribution of Au particles for the untreated and acid-pretreated pure Au/carbon catalysts. (**I**) Particle size distribution of Pd particles for the untreated and acid-pretreated pure Pd/carbon catalysts. The acid pretreatment shifts the Au and the Au-Pd particle size distribution toward the lower end of the size scale, whereas there is no tendency for acid pretreatment to alter the Pd particle size distribution.

imaging (fig. S5) (*18*) that intermediate and small particles are retained in the catalyst after the 98-hour aging treatment. Hence, the beneficial effect of the acid pretreatment is not short lived. We consider that with appropriate development and reaction engineering (i.e., scaling up using continuous flow reactors with pelleted or extruded catalyst formulations), our discovery, made using powdered catalysts in a small-scale batch autoclave reactor, can underpin the generation of H_2O_2 at the 3 to 8% concentration levels required in most chemical and medical applications

One benefit of the direct process (*24*) is that it will permit local synthesis on a small scale as and when required, thereby ensuring that H_2O_2 no longer needs to be stored or transported, both of which are potentially hazardous, as demonstrated by a recent road tanker explosion in the United Kingdom (*25*). In particular, the process lends itself to small-scale generation of H_2O_2, which could be of great value for the production of medical antiseptics where the H_2 would be generated from water by electrolysis.

References and Notes

1. H. T. Hess *et al.*, Eds., *Kirk-Othmer Encyclopedia of Chemical Engineering* (Wiley, New York, 1995).
2. J. Van Weynbergh, J. P. Schoebrechts, J. C. Colery, U.S. Patent 5447706, (1992).
3. J. H. Lunsford, *J. Catal.* **216**, 455 (2003).
4. D. P. Dissanayake, J. H. Lunsford, *J. Catal.* **206**, 173 (2002).
5. D. P. Dissanayake, J. H. Lunsford, *J. Catal.* **214**, 113 (2003).
6. V. R. Choudhary *et al.*, *Chem. Commun. (Camb.)* **2004**, 2054 (2004).
7. P. Landon *et al.*, *Phys. Chem. Chem. Phys.* **5**, 1917 (2003).
8. J. K. Edwards *et al.*, *J. Mater. Chem.* **15**, 4595 (2005).
9. M. J. Maraschino, U.S. Patent 5169618 (1992).
10. V. R. Choudhary, C. Samanta, *J. Catal.* **238**, 28 (2006).
11. V. R. Choudhary, P. Jana, *J. Catal.* **246**, 434 (2007).
12. V. R. Choudhary *et al.*, *Appl. Catal.* **317**, 234 (2007).
13. J. K. Edwards *et al.*, *Catal. Today* **122**, 397 (2007).
14. B. E. Solsona *et al.*, *Chem. Mater.* **18**, 2689 (2006).
15. J. K. Edwards *et al.*, *Faraday Discuss.* **138**, 225 (2008).
16. J. K. Edwards *et al.*, *J. Catal.* **236**, 69 (2005).
17. J. K. Edwards *et al.*, *Green Chem.* **10**, 388 (2008).
18. Materials and methods are available as supporting material on *Science* Online.
19. A. A. Herzing *et al.*, *Faraday Discuss.* **138**, 337 (2008).
20. Q. Liu *et al.*, *Angew. Chem. Int. Ed.* **47**, 6221 (2008).
21. M. Turner *et al.*, *Nature* **454**, 981 (2008).
22. A. A. Herzing *et al.*, *Science* **321**, 1331 (2008).
23. M. Chen *et al.*, *Science* **310**, 291 (2005).
24. *The Chemical Engineer* **766**, 16 (2005).
25. BBC News, 30 August 2005; http://news.bbc.co.uk/1/hi/england/london/4197500.stm

26. Supported by the Engineering and Physical Sciences Research Council of the United Kingdom and Johnson Matthey PLC (project ATHENA) and the European Union (project AURICAT, HPRN-CT-2002-00174). C.J.K. and A.A.H. are funded by: NSF DMR-0079996, NSF DMR-0304738, and NSF-DMR-0320906. A.A.H. thanks the NRC for support through the postdoctoral associate program. We thank A. Roberts and C. Blomfield (Kratos Analytical) for assistance with XPS measurements, and P. Collier, P. Ellis, and P. Johnston (Johnson Matthey) for discussions on analysis, provision of ICP analysis data, and design of the sequential experiments.

Supporting Online Material

www.sciencemag.org/cgi/content/full/323/5917/1037/DC1
Materials and Methods
SOM Text
Figs. S1 to S5
Table S1

25 November 2008; accepted 9 January 2009
10.1126/science.1168980

Strong Release of Methane on Mars in Northern Summer 2003

Michael J. Mumma,[1]* Geronimo L. Villanueva,[2,3] Robert E. Novak,[4] Tilak Hewagama,[3,5] Boncho P. Bonev,[2,3] Michael A. DiSanti,[3] Avi M. Mandell,[3] Michael D. Smith[3]

Living systems produce more than 90% of Earth's atmospheric methane; the balance is of geochemical origin. On Mars, methane could be a signature of either origin. Using high-dispersion infrared spectrometers at three ground-based telescopes, we measured methane and water vapor simultaneously on Mars over several longitude intervals in northern early and late summer in 2003 and near the vernal equinox in 2006. When present, methane occurred in extended plumes, and the maxima of latitudinal profiles imply that the methane was released from discrete regions. In northern midsummer, the principal plume contained ~19,000 metric tons of methane, and the estimated source strength (≥0.6 kilogram per second) was comparable to that of the massive hydrocarbon seep at Coal Oil Point in Santa Barbara, California.

The atmosphere of Mars is strongly oxidized, composed primarily of carbon dioxide (CO_2, 95.3%), along with minor nitrogen (N_2, 2.7%), carbon monoxide (CO, 0.07%), oxygen (O_2, 0.13%), water vapor (H_2O, 0 to 300 parts per million), and radiogenic argon (1.6%); other species and reduced gases such as methane (CH_4) are rare. CH_4 production by atmospheric chemistry is negligible, and its lifetime against removal by photochemistry is estimated to be several hundred years (*1*–*3*) or shorter if strong oxidants such as peroxides are present in the surface or on airborne dust grains (*4*). Thus, the presence of substantial amounts of CH_4 would require its recent release from subsurface reservoirs; the ultimate origin of this CH_4 is uncertain, but it could be either abiotic or biotic (*2*, *5*, *6*).

Before 2003, all searches for CH_4 were negative (*7*–*9*). Since then, three groups have reported detections of CH_4 (*10*–*18*); see (*19*–*24*) for discussion. Spectral data from the Mars Express mission contain five unidentified spectral features between 3000 and 3030 cm^{-1}, one of which coincides with the expected position of the CH_4 Q branch (*15*, *18*, *25*). The data span all seasons and extend over several years, but low S/N ratios require averaging the spectra over two of the three key dimensions (longitude, latitude, and time). Other searches featured low spatial coverage (*16*) or sparse seasonal coverage (*16*, *17*), and the results (CH_4 mixing ratios) are best interpreted as upper limits.

We report measurements of CH_4 in northern summer in 2003 and estimate its source strength and its (short) destruction lifetime. Our search covered about 90% of the planet's surface and spanned 3 Mars years (MYs) (7 Earth years). Our results (*10*–*14*) are based on the simultaneous detection of multiple spectrally resolved lines of CH_4, and each observation is spatially resolved, allowing examination of spatial and temporal effects. Our spatial maps reveal local sources and seasonal variations.

To search for CH_4 and other gases on Mars, we used the high-dispersion infrared spectrometers at three ground-based telescopes. Here we report data from CSHELL/IRTF (Hawaii) and NIRSPEC/Keck-2 (Hawaii) [supporting online material text 1 (SOM-1)]. Each spectrometer features a long entrance slit that is held to the central meridian of Mars (Fig. 1A) while spectra are taken sequentially in time (fig. S1). Pixelated spectra were acquired simultaneously at contiguous positions along the entire slit length, for each observation, providing 35 spectra at 0.2–arc second (arc sec) intervals (~195 km at disk center) when Mars' diameter is 7 arc sec (Fig. 1A). We binned these data (in groups of three along the slit) to provide latitudinally resolved spectra, and then in time (longitude) to improve the S/N ratio (SOM-1). Here we focus on three dates in 2003 [universal time (UT) 12 January, 19 March, and 20 March] and one in 2006 (UT 26 February) (Table 1).

Our spectra exhibit strong lines of terrestrial H_2O ($2\nu_2$ band) and CH_4 (ν_3) along with weaker lines of O_3 ($3\nu_3$) seen against the continuum (Fig. 1, B and C, top). We corrected the data for telluric extinction (SOM-2). At 3.3 μm, Mars is seen mainly in reflected sunlight, so the collected spectra also contain Fraunhofer lines (SOM-3). Removing these two components from a composite spectrum exposed the residual Mars atmospheric spectrum (Fig. 1, B and C) (*26*). One line of CH_4 and three distinct lines of H_2O are seen in each panel.

CH_4 consists of three separate nuclear spin species (A, E, and F) that act as independent

[1]NASA Goddard Space Flight Center, Mailstop 690.3, Greenbelt, MD 20771, USA. [2]Department of Physics, Catholic University of America, Washington, DC 20008, USA. [3]NASA Goddard Space Flight Center, Mailstop 693, Greenbelt, MD 20771, USA. [4]Department of Physics, Iona College, New Rochelle, NY 10801, USA. [5]Department of Astronomy, University of Maryland, College Park, MD 20742–2421, USA.

*To whom correspondence should be addressed. E-mail: michael.j.mumma@nasa.gov

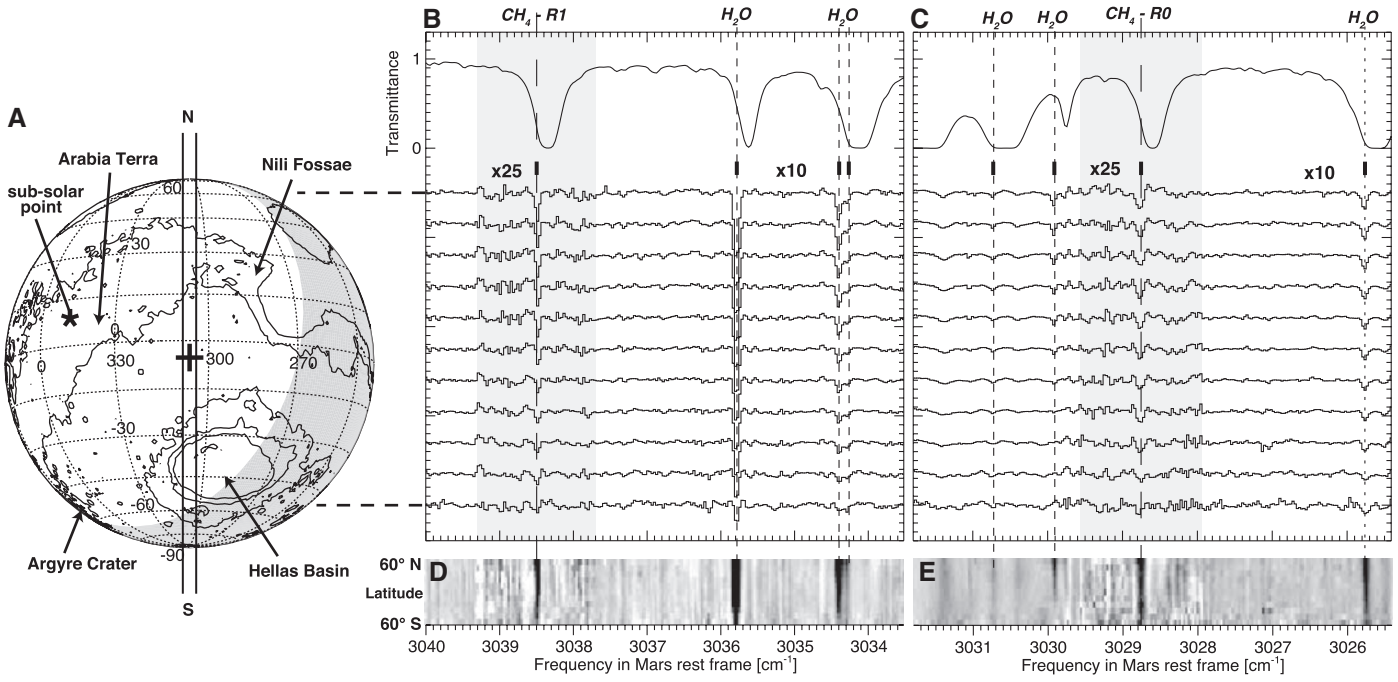

Fig. 1. Detections of CH_4 and water vapor on Mars on UT 19 and 20 March 2003. (**A**) Mars is shown as it appeared at the mean time of the R0 and R1 observations (Table 1). The subsolar (*) and sub-Earth (+) points are marked, along with several prominent features. Contours of constant altitude are shown at intervals of 3 km, and regions beyond the afternoon terminator (the night side) appear in gray. The entrance slit of the spectrometer was oriented north-south (N-S) on Mars along the central meridian and is shown to scale. (**B**) Spectra taken on 20 March were extracted at 11 equal intervals (0.6 arc sec each) along the slit (ranging from 70°N to 70°S), after binning over longitudes 277° to 323°W. At the sub-Earth position, the binned spectrum samples a footprint 3215 km (east-west) by 586 km (N-S) (see text and SOM-1). Strong lines of terrestrial water and CH_4 (labeled) and weak lines of ozone (3036 to 3038 cm^{-1}) appear in a typical spectrum, shown at the top of this panel. See SOM-3 for data reduction. Narrow spectral lines of H_2O (three lines, short dashes) and CH_4 (the R1 line, long dashes) are seen at the Doppler-shifted positions expected for this date. Corresponding Mars ozone (O_3) absorptions for this date are weak and would appear in the southern polar region (not sampled). (**C**) Spectra taken on 19 March are shown as in (B) but binned over the longitude range from 289° to 335°. Spectral lines of H_2O (three lines, short dashes) and CH_4 (the R0 line, long dashes) are seen. The longitude range sampled was systematically westward (by 12°) of that sampled for R1 (Table 1), owing to the slower rotation of Mars relative to Earth. The residual spectra shown in (B) and (C) are scaled by a factor of either 10 or 25 (gray background), to make the lines more apparent. (**D** and **E**) show residual intensities in a grayscale format, to more easily show the spatial distribution of the gases with latitude. The lines are displayed as measured; that is, corrections for two-way air mass on Mars (Sun to Mars surface and Mars surface to Earth), for Mars local topography, and for terrestrial transmittance have not yet been applied to the residuals (see Fig. 2).

spectral entities. The identification of two spectrally resolved CH_4 lines (R0 and R1, of the A and F species, respectively) and the good agreement (within measurement error) of the CH_4 column densities obtained independently from each line support our detection (systematic uncertainty and stochastic errors are discussed in SOM-2 and SOM-3). At a later season [areocentric longitude of the Sun (L_s) = 220°], we detected the P2 doublet, consisting of lines of the E and F species (SOM-1 and fig. S2). Detections (or upper limits) reported by others are based on the intensity summed over the frequencies of multiple unresolved lines [the Q branch (*15*, *18*)] or on the summed intensity of several undetected individual lines (*16*, *17*).

Column densities and mixing ratios for CH_4 obtained from the spectra of Fig. 1 show a broad CH_4 plume in late summer when averaged over 46° in longitude (Fig. 2, A and B) (SOM-3); more restricted longitudinal binning shows higher maxima (Fig. 2C, profile d). In early spring (profile a), the CH_4 mixing ratio was small at all latitudes and showed only a hint of the marked maximum seen in late summer. By early summer (profiles b and c), CH_4 was prominent but the maximum mixing ratio occurred at more northerly latitudes and was somewhat smaller than in late summer. The late summer profile (d) in Fig. 2C differs from the profile shown in Fig. 2B, owing to different longitudinal binning (*27*). The mixing ratios shown in Fig. 2C (profile d) represent a subset of the data of Fig. 1B, centered at central meridian longitude (CML) 310° (see aspect, Fig. 1A) and binned over only 30 min. Including the slit width, 30-min binning provides a footprint at the sub-Earth point that spans ~16° (948 km) in longitude and 10° (586 km) in latitude (fig. S1 and Table 1).

A quantitative release rate can be inferred by considering the observed temporal changes (with season) and measured spatial profiles. The summer mixing ratios (profiles b, c, and d) show a

Table 1. Observational searches for Mars CH_4 on selected dates. A complete listing of all dates searched, spanning 7 years, is available from the authors.

Date and observation range (UT)	Mars season (L_s, °)	Longitude range (CML, °)	Doppler shift (km s^{-1})	CH_4 line searched	Footprint* (°longitude by °latitude)
2003 – MY 26					
11 January 19:36–20:34	121.5	274–288	–14.7	R1	22° × 14°
12 January 17:20–20:18	121.9	231–274	–15.0	R1	22° × 14°
13 January 17:05–20:07	122.4	218–262	–15.0	R0	22° × 14°
19 March 15:41–18:50	154.5	289–335	–15.7	R0	16° × 10°
20 March 15:34–18:44	155.0	277–323	–15.6	R1	16° × 10°
2006 – MY 27 to 28					
16 January 04:49–07:03†	357.3	303–336	+16.1	R0, R1	
26 February 01:28–02:53	17.2	223–244	+17.1	R1	13° × 10°

*Centered on the sub-Earth point, binned over 30 min in time and 0.6 arc sec along the slit. †Using NIRSPEC/Keck-2 (SOM-3); all other listed observations used CSHELL/IRTF.

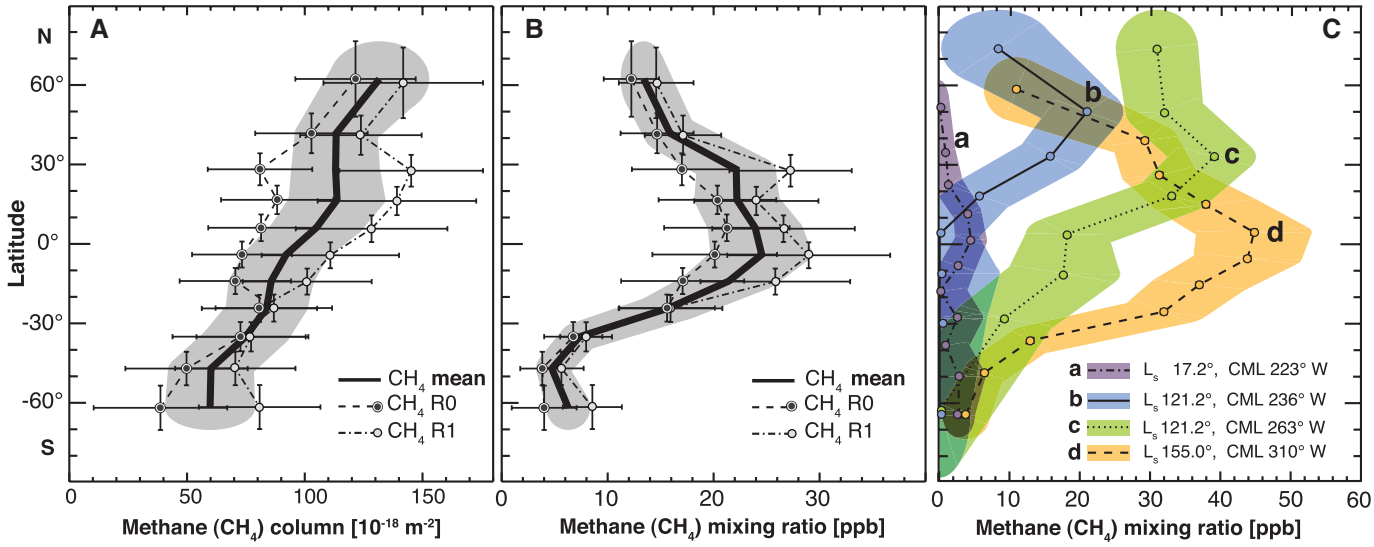

Fig. 2. Absolute abundances, spatial profiles, and seasonal changes of CH_4 on Mars. (**A**) The total CH_4 column density (in molecules per square meter) along a two-way path (Sun to Mars surface and Mars surface to Earth) needed to reproduce the measured lines (after correcting for terrestrial transmittance, SOM-2). The R0 (Fig. 1C) and R1 (Fig. 1B) lines were analyzed independently for a range of longitudes that spanned 46° but differed by 12° in mean longitude (312° for R0 versus 300° for R1, Table 1). The apparent differences in CH_4 column density seen at low latitudes (30°N to 15°S) reflect (in part) differences in mean topography sampled on the two dates. The confidence limits contain both systematic uncertainty and random error; the systematic uncertainty affects all extracted values in the same way whereas the random error introduces scatter among the individual points (SOM-2 and SOM-3). (**B**) The local mixing ratio (in parts per billion) of CH_4 obtained from the column density (A) in each footprint, after correcting for two-way air mass on Mars and for topography (SOM-3). The mixing ratios derived from R0 and R1 of CH_4 agree, within confidence limits. The remaining systematic difference at low latitudes is consistent with stronger weighting of local sources (Fig. 3) on 20 March (R1), when the longitude range sampled was more nearly centered over them. The differences in mixing ratio (R0 versus R1) should then have decreased with increasing distance from the source or sources, as they did (compare values at 60°N, 40°N, and 25°S, 35°S, 47°S, and 62°S). (**C**) Geographic and temporal variability of Mars CH_4. Latitudinal profiles of CH_4 mixing ratios for different longitudes and seasons are shown; the width of the color envelope represents the $\pm 1\sigma$ confidence envelope. The areocentric seasons (L_s) are early northern spring (a: 17°), early northern summer (b and c: 122°), and late northern summer (d: 155°) (Table 1). These extracts are taken from spectra centered at the indicated longitude (CML), and the sub-Earth footprints span longitude-latitude ranges (Table 1) with these physical dimensions: a, 770 km × 535 km; b and c, 1274 km × 818 km; d, 948 km × 586 km. The mixing ratios shown in profile d are larger than those shown in Fig. 2B, owing to different longitudinal binning, and they reflect the longitudinal maximum of the plume (SOM-1, figs. S1 and S6, and Fig. 3).

clear maximum for each north-south spatial profile (Fig. 2C). Moving southward by about 30° from the latitude of the peak, the mixing ratio decreased by a factor of 2 in each case, and for profile d the northward gradient was similar to the southward one. These latitudinal gradients suggest that there was a local source or sources and the resulting plume or plumes were being dispersed by atmospheric circulation.

We consider the dimension of the hypothesized CH_4 plume to be about 60° in latitude [full width at half maximum (FWHM); Fig. 2C, profile d] and assume a similar dimension in longitude. The latter view is weakly supported by profiles b and c, which differ by 27° in central longitude and by a factor of 2 in peak mixing ratio. It is also supported by the profile formed by binning over 46° in longitude (277° to 323°, Fig. 2B), which has a peak mixing ratio [24 parts per billion (ppb)] reduced by a factor of 2 from the peak value (45 ppb) obtained when binning over only 16° of longitude (302° to 318°, Fig. 2C, profile d). The slight increase of profile d near 40° N is consistent with enhanced CH_4 (perhaps owing to continued release at that latitude; compare profiles b and c), whereas the slight increase in profile c near 15°S suggests a small contribution from a source to the west (compare peak position, profile d). Together, these profiles suggest that there may be two local source regions, the first centered near 30°N, 260°W and the second near 0°, 310°W. The vapor plume from each is consistent with ~60° in both latitude and longitude.

The amount of trace gas present in each plume can be estimated from these parameters (SOM-4). In the central plume of profile d (FWHM diameter ~60°), the mean CH_4 mixing ratio is ~33 ppb (120 mol km^{-2}), and the plume contains ~1.17×10^9 mol of CH_4 (~1.86×10^7 kg, or ~19,000 metric tons). If seasonally controlled, the duration of release must be substantially shorter than 0.5 MYs, requiring a mean CH_4 release rate of ≥39 mol s^{-1} (≥0.63 kg s^{-1}). For comparison, the massive hydrocarbon seep field at Coal Oil Point in Santa Barbara, California, releases CH_4 at a rate of ~0.4 to 1.0 kg s^{-1} (*28*).

We considered three models for plume formation, to constrain aspects of CH_4 release and its migration in latitude and longitude (SOM-5). A model based on release from a central source region coupled with eddy diffusion fits the observed plume parameters. Models of meridional flow using a global circulation model suggest that released gas would move northward by ~3.3 cm s^{-1} at this season (*29*), for a total displacement by not more than ~170 km from its central source. If the mixing coefficients (K_x and K_y) in zonal and meridional directions are identical (K_h), a steady source would fill the plume (profile d) in 60 days if $K_h \sim 6.4 \times 10^8$ cm^2 s^{-1}. For this case, the required source strength would be ~3.66 kg s^{-1}. The filling time and K_h vary inversely, whereas K_h and source strength vary proportionately. For a filling time of 0.5 MYs (~344 Earth days), $K_h \sim 1.1 \times 10^8$ cm^2 s^{-1} and the source strength is ~0.63 kg s^{-1}. A reasonable limit for filling time (<120 days) requires $K_h \sim 3.2 \times 10^8$ cm^2 s^{-1} and source strength ~1.8 kg s^{-1}.

These parameters are consistent with release from a single central source region, followed by efficient eddy mixing (SOM-5). The central source could be activated thermally by warming of a surface zone, or by connecting subpermafrost regions to the atmosphere through seasonally opened pores in scarps or crater walls. The plume would reflect the gross morphology of active release zones (and their intensity), and the peak could suggest a region of enhanced release. For comparison, the subsolar latitude was 24°N at L_s = 122° (compare profiles b and c) and 10°N for L_s = 155° (profile d).

Additional information is obtained from a high-resolution map constructed from our data for mid-summer 2003 (Fig. 3 and fig. S1). CH_4 appears notably enriched over several localized areas: A (east of Arabia Terra, where we also measure greatly enriched water vapor), B_1 (Nili Fossae), and B_2 (the southeast quadrant of Syrtis Major). Unusual enrichments in hydrated minerals (phyllosilicates)

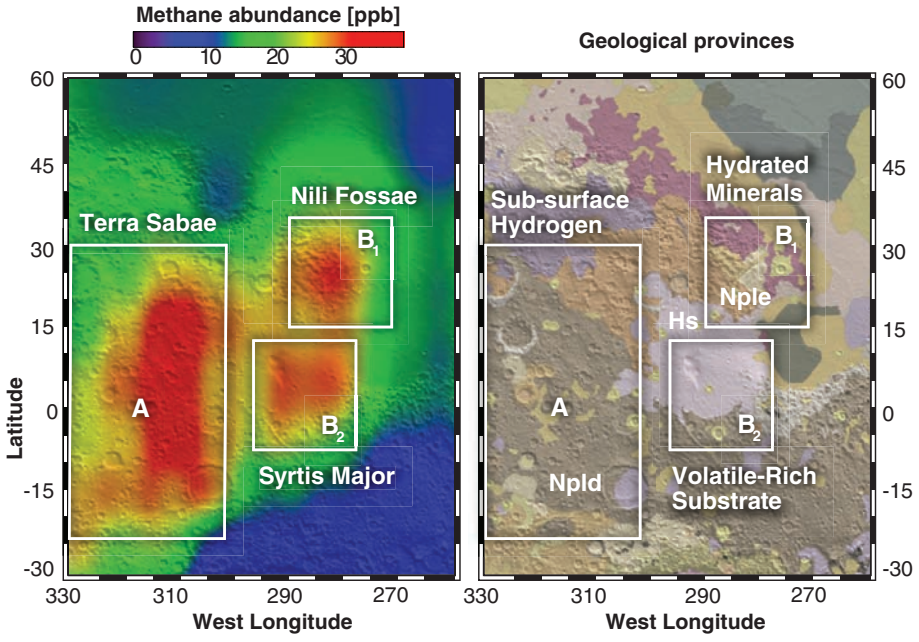

Fig. 3. Regions where CH_4 appears notably localized in northern summer (A, B_1, and B_2) and their relationship to mineralogical and geomorphological domains. (**A**) Observations of CH_4 near the Syrtis Major volcanic district. (**B**) Geologic map of Greeley and Guest (*45*) superimposed on the topographic shaded relief from the Mars Orbiter Laser Altimeter (*46*). The most ancient terrain units are dissected and etched Noachian plains (Npld and Nple) (~3.6 to 4.5 billion years old, when Mars was wet) and are overlain by volcanic deposits from Syrtis Major of Hesperian (Hs) age (~3.1 to 3.6 billion years old).

were identified in Nili Fossae by Mars Express (*30*, *31*) and by the Mars Reconnaissance Orbiter (*32*) (Fig. 3). The observed morphology and mineralogy (*33*, *34*) of this region suggest that these bedrock outcrops, rich in hydrated minerals, might be connecting with reservoirs of buried material rich in volatile species. The characteristic arcuate ridges in the southeast quadrant of Syrtis Major were interpreted as consistent with catastrophic collapse of that quadrant, from interaction with a volatile-rich substrate (*34*).

The low mean abundance measured in early spring 2006 (profile a) provides an important constraint on the CH_4 lifetime. The plume seen in March 2003 (19,000 tons, Fig. 2C, profile d) implies a global mean mixing ratio of ~2 ppb, if later spread uniformly over the planet. The content of the central plume of profile c is similar. Combining data for the entire region mapped during northern summer brings the total CH_4 to 42,000 tons, or 6 ppb if spread uniformly over the planet. However, the mean mixing ratio displayed in the early spring equinox in 2006 (profile a, Fig. 2C) was only 3 ppb (SOM-3). If CH_4 is not removed by other means, the implied destruction lifetime is ~4 Earth years if the 2003 event was singular, to as little as ~0.6 Earth years if the event repeats each MY. In either case, the destruction lifetime for CH_4 is much shorter than the time scale (~350 years) estimated for photochemical destruction (*16*). Another process thus must dominate removal of atmospheric CH_4 on Mars, and it must be more efficient than photochemistry by a factor ≥100.

Heterogeneous (gas-grain) chemistry is a strong candidate. The presence of strong oxidants in the soil was suggested first by the labeled-release experiment on Viking landers, and laboratory simulations suggested that peroxides (such as H_2O_2) were responsible; the apparent discovery of perchlorate ($XClO_4$) by the Phoenix lander (*35*, *36*) suggests the existence of another family of strong oxidants, although their presence at low latitudes has not been established. The lofting of oxidant-coated soil particles into the atmosphere could permit rapid oxidation of the CH_4 that collides with them. H_2O_2 is also produced photochemically and is a known trace gas in the atmosphere (*37*) and (being polar) might bind to aerosol surfaces. Electrochemical processes in dust storms may produce additional peroxide efficiently (*4*, *6*, *23*, *24*) (SOM-6). Peroxide-coated grains might provide an efficient sink for CH_4 for many years thereafter if they settle to the surface and are sequestered in the regolith (*6*, *24*). Sequestered oxidants should also efficiently destroy upward-diffusing CH_4, reducing the fraction that might escape to the atmosphere.

The most compelling question relates to the origin of CH_4 on Mars. The CH_4 we detected is of unknown age—its origin could be ancient (*38*) or perhaps recent. Both geochemical and biological origins have been explored, but no consensus has emerged. Most theses draw on known terrestrial analogs such as production in magma (*19*, *20*) or serpentinization of basalt (*39*), or production by psychrophilic methanogenic biota in Mars-analog cryoregimes such as permafrost (*21*). The annual release of CH_4 from an arctic tundra landscape on Earth (at 72°N) was measured to be 3.15 g m^{-2}, with midsummer CH_4 fluxes of typically 30 mg m^{-2} day^{-1} (*40*). If similar release rates applied to our midsummer plume, the tundra-equivalent area of (assumed uniform) release would be ~6000 km^2 compared with a plume footprint ~9.7×10^6 km^2. If CH_4 release were uniform over the plume footprint, the mean release rate could be smaller than the arctic rate by a factor of ~1600.

Of special interest are the deep biocommunities that reduce sulfate to sulfide using H_2 or abiotic CH_4 as the electron donor, releasing H_2S. These communities thrive at depths of 2 to 3 km in the Witwatersrand Basin of South Africa and have been isolated from the surface (and photosynthesis) for tens of millions of years (*41*, *42*). It might be possible for analogous biota (methanogens or methanotrophs) to survive for eons below the cryosphere boundary on Mars, where water is again liquid, radiolysis can supply energy, and CO_2 can provide a carbon source. Gases accumulated in such zones might be released to the atmosphere if pores or fissures open seasonally, connecting these deep zones to the atmosphere at scarps, crater walls, or canyons. The location of CH_4 maxima over the Syrtis Major shield volcano and the nearby Nili Fossae district suggests a possible relation to serpentinization and/or to the phyllosilicates discovered there (*43*, *44*).

References and Notes

1. H. Nair, M. Allen, A. D. Anbar, Y. L. Yung, R. T. Clancy, *Icarus* **111**, 124 (1994).
2. M. E. Summers, B. J. Lieb, E. Chapman, Y. L. Yung, *Geophys. Res. Lett.* **29**, 2171 (2002).
3. A.-S. Wong, S. K. Atreya, T. Encrenaz, *J. Geophys. Res. Planets* **108**, 7 (2003).
4. S. K. Atreya *et al.*, *Astrobiology* **6**, 439 (2006).
5. R. E. Pellenbarg, M. D. Max, S. M. Clifford, *J. Geophys. Res. Planets* **108**, GDS 23-1 (2003).
6. S. K. Atreya, P. R. Mahaffy, A.-S. Wong, *Planet. Space Sci.* **55**, 358 (2007).
7. W. C. Maguire, *Icarus* **32**, 85 (1977).
8. V. A. Krasnopolsky, G. L. Bjoraker, M. J. Mumma, D. E. Jennings, *J. Geophys. Res.* **102**, 6525 (1997).
9. M. Lellouch *et al.*, *Planet. Space Sci.* **48**, 1393 (2000).
10. M. J. Mumma *et al.*, *Bull. Am. Astron. Soc.* **35**, 937 (2003).
11. M. J. Mumma *et al.*, *Bull. Am. Astron. Soc.* **36**, 1127 (2004).
12. M. J. Mumma *et al.*, *Bull. Am. Astron. Soc.* **37**, 669 (2005).
13. M. J. Mumma *et al.*, *Bull. Am. Astron. Soc.* **39**, 471 (2007).
14. M. J. Mumma *et al.*, *Bull. Am. Astron. Soc.* **40**, 396 (2008).
15. V. Formisano, S. Atreya, T. Encrenaz, N. Ignatiev, M. Giuranna, *Science* **306**, 1758 (2004).
16. V. A. Krasnopolsky, J. P. Maillard, T. C. Owen, *Icarus* **172**, 537 (2004).
17. V. A. Krasnopolsky, *Icarus* **190**, 93 (2007).
18. A. Geminale, V. Formisano, M. Giuranna, *Planet. Space Sci.* **56**, 1194 (2008).
19. J. R. Lyons, C. E. Manning, C. E. Nimmo, *Geophys. Res. Lett.* **32**, L13201 (2005).
20. C. Oze, M. Sharma, *Geophys. Res. Lett.* **32**, L10203 (2005).
21. T. C. Onstott *et al.*, *Astrobiology* **6**, 377 (2006).
22. V. A. Krasnopolsky, *Icarus* **180**, 359 (2006).
23. W. M. Farrell, G. T. Delory, S. K. Atreya, *Geophys. Res. Lett.* **33**, L21203 (2006).
24. G. T. Delory *et al.*, *Astrobiology* **6**, 451 (2006).
25. V. Formisano *et al.*, *Planet. Space Sci.* **53**, 1043 (2005).
26. G. L. Villanueva, M. J. Mumma, R. E. Novak, T. Hewagama, *Icarus* **195**, 34 (2008).

27. We binned spectra over 46° of longitude (centered at CML 300°) for Fig. 1, B and C (and Fig. 2, A and B), but over only 16° for Fig. 2C. Profile d is centered at CML 310°, leading to lower mean mixing ratios in Fig. 2B as compared with Fig. 2C (profile d). See detailed map in Fig. 3.
28. S. Mau *et al.*, *Geophys. Res. Lett.* **34**, L22603 (2007).
29. M. A. Mischna, M. I. Richardson, R. J. Wilson, D. J. McCleese, *J. Geophys. Res.* **108**, 5062 (2003).
30. F. Poulet *et al.*, *Nature* **438**, 623 (2005).
31. J. P. Bibring *et al.*, *Science* **312**, 400 (2006).
32. J. F. Mustard *et al.*, *Nature* **454**, 305 (2008).
33. H. Hiesinger, J. W. Head III, *J. Geophys. Res.* **109**, E01004 (2004).
34. D. Baratoux *et al.*, *J. Geophys. Res.* **112**, E08S05 (2007).
35. M. H. Hecht *et al.*, *Eos* **89**, *Fall Meeting Suppl.*, U14A-04 (abstr.) (2008).
36. S. P. Kounaves *et al.*, *Eos* **89**, *Fall Meeting Suppl.*, U14A-05 (abstr.) (2008).
37. T. Encrenaz *et al.*, *Icarus* **195**, 547 (2008).
38. M. D. Max, S. M. Clifford, *J. Geophys. Res.* **105**, 4165 (2000).
39. D. S. Kelley *et al.*, *Science* **307**, 1428 (2005).
40. C. Wille, L. Kutzbach, T. Sachs, D. Wagner, E.-M. Pfeiffer, *Glob. Change Biol.* **14**, 1395 (2008).
41. T. C. Onstott *et al.*, *Geomicrobiol. J.* **23**, 369 (2006).
42. L.-H. Lin *et al.*, *Science* **314**, 479 (2006).
43. J.-P. Bibring *et al.*, *Science* **312**, 400 (2006).
44. J. F. Mustard *et al.*, *Nature* **454**, 305 (2008).
45. R. Greeley, J. E. Guest, *U.S. Geol. Surv. Map I-1802-B* (1987).
46. D. E. Smith *et al.*, *J. Geophys. Res.* **106**, 23689 (2001).
47. We thank T. C. Onstott and L. M. Pratt for helpful comments and two anonymous referees for their comments and suggestions. This work was supported by NASA [the Planetary Astronomy Program (RTOP 344-32-07 to M.J.M), Astrobiology Institute (RTOP 344-53-51, to M.J.M), and Postdoctoral Program (G.L.V.)] and by NSF (Research at Undergraduate Institutions Program AST-0505765 to R.E.N.). We thank the director and staff of NASA's InfraRed Telescope Facility (operated for NASA by the University of Hawaii) for exceptional support throughout our long Mars observing program. Data were also obtained at the W. M. Keck Observatory, operated as a scientific partnership by CalTech, the University of California Los Angeles, and NASA.

Supporting Online Material

www.sciencemag.org/cgi/content/full/1165243/DC1
SOM Text
Figs. S1 to S6
References and Notes

28 August 2008; accepted 6 January 2009
Published online 15 January 2009;
10.1126/science.1165243
Include this information when citing this paper.

Isotopic Evidence for an Aerobic Nitrogen Cycle in the Latest Archean

Jessica Garvin,[1] Roger Buick,[1]* Ariel D. Anbar,[2,3] Gail L. Arnold,[2] Alan J. Kaufman[4]

The nitrogen cycle provides essential nutrients to the biosphere, but its antiquity in modern form is unclear. In a drill core though homogeneous organic-rich shale in the 2.5-billion-year-old Mount McRae Shale, Australia, nitrogen isotope values vary from +1.0 to +7.5 per mil (‰) and back to +2.5‰ over ~30 meters. These changes evidently record a transient departure from a largely anaerobic to an aerobic nitrogen cycle complete with nitrification and denitrification. Complementary molybdenum abundance and sulfur isotopic values suggest that nitrification occurred in response to a small increase in surface-ocean oxygenation. These data imply that nitrifying and denitrifying microbes had already evolved by the late Archean and were present before oxygen first began to accumulate in the atmosphere.

All living organisms require fixed nitrogen for the synthesis of vital biomolecules, such as proteins and nucleic acids. Under low-oxygen conditions, nitrogen-fixing organisms meet this need by reducing dinitrogen gas (N_2) to ammonium (NH_4^+), which is readily incorporated into organic matter. All other organisms rely upon the degradation of N_2 fixers through ammonification to fulfill their nitrogen requirements. Although the evolved NH_4^+ is stable under anoxic conditions, the presence of O_2 in the surface ocean promotes nitrification, the microbial oxidation of NH_4^+ to nitrite (NO_2^-) or nitrate (NO_3^-). These oxidized species are either assimilated by organisms or, under low-oxygen conditions, biologically reduced and ultimately released to the atmosphere. The latter process provides a conduit for loss of fixed N from the ocean and proceeds via denitrification, the stepwise reduction of NO_3^- or NO_2^- to NO, N_2O, and finally N_2, or by anammox, the coupling of NH_4^+ oxidation to NO_2^- reduction. Because unique isotopic fractionations are imparted during many of these transformations, the nitrogen isotopic composition $\delta^{15}N$ (*1*) of organic matter preserved in ancient sediments provides information about the evolution of the N cycle. Here we report $\delta^{15}N$ and total nitrogen (TN) measurements, as well as $\delta^{13}C_{org}$ and total organic carbon (TOC) data, obtained at a resolution of approximately one data point per meter from ~100 m of continuous drill core through the ~2.5–billion-year-old Mount McRae Shale, Hamersley Group, Western Australia (*2*).

If the fixed N reservoir is a steady-state system, the $\delta^{15}N$ of fixed N input and output will be equal ($\delta^{15}N_{input} = \delta^{15}N_{output}$). The isotope effect ε (*3*) imparted during fixed N input is approximated by the difference in $\delta^{15}N$ between the atmospheric N_2 source and the fixed N product ($\varepsilon_{input} = \delta^{15}N_{dinitrogen} - \delta^{15}N_{input}$, where $\delta^{15}N_{dinitrogen} = 0$‰), whereas that of the fixed N output is approximated by the difference in $\delta^{15}N$ between the oceanic fixed N source and the N_2 product ($\varepsilon_{output} = \delta^{15}N_{fixed\ N} - \delta^{15}N_{output}$). Thus, the mean $\delta^{15}N$ of oceanic fixed N is roughly equal to the difference in ε between the output and input processes ($\delta^{15}N_{fixed\ N} = \varepsilon_{output} - \varepsilon_{input}$). In the modern ocean, N_2 fixation is the primary source of fixed N, and denitrification the primary sink. Although fractionation during N_2 fixation is minimal, with $\varepsilon_{N_2\ fixation} = -3$ to +4‰ (*4*, *5*), the isotope effect of denitrification from both NO_3^- and NO_2^- is large, with $\varepsilon_{denitrification} = +20$ to +30‰ (*4*). This results in a residual NO_3^- pool substantially enriched in ^{15}N. Thus, the +5‰ mean isotopic value of modern deep-ocean NO_3^- is attributed to the fractionation imparted during denitrification. Furthermore, because fixed N upwelled to the surface ocean is completely consumed by primary producers under most conditions (*6*), the $\delta^{15}N$ value of organic matter in well-preserved ancient sediments should record the mean $\delta^{15}N$ of oceanic fixed N.

The organic-rich Mount McRae Shale was deposited at 2.5 billion years ago (Ga), shortly before the main rise in O_2 2.45 to 2.22 Ga (*7*). Its geological setting, the sampling procedure, and analytical methods are described in the Supporting Online Material. In the lower portion of the sampled section (Fig. 1), $\delta^{15}N$ values average around +2.5‰ with relatively little variation (+1.3 to +3.8‰). They rise from +1.0‰ at ~161 m to a peak of +7.5‰ at 139 m, then fall back to +2.5‰. The rise in $\delta^{15}N$ roughly correlates with an enrichment in TOC between 153 and 126 m, from 3 to 16 weight percent (wt %). Additionally, atomic C/N ratios increase from ~150 to ~65 from base to top. $\delta^{13}C_{org}$ values vary little below 150 m, consistently falling between –36 and –42‰. There is no $\delta^{13}C_{org}$ excursion corresponding to the $\delta^{15}N$ spike. Instead, $\delta^{13}C_{org}$ values rise from –42 to –34‰ above 134 m, corresponding to a decrease in $\delta^{15}N$ values.

Given the low metamorphic grade (prehnite-pumpellyite facies to < 300°C) of the Mount McRae Shale (*8*), preferential $^{14}NH_4^+$ loss during high-temperature devolatilization should not have greatly affected $\delta^{15}N$ preservation (*9*). The direct relation between TN and $\delta^{15}N$ (Fig. 1) further supports minimal metamorphic $\delta^{15}N$ alteration because $^{14}NH_4^+$ loss would produce the opposite relation. The relatively high C/N ratios are typical of Precambrian organic matter (*10*) and reflect preferential degradation of organic N during diagenesis. The C/N decrease upsection may result from increased adsorption of diagenetically produced NH_4^+ onto clay minerals or its substitution for K^+ in K-bearing minerals. If so, the lack of covariation between $\delta^{15}N$ values and C/N ratios implies that diagenetic $\delta^{15}N$ alteration was

[1]Department of Earth and Space Sciences and Astrobiology Program, University of Washington, Seattle, WA 98195–1310, USA. [2]School of Earth and Space Exploration, Arizona State University, Tempe, AZ 85287, USA. [3]Department of Chemistry and Biochemistry, Arizona State University, Tempe, AZ 85287, USA. [4]Department of Geology, University of Maryland, College Park, MD 20742, USA.

*To whom correspondence should be addressed. E-mail: buick@ess.washington.edu

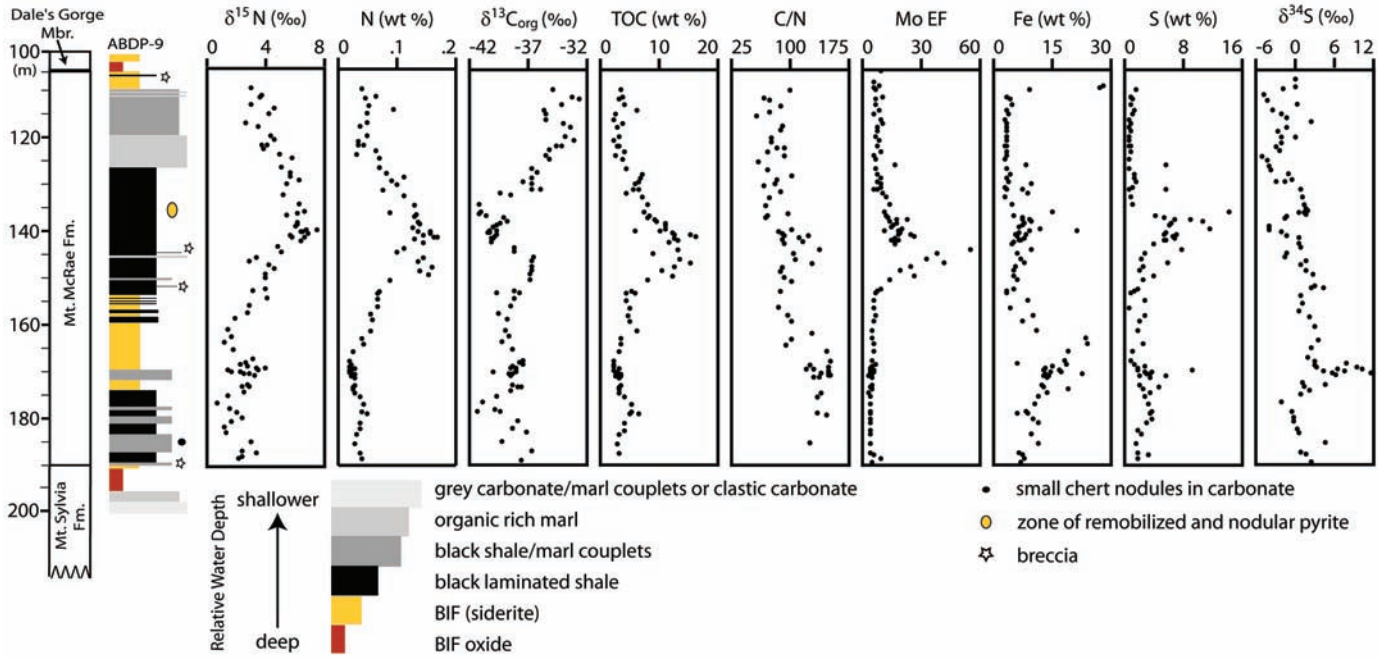

Fig. 1. Geochemistry of the Mount McRae stratigraphic section, including $\delta^{15}N$, TN, $\delta^{13}C_{org}$, TOC, atomic C/N, Fe and Mo enrichments, wt % S, and $\delta^{34}S$.

minimal. Furthermore, where bottom-water O_2 is low in the modern ocean, as it was during Mount McRae Shale deposition, there is little difference between the $\delta^{15}N$ of the original organic matter and that of diagenetically produced NH_4^+ (*11*). Thus, the $\delta^{15}N$ recorded in the Mount McRae kerogenous shales probably reflects the mean $\delta^{15}N$ of primary-producer biomass.

The $\delta^{15}N$ average of +2.5‰ below 161 m is less than the mean value of fixed N in the modern ocean (+5‰), indicating that little fractionation was imparted during fixed N input and output. This could reflect an environment similar to modern stratified basins where nitrification and denitrification are active and $\varepsilon_{denitrification}$ is underexpressed because NO_3^- is completely consumed at the oxic/anoxic interface (*12*). However, nitrification requires environmental O_2, but there is no evidence for its presence in this part of the core. In particular, the low amounts of sedimentary Mo below 161 m (despite high S and TOC contents, which should sequester any Mo if available) suggest that oxidative weathering of Mo-bearing sulfides in continental crust or detrital sediments was not active (*13*), precluding large amounts of atmospheric or oceanic O_2. Thus, it is more likely that the low $\delta^{15}N$ values below 161 m represent an anoxic N cycle with little fractionation imparted during microbial N_2 fixation and negligible fixed N loss (Fig. 2A).

The rise in $\delta^{15}N$ values to modern ocean values between 161 and 139 m indicates that fractionation occurred during fixed N loss. Although NH_3 loss to the atmosphere has an equilibrium isotope effect comparable to $\varepsilon_{denitrification}$ (*14*), this process should not have been favored because it is unlikely that Archean oceanic pH ever exceeded the limit (pH = 9.34) at which the NH_4^+-NH_3 equilibrium shifts toward gaseous NH_3 (*14*, *15*). Thus, increased expression of $\varepsilon_{denitrification}$ was evidently responsible for the increase in $\delta^{15}N$ values. The conversion of NO_3^- or NO_2^- to N_2 was probably biologically catalyzed because abiotic processes apparently reduce NO_3^- to NH_4^+ and not N_2 (*16*). Furthermore, expression of $\varepsilon_{denitrification}$ requires a large pool of NO_3^- or NO_2^- so that not all is consumed by denitrification. Thus, it is implausible that NO_2^- was a product of lightning combustion (*17*) because only a small amount of NO_2^- could have been produced by this process under late Archean conditions (*18*). Instead, it is most likely that microbial N_2 fixation introduced NH_4^+ to the ocean, and increased O_2 promoted the oxidation of NH_4^+ to NO_3^- or NO_2^-. Because high activation energy prevents NH_4^+ from abiotically oxidizing to NO_3^- or NO_2^- under Earth's surface conditions, nitrifying microbes evidently produced the NO_3^- or NO_2^-. Microbial denitrification then imparted a N isotope fractionation to the residual oxidized N pool, recorded in organic N (Fig. 2B)

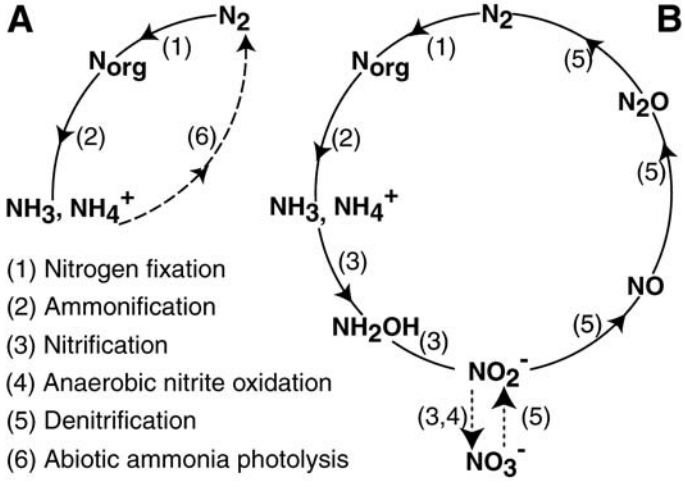

Fig. 2. Nitrogen cycle transformations. (**A**) Hypothesized anaerobic N cycle before Mount McRae $\delta^{15}N$ excursion and (**B**) hypothesized suboxic aerobic N cycle at peak of Mount McRae $\delta^{15}N$ excursion. The broken line indicates abiotic processes, and the dotted line indicates plausible but unproven processes.

Correlative redox-sensitive trace metal (*13*) and S isotopic (*19*) data imply that intensification of nitrification and denitrification during the $\delta^{15}N$ excursion corresponded to a rise in O_2 from $<10^{-6}$ to $\leq 10^{-5}$ present atmospheric level (PAL). Although increased oxygenation of the surface ocean may have limited N_2 fixation, and therefore productivity, during certain periods in Earth history (*20*), reduced N_2 fixation during the $\delta^{15}N$ excursion is unlikely. Although nitrogenase, the enzyme responsible for N_2 fixation, is irreversibly deactivated in the presence of molecular oxygen, inhibition is not apparent until the partial pressure of oxygen (P_{O_2}) > 0.2 to 0.5 PAL (*21*), which is

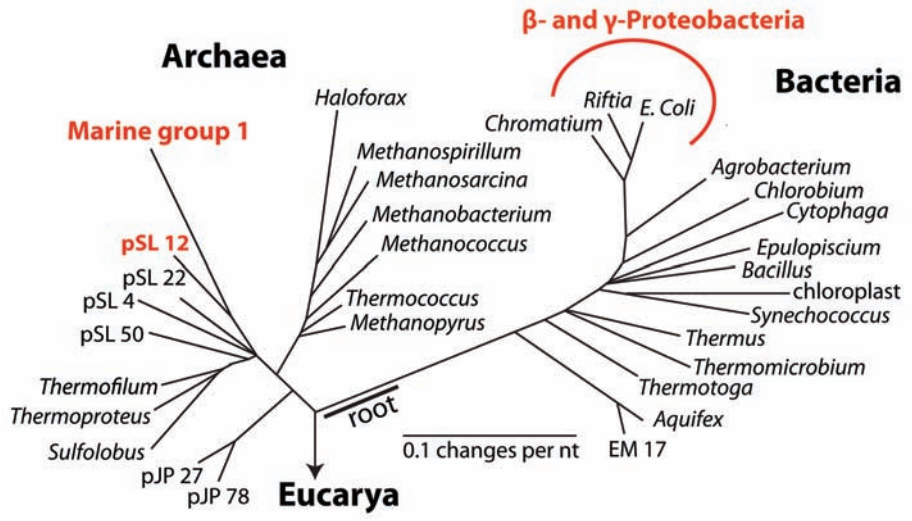

Fig. 3. The Tree of Life based on small subunit ribosomal RNA sequence analysis [modified from (*29*)]. Lineages in red represent known chemolithotrophic nitrifiers. The terminal position of Marine group 1 agrees with more recent widely accepted Archaeal trees [e.g., (*30*)].

much greater than the inferred maximum P_{O_2} of 10^{-5} PAL during the excursion. Furthermore, although Fe is a critical component of nitrogenase and the concentration of Fe^{2+} dropped during the $\delta^{15}N$ excursion (Fig. 1), cell culture experiments have shown that even under the low Fe concentrations characteristic of a fully oxygenated ocean, N_2 fixation rates are not lowered (*22*). Although NO_2^- may have been the most oxidized form of N attained under such low-oxygen conditions, incomplete nitrification would not have inhibited productivity because many microbes assimilate NO_2^- as effectively as NO_3^- (*23*). Thus, surface-ocean oxygenation during the $\delta^{15}N$ excursion was high enough to support nitrification, at least to NO_2^-, but not so high as to limit N_2 fixation, and therefore productivity.

The drop in $\delta^{15}N$ values above 139 m may indicate an increased proportion of sedimentary organic matter represented by N_2-fixing biomass. Alternatively, decreased $\delta^{15}N$ values may reflect decreased expression of $\varepsilon_{denitrification}$. This could have resulted from diminished nitrification (because denitrification should approach complete consumption as the size of the NO_2^- or NO_3^- pool decreases), diminished denitrification, or both diminished nitrification and denitrification. Although the drop in $\delta^{15}N$ values is difficult to explain, decreased Mo and Fe abundances during this interval without a corresponding decrease in S concentrations (Fig. 1) indicate that the deep ocean may have become euxinic (anoxic and sulfidic). Because both nitrification and denitrification are deactivated under euxinic conditions (*24*), the formation of euxinic bottom waters—a plausible response to slight surface-ocean oxygenation and increased $[SO_4^{2-}]$ during the $\delta^{15}N$ excursion (*20*)—may have caused the observed drop in $\delta^{15}N$ values.

We conclude that the 2.5-Ga Mount McRae section records an episode of increased nitrification and denitrification in response to slight surface-ocean oxygenation. Thus, an aerobic component to the N cycle was transiently active before the atmosphere became oxygen-rich after 2.45 Ga (*7*). Previously, Beaumont and Robert (*10*) observed a range of kerogen $\delta^{15}N$ in cherts from –6.2 to +13‰ between 3.5 and 2.8 Ga, and +0.3 to +10.1‰ between 2.1 and 0.7 Ga, which they attributed to a transition from an anaerobic to an aerobic N cycle. More recent $\delta^{15}N$ data has complicated this scenario. For example, Jia and Kerrich (*25*) reported a trend from high $\delta^{15}N$ kerogen (+15.3‰) in highly metamorphosed Archean shales to low (+3.5‰) values in Proterozoic counterparts, whereas Shen *et al.* (*26*) noted that the largest positive $\delta^{15}N$ shift occurs in banded iron formations (BIFs) between 2.7 and 2.6 Ga, and not during the transition to a fully oxygenated atmosphere. These contradictory results illustrate the difficulty of interpreting $\delta^{15}N$ data from diverse samples with low stratigraphic resolution. For example, because Archean cherts are often associated with hydrothermal systems where chemolithoautotrophs ($\delta^{15}N_{biomass}$ = –9.6 to +0.9‰) replace photosynthesizers as the primary producers (*26*), the ^{15}N-depleted ancient cherts reported by Beaumont and Robert may reflect incorporation of chemosynthetic biomass, and not the mean $\delta^{15}N$ of oceanic fixed N.

Although denitrifying microbes are widespread across the Archaea and Bacteria, nitrification is more restricted phylogenetically (Fig. 3). The high productivity indicated by the high TOC and the attendant large positive nitrogen isotope fractionations suggests that nitrification could have been performed only by chemolithotrophic nitrifiers, because heterotrophic nitrifiers are, and presumably always were, minor contributors to the marine pool of oxidized nitrogen species. Because marine chemolithotrophic nitrifiers are apparently restricted to the β- and γ-Proteobacteria and the low-temperature marine group I.1 Crenarchaeota [although there are hints that pSL 12 Crenarchaeota might also nitrify (*27*)], and as these dominant nitrifying groups are terminally branching subphyla of peripheral clades of the Bacteria and Archaea (Fig. 3), our data imply that most prokaryotic phyla in at least one of these domains must have been extant by the time these groups arose. Thus, the macroevolution of microbes in the bacterial and/or archaeal domains may have been largely complete by the end of the Archean.

References and Notes

1. $\delta^{15}N(‰) = [(^{15}N/^{14}N_{sample} \div {}^{15}N/^{14}N_{standard}) - 1] \times 1000$, where the $\delta^{15}N$ of the standard, represented by atmospheric N_2, is 0‰.
2. Geochronology constrains the age of the Mount McRae Shale to between 2501 ± 8 million years (*1*) and 2505 ± 5 million years (*28*).
3. $\varepsilon(‰) = {}^{14}\kappa/{}^{15}\kappa - 1) \times 1000$, where $^{14}\kappa$ and $^{15}\kappa$ are the rate coefficients of a reaction for the ^{14}N- and ^{15}N-containing reactants.
4. D. M. Sigman, K. L. Casciotti, in *Encyclopedia of Ocean Sciences*, J. H. Steele, K. K. Turekian, S. A. Thorpe, Eds. (Academic Press, London, 2001), pp. 1884–1894.
5. M. L. Fogel, L. A. Cifuentes, in *Organic Geochemistry*, M. H. Engel, S. A. Macko, Eds. (Plenum, New York, 1993), pp. 73–98.
6. M. A. Altabet, *Deep Sea Res. Part I Oceanogr. Res. Pap.* **35**, 535 (1988).
7. H. D. Holland, *Geochim. Cosmochim. Acta* **66**, 3811 (2002).
8. J. J. Brocks, R. Buick, G. A. Logan, R. E. Summons, *Geochim. Cosmochim. Acta* **67**, 4289 (2003).
9. G. E. Bebout, M. L. Fogel, *Geochim. Cosmochim. Acta* **56**, 2839 (1992).
10. V. Beaumont, F. Robert, *Precambrian Res.* **96**, 63 (1999).
11. M. A. Altabet *et al.*, *Deep Sea Res. Part I Oceanogr. Res. Pap.* **46**, 655 (1999).
12. R. C. Thunell, D. M. Sigman, F. Muller-Karger, Y. Astor, R. Varela, *Global Biogeochem. Cycles* **18**, GB3001 (2004).
13. A. D. Anbar *et al.*, *Science* **317**, 1903 (2007).
14. E. Wada, H. Hattori, *Nitrogen in the Sea: Forms, Abundances, and Rate Processes* (CRC Press, Boca Raton, FL, 1991).
15. D. L. Pinti, in *Lectures in Astrobiology*, M. Gargaud, B, Barbier, H. Martin, J. Reisse, Eds. (Springer, New York, 2005), vol. 1.
16. D. Summers, S. Chang, *Nature* **365**, 630 (1993).
17. Y. L. Yung, M. B. McElroy, *Science* **203**, 1002 (1979).
18. R. Navarro-Gonzalez, C. P. McKay, R. N. Mvondo, *Nature* **412**, 61 (2001).
19. A. J. Kaufman *et al.*, *Science* **317**, 1900 (2007).
20. A. D. Anbar, A. H. Knoll, *Science* **297**, 1137 (2002).
21. I. Berman-Frank, Y.-B. Chen, Y. Gerchman, G. C. Dismukes, P. G. Falkowski, *Biogeosci. Discuss.* **2**, 261 (2005).
22. A. L. Zerkle, C. H. House, R. P. Cox, D. E. Canfield, *Geobiology* **4**, 285 (2006).
23. J. P. Zehr, B. B. Ward, *Appl. Environ. Microbiol.* **68**, 1015 (2002).
24. W. A. Kaplan, in *Nitrogen in the Marine Environment*, E. J. Carpenter, D. G. Capone, Eds. (Academic Press, New York, 1983), pp. 139–190.
25. Y. Jia, R. Kerrich, *Terra Nova* **16**, 102 (2004).
26. Y. Shen, D. L. Pinti, K. Hashizume, in *Archean Geodynamic and Environments*, K. Benn, J.-C. Maraschel, K. C. Condie Eds. (American Geophysical Union, Washington, DC, 2005), pp. 309–320.
27. T. J. Mincer *et al.*, *Environ. Microbiol.* **9**, 1162 (2007).
28. B. Rasmussen, T. S. Blake, I. R. Fletcher, *Geology* **33**, 725 (2005).
29. N. R. Pace, *Science* **276**, 734 (1997).
30. C. Schleper, G. Jurgens, M. Jonuscheit, *Nat. Rev. Microbiol.* **3**, 479 (2005).

31. We thank L. C. Bonser, J. S. R. Dunlop, A. H. Hickman, M. van Kranendonk, the Geological Survey of Western Australia, P. van Loenhout, and Mount Magnet Drilling for assistance with core recovery; the NASA Astrobiology Drilling Program and NSF Geobiology and Low Temperature Geochemistry for funding; and A. H. Knoll, J. Farquhar, R. E. Summons, and T. W. Lyons for advice.

Supporting Online Material
www.sciencemag.org/cgi/content/full/323/5917/1045/DC1
Materials and Methods
Figs. S1 and S2
Table S1
References

9 September 2008; accepted 6 January 2009
10.1126/science.1165675

Zircon Dating of Oceanic Crustal Accretion

C. Johan Lissenberg,[1,2]*† Matthew Rioux,[3] Nobumichi Shimizu,[2] Samuel A. Bowring,[3] Catherine Mével[1]

Most of Earth's present-day crust formed at mid-ocean ridges. High-precision uranium-lead dating of zircons in gabbros from the Vema Fracture Zone on the Mid-Atlantic Ridge reveals that the crust there grew in a highly regular pattern characterized by shallow melt delivery. Combined with results from previous dating studies, this finding suggests that two distinct modes of crustal accretion occur along slow-spreading ridges. Individual samples record a zircon date range of 90,000 to 235,000 years, which is interpreted to reflect the time scale of zircon crystallization in oceanic plutonic rocks.

Nearly two-thirds of Earth's crust is formed at mid-ocean ridges. Crustal growth is controlled by the transfer of melt from the mantle to the crust. There has been extensive research on the rates and volume of extrusive volcanism, but the time scales of melt delivery from the mantle and the resulting patterns of intrusive magmatism in these settings are not well known. This is largely because of the inaccessibility of lower crustal sections and the limited spatial resolution of indirect methods such as seismic imaging.

Recently, U-Pb geochronology of samples from exposed lower crustal sections has begun to constrain the timing of intrusive magmatism beneath mid-ocean ridge spreading centers. Previous studies, from Atlantis Bank on the Southwest Indian Ridge (*1*) and Atlantis Massif on the Mid-Atlantic Ridge (*2*), used ion microprobe U-Pb geochronology of zircon to date the crystallization of igneous rocks intruded into the lower crust in these areas. These studies have provided considerable new insight into the time scales of magmatism at mid-ocean ridges, presenting evidence for protracted lower crustal growth, but the relatively low precision of ion microprobe spot analyses [1.5 to 43%, 2σ (*1*)] and the complex tectonic histories of these areas limit our understanding of magmatic processes at typical slow-spreading ridge segments.

We report chemical abrasion–thermal ionization mass spectrometry [CA-TIMS (*3*)] U-Pb zircon dates from the Vema lithospheric section (VLS), located at 11°N on the Mid-Atlantic Ridge. The single-grain CA-TIMS dates have an uncertainty of 0.07 to 0.79% (2σ), which corresponds to an error of ~10,000 to 106,000 years, more than an order of magnitude more precise than published ion microprobe dates on similar-age oceanic gabbros.

The VLS is exposed along the transverse ridge of the Vema Fracture Zone, which rises to ~450 m below sea level, and comprises lithosphere that was uplifted ~10 to 11 million years ago (Ma) as a result of plate flexure (*4*), thus exposing a full section of mantle peridotites, lower crustal gabbros, and basaltic upper crust formed along the Mid-Atlantic Ridge (Fig. 1). The studied samples come from a narrow (6 km) section of the VLS centered around 42°42′W (Fig. 1), which formed at ~13 Ma according to plate motion models (*5*). The crustal section exposed along the VLS in the study area represents the northern end of an ancient ridge segment ~60 km in length [the EMAR segment of (*4*, *6*)], and the section is thin [~2.2 km (*7*)] relative to the off-axis trace of the ancient segment center to the south (*6*). The crustal section, including the lower crust, is continuous, and is not composed of gabbro plutons intruding mantle peridotites, unlike the commonly inferred composition of slow-spreading segment ends (*8*). Gabbros exposed along the VLS in the study area commonly contain Fe-Ti oxides, indicating extensive differentiation.

We obtained U-Pb dates of 31 zircon grains and grain fragments separated from five gabbroic samples that were collected by submersible craft and by dredging along the VLS (*7*, *9*) (see supporting online material for sample descriptions, analytical techniques, and data). Individual zircon dates range from 13.75 to 13.25 Ma (Fig. 2) and show a good correlation with sample location

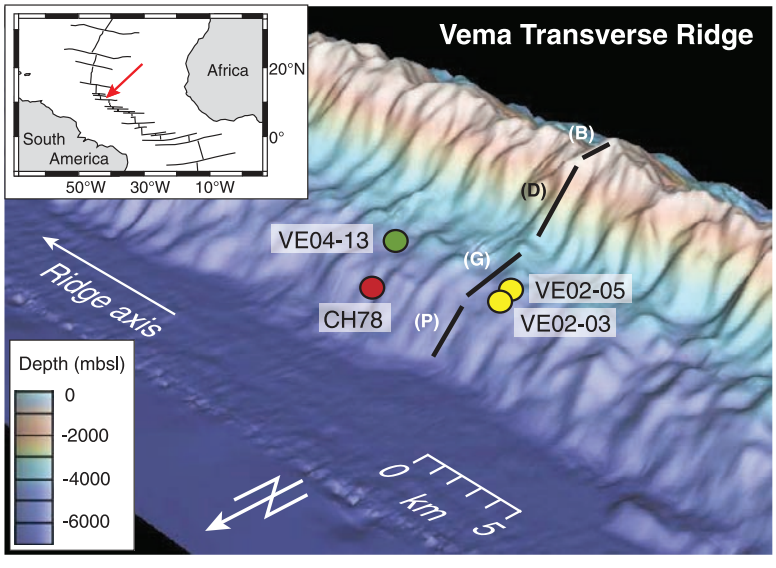

Fig. 1. Location of samples dated in this study. Inset shows location of VLS within the Atlantic Ocean. Schematic geological section of the VLS (black solid lines) after (*7*). Samples with prefix VE were sampled by the submersible Nautile during the Vemanaute cruise (*7*, *9*); samples with prefix CH were dredged during Jean Charcot Leg 78. On the basis of valley patterns observed in bathymetry, we estimate an along-axis uncertainty of 2 km for provenance of the dredged samples. P, peridotite; G, gabbro; D, dikes; B, basalt; mbsl, meters below sea level.

[1]Equipe de Géosciences Marines, Institut de Physique du Globe de Paris, 4 Place Jussieu, 75252 Paris Cedex 05, France. [2]Woods Hole Oceanographic Institution, Woods Hole, MA 02543, USA. [3]Department of Earth, Atmospheric, and Planetary Sciences, Massachusetts Institute of Technology, Cambridge, MA 02139, USA.

*Present address: School of Earth and Ocean Sciences, Cardiff University, Park Place, Cardiff CF10 3YE, UK.
†To whom correspondence should be addressed. E-mail: lissenbergcj@cardiff.ac.uk

(Fig. 3). The youngest zircon grains of each of the samples define a half-spreading rate of 15.8 ± 1.6 mm/year (Fig. 3), in agreement with the rate of 16.1 mm/year predicted by plate motion models (*5*).

Each sample has single-grain zircon dates that span 90,000 to 235,000 years, rather than a single population with equivalent dates (Fig. 2). Our interpretation is that these ranges reflect the time scale of zircon crystallization in mid-ocean ridge plutonic systems. In the dated gabbros, some zircons are included in amphibole (secondary after pyroxene) and plagioclase, whereas others occur along grain boundaries (fig. S1), consistent with an extended history of zircon growth. Individual zircon dates may therefore represent either discrete events or an average of a crystallization interval (with each grain capturing different parts of the growth history). As a result, the observed range in dates represents a minimum time scale of gabbro crystallization.

The Ti-in-zircon thermometer (*10*, *11*) indicates that zircon in individual oceanic gabbros may crystallize over a temperature range of ~60° to 120°C (fig. S2) (*12*). If this is the case for our samples, the intersample range in zircon dates we obtained indicates that the Vema gabbros cooled at rates of ~300° to 1300°C per million years, consistent with thermochronology-derived cooling rates of 800°C per million years determined for slow-spreading lower crust (*13*).

The extended time scales of zircon crystallization are also consistent with seismic velocity anomalies at slow-spreading ridges. For the half-spreading rate of 15.8 mm/year defined by the zircon dates, the age span observed in the Vema samples would correspond to 1.4 to 3.7 km of spreading. At slow-spreading ridge segments, lower crustal negative velocity anomalies, signaling the presence of partial melt, extend up to ±10 km across-axis (*14*, *15*), although this may have been less for the VLS owing to its proximity to a transform fault.

An alternative interpretation is that the observed range in zircon dates may reflect the assimilation of slightly older adjacent plutonic rocks during intrusion and cooling, a process that is commonly seen in continental crust. The date of each grain would then represent a mixture of a slightly older core and a younger magmatic rim; the range for each sample would reflect varying amounts and/or age of inherited components. However, cathodoluminescence and electron backscatter images of zircon from each sample, including grains that were subsequently analyzed, show no evidence for core/rim overgrowths or sharp breaks in composition, as would be expected in this model (Fig. 4). Thus, we prefer the model for protracted growth of zircon during solidification of the gabbroic plutons.

Results from the VLS are distinct from dating studies at Atlantis Bank (*1*) and Atlantis Massif (*2*), which suggests that there may be at least two different mechanisms of oceanic crustal accretion. At the VLS, the linear progression of ages away from the ridge axis (Fig. 3), combined with the continuous nature of the lower crust and scarcity of gabbroic plutons in the mantle section (*7*), suggest that the crust formed by highly regular, ridge-centered, shallow delivery of melt. In contrast, the data from Atlantis Bank and Atlantis Massif document the presence of inherited cores of up to 1.5 million years older than corresponding rims, with zircon dates as much as 2.5 million years older than the predicted magnetic ages for a given volume of crust. This extended time span of crustal growth was attributed to crystallization of gabbros in the mantle at depths of up to 18 km, followed by uplift to lower crustal depths and renewed magmatism (*1*, *2*). The different growth histories may relate to contrasting spreading histories. Atlantis Bank and Atlantis Massif expose sections of lower crust unroofed by low-angle

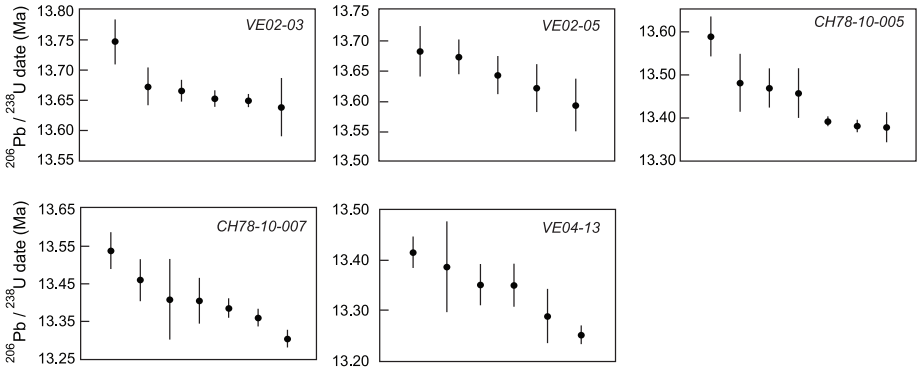

Fig. 2. CA-TIMS results for gabbros from the VLS. The single zircon grains (along the *x* axis) show a range in ^{206}Pb/^{238}U dates for each sample that exceeds the analytical uncertainties.

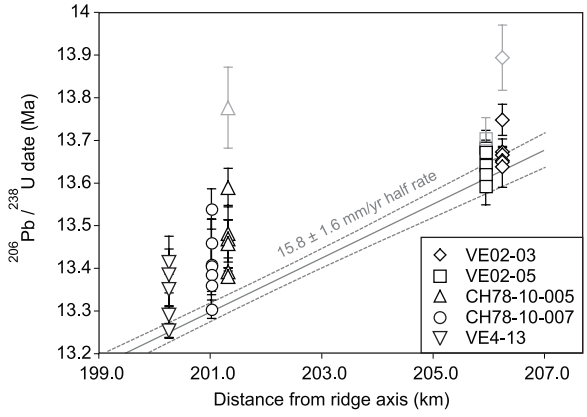

Fig. 3. ^{206}Pb/^{238}U dates of individual zircon crystals versus distance from the ridge axis. Half-spreading rate (defined by the youngest zircon in each of the samples) is shown by a gray line, with 2σ error envelope marked by dashed lines. Note that VE02-03 and VE02-05, as well as CH78-10-005 and CH78-10-007, were sampled from the same longitude but are separated by 300 m for clarity. There is a 2-km uncertainty in distance from the ridge axis for dredge samples CH78-10-005 and CH78-10-007. Grains for which common Pb exceeded 1 pg were excluded from the discussion (see supporting online material) and are shown in gray.

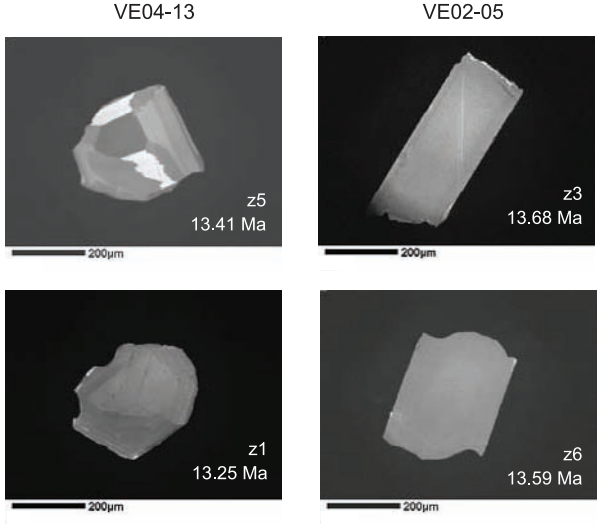

Fig. 4. Cathodoluminescence images of oldest and youngest zircon grains from Vema gabbros VE04-13 and VE02-05. Internal structures are consistent with growth during a single magmatic episode, lacking evidence for inherited cores overgrown by younger rims.

detachment faults [so-called oceanic core complexes (*16*–*18*)], typical of asymmetrically spreading ridge segments (*19*). The detachment faults are inferred to root in the lower crust or mantle beneath the ridge axis [e.g., (*20*, *21*)]. This would lead to an axial thermal structure, and hence a pluton emplacement pattern, that deviates considerably from that of a regular, symmetrically spreading ridge segment. In addition, plutons may intrude as the lower crust is exhumed (*22*), potentially leading to the juxtaposition of gabbros with different ages. Detachment faulting may thus substantially influence crustal accretion, possibly explaining the range of gabbro ages seen in Atlantis Bank and Atlantis Massif. The Vema samples come from an intact crustal section devoid of detachment faults, and the regular pattern of crustal accretion and absence of anomalously old ages may be typical of symmetrical accretion at slow-spreading ridges.

References and Notes

1. J. J. Schwartz *et al.*, *Science* **310**, 654 (2005).
2. C. B. Grimes, B. E. John, M. Cheadle, J. L. Wooden, *Geochem. Geophys. Geosyst.* **9**, Q08012 (2008).
3. J. M. Mattinson, *Chem. Geol.* **220**, 47 (2005).
4. E. Bonatti *et al.*, *Earth Planet. Sci. Lett.* **240**, 642 (2005).
5. R. D. Müller *et al.*, *Geochem. Geophys. Geosyst.* **9**, Q04006 (2008).
6. E. Bonatti *et al.*, *Nature* **423**, 499 (2003).
7. J.-M. Auzende *et al.*, *Nature* **337**, 726 (1989).
8. M. Cannat, *J. Geophys. Res.* **101**, 2847 (1996).
9. J. M. Auzende *et al.*, *Campagne Vemanaute 13/8/1989–16/9/1989, Cruise Report* (1988).
10. E. Watson, D. Wark, J. Thomas, *Contrib. Mineral. Petrol.* **151**, 413 (2006).
11. J. Ferry, E. Watson, *Contrib. Mineral. Petrol.* **154**, 429 (2007).
12. Calculated using data of (*23*–*25*) for samples with more than three zircon grains analyzed.
13. B. E. John *et al.*, *Earth Planet. Sci. Lett.* **222**, 145 (2004).
14. R. A. Dunn, V. Lekić, R. S. Detrick, D. R. Toomey, *J. Geophys. Res.* **110**, B09101 (2005).
15. J. P. Canales, J. A. Collins, J. Escartin, R. S. Detrick, *J. Geophys. Res.* **105**, 2699 (2000).
16. J. R. Cann *et al.*, *Nature* **385**, 329 (1997).
17. D. K. Blackman, J. R. Cann, R. Janssen, D. K. Smith, *J. Geophys. Res.* **103**, 21315 (1998).
18. H. J. B. Dick *et al.*, *Proc. ODP Sci. Res.* **118**, 359 (1991).
19. J. Escartin *et al.*, *Nature* **455**, 790 (2008).
20. B. E. Tucholke, J. Lin, M. C. Kleinrock, *J. Geophys. Res.* **103**, 9857 (1998).
21. B. J. deMartin, R. A. Sohn, J. P. Canales, S. E. Humphris, *Geology* **35**, 711 (2007).
22. H. J. B. Dick, M. A. Tivey, B. E. Tucholke, *Geochem. Geophys. Geosyst.* **9**, Q05014 (2008).
23. B. Fu *et al.*, *Contrib. Mineral. Petrol.* **156**, 197 (2008).
24. L. A. Coogan, R. W. Hinton, *Geology* **34**, 633 (2006).
25. C. B. Grimes *et al.*, *Geology* **35**, 643 (2007).

26. Supported by a grant from the Woods Hole Oceanographic Institution Deep Ocean Exploration Institute (N.S., C.J.L.). U-Pb geochronology was supported in part by NSF grant OCE-0727914 (S.A.B.). We thank H. Dick for discussions, J. Honnorez for providing CH78 cruise information, and two anonymous reviewers for their comments. Figure 1 was made using GeoMapApp. This is IPGP contribution 2457.

Supporting Online Material

www.sciencemag.org/cgi/content/full/1167330/DC1
SOM Text
Figs. S1 to S4
Tables S1 and S2
References

17 October 2008; accepted 15 December 2008
Published online 29 January 2009;
10.1126/science.1167330
Include this information when citing this paper.

A Self-Regulatory System of Interlinked Signaling Feedback Loops Controls Mouse Limb Patterning

Jean-Denis Bénazet,[1] Mirko Bischofberger,[2] Eva Tiecke,[1] Alexandre Gonçalves,[1] James F. Martin,[3] Aimée Zuniga,[1] Felix Naef,[2] Rolf Zeller[1]*

Embryogenesis depends on self-regulatory interactions between spatially separated signaling centers, but few of these are well understood. Limb development is regulated by epithelial-mesenchymal (e-m) feedback loops between sonic hedgehog (SHH) and fibroblast growth factor (FGF) signaling involving the bone morphogenetic protein (BMP) antagonist Gremlin1 (GREM1). By combining mouse molecular genetics with mathematical modeling, we showed that BMP4 first initiates and SHH then propagates e-m feedback signaling through differential transcriptional regulation of *Grem1* to control digit specification. This switch occurs by linking a fast BMP4/GREM1 module to the slower SHH/GREM1/FGF e-m feedback loop. This self-regulatory signaling network results in robust regulation of distal limb development that is able to compensate for variations by interconnectivity among the three signaling pathways.

Tissue morphogenesis depends on self-regulatory mechanisms that buffer genetic and environmental variations. With the exception of self-regulatory bone morphogenetic protein (BMP) signaling during gastrulation, the mechanisms endowing vertebrate development with robustness are largely unknown (*1*, *2*). The vertebrate limb bud is a classical model to study organogenesis, and its development is driven by signaling interactions between two instructive centers (*3*, *4*). The sonic hedgehog (SHH)/Gremlin1 (GREM1)/fibroblast growth factor (FGF) feedback loop (*5*–*7*) coordinates SHH signaling by the mesenchymal zone of polarizing activity (ZPA) with FGF signaling by the apical ectodermal ridge (AER) (*4*, *8*–*10*). In *Grem1*-deficient mouse limb buds, this feedback loop is not established, which disrupts both signaling centers and distal development as revealed by fusion of ulna and radius and loss of digits (Fig. 1A). Previous studies (*5*–*7*) suggested that GREM1-mediated antagonism of mesenchymal BMPs is key to SHH-mediated specification of digits 2 to 5 and proliferative expansion of the digit territory (autopod) (*8*, *10*). Three BMP ligands are expressed in limb buds (fig. S1) (*11*), and genetic studies revealed that mesenchymal BMP signaling inhibits anterior expansion of AER-*Fgf* expression and polydactyly (formation of additional digits) (*12*, *13*) and that a minimal BMP threshold is required to initiate chondrogenesis of posterior digits (*14*, *15*).

To identify the BMP ligand(s) antagonized by GREM1, we performed a genetic interaction screen in mouse embryos. Halving the *Bmp2* or *Bmp7* gene dosage only slightly improved limb development (Fig. 1A), whereas inactivation of one *Bmp4* allele restored the zeugopod (ulna and radius) and the posterior-most digits (Fig. 1B) (n = 24/24). Complete inactivation of *Bmp7* resulted in similar restoration (fig. S2), which indicates that GREM1 may reduce overall BMP activity. Cross-regulation among BMP ligands is unlikely because genetic lowering of one *Bmp* did not alter the expression of the others (figs. S1 and S2). Hindlimb development was also restored, but we only show forelimbs because the molecular alterations in $Grem1^{\Delta/\Delta}$ limb buds have been best characterized in forelimbs (*5*–*7*). In addition, the *Prx1*-Cre transgene was active in forelimb buds from an early stage.

Because genetic reduction of *Bmp4* in $Grem1^{\Delta/\Delta}$ embryos was most potent, we used a hypomorphic floxed *Bmp4* allele ($Bmp4^{hf}$) (*16*) with decreased activity (fig. S1) to reduce the *Bmp4* gene dosage in a stepwise manner. In this allelic series, forelimb development was progressively restored with proximal-to-distal and posterior-to-anterior

[1]Developmental Genetics, Department of Biomedicine, University of Basel, Mattenstrasse 28, CH-4058 Basel, Switzerland. [2]Computational Systems Biology Group, Ecole Polytechnique Federale de Lausanne, Swiss Institute for Experimental Cancer Research and Swiss Institute of Bioinformatics, AAB 0 21 Station 15, CH-1015 Lausanne, Switzerland. [3]Texas A&M Health Science Center, Institute of Biosciences and Technology, 2121 West Holcombe Boulevard, Room 907, Houston, TX 77030, USA.

*To whom correspondence should be addressed. E-mail: rolf.zeller@unibas.ch

sequence (Fig. 1B). In particular, low *Bmp4* levels restored pentadactyly in *Grem1*$^{\Delta/\Delta}$*Bmp4*$^{\Delta/hf}$ limb buds (Fig. 1B) (n = 10/14). About one-third of these limbs had five almost normal digits [Fig. 1B, right-most panel (n = 3/10) and fig. S3], whereas digits 2 and 3 remained proximally fused in all others [Fig. 1B (n = 7/10) and fig. S3]. This restoration is a likely consequence of rescuing cell survival and the distal *5'Hoxd* expression domains, which are disrupted in *Grem1*-deficient limb buds (fig. S4) (*5*–*7*).

To monitor BMP activity, we evaluated the transcription of *Msx2*, a direct and early target of BMP signal transduction in limb buds (*11*). *Msx2* expression was increased by a factor of about 2 in the mesenchyme of *Grem1*-deficient limb buds, whereas it was reduced to wild-type levels in *Grem1*$^{\Delta/\Delta}$*Bmp4*$^{\Delta/hf}$ limb buds (Fig. 2A and fig. S5). *Shh* expression and AER-*Fgf* expression were drastically reduced in *Grem1*-deficient limb buds (*5*–*7*) but were partially restored in *Grem1*$^{\Delta/\Delta}$*Bmp4*$^{\Delta/hf}$ limb buds (Fig. 2B and fig. S5). Thus, the aberrantly high BMP4 activity in *Grem1*$^{\Delta/\Delta}$ limb buds opposes distal limb development and specification of digit identities by interfering with transcriptional up-regulation of ZPA-SHH (*8*–*10*) and AER-FGF (*4*) signaling.

To probe these interactions further, we inactivated one *Shh* allele in *Grem1*-deficient embryos with reduced *Bmp4* gene dosage. In an otherwise wild-type context, inactivation of one *Shh* allele was completely compensated (Fig. 3A). In contrast, heterozygosity for *Shh* caused loss of an anterior digit in *Grem1*$^{\Delta/\Delta}$*Bmp4*$^{\Delta/hf}$ limb buds, as a likely consequence of further reducing SHH signal transduction (Fig. 3B) (n = 12/12). Posterior digit identities were lost in *Shh*$^{\Delta/+}$*Grem1*$^{\Delta/\Delta}$*Bmp4*$^{\Delta/+}$ embryos in concert with even lower SHH and increased BMP signal transduction (Fig. 3C) (n = 6/8). These results suggest that BMP and SHH activities are opposing one another and establish that intact epithelial-mesenchymal (e-m) feedback signaling buffers heterozygosity for *Shh* (Fig. 3A), whereas its disruption causes sensitivity to the *Shh* gene dosage (Fig. 3, B and C).

Similarly, reducing the *Bmp4* gene dosage alone did not alter limb skeletal patterning (fig. S6). However, *Grem1* expression was reduced in *Bmp4*$^{\Delta/hf}$ limb buds (Fig. 4A, B), which buffered BMP signal transduction such that *Msx2* was only slightly affected and *Shh* remained normal (fig. S6). It is known that BMPs up-regulate the expression of their antagonist *Grem1* (*17*, *18*), but the functional relevance of this self-regulatory interaction remained unclear. To determine the kinetics by which BMP4 and SHH coregulate *Grem1* expression (*5*, *6*, *18*), carrier beads soaked with recombinant ligands were implanted into cultured mouse limb buds. The initial response to BMP4 was detected within 1 hour (fig. S7) and *Grem1* was up-regulated within 2 hours (Fig. 4C and fig. S7), whereas SHH required about 6 hours (Fig. 4D). In turn, GREM1 required minimally 6 hours to up-regulate AER-*Fgfs* (fig. S7). Thus, the SHH/GREM1/FGF feedback loop (*5*–*7*) operates with a loop time of about 12 hours, whereas the BMP4/GREM1 feedback module is about 6 times as fast (Fig. 4E). The temporal dynamics of these dual-time feedback loops were simulated using an ordinary differential equation model (Fig. 4, F to H) (*15*, *19*) to probe the underlying network properties. These simulations indicated that BMP4, which functions upstream of *Grem1* and *Shh* (fig. S8), initiates *Grem1* expression around embryonic day (E) 9.0 (Fig. 4F). This increase in GREM1 rapidly lowered BMP4 activity, which in turn enabled the rise of SHH, GREM1, and AER-FGF activities (i.e., establishment of SHH/GREM1/FGF feedback signaling) in combination with low, but persistent, BMP4 activity (Fig. 4F). In particular, these equations were able to simulate the restoration of SHH activity in compound mutant limb buds (fig. S9). These results point to a switch from BMP4-dependent initiation to SHH-dependent progression of morphogenetic signaling (Fig. 4F). Indeed, simulations without the positive regulation of *Grem1* by BMP4 failed at initiation (Fig. 4G), whereas simulations without transcriptional input from SHH still enable up-regulation of morphogenetic signaling (Fig. 4H). This analysis identifies the BMP antagonist GREM1 as the critical node (*20*) linking the fast BMP4/GREM1 initiator module to the slower SHH/GREM1/FGF feedback loop.

We tested this predicted early requirement for BMP4 by *Prx1*-Cre mediated inactivation of the hypomorphic *Bmp4*^{hf} allele in *Bmp4*$^{\Delta/hf}$ embryos. This resulted in specific loss of forelimb mesenchymal *Bmp4* expression by about E9.0 (Fig. 5A and fig. S10) (*21*) and severe truncation of the forelimb skeleton (Fig. 5B). This early loss of

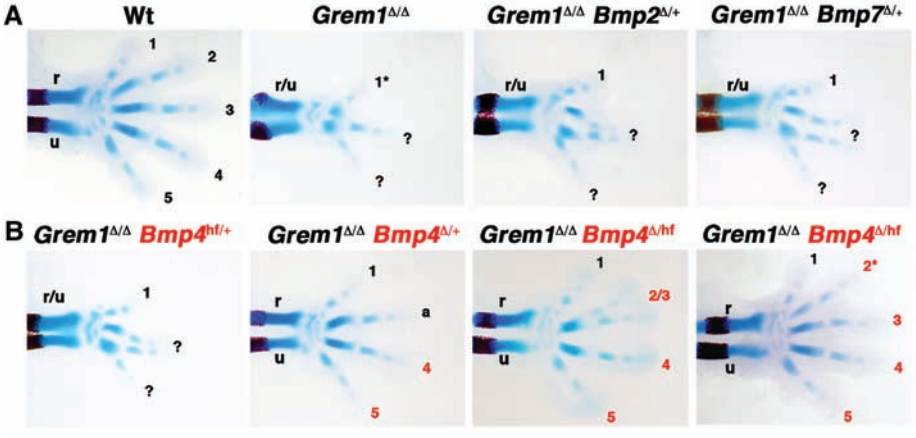

Fig. 1. Genetic reduction of BMP4 preferentially restores *Grem1*-deficient forelimb buds. Alcian blue and alizarin red stained skeletal preparations of mouse forelimbs at E14.5. Digit identities are indicated by numbers 1 (thumb, anterior) to 5 (little finger, posterior). Fused digits 2 and 3 are indicated as "2/3," digits with unclear anterior identity (digit 2 or 3) as "a," and hypoplastic digits with an asterisk. Question marks indicate digits with unknown identity, a hallmark of *Grem1*-deficient limbs. r, radius; u, ulna; r/u, fused radius and ulna. (**A**) Wt, wild-type; *Grem1*$^{\Delta/\Delta}$, *Grem1* deficient; *Grem1*$^{\Delta/\Delta}$*Bmp2*$^{\Delta/+}$ and *Grem1*$^{\Delta/\Delta}$*Bmp7*$^{\Delta/+}$, *Grem1*$^{\Delta/\Delta}$ embryos heterozygous for *Bmp2* or *Bmp7*, respectively. (**B**) Allelic series to reduce the *Bmp4* gene dosage in a stepwise manner in *Grem1*$^{\Delta/\Delta}$ forelimbs using both the hypomorphic *Bmp4*^{hf} and loss-of-function *Bmp4*$^{\Delta}$ alleles. The activity of the *Bmp4*^{hf} allele is reduced to slightly less than 50% (fig. S1). Digit identities were determined using morphological criteria in combination with carpal elements and *Sox9* expression (fig. S3). Digits with restored identity are indicated in red. All panels are oriented anterior to the top and posterior to the bottom.

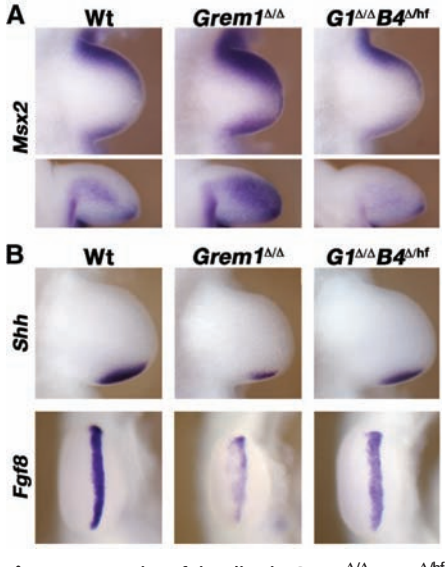

Fig. 2. Restoration of signaling in *Grem1*$^{\Delta/\Delta}$*Bmp4*$^{\Delta/hf}$ limb buds. (**A**) Detection of *Msx2* transcripts by in situ hybridization in wild-type, *Grem1*$^{\Delta/\Delta}$ and *Grem1*$^{\Delta/\Delta}$*Bmp4*$^{\Delta/hf}$ (*G1*$^{\Delta/\Delta}$*B4*$^{\Delta/hf}$) forelimb buds (35 somites). Bottom panels show posterior views (dorsal, top; ventral, bottom) of the limb buds in the top panels. (**B**) Detection of *Shh* (top, 37 somites) and *Fgf8* (bottom, 36 somites) transcripts.

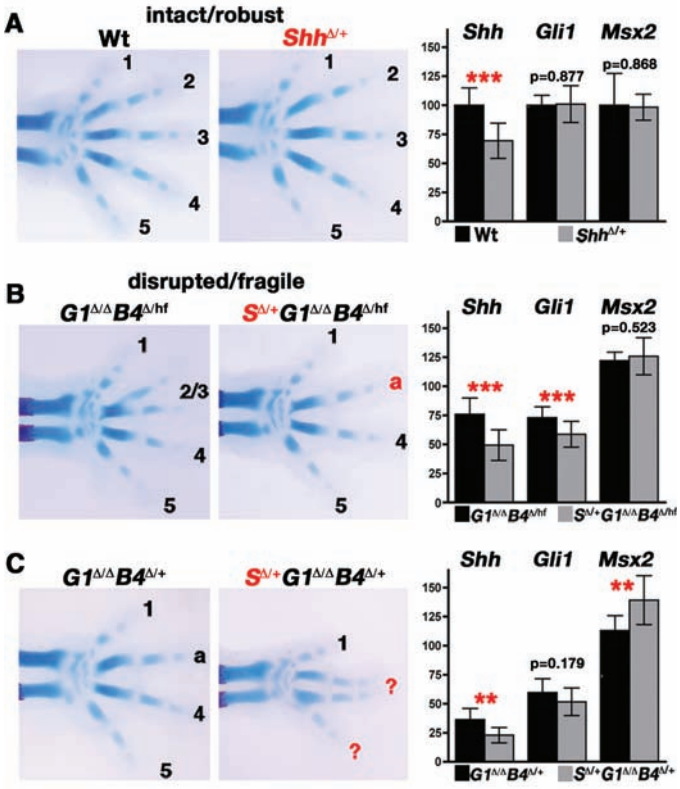

Fig. 3. Heterozygosity for *Shh* is no longer compensated in *Grem1*$^{\Delta/\Delta}$*Bmp4*$^{\Delta/hf}$ and *Grem1*$^{\Delta/\Delta}$*Bmp4*$^{\Delta/+}$ limb buds (*Shh*$^{\Delta/+}$*G1*$^{\Delta/\Delta}$*Bmp4*$^{\Delta/hf}$ and *Shh*$^{\Delta/+}$*G1*$^{\Delta/\Delta}$*Bmp4*$^{\Delta/+}$). Left and middle panels, forelimb skeletons at E14.5; right panels, QPCR quantification of the *Shh*, *Gli1*, and *Msx2* transcript levels; bars represent the average of nine limb bud pairs (34 to 38 somites) with SDs. (**A**) Heterozygosity for *Shh* (*Shh*$^{\Delta/+}$) does not affect digit specification or *Gli1* and *Msx2* transcription when e-m feedback signaling is intact. (**B** and **C**) Disruption of e-m feedback signaling renders digit specification and SHH and BMP signal transduction (assessed by *Gli1* and *Msx2* transcript levels) sensitive to the *Shh* gene dosage. The genotypes are indicated for *Shh* (*S*), *Grem1* (*G1*), and *Bmp4* (*B4*) as follows: *G1*$^{\Delta/\Delta}$*B4*$^{\Delta/hf}$, *Grem1*$^{\Delta/\Delta}$*Bmp4*$^{\Delta/hf}$; *S*$^{\Delta/+}$*G1*$^{\Delta/\Delta}$*B4*$^{\Delta/hf}$, *Shh*$^{\Delta/+}$*Grem1*$^{\Delta/\Delta}$*Bmp4*$^{\Delta/hf}$; *G1*$^{\Delta/\Delta}$*B4*$^{\Delta/+}$, *Grem1*$^{\Delta/\Delta}$*Bmp4*$^{\Delta/+}$; *S*$^{\Delta/+}$*G1*$^{\Delta/\Delta}$*B4*$^{\Delta/+}$, *Shh*$^{\Delta/+}$*Grem1*$^{\Delta/\Delta}$*Bmp4*$^{\Delta/+}$. *Shh* transcription is reduced about 30% when one *Shh* allele is inactivated (*Shh*$^{\Delta/+}$; *S*$^{\Delta/+}$*G1*$^{\Delta/\Delta}$*B4*$^{\Delta/hf}$; *S*$^{\Delta/+}$*G1*$^{\Delta/\Delta}$*B4*$^{\Delta/+}$). Error bars, mean ± SD. ***, $P < 0.001$; **, $P < 0.01$.

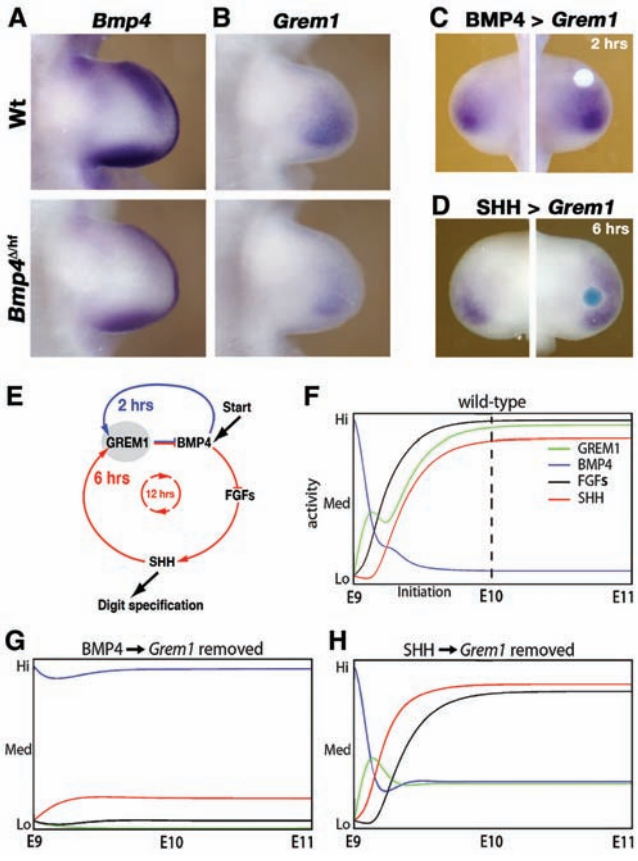

Fig. 4. GREM1-mediated interlinking of a fast GREM1/BMP4 module with the slower SHH/GREM1/FGF feedback loop. (**A** and **B**) Genetic lowering of *Bmp4* is compensated by down-regulation of *Grem1* expression at E10.75 (37 somites). (**C** and **D**) Differential transcriptional regulation of *Grem1* by BMP4 (C) and SHH (D). (C) BMP4 induces *Grem1* within 2 hours. (D) SHH induces Grem1 within 6 hours. (**E**) Scheme depicting how the GREM1 transcriptional node (shaded gray) interlinks the BMP4/GREM1 module and SHH/GREM1/FGF feedback loop. (**F**) Computer-aided simulations of the signaling activities in wild-type limb buds. The starting BMP4 activity was defined as high (Hi), whereas GREM1, SHH, and FGF are low (Lo). The initial increase of GREM1 is controlled by BMP4, whereas the second phase is controlled by SHH. Steady-state levels are reached by E10.0 and are characterized by high SHH/GREM1/FGF feedback loop and low BMP4/GREM1 module activities. (**G**) Disruption of BMP4-mediated up-regulation of *Grem1*. (**H**) Disruption of SHH-mediated up-regulation of *Grem1*.

Bmp4 disrupted *Grem1* (Fig. 5C), *Shh* activation (figs. S10 and S11), and formation of a functional AER as revealed by aberrant or lack of *Fgf8* expression (Fig. 5D). The predicted transient requirement of BMP4 was studied by inactivation from specific time points onward using a tamoxifen-inducible Cre transgene (*22*). Inactivation from E8.75 onward disrupted AER formation (Fig. 5E), whereas inactivation from E9.25 no longer impaired AER formation and *Shh* expression (Fig. 5F and fig. S10). However, *Fgf8* expression was expanded in these forelimb buds (Fig. 5F), indicating that the persistent low activity of the BMP4/GREM1 module is required to restrict AER length. This is relevant because anterior expansion of AER-FGF signaling causes digit polydactylies (*12*). Thus, BMP4 functions in the mesenchyme to initiate *Grem1* expression and signals to the ectoderm to regulate formation and length of the AER. The mesenchymal BMP4 signal is likely transduced in the AER by BMP receptor

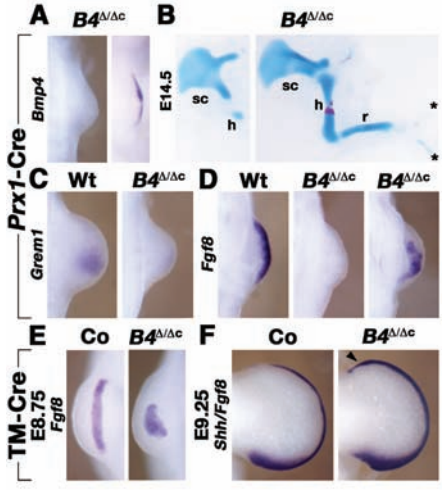

Fig. 5. BMP4 is required during initiation of limb bud development. (**A**) Detection of *Bmp4* transcripts in the mesenchyme (left) and AER (right) of *Bmp4*$^{\Delta/\Delta c}$ forelimb buds (26 somites). (**B**) Skeletal phenotypes of *Bmp4*$^{\Delta/\Delta c}$ forelimbs at E14.5 after inactivation of the *Bmp4*^{hf} allele by the *Prx1*-Cre transgene. (Left) Truncation distal to scapula (n = 8/14). (Right) Loss of posterior elements (n = 6/14). h, humerus; sc, scapula; r, radius; asterisks indicate rudimentary digits. (**C** and **D**) Detection of mesenchymal *Grem1* (28 somites, n = 6) and AER-*Fgf8* (26 somites) transcripts at E9.75. Note the patchy *Fgf8* expression (n = 8/10) or loss of *Fgf8* expression (n = 2/10). (**E**) Tamoxifen (TM)–Cre mediated inactivation of *Bmp4* by tamoxifen injection at about E8.75, i.e., before initiation of forelimb bud development. Detection of *Fgf8* transcripts in forelimb buds at E10.25 (32 somites, n = 6). Control, TM-Cre heterozygous embryo. (**F**) Detection of *Shh* and *Fgf8* transcripts in forelimb buds at E11.75 (50 somites) after tamoxifen injection at E9.25, i.e., after initiation of forelimb bud development (n = 4). Arrowhead points to the anterior expansion of *Fgf8* expression in *Bmp4*$^{\Delta/\Delta c}$ forelimb buds. Control: *Bmp4*$^{\Delta c/+}$TM-Cre forelimb bud.

1A (BMPR1A) because early AER-specific inactivation results in similar disruption of AER formation, whereas later inactivation alters AER-*Fgf* signaling (*23*, *24*). This early requirement of BMP4 (Fig. 5) may have been overlooked in previous studies because *Bmp4* was not inactivated early enough (*15*). In the limb bud mesenchyme, the BMP4 signal is likely also transduced by BMPR1A because its mesenchyme-specific inactivation disrupts *Grem1* up-regulation and distal limb development (*17*).

Our analysis provides evidence that linking the fast and self-regulatory BMP4/GREM1 initiator module to the slower SHH/GREM1/FGF feedback loop constitutes a crucial component of the limb patterning system. This system controls fail-safe specification of digit identities by coordinating the opposing SHH and BMP4 activities. Although genetic analysis in the mouse has not revealed major roles for BMP2 and BMP7 in the limb patterning system described here, they probably contribute to its robustness and might be more relevant for limb development in other vertebrate species (*18*, *25*). Another fascinating aspect of the SHH/GREM1/FGF feedback loop concerns its self-terminating properties, because the expanding population of *Shh* descendants is refractory to *Grem1* expression, which eventually disrupts e-m feedback signaling and autopod development (*18*, *26*). This refractoriness is caused by activation of an inhibitory FGF/GREM1 feedback loop in *Shh* descendants (*27*). Simulations reveal that the limb signaling system progresses in a self-regulatory manner from BMP4-dependent initiation by SHH-dependent digit specification and growth (propagation phase) to FGF-induced termination (fig. S12). This occurs because of the differential impact of BMP4, SHH, and FGF signal transduction on *Grem1* expression over time. Finally, our analysis reveals how variation can be compensated by so-called distributed robustness (*28*) due to interconnectivity between different signaling pathways and not simply by intrapathway compensation. During tetrapod evolution, fine-tuning the signaling interactions described here may have contributed to shaping and stabilizing the pentadactylous autopod (*15*).

References and Notes

1. M. Kerszberg, *Curr. Opin. Genet. Dev.* **14**, 440 (2004).
2. E. M. De Robertis, *Nat. Rev. Mol. Cell Biol.* **7**, 296 (2006).
3. C. Tickle, *Nat. Rev. Mol. Cell Biol.* **7**, 45 (2006).
4. F. V. Mariani, C. P. Ahn, G. R. Martin, *Nature* **453**, 401 (2008).
5. A. Zuniga, A. P. Haramis, A. P. McMahon, R. Zeller, *Nature* **401**, 598 (1999).
6. L. Panman *et al.*, *Development* **133**, 3419 (2006).
7. O. Michos *et al.*, *Development* **131**, 3401 (2004).
8. B. D. Harfe *et al.*, *Cell* **118**, 517 (2004).
9. M. Towers, R. Mahood, Y. Yin, C. Tickle, *Nature* **452**, 882 (2008).
10. J. Zhu *et al.*, *Dev. Cell* **14**, 624 (2008).
11. B. Robert, *Dev. Growth Differ.* **49**, 455 (2007).
12. J. Selever, W. Liu, M. F. Lu, R. R. Behringer, J. F. Martin, *Dev. Biol.* **276**, 268 (2004).
13. C. Hofmann, G. Luo, R. Balling, G. Karsenty, *Dev. Genet.* **19**, 43 (1996).
14. A. Bandyopadhyay *et al.*, *PLoS Genet.* **2**, e216 (2006).
15. Materials and methods and results are available as supporting material on *Science* Online.
16. H. Kulessa, B. L. Hogan, *Genesis* **32**, 66 (2002).
17. D. A. Ovchinnikov *et al.*, *Dev. Biol.* **295**, 103 (2006).
18. S. Nissim, S. M. Hasso, J. F. Fallon, C. J. Tabin, *Dev. Biol.* **299**, 12 (2006).
19. N. Ben-Haim *et al.*, *Dev. Cell* **11**, 313 (2006).
20. H. Kitano, *Nat. Rev. Genet.* **5**, 826 (2004).
21. M. Logan *et al.*, *Genesis* **33**, 77 (2002).
22. S. Hayashi, A. P. McMahon, *Dev. Biol.* **244**, 305 (2002).
23. K. Ahn, Y. Mishina, M. C. Hanks, R. R. Behringer, E. B. Crenshaw 3rd, *Development* **128**, 4449 (2001).
24. S. Pajni-Underwood, C. P. Wilson, C. Elder, Y. Mishina, M. Lewandoski, *Development* **134**, 2359 (2007).
25. D. Hockman *et al.*, *Proc. Natl. Acad. Sci. U.S.A.* **105**, 16982 (2008).
26. P. J. Scherz, B. D. Harfe, A. P. McMahon, C. J. Tabin, *Science* **305**, 396 (2004).
27. J. M. Verheyden, X. Sun, *Nature* **454**, 638 (2008).
28. A. Wagner, *Bioessays* **27**, 176 (2005).

29. We thank B. Hogan, C. Hoffmann, and G. Holländer for making *Bmp* mutant alleles available to us; F. Lehembre for help with quantitative polymerase chain reaction (QPCR); J. Lopez-Rios for input into the design of the network architecture; and M. Affolter, M. Kmita, and group members for input. This research is supported by the Swiss National Science Foundation (grants 3100A0-100240 and 3100A0-113866 to R.Z., grant 3100A0-113617 to F.N., and grant 3100A0-112607 to AZ), the Novartis Foundation (to R.Z. and E.T.), the NIH (grants 2R01DE12324-12 and R01DE16329 to J.F.M.), the FCT (SFRH/BD/24301/2005 to A.G.), and the University of Basel. The authors declare no competing financial interests.

Supporting Online Material

www.sciencemag.org/cgi/content/full/323/5917/1050/DC1
Materials and Methods
SOM Text
Figs. S1 to S13
Tables S1 to S4
References

19 November 2008; accepted 30 December 2008
10.1126/science.1168755

Trifurcate Feed-Forward Regulation of Age-Dependent Cell Death Involving *miR164* in *Arabidopsis*

Jin Hee Kim,[1]* Hye Ryun Woo,[1]* Jeongsik Kim,[1] Pyung Ok Lim,[2] In Chul Lee,[1] Seung Hee Choi,[1] Daehee Hwang,[3,4] Hong Gil Nam[1,4]†

Aging induces gradual yet massive cell death in higher organisms, including annual plants. Even so, the underlying regulatory mechanisms are barely known, despite the long-standing interest in this topic. Here, we demonstrate that ORE1, which is a NAC (NAM, ATAF, and CUC) transcription factor, positively regulates aging-induced cell death in *Arabidopsis* leaves. *ORE1* expression is up-regulated concurrently with leaf aging by *EIN2* but is negatively regulated by *miR164*. *miR164* expression gradually decreases with aging through negative regulation by *EIN2*, which leads to the elaborate up-regulation of *ORE1* expression. However, *EIN2* still contributes to aging-induced cell death in the absence of *ORE1*. The trifurcate feed-forward pathway involving *ORE1*, *miR164*, and *EIN2* provides a highly robust regulation to ensure that aging induces cell death in *Arabidopsis* leaves.

In most organisms, aging leads to organ- and organism-level senescence that eventually causes death and limits longevity. In plants, age-associated senescence and cell death are most dramatically observed in the leaves of annual plants and deciduous trees. Leaf senescence and the associated cell death are developmentally programmed processes that occur in an age-dependent manner, integrating multiple developmental and environmental signals (*1*, *2*). Age-associated cell death in plant leaves is a type of programmed cell death (PCD), but it occurs more slowly and massively than other acute PCD observed during tissue wounding or viral infection, for example. Although leaf senescence and the associated cell death are widely observed in nature and are regarded as a developmental strategy for plant fitness (*3*), the underlying molecular mechanisms remain elusive.

The *Arabidopsis oresara1-1* (*ore1-1*, *oresara* means "long-living" in Korean) mutant was ini-

[1]Division of Molecular Life Sciences, Pohang University of Science and Technology, Hyoja-dong, Pohang, Kyungbuk, 790-784, Republic of Korea. [2]Department of Science Education, Jeju National University, Jeju, 690-756, Republic of Korea. [3]Department of Chemical Engineering, Pohang University of Science and Technology, Hyoja-dong, Pohang, Kyungbuk, 790-784, Republic of Korea. [4]School of Interdisciplinary Biosciences and Bioengineering, Pohang University of Science and Technology, Hyoja-dong, Pohang, Kyungbuk, 790-784, Republic of Korea.

*These authors contributed equally to this work.
†To whom correspondence should be addressed. E-mail: nam@postech.ac.kr

tially identified as a delayed leaf senescence mutant (*4*). We isolated and genetically analyzed the *ore1-2* allele in this study (table S1) (*5*). Leaf yellowing due to the loss of chlorophyll is a typical characteristic of leaf senescence. The phenotype of the *ore1-2* mutant plants, with delayed loss of chlorophyll at a later age, is shown in Fig. 1A. We then examined age-associated characteristics in single leaves along their ages. Wild-type leaves showed a reproducible aging pattern; the third and fourth foliar leaves showed a life span of ~36 days from their emergence (Fig. 1, B and C). Delayed loss of chlorophyll content and of photochemical efficiency (Fv/Fm) (*6*) with leaf aging was observed in *ore1* mutants (Fig. 1, B and C) (*4*). The expression of the *chlorophyll a/b-binding protein 2* (*CAB2*) gene and the cystein protease-encoding *senescence-associated gene 12* (*SAG12*) exhibited delayed reduction and induction, respectively, with aging (Fig. 1D). We also found that aging-induced cell death was delayed in the *ore1* mutants, as shown by slower increases in membrane ion leakage (*7*) of the leaves with aging (Fig. 1E) and by the absence of trypan blue–stained cells (*7*) in aged (28-day-old) leaves (Fig. 1F). Thus, ORE1 is a positive regulator of aging-induced cell death and senescence in *Arabidopsis* leaves.

Map-based cloning of the *ORE1* locus with the use of *ore1-2* (fig. S1) revealed that the mutation was caused by a 5–base pair deletion in *At5g39610*, which encodes a NAC (NAM, ATAF, and CUC) transcription factor, AtNAC2 (fig. S2, A and B) (*8*). The nuclear localization of ORE1/AtNAC2 (fig. S2C) is consistent with its role as a transcription factor. A search of microarray data (*9*) revealed that *ORE1* expression increases in senescing leaves, and time-course analysis (Fig. 2, A and E) confirmed that *ORE1* expression increases with leaf aging. This result implies that *ORE1* regulates aging-induced cell death and senescence via its increased expression with leaf aging, which would, in turn, induce senescence-associated downstream genes as a transcription factor.

The *ORE1/AtNAC2* mRNA possesses a potential *miR164*-binding sequence in its third exon (fig. S2A) (*10*). The *miR164* family in *Arabidopsis* includes three isoforms [*miR164A*, *miR164B*, and *miR164C* (*11*)] and represses the expression of a group of *NAC* family genes by cleaving the target mRNAs (*12*–*15*). We found that the amount of *miR164* declined with leaf aging (Fig. 2A). The inverse correlation between the expression of *miR164* and *ORE1* with leaf aging led to the hypothesis that *miR164* negatively regulates *ORE1* mRNA, thereby antagonizing age-dependent senescence. We first tested if *ORE1* mRNA is a target of *miR164*-mediated cleavage. The level of *ORE1* mRNA increased and reduced, respectively, in the *mir164abc* triple mutant (Fig. 2E and fig. S3) (*14*) and in the *miR164B*-overexpressing lines (Fig. 2B and fig. S4). In the *miR164B*-overexpressing lines, a smaller transcript was found, which is probably a cleavage product of the full-length *ORE1* transcript (Fig. 2B). We found that several EST sequences of *ORE1* are truncated at the potential *miR164*-target sequence (Fig. 2C). Furthermore, in transgenic lines expressing a mutant version of *ORE1* (*mORE1*) where six mismatches were introduced into the potential *miR164*-binding sequence (Fig. 2C), the level of the mutant *ORE1* transcript was less affected by overexpression of *miR164B* (Fig. 2D). The minor reduction observed in the transgenic plants overexpressing mutant *ORE1* and *miR164B* is probably due to the cleavage of the endogenous wild-type *ORE1* mRNA present in the transgenic lines. These results confirmed that *ORE1* mRNA is a target of *miR164*-guided cleavage.

We then tested whether *miR164* controls the level of the *ORE1* transcript during leaf aging by examining its level in the *mir164abc* triple mutant. The differences in *ORE1* transcript levels between the wild type and the *mir164abc* mutant were greater in younger leaves and became negligible when the level of *miR164* was barely detectable in older leaves (Fig. 2, E and F). This result suggests that *ORE1* expression is negatively regulated by *miR164* at earlier stages, which is relieved at later stages because of the age-dependent down-regulation of *miR164* expression. This observation led us to test whether *miR164* functions as a negative regulator of aging-induced leaf cell death. Aging-induced cell death was accelerated in the *mir164abc* mutant, as indicated by a faster decline in chlorophyll content (fig. S5A) and photochemical efficiency and a faster increase in membrane ion leakage and *SAG12* expression with leaf aging (Fig. 3A). The opposite trends were observed in the *miR164A*- and *miR164B*-overexpressing lines (Fig. 3B and fig. S5B). Moreover, aging-induced cell death and senescence symptoms were more pronounced in the *mORE1* overexpression lines (fig. S6), where the *mORE1* transcript level was higher because of the escape from the *miR164*-guided cleavage (Fig. 2D). Therefore, *miR164* negatively regulates aging-induced cell death and senescence through down-regulation of *ORE1*.

Next, we asked how the age-dependent decline of *miR164* expression occurs. Because *miR164* negatively regulates leaf senescence, a genetic mutation in upstream regulatory elements that relieves age-dependent down-regulation

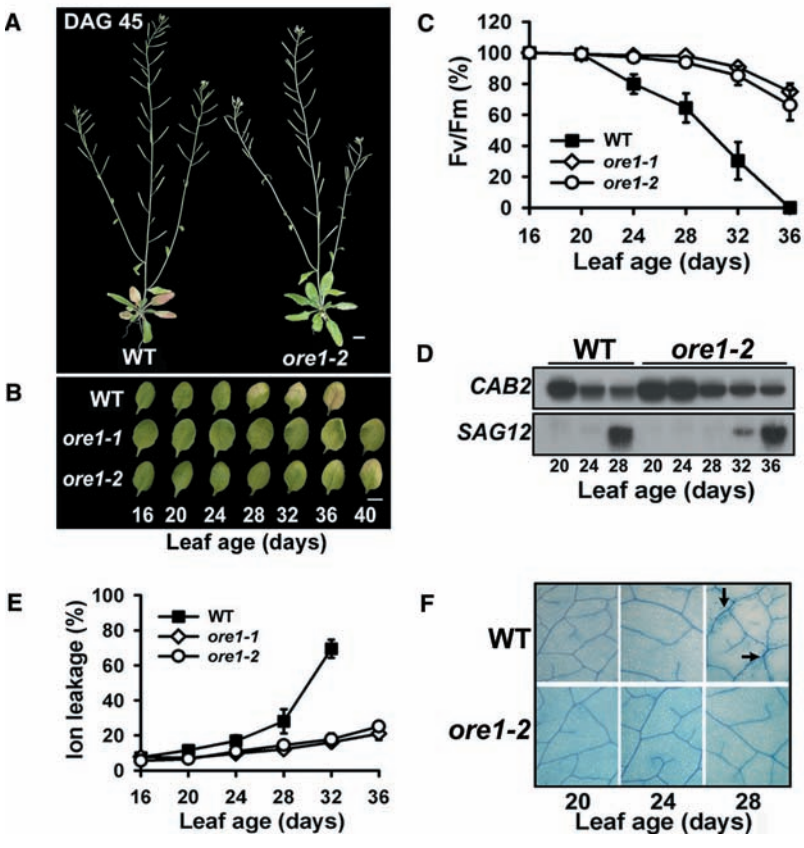

Fig. 1. Age-dependent cell death is delayed in the *ore1* mutants. (**A**) Whole plant phenotype of the wild type (WT) and *ore1-2* at 45 days after germination (DAG). WT, Col; scale bar, 1 cm. (**B**) Chlorophyll loss in WT, *ore1-1*, and *ore1-2* with leaf aging. The third rosette leaves at the indicated days after emergence (leaf age) are shown. Scale bar, 0.5 cm. (**C** to **F**) Photochemical efficiency (Fv/Fm) of photosystem II (C), expression of *CAB2* and *SAG12* (D), membrane ion leakage (E), and trypan blue staining (F) of WT and *ore1* leaves at the indicated leaf age. In (C) and (E), values are means ± 95% confidence intervals (± 95 CI; n = 12 to 14 leaves). In (F), WT leaves developed blue-colored patches of cells (arrows), indicating areas of dead or dying cells.

of *miR164* expression would lead to delayed senescence symptoms. We thus examined the age-dependent *miR164* expression in the delayed senescence mutants *ore1-1*, *ethylene insensitive 2-34* (*ein2-34*), *ore12-1*, and *ore7-1D* (Fig. 4A); *ein2-34* was originally isolated as *ore3-1* (*4*). Among the tested mutants, the *ein2-34* mutant alone exhibited the least difference in *miR164* expression between 8- and 20-day-old leaves. The age-dependent regulation of *miR164* expression by *EIN2* was examined in more detail at 4-day intervals (Fig. 4B). *miR164* expression was barely altered with aging in the *ein2-34* mutant. The results indicate that *EIN2* mediates age-dependent down-regulation of *miR164*.

EIN2 is required for salt-induced expression of *ORE1/AtNAC2* in seedlings (*8*). We found that age-dependent induction of *ORE1* relies on *EIN2*, as the level of *ORE1* transcript in the *ein2-34* mutant was only 12% of that in the wild type in 28-day-old plants (Fig. 4C). Thus, up-regulation of *ORE1* expression results from age-dependent induction through *EIN2*, as well as stabilization of *ORE1* mRNA due to the age-dependent down-regulation of *miR164* by *EIN2*. The functional relation between *ORE1* and *EIN2* in aging-induced leaf cell death was further examined using the *ore1-1 ein2-34* double mutant. In the double mutant, the loss of photochemical efficiency and the induction of *SAG12* expression exhibited a longer delay than did either of the single mutants (Fig. 4, D and E). Therefore, although age-dependent induction of *ORE1* critically depends on *EIN2*, *ore1-1* and *ein2-34* did not show a simple epistatic interaction but rather a partially additive effect.

Our study leads to a trifurcate feed-forward pathway for regulation of age-dependent cell death and senescence in *Arabidopsis* leaves (fig. S7): ORE1 is a transcription factor that functions positively in cell death. *ORE1* is induced in an age-dependent manner by *EIN2*. *ORE1* is negatively regulated by *miR164* at earlier stages, which is relieved at later stages because of the age-dependent down-regulation of *miR164* expression by *EIN2*. However, EIN2 also uses another pathway to regulate aging-induced cell death that does not include ORE1. Additionally, *miR164* may function in the age-dependent cell death pathway as a "brake" or "guard" against premature overexpression of *ORE1* and may finely tune the timing of senescence and cell death. We propose that the trifurcate pathway exists to ensure senescence and the accompanying cell death when leaves are aged. This trifurcate pathway contains an embedded coherent feed-forward loop (*16*). Mathematical modeling (fig. S8) of this pathway

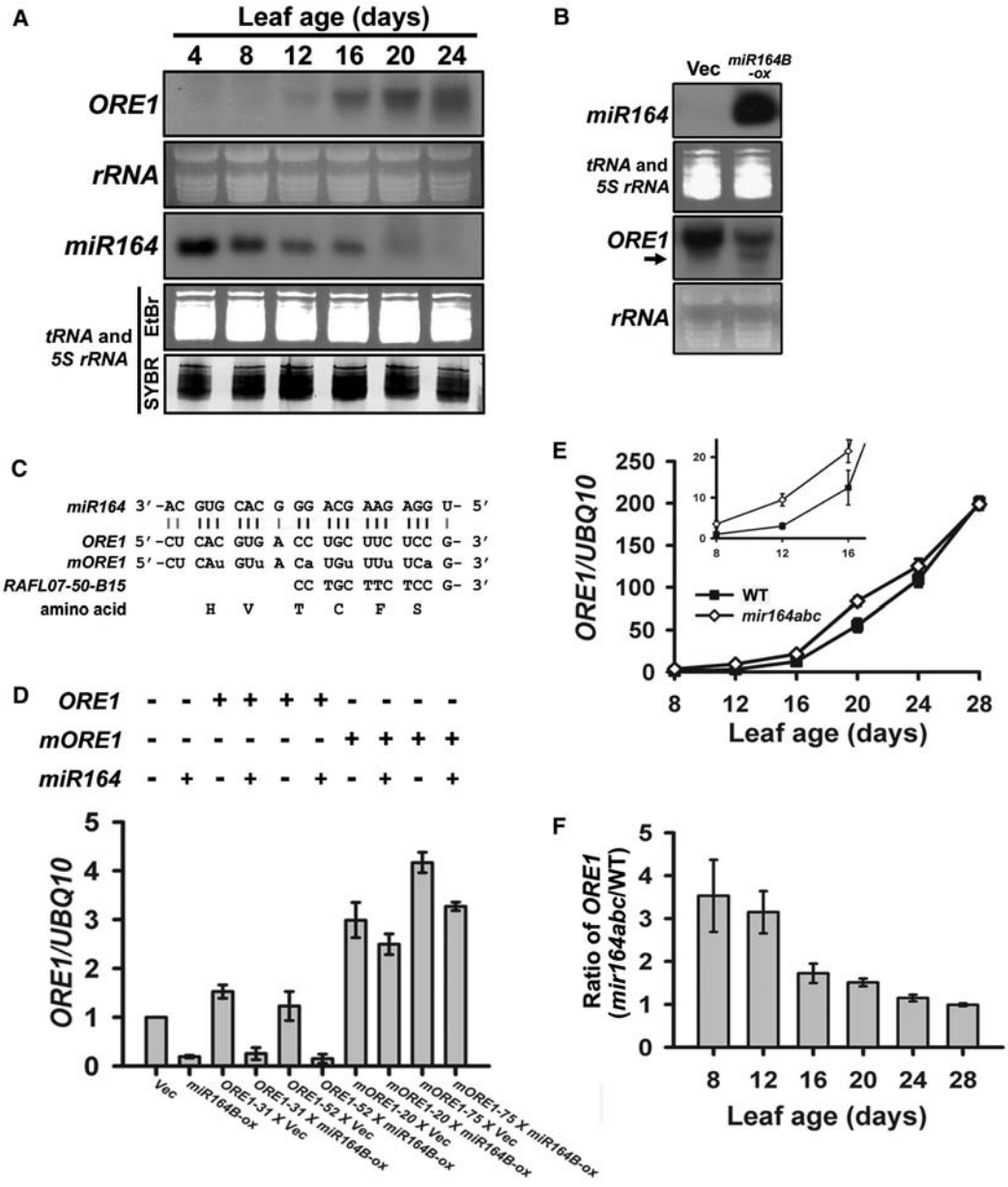

Fig. 2. *ORE1* mRNA is a target of *miR164*. (**A**) Inverse expression pattern of *ORE1* and *miR164* with leaf aging. rRNA and tRNA and 5S rRNA, loading controls; EtBr, ethidium bromide stain; SYBR, SYBR gold stain. (**B**) Expression of *ORE1* in control vector (Vec) and *miR164B*-overexpressing (*miR164B-ox*) lines. The arrow indicates a smaller fragment derived from the *ORE1* transcript. (**C**) Alignment of the *miR164* sequence with wild-type *ORE1* (*ORE1*), mutant *ORE1* (*mORE1*), and a truncated EST (*RAFL07-50-B15*). (**D**) Effect of *miR164*-target sequence on the level of *ORE1* mRNA. In 22-day-old leaves, *ORE1* mRNA levels were measured in the F_1 progenies of transgenic lines overexpressing wild-type (*ORE1-31xVec*, *ORE1-31xmiR164B-ox*, *ORE1-52xVec*, and *ORE1-52xmiR164B-ox*) or mutant *ORE1* (*mORE1-20xVec*, *mORE1-20xmiR164B-ox*, *mORE1-75xVec*, and *mORE1-75xmiR164B-ox*). (**E**) Level of *ORE1* mRNA in WT and the *mir164abc* mutant leaves with leaf age. (Inset) Smaller view of the graph at earlier ages. (**F**) Age-dependent decline of the ratio of *ORE1* level in the *mir164abc* mutant relative to that in WT. Error bars indicate SE of the mean in (D), (E), and (F).

showed that *SAG12* is gradually induced upon a systematic, persistent action of EIN2, but it is not induced upon nonsystematic variations of EIN2 action. EIN2, a component of the trifurcate pathway, regulates other functions including ethylene signaling, cell growth control, and stress responses as well as leaf senescence (*4*, *17*, *18*). *ORE1/AtNAC2* is also induced by salt as well as aging (*8*). Therefore, the age-dependent trifurcate pathway is probably interwoven with other developmental and environmental signals to tune leaf senescence and cell death processes.

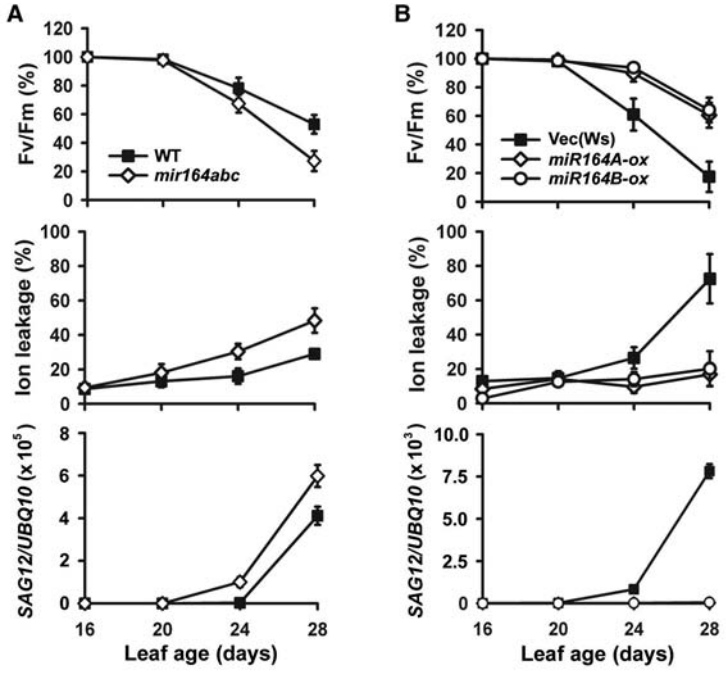

Fig. 3. *miR164* negatively regulates aging-induced cell death. (**A** and **B**) Photochemical efficiency (top), membrane ion leakage (middle), and transcript level of *SAG12* (bottom) in *mir164abc* (A) and *miR164A*- and *miR164B*-overexpressing leaves (B). The values of photochemical efficiency and ion leakage are means ± 95 CI (n = 12 to 18).

miRNAs are widespread and are involved in a variety of biological processes, in both animals and plants (*11*, *19*). Here, we place the function of the plant *miR164* in the context of age-dependent developmental pathways. The members of the *Arabidopsis miR164* target a group of *NAC* family genes (*CUC1*, *CUC2*, *NAC1*, *ORE1*, *At5g07680*, and *At5g61430*) and function in various developmental processes, including lateral root development and organ boundary formation in shoot meristem and flower development (*13*–*15*). Our study showed that *miR164* functions in regulation of age-dependent cell death in leaves through changes in its expression level over the life span of the leaves. Do the other *miR164*-binding *NAC* family genes also affect aging-induced cell death? Among the six *NAC* family genes, *NAC1*, *ORE1*, and *At5g61430* were induced with leaf aging (fig. S9A) and were down-regulated in *miR164*-overexpression lines (fig. S9B), implying that they are targets of *miR164* at the aged leaves. However, loss-of-function mutations of *CUC1*, *CUC2*, *NAC1*, and *At5g07680* did not noticeably alter age-dependent leaf senescence (see fig. S9C for a representative example of *NAC1*). Thus, at least the four *NAC* genes we tested may not have a critical function in age-induced leaf senescence, or their effect on leaf senescence may be negligible to be detected in a single mutation. Expression of *miR156* and *miR172* in *Arabidopsis* is also regulated along the developmental time to control heteroblasty and flowering, respectively (*20*, *21*). Thus, we note that miRNAs appear to participate in the regulation of a range of temporal events in plants. The mechanism presented here should provide insights into aging-induced cell death and senescence in plants as well as in other systems, including animals.

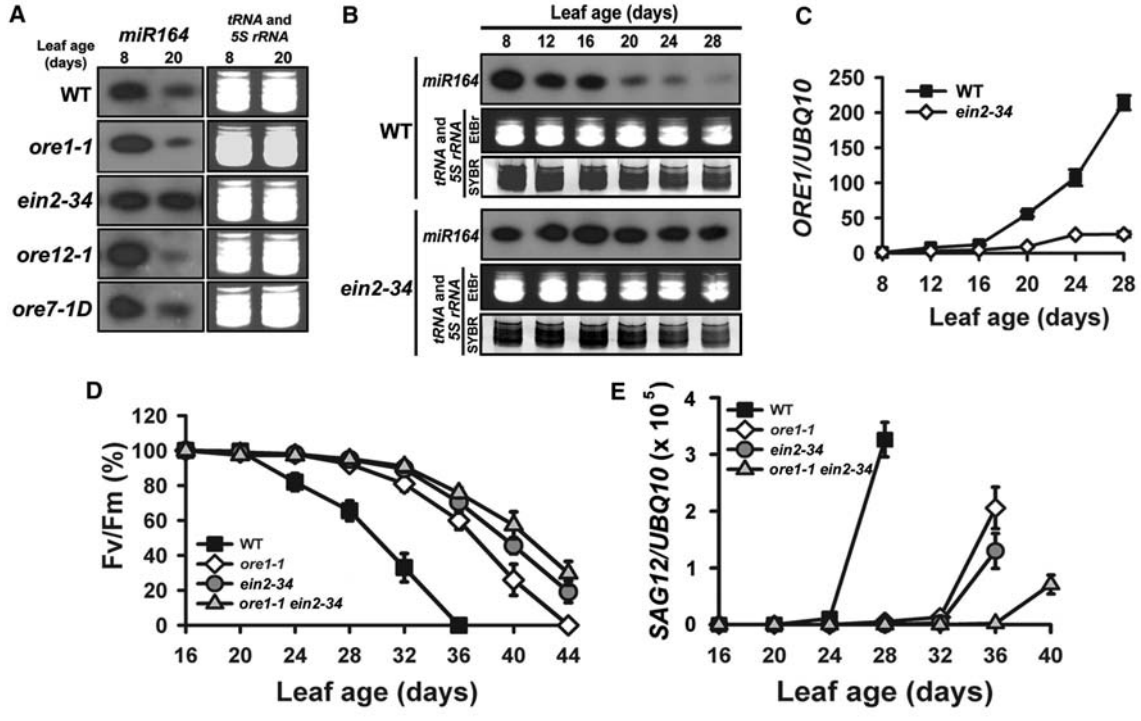

Fig. 4. A trifurcate feed-forward pathway controls age-dependent leaf cell death. (**A**) Comparison of *miR164* level between 8 and 20 days of leaf age in WT and delayed senescence mutant leaves. (**B**) Age-dependent expression of *miR164* in *ein2-34* leaves with aging. tRNA and 5S rRNA are loading controls. (**C**) Age-dependent expression level of *ORE1* mRNA in WT and *ein2-34* leaves. (**D** and **E**) Photochemical efficiency (D) and expression levels of *SAG12* (E) of WT, *ore1-1*, *ein2-34*, and *ore1-1 ein2-34* leaves. In (D), values are mean ± 95 CI (n = 12).

References and Notes

1. P. O. Lim, H. G. Nam, *Annu. Rev. Plant Biol.* **58**, 115 (2007).
2. Y. Guo, S. Gan, *Curr. Top. Dev. Biol.* **71**, 83 (2005).
3. E. Himelblau, R. M. Amasino, *J. Plant Physiol.* **158**, 1317 (2001).
4. S. A. Oh *et al.*, *Plant J.* **12**, 527 (1997).
5. Materials and methods are available as supporting material on *Science* Online.
6. H. R. Woo *et al.*, *Plant Cell* **13**, 1779 (2001).
7. M. A. Torres *et al.*, *Nat. Genet.* **37**, 1130 (2005).
8. X. J. He *et al.*, *Plant J.* **44**, 903 (2005).
9. V. Buchanan-Wollaston *et al.*, *Plant J.* **42**, 567 (2005).
10. R. Schwab *et al.*, *Dev. Cell* **8**, 517 (2005).
11. M. W. Jones-Rhoades, D. P. Bartel, B. Bartel, *Annu. Rev. Plant Biol.* **57**, 19 (2006).
12. M. W. Rhoades *et al.*, *Cell* **110**, 513 (2002).
13. A. C. Mallory, D. V. Dugas, D. P. Bartel, B. Bartel, *Curr. Biol.* **14**, 1035 (2004).
14. P. Sieber, F. Wellmer, J. Gheyselinck, J. L. Riechmann, E. M. Meyerowitz, *Development* **134**, 1051 (2007).
15. H. S. Guo, Q. Xie, J. F. Fei, N. H. Chua, *Plant Cell* **17**, 1376 (2005).
16. S. Mangan, U. Alon, *Proc. Natl. Acad. Sci. U.S.A.* **100**, 11980 (2003).
17. J. M. Alonso, T. Hirayama, G. Roman, S. Nourizadeh, J. R. Ecker, *Science* **284**, 2148 (1999).
18. W. H. Cao *et al.*, *Plant Physiol.* **143**, 707 (2007).
19. B. J. Reinhart *et al.*, *Nature* **403**, 901 (2000).
20. G. Wu, R. S. Poethig, *Development* **133**, 3539 (2006).
21. M. J. Aukerman, H. Sakai, *Plant Cell* **15**, 2730 (2003).

22. We thank E. M. Meyerowitz and P. Sieber for the *mir164abc* triple mutant line; J. Traas for the *miR164A-* and *miR164B-*overexpressing lines; and K. H. Suh, B. H. Kim, and Y. S. Park for technical assistance. This research was supported by grants from the Korea Science and Engineering Foundation National Core Research Center (no. R15-2004-033-05002-0) and the Crop Functional Genomics Frontier Research Program (CG3132) from the Korean government (Ministry of Education, Science, and Technology).

Supporting Online Material

www.sciencemag.org/cgi/content/full/323/5917/1053/DC1
Materials and Methods
Figs. S1 to S9
Tables S1 and S2
References

25 September 2008; accepted 22 December 2008
10.1126/science.1166386

HIN-200 Proteins Regulate Caspase Activation in Response to Foreign Cytoplasmic DNA

Tara L. Roberts,[1,2*] Adi Idris,[1*] Jasmyn A. Dunn,[1] Greg M. Kelly,[1] Carol M. Burnton,[1] Samantha Hodgson,[1] Lani L. Hardy,[1] Valerie Garceau,[1†] Matthew J. Sweet,[1,3] Ian L. Ross,[1] David A. Hume,[1†] Katryn J. Stacey[1,3‡]

The mammalian innate immune system is activated by foreign nucleic acids. Detection of double-stranded DNA (dsDNA) in the cytoplasm triggers characteristic antiviral responses and macrophage cell death. Cytoplasmic dsDNA rapidly activated caspase 3 and caspase 1 in bone marrow–derived macrophages. We identified the HIN-200 family member and candidate lupus susceptibility factor, p202, as a dsDNA binding protein that bound stably and rapidly to transfected DNA. Knockdown studies showed p202 to be an inhibitor of DNA-induced caspase activation. Conversely, the related pyrin domain–containing HIN-200 factor, AIM2 (p210), was required for caspase activation by cytoplasmic dsDNA. This work indicates that HIN-200 proteins can act as pattern recognition receptors mediating responses to cytoplasmic dsDNA.

Recognition of viral dsDNA is important in the initiation of antiviral responses, and is thought to occur in the cytoplasm (*1*–*3*). Transfection of DNA into the cytoplasm induces interferon-β (IFN-β) production, inflammasome activation, and cell death (*3*–*7*), all of which are specific responses to double-stranded DNA (dsDNA) and not single-stranded DNA (ssDNA). Several pathogen products and endogenous danger signals activate the inflammasome, a complex causing the clustering and activation of caspase 1, which subsequently cleaves pro–interleukin-1β (proIL-1β) and proIL-18 to their mature forms (*8*). Caspase 1 activation can also contribute to cell death in response to bacterial infection, in a process termed pyroptosis (*9*). Inflammasome responses to dsDNA require the adapter protein apoptosis-associated speck-like protein containing a caspase recruitment domain (ASC), which has a pyrin domain as well as a caspase recruitment domain (CARD) through which it binds caspase 1 (*5*). ASC itself is normally recruited via interactions between its pyrin domain and other pyrin domains on pathogen-sensing proteins such as Nod-like receptors. Thus, a pyrin domain–containing protein is likely to be involved in recognition of cytosolic dsDNA leading to inflammasome activation.

Primary macrophages and some macrophage cell lines die in response to transfection of dsDNA, and we proposed this as an antiviral defense (fig. S1) (*6*, *7*). In investigating the mechanism of DNA-induced cell death, we found that transfected DNA rapidly activated both caspase 3 and caspase 1, and members of the HIN-200 family of DNA binding proteins initiated and controlled this response.

The only well-characterized receptor for foreign DNA is Toll-like receptor 9 (TLR9) (*10*), which recognizes unmethylated CpG-containing DNA within the endosome (*11*). DNA-dependent IFN-β induction and inflammasome activation are independent of TLR9 (*3*–*5*), as is the DNA-dependent death of bone marrow–derived macrophages (BMMs) (Fig. 1A). The observed toxicity was a specific response to dsDNA and not ssDNA (Fig. 1B) (*6*), was abolished by deoxyribonuclease I (DNase I) treatment (Fig. 1C), and depended on the length of transfected DNA (Fig. 1D). Short ds oligonucleotides did not efficiently induce cell death (*6*), but 44–base pair (bp) DNA could kill cells when transfected at high concentration (fig. S2). In investigating the mechanism of cytoplasmic DNA-induced cell death, we found that an executioner caspase, caspase 3, was activated within 5 min of introduction of DNA (Fig. 1E) in cell types sensitive to DNA-induced cell death (fig. S3). DNA-dependent caspase 1 activation was also observed (Fig. 4A), but was not accompanied by IL-1β secretion, because there is negligible IL-1β mRNA in unprimed BMMs (fig. S4).

To identify candidate DNA receptors, we analyzed cytoplasmic extracts from BMMs for binding to a ds 44-bp oligonucleotide by electromobility shift assay (EMSA). A single strong DNA binding complex was found in the ultracentrifuged pellet of cytoplasmic extract (Fig. 2A). The fact that the DNA binding protein sedimented with ultracentrifugation (fig. S5A) suggests that it is attached to a membrane structure or cytoskeleton, but is released upon DNA binding; hence, the discrete band on EMSA. The candidate receptor bound specifically to dsDNA, with no competition by either ssDNA or dsRNA (Fig. 2A and fig. S5B). dsDNA binding showed no requirement for a sequence motif (Fig. 2B), but like the biological response to DNA, was length dependent; when tested in equal nanogram amounts, a 100-bp fragment of DNA was a more effective competitor than 44-bp DNA, and 22-bp DNA was a poor ligand (Fig. 2C and fig. S5C).

We purified the DNA binding protein from the ultracentrifuged pellet fraction by using dsDNA linked to Sepharose beads. Protein eluted from the beads showed one major 52-kD dsDNA-specific band, when binding to dsDNA-Sepharose and ssDNA-Sepharose was compared (Fig. 2D). This band was analyzed by mass spectrometry and identified from three tryptic fragments (VFNMDLK, LFTYDSIK, and VMVFEENLEK) (*12*) as the interferon-inducible protein p202. An antibody to p202 supershifted the protein-DNA complex on EMSA, whereas two control antibodies had little effect (Fig. 2E). When biotinylated DNA was electroporated into cells, p202 within the cell lysate was stably bound to plasmid, but not ss oligonucleotide (Fig. 2F).

Although p202 was previously shown to be a DNA binding protein, no function has been ascribed

[1]The University of Queensland, Institute for Molecular Bioscience, QLD 4072, Australia. [2]Queensland Institute of Medical Research, Brisbane, QLD 4029, Australia. [3]The University of Queensland, School of Chemistry and Biomolecular Science, QLD 4072, Australia.

*These authors contributed equally to this work.
†Present address: The Roslin Institute, University of Edinburgh, Roslin EH259PS, Scotland, UK.
‡To whom correspondence should be addressed. E-mail: k.stacey@imb.uq.edu.au

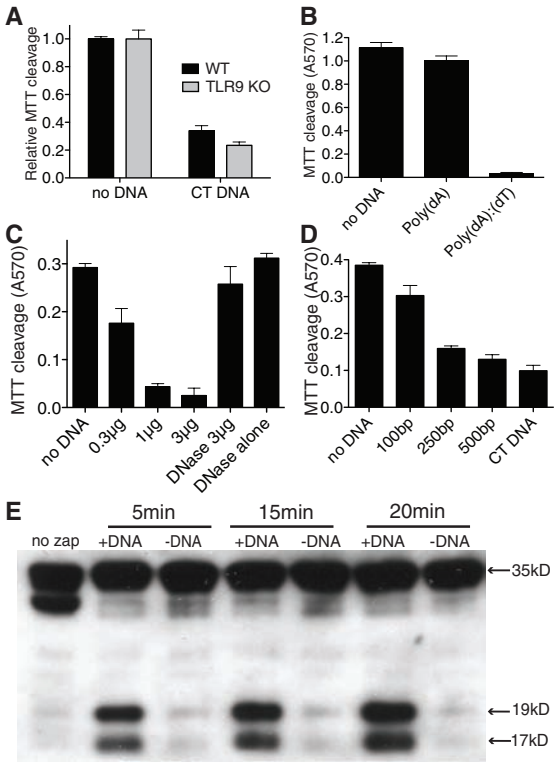

Fig. 1. Transfected DNA–induced BMM death is dependent on DNA length and strandedness and is independent of TLR9. Mitochondrial activity was measured by cleavage of the MTT reagent as an index of cell viability. Except as noted, the assay was performed at 24 hours after transfection, and bars show the mean and error bars the range of duplicate electroporations. Results are representative of two to five experiments. (**A**) Wild-type and TLR9$^{-/-}$ BMMs were electroporated either without DNA or with 10 μg of calf thymus genomic DNA (CT DNA). Results were normalized to the "no DNA" samples. (**B**) Cell death was caused by transfected dsDNA but not ssDNA. C57BL/6 BMMs were electroporated without DNA or with 10 μg of poly(dA) or poly(dA):(dT). (**C**) Loss of mitochondrial function occurred as early as 3 hours after transfection of poly(dA):(dT). TLR9$^{-/-}$ BMMs were electroporated either without DNA, with the indicated amounts of poly(dA):(dT), with 3 μg of DNase I–digested poly(dA):(dT) ("DNase 3μg"), or with DNase I in digestion buffer as a control ("DNase alone"). The assay was perfomed at 3 hours after electroporation. Bars show the mean and error bars the range of values from two independent experiments. (**D**) The length of electroporated DNA fragments determines the degree of cell death. BALB/c BMMs were electroporated without DNA or with 10 μg of polymerase chain reaction (PCR) products of various length, as indicated, or with CT DNA. (**E**) Caspase 3 is rapidly activated after electroporation with dsDNA. BALB/c BMMs were either untreated ("no zap") or electroporated alone ("–DNA") or with 20 μg of CT DNA ("+DNA"). Cells were harvested after 5, 15, or 20 min. Total caspase 3 was detected by Western blotting. Pro–caspase 3 is 35 kD in size and activated cleaved forms are 17 and 19 kD in size.

to this activity (*13*). To determine whether p202 can bind DNA alone, we expressed p202 with an N-terminal small ubiquitin-like modifier (SUMO)–His tag in *Escherichia coli* and purified the SUMO-p202 fusion protein. Full-length SUMO-p202 bound to dsDNA-beads, but truncated p202 products lacking the C-terminal end of the protein and a purified SUMO control did not (Fig. 2, G and H), showing the C-terminal to be essential for high-affinity binding to dsDNA. When analyzed by EMSA, recombinant p202 showed a dsDNA-specific binding activity (fig. S5D), consistent with the result for endogenous p202 (Fig. 2A).

p202 colocalization with microinjected Cy3–CT DNA (calf thymus DNA) occurred within 5 min (fig. S6 and Fig. 3). A 44-bp ds oligonucleotide also colocalized with p202, whereas there was little discernable colocalization of p202 with a 22-bp ds oligonucleotide (Fig. 3). This result corresponds with the higher affinity of p202 for long DNA (Fig. 2C). p202 also colocalized with electroporated Cy3-labeled plasmid (fig. S7).

In the absence of introduced DNA, p202 was diffuse in the cytoplasm (fig. S8). p202 was enriched in regions of the cell that stained strongly for the late endosomal/lysosomal marker LAMP-1 (lysosomal-associated membrane protein 1), but did not exclusively reside in this location (fig. S9A). After introduction of DNA, colocalization with LAMP-1 was lost (fig. S9B). Thus, a proportion of p202 may be bound to the cytoplasmic face of late endosomes/lysosomes and dissociate from this site upon DNA binding. This would explain the presence of p202 in the cytosolic ultracentrifuge pellet fraction and subsequent release to form a discrete band on EMSA.

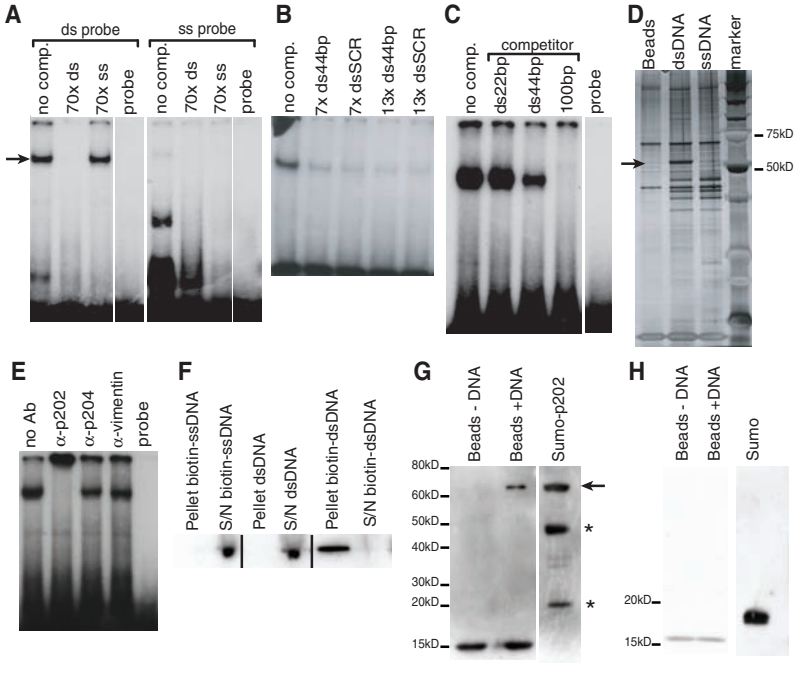

Fig. 2. p202 is a dsDNA-specific binding protein found in the ultracentrifuge pellet fraction of cytoplasmic extract. (**A**) EMSA shows that cytoplasmic extract contains a dsDNA-specific binding protein (arrow). Protein extract was bound to 44-bp dsDNA or 44-base ssDNA probe alone ("no comp.") or with a 70-fold molar excess of unlabeled ds or ss probe, showing that ssDNA did not compete for binding. "Probe" indicates probe without extract. (**B**) The dsDNA binding protein requires no specific sequence motif. Cytoplasmic protein was incubated with probe and 7- or 13-fold molar excess of competitors, either unlabeled probe (ds44bp) or a sequence-scrambled version (dsSCR). (**C**) Binding depends on DNA length. Cytoplasmic protein was incubated with 0.77 ng of 44-bp probe and 1.2 ng of unlabeled 22-, 44-, or 100-bp DNA (1.6-fold ng excess). (**D**) Purification of dsDNA-binding protein. Cytoplasmic extract was incubated with beads bound to either dsDNA, ssDNA, or no DNA ("beads"). Analysis of bound proteins revealed a 52-kD dsDNA binding protein (arrow). (**E**) EMSA supershift showing that the dsDNA-specific binding protein is p202. Cytoplasmic protein and probe were incubated with or without antisera against p202, p204, or vimentin. (**F**) p202 stably interacts with cytosolic DNA. Biotinylated plasmid DNA ("biotin-dsDNA"), unlabeled plasmid ("dsDNA"), or biotinylated 44-base oligonucleotide ("biotin-ssDNA") was electroporated into RAW264 cells stably expressing p202-V5. After 1 hour, cells were lysed and proteins associated with the biotinylated DNA were isolated by binding to streptavidin-Sepharose ("pellet"). The location of p202 in the biotinylated DNA-bound pellet fraction or unbound supernatant (S/N) was assessed by Western blotting for V5. (**G**) Purified recombinant SUMO-p202 binds directly to plasmid DNA. N-terminally SUMO/His-tagged p202 was incubated with streptavidin beads with or without bound biotinylated dsDNA. Bound protein was analyzed by Western blotting with anti-His. Analysis of input protein (right) shows full-length SUMO-p202 (arrow) and two C-terminal truncations (asterisks). A contaminating cross-reactive protein of 15kD bound nonspecifically to beads. (**H**) Purified SUMO tag does not bind to DNA. The experiment was performed as in (G).

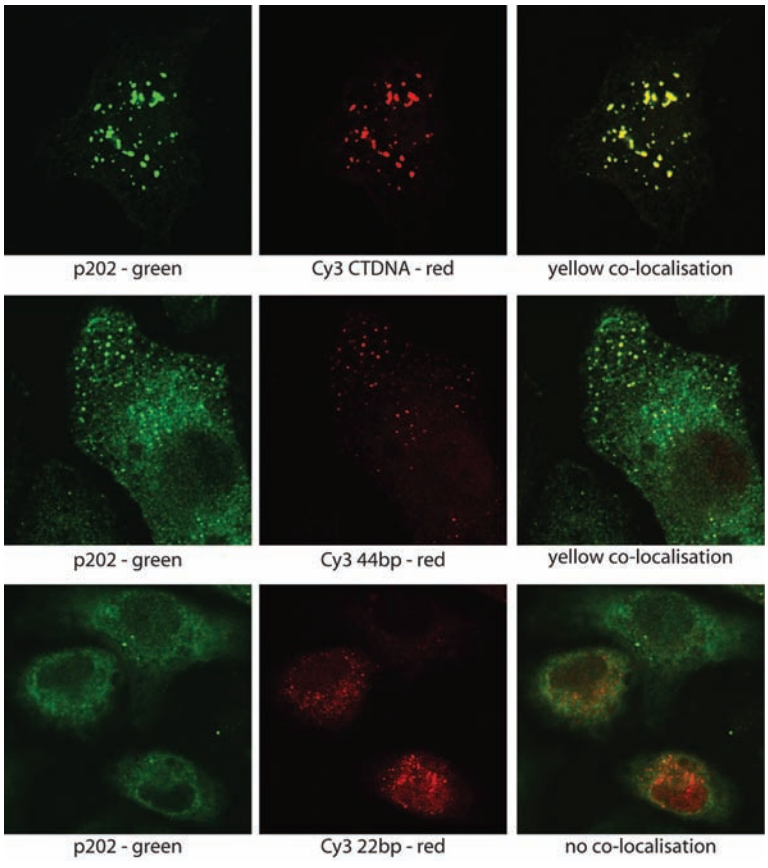

Fig. 3. Colocalization of microinjected Cy3-labeled CT DNA with p202. One hour after microinjection with labeled DNA, NZB BMMs were methanol fixed and antibody stained to show p202 localization. p202 (green, left panels) completely colocalized with CT DNA (red, center top panel) and slightly with ds44bp (red, center panel) and not at all with ds22bp (red, center bottom panel). Colocalization is indicated in yellow (right panels).

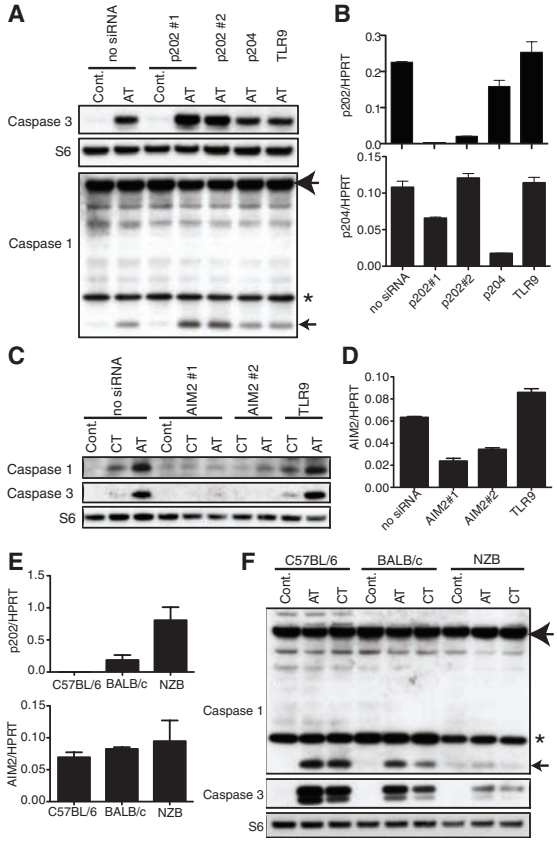

Fig. 4. HIN-200 factors regulate DNA-dependent caspase activation. (**A**) Knockdown of p202 enhances DNA-induced caspase 3 and caspase 1 activation. BALB/c BMMs were electroporated with the indicated siRNAs and left for 24 hours before electroporation with either no DNA ("cont.") or 1 μg of poly(dA):(dT) ("AT"). After 20 min, cells were lysed and protein extracts analyzed by Western blotting for cleaved caspase 3, S6 ribosomal protein as loading control, and caspase 1. A separate gel with the same samples is shown for caspase 1. The large arrow indicates full-length pro-caspase 1 (45kD), a small arrow the active cleaved product (10 kD), and the asterisk a nonspecific band. Results are representative of five experiments with three different siRNAs against p202 (fig. S10). (**B**) p202 and p204 mRNA expression relative to hypoxanthine-guanine phosphoribosyltransferase (HPRT) measured by real time PCR, 24 hours after electroporation with siRNAs used in (A). Bars show the mean of duplicate assays and error bars the SD as defined in the online methods. (**C**) Knockdown of AIM2 prevents DNA-induced caspase 3 and caspase 1 activation. BALB/c BMMs were electroporated with the indicated siRNAs and left for 24 hours before electroporation with either no DNA ("cont."), 10 μg of CT DNA ("CT"), or 1 μg of poly(dA):(dT) ("AT"). Samples were analyzed as in (A). Results are representative of four experiments. (**D**) AIM2 mRNA expression relative to HPRT measured by real time PCR as in (B), 24 hours after electroporation of siRNAs used in (C). (**E**) Expression of p202 and AIM2 mRNAs in BMMs from C57BL/6, BALB/c, and NZB mouse strains. Shown are the mean and range of results for two independent RNA preparations. (**F**) Activation of caspases in BMMs from three mouse strains electroporated with DNAs as in (C). Arrows and asterisk are as in (A).

To examine the function of p202, we knocked down (reduced) its expression using three different small interfering RNAs (siRNAs) (p202#1 to #3) and examined the response to electroporated DNA 24 hours later (Fig. 4, A and B, and fig. S10). Activation of both caspase 3 and caspase 1 was more pronounced with reduced p202, whereas use of siRNAs against the related protein p204, as well as TLR9, had no effect. Thus, p202 is not a DNA receptor mediating caspase activation, but instead antagonizes this pathway.

p202 is a member of the hematopoietic interferon-inducible nuclear protein HIN-200 family, a cluster of 13 or more interferon-inducible genes on mouse chromosome 1 (*14*–*16*). This family of proteins are characterized by the presence of one or two 200–amino acid HIN domains of poorly understood function, although the C-terminal HIN domain of p202 is required for dsDNA binding (Fig. 2G). All HIN-200 factors, apart from p202, contain an N-terminal pyrin domain, making them candidates for a DNA-dependent activator of caspase 1. Among the HIN-200 family, the pyrin domain of absent in melanoma 2 (AIM2 or p210) is the most similar to inflammasome-related pyrin domains (*17*). Further, AIM2 is the only family member with a clear human ortholog and is known to heterodimerize with p202 (*15*, *18*). Knockdown of AIM2 completely prevented activation of caspase 3 and caspase 1, even though the mRNA knockdown was only partial (Fig. 4, C and D). Sequestration of DNA by p202, or heterodimerization between p202 and AIM2, would inhibit AIM2-mediated responses, because the lack of a pyrin domain on p202 would reduce clustering of ASC and subsequent caspase 1 activation (fig. S11). Consequently, in the presence of p202, when the amount of AIM2 protein drops below a threshold, it would no longer signal.

Expression of p202 varies greatly between mouse strains (*19*). p202 mRNA was highly expressed in BMMs from NZB mice but barely detectable in those of C57BL/6 mice, whereas AIM2 expression was similar in all three strains tested (Fig. 4E). Consistent with the hypothesis that p202 regulates DNA-dependent caspase activation initiated by AIM2, caspase activation correlated inversely with the abundance of p202 in the three strains (Fig. 4F). p202 is suggested as a susceptibility factor for systemic lupus erythematosus (SLE), because it falls within the major susceptibility locus in NZB and BSXB mice and is overexpressed in these strains (*19*, *20*). SLE is an autoimmune disease in which DNA may act both as antigen and adjuvant (*21*), and results here suggest that p202 contributes to the SLE phenotype by modifying responses to cytoplasmic DNA. As well as DNA deriving from viruses or retrotransposons, cytoplasmic DNAs could be derived from phagocytosed self-DNA that has escaped into the cytoplasm.

In summary, the HIN-200 family proteins are a class of pattern recognition receptors, in which AIM2 promotes and p202 represses the activation of caspases in response to cytoplasmic dsDNA. The function of other members of the family awaits definition. The conservation seen among the HIN domains suggests they all have the potential to mediate responses to nucleic acids, perhaps differing in sequence specificity, localization, or effector function.

References and Notes

1. M. Nociari, O. Ocheretina, J. W. Schoggins, E. Falck-Pedersen, *J. Virol.* **81**, 4145 (2007).
2. J. Zhu, X. Huang, Y. Yang, *J. Virol.* **81**, 3170 (2007).
3. D. B. Stetson, R. Medzhitov, *Immunity* **24**, 93 (2006).
4. K. J. Ishii *et al.*, *Nat. Immunol.* **7**, 40 (2006).
5. D. A. Muruve *et al.*, *Nature* **452**, 103 (2008).
6. K. J. Stacey, I. L. Ross, D. A. Hume, *Immunol. Cell Biol.* **71**, 75 (1993).
7. T. J. Van De Parre, W. Martinet, D. M. Schrijvers, A. G. Herman, G. R. De Meyer, *Biochem. Biophys. Res. Commun.* **327**, 356 (2005).
8. F. Martinon, J. Tschopp, *Cell Death Differ.* **14**, 10 (2007).
9. K. Labbe, M. Saleh, *Cell Death Differ.* **15**, 1339 (2008).
10. H. Hemmi *et al.*, *Nature* **408**, 740 (2000).
11. E. Latz *et al.*, *Nat. Immunol.* **5**, 190 (2004).
12. Abbreviations for the amino acid residues are as follows: A, Ala; C, Cys; D, Asp; E, Glu; F, Phe; G, Gly; H, His; I, Ile; K, Lys; L, Leu; M, Met; N, Asn; P, Pro; Q, Gln; R, Arg; S, Ser; T, Thr; V, Val; W, Trp; and Y, Tyr.
13. D. Choubey, J. U. Gutterman, *Biochem. Biophys. Res. Commun.* **221**, 396 (1996).
14. B. Asefa *et al.*, *Blood Cells Mol. Dis.* **32**, 155 (2004).
15. L. E. Ludlow, R. W. Johnstone, C. J. Clarke, *Exp. Cell Res.* **308**, 1 (2005).
16. T. J. Hubbard *et al.*, *Nucleic Acids Res.* **35**, D610 (2007).
17. T. Liu, A. Rojas, Y. Ye, A. Godzik, *Protein Sci.* **12**, 1872 (2003).
18. D. Choubey, S. Walter, Y. Geng, H. Xin, *FEBS Lett.* **474**, 38 (2000).
19. S. J. Rozzo *et al.*, *Immunity* **15**, 435 (2001).
20. M. E. Haywood *et al.*, *Genes Immun.* **7**, 250 (2006).
21. A. Marshak-Rothstein, *Nat. Rev. Immunol.* **6**, 823 (2006).

22. This work was supported by grants from the National Health and Medical Research Council (NHMRC) of Australia (grants 455920 and 455882), and by the Cooperative Research Centre for Chronic Inflammatory Diseases. T.L.R. is the recipient of an NHMRC Peter Doherty Fellowship. Mass spectrometry facilities are supported by the Australian Research Council Special Research Centre for Functional and Applied Genomics. Confocal microscopy was performed at the Institute for Molecular Bioscience Dynamic Imaging Facility for Cancer Biology funded by the Australian Cancer Research Foundation. R. Johnstone and C. Clarke provided materials and valuable advice on the HIN-200 family proteins. S. Akira provided TLR9$^{-/-}$ mice. The work presented here is related to International Patent Application PCT/AU2007/001330.

Supporting Online Material

www.sciencemag.org/cgi/content/full/1169841/DC1
Methods
Figs. S1 to S11
References

4 June 2008; accepted 23 December 2008
Published online 8 January 2009;
10.1126/science.1169841
Include this information when citing this paper.

A Genetic Defect Caused by a Triplet Repeat Expansion in *Arabidopsis thaliana*

Sridevi Sureshkumar,[1,2]* Marco Todesco,[1]* Korbinian Schneeberger,[1] Ramya Harilal,[1] Sureshkumar Balasubramanian,[1,2]† Detlef Weigel[1]†

Variation in the length of simple DNA triplet repeats has been linked to phenotypic variability in microbes and to several human disorders. Population-level forces driving triplet repeat contraction and expansion in multicellular organisms are, however, not well understood. We have identified a triplet repeat–associated genetic defect in an *Arabidopsis thaliana* variety collected from the wild. The Bur-0 strain carries a dramatically expanded TTC/GAA repeat in the intron of the *ISOPROPYL MALATE ISOMERASE LARGE SUB UNIT1* (*IIL1*; At4g13430) gene. The repeat expansion causes an environment-dependent reduction in *IIL1* activity and severely impairs growth of this strain, whereas contraction of the expanded repeat can reverse the detrimental phenotype. The Bur-0 *IIL1* defect thus presents a genetically tractable model for triplet repeat expansions and their variability in natural populations.

Copy number variation in tandemly repeated, short DNA sequences can underlie phenotypic variability in microbes (*1*–*3*), and several human disorders are caused by expansions of trinucleotide (or triplet) repeats (*4*–*6*). DNA polymerase slippage and unequal crossing over affect repeat numbers (*7*, *8*), but how repeat variation arises and is maintained within a population is largely unknown.

To uncover cryptic genetic variation in *Arabidopsis thaliana,* we grew strains, collected from the wild, at 27°C and with short days—an environment not normally encountered by this species in its natural range (*9*). Most strains appeared normal (Fig. 1A), but the Bur-0 strain suffered from pleiotropic growth abnormalities and never progressed to the flowering stage. Because of the misshapen leaves (Fig. 1B), we refer to this phenotype as "*irregularly impaired leaves*" (*iil*). At 23°C, the *iil* defects disappeared (Fig. 1C), whereas the phenotype was even worse at 30°C (long days) (fig. S1) (*10*). Similarly, higher light intensity worsened the *iil* phenotype (Fig. 1, D and E). Leaf primordia arose normally (fig. S2, A and B), which suggested that the *iil* phenotype is due to abnormal leaf growth and expansion. The cellular architecture of the mesophyll was disrupted (Fig. 1F), whereas the overall organization of the vasculature was more normal (fig. S2, C to F).

[1]Department of Molecular Biology, Max Planck Institute for Developmental Biology, D-72076 Tübingen, Germany. [2]School of Biological Sciences, The University of Queensland, St. Lucia, QLD 4072, Australia.

*These authors contributed equally to the work.
†To whom correspondence should be addressed. E-mail: mb.suresh@uq.edu.au (S.B.), weigel@weigelworld.org (D.W.)

To determine the genetic basis of the *iil* defect, we crossed Bur-0 with another strain, Pf-0. F_1 plants were normal, but the *iil* phenotype reappeared in about 25% of F_2 plants. By linkage analysis in this population, we mapped the *IIL* locus to a 16.7-kilobase (kb) interval. In the sequenced strain Col-0, this region includes two genes fully, At4g13420 and At4g13430, and the first seven exons of At4g13410 (fig. S3). Because cDNA sequencing did not suggest causal polymorphisms in any of the three genes, we surveyed the mapping interval with the polymerase chain reaction (PCR). We discovered a dramatic expansion of a TTC/GAA triplet repeat from 23 copies in Col-0 and Pf-0 to more than 400 copies in the third intron of At4g13430 from Bur-0 (Fig. 2A). In humans, intronic TTC/GAA expansions reduce expression of the affected genes, with TTC repeats having weaker effects on transcript accumulation than GAA repeats (*11*–*14*). Consistent with this, At4g13430 RNA levels were ~50% lower in Bur-0 than in Pf-0 or Col-0 at 27°C (Fig. 2B). At 23°C, RNA levels did not differ between genotypes (Fig. 2B).

To test whether reduced At4g13430 RNA levels were the cause for the *iil* defects, we overexpressed the mature Bur-0 transcript in Bur-0 (fig. S4A). These plants no longer had the *iil* phenotype, and their growth habit was similar to that of other strains (Fig. 2, C and D). On the basis of these results, we concluded that At4g13430 is *IIL*.

IIL encodes a chloroplast-localized protein (*15*). Many other genes encoding chloroplast- and endomembrane-localized proteins were down-regulated in Bur-0 plants grown at 27°C, and this group of genes was overrepresented among all down-regulated genes [chi-square test, $P < 0.01$ (table S1)]. However, transmission electron microscopy did not reveal any major abnormalities in the chloroplasts of *iil* plants (fig. S5). IIL is the *A. thaliana* protein that is most closely related to fungal isopropyl malate dehydratase, an enzyme involved in leucine biosynthesis, and is henceforth referred to as ISOPROPYLMALATE ISOMERASE LARGE SUBUNIT 1, IIL1 (*16*) (fig. S6). Although irrigation of plants with a leucine solution did not ameliorate the *iil* defect, analysis of the amino

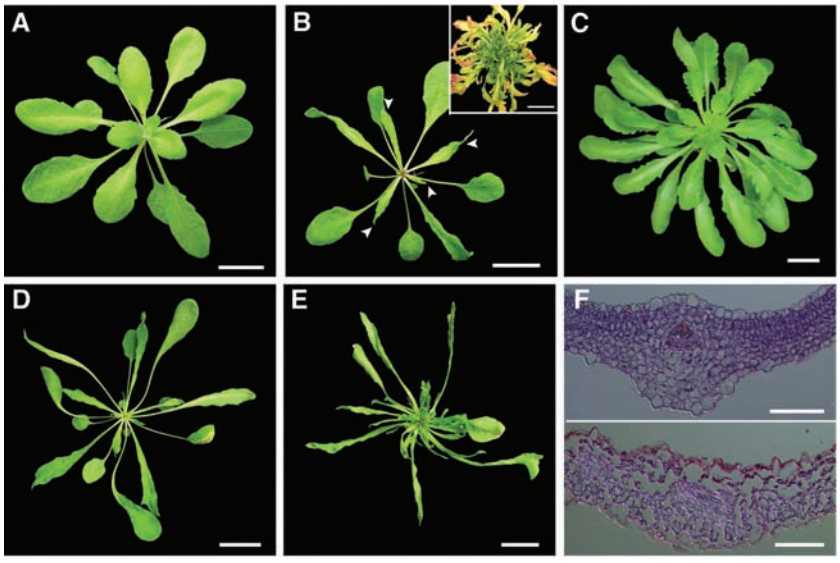

Fig. 1. The *iil* phenotype. (**A**) Four-week-old, normal-appearing Pf-0 plant grown at 27°C (short days). (**B**) Four-week-old Bur-0 plant at 27°C. Arrowheads indicate misshapen leaves, from about the seventh leaf onward. Inset shows progressive worsening of the phenotype after 10 weeks. (**C**) Ten-week-old, phenotypically normal Bur-0 plant at 23°C. (**D**) Six-week-old Bur-0 plant at 27°C, under photosynthetic photon flux density (PPFD) of 140 to 150 μmol m^{-2} s^{-1}. (**E**) Bur-0 plant under PPFD of 200 to 210 μmol m^{-2} s^{-1}. (**F**) Cross section of expanded leaves of Pf-0 (top) and Bur-0 at 27°C. Scale bars, 1.5 cm, except (F), 200 μm.

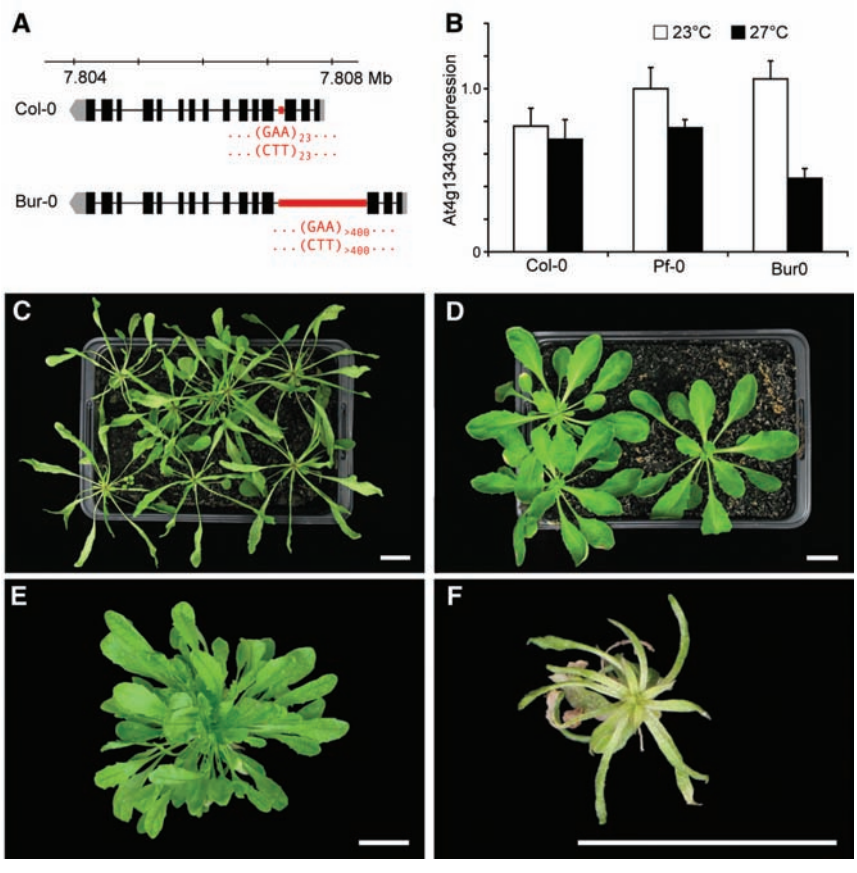

Fig. 2. Identification of At4g13430 as *IIL1*. (**A**) Location of expanded TTC/GAA repeats in At4g13430. See supporting information for details and fig. S3 for final mapping interval. (**B**) Real-time reverse transcriptase polymerase chain reaction (RT-PCR) analysis of At4g13430 RNA in leaves of 4-week-old plants, with at least two technical and eight biological replicates. Means ± SEM. Expression levels of Pf-0 and Bur-0 plants at 27°C differed significantly (Student's *t* test, $P < 0.0004$). (**C**) Five-week-old Bur-0 plants at 27°C. (**D**) Bur-0 plants harboring *35S:IIL1* Bur-0 transgene. (**E**) Ten-week-old *35S:amiR-IIL1* Bur-0 plant at 23°C. (**F**) Five-week-old *35S:amiR-IIL1* Bur-0 plant at 30°C (long days). Scale bars, 1.5 cm.

acid content of Col-0 plants with reduced IIL1 activity supports a similar role in *A. thaliana* (*17*).

Because a Col-0 line with a transferred DNA insertion at the 5′ end of *IIL1* (*10*) did not have the *iil* phenotype, we reduced steady-state levels of *IIL1* RNA by ~50% (fig. S4B) using an artificial microRNA (amiRNA) (*18*). AmiR-IIL1 introduction caused only a mild phenotype in Bur-0 and Pf-0 at 23°C, with slower growth and slightly paler leaves (Fig. 2 and fig. S7A). At elevated temperatures, the phenotype of Bur-0 or Pf-0 amiR-IIL1 plants became more severe, including high mortality (Fig. 2F and fig. S7, B and C). These observations indicated that Bur-0 and Pf-0 require more IIL1 activity as temperatures rise.

Defects caused by amiR-IIL1 were milder in the Col-0 background at all temperatures (fig. S7, D and E). The weaker effects of amiR-IIL1 in Col-0, compared with Bur-0 or Pf-0, were consistent with the segregation of the *iil* phenotype in a Col-0 × Bur-0 F_2 population. Only 23 out of 485 plants were affected, which suggested the presence of *iil* modifiers in the Col-0 genome. Further mapping in Bur-0 × Col-0 recombinant inbred lines (RILs) (*19*) revealed a region on chromosome 2 that may interact with the *IIL1* interval to produce the *iil* phenotype (Fig. 3, A and B).

In mammals, expanded TTC/GAA repeats often display extensive somatic variability (*20*–*22*). Likewise, we observed both between- and within-individual variability of repeat length in *IIL1* (Fig. 4A). We exploited this variability to demonstrate that the triplet repeat expansion causes the *iil* phenotype in Bur-0. We found 17 phenotypic revertants among 30,000 Bur-0 plants; all 17 showed a reduction in repeat length (Fig. 4B). Because ethyl methane sulfonate (EMS) can promote the contraction of triplet repeats (*23*, *24*), we also screened for suppression of the *iil* phenotype among 30,000 M_2 progeny of selfed, EMS-treated Bur-0 plants. We isolated 156 phenotypic revertants, 27 of which had reduced triplet copy number (Fig. 4B). Although EMS in this system did not strongly promote repeat contraction, the EMS population contained many phenotypically normal lines that had retained the expanded triplet repeats.

Stable phenotypic suppression was confirmed in the offspring of 13 spontaneous revertants. None had more than 120 triplet repeats left, which supported the hypothesis that the expanded triplet repeats caused the *iil* phenotype. In agreement, *IIL1* expression was increased in the revertants compared with the Bur-0 parent (Fig. 4, C and D, and fig. S4C). Reducing *IIL1* expression again in these lines with amiR-IIL1 resulted in a severe *iil* phenotype under higher temperatures (fig. S7F). We conclude that a decrease in *IIL1* expression caused by the expanded triplets, coupled with higher require-

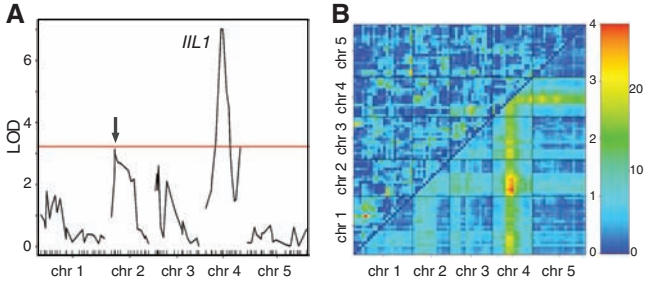

Fig. 3. Mapping of an *IIL1* modifier in Col-0. (**A**) Quantitative trait locus (QTL) analysis of *iil* phenotype in 164 Bur-0 × Col-0 RILs. Chromosome 2 has a LOD (logarithm of odds) peak (arrow) just below the significance threshold (red line). (**B**) Heat map for a two-dimensional genome scan with a two-QTL model. Upper triangle shows epistatic interactions (LOD scale on the left of the color bar), lower triangle additive interactions (scale on the right of the color bar). Although the LOD peak on chromosome 2 does not surpass the significance threshold on its own (A), this region appears to act additively with the *IIL1* QTL on chromosome 4.

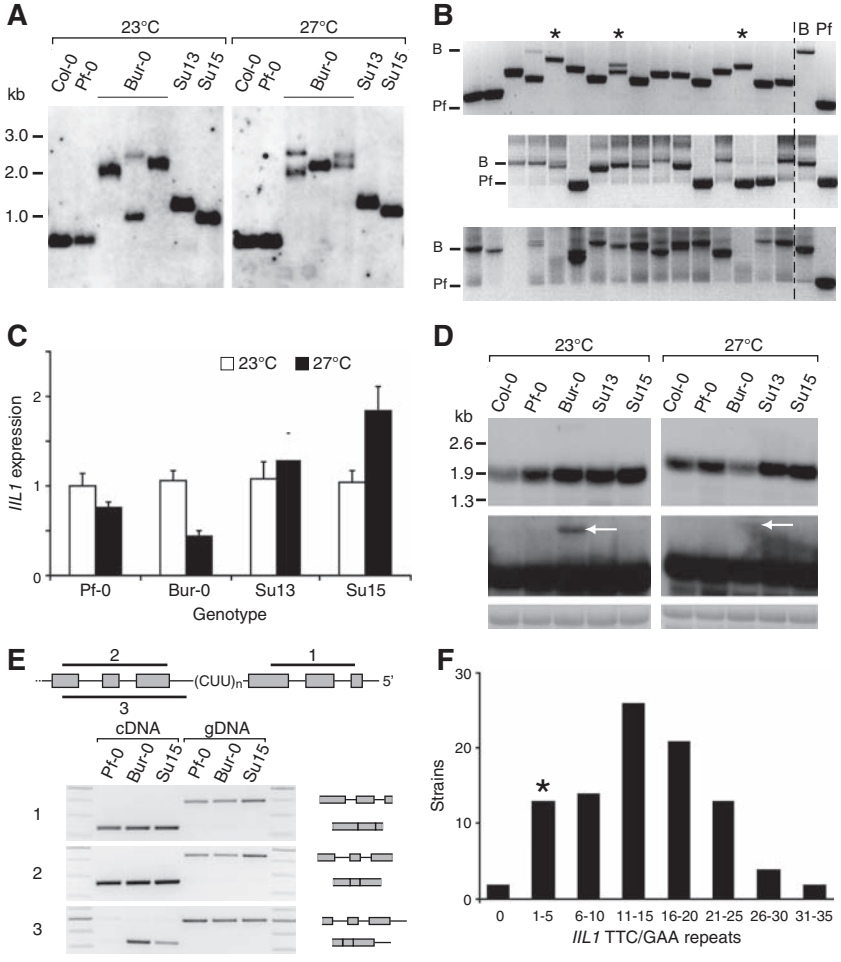

Fig. 4. Analysis of triplet repeat variation. (**A**) DNA blot analysis of *IIL1* triplet repeat–containing region. Su13 and Su15 are two spontaneous revertants in the Bur-0 background. (**B**) PCR analysis of *IIL1* repeat. Bur-0 [(B) ~2.3-kb fragment with over 400 repeats] and Pf-0 [(Pf) ~1.1 kb with 23 repeats] are always shown on the right. (Top) Sixteen spontaneous revertants are shown out of 17 spontaneous revertants in which phenotypic suppression was transmitted to the next generation. Asterisks indicate that ~50% of progeny regained the *iil* phenotype. (Middle) M_2 progeny of EMS-treated plants. All lacked the *iil* phenotype, but only a fraction had a shortened repeat. (Bottom) EMS M_2 progeny retaining the *iil* phenotype. (**C**) *IIL1* expression, measured by real-time RT-PCR. (**D**) RNA blots revealed a larger *IIL1* transcript isoform in Bur-0 (arrows): (top) after 30 min′, (middle) after 3.5 hours′ exposure. (Bottom) Ethidium bromide staining of the RNA shown to indicate loading. (**E**) RT-PCR analysis (30 cycles) of cDNA from plants grown at 27°C, with genomic DNA (gDNA) as control. Amplified fragments are indicated on top. Intron retention is reduced in Su15 compared to Bur-0, and not detected in Pf-0. Sequencing of the PCR product confirmed that the adjacent introns were not retained. See table S2 for the sequences of primers used. (**F**) Distribution of *IIL1* repeat copy number in 96 *A. thaliana* strains and in MN47 strain of *A. lyrata* (asterisk).

ments of *IIL1* activity under elevated temperatures, is the basis of the *iil* phenotype in Bur-0 plants.

RNA blots revealed longer *IIL1* transcript isoforms of minor abundance in Bur-0, independent of growth temperature (Fig. 4D). PCR analyses showed that this isoform retained only the intron containing the triplet expansion (Fig. 4E). The relatively weak effects are consistent with reports that GAA repeats are more likely than UUC repeats to affect splicing in mammalian cells (*25*). However, because normal splicing is not completely restored in a spontaneous revertant with an intermediate repeat length (Fig. 4E), the splicing defects alone cannot explain the observed differences in RNA expression levels. Nevertheless, inefficient splicing might contribute to reduced expression of mature *IIL1* transcripts, along with transcriptional defects, epigenetic changes, and post-transcriptional silencing (*26*–*28*).

If long repeats tended to be detrimental, as in the *IIL1* case, one would expect that these are rare in the genome. Indeed, less than 1% of all triplet repeats in the reference *A. thaliana* genome have six or more copies (table S3), and there is no expressed gene with more than 41 copies (table S4). The Bur-0 allele of *IIL1* itself seems to be rare, because we did not find it among 96 other *A. thaliana* strains nor in *Arabidopsis lyrata* (figs. S8 and S9). Several strains had either more (up to 36) or fewer than the 23 repeats in the Col-0 reference genome, and two strains had lost the triplets (Fig. 4F). These observations confirm the dynamic nature of the *IIL1* triplet repeat. Copy number variability in normal individuals is common for triplet expansion disorders in humans and often underlies genetic anticipation (*5*, *6*).

The *A. thaliana* Bur-0 allele of *IIL1* presents a genetically tractable model for the study of triplet repeat expansion and contraction across multiple generations. The recovery of phenotypic revertants that had retained the expanded *IIL1* repeat highlights the potential of the *IIL1* triplet repeat for future studies. Some of the apparent second-site mutations might act downstream of *IIL1*, but others might ameliorate the effects of the triplet repeat expansion itself. In addition, our findings support the argument that simple sequence repeats could be associated with phenotypic variability of evolutionary significance (*1*–*3*).

References and Notes

1. E. Levdansky *et al.*, *Eukaryot. Cell* **6**, 1380 (2007).
2. T. P. Michael *et al.*, *PLoS One* **2**, e795 (2007).
3. K. J. Verstrepen, A. Jansen, F. Lewitter, G. R. Fink, *Nat. Genet.* **37**, 986 (2005).
4. J. W. Fondon 3rd, E. A. Hammock, A. J. Hannan, D. G. King, *Trends Neurosci.* **31**, 328 (2008).
5. H. T. Orr, H. Y. Zoghbi, *Annu. Rev. Neurosci.* **30**, 575 (2007).
6. C. E. Pearson, K. Nichol Edamura, J. D. Cleary, *Nat. Rev. Genet.* **6**, 729 (2005).
7. L. Y. Brown, S. A. Brown, *Trends Genet.* **20**, 51 (2004).
8. R. D. Wells, R. Dere, M. L. Hebert, M. Napierala, L. S. Son, *Nucleic Acids Res.* **33**, 3785 (2005).
9. M. H. Hoffmann, *J. Biogeography* **29**, 125 (2002).
10. Supporting tables, figures, and materials and methods are available as supporting material on *Science* Online.
11. S. I. Bidichandani, T. Ashizawa, P. I. Patel, *Am. J. Hum. Genet.* **62**, 111 (1998).
12. E. Grabczyk, K. Usdin, *Nucleic Acids Res.* **28**, 2815 (2000).
13. K. Ohshima, L. Montermini, R. D. Wells, M. Pandolfo, *J. Biol. Chem.* **273**, 14588 (1998).
14. R. D. Wells, *FASEB J.* **22**, 1625 (2008).
15. B. Zybailov *et al.*, *PLoS ONE* **3**, e1994 (2008).
16. G. B. Kohlhaw, *Microbiol. Mol. Biol. Rev.* **67**, 1 (2003).
17. T. Knill, S. Binder, personal communication.
18. R. Schwab, S. Ossowski, M. Riester, N. Warthmann, D. Weigel, *Plant Cell* **18**, 1121 (2006).
19. M. Simon *et al.*, *Genetics* **178**, 2253 (2008).
20. R. M. Clark *et al.*, *Hum. Genet.* **120**, 633 (2007).
21. I. De Biase *et al.*, *Genomics* **90**, 1 (2007).
22. R. Sharma *et al.*, *Hum. Mol. Genet.* **11**, 2175 (2002).
23. V. I. Hashem *et al.*, *Nucleic Acids Res.* **32**, 6334 (2004).
24. V. I. Hashem, R. R. Sinden, *Mutat. Res.* **508**, 107 (2002).
25. M. Baralle, T. Pastor, E. Bussani, F. Pagani, *Am. J. Hum. Genet.* **83**, 77 (2008).
26. S. Al-Mahdawi *et al.*, *Hum. Mol. Genet.* **17**, 735 (2008).
27. R. Frisch *et al.*, *Mol. Genet. Metab.* **74**, 281 (2001).
28. E. Greene, L. Mahishi, A. Entezam, D. Kumari, K. Usdin, *Nucleic Acids Res.* **35**, 3383 (2007).

29. We are very grateful to T. Knill and S. Binder for sharing unpublished information. We acknowledge experimental support from our colleagues at the Max Planck Institute and University of Queensland. We also thank them as well as J. Carrington and D. Tautz for critical reading of the manuscript, and the European *Arabidopsis* Stock Centre and the French National Institute for Agricultural Research (INRA) at Versailles for seeds. Supported by an EMBO (*European Molecular Biology Organization*) Long-Term Fellowship (S.B.), Marie Curie Research Training Network SY-STEM, European Research Area—Plant Genomics (ERA-PG) Deutsche Forschungsgemeinschaft ARelatives Consortium, European Union Sixth Framework Programme for Research and Technological Development Integrated Project (EU FP6 IP) Agronomics (LSHG-CT-2006-037704), a Leibniz Award (DFG), and the Max Planck Society (D.W.). GenBank accession numbers are FJ665284 to FJ665378.

Supporting Online Material

www.sciencemag.org/cgi/content/full/1164014/DC1
Materials and Methods
Figs. S1 to S9
Tables S1 to S4
References

31 July 2008; accepted 11 December 2008
Published online 15 January 2009;
10.1126/science.1164014
Include this information when citing this paper.

Stress-Inducible Regulation of Heat Shock Factor 1 by the Deacetylase SIRT1

Sandy D. Westerheide,[1]* Julius Anckar,[2]* Stanley M. Stevens Jr.,[3] Lea Sistonen,[2] Richard I. Morimoto[1]†

Heat shock factor 1 (HSF1) is essential for protecting cells from protein-damaging stress associated with misfolded proteins and regulates the insulin-signaling pathway and aging. Here, we show that human HSF1 is inducibly acetylated at a critical residue that negatively regulates DNA binding activity. Activation of the deacetylase and longevity factor SIRT1 prolonged HSF1 binding to the heat shock promoter Hsp70 by maintaining HSF1 in a deacetylated, DNA–binding competent state. Conversely, down-regulation of SIRT1 accelerated the attenuation of the heat shock response (HSR) and release of HSF1 from its cognate promoter elements. These results provide a mechanistic basis for the requirement of HSF1 in the regulation of life span and establish a role for SIRT1 in protein homeostasis and the HSR.

Transient activation of heat shock factor 1 (HSF1) by diverse environmental and physiological stress is a multistep process that involves constitutive expression of an inert HSF1 monomer, conversion of the monomer to a DNA–binding competent trimer, increased phosphorylation of HSF1 at serine residues, enhanced transcription, and attenuation of HSF1 DNA binding and transcriptional activity (*1*). HSF1 activates the transcription of a large number of genes that regulate protein homeostasis including the molecular chaperones heat shock proteins 70 and 90 (Hsp70 and Hsp90, respectively). These chaperones associate with HSF1 to initiate a negative-feedback loop and to inhibit HSF1 transcriptional activity (*2*). However, HSF1 is not released from its target promoter sites (*3*); this suggests that additional mechanisms must exist to complete the HSF1 cycle.

Stress resistance and metabolic state are intimately coupled to protein homeostasis and increased life span. In *Caenorhabditis elegans*, the protective effects of reduced insulin signaling require HSF1 and the FOXO transcription factor DAF-16 to prevent damage by protein misfolding and to promote longevity (*4*, *5*). The beneficial effects of low caloric intake are mediated by the sirtuin family member Sir2, a deacetylase that is dependent on nicotinamide adenine dinucleotide (oxidized form) (NAD) and that is under metabolic control (*6*). The mammalian Sir2 homolog SIRT1 regulates the transcription factor FOXO3 among

[1]Department of Biochemistry, Molecular Biology and Cell Biology, Rice Institute for Biomedical Research, Northwestern University, Evanston, IL, 60208, USA. [2]Department of Biology, Turku Centre for Biotechnology, Åbo Akademi University, FI-20520 Turku, Finland. [3]University of Florida, Protein Chemistry Core Facility, Interdisciplinary Center for Biotechnology Research, Gainesville, FL 32610, USA.

*These authors contributed equally to this work.
†To whom correspondence should be addressed. E-mail: r-morimoto@northwestern.edu

other cellular protective pathways (*7*). We therefore tested whether the sirtuins, specifically SIRT1, regulate HSF1 activity and thereby provide a direct link between these three longevity factors.

We treated HeLa cells with the sirtuin inhibitor nicotinamide (*8*) and then exposed the cells to various stresses known to induce the heat shock response (HSR) (*9*). Nicotinamide treatment decreased abundance of the stress-induced mRNAs from all major classes of heat shock genes (hsp70, hsp90, hsp40, and hsp27) (Fig. 1A), which indicated that the sirtuins are required for full induction of the HSR. Of three nuclear sirtuins, SIRT1 has well-characterized targets (*10*). We

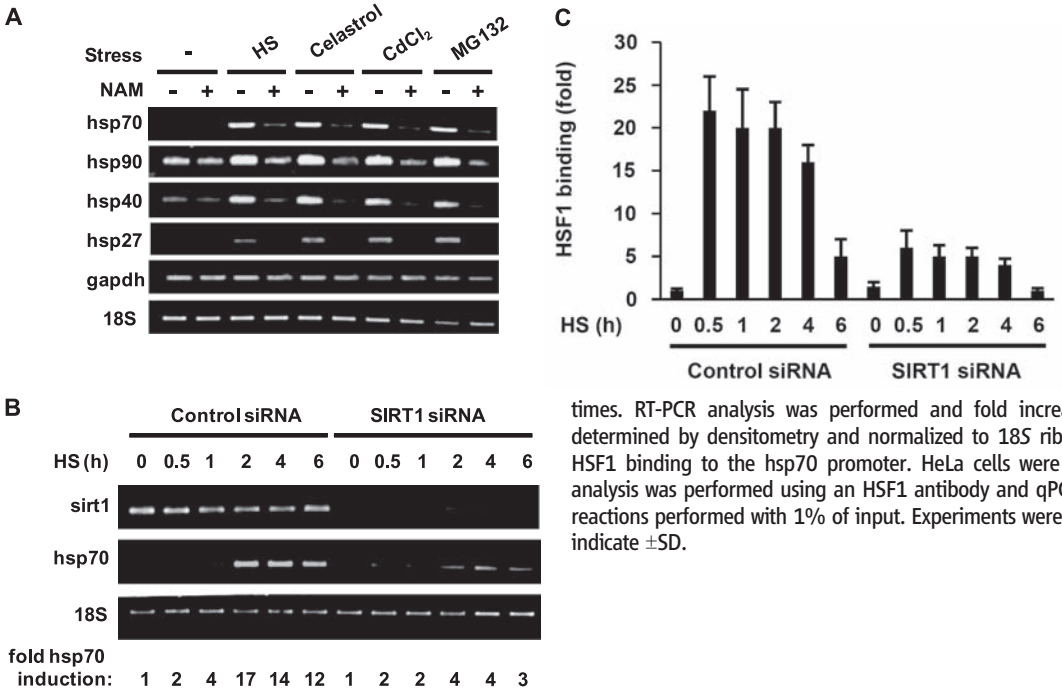

Fig. 1. Regulation of the HSR by sirtuins. (**A**) Effect of the sirtuin inhibitor nicotinamide on chaperone gene expression. HeLa cells were treated with nicotinamide (NAM) before exposure to heat shock (HS), celastrol, $CdCl_2$, or MG132, and reverse transcription (RT)–PCR analysis was performed with the indicated primers. (**B**) SIRT1 siRNA inhibits transcription of hsp70. HeLa cells transfected with siRNA against SIRT1 or a control siRNA were treated with heat shock for the indicated times. RT-PCR analysis was performed and fold increase in hsp70 mRNA abundance was determined by densitometry and normalized to 18*S* ribosomal RNA. (**C**) SIRT1 siRNA inhibits HSF1 binding to the hsp70 promoter. HeLa cells were treated as described above (B). ChIP analysis was performed using an HSF1 antibody and qPCR, and the results were normalized to reactions performed with 1% of input. Experiments were performed in triplicate, and error bars indicate ±SD.

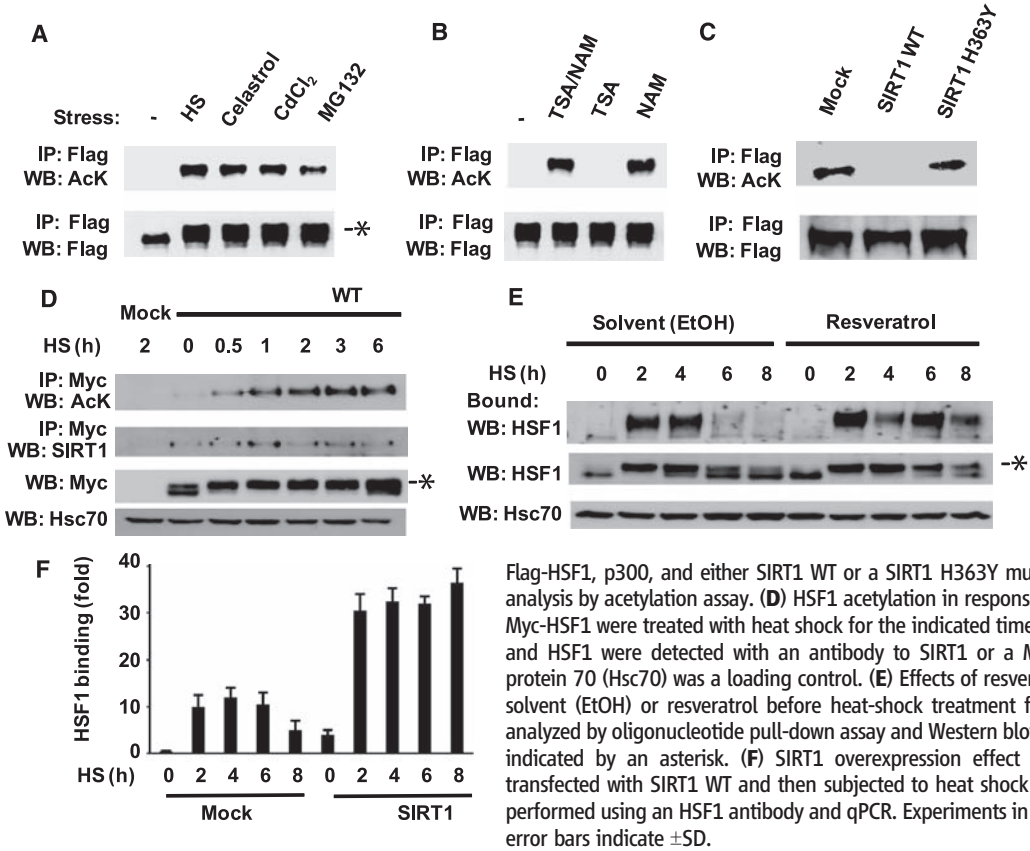

Fig. 2. Regulation of stress-induced acetylation of HSF1 by SIRT1. (**A**) Acetylation of HSF1 in response to HSR inducers. 293T cells transfected with Flag-HSF1 and p300 were treated with heat shock (HS), celastrol, $CdCl_2$ or MG132. Cell lysates were analyzed by acetylation assay using immunoprecipitation and Western blotting (*9*). Asterisk (*) indicates HSF1 that is slowly migrating because of increased phosphorylation (*17*). (**B**) Effects of nicotinamide and trichostatin A on HSF1 acetylation. 293T cells transfected with Flag-HSF1 and p300 were treated with trichostatin A (TSA), nicotinamide (NAM), or both, and exposed to heat shock, then cell lysates were analyzed by acetylation assay. (**C**) Wild-type SIRT1, but not a catalytic mutant, inhibits HSF1 acetylation. 293T cells were transfected with Flag-HSF1, p300, and either SIRT1 WT or a SIRT1 H363Y mutant before treatment with heat shock and analysis by acetylation assay. (**D**) HSF1 acetylation in response to heat shock. Cos7 cells transfected with Myc-HSF1 were treated with heat shock for the indicated times and analyzed by acetylation assay. SIRT1 and HSF1 were detected with an antibody to SIRT1 or a Myc-specific antibody. Heat-shock cognate protein 70 (Hsc70) was a loading control. (**E**) Effects of resveratrol. HeLa cells were treated with ethanol solvent (EtOH) or resveratrol before heat-shock treatment for the indicated times. Cell extracts were analyzed by oligonucleotide pull-down assay and Western blotting. Increased phosphorylation of HSF1 is indicated by an asterisk. (**F**) SIRT1 overexpression effect on HSF1 DNA binding. 293T cells were transfected with SIRT1 WT and then subjected to heat shock for the indicated times. ChIP analysis was performed using an HSF1 antibody and qPCR. Experiments in (A) to (G) were performed in triplicate, and error bars indicate ±SD.

therefore investigated SIRT1 as a candidate for regulation of the HSR. When SIRT1 was depleted by small interfering RNA (siRNA), the amount of hsp70 mRNA produced during a 6-hour heat shock was one-fourth of that in cells transfected with control siRNA (Fig. 1B).

To examine whether SIRT1 influences recruitment of HSF1 to the hsp70 promoter, we performed chromatin immunoprecipitation (ChIP) assays with cells transfected with control or SIRT1 siRNA before heat shock (Fig. 1C). In control siRNA-treated cells, binding of HSF1 to the hsp70 promoter occurs rapidly and begins to attenuate at 30 min of heat shock (*11*), with a gradual decline over a 6-hour period. However, in SIRT1 siRNA-transfected cells, about one-fourth as much HSF1 was associated with the promoter throughout the time course. These results support a role for SIRT1 as an in vivo regulator of HSF1 DNA binding activity and hsp70 expression.

To determine whether HSF1 is a direct target of SIRT1, we examined the acetylation status of HSF1. We transfected 293T cells with vectors encoding a Flag-HSF1 fusion protein and p300 and exposed them to several HSR inducers. Immunoprecipitated HSF1 was analyzed by Western blotting with an antibody that binds acetylated lysines. Acetylated HSF1 was not detected in untreated cells but was present in cells exposed to various stress conditions (Fig. 2A). The endogenous acetyltransferase that regulates HSF1 acetylation may be p300/CBP [adenosine 3′,5′-monophosphate (cAMP) response element–binding protein], as overexpression of either p300 or CBP, but not p300/CBP-associated factor, resulted in acetylation of HSF1 (fig. S1A), and p300 was recruited to the hsp70 promoter after heat shock (fig. S1B). SIRT1 also binds to the hsp70 promoter under both basal and stress conditions (fig. S1C).

Deacetylases are grouped into three families, with the class I and II histone deacetylase (HDAC) families inhibited by trichostatin A (*12*) and the nicotinamide adenine dinucleotide (NAD^+)–dependent class III sirtuin family inhibited by nicotinamide (*8*). Trichostatin A had no effect on deacetylation of HSF1, whereas nicotinamide inhibited deacetylation alone or in the presence of trichostatin A (Fig. 2B). Overexpression of SIRT1 WT, but not a point mutant with impaired NAD-dependent deacetylase activity [SIRT1 H363Y in which histidine at position 363 was replaced by tyrosine (*13*, *14*)], inhibited HSF1 acetylation (Fig. 2C), which supported a role

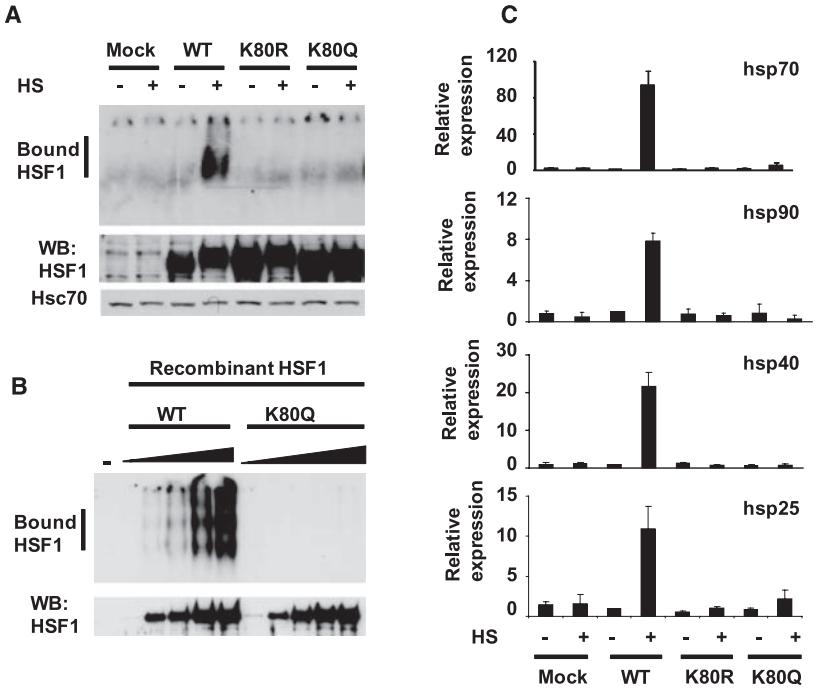

Fig. 3. Mutation of HSF1 K80 inhibits the HSR. (**A**) Mutation of HSF1 at K80 disrupts DNA binding activity. EMSA reactions were performed with extracts from *hsf1*$^{-/-}$ cells transfected with the indicated HSF1 constructs treated with or without heat shock (HS) (top). The EMSA probe contains the proximal HSE from the human hsp70 promoter. Western blot analysis was performed on the same samples to show HSF1 and Hsc70 levels. (**B**) Mutation of recombinant HSF1 at K80 disrupts DNA binding ability. EMSA reactions with increasing amounts (5, 20, 40, 80, or 120 ng) of recombinant WT HSF1 or HSF1 K80Q and a probe containing an HSE are shown (top). A sample without (–) HSF1 protein was a control. Western blot analysis was performed on the same samples to show HSF1 expression levels. (**C**) Failure of HSF1 mutated at K80 to rescue the HSR in *hsf1*$^{-/-}$ cells. *hsf1*$^{-/-}$ cells were transfected with the indicated versions of human HSF1 and treated with or without heat shock. RNA was quantified using qPCR with primers for the indicated genes. Data are normalized to values obtained for glyceraldehyde 3-phosphate dehydrogenase and are relative to the abundance of each mRNA in WT HSF1 cells treated without heat shock (value set as 1). Experiments in (A) to (C) were performed in triplicate, and error bars indicate ±SD.

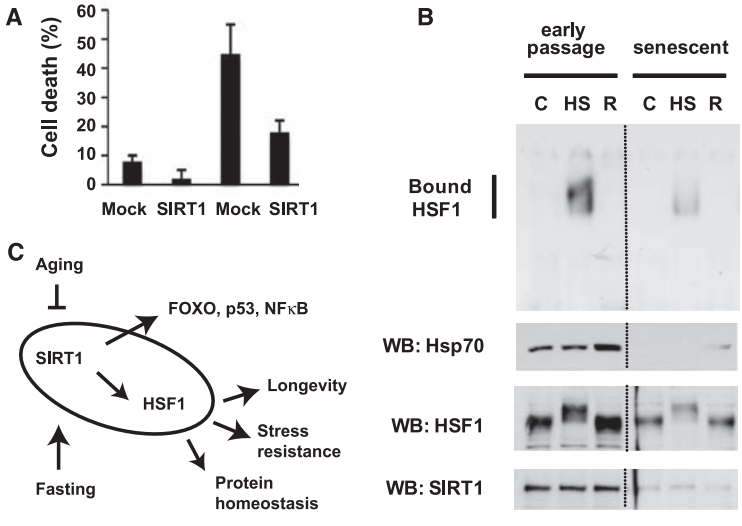

Fig. 4. Biological effects of SIRT1 on the HSR. (**A**) Protection of cells from severe stress by overexpressed SIRT1. 293T cells were transfected with empty vector (mock) or SIRT1 and treated with a 45°C heat shock for the indicated times, followed by recovery at 37°C. After 24 hours, cell death was determined by trypan blue uptake. The experiment was performed three times in triplicate, and error bars indicate ±SD. (**B**) Correlation of the age-dependent decline in the HSR with decreased abundance of SIRT1. Cell extracts from early passage (passage 21) and senescent (passage 44) WI-38 fibroblasts were treated with heat shock (HS) or heat shock followed by a 3-hour recovery at 37°C (R) and analyzed by EMSA with a probe containing an HSE (top). Western blot analysis was done on the same samples to show Hsp70, HSF1, and SIRT1 expression levels (bottom). (**C**) Model of the HSF1-SIRT1 regulatory network. The regulation of SIRT1 by aging and cellular metabolic state affects the activity of a network of transcription factors, including HSF1, to result in increased longevity and stress resistance.

for SIRT1 in HSF1 function. HSF1 acetylation was not cell type–specific, as it was detected in 293T and Cos7 cells, and although HSF1 acetylation was enhanced by p300 overexpression, it did not require p300 overexpression (Fig. 2, A and D). The kinetics of HSF1 acetylation do not match the kinetics of HSF1 activation. Acetylation is delayed and persists during the period when HSF1 activity and DNA binding have attenuated (*11*). In addition, an HSF1 in which 10 potentially phosphorylated serines were replaced with alanines remained competent for acetylation, which suggests that phosphorylation of HSF1 is not a prerequisite for acetylation (fig. S2).

The persistence of HSF1 acetylation during later time points of the HSR and the coimmunoprecipitation of SIRT1, together with HSF1 (Fig. 2D), led us to investigate whether SIRT1 has a role in attenuation of HSF1 activity. We treated HeLa cells with resveratrol, a small-molecule inducer of SIRT1 activity (*15*), and assayed HSF1 DNA binding activity in an oligonucleotide-based pull-down assay (*16*) (Fig. 2E). In cells treated with heat shock and vehicle alone, HSF1 DNA binding was induced within 2 hours and attenuated after 6 hours. The transient activation of HSF1 was reflected by altered mobility on SDS–polyacrylamide gel electrophoresis (SDS-PAGE), which detects the stress-induced phosphorylated state of HSF1 (*17*). In contrast, HSF1 in resveratrol-treated cells persisted in a DNA–binding competent and phosphorylated state even after 8 hours of continuous heat shock. In cells overexpressing SIRT1, HSF1 DNA binding was enhanced, and attenuation was suppressed as measured by ChIP experiments (Fig. 2F). These results suggest that changes in the abundance and activity of SIRT1 regulate the attenuation of the HSR.

To elucidate the mechanism by which acetylation regulates HSF1 DNA binding, we identified the sites of acetylation on HSF1 by mass spectrometry of peptides from Flag-HSF1 purified from 293T cells. At least nine lysines in HSF1 were acetylated in response to stress (fig. S3) of which K80, located in the DNA binding domain, was particularly intriguing because mutations of the corresponding lysine of yeast HSF cause a loss-of-function phenotype (*18*, *19*). Furthermore, analysis of the crystal structure of *Kluyveromyces lactis* HSF indicated that the lysine corresponding to human HSF1 K80 is located in a short domain that connects the main DNA binding helix to a flexible and solvent-exposed loop and forms a hydrogen bond with the DNA phosphate backbone (*20*). Comparative protein modeling of the HSF-HSE (HSF–heat shock element) crystal structure showed that human HSF1 K80 is in close contact with the DNA backbone (fig. S4), which suggests that neutralizing the positive charge of lysine by acetylation should interfere with DNA binding.

We therefore replaced K80 with a glutamine to mimic constitutive acetylation. In extracts from *hsf1*$^{-/-}$ fibroblasts (*21*) transfected with HSF1 wild-type (WT) and HSF1 K80Q expression constructs, the mutant protein failed to bind DNA in an electrophoretic mobility shift assay (EMSA) (Fig. 3A). The K80Q mutant, however, still assembled into heat shock–induced trimers, a hallmark of the DNA-bound state (fig. S5). Substitution of other amino acids at K80 [K80R, -A, -H, -N, and -T (*14*)] also resulted in defective DNA binding (Fig. 3A, fig. S6). In vitro, recombinant nonacetylated WT HSF1 readily bound to a synthetic HSE, but the K80Q mutant protein did not (Fig. 3B). We introduced WT and the K80 mutants into *hsf1*$^{-/-}$ fibroblasts and analyzed the heat shock–induced expression of HSF1 target genes by quantitative polymerase chain reaction (qPCR). Although WT HSF1 induced expression of heat shock protein mRNAs, HSF1 K80 mutants were nonfunctional (Fig. 3C). The mutants localized to the nucleus upon heat shock but were impaired in the relocalization into nuclear stress bodies that occurs in heat-shocked human cells (figs. S7 and S8) (*22*). An unmodified lysine side chain at residue 80 appears to be required for HSF1-HSE binding ability, relocalization into nuclear stress bodies, and expression of target genes. Therefore, we propose that acetylation of HSF1 K80 causes the regulated release of the HSF1 trimers from DNA and thus represents a regulatory step in the attenuation of the HSR (fig. S9).

To verify the biological significance of the regulation of the HSR by SIRT1, we used an assay of stress resistance in which the expression of chaperones confers increased thermotolerance (*23*). 293T cells were transfected with or without SIRT1, exposed to a 45°C heat shock for 20 or 30 min, allowed to recover for 24 hours, and analyzed for cell death. As expected, the 45°C heat shock resulted in cell death that increased with treatment time (Fig. 4A). At both time points, the cells overexpressing SIRT1 had about one-third as many cells undergo cell death (Fig. 4A). To examine whether age-regulated changes in SIRT1 affect HSF1 activity and the HSR, we used human WI-38 fibroblasts that have been widely used in studies on molecular changes in the aging process. When comparing early and late passage numbers, we found that aging resulted in a decreased HSR and reduced activation of HSF1 DNA binding activity that correlated with the reduced abundance of SIRT1 (Fig. 4B).

The finding that SIRT1 regulates HSF1 complements previous observations on the role of HSF1 in regulating life span (*4*, *5*). HSF1 appears to be at the hub of a regulatory network in which cell nutrition, stress, and life span are linked. Many SIRT1-regulated transcription factors, including FOXO3, p53, and nuclear factor–κB, have important roles in cellular stress responses (*7*, *24*, *25*). The addition of HSF1 to this stress regulatory network emphasizes the central role of protein homeostasis in SIRT1-mediated cellular protection (Fig. 4C) and may link the molecular response of the HSR to metabolic demands. A consistent observation in cell-based and animal studies has been the aging-related decline of the HSR (*23*), which may result, at least in part, from SIRT1 control of HSF1 activity. At the organismal level, we expect that regulation of HSF1 target genes may be influenced by diet and nutrition.

References and Notes

1. J. Anckar, L. Sistonen, *Adv. Exp. Med. Biol.* **594**, 78 (2007).
2. Y. Shi, D. D. Mosser, R. I. Morimoto, *Genes Dev.* **12**, 654 (1998).
3. S. K. Rabindran, J. Wisniewski, L. Li, G. C. Li, C. Wu, *Mol. Cell. Biol.* **14**, 6552 (1994).
4. A. L. Hsu, C. T. Murphy, C. Kenyon, *Science* **300**, 1142 (2003).
5. J. F. Morley, R. I. Morimoto, *Mol. Biol. Cell* **15**, 657 (2004).
6. S. Imai, C. M. Armstrong, M. Kaeberlein, L. Guarente, *Nature* **403**, 795 (2000).
7. A. Brunet *et al.*, *Science* **303**, 2011 (2004).
8. K. J. Bitterman, R. M. Anderson, H. Y. Cohen, M. Latorre-Esteves, D. A. Sinclair, *J. Biol. Chem.* **277**, 45099 (2002).
9. Materials and methods are available as supporting material on *Science* Online.
10. N. Dali-Youcef *et al.*, *Ann. Med.* **39**, 335 (2007).
11. M. P. Kline, R. I. Morimoto, *Mol. Cell. Biol.* **17**, 2107 (1997).
12. M. Yoshida, M. Kijima, M. Akita, T. Beppu, *J. Biol. Chem.* **265**, 17174 (1990).
13. E. Langley *et al.*, *EMBO J.* **21**, 2383 (2002).
14. Single-letter abbreviations for the amino acid residues are as follows: A, Ala; C, Cys; D, Asp; E, Glu; F, Phe; G, Gly; H, His; I, Ile; K, Lys; L, Leu; M, Met; N, Asn; P, Pro; Q, Gln; R, Arg; S, Ser; T, Thr; V, Val; W, Trp; and Y, Tyr.
15. K. T. Howitz *et al.*, *Nature* **425**, 191 (2003).
16. J. Anckar *et al.*, *Mol. Cell. Biol.* **26**, 955 (2006).
17. K. D. Sarge, S. P. Murphy, R. I. Morimoto, *Mol. Cell. Biol.* **13**, 1392 (1993).
18. S. T. Hubl, J. C. Owens, H. C. Nelson, *Nat. Struct. Biol.* **1**, 615 (1994).
19. F. A. Torres, J. J. Bonner, *Mol. Cell. Biol.* **15**, 5063 (1995).
20. O. Littlefield, H. C. Nelson, *Nat. Struct. Biol.* **6**, 464 (1999).
21. D. R. McMillan, X. Xiao, L. Shao, K. Graves, I. J. Benjamin, *J. Biol. Chem.* **273**, 7523 (1998).
22. C. Jolly *et al.*, *J. Cell Biol.* **156**, 775 (2002).
23. K. C. Kregel, *J. Appl. Physiol.* **92**, 2177 (2002).
24. H. Vaziri *et al.*, *Cell* **107**, 149 (2001).
25. F. Yeung *et al.*, *EMBO J.* **23**, 2369 (2004).

26. We thank N. Denslow, S. McClung, A. Schilling, and the Chicago Biomedical Consortium for assistance with the mass spectrometry; A. Mondragon for assistance with the molecular modeling; S. Raju for technical assistance; I. Benjamin for the *hsf1*$^{-/-}$ fibroblasts; and J. Brickner and members of the Morimoto laboratory for critical reading of the manuscript. This work was supported by an NIH training grant (S.D.W); Turku Graduate School of Biomedical Sciences (J.A.); Academy of Finland, Sigrid Juselius Foundation, and Åbo Akademi University (L.S.); and the National Institute for General Medical Science, the National Institute for Aging, and the Rice Institute for Biomedical Research (R.I.M.).

Supporting Online Material

www.sciencemag.org/cgi/content/full/323/5917/1063/DC1
Materials and Methods
Figs. S1 to S10
References

15 September 2008; accepted 9 December 2008
10.1126/science.1165946

Disruption of Vertical Motility by Shear Triggers Formation of Thin Phytoplankton Layers

William M. Durham,[1] John O. Kessler,[2] Roman Stocker[1]*

Thin layers of phytoplankton are important hotspots of ecological activity that are found in the coastal ocean, meters beneath the surface, and contain cell concentrations up to two orders of magnitude above ambient concentrations. Current interpretations of their formation favor abiotic processes, yet many phytoplankton species found in these layers are motile. We demonstrated that layers formed when the vertical migration of phytoplankton was disrupted by hydrodynamic shear. This mechanism, which we call gyrotactic trapping, can be responsible for the thin layers of phytoplankton commonly observed in the ocean. These results reveal that the coupling between active microorganism motility and ambient fluid motion can shape the macroscopic features of the marine ecological landscape.

Advances in underwater sensing technology over the past three decades have revealed the occurrence throughout the oceans of intense assemblages of unicellular photosynthetic organisms known as thin layers. Thin layers are centimeters to meters thick (*1*) and extend horizontally for kilometers (*2*). They often occur in coastal waters (*1*–*4*), in regions of vertical gradients in density where they are partially sheltered from turbulent mixing (*1*), and can persist for hours to days (*2*, *5*–*7*). Thin phytoplankton layers contain elevated amounts of marine snow and bacteria (*6*, *8*), enhance zooplankton growth rates (*7*), and provide the prey concentrations essential for the survival of some fish larvae (*9*). On the other hand, because many phytoplankton species found in these layers are toxic (*2*, *3*, *5*, *10*, *11*), thin layers can disrupt grazing, enhance zooplankton and fish mortality, and seed harmful algal blooms at the ocean surface (*2*, *5*, *10*). The large biomass found in thin layers can influence optical and acoustic signatures in the ocean (*1*, *6*, *8*). Understanding the mechanisms driving thin layer formation is critical for predicting their occurrence and ecological ramifications.

Phytoplankton species found in thin layers are often motile (*2*, *3*, *5*, *9*, *11*). The interplay between motility and fluid flow can result in complex and ecologically important phenomena, including localized cell accumulations (*12*, *13*) and directed swimming against the flow in zooplankton (*13*), bacteria (*14*), and sperm (*15*). Phytoplankton motility, coupled with shear, can lead to a striking focusing effect known as gyrotaxis (*12*). Shear, in the form of vertical gradients in horizontal fluid velocity, can be generated by tidal currents (*1*), wind stress (*1*), and internal waves (*16*) and is often enhanced within thin layers (*4*, *17*). Here, we propose a mechanism for thin layer formation in which a population of motile phytoplankton accumulates where shear exceeds a critical threshold: We have called this phenomenon gyrotactic trapping.

Many phytoplankton species exhibit gravitaxis, a tendency to swim upward against gravity. Gravitaxis can result from a torque caused by asymmetry in shape (*18*) or in distribution of body density (*12*) or through active sensing (*19*). Hydrodynamic shear imposes a viscous torque

[1]Department of Civil and Environmental Engineering, Massachusetts Institute of Technology (MIT), Cambridge, MA 02139, USA. [2]Department of Physics, University of Arizona, Tucson, AZ 85721, USA.

*To whom correspondence should be addressed. E-mail: romans@mit.edu

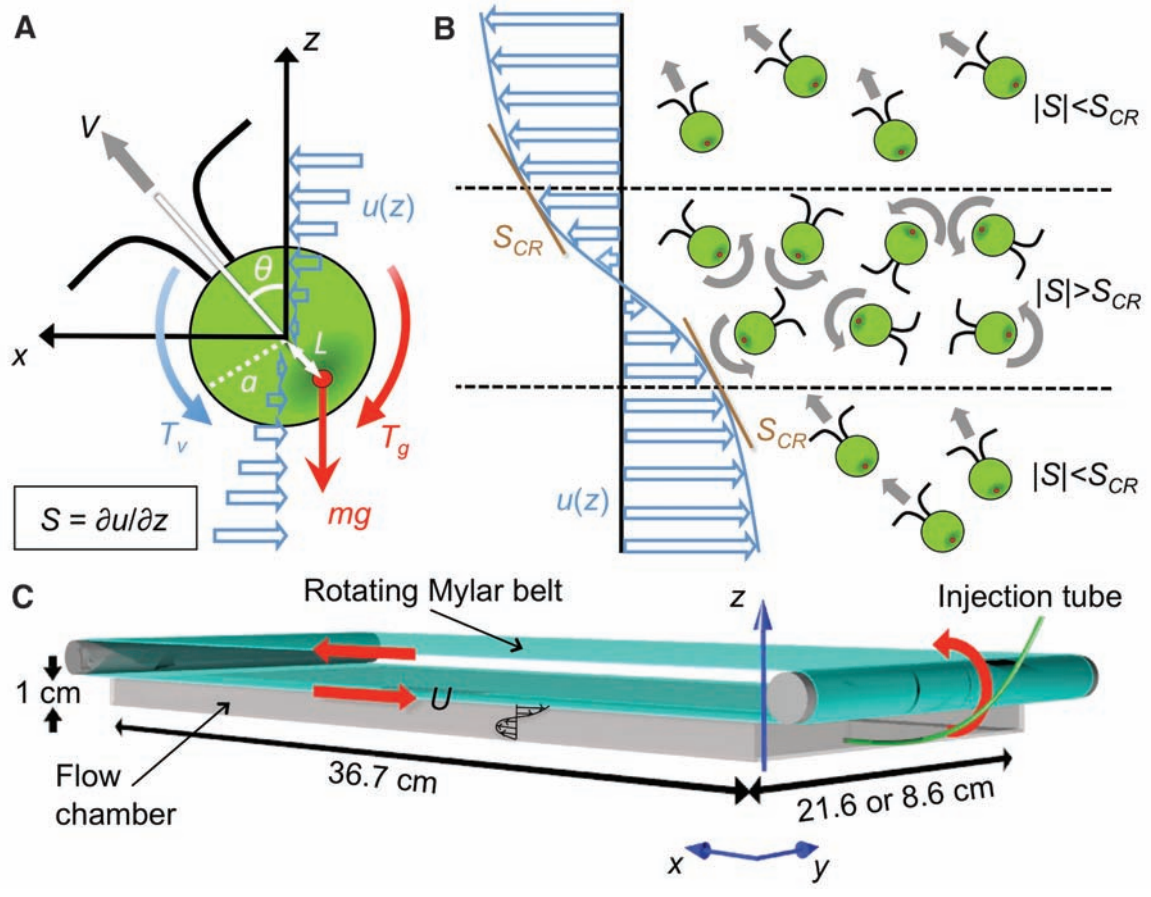

Fig. 1. Gyrotactic trapping. (**A**) A gyrotactic phytoplankton's center of mass (red) is displaced from its center of buoyancy ($x = z = 0$). As a result, the swimming direction θ in a shear flow, $u(z)$, is set by the balance of gravitational (T_g) and viscous (T_v) torques. V is swimming speed and m is mass. (**B**) Schematic of gyrotactic trapping. Cells can migrate vertically at low shear but tumble and become trapped where $|S| > S_{CR}$, accumulating in a thin layer. (**C**) Experimental apparatus to test gyrotactic trapping. The rotating belt generated a depth-varying shear $S(z)$ in the underlying flow chamber.

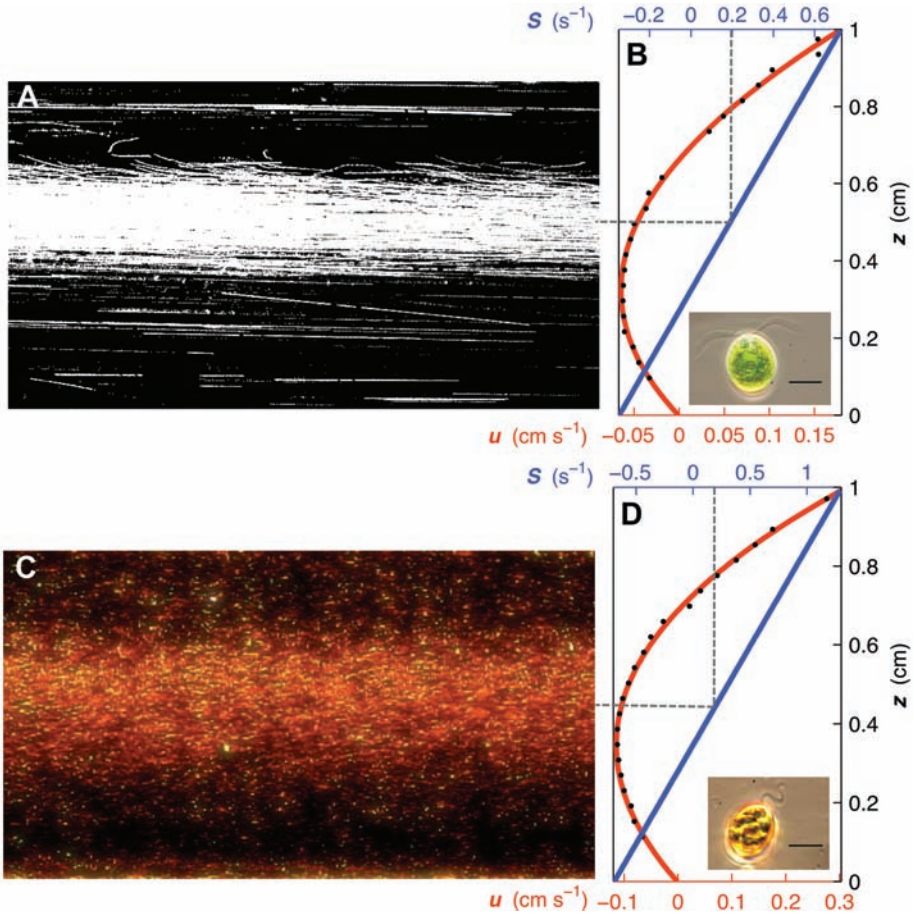

Fig. 2. Thin phytoplankton layers. (**A**) Multiple-exposure image showing a thin layer of *C. nivalis* (t = 12 min, x = 21.5 cm). Cells in high shear (z > 0.5 cm) were trapped, whereas those beneath ($|S| < S_{CR}$) swam upward, forming a thin layer. (**B**) Corresponding profile of measured flow velocities u (black dots), along with a quadratic fit (red) and the associated shear $S = \partial u/\partial z$ (blue). Because $u(z)$ was parabolic, S increased linearly with z. (Inset) *C. nivalis*, showing the two flagella used for swimming. Scale bar indicates 10 μm. (**C**) Thin layer of *H. akashiwo*. (**D**) Same as (B), for experiments in Fig. 2C. (Inset) *H. akashiwo*, showing one flagellum (a second resides in a ventral groove). Scale bar, 10 μm.

on cells. The swimming direction, θ, is then set by the balance of viscous and gravitactic torques (Fig. 1A), and cells are said to be gyrotactic (*12*). Consider a spherical cell of radius a and mean density ρ (Fig. 1A), with an asymmetric density distribution creating an offset, L, between its center of mass and its center of buoyancy (an equivalent L can be used to characterize gravitaxis resulting from shape or sensing). When exposed to shear S, the cell swims upward in the direction $\sin\theta = BS$ (*12*), where $B = 3\mu/\rho Lg$ is the gyrotactic reorientation time scale, μ the dynamic fluid viscosity, and g the acceleration of gravity. This results from the vorticity component of shear, whereas elongated cells would further be affected by the rate of strain component.

We show that vertical gradients ($S = \partial u/\partial z$) in horizontal velocity u can disrupt vertical migration of gyrotactic phytoplankton, causing them to accumulate in layers. When $|S| > S_{CR} = B^{-1}$, the stabilizing gravitational torque that acts to orient cells upward is overwhelmed by the hydrodynamic torque that induces them to spin: Upward migration is disrupted, because no equilibrium orientation exists ($|\sin\theta|$ must be ≤1), and cells tumble end over end, accumulating where they tumble (Fig. 1B). We demonstrated that gyrotactic trapping triggers layer formation by exposing the green alga *Chlamydomonas nivalis* and the toxic raphidophyte *Heterosigma akashiwo* (Fig. 2, B and D, insets) to a linearly varying shear, $S(z)$ (Fig. 2, B and D), in a 1-cm-deep chamber (Fig. 1C). *C. nivalis* is a classic model for gyrotaxis (*12*), whereas *H. akashiwo* has been the culprit of numerous large-scale fish kills and is known to form thin layers (*11*).

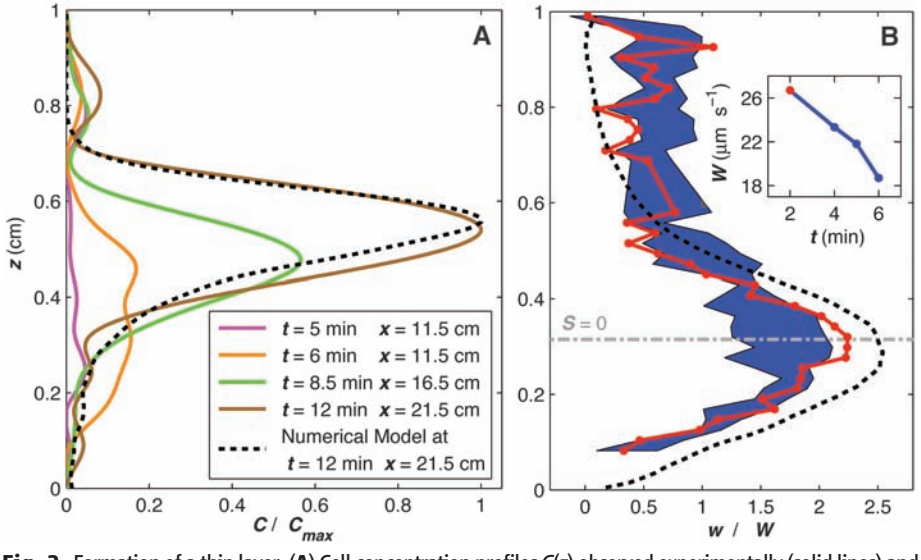

Fig. 3. Formation of a thin layer. (**A**) Cell concentration profiles $C(z)$ observed experimentally (solid lines) and numerically (dashed line), normalized by C_{max} observed at t = 12 min, x = 21.5 cm. (**B**) Upward swimming speed, w, at t = 2 min (red line) and standard deviation across four observations (blue strip and inset). W is the depth-averaged value of w. The dashed line shows the numerical simulation. The peak in $w(z)$ at $S \approx 0$ (gray line) and the deterioration in $w(z)$ for $|S| > 0$ are consistent with gyrotaxis and were responsible for layer formation. (Inset) W decreased with time, as the proportion of cells reaching their critical shear rate increased.

In our experiments, *C. nivalis* consistently formed intense thin layers (Fig. 2A). The dynamics

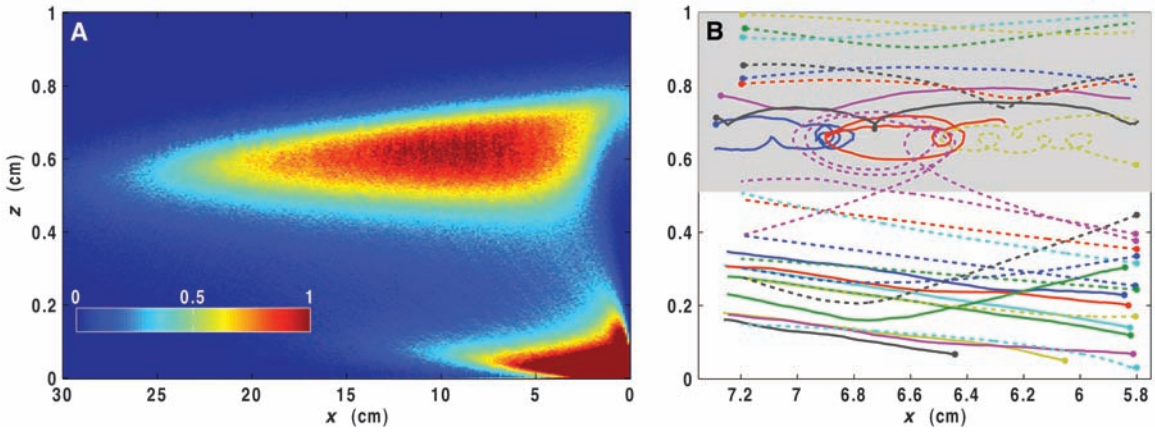

Fig. 4. Cell accumulation and trajectories. (**A**) Thin layer obtained from the numerical model at t = 12 min for conditions that simulated experiments with *C. nivalis* (Fig. 3A). Color denotes normalized cell concentration (the high concentrations at the lower right represent the region of injection). (**B**) Transition between two swimming regimes, demonstrated by experimental (solid) and numerical (dashed) trajectories. Where $|S| < S_{CR}$ (white background), cells migrated upward, whereas $|S| > S_{CR}$ (gray background) triggered tumbling and trapping. Shading represents the mean critical shear rate S_{CR} = 0.2 s^{-1}, although a statistical variability existed among cells. Dots mark beginning of trajectories.

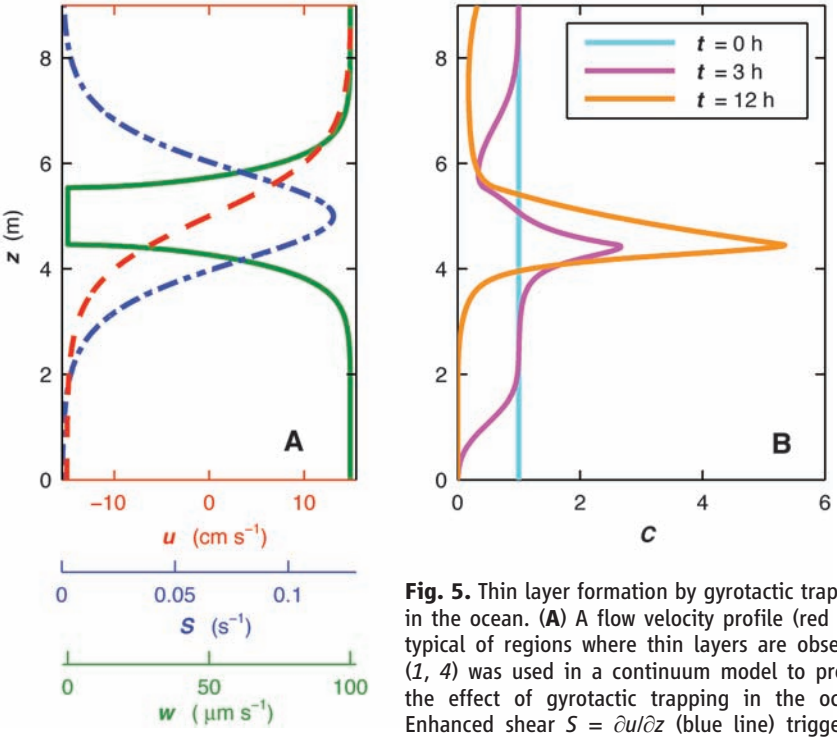

Fig. 5. Thin layer formation by gyrotactic trapping in the ocean. (**A**) A flow velocity profile (red line) typical of regions where thin layers are observed (*1*, *4*) was used in a continuum model to predict the effect of gyrotactic trapping in the ocean. Enhanced shear $S = \partial u/\partial z$ (blue line) triggers a reduction in upward swimming speed w (green line). (**B**) The model shows that an initially uniform population (cyan line) develops a localized accumulation within 3 hours (pink line) and forms an intense thin layer within 12 hours (orange line). Turbulence was parameterized by a vertical eddy diffusivity $D = 10^{-5}$ m^2 s^{-1}.

of thin layer formation were captured by using video microscopy (Fig. 3A). Initially (time t = 6 min, horizontal position x = 11.5 cm), cells entered the field of view with a broad distribution. Subsequently (t = 8.5 min, x = 16.5 cm), a 4-mm-wide thin layer formed as a result of the uppermost cells becoming trapped where $S_{CR} \approx 0.2$ s^{-1} and the cells beneath them still swimming upward. The location of cell accumulation corresponded to a gyrotactic reorientation time $B = 1/S_{CR} \approx 5$ s, in good agreement with previous literature values [$B \approx 1$ to 6 s (*20*, *21*, *22*)]. The thin layer grew more intense over time, peaking at t = 12 min. Importantly, motility was critical for layer formation: No layers were observed to form when we used dead cells. *H. akashiwo* also produced thin layers, which were so intense that they were visible to the naked eye (Fig. 2C), at a depth corresponding to $S_{CR} \approx 0.5$ s^{-1}.

Was gyrotaxis the mechanism underlying layer formation? According to theory, the mean upward speed, w, of a population of gyrotactic cells decreases with increasing shear. Measured vertical profiles of $w(z)$ from 70,000 *C. nivalis* trajectories (Fig. 3B) strongly support the occurrence of gyrotactic trapping: $w(z)$ peaked at $S = 0$ and decreased above and below. These observations were corroborated by numerical simulations of 50,000 cell trajectories under conditions mimicking the experiments (*23*) (movie S1). The simulations resulted in the formation of an intense thin layer (Fig. 4A), with cell concentration $C(z)$ closely matching observations (Fig. 3A). Furthermore, $w(z)$ decayed with increasing S, as in experiments (Fig. 3B).

Gyrotactic trapping requires a transition in swimming kinematics when $|S| = S_{CR}$ for a thin layer to form. To verify the existence of this transition, we tracked individual *C. nivalis* cells. Trajectories clearly revealed two distinct regimes (Fig. 4B and movie S2): for $|S| < S_{CR}$, cells swam upward, whereas for $|S| > S_{CR}$ they tumbled. Numerical and experimental trajectories exhibited clear similarities in the amplitude and frequency of tumbles, the rate of upward swimming for $|S| < S_{CR}$, and the presence of cells temporarily expelled from the lower side of the layer only to swim back upward moments later.

Can gyrotactic trapping contribute to layer formation in the ocean, where vertical distances are of the order of meters and turbulence may destroy vertical heterogeneity? To find out, we developed a continuum model of cell concentration, C, in the upper 10 m of the ocean, starting with a uniform distribution and accounting for turbulence intensities typical of thin layers (*24*) via a uniform eddy diffusivity, $D = 10^{-5}$ m^2 s^{-1}. Even for a conservatively low maximum upward swimming speed w_{max} = 100 μm s^{-1} (*11*, *25*), phytoplankton began to accumulate just beneath the depth of maximum shear within three hours, and the intensity of the layer strengthened over 12 hours (Fig. 5B). These time scales are consistent with field observations (*7*). Turbulence

subsequently eroded the layer, reducing peak concentration by 50% after 30 hours. Consideration of a local reduction in eddy diffusivity, typically encountered at the pycnocline, further increases layer intensity and duration. Importantly, we predict layer formation for shear rates ($S = 0.12\ s^{-1}$) comparable to those observed in thin layers (up to $S = 0.088\ s^{-1}$) (*1*, *4*), particularly considering that the latter likely underestimate peaks in shear because of coarse (meter-scale) sampling (*1*, *4*). Furthermore, recent high-resolution measurements find S in excess of $0.5\ s^{-1}$ in coastal waters (*26*), although the temporal coherence of these events remains to be determined.

Given the wide range of environmental conditions and species associated with thin layers, it is unlikely that a single mechanism is responsible for all layers (*27*). Although several mechanisms have been hypothesized, including in situ growth (*24*), buoyancy (*27*), and motility toward optimal resource levels (*5*), straining of a phytoplankton patch by shear is currently the most invoked (*4*, *16*, *24*, *27*). Our findings offer an alternative explanation of the role of shear: Regions of enhanced shear disrupt vertical motility and trigger sharp-peaked cell accumulations *ex novo* (Fig. 5B). This could occur routinely in natural water bodies because many species of phytoplankton are gyrotactic (*28*). Contrary to straining, gyrotactic trapping predicts that a mixture of phytoplankton species with differing gyrotactic behavior (e.g., B) will be sorted into multiple monospecific layers at different depths: Such vertical species separation is often observed in the ocean (*29*) and can affect zooplankton foraging and the spread of viral epidemics.

Gyrotactic trapping suggests that stabilization against tumbling might represent an evolutionarily selected trait for vertically migrating phytoplankton species. The parameter B^{-1} measures a cell's stability against overturning by shear. Whereas no stabilization ($B^{-1} = 0$) leaves the cell at the mercy of flow even at very small shear rates, stabilization is limited by biomechanical constraints (e.g., how bottom-heavy a cell can be) and excessive stabilization hinders maneuverability in exploiting nutrient patches and escaping predators. Although a simple model suggests that biomechanical constraints are not the only determinants of cell stability (*23*), further investigation is needed to establish the importance of stabilization in determining cell morphology.

The importance of motility in governing the spatial distribution of microorganisms in the ocean has been emphasized in recent years, chiefly for bacteria navigating patchy distributions of organic matter (*30*, *31*). Here we have demonstrated that motility and shear can generate intense thin layer accumulations of phytoplankton by gyrotactic trapping. By focusing resources, thin layers shape ecological interactions and can significantly affect trophic transfer and biogeochemical fluxes (*7*). Our results reveal how prominent macroscopic features of the marine landscape can originate from the microscopic coupling between flow and the motility of some of its smallest inhabitants.

References and Notes

1. M. M. Dekshenieks *et al.*, *Mar. Ecol. Prog. Ser.* **223**, 61 (2001).
2. T. G. Nielsen, T. Kiørboe, P. K. Bjørnsen, *Mar. Ecol. Prog. Ser.* **62**, 21 (1990).
3. D. W. Townsend, N. R. Pettigrew, A. C. Thomas, *Deep-Sea Res. Part II Top. Stud. Oceanogr.* **52**, 2603 (2005).
4. J. P. Ryan, M. A. McManus, J. D. Paduan, F. P. Chavez, *Mar. Ecol. Prog. Ser.* **354**, 21 (2008).
5. P. K. Bjørnsen, T. G. Nielsen, *Mar. Ecol. Prog. Ser.* **73**, 263 (1991).
6. M. A. McManus *et al.*, *Mar. Ecol. Prog. Ser.* **261**, 1 (2003).
7. T. J. Cowles, R. A. Desiderio, M. Carr, *Oceanography* **11**, 4 (1998).
8. A. L. Alldredge *et al.*, *Mar. Ecol. Prog. Ser.* **233**, 1 (2002).
9. R. Lasker, *Fish. Bull. (Washington)* **73**, 453 (1975).
10. P. L. Donaghay, T. R. Osborn, *Limnol. Oceanogr.* **42**, 1283 (1997).
11. S. Yamochi, T. Abe, *Mar. Biol. (Berl.)* **83**, 255 (1984).
12. J. O. Kessler, *Nature* **313**, 218 (1985).
13. A. Genin, J. S. Jaffe, R. Reef, C. Richter, P. J. S. Franks, *Science* **308**, 860 (2005).
14. J. Hill, O. Kalkanci, J. L. McMurray, H. Koser, *Phys. Rev. Lett.* **98**, 068101 (2007).
15. F. P. Bretherton, L. Rothchild, *Proc. R. Soc. London Ser. B* **153**, 490 (1961).
16. P. J. S. Franks, *Deep-Sea Res. Part I Oceanogr. Res. Pap.* **42**, 75 (1995).
17. T. J. Cowles, in *Handbook of Scaling Methods in Aquatic Ecology: Measurements, Analysis, Simulation*, L. Seuront, P. G. Strutton, Eds. (CRC, Boca Raton, FL, 2003), pp. 31–49.
18. A. M. Roberts, F. M. Deacon, *J. Fluid Mech.* **452**, 405 (2002).
19. M. Lebert, D. P. Häder, *Nature* **379**, 590 (1996).
20. M. S. Jones, L. Le Baron, T. J. Pedley, *J. Fluid Mech.* **281**, 137 (1994).
21. N. A. Hill, D. P. Häder, *J. Theor. Biol.* **186**, 503 (1997).
22. T. J. Pedley, N. A. Hill, J. O. Kessler, *J. Fluid Mech.* **195**, 223 (1988).
23. Materials and methods are available as supporting material on *Science* Online.
24. D. A. Birch, W. R. Young, P. J. S. Franks, *Deep-Sea Res. Part I Oceanogr. Res. Pap.* **55**, 277 (2008).
25. D. Kamykowski, R. E. Reed, G. J. Kirkpatrick, *Mar. Biol. (Berlin)* **113**, 319 (1992).
26. J. G. Mitchell, H. Yamazaki, L. Seuront, F. Wolk, H. Li, *J. Mar. Syst.* **69**, 247 (2008).
27. M. T. Stacey, M. A. McManus, J. V. Steinbuck, *Limnol. Oceanogr.* **52**, 1523 (2007).
28. J. O. Kessler, *Prog. Phycol. Res.* **4**, 257 (1986).
29. L. T. Mouritsen, K. Richardson, *J. Plankton Res.* **25**, 783 (2003).
30. R. Stocker, J. R. Seymour, A. Samadani, D. E. Hunt, M. F. Polz, *Proc. Natl. Acad. Sci. U.S.A.* **105**, 4209 (2008).
31. F. Azam, F. Malfatti, *Nat. Rev. Microbiol.* **5**, 782 (2007).

32. We thank P. Franks, W. Young, D. Grünbaum, T. Cowles, R. Bearon, M. Bees, D. Häder, D. Anderson, M. McManus, and L. Karp-Boss for helpful discussions; T. Peacock for the loan of experimental equipment; T. Clay and S. Stransky for developing BacTrack; R. A. Cattolico for providing *H. akashiwo*; and J. Mitchell, E. DeLong, S. Chisholm, M. Polz, H. Nepf, J. Seymour, J. Bragg, B. Kirkup, P. Reis, D. Birch, and S. Sunghwan for comments on the manuscript. W.M.D. acknowledges a National Defense Science and Engineering Graduate Fellowship. J.O.K. acknowledges support from Department of Energy grant W31-109-ENG38. R.S. acknowledges support from NSF (OCE 0526241 and OCE CAREER 0744641), MIT's Earth Systems Initiative, and a Doherty Professorship.

Supporting Online Material

www.sciencemag.org/cgi/content/full/323/5917/1067/DC1
Materials and Methods
References
Movies S1 and S2

17 October 2008; accepted 7 January 2009
10.1126/science.1167334

Cytosolic Viral Sensor RIG-I Is a 5′-Triphosphate–Dependent Translocase on Double-Stranded RNA

Sua Myong,[1]*† Sheng Cui,[2]* Peter V. Cornish,[3,4] Axel Kirchhofer,[2] Michaela U. Gack,[5,6,7] Jae U. Jung,[5,6] Karl-Peter Hopfner,[2]† Taekjip Ha[1,3,4]†

Retinoic acid inducible–gene I (RIG-I) is a cytosolic multidomain protein that detects viral RNA and elicits an antiviral immune response. Two N-terminal caspase activation and recruitment domains (CARDs) transmit the signal, and the regulatory domain prevents signaling in the absence of viral RNA. 5′-triphosphate and double-stranded RNA (dsRNA) are two molecular patterns that enable RIG-I to discriminate pathogenic from self-RNA. However, the function of the DExH box helicase domain that is also required for activity is less clear. Using single-molecule protein-induced fluorescence enhancement, we discovered a robust adenosine 5′-triphosphate–powered dsRNA translocation activity of RIG-I. The CARDs dramatically suppress translocation in the absence of 5′-triphosphate, and the activation by 5′-triphosphate triggers RIG-I to translocate preferentially on dsRNA in cis. This functional integration of two RNA molecular patterns may provide a means to specifically sense and counteract replicating viruses.

Retinoic acid inducible–gene I (RIG-I) is a cytosolic pattern-recognition receptor that senses pathogen-associated molecular patterns (PAMPs) on viral RNA and triggers an antiviral immune response by activating type-I interferons (IFN-α and -β) (*1*). A 5′-triphosphate moiety on viral RNA is a major PAMP detected by RIG-I as a viral signature (*2*, *3*). 5′-triphosphates arise during viral replication and are absent in most cytosolic RNA because of cleavage or capping

modifications (*4*–*6*). Another PAMP for RIG-I is double-stranded RNA (dsRNA), although it is less effective than 5′-triphosphate (*1*, *7*–*13*). It remains unclear, however, whether these distinct patterns trigger RIG-I signaling independently or whether they are integrated by RIG-I to increase specificity for viral RNA. RIG-I consists of two N-terminal tandem CARDs (caspase activation and recruitment domains), a central DExH box RNA helicase/adenosine triphosphatase (ATPase) domain, and a C-terminal regulatory domain (RD). The CARDs are ubiquitinated by tripartite motif-containing 25 (TRIM25) (*14*), and the ubiquitinated CARDs interact with the CARD on mitochondrial anti-viral signaling (MAVS; also called IPS-1, Cardif, or VISA) on the mitochondrial outer membrane to elicit downstream signaling that leads to IFN expression (*15*–*18*). The C-terminal RD inhibits RIG-I signaling in the absence of viral RNA (*8*) and senses the 5′-triphosphate in order to guide RIG-I to bind viral RNA with high specificity (*19*, *20*). Although the role of CARDs and RD has been characterized, the function of the ATPase domain remains elusive (*21*). A single-point mutation (Lys^{270}→Ala^{270}) in the ATPase site rendered RIG-I inactive in antiviral signaling (*1*), even though it retained RNA-binding ability (*22*). Furthermore, the ATPase activity of RIG-I correlates closely with the dsRNA-induced RIG-I signaling (*13*). However, it is unknown why the ATPase activity is required for RIG-I function.

RNA/DNA helicases usually unwind duplex nucleic acids by translocating on one of the product single strands by using adenosine 5′-triphosphate (ATP) hydrolysis, and their ATPase activity is consequently stimulated by single-stranded (ss) nucleic acids. In contrast, the ATPase activity of RIG-I is stimulated by dsRNA (*19*). We therefore examined whether RIG-I uses ATP hydrolysis to translocate on dsRNA. The dsRNA was made by annealing two complementary 25-nucleotide oligomer ssRNAs, one labeled with 3′-biotin and the other with a 3′-fluorescent label, DY547 (Dharmacon, Lafayette, CO). The dsRNA was tethered to a polymer-passivated quartz surface coated with neutravidin (Fig. 1A). The activity of RIG-I was monitored by a method termed protein-induced fluorescence enhancement (PIFE), which we found to be an effective alternative to fluorescence resonance energy transfer (FRET) (*23*, *24*). The method monitors changes in intensity of a single fluorophore that correlates with proximity of the unlabeled protein (more details and comparison of PIFE and FRET data for Rep helicase translocation are given in fig. S1) (*25*). PIFE can be used to study nucleic acids motors without fluorescent modification and even with high dissociation constant, which would prohibit single-molecule analysis of labeled proteins.

We first tested a RIG-I truncation mutant that lacks both of the CARDs, termed RIGh, because its ATPase activity is efficiently stimulated by dsRNA without the need for 5′-triphosphate on RNA (*19*). Binding of RIGh to dsRNA was visualized as an abrupt rise in the fluorescent signal of a single DY547 after the addition of protein (Fig. 1B). Most molecules (>90%) displayed a steady binding for 20 to 30 s, resulting in a strong fluorescence signal (Fig. 1E). The equilibrium-binding constant calculated from single-molecule binding data, which was collected from several hundred molecules, closely matched those determined using fluorescence anisotropy in bulk solution (fig. S2). When ATP was added together with RIGh, we detected a periodic fluorescence fluctuation, which is indicative of a repetitive translocational movement (Fig. 1, C and D; data obtained at 23°C). Translocation here is defined as directed movement of RIG-I along the axis of dsRNA without unwinding it. Under our conditions, RIG-I does not unwind dsRNA (fig. S3).

At 37°C, RIGh-induced fluctuation of the DY547 signal became more rapid (Fig. 2A). The time interval between successive intensity peaks, denoted by Δt, was determined from many molecules of RIGh translocating on 25–base pair (bp) and 40-bp dsRNA, and the resulting histograms show a single narrow peak with a longer average value for the longer dsRNA (2.9 s for 40 bp and 1.1 s for 25 bp) (Fig. 2B). When 100 nM wild-type RIG-I (wtRIG) was added with 1 mM ATP, the fluorescence signal also showed a gradual fluctuation at regular intervals but at a much-reduced frequency as compared with that of RIGh (Fig. 2C). Δt histograms are peaked at longer times for 40-bp as compared with 25-bp dsRNA (32.6 s versus 18.5 s), and their average values are 15 times higher than those of RIGh (Fig. 2D).

To test the role of ATP in the translocation reaction, the average of Δt, t_{avg}, was determined by Gaussian fitting of Δt histograms over a range of ATP concentrations (fig. S4). The inverse of t_{avg} was plotted versus ATP concentration and fitted well to the Michaelis-Menten equation, yielding K_m of 180 μM (Fig. 2G). The length dependence and ATP dependence show that the ATPase activity of RIG-I powers its translocation on the entire length of dsRNA. The contrast between the

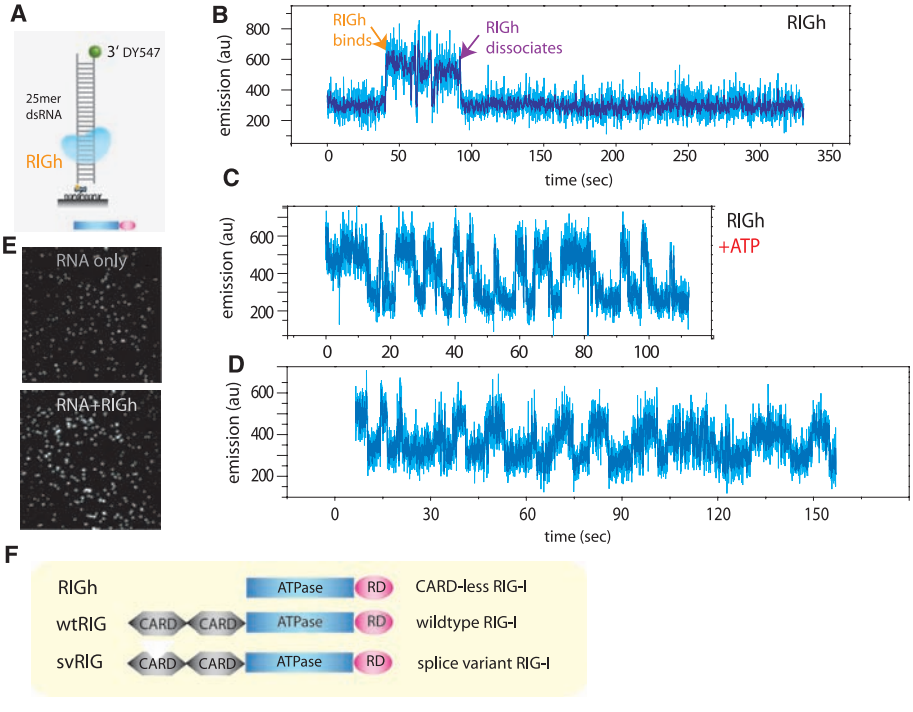

Fig. 1. PIFE visualization of RIG-I binding and translocation. (**A**) dsRNA (25-nucleotide oligomer) with single fluorophore (DY547) was tethered to surface via biotin-neutravidin. (**B**) Addition of RIGh (CARD-less mutant) resulted in an abrupt increase in emission of the fluorophore, indicating RIGh binding because of PIFE. (**C** and **D**) Addition of RIGh with ATP-induced periodic fluctuation of fluorophore. (**E**) The effect of PIFE is visible on the single-molecule imaging surface; fluorescence becomes substantially brighter upon adding RIGh protein. (**F**) Schematic representation of three RIG-I variants used in this study; wtRIG, RIGh, and svRIG are shown.

[1]Institute for Genomic Biology, University of Illinois at Urbana-Champaign, 1206 West Gregory Drive, Champaign, IL 61801, USA. [2]Center for Integrated Protein Science and Munich Center for Advanced Photonics at the Gene Center, Ludwig-Maximilians-University of Munich, Feodor-Lynen-Strasse 25, 81377 Munich, Germany. [3]Department of Physics and Center for the Physics of Living Cells, University of Illinois at Urbana-Champaign, Room 133, Loomis Laboratory, MC 704, 1110 West Green Street, Urbana, IL 61801, USA. [4]Howard Hughes Medical Institute, Urbana, IL, USA. [5]Department of Molecular Microbiology and Immunology, University of Southern California, Keck School of Medicine, Harlyne J. Norris Cancer Research Tower, 1450 Biggy Street, Los Angeles, CA 90033, USA. [6]Department of Microbiology and Molecular Genetics and Tumor Virology Division, New England Primate Research Center, Harvard Medical School, 1 Pine Hill Drive, Southborough, MA 01772, USA. [7]Institute for Clinical and Molecular Virology, Friedrich-Alexander-University Erlangen-Nuremberg, Schlossgarten 4, 91054 Erlangen, Germany.

*These authors contributed equally to this work.
†To whom correspondence should be addressed. E-mail: smyong@uiuc.edu (S.M.); hopfner@lmb.uni-muenchen.de (K.-P.H.); tjha@uiuc.edu (T.H.)

slow movement of wtRIG and the 15-fold accelerated movement of RIGh is consistent with the substantially higher stimulation of ATPase activity by dsRNA that was observed in RIGh than was in wtRIG (*19*) and with the report that CARDs inhibit the ATPase activity of RIG-I (*8*).

To further evaluate the regulatory role of CARDs, we tested the RIG-I splice variant, svRIG, which lacks amino acids 36 to 80 in the first CARD (*26*). svRIG confers dominant negativity in antiviral signaling, implying a loss of signaling function arising from a deficient CARD. The translocation activity of svRIG on dsRNA is highly similar to that of RIGh and is characterized by much more rapid fluctuations as compared with wtRIG (Fig. 2, A and F). svRIG translocation is also ATP-dependent with K_m of 114 μM similar to that of RIGh (fig. S5). Thus, CARD-mediated suppression of translocation activity requires complete CARDs.

Apart from dsRNA, a powerful PAMP for RIG-I is 5′-triphosphate (*2*, *22*). To examine if 5′-triphosphate influences the RNA translocation activity of RIG-I, we prepared 5′-triphosphate RNA (86-nucleotide oligomer) via in vitro transcription and annealed it to a complementary 20-nucleotide oligomer DNA strand. The DNA strand was modified with a 3′ fluorophore (Cy3) and 5′ biotin, which serves as a fluorescence reporter and a surface-tethering point, respectively (Fig. 3A). Addition of wtRIG and ATP to this substrate resulted in extremely rapid fluctuations in the fluorescence signal (Fig. 3, B and C). The rate of translocation, calculated as $(t_{avg})^{-1}$, was dependent on the ATP concentration, with a K_m value of 37 μM (fig. S6). RIGh showed translocation activity on 5′-triphosphate RNA with a rate comparable with wtRIG (Fig. 3, D and E).

wtRIG's translocation on 5′-triphosphate RNA is over 20 times faster than on dsRNA (t_{avg} of 18.5 s versus 0.85 s) (Figs. 1C and 3C). Combined with the data on RIGh and svRIG that showed rapid dsRNA translocation activity regardless of the presence of 5′-triphosphate, we conclude that (i) intact CARDs are necessary to negatively regulate the dsRNA translocation activity of RIG-I and (ii) recognition of 5′-triphosphate by RD completely lifts the suppression by CARDs. Therefore, RNA translocation of RIG-I is regulated by its N-terminal (CARD) and C-terminal (RD) domains. Because the immobilized RNA molecules are more than 1 μm apart from each other, the effect of 5′-triphophate must be in cis; that is, RIG-I translocates rapidly on the same RNA that presents 5′-triphosphate. Adding up to 100 times molar excess of 5′-triphosphate–containing ssRNA strand did not increase the translocation rate of wtRIG on dsRNA (fig. S7).

The 5′-triphosphate RNA we used has both single-stranded and double-stranded portions, and the double-stranded portion is a RNA/DNA heteroduplex. Studies on various nucleic acid substrates showed that RIG-I is an RNA-specific translocase that tracks one RNA strand either on dsRNA or RNA/DNA heteroduplexes (figs. S8 and S9). Does RIG-I, upon recognition of 5′-triphosphate, translocate on the ssRNA, the duplex region, or both? To answer this question, we progressively lengthened the duplex from 20 to 50 bp while progressively shortening the single-stranded region proximal to 5′-triphosphate from 66 to 36 nucleotides (nt) (Fig. 4A). t_{avg} of both wtRIG and RIGh increased linearly with the duplex length, demonstrating translocation on duplex rather than ssRNA (Fig. 4B and fig. S10). Varying the ssRNA tail length while keeping the same length dsRNA did not change t_{avg} (Fig. 4, C and D, and fig. S11). The asymmetric PIFE signal on the heteroduplexes indicates 5′ to 3′ translocation directionality (fig. S12).

The highly periodic repetitive nature of the translocation signal, reminiscent of *Escherichia coli* Rep and Hepatitis C virus NS3 helicases (*27*, *28*), suggests that a single unit of RIG-I repeatedly moves on one RNA without dissociation. This was further verified by washing the reaction chamber with ATP-containing buffer devoid of protein, which left a majority of molecules still in repetitive motion (fig. S13). As a further test, we labeled RIGh nonspecifically with the acceptor fluorophore, and performed single-molecule FRET experiments on the donor-labeled RNA. Periodic anticorrelated changes of the donor and acceptor intensities, consistent with RIG-I translocation on RNA (fig. S14), were observed.

The dsRNA translocation activity on RNA that contains 5′-triphosphate would serve as a signal verification mechanism by activating the ATPase only if the RNA features both PAMPs, the 5′-triphosphate, and dsRNA. Thus, our data not only suggest a functional connection between the apparently different PAMPs but also indicate that integration of more than one PAMP in a single activation mechanism could be important for the selective distinction of host from viral RNA.

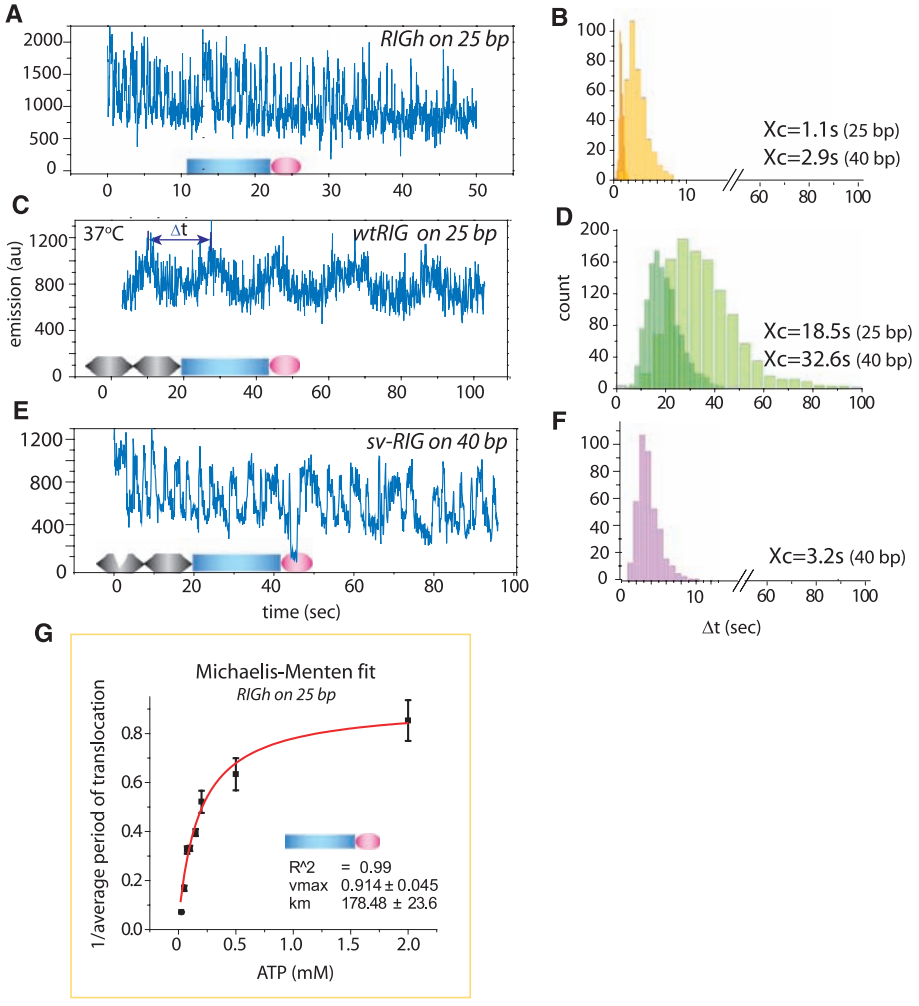

Fig. 2. RIG-I translocates on dsRNA, and CARD is inhibitory. (**A**, **C**, and **E**) 100 nM RIGh, wtRIG, and svRIG were added with 1 mM ATP, respectively, at 37°C. The signal fluctuation represents RIG-I movement along the dsRNA substrate. (**B**, **D**, and **F**) Dwell-time analysis of periods denoted by Δ*t* with a double arrow (C) was measured for many molecules and plotted as histograms for RIGh (B), wtRIG (D), and svRIG (F) for 25-bp and 40-bp dsRNA. (**G**) The inverse of average Δ*t*, $(t_{avg})^{-1}$, was plotted against an axis of ATP concentration and fitted to the Michaelis-Menten equation. The error bars denote SD from three separate experiments each. The maximum velocity (V_{max}) and substrate concentration at half maximal velocity (K_m) values were 0.91 and 179 μM, respectively.

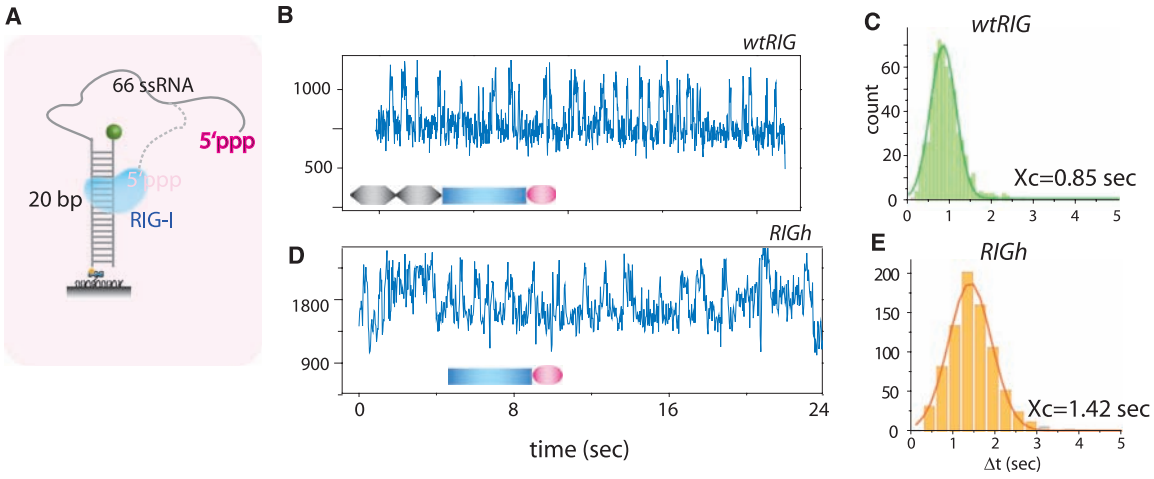

Fig. 3. 5′-triphosphate accelerates RIG-I translocation activity. (**A**) The translocation assay was performed on a 5′-triphosphate–containing substrate that consists of 86-nucleotide oligomer ssRNA from in vitro transcription annealed to complementary 20-nucleotide oligomer ssDNA with 3′ Cy3 and 5′ biotin. (**B** and **D**) Activity of wtRIG was greatly stimulated by the presence of 5′-triphosphate. The data shown were taken at room temperature because of an extremely fast kinetic rate observed at 37°C. RIGh also showed robust translocation activity on this substrate. (**C** and **E**) Dwell-time analysis indicates that wtRIG showed a slightly higher rate of translocation than did RIGh.

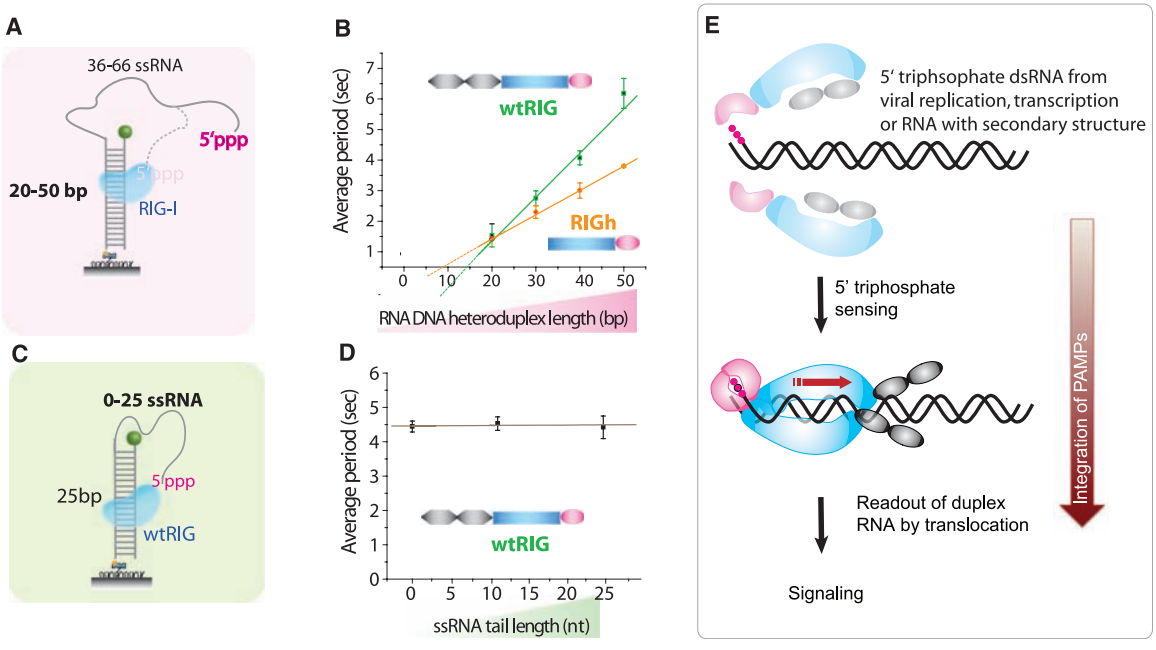

Fig. 4. RIG-I translocates on a double strand of 5′-triphosphate RNA. (**A**) To identify the region of translocation, the double-strand length was varied from 20 to 50 bp, whereas the ssRNA length was varied from 66 to 36 nt, respectively. (**B**) t_{avg} versus duplex length. (**C**) Three constructs were prepared with the fixed dsRNA length of 25 bp and variable ssRNA tail length of 0, 10, and 25 nt. (**D**) t_{avg} versus ssRNA tail length. Error bars denote SD from three separate experiments each. (**E**) Proposed mechanism for PAMP signal integration by RIG-I. Binding of RIG-I regulatory domain (pink) to RNA 5′ triphosphates(for example, arising from virus replication or transcription) dimerizes RIG-I and activates the translocase domain (blue). Further recognition of dsRNA stimulates ATPase activity, resulting in translocation (red arrow), a process that may induce a signaling conformation with exposed CARDs (gray). Precise domain arrangements are speculative and depicted here for illustrative purposes.

What is the molecular function of the translocase activity? Translocation might effectively interfere with viral proteins by preventing them from binding, blocking their progression, or displacing them, thus actively interfering with viral replication (*29*). However, such a function does not explain why an ATPase-deficient mutation of RIG-I lacks signaling activity. Perhaps repetitive shuttling at dsRNA regions of the viral genome, which may arise from genome replication, transcription, or stable secondary structures, could provide a structural conformation in RIG-I with exposed CARDs to attract the next players in the signaling cascade (Fig. 4E). The signal strength is likely related to the amount of time spent in translocation mode and therefore to the length of RNA. This might explain how RIG-I and melanoma differentiation-associated protein-5 (MDA5) may differentially read out very long dsRNA regions (*13*). Finally, our finding of RIG-I as a dsRNA translocase completes the range of activities in superfamily 2 DExH box ATPases, which now include single-strand– and double-strand–specific translocases for both RNA and DNA (*30*).

References and Notes

1. M. Yoneyama *et al.*, *Nat. Immunol.* **5**, 730 (2004).
2. V. Hornung *et al.*, *Science* **314**, 994 (2006).
3. A. Pichlmair *et al.*, *Science* **314**, 997 (2006).
4. A. J. Shatkin, J. L. Manley, *Nat. Struct. Biol.* **7**, 838 (2000).
5. M. Fromont-Racine, B. Senger, C. Saveanu, F. Fasiolo, *Gene* **313**, 17 (2003).
6. R. Singh, R. Reddy, *Proc. Natl. Acad. Sci. U.S.A.* **86**, 8280 (1989).
7. R. Sumpter Jr. *et al.*, *J. Virol.* **79**, 2689 (2005).
8. T. Saito *et al.*, *Proc. Natl. Acad. Sci. U.S.A.* **104**, 582 (2007).
9. J. T. Marques *et al.*, *Nat. Biotechnol.* **24**, 559 (2006).
10. P. Gee *et al.*, *J. Biol. Chem.* **283**, 9488 (2008).
11. C. E. Samuel, *Clin. Microbiol. Rev.* **14**, 778 (2001).
12. H. Kato *et al.*, *Nature* **441**, 101 (2006).
13. H. Kato *et al.*, *J. Exp. Med.* **205**, 1601 (2008).
14. M. U. Gack *et al.*, *Nature* **446**, 916 (2007).
15. E. Meylan *et al.*, *Nature* **437**, 1167 (2005).
16. R. B. Seth, L. Sun, C. K. Ea, Z. J. Chen, *Cell* **122**, 669 (2005).
17. L. G. Xu *et al.*, *Mol. Cell* **19**, 727 (2005).
18. T. Kawai *et al.*, *Nat. Immunol.* **6**, 981 (2005).
19. S. Cui *et al.*, *Mol. Cell* **29**, 169 (2008).
20. K. Takahasi *et al.*, *Mol. Cell* **29**, 428 (2008).

21. M. Yoneyama, T. Fujita, *Immunity* **29**, 178 (2008).
22. S. Plumet *et al.*, *PLoS One* **2**, e279 (2007).
23. G. Luo, M. Wang, W. H. Konigsberg, X. S. Xie, *Proc. Natl. Acad. Sci. U.S.A.* **104**, 12610 (2007).
24. C. J. Fischer, N. K. Maluf, T. M. Lohman, *J. Mol. Biol.* **344**, 1287 (2004).
25. Materials and methods are available as supporting material on *Science* Online.
26. M. U. Gack *et al.*, *Proc. Natl. Acad. Sci. U.S.A.* **105**, 16743 (2008).
27. S. Myong, I. Rasnik, C. Joo, T. M. Lohman, T. Ha, *Nature* **437**, 1321 (2005).
28. S. Myong, M. M. Bruno, A. M. Pyle, T. Ha, *Science* **317**, 513 (2007).
29. E. Jankowsky, C. H. Gross, S. Shuman, A. M. Pyle, *Science* **291**, 121 (2001).
30. H. Durr, C. Korner, M. Muller, V. Hickmann, K. P. Hopfner, *Cell* **121**, 363 (2005).
31. We thank C. Joo and K. Ragunathan for careful review of the manuscript. This work was supported by NIH grant R01-GM065367 and NSF Physics Frontiers Center grant 0822613 to T.H., NIH grant CA82057 to J.U.J., and a Human Frontiers of Science grant to T.H. and K.-P.H. K.-P.H. acknowledges support from the German Excellence Initiative. S.C. is supported by Deutsche Forschungsgemeinschaft (DFG) program project 455 to K.-P.H. A.K. acknowledges support from the DFG graduate school 1202. T.H. is an investigator with the Howard Hughes Medical Institute. S.M. is a fellow at the Institute for Genomic Biology.

Supporting Online Material
www.sciencemag.org/cgi/content/full/1168352/DC1
Materials and Methods
Figs. S1 to S14
References

11 November 2008; accepted 15 December 2008
Published online 1 January 2009;
10.1126/science.1168352
Include this information when citing this paper.

Neuronal Activity–Induced Gadd45b Promotes Epigenetic DNA Demethylation and Adult Neurogenesis

Dengke K. Ma,[1,2*†] Mi-Hyeon Jang,[1,3*] Junjie U. Guo,[1,2] Yasuji Kitabatake,[1,3] Min-lin Chang,[1,3] Nattapol Pow-anpongkul,[1] Richard A. Flavell,[4] Binfeng Lu,[5] Guo-li Ming,[1,2,3] Hongjun Song[1,2,3†]

The mammalian brain exhibits diverse types of neural plasticity, including activity-dependent neurogenesis in the adult hippocampus. How transient activation of mature neurons leads to long-lasting modulation of adult neurogenesis is unknown. Here we identify *Gadd45b* as a neural activity–induced immediate early gene in mature hippocampal neurons. Mice with *Gadd45b* deletion exhibit specific deficits in neural activity–induced proliferation of neural progenitors and dendritic growth of newborn neurons in the adult hippocampus. Mechanistically, *Gadd45b* is required for activity-induced DNA demethylation of specific promoters and expression of corresponding genes critical for adult neurogenesis, including brain-derived neurotrophic factor and fibroblast growth factor. Thus, Gadd45b links neuronal circuit activity to epigenetic DNA modification and expression of secreted factors in mature neurons for extrinsic modulation of neurogenesis in the adult brain.

Adult neurogenesis represents a prominent form of structural plasticity through continuous generation of new neurons in the mature mammalian brain (*1*, *2*). Similar to other neural activity-induced plasticity with fine structural changes within individual neurons, adult neurogenesis is modulated by a plethora of external stimuli (*1*, *2*). For example, synchronized activation of mature dentate neurons by electroconvulsive treatment (ECT) in adult mice causes sustained up-regulation of hippocampal neurogenesis (*3*) without any detectable cell damage (fig. S1). How transient activation of mature neuronal circuits modulates adult neurogenesis over days and weeks is largely unknown.

Epigenetic mechanisms potentially provide a basis for such long-lasting modulation (*4*). We examined the expression profiles of known epigenetic regulators in response to ECT, including those involved in chromatin modification (*5*). One gene that we found to be strongly induced by ECT was *Gadd45b* (Fig. 1A) (*6*), a member of the *Gadd45* family previously implicated in DNA repair, adaptive immune response (*7*–*10*), and DNA 5-methylcytosine excision in cultured cells (*11*). We first characterized *Gadd45b* induction by neuronal activity in the adult hippocampus (*5*). Analysis of microdissected dentate gyrus tissue showed robust, transient induction of *Gadd45b* expression by a single ECT (Fig. 1A, fig. S2, and table S1). In situ analysis revealed induction largely in $NeuN^+$ mature dentate granule cells (Fig. 1B and fig. S3). Spatial exploration of a novel environment, a behavioral paradigm that activates immediate early genes (IEGs) (*12*), also led to significant induction of *Gadd45b*, but not *Gadd45a* or *Gadd45g* (Fig. 1, C and D). Most Gadd45b-positive cells also expressed Arc (Fig. 1D) (88 ± 3%, $n = 4$), a classic activity-induced IEG. Thus, physiological stimulation is sufficient to induce *Gadd45b* expression in dentate granule cells. Experiments with pharmacological manipulations of primary hippocampal neurons further suggested that *Gadd45b* induction by activity requires the *N*-methyl-D-aspartate receptor (NMDAR), Ca^{2+}, and calcium/calmodulin-dependent protein kinase signaling (fig. S4 and supporting text). In vivo injection of the NMDAR antagonist +3-(2-carboxypiperazin-4-yl)-propyl-1-phosphonic acid (CPP) abolished ECT-induced *Gadd45b* and *Arc* expression in the adult dentate gryus (Fig. 1E). Together, these results suggest that *Gadd45b* shares the same induction pathway as classic activity-induced IEGs (*13*).

We next assessed whether *Gadd45b* induction is required for neural activity–dependent adult neurogenesis. Adult *Gadd45b* knockout (KO) (*10*) mice appeared anatomically normal (fig. S5) and exhibited identical NMDAR-dependent induction of known IEGs at 1 hour after ECT (Fig. 1E). To examine neural progenitor proliferation, adult mice at 3 days after ECT or sham treatment were injected with bromodeoxyuridine (BrdU) and killed 2 hours later (*5*). Stereological counting showed similar densities of $BrdU^+$ cells in the dentate gyrus between wild-type (WT) and KO mice without ECT (Fig. 2). After ECT, however, there was a 140% increase in the density of $BrdU^+$ cells in WT mice and only a 40% increase in KO littermates (Fig. 2). Little caspase-3 activation was detected within the dentate gyrus under all these conditions (figs. S1 and S6), ruling out a potential contribution from cell death. To confirm this finding with a manipulation of better spatiotemporal control, we developed effective lentiviruses to reduce the expression of endogenous *Gadd45b* with short-hairpin RNA (shRNA) (fig. S7). Expression of shRNA-*Gadd45b* through stereotaxic viral injection largely abolished ECT-induced proliferation of adult neural progenitors, whereas the basal proliferation was similar to that of shRNA-control (fig. S7). We also examined exercise-induced adult neurogenesis, a physiological stimulation that induced a modest increase in *Gadd45b* expression (fig. S8A). A 7-day running program led to a marked increase of neural progenitor proliferation in adult WT mice, but was significantly less effective in their KO littermates (fig. S8B). Together, these results demonstrate a specific and essential role of *Gadd45b* in activity-induced, but not basal, proliferation of neural progenitors in the adult dentate gyrus.

We next examined the role of *Gadd45b* induction in the dendritic development of newborn

[1]Institute for Cell Engineering, Johns Hopkins University School of Medicine, 733 North Broadway, Baltimore, MD 21205, USA. [2]The Solomon H. Snyder Department of Neuroscience, Johns Hopkins University School of Medicine, 733 North Broadway, Baltimore, MD 21205, USA. [3]Department of Neurology, Johns Hopkins University School of Medicine, 733 North Broadway, Baltimore, MD 21205, USA. [4]Department of Immunobiology, Howard Hughes Medical Institute, Yale University School of Medicine, 300 Cedar Street, New Haven, CT 06520, USA. [5]Department of Immunology, University of Pittsburgh, School of Medicine, Pittsburgh, PA 15261, USA.

*These authors contributed equally to this work.
†To whom correspondence should be addressed. E-mail: shongju1@jhmi.edu (H.S.); dma2@jhmi.edu (D.K.M.)

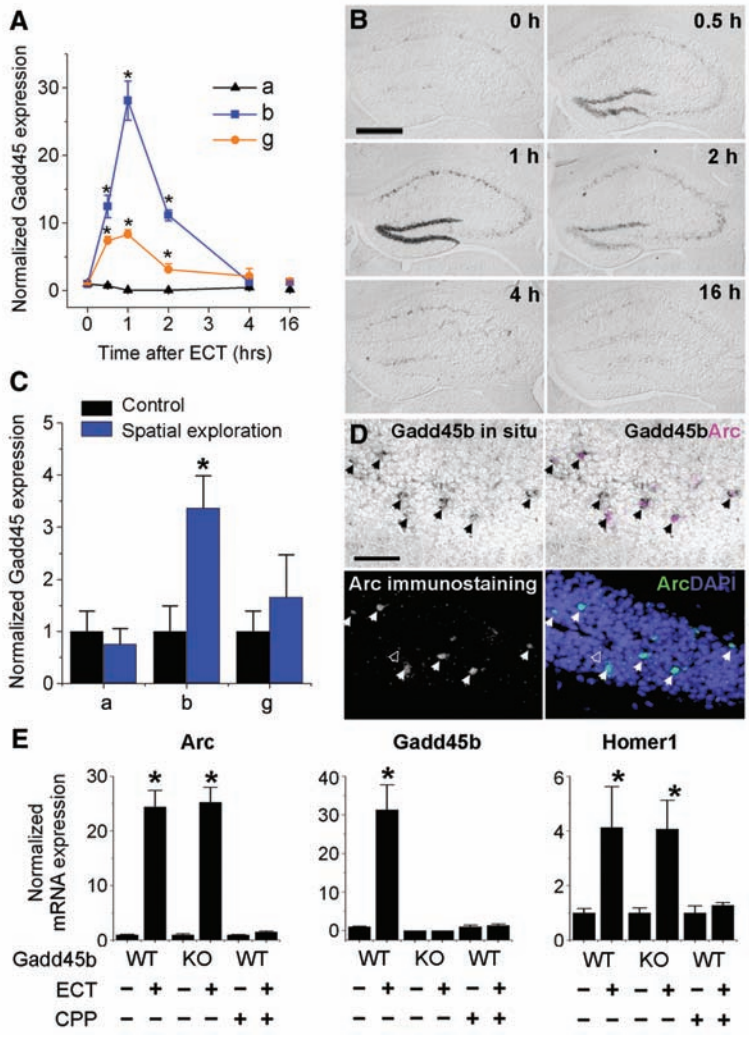

Fig. 1. Activity-induced neuronal *Gadd45b* expression. (**A**) Quantitative polymerase chain reaction (Q-PCR) analysis of ECT-induced expression of *Gadd45a*, *Gadd45b*, and *Gadd45g* in the adult dentate gyrus after a single ECT. (**B**) Sample images of *Gadd45b* in situ hybridization of the adult hippocampus after ECT. Scale bar: 0.5 mm. (**C** and **D**) *Gadd45* induction in the dentate gyrus after 1 hour of spatial exploration of a novel environment. (C) A summary from Q-PCR analysis. (D) Sample confocal images of *Gadd45b* in situ hybridization, and 4′,6-diamidino-2-phenylindole (DAPI) and Arc immunostaining. Most of the Gadd45b-positive cells (open and closed arrowheads) were Arc-positive (closed arrowheads). Scale bar: 50 μm. (**E**) NMDAR-dependent induction of *Gadd45b*, *Arc*, and *Homer1* in the adult dentate gyrus at 1 hour after ECT. The NMDAR antagonist CPP was injected intraperitoneally at 1 hour before ECT (10 mg per kg of body weight). Values represent mean ± SEM [n = 4 animals; $^{*}P < 0.01$, analysis of variance (ANOVA)].

neurons. Retroviruses expressing green fluorescent protein (GFP) were stereotaxically injected into the dentate gyrus of adult WT and KO mice to label proliferating neural progenitors and their progeny (*5*, *14*). A single ECT was given at 3 days after injection, when most GFP-labeled cells have already become postmitotic neurons (*14*). Quantitative analysis showed that ECT markedly increased the total dendritic length and complexity of GFP^{+} newborn neurons at 14 days after retroviral labeling (Fig. 3). This ECT-induced dendritic growth was significantly attenuated in KO mice, whereas the basal level of dendritic growth was similar (Fig. 3). Thus, *Gadd45b* is also essential for activity-induced dendritic development of newborn neurons in the adult brain.

How does transient *Gadd45b* induction regulate activity-dependent adult neurogenesis over the long-term? *Gadd45a* has been implicated in promoting global DNA demethylation in cultured cells, yet the finding remains controversial (*11*, *15*). To examine whether *Gadd45b* induction may confer long-lasting epigenetic modulation in the expression of neurogenic niche signals, we analyzed DNA methylation status using microdissected adult dentate tissue enriched in $NeuN^{+}$ mature neurons (*5*). No significant global DNA demethylation was detected after ECT in vivo (figs. S9 and S10B and supporting text). We next used methylated DNA immunoprecipitation (MeDIP) analysis in a preliminary screen for region-specific DNA demethylation, with a focus on growth factor families that have been implicated in regulating adult neurogenesis (*2*). Significant demethylation was found at specific regulatory regions of brain-derived neurotrophic factor (*Bdnf*) and fibroblast growth factor–1 (*Fgf-1*) (fig. S10B). Bisulfite sequencing analysis further confirmed ECT-induced demethylation within the regulatory region IX of *Bdnf* (*16*) and the brain-specific promoter B of *Fgf-1* (*17*) (Fig. 4, A and B; fig. S11 and table S2). Every CpG site within these regions exhibited a marked reduction in the frequency of methylation (Fig. 4A). Time-course analysis further revealed the temporal dynamics of DNA methylation status at these CpG sites (figs. S12 and S13). In contrast, no significant change was induced by ECT in the pluripotent cell-specific *Oct4* promoter or the kidney and liver-specific *Fgf-1G* promoter (*18*)

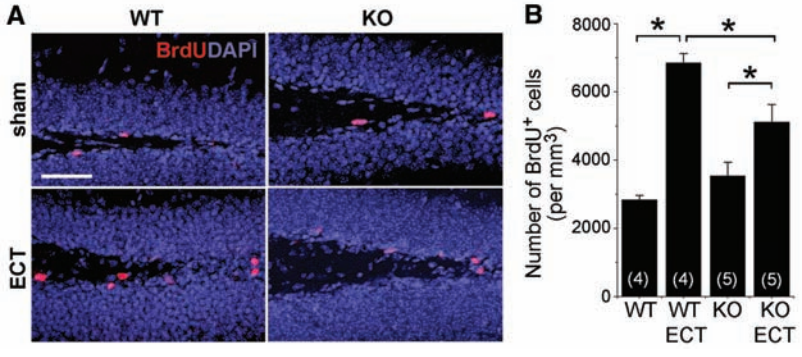

Fig. 2. Essential role of *Gadd45b* in activity-induced proliferation of adult neural progenitors. (**A**) Sample projected confocal images of BrdU immunostaining (red) and DAPI (blue). Scale bar: 50 μm. (**B**) Summary of stereological quantification of $BrdU^{+}$ cells in the dentate gyrus. Values represent mean ± SEM (n = 4 or 5 animals as indicated; $^{*}P < 0.01$, ANOVA).

(Fig. 4B and fig. S11B). Comparison of adult *Gadd45b* WT and KO mice without ECT showed no significant difference in the basal levels of DNA methylation within *Bdnf* IX and *Fgf-1B* regulatory regions (Fig. 4B and fig. S14). In contrast, ECT-induced DNA demethylation of these regions was almost completely abolished in KO mice (Fig. 4, A and B, and figs. S10C and S11A). In addition, overexpression of *Gadd45b* appeared to promote DNA demethylation in vivo (Fig. 4C) and to activate methylation-silenced reporters in cultured postmitotic neurons (fig. S15). Chromatin immunoprecipitation analysis further showed specific binding of Gadd45b to the *Fgf-1B* and *Bdnf* IX regulatory regions (fig. S16). ECT-induced gene expression from these regions and total expression of *Bdnf* and *Fgf-1* were largely absent in *Gadd45b* KO mice at 4 hours (Fig. 4D and fig. S17), consistent with a critical role of DNA methylation status in regulating gene expression. Thus, *Gadd45b* is essential for activity-dependent demethylation and late-onset expression of specific secreted factors in the adult dentate gyrus.

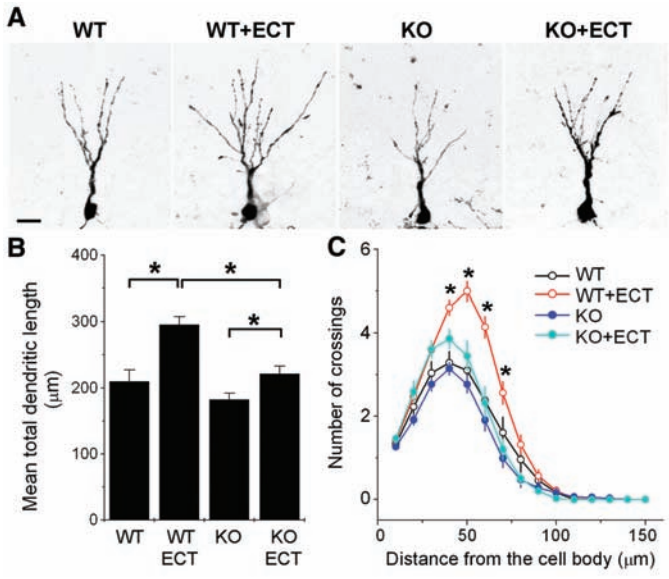

Fig. 3. Essential role of *Gadd45b* in activity-induced dendritic development of newborn neurons in the adult brain. (**A**) Sample projected Z-series confocal images of GFP$^+$ dentate granule cells at 14 days after viral labeling. Scale bar: 50 μm. (**B**) Quantification of the total dendritic length of GFP$^+$ dentate granule cells. Values represent mean ± SEM (n = 23 to 45 neurons for each condition; $^*P$ < 0.01, ANOVA). (**C**) Analysis of dendritic complexity of the same group of cells as in (B). Values represent mean ± SEM ($^*P$ < 0.01, Student's t test).

In summary, Gadd45b links neuronal circuit activity to region-specific DNA demethylation and expression of paracrine neurogenic niche factors from mature neurons in controlling key aspects of activity-dependent adult neurogenesis (fig. S18). As endogenous target of *Gadd45b*-dependent demethylation pathway, BDNF is known to promote dendritic growth of neurons in vivo, and FGF-1 exhibited as robust mitogenic activity as FGF-2 on neural progenitor proliferation in vitro (fig. S19). The presence of Gadd45b in chromatin associated with *Bdnf* IX and *Fgf-1B* regulatory regions in neurons (fig. S16) points to its direct role in gene regulation and potentially in a demethylation complex (fig. S18) (*11*, *19*). The known role of the *Gadd45* family in 5-methylcytosine excision (*7*, *8*, *11*) is consistent with the emerging notion that region-specific demethylation can be mediated through DNA repair–like mechanisms, as supported by genetic and biochemical studies in both *Arabidopsis* and mammalian cells (*20*, *21*) (supporting text).

How transient neuronal activation achieves long-lasting effects in neural plasticity and memory has been a long-standing question; enzymatic modification of cytosine in DNA was proposed as a means to provide such necessary stability with reversibility (*22*). Although DNA demethylation can occur passively during cell division, emerging evidence suggests the existence of active demethylation in postmitotic cells (*23*–*25*). DNA demethylation in neurons represents an extra layer of activity-dependent regulation, in addition to transcription factors and histone-modifying enzymes (*13*). *Gadd45b* expression is altered in some autistic patients (*26*) and is induced by light in the suprachiasmatic nucleus (*27*), by induction of long-term potentiation in vivo (*28*). *Gadd45b* is also associated with critical-period plasticity in the visual cortex (*29*). Thus, *Gadd45b* may represent a common target of physiological stimuli in different neurons in vivo, and mechanisms involving epigenetic DNA modification may be fundamental for activity-dependent neural plasticity.

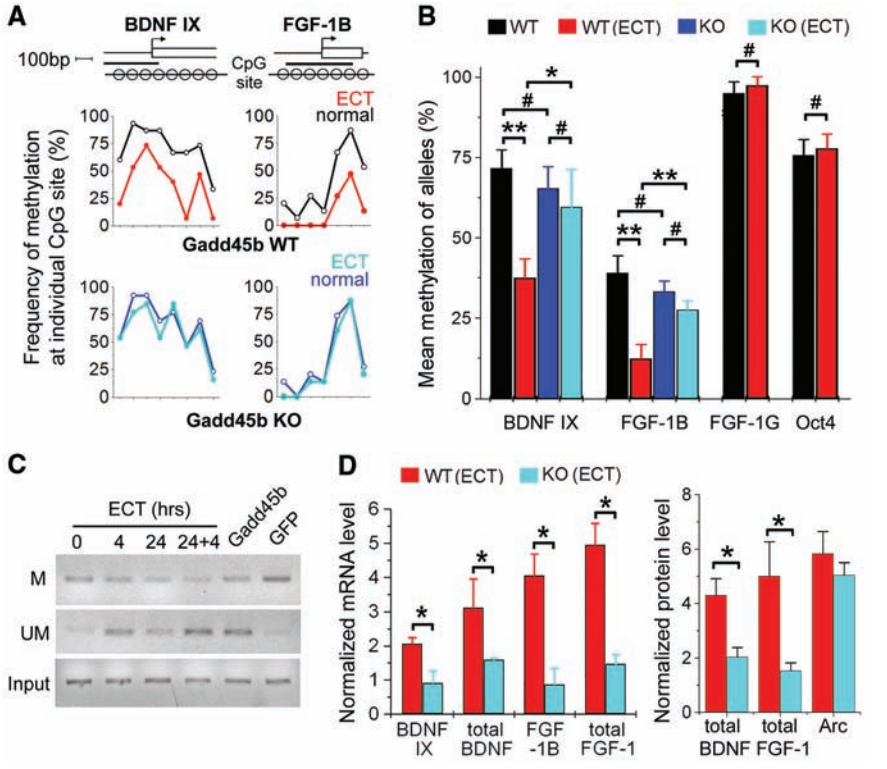

Fig. 4. Essential role of *Gadd45b* in activity-induced specific DNA demethylation and gene expression in the adult dentate gyrus. (**A** and **B**) Bisulfite sequencing analysis of adult dentate gyrus tissue before or at 4 hours after ECT. (A) A schematic diagram of the genomic region subjected to analysis and a summary of methylation frequency at individual CpG sites. (B) A summary of mean DNA methylation levels of individual alleles. Values represent mean ± SEM (n = 10 to 15 reads; $^{**}P$ < 0.01, $^*P$ < 0.05, $^\#P$ > 0.1, ANOVA; exact P values are given in table S2). (**C**) Methylation-specific PCR analysis from the dentate gyrus of WT mice after one or two ECTs ("24+4": 4 hours after two ECTs at 24 hours apart) or 7 days after lentivirus-mediated expression of Gadd45b-GFP or GFP alone without ECT. Primers are specific for methylated (M) and unmethylated alleles (UM) of the *Fgf-1B* promoter, or for bisulfite sequencing without CpGs (Input). (**D**) Summary of the mRNA and protein expression in the dentate gyrus of adult *Gadd45b* WT and KO mice at 4 hours after ECT and sham controls. Values represent mean ± SEM (n = 4 animals; $^*P$ < 0.01, ANOVA).

References and Notes

1. G. Kempermann, H. van Praag, F. H. Gage, *Prog. Brain Res.* **127**, 35 (2000).
2. G. L. Ming, H. Song, *Annu. Rev. Neurosci.* **28**, 223 (2005).
3. T. M. Madsen *et al.*, *Biol. Psychiatry* **47**, 1043 (2000).
4. R. Jaenisch, A. Bird, *Nat. Genet.* **33** (suppl.), 245 (2003).
5. Materials and methods and supporting data are available on *Science* Online.
6. J. E. Ploski, S. S. Newton, R. S. Duman, *J. Neurochem.* **99**, 1122 (2006).
7. H. J. Jung *et al.*, *Oncogene* **26**, 7517 (2007).
8. H. Tran *et al.*, *Science* **296**, 530 (2002).
9. M. C. Hollander, A. J. Fornace Jr., *Oncogene* **21**, 6228 (2002).
10. B. Lu, A. F. Ferrandino, R. A. Flavell, *Nat. Immunol.* **5**, 38 (2004).
11. G. Barreto *et al.*, *Nature* **445**, 671 (2007).
12. V. Ramirez-Amaya *et al.*, *J. Neurosci.* **25**, 1761 (2005).
13. S. W. Flavell, M. E. Greenberg, *Annu. Rev. Neurosci.* **31**, 563 (2008).
14. S. Ge *et al.*, *Nature* **439**, 589 (2006).
15. S. G. Jin, C. Guo, G. P. Pfeifer, *PLoS Genet.* **4**, e1000013 (2008).
16. T. Aid, A. Kazantseva, M. Piirsoo, K. Palm, T. Timmusk, *J. Neurosci. Res.* **85**, 525 (2007).
17. K. Y. Alam *et al.*, *J. Biol. Chem.* **271**, 30263 (1996).
18. Y. Zhang, F. Madiai, K. V. Hackshaw, *Biochim. Biophys. Acta* **1521**, 45 (2001).
19. N. Cervoni, M. Szyf, *J. Biol. Chem.* **276**, 40778 (2001).
20. M. Gehring *et al.*, *Cell* **124**, 495 (2006).
21. R. Métivier *et al.*, *Nature* **452**, 45 (2008).
22. R. Holliday, *J. Theor. Biol.* **200**, 339 (1999).
23. K. Martinowich *et al.*, *Science* **302**, 890 (2003).
24. I. C. Weaver *et al.*, *Nat. Neurosci.* **7**, 847 (2004).
25. F. D. Lubin, T. L. Roth, J. D. Sweatt, *J. Neurosci.* **28**, 10576 (2008).
26. K. Garbett *et al.*, *Neurobiol. Dis.* **30**, 303 (2008).
27. V. M. Porterfield, H. Piontkivska, E. M. Mintz, *BMC Neurosci.* **8**, 98 (2007).
28. D. Hevroni *et al.*, *J. Mol. Neurosci.* **10**, 75 (1998).
29. M. Majdan, C. J. Shatz, *Nat. Neurosci.* **9**, 650 (2006).

30. We thank D. Ginty, S. Synder, and members of Ming and Song laboratories for help and critical comments and L. Liu and Y. Cai for technical support. This work was supported by NIH, McKnight, and NARSAD (to H.S.) and by NIH, March of Dimes, and Johns Hopkins Brain Science Institute (to G-l.M.). R.A.F. is an investigator with the Howard Hughes Medical Institute.

Supporting Online Material

www.sciencemag.org/cgi/content/full/1166859/DC1
Materials and Methods
SOM Text
Figs. S1 to S19
Tables S1 and S2
References

6 October 2008; accepted 16 December 2008
Published online 1 January 2009;
10.1126/science.1166859
Include this information when citing this paper.

Harmonic Convergence in the Love Songs of the Dengue Vector Mosquito

Lauren J. Cator,[1]* Ben J. Arthur,[2]* Laura C. Harrington,[1] Ronald R. Hoy[2]†

The familiar buzz of flying mosquitoes is an important mating signal, with the fundamental frequency of the female's flight tone signaling her presence. In the yellow fever and dengue vector *Aedes aegypti*, both sexes interact acoustically by shifting their flight tones to match, resulting in a courtship duet. Matching is made not at the fundamental frequency of 400 hertz (female) or 600 hertz (male) but at a shared harmonic of 1200 hertz, which exceeds the previously known upper limit of hearing in mosquitoes. Physiological recordings from Johnston's organ (the mosquito's "ear") reveal sensitivity up to 2000 hertz, consistent with our observed courtship behavior. These findings revise widely accepted limits of acoustic behavior in mosquitoes.

Mosquito-borne diseases such as malaria, yellow fever, and dengue continue to afflict millions, even after decades of work to control vector populations. Despite this effort, basic aspects of mosquito biology are not fully understood, including mating behavior, an important target for vector control. We describe investigations in *Aedes aegypti* that require revision of the current understanding of mosquito mating behavior. Since Johnston (*1*) first suggested in 1855 that mosquitoes could perceive sound, over 14 studies have been published on sound production and hearing in *A. aegypti* (*2*–*17*) (table S1). The buzz of a flying female mosquito acts as a mating signal, attracting males. Typically, the behaviorally salient frequency component of flight tone is the fundamental frequency of wing beat, which is between 300 to 600 Hz depending on species (*8*). However, mate attraction is not simply a matter of a male passively hearing and homing in on a 400-Hz tone. For example, males and females of the non–blood-feeding mosquito *Toxorhynchites brevipalpis* modulate their 300- to 500-Hz wing beat frequencies to match each other (*18*). Thus, acoustically mediated mate attraction involves active modulation by both sexes, creating a duet.

We show that males and females of the dengue and yellow fever vector *A. aegypti* also modulate their flight tones when brought within a few centimeters of each other. This modulation, however, does not match the fundamental wing beat frequency of around 400 Hz (female) or around 600 Hz (male) but a shared harmonic frequency of around 1200 Hz (Fig. 1). Consistent with this, a neurophysiological examination of the ears of *A. aegypti* shows response in both males and females up to 2000 Hz (Fig. 2). These results are unexpected because over 5 decades of behavioral and physiological studies had concluded that male mosquito ears (antennae and associated Johnston's organ) are tuned to 300 to 800 Hz and deaf to frequencies above 800 Hz (*8*, *19*). The present study also directly addresses the issue of auditory competence in female mosquitoes. Acoustic duetting behavior in the nonvector mosquito *T. brevipalpis* (*18*) would seem to imply active audition in both sexes, and laser vibrometry studies of the Johnston's organ in that species and *A. aegypti* (*16*, *17*) indicate that they respond mechanically to salient sounds. Moreover, female frog-biting mosquitoes are reported to be attracted by the sounds of their singing hosts (*20*). The auditory physiology on *A. aegypti* provides direct evidence that females can hear and puts to rest textbook wisdom that females are deaf (*8*, *9*).

For behavioral experiments, we tethered each mosquito to the end of an insect pin. When suspended in midair, flies initiated bouts of wing-flapping flight. We recorded flight tones with a particle velocity microphone. Acoustic interaction was demonstrated by moving a tethered flying mosquito past a stationary tethered flying partner (movie S1 with audio). Females were brought in and out of the male hearing range (2 cm) for 10-s fly-bys. Recordings revealed acoustic interaction: In 14 of 21 (67%) pairs, both sexes altered their flight tones so that the male's second harmonic [fundamental (F0) = 636.7 ± 15.1, second harmonic (F1) = 1238.3 ± 31.0 (SEM) Hz] matched the female's third harmonic [F0 = 430.6 ± 10.8, F2 = 1356.2 ± 29.2 (SEM) Hz] (Fig. 1, A to C). The period of synchronization lasted an average of 9.71 ± 1.05 (SEM) s with the synchronization frequency averaging 1354.5 ± 31.5 (SEM) Hz. *A. aegypti* do not shift their flight tones in the absence of acoustic stimulation, as tested both by deafening the mosquitoes [and stimulating with tones, Fisher' exact test, males $P = 0.02$, females $P = 0.04$ (*21*)] and flying intact control subjects in silence [Fisher's exact test, males $P = 0.02$, females $P = 0.04$ (*21*)].

The presence of the fundamental frequency tone was not necessary for harmonic matching. We stimulated tethered mosquitoes with electronically generated pure sinusoidal tones as well as with harmonic combinations of pure tones lacking the fundamental frequency (Fig. 1, D to F). The intensity of the pure tones was set at a particle velocity of 0.024 mm/s corresponding to 54 dB sound pressure level (relative to 20 μPa) when played through an ear bud speaker positioned 1.5 cm in front of the test mosquito. This intensity is well within the response range of *A. aegypti*'s Johnston's organ, as measured by Doppler vibrometry (*17*). Stimuli were played in 10- to 15-s bursts with 5- to 20-s recovery periods. Playback experiments with pure-tone combinations

[1]Department of Entomology, Cornell University, Ithaca, NY 14853, USA. [2]Department of Neurobiology and Behavior, Cornell University, Ithaca, NY 14853, USA.

*These authors contributed equally to this work.
†To whom correspondence should be addressed. E-mail: rrh3@cornell.edu

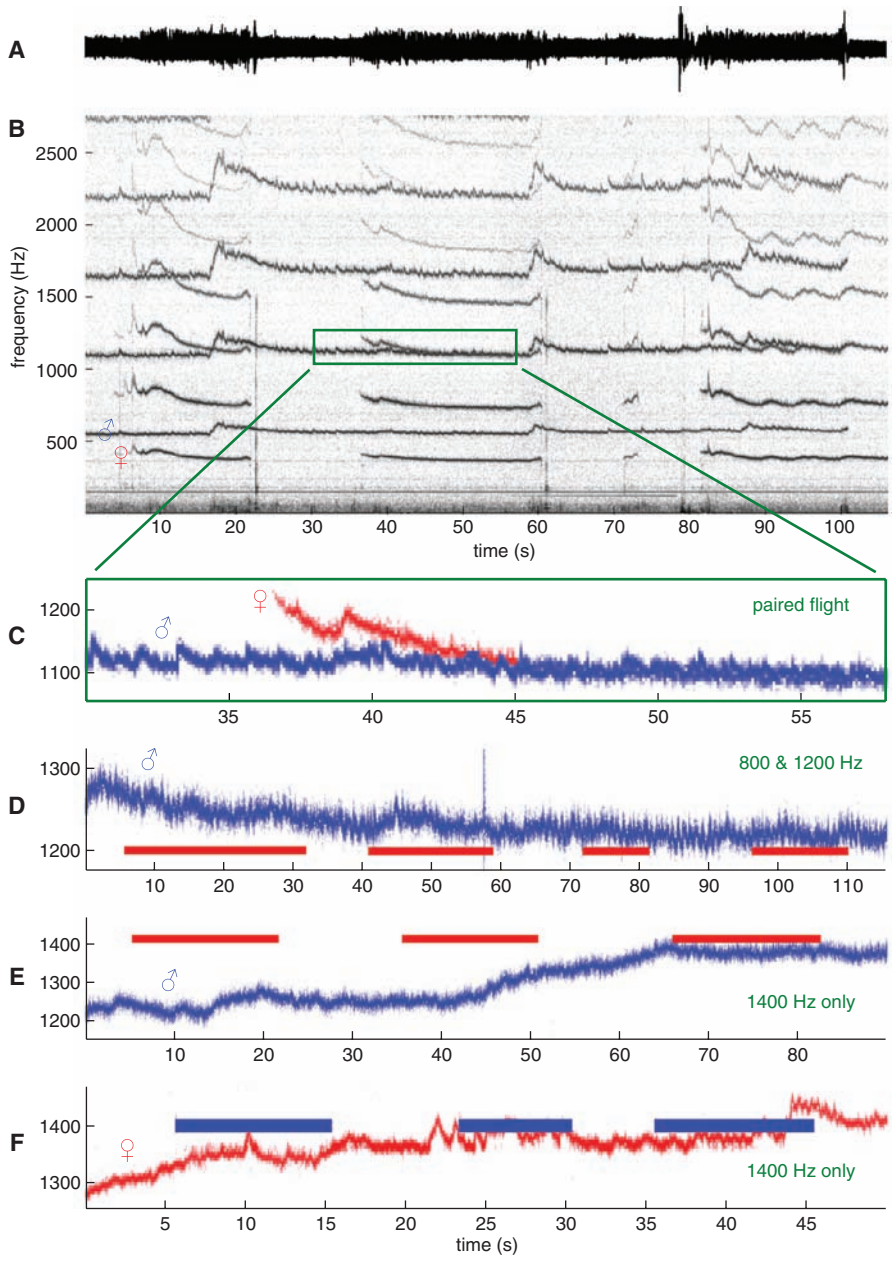

Fig. 1. (**A**) An oscillogram from a sound clip of a tethered male and female duetting. (**B**) A spectrogram depicting the harmonic stack of the same sound clip. The male was held in a fixed position and sang continuously for nearly 2 min. The female was brought within 2 cm of the male on three separate occasions. (**C**) An expanded view of (B) showing the synchronization of the flight tone at the second harmonic of the male (blue) and the third of the female (red). At t = 45 s, the two tones converge to the extent that they cannot be readily distinguished. (**D**) A separate recording of a tethered male (blue) flying solo and synchronizing to a loud speaker stimulus consisting of a simulated female flight tone with a missing fundamental (red). (**E**) A recording of a tethered male flying solo (blue) modulating his flight tone to match the playback of a simulated third harmonic of a female. (**F**) A female flying solo (red) matches a simulated second harmonic of a male (blue) playback tone.

demonstrated that 11 of 28 (39%) males could synchronize their 1200-Hz second harmonic to the simulated female's 1200-Hz third harmonic in the absence of the 400-Hz fundamental tone of an actual female. Furthermore, 12 of 54 (22%) males could match a pure 1200-Hz tone (the third harmonic of female flight tone) in the absence of the fundamental and any other harmonic components. We also tested the ability of females to synchronize to playback of pure tones mimicking male sound. Six of 20 (30%) unmated females matched the second harmonic of their flight tone to a complete stack of tones (F0 to F3, 700 to 2800 Hz). When unmated females were stimulated with a pure 1400-Hz tone, 7 of 20 (35%) responded by matching with their third harmonic. In contrast, only 2 of 18 (11%) previously mated females (confirmed by the presence of sperm in the female's sperm storage organs) performed a frequency match to playback of complete male songs, suggesting that mating decreases sensitivity to male stimuli.

Physiological data from the mosquito's auditory organ were obtained by impaling Johnston's organ with tungsten electrodes and recording acoustically evoked field potentials. The Johnston's organ of both males and females responded to 0.5-s cosine-enveloped pure-tone pulses at all frequencies tested (125 to 2000 Hz), including the shared harmonic of their flight tones at 1200 Hz (Fig. 2). The response consists of a sustained voltage deflection, which is negative with respect to the thoracic ground electrode, and a concurrent periodic oscillation at the stimulation frequency and its harmonics, a form of neural encoding that bears resemblance to that seen in the mammalian cochlea (*22*). It is the amplitude of the sustained deflection that remains significantly higher than prestimulus background noise and thoracic control recordings up to 2000 Hz (t test, $P < 0.001$ in both males and females); the amplitude of the periodic oscillation is about an order of magnitude smaller and remains higher than background and controls only up to 1000 Hz, in the case of the stimulus's fundamental, and 700 Hz, for its second harmonic (t test, $P < 0.01$). These recordings confirm earlier studies that the mosquito Johnston's organ is sensitive to 100- to 500-Hz tones and extend the upper limit of hearing to at least 2000 Hz. Earlier physiological studies of Johnston's organ that failed to report a high-frequency response are likely due to filter bandwidths set at the time of recording. We recorded high-frequency responses only when we set the high-pass filter to 1 Hz or less, not the customary 100 Hz or higher used in extracellular recording.

Tone-matching behavior does not require that a tethered, flying mosquito hear a live partner. Either a male or a female *A. aegypti* can modulate its flight tone harmonics to match electronically generated pure-tone probes (Fig. 1). Frequency match is elicited to a probe that simulates a natural flight tone stripped of its fundamental frequency and even to a probe that contains only a single harmonic. Moreover, mosquitoes can modulate their flight tone harmonics to match the probe tone whether the probe frequency is set above or below the fly's actual flight tone. This directly demonstrates that both sexes of this species (and likely other mosquito species) can hear and respond to high-frequency tones alone. These behavioral findings are supported by sensory physiology (Fig. 2). Extracellular recordings of acoustically evoked field potentials from the Johnston's organ elicited clear responses not only to frequencies of the fundamental (400 to 600 Hz), as expected, but into the kilohertz range, where males and females perform active acoustic modulation of their flight tone harmonics. Thus, both behavioral and physiological experiments establish that *A. aegypti* signal to each other by using frequen-

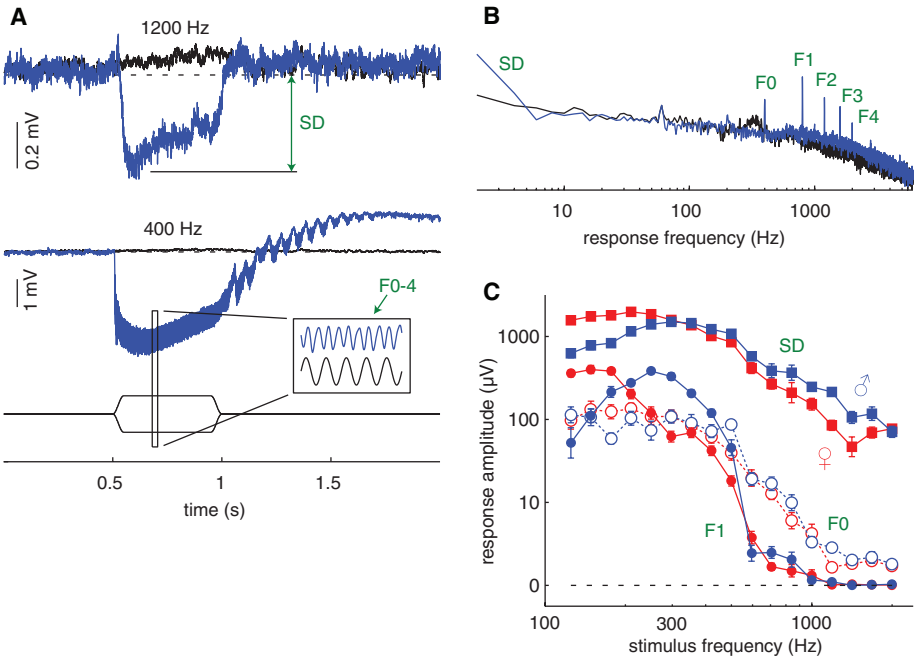

Fig. 2. (**A**) Acoustically evoked field potentials recorded from Johnston's organ exhibit periodic oscillations (inset, F0 to F4) riding on top of a sustained deflection (SD). Shown are averages of 10 and 5 repetitions to 1200 and 400 Hz, respectively, in a male. Thoracic control recordings are in black; the stimulus envelope is at bottom. (**B**) Spectral analysis of the response to the 400-Hz tone in (A) shows substantial power at low frequencies (SD) during the stimulus (blue) compared with a prestimulus background period (black), as well as peaks at multiple harmonics (F1 to F4) of the stimulus's fundamental frequency (F0). (**C**) Averaged across 12 males (blue) and 15 females (red), the amplitude (mean ± SEM) of the sustained deflection (SD, solid squares) remains higher than that of prestimulus background noise (dashed line at zero) up to 2000 Hz, whereas the amplitudes of F0 and F1 (open and solid circles, respectively) are substantially smaller.

cies in the kilohertz range and can detect these with their auditory organs. Taken together, these data call for revision of our understanding of acoustically mediated mating behavior in mosquitoes and, in particular, removal of the long-accepted benchmark ceiling for hearing in mosquitoes.

Lastly, once mated, females are much less responsive to male flight tones and less likely to perform tone matching. These results are consistent with the observation that, once mated, *A. aegypti* females are not responsive to additional matings for the duration of one or more egg-laying cycles (*23*, *24*). This implies that an initial mating depresses the likelihood of subsequent matings. Thus, releasing sterile male mosquitoes into the wild might adversely affect the reproductive potential of virgin females, providing a rationale for controlling these disease vectors through diminishing mating potential. Other vector and pest species of flies have been controlled by the release of sterile males (*25*–*27*). Our investigation connects control to signal function. We hypothesize that the ability of males to modulate their flight tones to females is the result of sexual selection. Hence, harmonic convergence could be a measure of a male's reproductive fitness and the ability of lab-reared, sterilized or genetically modified males to modulate their flight tones could be a useful behavioral bioassay for the sterilization program (*28*, *29*). At the very least, our findings open the door to a new understanding of their mating behavior, one that stresses acoustic interactivity between the sexes at frequencies thought previously to be beyond their range of hearing.

References and Notes

1. C. Johnston, *Q. J. Microsc. Sci.* **3**, 97 (1855).
2. P. Belton, in *Experimental Analysis of Insect Behavior*, L. B. Browne, Ed. (Springer-Verlag, Berlin, 1974), pp. 139–147.
3. P. Belton, in *Insect Flight: Dispersal and Migration*, W. Danthanarayana, Ed. (Springer-Verlag, Berlin, 1986), pp. 60–70.
4. P. Belton, *Can. J. Zool.* **67**, 2625 (1989).
5. P. Belton, *J. Am. Mosq. Control Assoc.* **10**, 297 (1994).
6. P. Belton, R. A. Costello, *Entomol. Exp. Appl.* **26**, 105 (1979).
7. K. S. Boo, A. G. Richards, *J. Insect Physiol.* **21**, 1129 (1975).
8. A. N. Clements, *The Biology of Mosquitoes: Sensory Reception and Behaviour* (CABI, Wallingford, UK, 1999), p. 740.
9. J. A. Downes, *Annu. Rev. Entomol.* **14**, 271 (1969).
10. P. T. Haskell, in *The Physiology of Insecta*, M. Rockstein, Ed. (Academic Press, New York, ed. 2, 1974), vol. 2, pp. 353–410.
11. M. C. Kahn, W. Offenhauser Jr., *Am. J. Trop. Med. Hyg.* **29**, 811 (1949).
12. A. M. Mayer, *Am. Nat.* **8**, 577 (1874).
13. L. M. Roth, *Am. Midl. Nat.* **40**, 265 (1948).
14. J. Schwartzkopff, in *The Physiology of Insecta*, M. Rockstein, Ed. (Academic Press, New York, ed. 2, 1974), vol. 2, pp. 273–352.
15. M. C. Göpfert, D. Robert, *Proc. R. Soc. London Ser. B* **268**, 333 (2001).
16. M. C. Göpfert, D. Robert, *Proc. R. Soc. London Ser. B* **267**, 453 (2000).
17. M. C. Göpfert, H. Briegel, D. Robert, *J. Exp. Biol.* **202**, 2727 (1999).
18. G. Gibson, I. Russell, *Curr. Biol.* **16**, 1311 (2006).
19. G. Wishart, C. F. Riordan, *Can. Entomol.* **91**, 181 (1959).
20. A. Borkent, P. Belton, *Can. Entomol.* **138**, 91 (2006).
21. Materials and methods are available as supporting material on *Science* Online.
22. A. R. Palmer, I. J. Russell, *Hear. Res.* **24**, 1 (1986).
23. R. Williams, A. Berger, *Mosq. News* **40**, 597 (1980).
24. A. Young, A. Downe, *Physiol. Entomol.* **7**, 467 (1982).
25. M. J. B. R. Vreysen, A. S. Hendrichs, in *Area-Wide Control of Insect Pests from Research to Field Implementation*, M. J. B. R. Vreysen, A. S. Hendrichs, Eds. (Springer, Dordrecht, Netherlands, 2007), p. 792.
26. E. S. Krafsur, *J. Agric. Entomol.* **15**, 303 (1998).
27. R. C. Bushland, A. W. Lindquist, E. F. Knipling, *Science* **122**, 287 (1955).
28. M. Q. Benedict, A. S. Robinson, *Trends Parasitol.* **19**, 349 (2003).
29. T. W. Scott, L. C. Harrington, B. G. J. Knols, W. Takken, in *Transgenesis and Management of Vector-Borne Disease*, S. Aksoy, Ed. (Landes Bioscience, Austin, TX, 2008), pp. 151–168.

30. We thank B. Wyttenbach for the suggestion to look for sustained deflections in the neural response and are grateful to L. Ristroph and I. Cohen for high-speed video of males and females in free flight. Support was provided (to L.C.H.) from the Foundation for the National Institutes of Health through the Grand Challenges in Global Health Initiative and Hatch Project NYC-139432.

Supporting Online Material

www.sciencemag.org/cgi/content/full/1166541/DC1
Materials and Methods
Fig. S1
Table S1
References
Movie S1

29 September 2008; accepted 22 December 2008
Published online 8 January 2009;
10.1126/science.1166541
Include this information when citing this paper.

PREPARING THE PROTEOME FOR MASS SPECTROMETRY

Preparing samples for mass spectrometry analysis is not as simple as merely isolating total protein from its biological source. They also need to be in a chemical environment that is MS friendly and allows their interrogation. Often enzymatic digestion and/or depletion/partitioning/enrichment are required to obtain a usable sample; but what are the best sample preparation methods, and how might they impact experiments? **By Gautam Thor**

Until the early 1990s, mass spectrometry (MS) researchers were generally restricted to the study of small, thermostable molecules that could be easily ionized. Two breakthroughs occurred in quick succession in the late 1980s when John Fenn (who received part of the 2002 Nobel Prize in Chemistry) developed electrospray ionization (ESI) and Koichi Tanaka introduced matrix associated laser desorption ionization (MALDI) for large molecules, based on the work of Franz Hillenkamp and Michael Karas. These methodologies enabled MS analysis of a much broader range of biological molecules, without any need for chemical derivatization.

Finding the Needle in a Haystack

Now, the way in which samples are prepared for MS experiments is frequently determined by, and can have significant impact on, the subsequent steps in the procedure.

Sample preparation procedures prior to MS need to serve dual functions in proteomic studies. First, they must provide adequate isolation of the protein(s) of interest, and second, the buffers used should provide a suitable environment for subsequent MS analysis. One of the biggest challenges, particularly in clinical, diagnostic, and prognostic applications such as those associated with biomarker discovery, is dealing with both the sheer complexity and the large dynamic range of the samples used. Jerald Feitelson, business development, intellectual property, and alliance manager at **Beckman Coulter,** points out that "although any single protein preparation technology is unlikely to be ideal for all samples, the more one can simplify the sample, reduce the dynamic range of protein concentrations, enrich for medium and low abundance proteins, and remove interfering peptide mass fingerprints the better the mass spectrometry results will be and the deeper one can dig into the proteome."

Fluids like blood, saliva, and urine can contain many thousands of proteins and protein fragments that cover a dynamic range of 10 or more orders of magnitude, whereas most MS workflows are restricted to three or four logs of concentration, at best. Roughly 85 percent by mass of the human serum proteome is comprised of only six highly abundant proteins, including albumin, immunoglobulins of the G and A subtypes, transferrin, haptoglobin, and α1-antitrypsin. But this handful of components can mask the mass spectra of the low abundance (and often more interesting) proteins. In fact, early research in biomarker discovery using low resolution, but rapid, MS technologies such as surface enhanced laser desorption ionization (SELDI) was unable to establish any reproducible or clinically valid biomarkers (most of the signature differences turned out to be nonspecific components of the proteome). In order to overcome this hurdle, several approaches to sample preparation were developed that rely on depleting samples of highly abundant proteins.

Depletion procedures often involve immunoaffinity-based methods using polyclonal or monoclonal antibodies—immobilized on a solid phase—to capture and retain the most abundant proteins. "The Multiple Affinity Removal System was designed to be highly selective for the removal of 14 highly abundant continued >

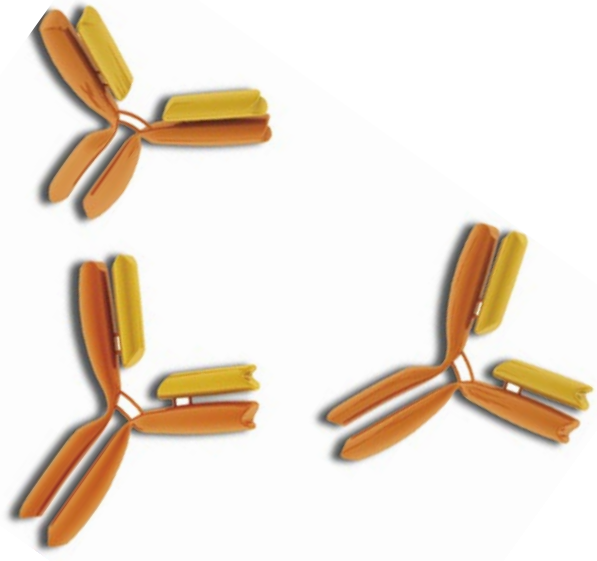

"The more one can simplify the sample, reduce the dynamic range of protein conentrations, enrich for medium and low abundance proteins, and remove interfering peptide mass fingerprints the better the results will be."

Look for these **Upcoming** Articles

In Vivo Imaging — March 6
Genomics 1 — April 10
Molecular Diagnostics — May 8

Inclusion of companies in this article does not indicate endorsement by either AAAS or Science, *nor is it meant to imply that their products or services are superior to those of other companies.*

proteins from human serum or plasma," states Scott O'Brien, product line manager at **Stratagene**, an **Agilent Technologies** division. The kit makes use of a specifically formulated buffer "to minimize protein-protein interactions and ensure efficient capture and release of targeted proteins," says O'Brien.

Immunoaffinity capture using avian antibodies may provide higher selectivity and lower cross-reactivity than other comparable products, since chicken antibodies display less cross-reactivity with mammalian proteins. **GenWay Biotech** (recently acquired by **Sigma-Aldrich**) provides Seppro affinity depletion technology built from a library of 700 chicken-derived IgY antibodies, while Beckman Coulter has been offering, for research use only, ProteomeLab IgY-12 spin and liquid chromatography column kits that are able to selectively partition 12 highly abundant proteins found in plasma or serum, enriching the sample up to 25-fold.

Calbiochem (part of **EMD Biosciences**) makes use of a different methodology: the company's ProteoExtract kit includes an albumin/IgG removal component which uses a combination of the albumin-specific resin and an immobilized protein A polymeric resin. After removal of the high abundance proteins, the kit allows for the selection of partial or full proteome extraction, a precipitation step to concentrate the sample, and an enzymatic digestion if required. **Novagen's** (also a part of EMD Biosciences) ProteoEnrich CAT-X kit separates proteins under nondenaturing conditions based on their binding to the strong cation exchange resin. Almost the entire proteome should bind to the matrix under slightly acidic conditions, and partial proteomes can be eluted using a salt gradient.

One profound drawback of depletion strategies results from the tendency for abundant proteins, particularly albumin, to bind other serum proteins and protein fragments. Thus it is possible that depletion of highly abundant proteins might also remove desirable ones. **Bio-Rad** addresses this problem with its ProteoMiner technology, which provides a large and highly diverse library of hexapeptides bound to a chromatographic support, allowing each unique hexapeptide to bind to a unique protein sequence. When the sample is added, the limiting binding capacity of the beads enables high abundance proteins to rapidly saturate their ligands, and excess protein is washed out. In contrast, the low abundance proteins are concentrated on their specific ligands. Following elution from the beads, the dynamic range of proteins in the sample is greatly reduced. Kate Smith, Bio-Rad's product manager for expression proteomics, explains that "since our depletion strategy does not entirely discard all the high abundant proteins, we get a quantitative analysis of the low abundance proteins and limit the potential codepletion of proteins associated with the highly abundant proteins."

The procedure described above not only depletes abundant proteins but also provides a means to segment the sample, demonstrating an alternative strategy for protein sample preparation: enrichment.

Separating the Wheat from the Chaff

In contrast to depletion strategies for sample preparations, enrichment processes allow for the preparation of specific subsets of proteins. These can be achieved either through affinity purification using posttranslational chemical modifications (for example, glycosylation or phosphorylation) or by the isolation of cellular subpopulations (such as organelles or plasma membrane fractions).

"Most biofluid samples for clinical discovery experiments need to be reduced, alkylated and trypsin digested, and then subjected to a sample cleanup by reverse phase HPLC [high performance liquid chromatography]," says Mary F. Lopez, director, biomarker research initiatives in mass spectrometry at **Thermo Fisher Scientific.** In her

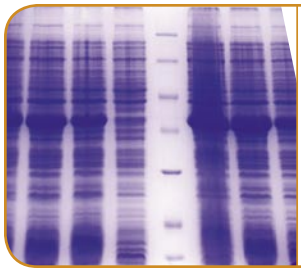

"The necessary sensitivity level in blood, urine, or even tissue extracts is often achievable only through an enrichment strategy."

opinion, the most successful approaches seem to be enrichment strategies for target pathways rather than depletion of interfering proteins. However, she also says that "the choice of targeted-enrichment strategy depends on how much is known about the protein or family of proteins of interest." Lopez indicates that proteomics-based identification of relevant biomarkers is a very active area of research. "The objective is biomarker candidates or signatures that can be used in a targeted, clinically relevant quantitative assay. However, the necessary sensitivity level in blood, urine, or even tissue extracts is often achievable only through an enrichment strategy."

Enrichment strategies frequently use solid-phase extraction (SPE), a standard biochemical technique that uses the affinity of solutes within a liquid (mobile) phase for the solid (stationary) phase over which that sample is passed. Either the desired analytes of interest are collected in the flow through or, if they are retained on the stationary phase, they can then be removed with an appropriate eluent.

Jeff Zonderman, director of clinical and toxicology LC/MC from Thermo Fisher Scientific, points out that "the most widely used pre-MS clinical sample preparation method is probably SPE due to its large selectivity." However, he acknowledges that researchers frequently use more than one selective technology to adequately reduce the complexity of a sample. One example is Thermo's Transcend system with TurboFlow technology, which puts a unique spin on pre-MS chromatographic separation. As Zonderman explains, introducing turbulence into the system—by running cartridges at predetermined high speeds—creates a more uniform velocity profile across the column, and "provides a means to obtain high volume, high demand separation."

Varian's OMIX product line uses SPE in a pipette tip to provide a high throughput application for microextraction of proteins and peptides. The company claims that the small sorbent bed makes for a cleaner elution into a smaller volume. A similar product from **Millipore,** the ZipTip, is made to be compatible with a number of automated liquid handling systems and, according to the company literature, "provides a reproducible, high recovery method for concentrating and purifying femtomoles to picomoles of peptides, proteins, and oligonucleotides."

"Selective enrichment is an area we are pursuing vigorously," states Andrew Emili, professor at the Donnelly Centre for Cellular and Biomolecular Research, at the **University of Toronto,** Canada. "For example, we are using both HPLC and aptamer phage display to physically isolate targets of interest from complex mixtures prior to MS detection." Emili claims that their approach, which is still in the research phase, is faster and cheaper for isolating proteins or peptides than raising antibodies for immunoenrichment.

Teasing Apart the Cell

If depletion strategies are too blunt an instrument and enrichment procedures too specific, the limitations introduced by the complexity of the MS samples could be addressed, at least in part, continued >

by the use of strategies targeting information-rich subsets of the proteome. This includes using standard subcellular fractionation technologies such as Poppers kits from **Pierce** (now a part of Thermo Fisher Scientific) and EMD Bioscience's ProteoExtract Subcellular Proteome Extraction kit, both of which are capable of enriching for nuclear, cytoplasmic, and mitochondrial proteins.

The Qproteome kits from **Qiagen,** in contrast to straightforward differential centrifugation methods, promise to provide high purity of isolated subcellular fractions and soluble proteins, with concomitant depletion of high-abundant proteins such as IgG and albumin. "At the same time," says Ute Boronowsky, global product manager, "the procedure is very gentle, using only a benchtop centrifuge, leaving subcellular organelles such as mitochondria and plasma membranes intact, and retaining proteins in a native conformation with full biological activity."

Although it is predicted that nearly 30 percent of all proteins are phosphorylated, phosphoproteins tend to be of low abundance and often with multiple phosphorylation sites of varying stoichiometries, which presents several challenges for MS analysis. Enrichment of phosphoproteins from complex mixtures can be performed by affinity chromatography using immobilized antibodies specific for phosphoserine, phosphothreonine, and phosphotyrosine residues, obtainable as commercial kits. Another technique more amenable to MS analysis is the use of immobilized metal affinity chromatography (IMAC) as it relies on the affinity of phosphate groups for certain metal ions (e.g., Fe^{3+} or Ga^{3+}) bound to tethered chelating reagents presented on solid phase supports. Pierce's Phosphopeptide Isolation kit and Sigma-Aldrich's PhosphoProfile I Phosphopeptide Enrichment kit are both designed to simplify the isolation and identification of phosphopeptides from protein digests through the specific interaction of phosphate groups with immobilized gallium. Using a different process involving magnetic beads as the carrier and zirconium ions for capture, Calbiochem's ProteoExtract Phosphopeptide Capture kit enables isolation of phosphorylated peptides for downstream identification by MS. The company also produces the ProteoEnrich ATP-Binders kit which uses a novel resin with covalently bound ATP on a flexible linker to obtain samples enriched for protein kinases and other ATP-binding proteins.

Other subproteomes often targeted are those of the intracellular and plasma membranes, of particular interest because they are the location of many proteins involved in cell signaling. However, these proteins have proved difficult to analyse, as their hydrophilic regions are preferentially detected by commonly used MS preparative methods. This necessitates high sequence coverage in order to accurately map sites of posttranslational modification and agonist/antagonist binding, elucidate stoichiometry, and identify sites of protein-protein interaction. Reagents that can increase sequence coverage of hydrophobic proteins are therefore in great demand. Novagen's ProteoExtract Native Membrane Protein Extraction kit is designed for the isolation of membrane proteins from mammalian cells and tissues. The extremely mild procedure yields a solution of integral membrane and membrane-associated proteins in their nondenatured state. **Life Technology's** (previously Invitrogen) Invitrosol MALDI Protein Solubilizer includes the ability to prepare both hydrophobic and hydrophilic proteins and peptides directly for MALDI time-of-flight MS analysis without the need for subsequent acid hydrolysis.

Pushing the Limits of Technology

Sample preparation methods are highly dependent on the proteomic query of interest. Generally, protein purification procedures require nonvolatile buffers, solubilizing agents, EDTA, and detergents to ensure that the proteins retain their native conformation. Some MS applications might require relatively harsh treatments to expose certain structures or hydrophobic components, while others, such as ESI-MS, might require more gentle buffers that retain macromolecular associations, but could require meticulous cleanup of interfering reagents prior to MS analysis. Although approaches relying on the depletion of potentially interfering, highly abundant proteins in clinical samples are often used, the approach runs the risk of throwing out the proverbial baby with the bathwater, since some of these high abundance proteins might have proteins of interest associated with them.

These issues can be overcome by partitioning procedures that not only separate out the unwanted proteins, but also allow for the analysis of the bound sets of fragments, too. The combination of proteome partitioning and fractionation allows for the enrichment of low abundant proteins, as well as abrogation of the masking effect created by peptides derived from highly abundant proteins. Complementary biochemical manipulations for sample preparative methods include enrichment strategies that target subsets of the proteome such as cellular organelles or functional groups—the choice being determined by the specific target in mind.

Although preparative technologies for MS have improved dramatically in the past decade, ironically the extraordinary ability and power of MS instruments is still being held back by the seemingly mundane biochemical limitations imposed by the procedures for sample preparation.

Featured Participants

Agilent Technologies
www.agilent.com

Beckman Coulter
www.beckman.com

Bio-Rad
www.bio-rad.com

Calbiochem
www.calbiochem.com

EMD Biosciences
www.emdbiosciences.com

GenWay Biotech
www.genwaybio.com

Life Technologies
www.lifetech.com

Millipore
www.millipore.com

Novagen
www.novagen.com

Pierce
www.piercenet.com

Qiagen
www.qiagen.com

Sigma-Aldrich
www.sigmaaldrich.com

Stratagene
www.stratagene.com

Thermo Fisher Scientific
www.thermofisher.com

University of Toronto
www.utoronto.ca

Varian
www.varian.com

Guatam Thor has a Ph.D. in Neurobiology and is currently a freelance writer based in San Diego, California.

DOI: 10.1126/science.opms.p0900032

Mass Spectrometer

The AB Sciex Qtrap 5500 System is a next-generation mass spectrometer that combines high sensitivity, scanning speed, and capacity to analyze a greater number of compounds, proteins, and contaminants in a single run than previously possible. The system integrates triple quadrupole capabilities with an innovation in ion trap technology called Linear Accelerator Trap for combined quantitative and qualitative analysis. The system supports multiple experiments on the same instrument through a proprietary innovation, called TripleTrap Scanning, that allows scientists to move from sensitive, specific, triple quadrupole scan modes to highly sensitive full-scan ion trap mode in less than one millisecond.

Applied Biosystems
For information 800-327-3002
www.appliedbiosystems.com

SFC Columns

A new line of supercritical fluid chromatography (SFC) columns brings new phases and selectivities to SFC separations, expanding the use of this technology to analytical and preparative applications. SFC offers several advantages over high-performance liquid chromatography, including improved resolution, faster separations, and higher throughput. SFC also reduces the use of toxic solvents. SFC columns have applications in pharmaceutical and academic research as well as medicinal chemistry. Phenomenex's new SFC offerings include the Luna HILIC (hydrophilic interaction liquid chromatography) columns with unique, cross-linked diol chemistry for analysis of polar metabolites; Synergi Polar-RP (ether-linked phenyl phase) for polar and aromatic analysis; and Lux chiral phases.

Phenomenex
For information 310-212-0555
www.phenomenex.com

Liquid Chromatography System

The AKTAready liquid chromatography system is designed for process scale-up and production for drug development and full-scale production following good laboratory practice and good manufacturing practice standards. The system can improve cost efficiency and productivity by saving time and expenditures for startup, labor, and consumables. AKTAready operates with ready-to-use, disposable flow paths, eliminating the risk of cross-contamination and the need for cleaning and validation of cleaning procedures. The system includes the chromatography unit, Unicorn software, and a disposable ReadyToProcess Flow Kit including sensors and detection flow cells. The software includes an installation wizard with instructions and reports for column installation. The system is supported by extensive regulatory product documentation and services, including validation documentation, product documentation, and more.

GE Healthcare
For information 800-526-3593
www.gelifesciences.com

Stain-Free Imaging

The Criterion Stain Free imaging system for detection and quantitation of proteins consists of a new formulation of Bio-Rad's Criterion precast gels, a Criterion Stain Free imager, and Image-Lab software. The new system enables scientists to bypass the staining and destaining steps of sodium dodecyl sulfate-polyacrylamide gel electrophoresis and visualize protein samples in 2.5 minutes after electrophoresis. In addition, the system captures digital images of gels to make record-keeping easy, with no need for a gel drying step. Benefits of the system include one-touch instrument operation, equal or improved sensitivity compared with a Coomassie stain, compatibility with protein immunoblotting and mass spectrometry, and digital images and data that are easy to share, print, and store. There is no organic waste.

Bio-Rad Laboratories
For information 800-424-6723
www.bio-rad.com

Antibody Purification Tools

The PureProteome Protein A and Protein G Magnetic Beads enable researchers to perform small-scale purifications faster and more easily. The beads provide high binding capacity for high recovery of protein. The beads also ensure reproducible separation of immunoglobulins (IgG) by allowing for total removal of buffers and complete recovery of beads. Magnetic beads were developed to ensure rapid and reproducible purifications by immobilizing the beads to the side of the tube allowing for total removal of buffers with no loss of sample. In the past, magnetic beads have had significantly lower binding capacities than other bead-based purification media, but PureProteome beads overcome this by binding higher amounts of IgG. PureProteome beads are available with an optional magnetic rack that immobilizes the beads against the side of the tube in seconds, allowing for reproducible purifications to be performed quickly and easily.

Millipore
For information 978-762-5170
www.millipore.com

Fluorescent Detection Kit

The DetectX Glutathione Fluorescent Detection Kit is designed to quantitatively measure free and oxidized glutathione in a single sample. The kit makes use of a proprietary molecule, ThioStar, that covalently binds to the free thiol group on glutathione to yield a highly fluorescent product. After mixing the sample with ThioStar for 15 minutes, the user reads the glutathione-generated signal at 510 nm in a fluorescent plate reader. Addition of the provided reaction mixture to the wells converts all the glutathione disulfide into free glutathione, which then reacts with the excess ThioStar during a second 15-minute incubation to detect total glutathione.

Luminos
For information 734-677-1774
www.LuminosAssays.com

Electronically submit your new product description or product literature information! Go to **www.sciencemag.org/products/newproducts.dtl** for more information.

Newly offered instrumentation, apparatus, and laboratory materials of interest to researchers in all disciplines in academic, industrial, and governmental organizations are featured in this space. Emphasis is given to purpose, chief characteristics, and availabilty of products and materials. Endorsement by *Science* or AAAS of any products or materials mentioned is not implied. Additional information may be obtained from the manufacturer or supplier.

Gordon Research Conferences

2009 Meeting Schedule

Session II (June-September)

Photo: Poster Session at Proctor Academy in Andover, NH

For over 75 years, GRC's high-quality, cost-effective meetings have been recognized as the world's premier scientific conferences, where leading investigators from around the globe discuss their latest work and future challenges in a uniquely informal, interactive format. Session II 2009 meetings will be held in New England in the United States and internationally in Italy, China, Switzerland, and the United Kingdom. Apply to a Gordon Research Conference now and see why attendees consistently rate them "the best conference I've attended this year". For full programs, fees and site/travel information, please visit our web site.

visit the frontiers of science: www.grc.org

*The list of meetings begins below. Discussion leaders are noted in italics. New meetings are highlighted with the word "**new**" in red text. Gordon Research Seminars (2-day meetings for graduate students and post-docs) are listed in **green text** beneath their corresponding Gordon Conference.*

ADHESION, SCIENCE OF
Jul 26-31, 2009
Colby-Sawyer College
New London, NH
Chair: Jeffrey T. Koberstein
Vice Chair: Chung-Yuen Hui

- **New Concepts in Adhesion**
  (*Russell Composto* / Jurgen Rühe / Lubwik Leibler)
- **Wetting**
  (*Kai Li, Ryan Hayward* / Judith Stein / Shu Yang / Atsushi Takahara)
- **Developments in Adhesion Chemistry**
  (*Dale Huber* / Philip Klemarczyk / M.G. Finn)
- **Bioadhesives and Bioadhesion**
  (*Elie Rafael, Phillip Messersmith* / Christopher Ober / Paul Foreman / Anthony Brennan)
- **Bio-Inspired Adhesion**
  (*Eduard Arzt* / Animangsu Ghatak / Ali Dhinojwala)
- **Adhesive Properties and Mechanics**
  (*Kelly Anderson, Chris White* / Samuel Kenig / Hanna Dodiuk / Kenneth Shull / Zhigang Suo)
- **Molecular Aspects of Polymer Friction/Adhesion**
  (*Kathy Wahl* / Lilian Leger / Matthew Tirrell)
- **Aspects of Cellular Adhesion**
  (*Simcha Srebnik, Wendy Thomas* / Jennifer Elisseeff / Viola Vogel / Evan Evans)
- **Cell and Tissue Adhesion**
  (*Chung-Yuen "Herbert" Hui* / Jeffrey Karp)
- **Panel Discussion: Quantitative Challenges in Biological Adhesion**
  (*Wendy Thomas*)

NEW! AMYGDALA IN HEALTH & DISEASE
Contributions To Emotional Memories
Jul 12-17, 2009
Colby College
Waterville, ME
Chairs: Denis Pare & Gregory J. Quirk
Vice Chair: Raymond Dolan

- **Developmental Regulation of Fear Learning**
  (*Jocelyne Bachevalier* / C.P. Wiedenmayer / Regina M. Sullivan / Rick Richardson)
- **Plasticity Induced in the Amygdala and Related Structures by Fear Learning and Stress**
  (*Sheena Josselyn* / Pankaj Sah / Vadim Y. Bolshakov / Ki A. Goosens / Sumantra Chattarji / Mike Davis)
- **Primate and Human Amygdala**
  (*Elizabeth A. Murray* / C. Daniel Salzman / Jocelyne Bachevalier / Elizabeth A. Phelps / Ralph Adolphs)
- **Amygdala and Reward: Prefrontal Interactions**
  (*Gregory J. Quirk* / Elizabeth A. Murray / Stan B. Floresco / Geoffrey Schoenbaum / Bernard W. Balleine / Patricia H. Janak)
- **Anxiety Disorders: Human Studies and Animal Models**
  (*Kerry J. Ressler* / Charles B. Nemeroff / Jorge Armony / Ned H. Kalin / Andrew Holmes)
- **Formation and Consolidation of Aversive Memories**
  (*Mike Davis* / Mark Mayford / Sheena Josselyn / Kay Jungling / Fred J. Helmstetter / Hugh Blair / Stephane Ciocchi)
- **Cellular and Network Interactions of the Amygdala**
  (*Pankaj Sah* / Hans Christian Pape / Andrei T. Popescu / John Powers / Rony Paz)
- **Extinction: Emerging Trends**
  (*Rick Richardson* / Gregory J. Quirk / Andreas Luthi / Taiju Amano / Steve Maren / Satish S. Nair / Ray J. Dolan)
- **Involvement of the Amygdala in Autism and Anxiety Disorders**
  (*Elizabeth A. Phelps* / David G. Amaral / Mohamed R. Milad / Kerry J. Ressler / Kevin La Bar)

DETECTING ILLICIT SUBSTANCES: EXPLOSIVES & DRUGS
Sampling, Signatures and Clutter - Unconventional And Novel Approaches To Age Old Problems
Jun 14-19, 2009
Les Diablerets Conference Center
Les Diablerets, Switzerland
Chairs: Louis S. Wasserzug & Shabana Haque
Vice Chair: David A. Atkinson

- **Transition from Concept to Field Deployable Kit** (*Josh Rubinstein*)
- **Innovative Methods in Sampling Analytes of Interest** (*Rasmus Schulte Ladbeck*)
- **Policy Impact of Innovative Technologies** (*Susan Hallowell*)
- **Deciphering Target Signatures for Explosives and Drugs**
- **Impact of Clutter / Interference in Obtaining Adequate Signal for Detection** (*Steve Smith*)
- **Materials for Novel Sources and Detectors**
- **Applicability of Biosensors for Detection of Explosives** (*Helen Almey*)
- **Translating Test Standards to Applications** (*Greg Gillen*)
- **Selected Posters Demonstrating Innovative Research in Explosives Detection** (*Samantha Ollerton*)

DEVELOPMENTAL BIOLOGY
Jun 21-26, 2009
Proctor Academy
Andover, NH
Chair: Alexander Schier
Vice Chair: Claude R. Desplan

- **Asymmetry and Growth** (*Barbara Meyer* / Juergen Knoblich / Magdalena Zernicka-Goetz / Dominique Bergmann)
- **Morphogen Gradients and Positional Information** (*Denise Montell* / Eric Wieschaus / James Briscoe / Lewis Wolpert / Shigeru Kondo)
- **Signaling** (*Lee Niswander* / Trudi Schuepbach / Alex Schier / Kathryn Anderson)
- **Evolution** (*Piali Sengupta* / Marie Anne Felix / Arkhat Abzhanov / Claude Desplan / Hopi Hoekstra)
- **Stem Cells and Regeneration** (*Magdalena Zernicka-Goetz* / Ken Poss / Alejandro Sánchez Alvarado / Amy Wagers)
- **Morphogenesis** (*Trudi Schuepbach* / Jeremy Nance / Erez Raz / Ken Irvine / Will Talbot)
- **Transcriptional Control** (*Marion Walhout* / Richard Mann / Denis Duboule / Soo-Kyung Lee)
- **Regulatory Networks and Epigenetics** (*Kathryn Anderson* / Barbara Meyer / Denise Barlow / Sui Huang / Marion Walhout)
- **Organogenesis** (*Amy Wagers* / Piali Sengupta / Denise Montell / Lee Niswander)

NEW! DRINKING WATER DISINFECTION BY-PRODUCTS
Aug 9-14, 2009
Mount Holyoke College
South Hadley, MA
Chair: Ben Blount
Vice Chair: Manolis Kogevinas

- **Roadmap for Interdisciplinary Research on Water Disinfection By-Products** (*Rex Pegram* / Susan Richardson / David DeMarini)
- **DBP Formation and Occurrence** (*Xing-Fang Li* / William Mitch / David Reckhow / Shane Snyder)
- **DBP Fate, Transport and Monitoring** (Paul Westerhoff / Stuart Krasner)
- **Toxicological Studies** (*Jane Ellen Simmons* / Michael Plewa / Sid Hunter / Peter Goebell)
- **Assessing DBP Exposure** (*Cristina Villanueva* / Cliff Weisel / Lesa Aylward / Sean Hays)
- **Epidemiological Studies of DBPs** (*Sylvaine Cordier* / Mark Nieuwenhuijsen / Ken Cantor / Will King)
- **Swimming Pool-Related DBP Exposure and Health Studies** (*Cliff Weisel* / Ernest Blatchley / Manolis Kogevinas)
- **DBP Regulation and Perspectives** (*Linda Teuschler* / Rita Schoeny / Charles Haas / Jamie Bartram)
- **Discussion of Emerging DBPs** (*Philip Singer, Ben Blount* / Susan Richardson / David DeMarini / Ken Cantor / Michael Plewa / Rita Schoeny)

DRUG METABOLISM
The Past Is Prologue: Learning From The Past And Applying To Solve New Problems
Jul 5-10, 2009
Holderness School
Holderness, NH
Chair: Donald J. Tweedie
Vice Chair: Kenneth E. Thummel

- **Keynote Presentation: Making Shakespeare Proud - Let's Get to a Regulatory Perspective on Drug Metabolism** (Lawrence Lesko)
- **Drug-Drug Interactions: Are We Providing Solutions?** (*Lisa Shipley* / Kellie Reynolds / Donghui Cui / Lewis Klunk / Lan Ni)
- **Translating Nonclinical and Clinical Knowledge: Using the Quantitative Model Based Development Approach** (*Sandy Allerheiligen* / Doug Lauggenburger / Joe Balthazar)
- **Drug Transporters: Potential for Drug-Drug Interactions and Correlation with Organ Toxicity** (*Raymond Evers*)
- **Transporter / Phase II Drug Metabolizing Enzyme Interplay** (*K. Sandy Pang* / Huadong Sun / Kim Brouwer / Dietrich Keppler)
- **Pathophysiological Regulation of Drug Disposition Protein Turnover** (*Bernard Murray* / Almeia Correia / Yanan Tian / Magang Shou)
- **Student and Post-Doc Presentations** (*Henry Strobel*)
- **Models and Biomarkers of DILI** (*Bob Roth* / Rusty Thomas / Ivan Rusyn / Patti Ganey / Jim Xu)
- **Preclinical Identification of Reactive Intermediates: Defining the Clinical Value** (*Donald Tweedie* / Scott Obach / Yan Li / Kevin Park / Deborah Nicoll-Griffith)

DYNAMICS AT SURFACES
Dynamics At Gas-Liquid, Gas-Solid And Liquid-Solid Interfaces; Dynamics Of Liquid And Solid Surfaces
Aug 9-14, 2009
Proctor Academy
Andover, NH
Chair: Sylvia T. Ceyer
Vice Chair: Geert-Jan Kroes

- **State to State Dynamics** (*Greg O. Sitz* / Art L. Utz / Bret Jackson)
- **Non-Adiabatic Effects I** (*Cristina Diaz* / Hermann Nienhaus / Daniel J. Auerbach / Maite Alducin)
- **Non-Adiabatic Effects II** (*Aart W. Kleyn* / Konstantinos P. Giapis / David Bird)
- **Reaction Dynamics** (*Steven J. Sibener* / Liv Hornekaer / Daniel Farias / Jens K. Norskov)
- **Ultra-Fast Surface Dynamics** (*Kurt W. Kolasinski* / R.J. Dwayne Miller / Klaus Sokolowski-Tinten)
- **Dynamics at the Water Interface** (*John R. Morris* / Suzi Jarvis / Mischa Bonn / James Skinner)
- **Single Molecule Dynamics** (*Robert J. Hamers* / Maki Kawai / Miquel B. Salmeron)
- **Dynamics of Photodesorption** (*Richard Osgood, Jr.* / Nicholas Camillone / Thorsten Kluner / Dietrich Menzel)

ELASTIN & ELASTIC FIBERS
Jul 26-31, 2009
University of New England
Biddeford, ME
Chair: Anthony S. Weiss
Vice Chair: Richard A. Pierce

- **Molecules of the Elastic Fiber** (*Elaine Davis* / Clair Baldock / Penny Handford / Sacha Jensen / Antonio Tamburro / Stuart Cain)
- **Microfibril and Elastin Ultrastructure, Function and Assembly** (*Cay Kielty, Dieter Reinhardt* / Francesco Ramirez / Cay Kielty / Tim Wess / Dieter Reinhardt / Suzanne Mithieux / Tomoyuki Nakamura)
- **Molecular Determinants of Elastogenesis and Elastin Destruction** (*Francesco Ramirez* / Hiromi Yanagisawa / Pascal Sommer / Alek Hinek / Kohji Itoh / Suneel Apte)
- **Regulation of Elastic Fiber Gene Expression** (*Bob Mecham* / Judi Foster / Branka Dabovic / John Couchman / Philip Trackman)
- **Cell Signaling and the Elastic Fiber** (*Lynn Sakai* / Clarissa Craft / Daniel Bax / Lynn Sakai)

- **Elastic Fibers and Vascular Development**
  (*Giorgio Bressan* / Brenda Rongish / Giorgio Bressan / Mark Majesky / Virginie Mattot)
- **Elastic Tissues: Disorders and Disease**
  (*Zsolt Urban* / Zsolt Urban / Jouni Uitto / Hal Dietz / Lucy Osborne / Dianna Milewicz)
- **Therapeutic Advances and Elastic Tissues**
  (*Rich Pierce* / Rich Pierce / Bela Suki / Rae Yeung / John Curchi / Marlene Rabinovitch)
- **New Advances in Elastogenic Tissue Repair: Biomaterials and Bioengineering**
  (*Fred Keeley* / Fred Keeley / Steven Wise / Willeke Daamen)

ELECTRONIC SPECTROSCOPY & DYNAMICS

Jul 19-24, 2009
Colby College
Waterville, ME
Chairs: Mark Maroncelli & Timothy S. Zwier
Vice Chairs: Edward R. Grant & Bern Kohler

- **Electronic Spectroscopy at High-Resolution I: Few-Atom Systems**
  (*Edward Grant* / Thomas Udem / Wim Ubachs)
- **Electronic Spectroscopy at High-Resolution II: Larger Molecules & Interactions**
  (Frédéric Merkt / Tim Softley / Robert Field / John Maier)
- **Theory for Electronically Excited States**
  (John Stanton / Anna Krylov)
- **Excited-State Dynamics**
  (Laurie Butler / Hanna Reisler / Scott Kable / Toshi Suzuki)
- **Biological Molecules in the Gas Phase**
  (*Donald Levy* / Oleg Boyarkin / Takayuki Ebata)
- **Single Molecule and Multi-Chromophore Systems**
  (*Piotr Piotrowiak* / Niek van Hulst / Carl Hayden / Paul Barbara / David Blank)
- **Multi-Chromophore Systems & Exciton Dynamics**
  (*Eric Bittner* / Gregory Scholes / Xiaoyang Zhu)
- **Electronic Coupling and Conical Intersections**
  (*Jeffrey Cina* / David Plusquellic / Spiridoula Matsika / James Hynes / David Jonas)
- **Excited State Dynamics in Solution**
  (*Berne Kohler* / Benjamin Schwartz / Richard Mathies)

ENZYMES, COENZYMES & METABOLIC PATHWAYS

Discovery And Therapeutic Targeting Of New Enzyme Reactions And Pathways

Jul 5-10, 2009
Waterville Valley Resort
Waterville Valley, NH
Chairs: Joseph Martin Bollinger & Philip A. Cole
Vice Chairs: Bruce A. Palfey & Thomas D. Meek

- **Enzymes in Medicine**
  (*Jack Kirsch* / Jill Milne / Jay Grobler / Theodore Holman)
- **Discovery and Elucidation of Enzymatic Pathways**
  (*Anthony Sauve* / Charles Brenner / Tracey Rouault / Eric Brown / Benjamin Cravatt)
- **Phosphorylation in Cell Signaling**
  (*Karen Allen* / Louise Johnson / Jin Zhang / Zhong-Yin Zhang)
- **Antibiotic Development**
  (*Pinghua Liu* / John Blanchard / Suzanne Walker / Jon Clardy)
- **Chromatin Remodeling and Transcription**
  (*Weiping Zheng* / Jerry Workman / Ali Shilatifard / Paul Thompson / Tom Muir)
- **Novel Reactions and Mechanisms**
  (*Liviu Mirica* / Wilfred van der Donk / Jacqueline Barton / Jennifer Dubois)
- **Principles of Enzyme Catalysis**
  (*Audrey Lamb* / John Richard / Stephen Benkovic / Dan Herschlag)
- **Nucleic Acid Enzymology**
  (*Irene Lee* / Craig Cameron / Jim Stivers / Alex Drohat)
- **Design and Discovery of New Activities**
  (*Gary Dotson* / John Gerlt)

EPIGENETICS

The Role Of The Environment And Epigenetic Mechanisms In Behavior, Health, And Disease

Aug 9-14, 2009
Holderness School
Holderness, NH
Chairs: Jeannie T. Lee & Ueli Grossniklaus
Vice Chairs: Marisa S. Bartolomei & Craig S. Pikaard

- **Defining Epigenetic Phenomena**
  (*Eric Richards, Denise Barlow* / Ting Wu / Vicki Chandler / Paul Soloway / Andreas Houben / Tetsuji Kakutani)
- **Germline and Transgenerational Inheritance**
  (*William Kelley, Jean Finnegan* / Brad Cairns / Emma Whitelaw / Marisa Bartolomei / James Turner / Patrick Shiu / Orturn Mittelsten Scheid)
- **Epigenetic Reprogramming**
  (*Robert Feil, Ueli Grossniklaus* / Anne Ferguson-Smith / Wolf Reik / Daniel Grimanelli / Rudolf Jaenisch)
- **Balancing the Epigenome**
  (*Peter Becker, Asifa Akhtar* / Steve Henikoff / Jim Birchler / Barbara Meyer / Jenny Graves / Jeffrey Chen / Craig Pikaard)
- **Epigenetics in Health and Disease**
  (*Marisa Bartolomei, Jeannie Lee* / Fred Gage / Steve Baylin / Amar Klar / Rosanna Weksberg)
- **Environmental Epigenetics and Behavior**
  (*Howard Cedar, Jeannie Lee* / Randy Jirtle / Moshe Szyf / Pat Hunt / Marcus Pembrey / Catherine Dulac)
- **Chromatin Modifiers**
  (*Vincenzo Pirrotta, Judith Bender* / Steve Jacobsen / Marjorie Matzke / Hiro Sasaki / Tim Bestor / Renato Paro / Danesh Moazed)
- **Transposons and Prions**
  (*Sally Elgin, Doug Ruden* / Jim Goodrich / Rob Martienssen / Shiv Grewal / Susan Linquist / Reed Wickner)
- **Nuclear Organization**
  (*Thomas Cremer, Ueli Grossniklaus* / Alexandre Reymond / Peter Fraser / Edith Heard / Wendy Bickmore / Paul Fransz)

EPITHELIAL DIFFERENTIATION & KERATINIZATION

Jun 21-26, 2009
Les Diablerets Conference Center
Les Diablerets, Switzerland
Chair: Pierre A. Coulombe
Vice Chair: Raphael Kopan

- **Perspectives on New Paradigms**
  (*Raphael Kopan* / Denis Duboule / Hans Clevers / Paul Martin)
- **Stem Cells: Mobilization, Regulation and Disease Regulation**
  (*George Cotsarelis* / Elaine Fuchs / Fiona Watt / George Cotsarelis / Yann Barrandon / Jonathan Vogel / Carlos Lopez-Otin)
- **Genome Biology**
  (*Howard Chang* / Harinder Singh / Julie Segre / Bogi Andersen / Howard Chang)
- **New Insight in Keratinocyte and Skin Biology**
  (*Sabine Werner* / Michael Caterina / Randall Johnson / Janice Brissette / Anthony Oro / Zena Werb / Sabine Werner)
- **Issues Arising I (Poster Discussion)**
  (*Tudorita Tumbar / Angela Christiano*)
- **Signaling in Development and Tissue Homeostasis**
  (*Cheng-Ming Chuong* / Irma Thesleff / Briuce Morgan / Sarah Millar / Raphael Kopan / Paolo Dotto / Cheng-Ming Chuong)
- **Mechanistic Insight into Complex Cellular Processes**
  (*Kathleen Green* / Stuart Yuspa / Dennis Roop / Paul Khavari / Kathleen Green)
- **Disease Pathophysiology and Therapeutic Approaches**
  (*David Woodley* / Steven Young / Michele DeLuca / David Woodley / Irwin McLean / Shigetoshi Sano / Masa Amagai)
- **Issues Arising II (Poster Discussion)**
  (*Rhadika Atit / Anj Dlugosz*)

EVOLUTIONARY & ECOLOGICAL FUNCTIONAL GENOMICS

Jul 12-17, 2009
Tilton School
Tilton, NH
Chair: Scott Edwards
Vice Chair: Loretta C. Johnson

- **Keynote Presentation: Genes and Social Behavior**
  (Gene Robinson)
- **Population Genomics**
  (*Andrew Whitehead* / Maitreya Dunham / Andres Aguilar / John Novembre)
- **Evolutionary Developmental Biology**
  (*Gretchen Hofmann* / Todd Streelman / Gro Amdam / Arkhat Abzhanov / Nicole Valenzuela)
- **Plant Ecological Genomics**
  (*Loretta Johnson* / Ian Baldwin / Justin Borevitz / John McKay)
- **Global Change Genomics**
  (*Gro Amdam* / Erica Rosenblum / Gretchen Hofmann / Thorsten Reusch)
- **Emerging Approaches in Ecological and Evolutionary Genomics**
  (*Ian Baldwin*)
- **Comparative Genomics**
  (*Erica Rosenblum* / Joana Silva / John Colbourne)

- **Hydration**
  (*Mark Johnson* / Simon Ebbinghaus / Evan Williams / Shekhar Garde)
- **Peptides and Proteins**
  (*Lars Konermann* / David Clemmer / Ryan Julian / H.-F. Chan)
- **Enzymes**
  (*Rebecca Jockusch* / Katie Henzler-Wildman / Ben Schuler / Sharon Hammes-Schiffer)
- **Nucleic Acids**
  (*Mattanjah de Vries* / Danielle Fabris / Jiri Sponer / Valerie Gabelica)
- **Energy Transduction**
  (*Ralph Jimenez* / Steve Boxer / David Beratan / Carolo Bustamante)
- **Carbohydrates**
  (*Mark Wormald* / John Simons / Rob Woods / Julie Leary)
- **Functioning Biological Systems**
  (*Perdita Barran* / Mike Bowers / Christoph Braeuchle / Ruben Gonzalez)
- **Molecular Diamonds: Building Multifaceted Peptides**
  (*Isaac Carrico* / Dehua Pei / Felicia Etzkorn / John Robinson / Helma Wennemers)
- **Tracking Cancer And Putting On The Brakes**
  (Lisa Shewchuk / Patrick Zarrinkar / Elizabeth Buck)
- **Bacterial Scourges: Trying to Outsmart Them**
  (*Danica Fujimori* / Eric Brown / Carl Nathan / Ann Eakin)
- **Monitoring Metabolites: Needle in the Haystack**
  (Amy Palmer / Michelle Reyzer / Peter Beal)
- **Invasion of Molecular Synthesis: To Activators & Beyond!**
  (*Rami Hannoush* / Jim Hartman / Sergey Kozmin / Qing Lin / Orion Jankowski)
- **Frontiers in Chemical Biology**
  (*Tamara Hendrickson* / Barbara Imperiali / Joanna Fowler / Carolyn Bertozzi)

BIOMATERIALS: BIOCOMPATIBILITY / TISSUE ENGINEERING
The Engineering Of Healing: From Molecular Mediation To Tissue Constructs

Jul 19-24, 2009
Holderness School
Holderness, NH
Chair: William M. Reichert
Vice Chair: Joyce Y. Wong

- **Masters of Biomaterials and Wound Healing**
  (*Monty Reichert* / Jan Feijan / Luisa DiPietro)
- **Surface Ligands and Molecular Architecture**
  (*Ashutosh Chilkoti* / Vladimir Hlady / Roger Marchant / David Grainger)
- **Cell Signaling Networks**
  (*Edward Botchwey* / Don Elbert / Jason Haugh)
- **Materials for Molecular Mediation**
  (*Tony Giuseppi-Elie* / Mark Saltzman / Kam Leong / Valerie Ashby)
- **Molecular Mediation of Tissues and Cells**
  (*Kevin Healy* / Francis Moussy / Jennifer West)
- **Assembling Tissue Constructs**
  (*Michael Sefton* / William Wagner / Karen Burg / Christine Schmidt)
- **Whole Organ Tissue Engineering**
  (*Guillermo Ameer* / Tony Atala / Doris Taylor)
- **Mediating Inflammation and Infection**
  (*Newell Washburn* / Samir Mitragotri / Roman Stocker / James Bryers)
- **Outstanding Poster Presentations**
  (*Joyce Wong*)

BIOORGANIC CHEMISTRY

Jun 14-19, 2009
Proctor Academy
Andover, NH
Chairs: Nicole S. Sampson & Stewart L. Fisher
Vice Chairs: Christine S. Chow & Arthur M. Hanel

- **Viral Scourges: Advancing Drug Design**
  (*Alexey Lugovsky* / Ann Kwong / Edward Driggers / Carlos Simmerling)
- **Bacterial Treasure Troves: Making The Gold**
  (Joseph Noel / David Cane / Brian Bachman)
- **New Materials: Blood, Sweat & Tears**
  (Jerry Yang / Gregory Tew / Ron Kluger)

BONES & TEETH
Stem Cells And Regulation Of Bone Modeling And Regeneration

Jul 12-17, 2009
University of New England
Biddeford, ME
Chair: Brendan F. Boyce
Vice Chair: Bjorn R. Olsen

- **Cartilage Biology and Disease**
  (*Bjorn Olsen* / Veronique Lefebvre / Danny Chan)
- **Skeletal Development**
  (*Yingzi Yang* / Hank Kronenberg / Xu Cao / Roland Baron)
- **Dental Development**
  (*Laurie McCauley* / Yang Chai / Jan Hu)
- **Genetics and Bone Diseases**
  (*Brendan Lee* / Fanxin Long / Dan Cohn / Valerie Cormier Daire)
- **Osteoblastic and Hematopoietic Stem Cells**
  (*Paul Simmons* / Linheng Li / Paulo Bianco)
- **Osteoimmunology**
  (*Yongwon Choi* / Hiroshi Takayanagi / Michael Cancro / Georg Schett)
- **Bone Repair and Regeneration**
  (*Regis O'Keefe* / Johnny Huard / Vicki Rosen)
- **The Biological Basis of Bone Therapies**
  (*Sundeep Khosla* / Tom Clemens / Mark Johnson / Merry Jo Oursler)

NEW! BONES & TEETH (GORDON-KENAN RESEARCH SEMINAR)
Advances In The Understanding Of Bone And Cartilage Development

Jul 11-12, 2009
University of New England
Biddeford, ME
Chairs: Jean B. Regard & Lea Gunnell

- **Keynote Presentation: Milestones in Bone Cell Biology Over Four Decades**
  (Thomas John "Jack" Martin)
- **Development of the Skeletal System**
  (*Thomas John "Jack" Martin*)
- **Bone Cell Differentiation**
  (*Pamela Robey*)

The Gordon Research Seminar on Bones & Teeth is a two-day Gordon Conference-style meeting exclusively for graduate students, post-docs, and other scientists with comparable levels of experience and education. Speakers will be chosen from among the attendees. The associated Gordon Research Conference will take place at the same location, immediately following the Seminar.

CAG TRIPLET REPEAT DISORDERS

May 31 - Jun 5, 2009
Waterville Valley Resort
Waterville Valley, NH
Chair: Jang-Ho Cha
Vice Chair: Laura Ranum

- **Keynote Presentation: Biochemical and Physiological Deficits in a Polyglutamine Disease**
  (Harry Orr)
- **Clinical Presentation Setting Stage for Preclinical Opportunities (HD and SCAs)**
  (Stefano Di Donato / Marian DiFiglia / Jane Paulsen)
- **Inflammation in CAG Triplet Repeat Disorders**
  (Maria Bjorkqvist / Thomas Moeller)
- **Transcription: Mechanism and Therapy**
  (Gillian Bates / Joel Gottesfeld / Ruth Luthi-Carter)
- **Circuitry Malfunction and Synaptic Pathology**
  (*Kerry Murphy* / Xiao-Jiang Li / George Rebec)
- **RNA Gain of Function CUG and CAG Mechanisms and Bidirectional Expression**
  (*Maurice Swanson* / Tom Cooper / Al La Spada)
- **Repeat Instability**
  (Vanessa Wheeler / Chris Pearson)
- **Neuroimaging Studies**
  (Gülin Öz)
- **Genetic Modifiers**
  (Juan Botas / Darren Monckton)

NEW! CAG TRIPLET REPEAT DISORDERS (GORDON-KENAN RESEARCH SEMINAR)

May 30-31, 2009
Waterville Valley Resort
Waterville Valley, NH
Chair: Mary Y. Heng

- **Keynote Presentation: Polyglutamine Protein Biology**
  (Paul Taylor)
- **Mechanisms of Neuronal Dysfunction and Neuronal Loss**
  (*Diane Merry*)
- **Pathogenesis and Therapeutics of Polyglutamine Diseases**
  (*Harry Orr*)

The Gordon Research Seminar on CAG Triplet Repeat Disorders is a two-day Gordon Conference-style meeting exclusively for graduate students, post-docs, and other scientists with comparable levels of experience and education. Speakers will be chosen from among the attendees. The associated Gordon Research Conference will take place at the same location, immediately following the Seminar.

- **Microbial Genomics and Symbiosis**
  (*Maitreya Dunham* / Colleen Cavanaugh / Monica Medina / Pilar Francino)
- **Ecological and Physiological Genomics**
  (*Andres Aguilar* / Sean Rogers / Andrew Whitehead)

EXCITATORY SYNAPSES & BRAIN FUNCTION

Sep 6-11, 2009
Les Diablerets Conference Center
Les Diablerets, Switzerland
Chairs: Gary L. Westbrook & Christophe Mulle
Vice Chairs: Andres Villu Maricq & Katherine W. Roche

- **Keynote Presentations: Synaptic Vesicles as Fusion Machines / Homeostatic Synaptic Scaling**
  (Reinhard Jahn / Gina Turrigiano)
- **New Insights in Glutamate Receptor Structure & Excitatory Synaptic Complexes**
  (Eric Gouaux / Xiaobing Chen / Jean-Philippe Pin)
- **Trafficking and Molecular Organization at Excitatory Synapses**
  (Michael Ehlers / Daniel Choquet / Katherine Roche)
- **Vesicular and Presynaptic Mechanisms at Excitatory Synapses**
  (Richard Tsien / Robert Edwards / Yukiko Goda)
- **Excitatory Synapses - Insights from Model Systems**
  (Andres Villu Maricq / Kang Shen / Stephan Sigrist / Yishi Jin)
- **Glutamate Receptor Signaling and Modulation at Excitatory Synapses**
  (Ryodei Yasuda / Lu Chen / Roger Nicoll / Hannah Monyer)
- **Structural and Functional Synaptic Plasticity**
  (Bernardo Sabatini / Valentin Nägerl / Suzanne Zukin / Christian Lüscher)
- **Patterns of Synaptic Dysfunction and Disease**
  (Timothy Murphy / Monica DiLuca / Nils Brose / Claudia Bagni)
- **The Next Frontier - Approaches to Signaling Complexes and Networks**
  (Seth Grant / Michael Häusser / Edvard Moser)

FERTILIZATION & ACTIVATION OF DEVELOPMENT

Jul 12-17, 2009
Holderness School
Holderness, NH
Chair: Alberto Darszon
Vice Chair: Janice P. Evans

- **Gamete Differentiation**
  (*Mariana Wolfner* / Renee Reijo Pera / Tim Schedl / Julie Brill)
- **Sperm Epididymal Maturation and Capacitation**
  (*Pablo Visconti* / Sylvie Breton / Betsy Navarro)
- **New Approaches to Gamete and Embryo Biology**
  (*Michael Whitaker* / Daniel Sánchez / Hitoshi Sawada / Takeharu Nagai)
- **Fertilization and Activation of Development**
  (*Janice P. Evans* / Keith Jones / John Parrington / Luigia Santella)
- **Sperm Flagellar Regulation**
  (*Susan Suarez* / Benjamin Kaupp / Ritsu Kamiya / Steve Publicover)
- **Egg and Embryo Polarity**
  (*Christian Sardet* / Tsuyoshi Momose / Geraldine Seydoux / John Carroll / Colin Brownlee)
- **Keynote Presentation: Evolution of Gamete Recognition Proteins**
  (*Vic Vacquier* / Willie Swanson)
- **Egg Envelopes and the Sperm Acrosome Reaction**
  (*Luís Mayorga* / Barbara Wakimoto / George Gerton / David J. Miller / Luca Jovine)
- **Embryogenesis and Epigenetics**
  (*Richard M. Schultz* / Jacquetta Trasler / Antoine H.M. Peters / Wolf Reik)

FLORAL & VEGETATIVE VOLATILES
Ecology, Analytics, Genomics, Sensory Perception And Linguistics

Aug 9-14, 2009
Magdalen College
Oxford, United Kingdom
Chairs: Ian T. Baldwin & Joerg Bohlmann
Vice Chairs: Jonathan Gershenzon & Florian Schiestl

- **Plant Volatiles in Human Affairs: Linguistics, Mate Choice and Food Selection**
  (*Harry Klee* / Asifa Majid / Boris Schilling)
- **Metabolomics and Analytics of Plant Volatiles: *In situ* Analytics**
  (*Aleš Svatoš* / Akos Vertes / Zheng Ouyang / Benjamin Dietzek)
- **Metabolomics and Analytics of Plant Volatiles - Metabolic Profiling and Bioinformatics**
  (*Aleš Svatoš* / Renato Zenobi / Kirsten Skogerson)
- **Mechanisms of Volatile Production**
  (*Jonathan Gershenzon* / C.S. Raman / Philippe Hugueney)
- **Mechanisms of Volatile Production and Release**
  (*Jonathan Gershenzon* / Jörg-Peter Schnitzler / Sylvie Baudino)
- **Perception of Volatiles I**
  (*Bill Hansson* / Peter Mombaerts / Pablo Guerenstein / Neil Vickers)
- **Perception of Volatiles II**
  (*Bill Hansson* / Christian Margot / Silke Sachse / Teun Dekker)
- **Plant Behavior in the Headspace: Plant VOCs in Ecological Interactions with Plants, Insects and Microorganisms - Signal Evolution and Diversity**
  (*Robert Raguso / André Kessler* / Andrew Stephenson / Arthur Zangerl / May Berenbaum / Rick Karban)
- **Plant Behavior in the Headspace: Plant VOCs in Ecological Interactions with Plants, Insects and Microorganisms - Signal Manipulation and Exploitation**
  (*Joerg Bohlmann* / Manfred Ayasse / Bitty Roy / Paul W. Paré)

FUEL CELLS

Jul 26-31, 2009
Bryant University
Smithfield, RI
Chairs: John F. Elter & Felix N. Büchi
Vice Chairs: Shyam S. Kocha & Yu Morimoto

- **Fuel Cells: Challenges and Ideas**
  (*John Elter / Felix Büchi* / Tom Jarvi)
- **Catalysis**
  (*Shyam Kocha* / Timo Jacob / Elena Savinova / Nenad Markovic)
- **Degradation Issues**
  (*Bryan Pivovar* / Karen Swider-Lyons / Greg Haugen)
- **Membrane Developments**
  (*Tom Zawodzinski* / Biswajit Choudhury / Frank Coms / Lorenz Gubler)
- **New Concepts and Materials**
  (*Shimshon Gottesfeld* / Hubert Gasteiger / Hiroyuki Yanangi)
- **Model Based Developments**
  (*Jon Pharoah* / Wolfgang Bessler / Shunsuke Yamakawa / Michael Eikerling)
- **Transport Processes**
  (*Yu Morimoto* / Daniel Schwartz / Yuchihiro Tabuchi)
- **System Issues and Hydrogen**
  (*Byung Ki Ahn* / Matt Fronk / Herwig Haas / Kathy Ayers)
- **Fuel Cell Visions**
  (*John Elter / Felix Büchi* / Tom Zawodzinski / Chris Guzy)

GENETIC TOXICOLOGY

Aug 9-14, 2009
Colby-Sawyer College
New London, NH
Chair: Samuel H. Wilson
Vice Chair: Jessica A. Downs

- **Keynote Presentations**
  (*Samuel Wilson, Jessica Downs* / Anthony Carr / Myron Goodman)
- **Environment & Genotoxic Stress**
  (*Stephen Lloyd, David Hunter* / David Hunter / Frederica Perera / Stephen Lloyd / Nick Geacintov / Gerd Pfeifer)
- **Endogenous Genotoxic Stress**
  (*Leona Samson, Susan Wallace* / Leona Samson / Susan Wallace / Keith Caldecott / Ben Van Houten)
- **Mutagenesis & Lesion By-Pass I**
  (*Thomas Kunkel, Larry Loeb* / Marietta Lee / Thomas Kunkel / Andrei Chabes / Julian Sale / Joann Sweasy)
- **Mutagenesis & Lesion By-Pass II**
  (*Roger Woodgate, Alan Lehmann* / Alan Lehmann / Roger Woodgate / Shunichi Takeda / Larry Loeb)
- **Chromatin & Links to Genotoxicity I**
  (*Jessica Downs, Michael Smerdon* / Jessica Downs / Michael Smerdon / Michael Bustin / Craig Peterson)
- **Chromatin & Links to Genotoxicity II**
  (*Ben Van Houten, Michael Bustin* / Wim Vermeulen / K.J. Myung / Sang Eun Lee)
- **DNA Damage & Cellular Decisions I**
  (*Yosef Shiloh, Anthony Carr* / Yosef Shiloh / William Dunphy / David Cortez / Michael Yaffe / Dan Durocher)

- **DNA Damage & Cellular Decisions II**
  (*Penny Jeggo, Michael Resnick* / Junjie Chen / Penny Jeggo / Michael Resnick / Thomas Helleday)

HETEROCYCLIC COMPOUNDS

Jun 28 - Jul 3, 2009
Salve Regina University
Newport, RI
Chair: Christopher J. Moody
Vice Chair: J. Ramon Vargas

- **New Methodology in the Synthesis of Heterocyclic Compounds I**
  (*J Ramon Vargas* / Jeffrey Aubé / Louis Barriault)
- **New Routes to Biologically Active Heterocycles I**
  (*Julia M. Clay* / Tom G. Driver / Scott Coffey / Jon Rainier)
- **Catalysis in Heterocyclic Chemistry**
  (Janis Louie / Gregory C. Fu)
- **Synthesis of Heterocyclic Natural Products**
  (Tehshik P. Yoon / Mercedes Álvarez / Viresh Rawal)
- **Heterocyclic Natural Products: Biosynthesis and Biomimetic Synthesis**
  (Sarah E. O'Connor / Robert M. Williams)
- **New Strategies Towards Heterocyclic Compounds**
  (Anna Mapp / Thorsten Bach / Donald Craig)
- **New Methodology in the Synthesis of Heterocyclic Compounds II**
  (Helena Malinakova / Sam Zard)
- **New Routes to Biologically Active Heterocycles II**
  (Brian Shook / Richmond Sarpong / Stephen F. Martin)
- **A Perspective On Heterocyclic Chemistry: The Challenges Posed By the Synthesis of Biologically Important Heterocyclic Compounds**
  (*Chris Moody* / Samuel J. Danishefsky)

HIGH TEMPERATURE CORROSION

Jul 26-31, 2009
Colby-Sawyer College
New London, NH
Chair: John R. Nicholls
Vice Chair: Peter F. Tortorelli

- **Transient Oxidation**
  (*Michael Graham* / Judith C. Yang / David B. Hovis)
- **Segregation Processes During Oxidation**
  (*Peggy Hou* / Gordon Tatlock)
- **Ultra High Temperature Oxidation**
  (*Bo Jonsson* / David J. Young / Mats Halvarsson)
- **Materials Issues for Solid Oxide Fuel Cells**
  (*Alan Atkinson* / Toshio Maruyama / W. Joe Quadakkers)
- **Water Vapour Effect on Oxidation: Oxidation in Steam Environments**
  (*Bruce Pint* / Alain Galerie / Alina Aguero)
- **Corrosion Under Aggressive Service Conditions**
  (*Michael Schütze* / Nigel J. Simms / Bettina Bordenet)
- **Oxidation/Corrosion Resistant Coating Systems**
  (*Brian Gleeson* / Daniel Monceau / Toshio Narita)
- **Thermal Barrier Coatings**
  (*Hugh Evans* / Daniel Renusch / David Rickerby)
- **Keynote Presentation: Type II Hot Corrosion, its Discovery, Science and Industrial Impact**
  (Fred Pettit)

NEW! HORMONE ACTION IN DEVELOPMENT & CANCER

Hormonal Regulation Of Development & Cancer: Common Signaling Pathways

Jul 26-31, 2009
Holderness School
Holderness, NH
Chairs: Gail S. Prins & Kevin White
Vice Chairs: Jose Russo & Henry Krause

- **Keynote Presentations: Nuclear Receptors in Differentiation and Cancer**
  (*Gail Prins, Kevin White* / M. Geoffrey Rosenfeld / Benita Katzenellenbogen)
- **Recent Advances in Steroid Hormone Action**
  (*Geoffrey Greene, Ken Korach* / Geoffrey Greene / Carol Lange / Gordon Hager / Fraydoon Rastinejad)
- **Hormonal Regulation of Development**
  (*Henry Krause, Jose Russo* / Adam Antebi / Wellington Cardosa / Liang Ma)
- **Steroid Action in Breast and Prostate Cancer**
  (*Suzanne Fuqua, Maarten Bosland* / Karen Knudsen / Patricia Elizalde / Ken Korach / Judy Bolton)
- **Hormonal Carcinogenesis: Alternate Pathways and Sites**
  (*Shiuan Chen, Cheryl Walker* / Lois Mulligan / Leslie Gold / Marja Nevalalainen)
- **Developmental Pathways Gone Awry in Cancer**
  (*Gail Prins, Susan Kasper* / Kornelia Polyak / Wade Busman / Randall Moon / Sara Sukumar)
- **Environmental Hormones: Effects on Development and Cancer**
  (*John McLachlan, Michael Gallo* / David Crews / Anna Soto / John McLachlan)
- **Epigenomic Mechanisms Regulating Development and Cancer**
  (*Shuk-mei Ho, Gerry Coetzee* / John McCarrey / Tim Huang / Cheryl Walker / Ralph de Vere White)
- **Novel Approaches for Translational Research**
  (*Kevin White, Wade Bushman* / Randall Peterson / Myles Brown / Suzanne Fuqua)

HUMAN GENETICS & GENOMICS

Jul 19-24, 2009
University of New England
Biddeford, ME
Chair: Evan Eichler
Vice Chair: Susan A. Slaugenhaupt

- **The Future of Human Genetics and Genomics**
  (Eric Lander / Mary-Claire King)
- **Genetics of Human Disease**
  (*Mary-Claire King* / Aravinda Chakravarti / Leena Peltonen-Palotie / David Altshuler / David Goldstein)
- **Human Evolution and Diversity**
  (*Aravinda Chakravarti* / Jim Noonan / Carlos Bustamante / Haig Kazazian)
- **Chromosome Dynamics**
  (*Evan Eichler* / David Page / Hunt Willard / Gil McVean / Wendy Bickmore)
- **Copy Number Variation and Disease**
  (*David Page* / Jim Lupski / Evan Eichler / Steve Scherer)
- **Personalized Genomes and Genome Technology**
  (*Len Pennacchio* / George Church / Debbie Nickerson / Eric Green / Gonçalo Abecasis)
- **Functional Characterization of the Human Genome**
  (*Hunt Willard* / Len Pennacchio / Rick Myers / Vivian Cheung / Eran Segal)
- **Models of Disease and Therapeutics**
  (*Rick Lifton* / Steve Warren / Niko Katsanis / Stephanie Sherman / Sue Slaugenhaupt)
- **Keynote Presentation: From Disease to Genes**
  (*Sue Slaugenhaupt* / Rick Lifton)

HYDROGEN-METAL SYSTEMS

Jul 12-17, 2009
Il Ciocco Hotel and Resort
Lucca (Barga), Italy
Chairs: Gary D. Sandrock & Etsuo Akiba
Vice Chairs: Scott W. Jorgensen & Astrid Pundt

- **National Perspectives on H-M R&D**
  (*Gary Sandrock* / Etsuo Akiba / Ned Stetson)
- **Complex Hydrides I: Alanes & Thermodynamics**
  (*Sabrina Sartori* / Jason Graetz & Ragaiy Zidan / Andreas Züttel)
- **Complex Hydrides II: Theory & Modeling**
  (*Chris Wolverton* / Mei-Yin Chou / Tejs Vegge)
- **Complex Hydrides III: Borohydrides**
  (*Ewa Rönnebro* / Magnus Sørby / Youngwhan Cho / Martin Dornheim)
- **Neutron Studies**
  (*Peter Vajda* / Craig Brown / Bill David)
- **Hydrogen Effects on Structural Metals**
  (Brian Somerday / David Delafosse)
- **Metallic Hydrides**
  (*Robert Bowman* / Diagoro Mori / Michel Latroche)
- **Special Hydrogen-Metal Systems**
  (*Rosario Cantelli* / Andrea Baldi / Gerd Ganteför / Tony Burrell)
- **M-Containing Hydrogen Adsorbents**
  (*Channing Ahn* / Theodore Steriotis / Joe Zhou)

NEW! INHIBITION IN THE CNS

Jul 26-31, 2009
Colby College
Waterville, ME
Chair: Hannah Monyer
Vice Chair: Neil Harrison

- **Keynote Presentation I: Inhibitory Control of the Mossy Fiber-CA3 System**
  (*Hannah Monyer* / Chris J. McBain)
- **GABA and GABAergic Interneurones During Development**
  (*Gordon Fishell* / Rustem Khazipov / Oscar Marin / Stewart A. Anderson / Yves Barde / Josh Kaplan)
- **Interneurones in the Olfactory Bulb**
  (*Istvan Mody* / Ben W. Strowbridge / Zoltan Nusser / Gary Westbrook / Pierre-Marie Lledo / Thomas Kuner)
- **Interneurons in the Cortex and Hippocampus**
  (*Alex Thomson* / Yasuo Kawaguchi / Dimitri M. Kullmann / Peter Jonas / Peter Somogyi / Henry Markram)
- **More on Interneurons in the Forebrain and Cerebellum**
  (*Tamas Freund* / Javier DeFelipe / Angus Silver / Stefano Vicini / Viktor Varga / Elly Nedivi)
- **Interneurones and Network Activity**
  (*Roger Traub* / Kamran Diba / Ed Mann / Norbert Hajos / Jozsef Csicsvari / Elke Fuchs / Nancy Kopell)
- **Receptor Expression, Modulation and Trafficking**
  (*Peter Seeburg* / Antoine Triller / Stephen Moss / Hanns Ulrich Zeilhofer / Trevor Smart / Uwe Rudolph / Yael Stern-Bach)
- **Pathology of Inhibition**
  (*Neil Harrison* / Frederique Varoqueaux / Takao Hensch / Miles Whittington / Jorge J. Palop / Andrew Trevelyan)
- **Keynote Presentation II: Constructing Inhibitory Synapses - Roles of Receptor- and Transporter-Associated Proteins**
  (*Neil Harrison* / Heinrich Betz)

INORGANIC CHEMISTRY
The New Frontiers

Jun 21-26, 2009
University of New England
Biddeford, ME
Chair: Gregory Girolami
Vice Chair: John R. Lockemeyer

- **Coordination Clusters and Polymers**
  (*Gregory Girolami* / Achim Müller / Kim Dunbar / Lan-Sun Zheng)
- **Solids, Films, and Nanoparticles**
  (*Richard Kemp* / Mercouri Kanatzidis / Lisa McElwee-White / Catherine Murphy / Christopher Marshall)
- **Chemically Active Porous Networks**
  (Wenbin Lin / Omar Yaghi / Joseph Hupp)
- **New Ventures in Catalysis**
  (Robert Crabtree / Guido Pez / Richard Eisenberg)
- **Chemistry of the Main Group Elements**
  (*Kun Wang* / Gregory Robinson / Oleg Ozerov / Scott Weinert)
- **Inorganic Compounds in Biology**
  (*Alan Heyduk* / Ivano Bertini / Elizabeth Theil / Ann Valentine)
- **Bioinspired and Biomedical Inorganic Chemistry**
  (Marcetta Darensbourg / Julia Brumaghim)
- **Chemical Dynamics**
  (*Jaqueline Kiplinger* / Janet Bluemel / Lisa Hope-Weeks / Roman Boulatov / Paula Diaconescu)
- **New Directions in Inorganic Chemistry**
  (*John Lockemeyer* / Keith Watson / Peter Wolczanski)

NEW! INORGANIC CHEMISTRY (GORDON-KENAN RESEARCH SEMINAR)

Jun 20-21, 2009
University of New England
Biddeford, ME
Chairs: Matthew S. Varonka & Marie M. Melzer

- **Keynote Presentation**
  (Thomas Meade)
- **Biologically Inspired Inorganic Chemistry**
  (*Thomas Meade*)
- **Material and Organometallic Chemistry**
  (*Kim Johnson*)

The Gordon Research Seminar on Inorganic Chemistry is a two-day Gordon Conference-style meeting exclusively for graduate students, post-docs, and other scientists with comparable levels of experience and education. Speakers will be chosen from among the attendees. The associated Gordon Research Conference will take place at the same location, immediately following the Seminar.

INTERIOR OF THE EARTH

Jun 14-19, 2009
Mount Holyoke College
South Hadley, MA
Chair: Bruce Buffett
Vice Chair: Carolina R. Lithgow-Bertelloni

- **Seismic Tomography: Intrepreting the Images**
  (*Guy Masters* / Lars Stixrude / Thorsten Becker / Barbara Romanowicz)
- **Geochemical Heteroegneity: Sources, Sinks, and Storage**
  (*Louise Kellogg* / Peter van Keken / Sujoy Mukhopadhyay)
- **Plate Tectonics and the Radial Structure of Convection**
  (*Magali Billen* / Jeannot Trampert / Allen McNamara)
- **Core-Mantle Boundary Region: Chemistry, Structure, and Dynamics**
  (*Ed Garnero* / Christine Thomas / Dan Shim / Paul Asimow)
- **Structure and Dynamics of the Core: Earth's Foundry**
  (*Andy Jackson* / Julien Aubert / Arwen Deuss)
- **Early Earth: Vestiges of a Distant Past**
  (*Stephane Labrosse* / Rick Carlson / Stein Jacobsen)
- **Planetary Interiors and Magnetic Fields**
  (*Sabine Stanley* / Sean Solomon / Ulrich Christensen / Jie Li)
- **Trends in Scientific Computing and Numerical Simulations**
  (*Mike Gurnis* / Georg Stadler / Heiner Igel / Ron Cohen)
- **Unsolved Problems**
  (*Peter Olson* / David Stevenson / Alex Halliday / Rob van der Hilst)

LASER DIAGNOSTICS IN COMBUSTION

Aug 16-21, 2009
Waterville Valley Resort
Waterville Valley, NH
Chair: Volker Sick
Vice Chair: Andreas Dreizler

- **New Sources**
  (*Pascale Desgroux* / Margaret Murnane)
- **Surface Diagnostics**
  (*Marcus Alden* / Robert Schlögl / Roger Farrow / Arnulf Materny)
- **Non-Linear Techniques**
  (*Paul Ewart* / James Gord / Thomas Settersten)
- **Coupling Experiments and Simulations**
  (*Rob Barlow* / Josette Bellan / Andreas Kempf / Blair Connelly)
- **Applications to Engines Research**
  (*Min Xu* / Stefan Arndt / Mattias Richter)
- **High-Speed Imaging Diagnostics**
  (*Jeffrey Sutton* / Claudia Fajardo / Isaac Boxx / Adam Steinberg)
- **Spray Diagnostics**
  (*Cam Tropea* / Mark Linne / Scott Parrish)
- **Advanced Applications of Tunable Diode Lasers**
  (*Volker Ebert* / Rob Cook / Kevin Sholes / Skip Williams)
- **Particulate Diagnostics**
  (*Hope Michelsen* / Christof Schulz / Greg Smallwood)

LIPIDS, MOLECULAR & CELLULAR BIOLOGY OF

Jul 19-24, 2009
Waterville Valley Resort
Waterville Valley, NH
Chair: David W. Russell
Vice Chair: Judy Storch

- **Keynote Presentations: Intracellular Signaling by Phosphoinositides**
  (*David Russell* / Jack Dixon / Lewis Cantley)
- **Regulation of Lipid Metabolism by Nuclear Receptors**
  (Fraydoon Rastinejad / David Mangelsdorf / Bruce Spiegelman / Peter Tontonoz)
- **Bacterial Lipid Synthesis and Catabolism**
  (Chris Raetz / William Mohn / Charles Rock)
- **Genetics of Lipid Metabolizing Enzymes**
  (Bo Shen / Helen Hobbs / Karen Reue / Robert Farese)
- **Enzymes of Lipid Metabolism**
  (Russell DeBose-Boyd / Jay Horton / George Carman)
- **Trafficking of Lipids and Proteins**
  (*Judith Storch* / Vytas Bankaitis / Dennis Voelker / Monilola Olayioye / Scott Emr / Christoph Benning)
- **Protein Structure in the Lipid Bilayer**
  (*William Dowhan* / Hans Diesenhofer / Will Prinz / Thomas Walz)
- **Mammalian Lipid Metabolism**
  (John Dietschy / Steve Young / Daniel Lane / Maurine Linder)
- **Lipid Localization and Structure**
  (Robert Murphy / William Robinson / Sergio Grinstein)

ANGIOGENESIS
Aug 2-7, 2009
Salve Regina University
Newport, RI
Chair: Donald M. McDonald
Vice Chair: Lena Claesson-Welsh

- **Keynote Presentation: Angiogenesis - Puzzles, Paradoxes & Controversies** (Kari Alitalo)
- **Advances in Endothelial Cell Biology in Angiogenesis** (Lena Claesson-Welsh / Eckhard Lammert / Raghu Kalluri / Michael Detmar / Shahin Rafii)
- **Advances in VEGF Biology in Angiogenesis** (Masabumi Shibuya / Luisa Iruela-Arispe / Holger Gerhardt / Napoleone Ferrara)
- **Advances in Non-VEGF Driven Angiogenesis** (Christer Betsholtz / Hellmut Augustin / Ralf Adams / Gou Young Koh / Michele De-Palma)
- **Advances in Signaling in Angiogenesis** (Michael Simons / Peter Carmeliet / Jan Kitajewski / Laura Benjamin)
- **Advances in Angiogenesis in Development** (Roy Bicknell / Brant Weinstein / Anne Eichmann / Dean Li / Eli Keshet)
- **Advances in Endothelial Barrier Function** (Harold Dvorak / David Cheresh / Dietmar Vestweber / Elisabetta Dejana)
- **Advances in Angiogenesis in Tumor Invasion & Metastasis** (Gavin Thurston / Peter Friedl / Oriol Casanovas / Gabriele Bergers / Sandra McAllister)
- **Advances in Angiogenesis Inhibition** (Gerhard Christofori / Robert Kerbel / Rakesh Jain / Herb Hurwitz)

NEW! ANTIGEN CROSS-PRESENTATION
Jun 14-19, 2009
Il Ciocco Hotel and Resort
Lucca (Barga), Italy
Chairs: Stephen Schoenberger & Sebastian D. Amigorena
Vice Chairs: Pam Ohashi & William Heath

- **The Immunobiology of Cross-Presentation** (*Peter Cresswell* / Michael Bevan / Hidde Ploegh / Nilabh Shastri)
- **Cross Presentation in Health and Disease** (*Hyam Levitsky* / Vincenzo Barnaba / Anne Hosmalin / Karolina Palucka / Marina Botto)
- **Innate Immunity and Cross-Presentation I** (*Michael Lotze* / Greg Barton / Edith Janssen / Dana Philiopott)
- **Innate Immunity and Cross-Presentation II** (*Matthew Albert* / Michel Gilliet / Laurence Zitvogel)
- **The Cell Biology of Cross-Presentation I** (*Jacques Neefjes* / Serge Grinstein / David Russell / Peter ven Endert)
- **The Cell Biology of Cross Presentation II** (*Michel Desjardins* / Christian Kurts / Christian Munz / Ira Mellman / Greg Lemke)
- **Cell Death and Cross-Presentation** (*Pramod Srivastava* / Doug Green / Guido Kroemer / Shigekazu Nagata)
- **Adaptive Immunity and Cross-Presentation I** (*Shannon Turley* / Frank Carbone / Jose Villandangos / Pramod Srivatstava / Ken Murphy)
- **Adaptive Immunity and Cross-Presentation II** (*Jorge Geffner* / Brigitta Stockinger / Thomas Brocker / Kenneth Rock)

APOPTOTIC CELL RECOGNITION & CLEARANCE
Worm-Fly-Vertebrate-Human Clearance And Failure
Jun 28 - Jul 3, 2009
Colby-Sawyer College
New London, NH
Chairs: Martin Herrmann & Yoshinobu Nakanishi
Vice Chairs: Adam Lacy-Hulbert & Chris Gregory

- **The Beginnings: The Mechanisms and Consequences of Apoptotic Cell Clearance (Keynote Presentations)** (*Robert Schlegel* / John Savill / Donna Bratton)
- **The Recognition: The Way Phagocytes Find Their Targets** (*David Ucker* / Pat Williamson / Ding Xue / Shige Nagata / In-San Kim / Kodi Ravichandran)
- **The Response: Maintenance of Tissue Homeostasis through Removal of Dying Cells** (*Angelo Manfredi* / Stephen P. Schoenberger / Patrizia Rovere-Querini / Kerstin Sarter / Udo S. Gaipl / Masato Tanaka)
- **The Players: Newly Identified Molecules Working at the Onset of Clearance** (*Yoshiro Kobayashi* / Nathalie Franc / Zheng Zhou / Michael Hengartner / Marc Freeman / Estee Kurant / Takayuki Kuraishi)
- **The Failure: Diseases Developed from Inefficient Removal of Apoptotic Cells** (*Chris Gregory* / Reinhard E. Voll / Alexander Gabibov / Johan van der Vlag / Ole Petter Rekvig)
- **The Alternatives: The Meaning of Apoptotic Cell Clearance in Physiologic State** (*Nathalie Franc* / Mike Overholtzer / Nick Baker / Silvia Finnemann / Eric Baehrecke / Jason Mercer)
- **The Consequences: The Meaning of Apoptotic Cell Clearance in Sub-Physiologic State** (*Adam Lacy-Hulbert* / Adam Lacy-Hulbert / Chris Gregory / Ian Dransfield)
- **The Effects: Positive and Negative Regulation of Apoptotic Cell Clearance** (*Kirsten Lauber* / Xiaojing Ma / Kirsten Lauber / Dennis Discher / Jerry Levine / Luis E. Munoz)
- **The Use: Clinical Application of Apoptotic Cell Clearance** (*Sandra Franz* / James George / Scott Marshall / Thomas Schwarz)

APPLIED & ENVIRONMENTAL MICROBIOLOGY
From Single Cells To The Environment
Jul 12-17, 2009
Mount Holyoke College
South Hadley, MA
Chair: Nicole Dubilier
Vice Chair: Max M. Haggblom

- **Keynote Presentation: From Single Cells to the Environment** (*Antje Boetius* / Kenneth Nealson)
- **Single Cell Imaging** (*Martin Keller* / Michael Wagner / Marcel Kuypers / Mark Ellismann)
- **Single Cell Genomics** (*Roger Lasken* / Tanja Woyke / Paul Blainey)
- **From Clonal to Global Diversity** (*Harold Drake* / William Hanage / Martin Polz / Jessica Green)
- **Biodegradation and Bioremediation** (*Carl Cerniglia* / Hauke Harms / Frank Loeffler)
- **Symbiosis** (*Claudia Lupp* / Jared Leadbetter / Nancy Moran / Edward Ruby)
- **The Human Microbiota** (*Janet Jansson* / Ruth Ley / Joel Doré)
- **Meta'omics'** (*Gerard Muyzer* / Gregory Dick / Gene Tyson / Robert Hettich)
- **Keynote Presentation: From Single Cells to the Environment and Back Again** (*Alexis Tempelton* / Brad Tebo)

ARCHAEA: ECOLOGY, METABOLISM & MOLECULAR BIOLOGY
Jul 26-31, 2009
Waterville Valley Resort
Waterville Valley, NH
Chairs: Julie Maupin-Furlow & Bettina Siebers
Vice Chairs: Kenneth M. Stedman & Haruyuki Atomi

- **Keynote Presentation: Genomics and Metabolism of Halophilic Archaea** (*Julie Maupin-Furlow* / Dieter Oesterhelt)
- **Systems Biology and Genome Function** (*Bettina Siebers* / Michael W.W. Adams / James G. Ferry)
- **Ecology & Diversity of Archaea & Their Viruses** (*Karl O. Stetter* / Anna-Louise Reysenbach / Christa Schleper / Aharon Oren / David Prangishvili / Ken Stedman / James G. Elkins)
- **Enzyme Structure & Function** (*Imke Schröder* / Volker Müller / Shigeyuki Yokoyama / Michael Terns / Robert H. White)
- **Transcription & Gene Regulation** (*Charles J. Daniels* / Felicitas Pfeifer / Shiladitya DasSarma / Michael Thomm / Elizabeth A. Karr / John Leigh / Elisabetta Bini)
- **Translation & Post-Transcriptional Modification** (*Jerry Eichler* / Jörg Soppa / Mecky Pohlschröder / Sonja-Verena Albers / Paola Londei)
- **Physiology & Regulation of Metabolism** (*William B. Whitman* / Harald Huber / William W. Metcalf / Ruth Schmitz-Streit / David E. Graham / Haruyuki Atomi)
- **Extremophiles & Biotechnology Applications** (*Rolf Thauer* / John van der Oost / Garo Antranikian / Robert M. Kelly / Norbert Hampp)
- **Evolution & the Tree of Life** (*Gary J. Olsen* / Patrick Forterre / Eugene V. Koonin)
- **Replication, Repair & Recombination** (*Francine Perler* / Thorsten Allers / Zvi Kelman / Bernard A. Connolly / Malcolm F. White)

- **Alexander M. Cruickshank Lecture: DNA Replication and Cell Division in the Third Domain**
  (*Malcolm F. White* / Stephen D. Bell)
- **Student and Post-Doctoral Presentations**
  (*John Reeve*)

ASSISTED CIRCULATION

Sep 6-11, 2009
Waterville Valley Resort
Waterville Valley, NH
Chair: John Watson
Vice Chairs: John T. Baldwin & Michael Acker

- **MCS & Heart Failure**
  (*James Kirklin, Michael Acker*)
- **Designing Bleeding, Thrombosis and Infection Away?**
  (*Harvery Borovetz, Mariell Jessup*)
- **Continuous Flow Biomechanics and Biology: Clinical and Bioengineering**
  (*Dan Burkhoff, Heinrich Schima*)
- **Planning Neonatal, Pediatric and Adult Clinical Trials**
  (*Leslie Miller*)
- **Temporary MCS: Reversing Acute Heart Failure**
  (*Frank Pagani*)
- **Repair, Recovery, and Remission: Route to a Happy Heart**
  (*Emma Birks, Doris Taylor*)
- **Patient, Family and Coordinator Factors**
  (*Karen May-Newman*)
- **Regulatory, Payment, Hospital and Industry: Different Mission - Same Goal**
  (*J. Timothy Baldwin*)
- **Total Replacement: Quality of Life**
  (*Michael Acker, John Watson*)

ATHEROSCLEROSIS
The Artery Wall And Beyond

Jun 21-26, 2009
Tilton School
Tilton, NH
Chairs: Martha K. Cathcart & Linda L. Demer
Vice Chair: John M. Chapman

- **Macrophage Heterogeneity and Atherosclerosis**
  (*Siamon Gordon* / Siamon Gordon / Mikael Pittet / Frederic Geissmann)
- **Genomics and Genetics**
  (*Ruth McPherson* / Ruth McPherson / Karen Mohlke / Sekar Kathiresan / Bev Paigen)
- **Systems Biology of Atherosclerosis**
  (*Alan Adrerem* / Alan Aderem / Stan Hazen / Rita Upmacis)
- **Calcific Vasculopathy and Valvulopathy**
  (*Dwight Towler* / Elena Aikawa / Robert Terkeltaub / Dwight Towler / Nalini Rajamannan / Jordan Miller)
- **Nanotechnology for Atherosclerosis**
  (*Sam Wickline* / John Bulte / Tillmann Cyrus / Dennis Buxton)
- **Lipoproteins and Dysmetabolic Conditions**
  (*Stan Hazen* / Jonathan Smith / Clay Semenkovich / Kerry-Anne Rye)
- **Plaque Dynamics**
  (*Rich Lee* / Hanjoong Jo / Guillermo Garcia-Cardena / Craig Simmons)
- **Atherosclerosis Progression and Regression**
  (*Ed Fisher, Elaine Raines* / Ira Tabas / Guo-Ping Shi / Elaine Raines / Ed Fisher / Collin Stultz)
- **Stem Cells and Lineage Acquisition**
  (*Qingbo Xu* / Qingbo Xu / Hiroaki Matsubara / Ann Canfield)

ATMOSPHERIC CHEMISTRY

Aug 23-28, 2009
Waterville Valley Resort
Waterville Valley, NH
Chair: Paul O. Wennberg
Vice Chairs: Kristie A. Boering & Jonathan Abbatt

- **Geoengineering for Climate Change Mitigation**
  (*Paul Crutzen* / Philip Rasch / David Keith)
- **Atmospheres of the Past**
  (*Kristie Boering* / Margaret Tolbert / Mark Thiemens / William Ruddiman)
- **Air Pollution and Human Health**
  (*James Pitts* / Petros Koutrakis)
- **Biogenic Emissions to the Atmosphere**
  (*Mary Barth* / Lucy Carpenter / Thomas Sharkey)
- **New Discoveries in Oxidative Chemistry**
  (*Andreas Hofzumahaus* / Ronald Cohen / Jos Lelieveld)
- **China: The Olympics and Air Pollution Abatement**
  (*David Streets* / Qi Zhang / Andreas Richter / Gregory Carmichael)
- **Fire**
  (*Christine Wiedinmyer* / Robert Yokelson / Anthony Clarke / Jennifer Logan / James Randerson)
- **Aerosols: Chemistry & Climate Interactions**
  (*Jonathan Abbatt* / Kimberly Prather / Jesse Kroll / Rushan Gao / Peter Adams)

ATOMIC PHYSICS

Jun 28 - Jul 3, 2009
Tilton School
Tilton, NH
Chair: Protik K. Majumder
Vice Chair: John M. Doyle

- **Precision Measurements and Fundamental Tests**
  (*Michael Romalis* / Norval Fortson / Chris Stubbs)
- **Quantum Information Science**
  (*Chris Monroe* / Rainer Blatt)
- **Cold Molecules**
  (*David DeMille* / Rudy Grimm / Jun Ye)
- **Cavity QED and Quantum Optics**
  (*Micheal Chapman* / Rob Schoelkopf / Serge Haroche)
- **Optical Lattices**
  (*Trey Porto* / Wolfgang Ketterle)
- **Mesoscopic Physics**
  (Jack Harris / Misha Lukin)
- **Atomic and Molecular Colliisions and Interactions**
  (Roman Krems / Heather Lewandowski)
- **Bose and Fermi Gases**
  (Masahito Ueda)
- **Ulltrafast and X-Ray Physics**
  (*Linda Young* / Margaret Murnane / Kenji Ohmori)

BARRIER FUNCTION OF MAMMALIAN SKIN
Molecular, Biophysical & Biomechanical Understanding Of Skin Barrier Formation, Function & Disease

Aug 9-14, 2009
Waterville Valley Resort
Waterville Valley, NH
Chairs: Walter M. Holleran & Neil Kitson
Vice Chairs: Gopinathan K. Menon & Juergen Lademann

- **Molecular Regulation and Matrix Signaling in Epidermal Barrier Generation**
  (*Kenneth Feingold, Theodora Mauro* / Alan R. Brash / Pierre Chambon / Dennis Roop)
- **Barrier Structure and Function: Insights from Novel Technologies & Applications**
  (*Reinhard Neubert, Jerry Kasting* / Luis Bagatolli / Joke Bouwstra / Annett Ruettinger / Sunney Xie)
- **Membrane Biophysics and Skin Biomechanics**
  (*Jennifer Theiwalt, Juergen Lademann* / Pieter Cullis / Evan Evans / Michel Lafleur)
- **Membrane Lipids and Trafficking in Barrier Formation and Function**
  (*Lars Norlen, Philip Wertz* / Masashi Akiyama / Gerrit van Meer / Michel Simon / Akemi Ishida-Yamamoto)
- **Skin Barrier as Biosensor: Neural-Epidermal Connections**
  (*Steven Hoath, Anthony Rawlings* / John Ansel / Mitsuhiro Denda / Randall Johnson)
- **Crossing Epidermis and Other Barriers: Lessons from Lung, Brain, & GI Barriers**
  (*Nancy Monteiro-Riviere, Annette Bunge* / Jesus Perez-Gil / Samir Mitragotri / Sabine Nuding / Nadine Barrie Smith)
- **Emerging Barrier Functions & Technologies: Hot Topics Session**
  (*Kevin Mills, Mike Roberts*)
- **Stratum Corneum Structure, Function and Disease**
  (*Peter Elias, Seung-Hun Lee* / Lilly Bourguignon / Jean-Pierre Hachem / Edith Hummler / Jens Schroder)
- **Insights from Alternate Perspectives: Math vs. Mouse Debate**
  (*Keith Brain* / Richard Guy / John Sundberg)

BIOLOGICAL MOLECULES IN THE GAS PHASE
And In Solution...

Jul 5-10, 2009
Tilton School
Tilton, NH
Chairs: David Pratt & Joan-Emma Shea
Vice Chair: Lars Konermann

- **Keynote Presentation: Setting the Stage**
  (*Joan-Emma Shea, David Pratt* / Tim Zwier / Alan Marshall / Chris Dobson)
- **Noncovalent Interactions**
  (*Steve Scheiner* / Michel Mons / Joel Moreno Ireta / Martin Jarrold)

CALCIUM SIGNALLING

Jun 21-26, 2009
Il Ciocco Hotel and Resort
Lucca (Barga), Italy
Chair: Alexei V. Tepikin
Vice Chair: J. Kevin Foskett

- **State of the Field**
  (*Alexei Tepikin, Kevin Foskett* / Tullio Pozzan)
- **Calcium Signaling in Bioenergetics and Apoptosis**
  (*Tullio Pozzan* / Michael Duchen / Rosario Rizzuto)
- **Calcium Signaling in Disease and Aging**
  (*Ernesto Carafoli* / Stephen Pandol / Natalia Prevarskaya / Llewelyn Roderick / Grace Stutzmann)
- **Calcium Stores and Calcium Release Channels**
  (*Susan Hamilton* / Barbara Ehrlich / Antony Galione / Colin Taylor)
- **Mechanisms of Calcium Entry**
  (*Anjana Rao* / Indu Ambudkar / Berndt Nilius / Richard Lewis / Anant Parekh)
- **Are TRP Channels Involved in Store-Operated Ca^{2+} Entry?**
  (*Kevin Foskett* / Shmuel Muallem / Jim Putney)
- **Interacting Second Messenger Cascades**
  (*Indu Ambudkar* / Aldebaran Hofer / David Yule)
- **Comparative Physiology of Calcium Signaling**
  (*Michael Berridge* / Luigia Santella / Alex Webb)
- **Downstream from Calcium Signaling: The Philosophy of Calcium Sensors**
  (*Bob Burgoyne* / Annete Draeger / Mitsu Ikura / Richard Tsien / David Yue)
- **Keynote Presentation: Calcium Signaling from Endoplasmic Reticulum to the Plasma Membrane**
  (*Ole Petersen* / Tobias Meyer)

NEW! CANNABINOID FUNCTION IN THE CNS

Aug 2-7, 2009
University of New England
Biddeford, ME
Chairs: Daniele Piomelli & Brad Alger
Vice Chairs: Beat Lutz & Vincenzo Di Marzo

- **Keynote Presentation: Cannabis and Schizophrenia**
  (Robin Murray)
- **New Chemical Probes and Ligands**
  (Marco Mor / Mauro Mileni / Alexandros Makriyannis / Natsuo Ueda / Larry Marnett / Ben Cravatt)
- **Endocannabinoids and Synaptic Plasticity**
  (Mauro Maccarrone / David Lovinger / Giovanni Marsicano / Ivan Soltesz / Abdel El Manira / Pablo Castillo)
- **Endocannabinoids and Neuronal Circuitry**
  (Olivier Manzoni / Istvan Katona / Shaul Hestrin / Wade Regehr / Masanobu Kano)
- **Endocannabinoids and Control of Energy Balance**
  (Jaideep Bains / Vincenzo di Marzo / Matthias Tschoep / Blerina Kola)
- **Endocannabinoid Signals in Neural Development and Survival**
  (Manuel Guzman / Tibor Harkany / Ravi Iyengar)
- **Endocannabinoid Modulation of Stress and Emotion**
  (Jeffrey Tasker / Beat Lutz / Cecilia Hillard)
- **Cannabinoids in Pain and Reward**
  (Andrea Hohmann / Rohini Kuner / Hans-Urlich Zeilhofer/ Steven Goldberg / Margaret Haney)
- **Cannabinoids, Endocannabinoids, and Schizophrenia**
  (Daniela Parolaro / Koen Van Laere / Markus Leweke)

CARBOHYDRATES

Jun 14-19, 2009
Tilton School
Tilton, NH
Chairs: Peter H. Seeberger & Stephen G. Withers
Vice Chairs: Robert J. Woods & Nicola Pohl

- **Carbohydrate Synthesis I**
  (Todd Lowary / Shino Manabe / Timor Baasov)
- **Glycobiology I**
  (Carolyn Bertozzi / Mike Ferguson)
- **Renewable Resources**
  (Bernard Henrissat / Harry Brumer)
- **Structural Biology**
  (Jim Prestegaard / Thilo Stehle / Julie Leary / Ken Ng)
- **Carbohydrates in Industry**
  (Stewart Campbell / Stefan Goletz / Gavin Painter)
- **Carbohydrate Synthesis II**
  (Koichi Fukase / Spencer Williams / Kwan Soo Kim / Biao Yu)
- **Glycobiology II**
  (*Nicola Pohl* / Chris Raetz / Chris Whitfield)
- **Young Investigator Presentations**
  (*Robert Woods* / Mario Feldmann / Lara Mahal / Kevin Yarema / Daniel Werz / Mark Nitz / Jian Liu)
- **Carbohydrate Engineering**
  (T.H. Van Kuppelt / Peng George Wang / Jon Thorson)

CARTILAGE BIOLOGY & PATHOLOGY

Jun 7-12, 2009
Les Diablerets Conference Center
Les Diablerets, Switzerland
Chairs: Bjorn R. Olsen & Dick K. Heinegard
Vice Chairs: Karen M. Lyons & Kathryn S. Cheah

- **Development / Evolution of Cartilage**
  (*Karen Lyons* / Raymond Boot-Handford / Ryan Kerney / Matthew Harris)
- **Signaling and Control Mechanisms**
  (*Andrea Vortkamp* / Fanxin Long / Elazar Zelzer / Susan Mackem / Deborah Krakow)
- **Genetic Mechanisms of Disease**
  (*Matthew Warman* / Stefan Mundlos / Christine Hartmann / Shiro Ikegawa)
- **Molecular Structure**
  (*Erhard Hohenester* / Hideaki Nagase / Anthony Day / Erhard Hohenester / Anders Aspberg)
- **Mechanobiology**
  (*Christopher S. Chen* / Dennis Discher / Sudha Agarwal)
- **Degenerative Disorders**
  (*Amanda Fosang* / Elisabeth Morris / Danny Chan / Yefu Li / Tonia L. Vincent)
- **Cellular Mechanobiology and Immune Mechanisms in Disease**
  (*Rocky Tuan* / Christopher S. Chen / Rikard Holmdahl)
- **Repair, Regeneration and Tissue Engineering**
  (*Vicki Rosen* / Rocky Tuan / Ichiro Sekiya / Anthony Hollander)
- **New Directions**
  (*Kathryn Cheah* / David Cox)

CATCHMENT SCIENCE: INTERACTIONS OF HYDROLOGY, BIOLOGY & GEOCHEMISTRY
Thresholds, Tipping Points, And Non-Linearity: Integrated Catchment Science For The 21st Century

Jul 12-17, 2009
Proctor Academy
Andover, NH
Chairs: Keith N. Eshleman & Penny J. Johnes
Vice Chair: Irena F. Creed

- **Hydrological Responses of Catchments to Environmental Change: Extreme Events and Their Magnitude, Frequency, and Predictability**
  (Muratha Sivapalan / Nigel Arnell / Doerthe Tetzlaff / Peter Troch)
- **Hydrochemical Responses of Catchments to Environmental Change: Coupling and Decoupling of Biogeochemical Cycles**
  (Bill McDowell / Myron Mitchell / Pirkko Kortelainen / Gunnar Lischeid)
- **Catchment Scale Responses of Acidification and Recovery**
  (Shelly Arnott / Don Monteith / Norman Yan)
- **Catchment Responses to Nutrient Loadings from Headwaters to Regional Scales**
  (David Hamilton / J. Iwan Jones / Mike Kemp)

CATECHOLAMINES

Aug 9-14, 2009
University of New England
Biddeford, ME
Chair: Patricio O'Donnell
Vice Chair: Regina M. Carelli

- **Keynote Presentations**
  (James Surmeier / Eric Nestler)
- **Catecholamines: Novel Views on Anatomical Organization**
  (*Susan Sesack* / Suzanne Haber / Satoshi Ikemoto / Gloria Meredith / Elizabeth Van Bockstaele)
- **Catecholamines and Synaptic Transmission**
  (Marina Wolf / Mark Thomas / Kuei-Yuan Tseng / Antonello Bonci)
- **Catecholamine Pharmacology: Receptor Heterodimers and Novel Mechanisms**
  (*David Weinshenker* / Susan George / Kjell Fuxe)
- **Catecholamines in Reward and Drug Addiction**
  (*Nathaniel Daw* / Sue Grigson / Toni Shippenberg / Geoffrey Schoenbaum / Paul Phillips / Paul Shepard / Athina Markou)

- **Cognitive Effects of Catecholamines** (*Trevor Robbins* / Stan Floresco / John Salamone / Earl Miller / Barry Waterhouse)
- **Catecholamines in Neurodegenerative Disease** (*Mark Wightman* / Michael Zigmond / Gustavo Murer)
- **Catecholamines and Mental Disorders** (Daniel Weinberger / Michael Frank / Rita Valentino)
- **Sex Differences and Catecholamines** (*Barry Levin* / David Standaert / Victoria Luine / Jill Becker)
- **Transgenic Approaches: Modeling Disease** (*Randy Blakely* / Richard Palmiter / Xiaoxi Zhuang / Steve Thomas)
- **Adolescence** (Susan Andersen / Adriana Galvan)

NEW! CATECHOLAMINES (GORDON RESEARCH SEMINAR)

Aug 8-9, 2009
University of New England
Biddeford, ME
Chairs: Cheryse A. Furman & Joshua L. Jones

- **Introduction to GRS Catecholamines & Data Blitz** (*GRS Committee*)
- **Cellular and Molecular Regulation of Catecholamine Transmission** (*Antonello Bonci*)
- **Catecholamines in Brain Circuitry** (*Stan Floresco*)

The Gordon Research Seminar on Catecholamines is a two-day Gordon Conference-style meeting exclusively for graduate students, post-docs, and other scientists with comparable levels of experience and education. Speakers will be chosen from among the attendees. The associated Gordon Research Conference will take place at the same location, immediately following the Seminar.

CELL BIOLOGY OF METALS
Metal Metabolism And Disease

Aug 9-14, 2009
Salve Regina University
Newport, RI
Chairs: Valeria Culotta & Walter Schaffner
Vice Chairs: David P. Giedroc & Nancy C. Andrews

- **Metals and Cancer** (*Valeria Culotta* / Thomas O'Halloran / Steve Lippard)
- **Metals and Oxidative Stress** (*Sabeeha Merchant* / Michael Daly / Vadim Gladyshev / Wayne Outten / Jim Imlay)
- **Metals and Neurodegeneration** (*Leah Harris* / Gerd Multhaup / Jonathan Gitlin / Michael Ashner)
- **Cell Biology of Iron Disorders** (*Jodie Babitt* / Randall Peterson / Andrew Dancis / Jan Abkowitz / Caroline Philpott)
- **Metals in Microbial Pathogenicity and Immunity** (*Philippe Gros* / Norma Andrews / David Giedroc / Michael Petris)
- **Monitoring Metals in Cells** (*David Eide* / Jim Penner-Hahn / Amy Palmer / Christoph Fahrni / Chris Chang)
- **Metal Ion Selectivity in Cells** (*Megan McEvoy* / Nigel Robinson / Jaekwon Lee / Barry Rosen)
- **Metal Co-Factor Biogenesis** (*Andrew Dancis* / William Walden / Dennis Dean / Dennis Winge / Janneke Balk)
- **Metal Metabolism and Development** (*Walter Schaffner* / Jerry Kaplan / Dennis Thiele)

CELL CONTACT & ADHESION
Cell-Cell Junction Functions, Polarity And Morphogenesis

Jun 28 - Jul 3, 2009
Waterville Valley Resort
Waterville Valley, NH
Chair: Pierre McCrea
Vice Chair: Alpha S. Yap

- **Opening Views Upon Cell-Cell Junction Functions** (*Pierre McCrea, Alpha Yap* / W. James Nelson / Joan Brugge)
- **Cell Polarity Within Tissues** (Marek Mlodzik / Ulrich Tepass / Lou Reichardt / Yokiko Goda / Erin Schuman / Jeff Axelrod)
- **Cytoskeletal Interplay with Cell-Cell Contacts** (Alpha Yap / Chris Wylie / John Collard / Masatoshi Takeichi)
- **Tight, Desmosome & Gap Junctions** (Kathy Green / Ben Margolis / Asma Nusrat / Klaus Willecke)
- **Molecular Mechanisms Modulating Cell-Cell Adhesive Processes** (Larry Shapiro / Andrew Kowalczyk)
- **Developmental Roles of Adhesive-Complex Proteins** (Rolf Kemler / Elisabetta Dejana / Barry Gumbiner / Valera Vasioukhin)
- **Cancer/Pathology and Cell-Cell Junction Components** (Pamela Cowin / Keith Johnson / Michael Brenner)
- **Catenins in Physiologic/Pathologic Contexts** (*Cara Gottardi* / Walter Birchmeier / Juliet Daniels / Frans van Roy / Albert Reynolds)
- **Morphogenesis I: Formation of Epithelia** (Keith Mostov / Thomas Lecuit)
- **Morphogenesis II: Dynamics of Cell-Cell and Tissue Organization in Animal Models** (Mark Peifer / Carl-Philipp Heisenberg / Jennifer Zallen)

CELL GROWTH & PROLIFERATION

Jul 5-10, 2009
Colby College
Waterville, ME
Chair: Sally Kornbluth
Vice Chair: Johannes Walter

- **Keynote Presentation: Mechanisms of DNA Replication** (John Diffley)
- **Cell Cycle Engines** (Steve Reed / Fred Cross / Steve Haase)
- **Genome Stability and Chromsome Dynamics** (Angelika Amon / Frank Uhlmann / David Pellman)
- **G1 Control and Chromosomal Replication** (Nick Dyson / Bryan Dynlacht / David MacAlpine / Anindya Dutta / Mary Lilly / Maki Asano)
- **DNA Damage and Cell Cycle Checkpoints** (Helen Piwinica-Worms / Daniel Lew / Jean Gautier / Anja Bielinsky / Michael Yaffe / Robert Abraham)
- **Mitosis I** (Peter Jackson / Jonathon Pines / Mary Dasso / Todd Stukenberg)
- **Oncogenes, Tumor Suppressors, and Growth Control I** (Gerard Evan / Iswar Hariharan / Andrea McLatchey / Hermann Steller / Eileen White)
- **Mitosis II** (Hongtao Yu / Kerry Bloom / Orna Cohen-Fix / Andrea Mussachio)
- **Oncogenes, Tumor Suppressors, and Growth Control II** (Jing Yang / Kornelia Polyak / Jacqueline Lees / Chi Dang / Tak Mak)

NEW! CELL-CELL FUSION
From Natural History To Molecular Physics And Medical Applications

Jul 19-24, 2009
Colby-Sawyer College
New London, NH
Chair: William A. Mohler
Vice Chair: Benjamin Podbilewicz

- **Keynote Presentation: Protein-Induced Stress and Strain Within Lipid Bilayers - A Route to Membrane Fusion** (*William A. Mohler* / Harvey T. McMahon)
- **Cell-Cell Fusogens: Viral and Developmental Fusion Proteins** (*Benjamin Podbilewicz* / Judith M. White / Amir Sapir / Joshua Zimmerberg)
- **Fertilization and Gamete Fusion** (*Laurinda A. Jaffe* / Laurinda A. Jaffe / Andrew W. Singson / Kenji Miyado)
- **Myoblast and Mesenchymal Fusion** (*Elizabeth H. Chen* / Charles A. Ettensohn / Grace K. Pavlath / Renate Renkawitz-Pohl)
- **Fusion in Epithelia** (*William A. Mohler* / Steven Bassnett / Valery I. Shestopalov / Michael J. Galko / Thomas E. Spencer)
- **Models of the Physicochemical Pathway to Membrane Fusion** (*Leonid V. Chernomordik* / Michael M. Kozlov / Michael Schick / Huey W. Huang)
- **Monocytic Cells: Fusion and Nanotubular Communication** (*Agnès Vignery* / Markus Grompe / Agnès Vignery / Simon C. Watkins)
- **Fusion in Fungal and Plant Species** (*Eric Grote* / Aska Goverse / Thomas J. Baum / Mark D. Rose)
- **Applications of Induced Cell Fusion in Medicine** (*Richard Borgens* / David E. Avigan / Jose Alexandre M. Barbuto / Richard B. Borgens)

CELLULAR OSMOREGULATION & MECHANOTRANSDUCTION
Sensation, Transduction And Integration Of Osmotic And Mechanical Signals
Jul 5-10, 2009
University of New England
Biddeford, ME
Chair: Bert Poolman
Vice Chair: Boris Martinac

- **Keynote Presentations: Osmotic Balancing and Cellular Roles of Aquaporins**
  (*Bert Poolman* / Ian Booth / Alan Verkman)
- **Cellular Responses to Osmotic Stress**
  (*Gloria Muday* / Frank Wehner / Jian-Kang Zhu / Julian Schroeder / Thomas Record)
- **Osmosensing and Transduction**
  (*Miriam Goodman* / Armagan Kocer / Kevin Strange / Janet Wood)
- **Signal Transduction Cascades in Animals and Plants**
  (*Maurice Burg* / Natalia Dmitrieva / Ben Ko / Moo Kwon)
- **Mechanism and Physics of Mechanotransduction**
  (*Paul Blount* / Ching Kung / Sergei Sukharev / Masahiro Sokabe / Eric Honoré)
- **Biophysical Chemistry of (Macro)Molecule-Water Interactions**
  (*Wayne Bolen* / Zoya Ignatova / Frederick Sachs / Matthew Auton)
- **System Analysis of Cell Volume Regulation (Omics, *etc*)**
  (*Rainer Hedrich* / Elizabeth Haswell)
- **Cell Morphogenesis**
  (*Paul Yancey* / Patrick Masson / Kerwin Casey Huang / Christine Jacobs Wagner)
- **Structural Analysis of Osmoregulatory Channels and Transporters**
  (*Reinhard Kramer* / Eduardo Perozo / Preben Morth / Christine Ziegler / Anthony Lee)

CELLULOSOMES, CELLULASES & OTHER CARBOHYDRATE MODIFYING ENZYMES
Jul 26-31, 2009
Proctor Academy
Andover, NH
Chair: Harry J. Gilbert
Vice Chair: Colin Mitchinson

- **Keynote Presentation: Understanding Plant Cell Walls: Improved Biomass Conversion and New Materials**
  (*Edward Bayer* / Mike Himmel)
- **Keynote Presentation: New Perspectives of Protein Carbohydrate Recognition**
  (*Edward Bayer* / Alisdair Boraston)
- **Cell Wall Architecture and Display**
  (*Tuula Teeri* / Vincent Bulone / Paul Knox / Debra Mohnen / Claire Halpin)
- **Plant Cell Wall Hydrolase Structure and Function: Cellulosomal Module Interactions**
  (*Stephen Smith* / Henri-Pierre Fierobe / Ilit Noach / Michael Crowley / Elizabeth Ficko-Blean)
- **Plant Cell Wall Hydrolase Structure and Function: Catalytic Modules**
  (*Mirjam Czjzek* / Cecile / Herve / Peter Biely / Richard Pickersgill / Jocelyn Rose / Mats Sandren / Vincent Eijsink / Kiyohiko Igarashi)
- **Regulation of Gene Expression**
  (*Merja Penttilä* / Eric Martens / David Bolam / Yuval Shoham / Chrisitan Kubicek)
- **Rational Design, Directed Evolution and Prospecting for Superior Enzymes**
  (*Harry Brumer* / Suzanne Lantz / Andres Anders Viksø-Nielsen / Justin Siege)
- **Genomes**
  (*Bernard Henrissat* / Pedro Coutino / Mark Morrison)

CHEMICAL OCEANOGRAPHY
Process, Dynamics, And Change In The Anthropocene Ocean
Aug 2-7, 2009
Tilton School
Tilton, NH
Chair: Robert C. Aller
Vice Chair: David J. Burdige

- **Open Ocean Carbon Cycling and Fluxes**
  (*Cindy Lee* / Steven R. Emerson / Ellen R.M. Druffel)
- **Ocean Acidification, Carbonates, and Biogeochemical Responses**
  (*Frank J. Millero* / Richard A. Feely / John W. Morse / Anja Engle)
- **Biomineralization and Ocean Process / State Proxies**
  (*Jess F. Adkins* / Jonathan Erez / Laura F. Robinson)
- **Metals, Volatiles: Inputs, Outputs, and Interior Ocean Processing**
  (*Silke Severmann* / Derek Vance / Seth G. John / William E. Seyfried, Jr.)
- **Biogeochemical Mechanisms of Elemental Cycling in the Water Column**
  (*Mark L. Wells* / Kathy Barbeau / Kay D. Bidle)
- **Organic Tracers of Biogeochemical and Oceanic Processes**
  (*Ann Pearson* / Timothy I. Eglinton / Anitra E. Ingalls / Marco Coolen)
- **Physical Structure / Dynamics - Biogeochemical Coupling**
  (*Kathleen C. Ruttenberg* / Phyllis Lam / Curtis Deutsch)
- **Benthic Systems**
  (*David J. Burdige* / Peter Berg / Christopher S. Martens / Maria Pokopenko)
- **Coastal Ocean Biogeochemical Processing and Exchange**
  (*Paula G. Coble* / Joseph A. Needoba / Wei-Jun Cai)

CHEMISTRY EDUCATION RESEARCH & PRACTICE
Jun 21-26, 2009
Colby College
Waterville, ME
Chair: Thomas J. Greenbowe
Vice Chair: Marcy Hamby Towns

- **The Role of Multimodal Representations in Chemistry Education**
  (*Chris Bauer* / Maria Oliver-Hoyo / Brian Hand)
- **Advances in Learning Theories**
  (*Gabriela Weaver* / David Jonassen / David Brooks)
- **Using Case Studies To Investigate Student Understanding**
  (*Jennifer Lewis* / Tina Overton / Peter Mahaffy)
- **Research on Learning by Inquiry**
  (*Guy Ashkenazi* / Renee Cole / Ellen Yezierski / Debbie Herrington / Hannah Sevian)
- **Enhancing Conceptual Understanding of Chemistry Using Practical Applications**
  (*Stacey Lowery Bretz* / Scott Donnelly / Steve Fleming)
- **Learning with Technology**
  (*Shelia Woodgate* / Robert Beichner / Vickie Williamson / Mike Sanger)
- **Chemistry Education Beyond the Freshmen Year**
  (*Norb Pienta* / Georgios Tsaparlis / George Bodner)
- **Research Based Curriculum Development**
  (*Bryce Hach* / Melanie Cooper / Mike Klymkowsky / Judi Dori / Rick Moog)
- **Future Directions in Chemistry Education Research**
  (*Marcy Towns* / Tom Holme)

CHRONOBIOLOGY
Molecular Mechanisms Of Circadian Clocks
Jul 19-24, 2009
Salve Regina University
Newport, RI
Chair: Joseph S. Takahashi
Vice Chair: Martha Merrow

- **Dynamics of Transcription and Cell Cycles**
  (*Joseph Takahashi* / James McNally / Sharad Ramanathan)
- **Molecular Clock Mechanisms / Hot Topics I**
  (*Susan Golden / Martha Merrow* / Takao Kondo / Carl Johnson / Ueli Schibler / Jay Dunlap)
- **Human Clock Genetics**
  (*Michael Young* / Till Roenneberg / Thomas Bourgeron / Ying-Hui Fu / Juliane Winkelmann)
- **Clocks and Metabolism / Hot Topics II**
  (*Joe Bass* / Benjamin Tu / Z. Jeffrey Chen / Charles Weitz)
- **Emerging Roles for Clock Genes**
  (*Carla Green* / Paul Frenette / Bogi Anderson / Andrew C. Oates)
- **Genetics of Drosophila Clocks / Hot Topics III**
  (*Amita Sehgal / Ignacio Provencio* / Trudy McKay / Paul Taghert / Ravi Allada / Michael Nitabach)
- **Systems Biology of Circadian Clocks**
  (*Hiroki Ueda* / Steve Kay / John Hogenesch / Achim Kramer)
- **Mammalian Clocks and the SCN / Hot Topics IV**
  (*Martha Gillette* / Michael Hastings / Samer Hattar / Sato Honma / Erik Herzog)
- **Perspectives**
  (*Martin Zatz* / Michael Rosbash / Charalambos Kyriacou)

CLUSTERS, NANOCRYSTALS & NANOSTRUCTURES

Jul 19-24, 2009
Mount Holyoke College
South Hadley, MA
Chairs: Hellmut H. Haberland & David J. Norris
Vice Chairs: Lai-Sheng Wang & Richard E. Palmer

- **Energy I**
  (*Louis Brus* / Paul Alivisatos / John Rogers)
- **Carbon**
  (*Lai-Sheng Wang* / Richard Kaner / Eleanor Campbell)
- **Growth & Assembly**
  (*Taeghwan Hyeon* / Dmitri Talapin / Peter Reiss / Frances Ross / Simon Brown)
- **Plasmonics**
  (*Ulrike Woggon* / Thomas Ebbesen / Teri Odom)
- **Young Investigator Presentations**
  (*Richard Palmer*)
- **Theoretical Insights**
  (*Catherine Bréchignac* / Uzi Landman / Alexander Efros)
- **Spectroscopy I**
  (*Ori Cheshnovsky* / Daniel Neumark / Todd Krauss / Tobias Lau)
- **Phase Transitions**
  (*Martin Schmidt* / Martin Jarrold / Jean-Marc L'Hermite)
- **Energy II**
  (*Song Jin* / Peidong Yang / Yi Cui)
- **Spectroscopy II**
  (*Will Castleman* / Markus Arndt / Akira Terasaki)
- **Carrier Multiplication Controversy I**
  (*Arthur Nozik* / Moungi Bawendi / Sanford Ruhman)
- **Carrier Multiplication Controversy II**
  (*Philippe Guyot-Sionnest* / Victor Klimov / Eran Rabani)

COASTAL OCEAN CIRCULATION

Jun 7-12, 2009
Colby-Sawyer College
New London, NH
Chair: James O'Donnell
Vice Chair: Mark Stacey

- **Shelf Dynamics**
  (*John Allen* / Steve Lentz / Chris Edwards)
- **Inner Shelf Dynamics**
  (*Jack Barth* / Stephen Monismith / Geno Pawlak / Melanie Fewings)
- **Nearshore Dynamics**
  (*Tuba Ozkan-Haller* / Falk Feddersen / Britt Raubenheimer)
- **Buoyancy-Driven Flows**
  (*Glen Gawarkiewicz* / Lars Umlauf / Rob Hetland / Tom Hsu)
- **Air-Sea Interactions**
  (*Jim Edson* / Roger Samelson / Andy Jessup)
- **Ecosystem Dynamics**
  (*Johnathan Sharples* / Neil Banas / Katja Fennel / Tom Rippeth)
- **Coastal Mixing**
  (*Jen MacKinnon* / Mike Gregg / Phil Wiles)
- **Estuarine Dynamics**
  (*Rocky Geyer* / David Ralston / Malcolm Scully / Elizabeth North)
- **Topography and Mixing**
  (*M. Stacey* / Parker McCready / Mark Inall)

COLLAGEN

The Functional Continuum Of Cells And Matrix

Jul 19-24, 2009
Colby-Sawyer College
New London, NH
Chair: Leena Bruckner-Tuderman
Vice Chair: Billy G. Hudson

- **Biosynthesis and Regulation of Collagens**
  (*Johanna Myllyharju* / Hank Qi / Janice Vranka)
- **Molecular Collagen Assembly**
  (*Hans Peter Bächinger* / Sergei Boudko / Yujia Xu / Jeff Hartgerink / Taina Pihlajaniemi)
- **Collagen Receptors**
  (*Ambra Pozzi* / Thomas Bugge / Birgit Leitinger)
- **Collagen Suprastructures and ECM Ligand Interactions**
  (*David Birk* / Ake Oldberg / Michael Yu)
- **ER Stress and Quality Control of Collagens**
  (*John Bateman* / Kazuhiro Nagata / Ray Boot-Handford)
- **Fibroblasts and ECM Mechanoreception**
  (*Boris Hinz* / Paul Janmey / Joachim Spatz / Melody Swartz)
- **Functions of ECM in Stem Cell Niches**
  (*Marion Young* / Jennifer Elisseeff / Xiao-Dong Chen)
- **Collagen and ECM Diseases and Novel Therapeutic Strategies**
  (*Danny Chan* / Manuel Koch / Raili Myllylä / Markus Moser)
- **Hot Topics**
  (*Billy Hudson*)

COMBINATORIAL CHEMISTRY

High Throughput Chemistry & Chemical Biology

Jun 7-12, 2009
Colby-Sawyer College
New London, NH
Chair: Joseph M. Salvino
Vice Chair: Michael A. Foley

- **Frontiers in Drug Discovery / Chemical Biology**
  (*Oliver Reiser* / Mikel Moyer / Stuart Schreiber)
- **Hit to Lead / Medicinal Chemistry / Synthesis**
  (*Roland E. Dolle* / Karin Worm / Horst Hemmerle / Scott Wolkenberg / Mario Rottländer / Simon MacDonald)
- **Synthesis and New Directions in Medicinal Chemistry**
  (*Scott Wolkenberg* / M. Christina White / Paul Anderson)
- **High Throughput Technologies**
  (*Greg Roth* / David Spring / Richard Hartley / Ann Kelly / Marco Schmidt / Benjamin Miller)
- **Chemical Methodologies and Library Development I**
  (*Padmakumar A. Kaimal* / John Porco / Amos B. Smith III)
- **Chemical Methodologies and Library Development II**
  (*Michael Lawrence* / Scott A. Snyder / Greg Roth / Aaron Beeler / Anna Mapp / Paul Floreancig)
- **Chemical Biology and Methodology**
  (*Scott A. Snyder* / Kevin Burgess / Annaliese Franz / Anthony Czarnik)
- **High Throughput Technologies / Hit to Lead**
  (*Annaliese Franz* / Hong Liu / Craig Thomas / Michael Lawrence / Paul Fleming / Alex Kiselyov)
- **Frontiers in Drug Discovery**
  (*Anna Mapp* / Alexis Borisy / Edward Scolnick)

NEW! COMBINATORIAL CHEMISTRY (GORDON-KENAN RESEARCH SEMINAR)

High Throughput Chemistry & Chemical Biology

Jun 6-7, 2009
Colby-Sawyer College
New London, NH
Chairs: Alan Rolfe & Thiwanka B. Samarakoon

- **Keynote Presentation**
  (Jared Shaw)
- **Molecular Libraries, Natural Products and Probes**
  (Matt Boxer / Wei Wang)
- **Chemical Methodologies and Library Development**
  (Catherine Smith / Jennifer Treece / Won-Suk Kim)

The Gordon Research Seminar on Combinatorial Chemistry is a two-day Gordon Conference-style meeting exclusively for graduate students, post-docs, and other scientists with comparable levels of experience and education. All attendees are strongly encouraged to present posters and are urged to submit an abstract of the work being presented. From these submitted poster abstracts, 10 individuals will be selected to give an oral presentation. The associated Gordon Research Conference will take place at the same location, immediately following the Seminar.

COMPUTER AIDED DRUG DESIGN

Experiment Meets Modeling: Where Are We Now, Where Are We Going

Jul 19-24, 2009
Tilton School
Tilton, NH
Chair: Brian K. Shoichet
Vice Chair: Gerhard Klebe

- **Success Stories from Drug Design**
  (*Hugo Kubinyi* / Jay Pandit / Sandra Jacob-Cowan)
- **The Ribosome as a Drug Target**
  (*Holger Gohlke* / Tom Steitz / Erin Duffy)
- **RNA and Aptamers in Drug Research**
  (*Jennifer Kumrine* / Eric Westhof / Thomas Hermann)
- **Thermodynamics and Ligand Binding**
  (*Jeremy Tame* / John Ladbury / Steve Homans / Glyn Williams)
- **Selectivity and Residence Time**
  (*Katharine Holloway* / Helena Danielson)
- **Merging Chemical and Biological Space**
  (*Ruben Abagyan* / Jean-Louis Reymond / Christine Orengo / Jordi Mestres)
- **Protein Networks and Systems Biology**
  (*Tanja Kortemme* / Hans-Werner Mewes / Patrick Aloy)
- **Electrostatics as a Major Obstacle in Computational Drug Design**
  (*Curt Breneman* / Jens-Eric Nielsen / Thomas Simonson / Jay W. Ponder)
- **Keynote Presentation: Water as a Major Obstacle in Computational Drug Design**
  (*Leslie Kuhn* / Gerhard Hummer / Ken Dill)

LIQUID CRYSTALS
Jun 14-19, 2009
Colby-Sawyer College
New London, NH
Chair: Peter J. Collings
Vice Chair: L.C. Chien

- **Synthesis and Characterization of New Liquid Crystals**
  (*Anselm Griffin* / Robert Lemieux / George Mehl)
- **Colloids, Self-Assembly, and Molecular Aggregation**
  (*David Van Winkle* / Zvonimir Dogic / Daniel Needleman / Gordon Tiddy)
- **Theory, Modeling, and Computation**
  (*Tom Lubensky* / Randall Kamien / Robin Sellinger / Julia Yeomans)
- **Nanoparticle and Nanotube Dispersions**
  (*Oleg Lavrentovitch* / Jan Lagerwall / Peter Palffy-Muhoray)
- **Biaxial Nematics**
  (*David Allender* / Helen Gleeson / Antal Jakli)
- **Lasers, Photonics, Electro-Optics**
  (*Robert Meyer* / Scott Davis / Byoungho Lee)
- **Liquid Crystal Sensors**
  (*Suk-Wah Tam-Chang* / Bharat Acharya / Daniel Schwartz)
- **Liquid Crystal Ordering and Biological Function**
  (*Mohan Srinivasarao* / Noel Clark / Cyrus Safinya)
- **Bio-Inspired Materials**
  (*Linda Hirst* / Tomiki Ikeda / Julia Kornfield / B. Ratna)

LIQUIDS, CHEMISTRY & PHYSICS OF
Aug 2-7, 2009
Holderness School
Holderness, NH
Chair: Steve Granick
Vice Chair: Peter Harrowell

- **Biomolecular**
  (David Nelson / Tobias Baumgart)
- **Spectroscopy, Scattering**
  (Mike Fayer / Mischa Bonn / Miquel Salmeron)
- **The Energy Problem**
  (Nitash Balsara / David Chandler)
- **Complex Fluids**
  (Jerome Bibette / Erik Luijten / Hajime Tanaka)
- **Interfacial Fluids**
  (Daniel Bonn / Elisa Riedo)
- **Molecular and Biomolecular Assembly**
  (Sharon Glotzer / Igal Szleifer / Helmuth Möhwald)
- **From Glasses to Vibrational Relaxation**
  (Laura Kaufmann / Rich Stratt)
- **Phase Transitions**
  (Daan Frenkel / Andrea Liu / Tim Lodge)
- **Keynote Presentation: Theory of Liquids**
  (Ben Widom)

MAGNETIC RESONANCE
Jun 14-19, 2009
University of New England
Biddeford, ME
Chair: Beat H. Meier
Vice Chair: Jeffrey A. Reimer

- **Structure Determination and Dynamics in Biosolids**
  (*Beat H. Meier* / Nicolai R. Skrynnikov / Anja Böckmann)
- **Folding and Misfolding of Protein**
  (*Kurt W. Zilm* / Robert Tycko / Hartmut Oschkinat / Christopher P. Jaroniec / Yoshitaka Ishii)
- **Electron Paramagnetic Resonance**
  (*Brian M. Hoffman* / Daniela Goldfarb / Gunnar Jeschke)
- **Microscopy and Imaging**
  (*Alexander Pines*)
- **NMR of Materials**
  (*Jeffrey A. Reimer* / Roderick E. Wasylishen / Josef W. Zwanziger)
- **Alternative Detection and Hyperpolarization**
  (*John S. Waugh* / Robert G. Griffin / Son-I Han / Walter Köckenberger / Jörg Wrachtrup)
- **Large Systems**
  (*Chad M. Rienstra*)
- **New Developments**
  (Sophia E. Hayes)
- **New Methodological Developments**
  (Lyndon Emsley / Geoffrey Bodenhausen)

NEW! MAGNETIC RESONANCE (GORDON-KENAN RESEARCH SEMINAR)
Foundations Of NMR
Jun 13-14, 2009
University of New England
Biddeford, ME
Chairs: Adam Lange & Paul Hudson

- **Structure and Dynamics of Solid- and Solution-Phase Proteins**
  (*Adam Lange / Paul Hudson* / Manuel Etzkorn / Nils Lakomek)
- **Novel Methodologies in Material Studies**
  (*Brian Mayer*)
- **Hyperpolarization and Enhanced Detection Techniques**

The Gordon Research Seminar on Magnetic Resonance is a two-day Gordon Conference-style meeting exclusively for graduate students, post-docs, and other scientists with comparable levels of experience and education. Speakers will be chosen from among the attendees. The associated Gordon Research Conference will take place at the same location, immediately following the Seminar.

MALARIA
Parasite Biology And Host-Parasite Interactions
Sep 6-11, 2009
Magdalen College
Oxford, United Kingdom
Chair: Chetan E. Chitnis
Vice Chair: Patrick Duffy

- **Molecular Aspects of Hepatocyte Infection by Sporozoites**
  (Maria Mota / Robert Menard / Volker Heussler)
- **Molecular Mechanisms Involved in Red Cell Invasion by Merozoites**
  (*Tony Holder* / Michael Blackman / Jake Baum / David Sibley / Pushkar Sharma)
- **Transmission of Parasites from Host to Vector**
  (*Robert Sinden* / Oliver Bilker / Elena Levashina / Ken Vernick)
- **Immunity to Malaria**
  (*Carole Long* / Fidel Zavala / Eleanor Riley / Dominic Kwiatkowski / Kevin Marsh)
- **Molecular Basis of Pathogenic Mechanisms**
  (*Patrick Duffy* / Pierre Buffet / Kasturi Haldar / Ali Salanti)
- **Novel Approaches to Malaria Vaccine Development**
  (*Alan Thomas* / Stefan Kappe / Brendan Crabb / Adrian Hill / Richard Pleass)
- **Drug Targets and Mechanisms of Drug Resistance**
  (*Timothy Wells* / Yongyuth Yuthavong / David Fidock / Margaret Phillips)
- **Plasmodium Genomes and Post-Genome Biology**
  (*Chris Newbold* / Sarah Volkman / Jane Carlton / Amit Sharma / Christian Doerig)
- **Control of Gene Expression**
  (*Pradip Rathod* / Artur Scherf / Kirk Deitsch / Andy Waters)

MAMMALIAN GAMETOGENESIS & EMBRYOGENESIS
Aug 2-7, 2009
Waterville Valley Resort
Waterville Valley, NH
Chair: Michael K. Skinner
Vice Chair: Robert E. Braun

- **Stem Cells: Germline & Embryonic**
  (*Erika Matunis* / Wolfgang Engel / Kyle Orwig / Michael Roberts)
- **sRNA in Gametogenesis and Embryogenesis**
  (*Haifan Lin* / Wei Yan / Deborah Boure'his)
- **Epigenetic Programming During Gametogenesis and Embryogenesis**
  (*John McCarrey* / Alex Meissner / Wolf Reik / Kevin Eggan)
- **Environmental Impacts on Embryogenesis and Development**
  (*Pat Hunt* / Robert Waterland / Kevin Sinclair)
- **Integrated Genomics and Epigenetics**
  (*Marisa Bartolomei* / Laurie Boyer / Marisa Bartolomei)
- **Gonadal Development and Sex Determination**
  (*Andrea Cupp* / Andrew Sinclair / David Page / Blanche Chapel)
- **Gene Networks and Transcriptional Regulation**
  (*Miles Wilkinson* / Andrew Kasarskis / Bill Kelly / Allyson Spence)
- **Assisted Reproductive Technologies and Stem Cells**
  (Derek McLean / Carmen Sapienza / Jiyoung Lee)
- **Keynote Presentations**
  (*MaryAnn Handel* / Eva Eicher / Janet Rossant / John Eppig)

MAMMARY GLAND BIOLOGY
Jun 14-19, 2009
Salve Regina University
Newport, RI
Chair: D. Joseph Jerry
Vice Chair: Chris Ormandy

- **Regulation of Development by Hormones and Growth Factors**
  (*Christopher Ormandy* / John Lydon / Christine Watson / Sean Egan)
- **Stem Cells: Puppets or Puppeteers?**
  (*Jeff Rosen* / Lola Reid / Amar Klar)
- **Parity: Prevention or Promotion of Breast Cancer?**
  (*Daniel Medina* / Melissa Troester / Pepper Schedin / Kornelia Polyak)
- **Breast Cancer Pathways**
  (*John Hilkens* / Andrew Futreal / Jeffrey Green)
- **DNA Repair and Breast Cancer Risk**
  (*D. Joseph Jerry* / Lisa Wiesmüller / David Livingston / Vivian Cheung)
- **Environmental Factors in Mammary Gland Development and Carcinogenesis**
  (*Weston Porter* / Mary-Helen Barcellos-Hoff / Cheng Chi Lee)
- **Metabolic Adaptations During Development**
  (*Russell Hovey* / Vassiliki Karantza-Wadsworth / Sylvaine Cases)
- **Prolactin in Breast Development and Cancer**
  (*D. Joseph Jerry* / Barbara K. Vonderhaar)

MATRIX-ISOLATED SPECIES, PHYSICS & CHEMISTRY OF
Jul 19-24, 2009
Magdalen College
Oxford, United Kingdom
Chairs: Nigel Young & Steve Ogden

- **Matrix Isolation: Where is it Going?**
  (*Nigel Young* / Matthew Almond)
- **Matrix Dynamics and Quantum Hosts**
  (*Mika Pettersson* / Benny Gerber / Mario Fajardo)
- **Bring and Share Technical Session**
  (*Lester Andrews* / Laurent Manceron / Adam Bridgeman)
- **New Organic Species and Biomolecules**
  (*Ian Dunkin* / Rui Fausto / Thomas Bally / Wolfram Sanders / György Tarczay)
- **Laser Ablation as a Route to New Species**
  (*Takamasa Momose* / Lester Andrews / Qiang Xu / Mingfeng Zhou)
- **Astrochemistry**
  (Ralf Kaiser / Helen Fraser)
- **Atmospheric Chemistry**
  (John Sodeau / Bruce Ault)
- **High Temperature and Unstable Inorganic Species**
  (*Mark Parnis* / Magdolna Hargittai / Helge Willner / Markku Räsänen)

MATRIX METALLOPROTEINASES
Signalling Scissors In Development And Disease
Aug 30 - Sep 4, 2009
Les Diablerets Conference Center
Les Diablerets, Switzerland
Chair: Carl P. Blobel
Vice Chair: Rafael A. Fridman

- **Regulation of Development and Nociceptive Responses by MMPs**
  (*William Parks* / Zena Werb / Carlos Lopez-Otin)
- **Structure and Biochemistry of Metalloproteinases**
  (*Irit Sagi* / Irit Sagi / Gillian Murphy / Xavier Gomis-Rüth / Claudio Luchinat)
- **Metalloproteinases in Development**
  (*Zena Werb* / Douglas DeSimone / Margarete Heck / Mikala Egblad)
- **Cell Biology and Substrate Identification**
  (*Chris Overall* / Geraldine Weinmaster / Judith Bond / Stephen Weiss / Peter Friedl / Christopher Overall)
- **Metalloproteinases as Mediators of Inflammation**
  (*Lisa Coussens* / Lisa Coussens / Rama Khokha / Barbara Fingleton)
- **Contributions of Metalloproteinases to Human Disease**
  (*Suneel Apte* / Christian Haass / John Sandy / Suneel Apte / Daniel McCulloch / Valerie Cormier-Daire)
- **Metalloproteinase Inhibitors**
  (*Vincent Dive* / Vincent Dive / Shahriar Mobashery / Anne-Marie Malfait)
- **Metalloproteinases in Cancer and Angiogenesis**
  (*Luisa Iruela-Arispe* / George Davis / Luisa Iruela-Arispe / Yasunori Okada / Howard Crawford / James Quigley / Conor Lynch)
- **ADAMTS13 and its Role in Thrombotic Thrombocytopenic Purpura**
  (*William Parks* / David Ginsburg)

MECHANISMS OF CELL SIGNALLING
Towards Understanding Signalling Networks
Aug 23-28, 2009
Magdalen College
Oxford, United Kingdom
Chair: Christopher J. Marshall
Vice Chair: John Sondek

- **Keynote Presentation: Modular Protein Interactions and Network Biology**
  (*Chris Marshall* / Tony Pawson)
- **Activation of Small GTPases**
  (*Erik Sahai* / Michiyuki Matsuda / John Sondek / Giorgio Scita / Klaus Hahn)
- **Cell Polarity**
  (*Martin Schwartz* / Alan Hall / Shuh Narumiya / Ian Macara / Kozo Kaibuchi)
- **Signalling at the Network Level**
  (*Tony Pawson* / Doug Lauffenburger / Forest White / Matthias Mann / Rune Linding / John Hancock)
- **Sensing the Physical Environment**
  (*Linda van Aelst* / Alexander Bershadsky / Michael Eyck / Martin Schwartz)
- **Ubiquitin Networks**
  (*Dafna Bar-Sagi* / Ivan Dikic / Ron Hay)
- **Organismal Biology and Development**
  (*Richard Marais* / Luis Parada / Linda van Aelst / Benny Shilo / Jean-Francois Cote)
- **Cell Adhesion and Migration**
  (*Alan Hall* / Jonanthan Chernoff / Michael Sixt / Erik Sahai / Margaret Frame / Anne Ridley)
- **Signalling and Cancer**
  (*Margaret Frame* / Dafna Bar Sagi / Channing Der / Richard Marais / Julian Downward)

MECHANISMS OF MEMBRANE TRANSPORT
Jun 14-19, 2009
Colby College
Waterville, ME
Chair: Amy L. Davidson
Vice Chair: Joseph A. Mindell

- **Regulation of Channels and Transporters**
  (*William Zagotta* / Rachelle Gaudet / David Yue / William Zagotta)
- **Neurotransmitters**
  (*Joseph Mindell* / Baruch Kanner / Olga Boudker / Gray Rudnick)
- **ABC Transporters**
  (*Amy Davidson* / David Clarke / Lydia Aguilar-Bryan / Jue Chen)
- **Ion Channels**
  (*Rod Mackinnon* / Raimund Dutzler / Rod Mackinnon)
- **Ion Motive Force-Dependent Transporters**
  (*Nancy Carrasco* / Ron Kaback / Joseph Mindell / Chris Miller / Nancy Carrasco)
- **Lipid-Protein Interactions**
  (*Stephen White* / Alexey Ladokhin / Zhe Lu / Stephen White)
- **P-Type Transport ATPases**
  (*Chris Miller* / Miguel Holmgren / David Gadsby / Svetlana Lutsenko / Jesper Møller)
- **Membrane Protein Transport and Assembly**
  (*William Skach* / Arnold Driessen / Nils Wiedemann / Jochen Zimmer / William Skach)

MEDICINAL CHEMISTRY
Aug 2-7, 2009
Colby-Sawyer College
New London, NH
Chair: Albert J. Robichaud
Vice Chair: Mary M. Mader

- **Pathway and Phenotypic Screening in Target and Drug Discovery**
  (*Young Shin Cho* / Patrick Harran / Sergey Kozmin / John Tallarico)
- **New Prospects for the Treatment of Type 2 Diabetes**
  (*Scott Hecker* / Max Dang / Ramakanth Sarabu / Rob Jones / Bob Dow)
- **Antivirals**
  (*Manoj Desai* / Paul M. Scola / John McCauley / Mike Peel)
- **Targeting the P13K/AKT Pathway for Oncology: Recent Advances in Drug Discovery**
  (*Jean-Christophe Harmange* / Phil Sanderson / Carlos Garcia-Echeverria / Kevin Freeman-Cook / John Allen)

- **Sphingosine-1-Phosphate Signaling and Immunomodulation**
  (*Zoran Rankovic* / Hugh Rosen / Nigel Cooke / Kevin Cusack)
- **Preclinical Screening and Design Principles for Improved Drug Safety**
  (*Mark C. Noe* / Martin Edwards / Jim Empfield / David Goldstein / Tom Baillie)
- **New Targets for Oncology**
  (*Matthew Marx* / Shawn Qian / Mike Koehler / Ashvin Gavia)
- **Late Breaking Topics**
  (*Sandra Filla*)
- **Keynote Presentation**
  (*Albert J. Robichaud* / Paul Reider)

MICROBIAL ADHESION & SIGNAL TRANSDUCTION

Jul 26-31, 2009
Salve Regina University
Newport, RI
Chairs: Michael Starnbach & Alain A. Filloux
Vice Chairs: Michael S. Gilmore & Lotte Sogaard-Andersen

- **Sporulation, Cell Division and the Cytoskeleton**
  (*Richard Losick* / Jeff Errington / Lotte Sogaard-Andersen / David Rudner)
- **Toxins, Secretion Systems, and Virulence Factors**
  (*Guy Cornelis* / Samuel Miller / John Mekalanos / Wim Hol)
- **The Bacterial Cell Envelope**
  (*Jan Tommassen* / Chris Whitfield / Gabriel Waksman)
- **Cell-Cell Communication and Regulatory Networks**
  (*Paul Williams* / Stephen Lory / Hanah Engelberg-Kulka)
- **Biofilms and Microbial Communities**
  (*Jean-Marc Ghigo*)
- **Infection and Immunity**
  (*Philippe Sansonetti* / Michael Gilmore / Benoit Marteyn / Fidel Zavala / Joanne Flynn / Sarkis Mazmanian / Suzana Salcedo)
- **Intracellular Survival**
  (*Pascale Cossart* / Christophe Dehio / Craig Roy)
- **Modulation of Host Cell Responses by Pathogens**
  (*Stephane Meresse* / Brad Cookson / Alexis Kalergis / Michael Way / Richard Ferrero / Leigh Knodler)
- **Models to Study Host-Pathogen Interactions**
  (*Gad Frankel* / Gordon Dougan / Raphael Valdivia)

MICROBIAL POPULATION BIOLOGY

Jul 19-24, 2009
Proctor Academy
Andover, NH
Chair: Antony M. Dean
Vice Chair: James J. Bull

- **Microbes and Ecosystem Function**
  (*Jed Furhman* / Nicole King / Susan Rosenberg / Nelson Hairston)
- **Community Dynamics**
  (*Larry Fourney* / Larry Fourney / Pilar Francino / Sheri Simmons / Jed Furhman)
- **Social Evolution**
  (*Greg Velicer* / Joan Strassman / Stuart West / Duncan Greig)
- **Experimental Evolution**
  (*Tim Cooper* / David Gresham / Chris Marx / Tom Ferenci / Trish Wittkopp)
- **Adaptive Landscapes**
  (*Holly Wichman* / Dan Weinreich / Sander Tans / Darin Rokyta)
- **Evolution of Disease**
  (*Mary Poss* / Katia Koelle / Dusty Brissom / Sarah Sawyer / Marilyn Roosnick)
- **Protein Evolution**
  (*Yousif Shamoo* / Danny Tawfick / Shelly Copley / Matt Cordes)
- **Symbiosis**
  (*Ellen Simms* / Ellen Simms / Margaret McFall-Ngai / Toby Kiers)
- **Epigenetics**
  (*Ben Kerr* / Laura Landweber / Oscar Kuipers)

MICROFLUIDICS, PHYSICS & CHEMISTRY OF

Jun 28 - Jul 3, 2009
Il Ciocco Hotel and Resort
Lucca (Barga), Italy
Chairs: Juan Santiago & Amy E. Herr
Vice Chairs: James P. Landers & Brian J. Kirby

- **Multifunctional Microfluidic Devices**
  (*Paul Yager* / Mark Shannon / Jaap M.J. den Toonder)
- **Probing the Role of Cellular Response**
  (*Jean-Louis Viovy* / Peter Gascoyne / Hywel Morgan / Vincent Studer)
- **Unraveling Complex DNA & Protein Systems**
  (*Harold Craighead* / Eric Shaqfeh / P.G. Righetti)
- **Harnessing Electrokinetics for Novel Separations**
  (*Sabeth Verpoorte* / David Ross / Koji Otsuka / Stephen Jacobson)
- **Pushing the Limits: Nanochannels and Nanoparticles**
  (Jan Eijkel / Nadine Aubry)
- **Young Investigator Presentations**
  (Hang Lu / Aaron Wheeler / Shelley Anna / Todd Squires)
- **Multiphase Microfluidics**
  (Sandra Troian / Takehiko Kitamori)
- **Single-Cell Assays**
  (Steve Quake / Chih-Ming Ho / Robert Austin)
- **Panel Discussion: Translation to the Commercial Sector**
  (Andrei Dukhin / M. Allen Northrup / Holger Becker)

MOLECULAR & CELLULAR BIOENERGETICS
From Crystal Structures To Human Disease

Jun 7-12, 2009
Proctor Academy
Andover, NH
Chair: David G. Nicholls
Vice Chair: Brian D. Cain

- **F1Fo ATPase**
  (*Stanley Dunn* / John Walker / Christoph von Ballmoos / Robert Fillingame / Joachim Weber)
- **Focus on Complex I Structure and Function**
  (*Judy Hirst* / Ulrich Brandt / Michael Ryan / Claire Remacle / Thorsten Friedrich)
- **V- and P-ATPases**
  (*Patty Kane* / Michael Forgac / Poul Nissen / Stephan Wilkens)
- **Electron Transport Chain Dysfunction in Neurodegenerative Disease**
  (*Tim Greenamyre* / Hemachandra Reddy / Leo Pallanck / Emmanuel Brouillet / Brad Gibson)
- **New Aspects of Mitochondrial Metabolism**
  (*Ferdinando Palmieri* / Hindrik Mulder / Pete Pedersen / Anthony Civitarese)
- **Molecular Mechanisms in Complexes III and IV**
  (*Fevzi Daldal* / Mårten Wikström / Leslie Dutton / Bob Gennis)
- **Mitochondria, Oxidative Stress and Aging**
  (*Martin Brand* / Nils-Göran Larsson / Doug Turnbull / Eric Schon / Norbert Dencher)
- **Fission, Fusion and Function**
  (*Richard Youle* / Peter Hollenbeck / Luca Scorrano / Jodi Nunnari)

MOLECULAR MEMBRANE BIOLOGY

Jul 5-10, 2009
Proctor Academy
Andover, NH
Chair: Sean Munro
Vice Chair: Charlie K. Barlowe

- **Translocation and Folding in the Endoplasmic Reticulum**
  (Tom Rapoport / Ramanujan Hegde / Peter Walter / Ineke Braakman / Jonathan Weissman)
- **Exit from the ER in Health and Disease**
  (Randy Schekman / Ben Glick / William Balch)
- **Membrane Traffic in the Golgi Apparatus**
  (Fred Hughson / Graham Warren / Susan Ferro-Novick / Jennifer Lippincott-Schwartz)
- **Small G Proteins in Membrane Dynamics**
  (David Lambright / Karin Reinisch / Suzanne Pfeffer / Francis Barr)
- **Membrane Bending and Fusion**
  (Bill Wickner / Bruno Antonny / Sandy Schmidt / Elizabeth Chen / David Chan)
- **Vacuoles and Autophagy**
  (Scott Emr / Tamotsu Yoshimori / Elizabeth Conibear)
- **New Technology for Membrane Biology**
  (Lucas Pelkmans / Xiaowei Zhuang / Maya Schuldiner)
- **Lipid Biology and Pathogens**
  (Sergio Grinstein / Gisou van der Goot / Joost Holthuis / Sarah Keller / Kai Simons)
- **Organelles and the Motors that Move Them**
  (Anna Akhmanova / Steven Gross / Gillian Griffiths)

MOLECULAR PHARMACOLOGY
Recent Advances In Basic And Translational Research On G Protein-Coupled Receptors And Signaling

May 31 - Jun 5, 2009
Il Ciocco Hotel and Resort
Lucca (Barga), Italy
Chairs: Susanna Cotecchia & Joel Bockaert
Vice Chair: Paul Insel

- **Towards Crystal Clear Views of Receptors** (*Klaus-Peter Hofmann* / Brian Kobilka / Gebhard Schertler / Hisato Jingami)
- **Activation and Molecular Dynamics of Signaling Proteins** (*Michel Bouvier* / Martin Lohse / Jean-Philippe Pin / Akihoro Kusumi / Francesca Fanelli)
- **Molecular Organization of Signaling Proteins** (*Mark von Zastrow* / Roger Sunhara / Jean-Louis Baneres / Francoise Bachelerie)
- **Signaling: A Space and Time Perspective** (*Stefano Marullo* / Michel Bouvier / Graeme Milligan / Gerald Zamponi / Eric Trinquet)
- **Regulatory Mechanisms and Trafficking of Receptors** (*Mark Rasenick* / Mark von Zastrow / Jeffrey Benovic / JoAnn Trejo)
- **Diversity of Physiological and Pathological Implications** (*Joan Heller-Brown* / Silvio Gutkind / Martine Smit / Diane Barber / Sivia Costagliola)
- **Keynote Presentation: Evolving Concepts in GPCR-Mediated Signaling** (Robert Lefkowitz)
- **Drug Diversity and the Receptorome** (*Thue Schwartz* / Bryan Roth / Guy Servant)
- **Regulation of Brain Functions and Metabolism in Animal Models** (*Michael Freissmuth* / Marc Caron / Brigitte Kieffer / Bernhard Bettler / Jurgen Wess)

MOLYBDENUM & TUNGSTEN ENZYMES

Jul 5-10, 2009
Il Ciocco Hotel and Resort
Lucca (Barga), Italy
Chairs: Maria João Romão & Martin L. Kirk
Vice Chairs: Joel Weiner & Charles G. Young

- **Keynote Presentation: The Inhibitors of Xanthine Oxidoreductase - Mechanism of Inhibition and Their Application to Disease** (*Maria João Romão* / Takeshi Nishino)
- **Molybdenum Cofactor: Biosynthesis, Transport and Insertion** (*Ralf Mendel* / K.V. Rajagopalan / Axel Magalon / Silke Leimkühler / Elizabeth Regulski / Chantal Iobbi-Nivol)
- **Mo and W Homeostasis** (*Jan Andreesen* / Vadim N. Gladyshev / Kaspar P. Locher / Emilio Fernandez)
- **Synthetic Analogue Studies of Mo and W Active Sites** (*Charles Young* / Partha Basu / Hideki Sugimoto / Carola Schulzke / Nadia Mösch- Zanetti)
- **Applications of Spectroscopy for Studying Enzyme Function** (*Isabel Moura* / John Enemark / Wilfred R. Hagen / Graham N. George)
- **Medical, Environmental, and Agricultural Aspects of Mo Enzymes** (*Joanne Santini* / Enrico Garatini / Wolfgang Nitschke / Günter Schwarz / Jeff Jones)
- **Reactions Mechanisms and Mechanistic Enzymology** (*David Garner* / Joel Weiner / Russ Hille / Matthias Boll)
- **Novel Mo Enzymes and Key Enzymes Crystal Structures** (*Caroline Kisker* / Mika Jormakka / Holger Dobbek / Petra Hänzelmann / Roel M. Schaaper / Florian Bittner)
- **Keynote Presentation: The Electronic Structure of Tris(dithiolene) Metal Complexes as Established by X-ray Absorption Spectroscopy** (*Martin Kirk* / Karl Wieghardt)

MOTILE & CONTRACTILE SYSTEMS
Mechanical Basis Of Cellular Function

Jul 12-17, 2009
Colby-Sawyer College
New London, NH
Chair: Kerry Bloom
Vice Chair: Dyche Mullins

- **Keynote Presentation: Matrix Elasticity Modulates Contractility and Directs Differentiation and De-Differentiation Processes** (Dennis Discher)
- **Mechanisms of Motor Proteins** (*Enrique de la Cruz* / Sarah Rice / Jon Scholey)
- **Mechanisms of Chromosome Movement** (*Trisha Davis* / Chip Asbury / Maria Schumacher)
- **Organelle and Chromosome Dynamics** (*Erica Holzbaur* / Iva Tolic-Norrelykke / Linda Wordeman)
- **Novel Roles for Cellular Actin** (*Yu-Li Wang* / Rong Li / Snezhka Oliferenko)
- **Cell and Subcellular Orientation** (*Gregg Gundersen* / Valerie Weaver / Anna Skop / Phong Tran)
- **Polymer Dynamics** (*Alexi Khodjakov* / Dan Fletcher / David Odde)
- **Spatial Regulation of Development and Division** (*Rebecca Heald* / Martin Loose / Peter Lenart)
- **Cell Separation** (*David Burgess* / Bill Sullivan / Harold Erickson / Amy Maddox)

MUSCLE: EXCITATION / CONTRACTION COUPLING

Jun 14-19, 2009
Waterville Valley Resort
Waterville Valley, NH
Chair: Kurt Beam
Vice Chairs: Paul D. Allen & Francesco Zorzato

- **Ultrastructural Basis for Excitation-Contraction Coupling** (*Clara Franzini-Armstrong* / Irina Serysheva / Montserrat Samso)
- **Reciprocal Signaling Between the DHPR and RyR1** (Johann Schredelseker)
- **Calcium Movements During Excitation-Contraction Coupling** (*Eduardo Rios* / Martin Schneider)
- **Calcium Dysregulation, Fatigue** (*Paul Allen* / Graham Lamb / Simona Boncampagni)
- **Muscle Diseases** (*Susan Hamilton* / Kevin Campbell)
- **"Other" Regulators of Calcium Homeostasis** (Peace Cheng / Robert Dirksen / Masamitsu Iino)
- **Calcium Signaling During Muscle Development and Adaptation** (*Jianje Ma*)
- **Proteins Regulating Triad Formation and Function** (Hiroshi Takeshima / Jon Abramson)
- **Aging, Damage and Muscle Membrane Repair** (*Francesco Zorzato* / Noah Weisleder)

MYCOTOXINS & PHYCOTOXINS

Jun 21-26, 2009
Colby-Sawyer College
New London, NH
Chairs: Robert W. Dickey & Barbara A. Blackwell
Vice Chairs: James J. Pestka & Vera L. Trainer

- **Toxic Events in Response to a Changing World** (*Tracey Villareal, David Miller* / Richard Spinrad / Charles Bacon / Benjamin Suarez)
- **New Hazards from New and Known Toxins** (*Michael Quilliam, Ken Voss* / Alison Robertson / John Berry / Rudi Kryska / Tineke Kuiper-Goodman)
- **Detection Technologies for Organisms and Toxins** (*Stacey Etheridge, Uwe Lauber* / Tom Rand / Betsy Yakes / Corrado Fanelli)
- **Biogeographic Patterns of Toxin Production** (*Don Anderson, John Gilbert* / Juli Dyble-Bressie / Uwe John / Linda Kohn / Todd Ward)
- **Predictive Technologies and Models** (*Vera Trainer, Jim Pestka* / Lisa Campbell / Art Schafssma)
- **Mechanisms of Toxicity and Detoxification** (*Kathi Lefebvre, Wentzel Gelderblom* / Isabelle Oswald / Peter Mantle / Kelly Rein / Mark Hahn)
- **Myco- and Phyco-Economics in Global Commerce** (*Porter Hoagland, Felicia Wu* / Alejandra Engler / Hauke Kite-Powell)
- **Genomics, Proteomics and the Phylogenetic Basis of Toxicity** (*Allen Place, Nancy Keller* / Micaela S. Parker / Brett Neilen / Nancy Alexander / John Linz)
- **Public Health and Epidemiology: Outbreak Investigations Informing Science** (*Jonathan Deeds, Lauren Lewis* / Ray Granade / Allan Merrill / Aurelia Tubaro / Tim Phillips)

NATURAL PRODUCTS
Jul 26-31, 2009
Tilton School
Tilton, NH
Chair: Marvin M. Hansen
Vice Chair: Jef K. De Brabander

- **Synthesis and Synthetic Methodology** (Kay Brummond / Barry Trost)
- **Catalysis and Synthetic Methodology** (Amir Hoveyda / Veronique Gouverneur / John Hartwig)
- **Chemical Biology** (Jennifer Kohler / Laura Kiessling / Stuart Schreiber)
- **Chemistry and Biology of Natural Products** (David Sherman / Rolf Müller / Carole Bewley)
- **Natural Product Synthesis** (Raymond Funk / Amos Smith)
- **Synthesis, Chemistry and Natural Products** (Michael Krische / Kyoko Nozaki / Richard Taylor / Markus Kalesse)
- **Methodology and Synthesis** (Zhu-Jun Yao / William Roush)
- **Synthesis, Chemistry and Biology of Natural Products** (Michael VanNieuwenhze / Martin Banwell / Paul Hergenrother / Peter Seeberger)
- **Natural Product Synthesis** (Dirk Trauner / Peter Wipf)

NEURAL CIRCUITS & PLASTICITY
Jun 7-12, 2009
Salve Regina University
Newport, RI
Chair: Takao K. Hensch
Vice Chair: Matthew Wilson

- **Keynote Presentation: Integrative and Regulatory Mechanisms of Synaptic Transmission in the Neural Network** (Shigetada Nakanishi)
- **Development** (Yishi Jin / Gord Fishell / Holly Cline)
- **Cerebellum** (Masanobu Kano / Michael Hausser)
- **Hot Topics: Optical Probing of Neural Dynamics** (Florian Engert / Mark Schnitzer / Karel Svoboda)
- **Limbic System** (Thomas Klausberger / Rene Hen / Andreas Luthi)
- **Auditory System** (Xiaoqin Wang / Dan Sanes)
- **Chemical Senses** (Donald Katz / Catherine Dulac / Liqun Luo)
- **Cognition / Disorder** (Tony Zador / Daphne Bavelier / Okihide Hikosaka / David Lewis)
- **Keynote Presentation: Social Context and Neural Coding in a Basal Ganglia Circuit Essential for Vocal Plasticity** (Allison Doupe)
- **Computation** (Sebastian Seung / Alex Pouget / Misha Tsodyks)
- **Neocortex** (Alison Barth / Gina Turrigiano / Li Zhang / Yang Dan / Rafa Yuste)
- **Hot Topics: Epigenetics** (Frances Champagne / Lisa Monteggia / Li-huei Tsai)

NEUROTROPHIC FACTORS
Jun 21-26, 2009
Salve Regina University
Newport, RI
Chair: William Mobley
Vice Chair: Carlos Ibanez

- **Neurotrophic Factor Synthesis, Secretion and Signaling I** (*Nancy Ip* / Biaoji Xu / Teiichi Furuichi / Jonah Chan)
- **Neurotrophic Factors and Stem Cells: Defining Mechanisms and Exploring Possibilities** (*Yi Sun* / Patrik Ernfors / Freda Miller / Yves Barde / Arnold Kriegstein)
- **Neurotrophic Factors and Development I** (*Alun Davies* / Susana Cohen-Cory / Kim McAllister / Lou Reichardt / Rosalind Segal)
- **Neurotrophins and Behavior** (*Bai Lu* / Eero Castren / Sadaf Farooqi / Mu-ming Poo)
- **Neurotrophic Factors and Circuit Modulation / Plasticity** (Mike Greenberg / Chinfei Chin)
- **Neurotrophic Factor Synthesis, Secretion and Signaling II** (*Bruce Carter* / Phil Barker / Greg O'Sullivan / Moses Chao / Sami Jaffrey / Jeff Milbrandt)
- **Neurotrophic Factors and Development II** (*William Snider* / David Ginty / Haruo Kasai / Wilma Friedman)
- **New Tools to Study Neurotrophic Factors** (Bianxiao Cui / Karl Deisseroth)
- **Neurotrophic Factors and Disease** (Pietro Callisano / Ernest Arenas / Frederic Sadou / Donna Senger / Michael Fanizilber)

NONLINEAR SCIENCE
Jun 28 - Jul 3, 2009
Mount Holyoke College
South Hadley, MA
Chair: Robert P. Behringer
Vice Chair: Stephen Morris

- **Biological Complexity and Dynamics I** (Beate Schmittmann / Joshua Socolar)
- **Fluids and Turbulence I** (Martine Ben Amar / Bruno Eckart / Nigel Goldenfeld)
- **Novel Dynamical Systems I** (Troy Shinbrot / Bill McKelvey)
- **Biological Complexity and Dynamics II** (Jane Wang / Bernd Blasius / Andrea Bertozzi)
- **Novel Dynamical Systems II** (Eran Sharon / Edgar Knobloch)
- **Fluids and Turbulence II** (Predrag Cvitanovic / Tom Mullin)
- **Novel Dynamical Systems III** (Laurette Tuckerman / Tom Solomon)
- **Biological Complexity and Dynamics III** (Will Ryu / Kalin Vetsigian)
- **Novel Dynamical Systems IV** (Michael Brenner / Jun Zhang)

NUCLEAR CHEMISTRY
Frontiers Of Nuclear Structure Through Spectroscopy And Reactions
Jun 21-26, 2009
Colby-Sawyer College
New London, NH
Chair: Andrew E. Stuchbery
Vice Chair: Francesca Gulminelli

- **Structure of Light Nuclei: *Ab Initio* Calculations and Clustering** (*Bruce Barrett* / Libby McCutchan / Thomas Neff / Sofia Quaglioni / Grisha Rogachev)
- **Nuclear Structure Near Exotic Shell Closures** (*Reiner Krücken* / Thomas Faestermann / Kieran Flanagan / Robert Grzywacz / Morten Hjorth-Jensen / Taka Otsuka / Darek Seweryniak)
- **Structure of Exotic Nuclei from Spectroscopy and Reactions** (*John Schiffer* / Alexandra Gade / Tohru Motobayashi / Maurycy Rejmund / Tomas Rodriguez / Enrico Vigezzi)
- **Nuclear Shapes, Phonon Excitations: Nuclear Structure at Low and High Spin** (*John Sharpey-Schafer* / Mitch Allmond / Rob Bark / Mark Caprio / Paul Garrett / Daryl Hartley / David Kulp / Zsolt Podolyak)
- **Production and Spectroscopy of the Heaviest Nuclei** (*Rodi Herzberg* / Paul Greenlees / Henrik Jeppesen / Sasha Yeremin)
- **Advances in Nuclear Astrophysics** (*Jeff Blackmon* / Adriana Banu / Phil Woods / Remco Zegers)
- **Exotic Decay Modes, Nuclear Moments, and Weak Interactions** (*Dimiter Balabanski* / Andrei Andreyev / Jean-Michel Daugas / Yuri Litvinov / Hideki Ueno / Paul Vetter)
- **New Instruments and New Opportunities with Radioactive Beams** (*John Simpson* / Thomas Glasmacher / Wolfram Korten / I-Yang Lee)
- **Keynote Presentation: Imaginary Weapons - The Hafnium Saga** (*Francesca Gulminelli* / Jerry Wilhelmy)

NUCLEAR PHYSICS
Jul 12-17, 2009
Bryant University
Smithfield, RI
Chair: Steve Vigdor
Vice Chair: Zein-Eddine Meziani

- **Nuclear Astrophysics Theory** (Adam Burrows / Baha Balantekin)
- **New Results in Nucleon Structure** (Marco Stratmann / Feng Yuan / Charles Hyde-Wright / Harvey Meyer)
- **New Results in Nuclear Structure I** (Douglas Higinbotham / Steffen Strauch / Joe Carlson)
- **Frontiers in Neutrino Physics** (Bruce Vogelaar / Reina Maruyama / Mary Bishai)
- **Nuclear Astrophysics Experiment** (Hendrik Schatz / Daniela Leitner / Brenda Dingus)
- **Relativistic Heavy Ion Collisions** (Jamie Nagle / Fuqiang Wang / John Harris / Volker Koch / Zoltan Fodor)

- **New Results in Nuclear Structure II**
  (Robert Janssens / Yuri Litvinov / Chuck Horowitz)
- **Searching for Physics Beyond the Standard Model**
  (Paul Reimer / Jen-Chieh Peng / Yannis Semertzidis / Brad Plaster / Daniel Chung)
- **Gluon-Dominated Matter**
  (Francois Gelis / Les Bland / Thomas Ullrich)

NEW! NUCLEAR PHYSICS (GORDON-KENAN RESEARCH SEMINAR)

Jul 11-12, 2009
Bryant University
Smithfield, RI
Chair: Sean M. Tulin

- **Neutrinos, Astrophysics, and Beyond the Standard Model**
  (*Brad Plaster*)
- **QCD: From Quarks to the Nuclei**
  (*Joe Carlson*)

The Gordon Research Seminar on Nuclear Physics is a two-day Gordon Conference-style meeting exclusively for graduate students, post-docs, and other scientists with comparable levels of experience and education. Speakers will be chosen from among the attendees. The associated Gordon Research Conference will take place at the same location, immediately following the Seminar.

NUCLEIC ACIDS

May 31 - Jun 5, 2009
University of New England
Biddeford, ME
Chairs: Leemor Joshua-Tor & Kristen W. Lynch
Vice Chairs: Christopher D. Lima & Roland Kanaar

- **Keynote Presentations: Understanding and Using the Human Genome**
  (Richard M. Myers / Robert Cook-Deegan)
- **Genome Integrity**
  (*Gregory L. Verdine* / Anja-Katrin Bielinsky / Roland Kanaar / Hongtao Yu / John A. Tainer)
- **Replication**
  (*Stephen P. Bell* / Michael Botchan / Johannes Walter / John Kuriyan)
- **Transcription and Chromatin Dynamics**
  (*Robert Kingston* / Nouria Hernandez / Karolin Luger / Shelley L. Berger / Ronald Breaker)
- **Post Transcriptional Regulation**
  (*Brenton R. Graveley* / Tracy Johnson / Holger Stark / Robert B. Darnell)
- **ncRNA: Diverse Effects on DNA and RNA**
  (*Gary Ruvkun* / Janet F. Partridge / Robert Martienssen / Alain Bucheton)
- **RNA Fate Decisions: Stability and Export**
  (*Lynne E. Maquat* / Jeremy Sanford / Chrisopher D. Lima / David L. Spector)
- **Ribosome Biogenesis, Function, and Regulation**
  (*Rachel Green* / Taekjip Ha / Juli Feigon / Harry F. Noller)
- **RNA Catalysis**
  (*Anna Marie Pyle* / Samuel E. Butcher / Joseph A. Piccirilli / Saba Valadkhan)

NUCLEOSIDES, NUCLEOTIDES & OLIGONUCLEOTIDES

Jul 5-10, 2009
Salve Regina University
Newport, RI
Chair: Varsha Gandhi
Vice Chair: Piet Herdewijn

- **Keynote Presentation: DNA Polymerases**
  (*Robert Kuchta* / Thomas Kunkel)
- **DNA Repair**
  (*Bill Plunkett* / Lawrence Loeb / Peggy Hsieh / Bradley Preston)
- **Target Enzymes: SAR**
  (*Donna Shewach* / Chris Dealwis / Arnon Lavie)
- **Gene Expression and Silencing**
  (*Victor Marquez* / Masad Damha / George Calin / Peter Jones)
- **Other Uses of Nucleosides**
  (*Steven Graham* / Hon Cheung Lee / Michael Williams)
- **Nucleoside Imaging, Transport and Analog Actions**
  (*William Parker* / Eric Kool / Carol Cass / Yung-chi Cheng)
- **mRNA Recognition and mRNA Polyadenylation**
  (*Jyoti Chattopadhyaya* / Dinshaw Patel / James Manley)
- **Synthetic Strategies for Analogs**
  (*Barbara Ramsey Shaw* / Chong Kim / Chris Meier / Michael Sofia)
- **Best Abstract Presentations**
  (*Piet Herdewijn*)

ORGANIC REACTIONS & PROCESSES

Jul 19-24, 2009
Bryant University
Smithfield, RI
Chairs: Yannis N. Houpis & Jerry A. Murry
Vice Chair: Richard P. Hsung

- **Synthesis and Metal Catalysis**
  (*Michael Harmata* / Tohru Fukuyama / Barry Trost)
- **Industrial Biotransformations**
- **Biocatalysis**
  (*Fraser Fleming, Kathleen Crudden* / Don Hilvert / Chi huey Wong / Oliver May / Owen Goodwin / Jake Janey / Nicholas Turner)
- **Synthetic Methods and Processes**
  (*Rob Dancer, Rod Parsons* / Mimi Hii / Jon Antilla / Scott Snyder)
- **Molecular Catalysis**
  (*Robert Hinkel* / David MacMillan / Shu Kobayashi)
- **Metal Catalysis**
  (*Neal Anderson, Michel Couturier* / Justin Dubois / Jean Suffert / Jeff Song)
- **Synthetic Methods**
  (*Mimi Hee* / Dean Toste / P. Andrew Evans)
- **Synthesis and Catalysis**
  (*Yi-Yin Ku, Kai Rossen* / Scott Denmark / Jim Leighton)
- **At the Interface of Chemistry and Biology**
  (*Richard Hsung* / Peter Schreiner / Stuart Schreiber)

ORGANOMETALLIC CHEMISTRY

Jul 12-17, 2009
Salve Regina University
Newport, RI
Chair: John F. Walzer
Vice Chair: Richard F. Jordan

- **Ligand Platforms**
  (*Rich Jordan* / David Milstein / Adam Veige)
- **Applications to Organic Synthesis I**
  (*Bernadette Donovan-Merkert* / Keith Fagnou / Hélène Lebel / John Hartwig)
- **Novel Reactivity and Transformations**
  (*James Mayer* / Miguel Esteruelas / Christopher Cummins / Karen Goldberg)
- **Theory and Mechanism**
  (*Gary Silverman* / Andrei Vedernikov / Tom Cundari / Brooke Small)
- **Organometallic Approaches to a Post-Petroleum World**
  (*Jeff Yoder* / Daniel DuBois / Roy Periana / Jay Labinger)
- **Catalytic Transformations of Olefins**
  (*Ted Betley* / Deryn Fogg / Jerzy Klosin / Matthew Overett)
- **Applications to Organic Synthesis II**
  (*Jamie Strickler* / Mitch Smith / Jennifer Love / Albert Casalnuovo)
- **New Molecular Architectures**
  (*William Hersh* / Andrew Weller / Makoto Fujita / Didier Bourissou)
- **Back to the Future**
  (*Greg Hillhouse* / Clifford Kubiak / William D. Jones)

NEW! ORGANOMETALLIC CHEMISTRY (GORDON RESEARCH SEMINAR)

Jul 11-12, 2009
Salve Regina University
Newport, RI
Chair: Jason Gavenonis
Vice Chair: Tiffany R. Maher

- **Keynote Presentation: Studying Polar Molecules in the Great White North**
  (Tom Baker)
- **Synthetic Advances in Organometallic Chemistry**
  (*Rich Jordan* / Guy Bertrand)
- **Applications of Organometallic Chemistry**
  (*Peter Wolczanski*)

The Gordon Research Seminar on Organometallic Chemistry is a two-day Gordon Conference-style meeting exclusively for graduate students, post-docs, and other scientists with comparable levels of experience and education. Speakers will be chosen from among the attendees. The associated Gordon Research Conference will take place at the same location, immediately following the Seminar.

ORIGINS OF SOLAR SYSTEMS

Jul 5-10, 2009
Mount Holyoke College
South Hadley, MA
Chair: Sara S. Russell
Vice Chair: Michael R. Meyer

- **Initial Cosmic Abundances**
  (Martin Asplund / Trevor Ireland)
- **Timescales of Disks**
  (*Alycia Weinberger* / Jerome Bouvier / David Wilner / Noriko Kita)

- **Disk Chemistry**
  (*Joan Najita* / Ilaria Pascucci / Phil Bland)
- **Planet Formation**
  (Edward Thommes / David O'Brien)
- **Distribution of Isotopes in the Solar System**
  (*Stein Jacobsen* / Tim Elliott / Jonathan Williams)
- **Dust to Planetesimals**
  (*Conel Alexander* / Qing-Zhu Yin / Anders Johansen / Denton Ebel)
- **Planets to Dust**
  (Klaus Mezger / Stu Weidenschilling)
- **Planet Structure and Evolution**
  (Isabelle Baraffe / Francis Albarede)
- **Comparative Planetology**
  (*Josh Winn* / Christian Marois)

PERIODONTAL DISEASES

Aug 2-7, 2009
Colby-Sawyer College
New London, NH
Chair: Denis F. Kinane
Vice Chair: Jeffrey L. Ebersole

- **Microbial Complexity: Commensals, Pathogens and Biofilms**
  (*Bruce Paster* / David Relman / Ann Griffen / Bernie Guggenheim)
- **Microbial Virulence**
  (*Mike Curtis* / Hansel Fletcher / Eric Reynolds / Dan Fine / Jan Potempa)
- **Microbe Mucosal Interactions**
  (*Richard Lamont* / Yousef Abu-Kwaik / Julio Scharfstein)
- **Host Cell - Microbe Recognition**
  (*George Hajishengallis* / Kathy Triantafilou / Richard Tapping / Gabriel Naussbaum)
- **Stem Cells: Tissue Engineering**
  (*David L. Cochran* / Pamela Robey / Songtao Shi / David Mooney)
- **Toll Like Receptor Signaling**
  (*Caroline Genco* / Mike Martin / Douglas Golenbock / Kate Fitzgerald)
- **Host Response in Periodontal Disease / Host Microbe Interactions**
  (*Jeff Ebersole*)
- **Controlling Systemic Inflammation**
  (*Steven Offenbacher* / F.Y. "Eddie" Liew / Charles Serhan)
- **Control of Cellular Responses: miRNA, Tolerance; Epigenetics**
  (*Dana Graves* / Bayar Dahshevig / Tom Knudsen / Jackson Egen)

PHAGOCYTES
Innate Immune Cell: Pathogen Interactions

Jun 7-12, 2009
Waterville Valley Resort
Waterville Valley, NH
Chair: Linda C. McPhail
Vice Chair: Sergio Grinstein

- **Novel Technologies**
  (*Sam Silverstein* / Joel Swanson / Steffen Jung / Jackson Egen)
- **Cell Migration**
  (*Gary Bokoch* / Tobias Meyer / Klaus Ley / Chuck Parkos)
- **Pattern Recognition Receptors**
  (*David Underhill* / Kate Fitzgerald / Paul Heyworth)
- **Phagocytosis**
  (*Joel Swanson* / Julie Blander / Lynda Stuart / John Brumell / Nathalie Franc)
- **Innate and Adaptive Immunity**
  (*Alberto Mantovani* / Luigina Romani / Hidde Pleogh)
- **Redox Regulation**
  (*Mary Dinauer* / Rachel Levy / Ariel Savina / Erzsebet Ligeti)
- **Pathogen Effects on Innate Immune Cells**
  (*Lee-Ann Allen* / David Mosser / Lalita Ramakrishnan)
- **Innate Immune Cells in Inflammation**
  (*Bill Nauseef* / Charles Serhan / Sankar Ghosh / Donna Bratton / Moira Whyte)
- **Innate Immune Cells and Disease**
  (*Peter Ward* / Gwen Randolph / Guillermina Girardi / Joseph El-Khoury)

NEW! PHAGOCYTES
(GORDON-KENAN RESEARCH SEMINAR)
Innate Immune Cell: Pathogen Interactions

Jun 6-7, 2009
Waterville Valley Resort
Waterville Valley, NH
Chairs: Xing Jun Li & Justin T. Schwartz

- **Phagocytes and Innate Immunity**
  (*Justin T. Schwartz*)
- **Effects of Pathogens on Innate Immune Cells**
- **Effects of Innate Immune Cells on Pathogens**
  (*William M. Nauseef*)

The Gordon Research Seminar on Phagocytes is a two-day Gordon Conference-style meeting exclusively for graduate students, post-docs, and other scientists with comparable levels of experience and education. Speakers will be chosen from among the attendees. The associated Gordon Research Conference will take place at the same location, immediately following the Seminar.

PHOSPHORYLATION & G-PROTEIN MEDIATED SIGNALING NETWORKS

Jun 7-12, 2009
University of New England
Biddeford, ME
Chairs: T Kendall Harden & Rick Neubig
Vice Chairs: Brendan D. Manning & Jin Zhang

- **Keynote Presentation: Structure of G Protein-Coupled Receptors**
  (*Rick Neubig* / Brian Kobilka)
- **Regulation of GPCR**
  (*Roger Sunahara* / Jeffrey Benovic / JoAnn Trejo / Laura Bohn)
- **G Protein-Independent Signaling of GPCR**
  (*Stephen Lanier* / Randy Hall / X.Y. Huang / Kodi Ravichandran)
- **G Protein-Regulating Proteins**
  (*John Tesmer* / Kendall Blumer / Kiril Martemyanov / John Hepler / Stephen Lanier)
- **Subcellular Targeting**
  (*James Putney* / Maurine Linder / Renolds Ostrom / Tobias Meyer)
- **Effectors and Downstream Signaling Pathways**
  (*Joan Heller Brown* / Dianqing Wu / James Putney / Jin Zhang)
- **GPCR-Promoted Ras GTPase Signaling**
  (*John Sondek* / Joan Heller Brown / Stefan Offermanns / Heidi Hamm / Brendan Manning)
- **Structural Basis of G Protein Signaling**
  (*Heidi Hamm* / John Tesmer / John Sondek / Roger Sunahara / Gebhard Schertler)
- **GPCR Drug Discovery**
  (*Randy Hall* / Arthur Christopoulos / Larry Sklar / Jeffrey Conn)

PHOTOCHEMISTRY

Jul 5-10, 2009
Bryant University
Smithfield, RI
Chairs: Michael R. Wasielewski & Bruce A. Armitage
Vice Chairs: Cornelia Bohne & Gerald J. Meyer

- **Solar Energy Conversion**
  (*Ana Moore* / Leif Hammarström / Devens Gust / Emily Weiss)
- **Reactions and Mechanisms**
  (*Michael Wasielewski* / Samir Farid / Andrei Kutateladze / Igor Alabugin / Willie Leigh)
- **Supramolecular Photochemistry**
  (*Linda Shimizu* / Frank Würthner / Dirk Guldi)
- **Biological Photochemistry and Imaging**
  (*Sarah Schmidtke* / Linda Johnston / Alex Deiters / Bern Kohler / Dmitry Matyushov)
- **Single Molecule Photochemistry**
  (*Jason Kahn* / Marcel Bruchez / Johan Hofkens)
- **Spectroscopy and Dynamics**
  (*Torsten Fiebig* / David McCamant / Lin Chen / David Jonas)
- **Spin Effects in Photochemistry**
  (*Tijana Rajh* / Christiane Timmel / David Schultz / Malcolm Forbes)
- **Materials Photochemistry**
  (*Pavel Anzenbacher* / Uwe Bunz / Elizabeth Harbron / Zhigang Shuai / Thuc-Quyen Nguyen)
- **New Frontiers in Photochemistry**
  (*Francisco Raymo* / Klaus Hahn / Valentina Emiliani)

PHOTOSYNTHESIS

Jun 28 - Jul 3, 2009
Bryant University
Smithfield, RI
Chair: Doug Bruce
Vice Chair: Krishna K. Niyogi

- **Bioenergy I: Hydrogen**
  (*Tom Moore* / Fraser Armstrong / Cara Lubner)
- **Water Splitting, the Oxygen Evolving Complex**
  (*Gary Brudvig* / Warwick Hillier / David Britt / Sergej Vassiliev / Alain Boussac)
- **Photosystem II. Primary Processes, Secondary Pathways and Regulation**
  (*Bill Rutherford* / T. Renger)
- **Antenna and Regulation**
  (*Roberta Croce* / Rienk van Grondelle / Naomi Ginsberg)

- **Type I Reaction Centers**
  (*Kevin Redding* / Lisa Utschig)
- **Bioenergy II: Solar Energy Devices and Artificial Photosynthesis**
  (*John Golbeck* / Klaus Lips / Ana Moore)
- **Electron and Proton Transport**
  (*Marilyn Gunner* / Fabrice Rappaport)
- **Putting It All Together, Supermolecular Complexes and Assembly**
  (*Conrad Mullineaux* / Klaus Schulten / Sascha Rexroth / Lu-Ning Liu)
- **Young Investigator Presentations**
  (*Jim Barber*)

PHYSICAL METALLURGY
Integrating Computational Materials Science And Engineering

Aug 2-7, 2009
Proctor Academy
Andover, NH
Chairs: Kevin Hemker, John Allison & Hamish Fraser
Vice Chairs: Mark D. Asta, Emmanuelle A. Marquis, Dallas R. Trinkle & Peter W. Voorhees

- **ICMSE: The Payoff**
  (Leo Christodoulou / Robert Shafrik)
- **Developing Processing-Structure Relations**
  (Peter Lee / Gunther Gottstein / Tresa Pollock / Carlos Levi)
- **Poster Synopses**
  (*Kevin Hemker*)
- **Developing Structure-Properties Relations**
  (Chris Wolverton / Paul Krajewski / Johns Hutchinson / Michael Mills)
- **New Modeling Tools**
  (Junzhi Wang / Liz Holm)
- **New Experimental Tools**
  (George Spanos / Barry Muddle)
- **ICMSE Integration Success Stories and Challenges I**
  (Mei Li / Jurgen Hirsch / Anthony Evans)
- **ICMSE Integration Success Stories and Challenges II**
  (Deb Whitis / Steve Fox)
- **ICMSE Integration Success Stories and Challenges III**
  (James Williams)

PHYSICAL ORGANIC CHEMISTRY
Molecular Design And Synthesis

Jun 28 - Jul 3, 2009
Holderness School
Holderness, NH
Chair: Peter R. Schreiner
Vice Chair: Luis Echegoyen

- **Alkane C-H Bond Activation**
  (*G.K. Surya Prakash* / Helmut Schwarz / Armando J.L. Pombeiro / Melanie S. Sanford)
- **Radicals, Electron Transfer, and Photochemistry**
  (*Nathaniel Finney* / John A. Murphy / Angelo Albini / Burkhard König / Dario Bassani)
- **Synthesis and Reactivity**
  (*Robert A. Pascal Jr.* / Alison J. Frontier / G. Narahari Sastry / Detlef Schröder)
- **Carbon Materials**
  (*Jeremy E.P. Dahl* / Michael M. Haley / Michael Bendikov / Lawrence T. Scott / Robert M.K. Carlson)
- **Materials and Function**
  (*Kim Baldridge* / Rainer Herges / Jean-Cyrille Hierso / Matthias Bremer)
- **Radicals**
  (*Uta Wille* / Carl Schiesser / Armido Studer / Shunichi Fukuzumi / Igor Alabugin)
- **Biradicals, Carbenes, and More**
  (*Carol Parish* / Vladimir Popik / Michael Schmittel)
- **Computation Meets Experiment**
  (*Raghavan B. Sunoj* / Götz Bucher / Manabu Abe / Alexander Greer / Wesley D. Allen)
- **Poster Session Presentations**
  (*Luis Echegoyen*)

PLANT CELL WALLS
Plant Cell Wall Biosynthesis

Aug 2-7, 2009
Bryant University
Smithfield, RI
Chair: Debra Mohnen
Vice Chair: Jocelyn K. Rose

- **Keynote Presentations: Understanding Plant Cell Wall Structure - The Challenge to Meet Future Biofuel and Natural Product Needs**
  (*Kenneth Keegstra* / Alan Darvill / Tuula Terri)
- **The Entire Plant Cell Wall: Polysaccharides, Proteins, Lignin and Waxes**
  (*Paul Knox* / Jocelyn Rose / John Ralph / Michael Hahn / Tatyana Gorshkova)
- **Evolution and Wall Structural Diversity**
  (*Malcolm O'Neill / Jim Wade* / Zoë Popper / William Willats / Stephen Fry)
- **Wall Biosynthesis: Emerging Paradigms**
  (*Kanwalpal Dhugga / Henrik Scheller* / Maor Bar-Peled / Vincent Bulone / Seth Debolt / William York / Taku Demura)
- **Systems Biology of Cell Walls - What Do We Need to Get There?**
  (*Steve Thomas / William York* / Bernard Henrissat / Gerald Tuskan / Marcia Kieliszewski)
- **Role of Wall in Plant Development & Defense**
  (*Bruce Link / Mary Tierney* / Karl Oparka / Simon Turner / Norman Lewis)
- **Keynote Presentations: Plant Cell Walls - Where Have We Been & Where We Need to Go**
  (*Nick Carpita* / Geoff Fincher / Tony Bacic / Herman Hofte)
- **3D Structure and Function of Wall Modifying Enzymes**
  (*Barry McCleary / Harry Brummer* / Harry Gilbert / Matt Ohlin / Dan Cosgrove)
- **Walls as Biomass for Biofuels**
  (*Maud Hinchee / Markus Pauly* / Kenneth Keegstra / Henrik Scheller / Richard Dixon)

NEW! PLANT CELL WALLS (GORDON-KENAN RESEARCH SEMINAR)
Unraveling The Wall From Plant Cell Wall Biosynthesis To Lignocellulosic Bioethanol Production

Aug 1-2, 2009
Bryant University
Smithfield, RI
Chair: Zhangying Hao

- **Keynote Presentation: The Rapidly Expanding Field of Plant Cell Walls - History, Present, And The Future**
  (Tony Bacic)
- **Plant Cell Wall Biosynthesis, Structure and Function**
  (*Mary Tierney / Staffan Persson*)
- **Progress in Lignocellulosic Bioethanol Production: From Theory to Industry**
  (*Henrik V. Scheller / Tina Jeoh*)

The Gordon Research Seminar on Plant Cell Walls is a two-day Gordon Conference-style meeting exclusively for graduate students, post-docs, and other scientists with comparable levels of experience and education. Speakers will be chosen from among the attendees. The associated Gordon Research Conference will take place at the same location, immediately following the Seminar.

NEW! PLANT METABOLIC ENGINEERING

Jul 12-17, 2009
Waterville Valley Resort
Waterville Valley, NH
Chair: Joe Chappell
Vice Chair: Natalia Dudareva

- **Systems Biology Approaches and Metabolic Networks**
  (*Dirk Inze* / Lothar Willmitzer)
- **Organization and Evolution of Metabolic Pathways**
  (*Eran Pichersky* / Anne Osbourn / Thomas Mitchell-Olds)
- **Enzyme Plasticity: The Engine for Metabolic Engineering, Evolution and Chemical Diversification?**
  (*Jonathan Gershenzon* / Dan Tawfik / Sarah O'Connor)
- **Regulatory Factors for Metabolic Engineering**
  (Rick Dixon / Pierre Broun)
- **Integrating Metabolism and Cell Biology**
  (*Peter Facchini* / Erich Grotewold / Elison Blancaflor)
- **Harvesting Energy and Bioconversion**
  (*Clint Chapple* / Steve Mayfield / Debra Mohnen)
- **Understanding Complex Metabolic Traits**
  (*Andrew Hansen* / Tom Leustek / Teruhiro Takabe)
- **Plant Metabolic Engineering for Human Health**
  (*Charile Arntzen* / Cathie R. Martin / Dean Della Penna)
- **Windows to the Future for Metabolic Engineering**
  (*Wolf Frommer*)

NEW! PLANT METABOLIC ENGINEERING (GORDON RESEARCH SEMINAR)

Jul 11-12, 2009
Waterville Valley Resort
Waterville Valley, NH
Chairs: Ezekiel Nims & David K. Liscombe

- **Deciphering the Code of Nature's Best Chemists: Progress in Understanding the Chemistry and Biology of Plant Metabolism**
  (*Ezekiel Nims*)
- **Modulation, Redesign, and Reconstitution of Plant Metabolic Pathways**
  (*David Liscombe*)

- **Combinatorial Biosynthesis: Algal, Bacterial and Fungal Tools Being to Produce Novel Medicinal Compounds in Higher Plants**

The Gordon Research Seminar on Plant Metabolic Engineering is a two-day Gordon Conference-style meeting exclusively for graduate students, post-docs, and other scientists with comparable levels of experience and education. Speakers will be chosen from among the attendees. The associated Gordon Research Conference will take place at the same location, immediately following the Seminar.

POLYAMINES
Polyamine Genetics, Metabolism, Cellular Homeostasis And Drug Discovery
Jun 21-26, 2009
Waterville Valley Resort
Waterville Valley, NH
Chairs: Patrick M. Woster & Senya Matsufuji
Vice Chairs: Lisa M. Shantz & Enzo Agostinelli

- **The Genetics and Epigenetics of Polyamine Metabolism**
  (*Robert A. Casero, Jr.* / Yi Huang / Olivier Namy / Chaim Kahana)
- **Polyamines in Cellular Homeostasis and Physiology**
  (*Leena Alhonen* / Myung Hee Park / Keiko Kashiwagi / Jian-Ying Yang / Keith Wilson)
- **Polyamine Biosynthesis: Enzyme Structure, Function and Control**
  (*Kazuei Igarashi* / Steven Ealick / David Hoffman)
- **Polyamine Catabolism and Transport**
  (*Heather Wallace* / Susan Gilmour / Lisa Shantz / Takeshi Uemura)
- **Polyamine Function in Plants and Lower Eukaryotes**
  (*Anthony Michael* / Autar Mattoo / Kiyotaka Hitomi)
- **Polyamine Drug Discovery and Development**
  (*Natalia Ignatenko* / Ian Blagbrough / Heinz Gehring)
- **Clinical Application of Drugs Targeting Polyamine Metabolism**
  (*Laurence Marton* / Andre Bachmann / John Cleveland)
- **Polyamine Metabolism as a Target for Antiparasitic Chemotherapy**
  (*Sigrid Roberts* / Lynn Soong / Annette Kaiser / Lyn-Marie Birkholz)
- **Keynote Presentation: Perspectives on Past, Present & Future Polyamine Research**
  (*Anthony Pegg* / Olle Heby / Carl Porter)

NEW! POLYAMINES
(GORDON RESEARCH SEMINAR)
Jun 20-21, 2009
Waterville Valley Resort
Waterville Valley, NH
Chairs: Andrew Goodwin & Takeshi Uemura

- **Keynote Presentation**
  (Laurence J. Marton)
- **Biochemical, Structural, and Enzymatic Studies of Polyamine Metabolic Pathways**
- **Applications of Polyamine Research in Human Health and Disease**

The Gordon Research Seminar on Polyamines is a two-day Gordon Conference-style meeting exclusively for graduate students, post-docs, and other scientists with comparable levels of experience and education. Speakers will be chosen from among the attendees. The associated Gordon Research Conference will take place at the same location, immediately following the Seminar.

POLYMERS
Responsive And Multifunctional Polymers Enabling Emerging Technologies
Jun 21-26, 2009
Mount Holyoke College
South Hadley, MA
Chair: Timothy E. Long
Vice Chair: Stuart J. Rowan

- **Trends in the Design of Responsive Polymers**
  (*LaShanda T.J. Korley* / Anna Balazs / Jeffrey Moore)
- **Polymer Design at the Interface of Biology**
  (*Joseph Rule* / Mark Van Dyke / Joseph DeSimone / Theresa Reineke)
- **Polymers for Alternate Energy**
  (*Kate Beers* / Hiro Nishide / Deborah Jones)
- **Novel Polymer Synthetic Strategies**
  (*Anne McNeil* / Rint Sijbesma / Greg Tew / Craig Hawker)
- **New Directions in Multifunctional Polymer Characterization**
  (*Sheng Lin-Gibson* / Karen Winey / Stephen Cheng)
- **Polymers at the Engineering Interface**
  (*Martha Grover* / David Tirrell / Ann-Christine Albertsson / Tony Ryan)
- **Tailoring Polymer Surfaces**
  (*Qian Wang* / Thomas Epps / Joy Cheng)
- **Polymer Design for Sustainability**
  (*Astrid Rosario* / Timothy Lodge / Jerry White / Luc Leemans)
- **Polymers for Emerging Technologies**
  (*Dan Knauss* / Scott Grayson / Karen Wooley)

NEW! POLYMERS
(GORDON-KENAN RESEARCH SEMINAR)
Excellence In Polymer Graduate Research
Jun 20-21, 2009
Mount Holyoke College
South Hadley, MA
Chairs: Emily B. Anderson & Timothy Merkel

- **Defining Directions for Graduate Research**
  (*Takeo Suga*)
- **Polymers at the Interface with Life Science**
  (*Sean Ramirez*)
- **Responsive Polymers for Technology**
  (*Stuart Williams*)

The Gordon Research Seminar on Polymers is a two-day Gordon Conference-style meeting exclusively for graduate students, post-docs, and other scientists with comparable levels of experience and education. Speakers will be chosen from among the attendees. The associated Gordon Research Conference will take place at the same location, immediately following the Seminar.

PROTEINS
Jun 21-26, 2009
Holderness School
Holderness, NH
Chairs: Jacquelyn S. Fetrow & Terrence G. Oas
Vice Chairs: James U. Bowie & Patricia L. Clark

- **Keynote Presentation: Post Reductionist Protein Science**
  (*Lila Gierasch* / Tom Kerppola)
- **Role of Co-Solutes and Water in Protein Stability**
  (*George Rose* / Wayne Bolen / Bertil Halle / Adrian Elcock / Janet Wood)
- **Protein-RNA Biology**
  (*Ignacio Tinoco* / Jamie Williamson / Ruben Gonzalez, Jr.)
- **The Hydrogen Bond and Hydrophobicity, Revisited**
  (*Robert "Buzz" Baldwin* / Michele Vendruscolo / Joseph Dannenburg / Bertrand Garcia-Moreno / Stephen White)
- **Visualization of Proteins in the Cell**
  (*Enrico Gratton* / Ahmet Yildez / Catherine Royer)
- **Functional Consequences of Protein Heterogeneity**
  (*Ken Dill* / Sharon Hammes-Schiffer / Vincent Hilser / Elan Eisenmesser / Floyd Romesburg)
- **Theory of Amyloid Formation**
  (*Harold Scheraga* / Devarajan Thirumalai / Charles Brooks)
- **Structural and Functional Proteomics**
  (*Jane Richardson* / Benjamin Cravatt / Adam Godzik / Richard Hanson / Patricia Babbitt)
- **Keynote Presentation: Experiments with Single Protein Molecules**
  (*Terry Oas* / Carlos Bustamante)

QUANTUM CONTROL OF LIGHT & MATTER
Aug 2-7, 2009
Mount Holyoke College
South Hadley, MA
Chair: Yaron Silberberg
Vice Chairs: Gustav G. Gerber & Ronald B. Kosloff

- **Photons**
  (*Moshe Shapiro* / Steve Harris / Ian Walmsley)
- **Atoms**
  (*Bertrand Girard* / Mark Raizen / Tommaso Calarco)
- **Molecules I**
  (*Misha Ivanov* / Albert Stolow / Ilya Averbukh or Yehiam Prior / Stephane Guerin)
- **Molecules II**
  (*Ludger Woeste* / Nikolai Vitanov / Niek van Hulst / Matthias Weidemuller)
- **Attoseconds and High Harmonics**
  (Margaret Murnane or Henry Kapteyn / Olga Smirnova / Phillip Bucksbaum)
- **Control and Controllability**
  (*David Tannor* / Hersch Rabitz / Paul Brumer / Lorenza Viola)
- **Techniques**
  (*Tobias Brixner* / Jean-Pierre Wolf / Andrew Weiner)
- **Applications**
  (*Keith Nelson* / Marcus Motzkus / Robert Gordon)

- **Control with Strong Fields**
  (Thomas Weinacht / Valery Milner / Zohar Amitay)

RADIATION & CLIMATE

Jul 5-10, 2009
Colby-Sawyer College
New London, NH
Chairs: Qiang Fu & Christian Jakob
Vice Chairs: Robert Wood & Alexander Marshak

- **Keynote Presentation: Grand Challenges in Radiation and Climate**
  (*V. Ramaswamy* / Susan Solomon / Bruce A. Wielicki)
- **Radiative Forcing in Climate Change I**
  (*Thomas P. Ackerman* / James M. Haywood / Joyce E. Penner / Stephen G. Warren)
- **Radiative Forcing in Climate Change II**
  (*Warren J. Wiscombe* / Piers M. Forster / Ka-Kit Tung)
- **Analysis of Climate Feedbacks**
  (*Thomas P. Charlock* / Andrew E. Dessler / Alex Hall / Christopher S. Bretherton)
- **Hydrological Cycle in Changing Climate**
  (*Graeme L. Stephens* / Yukari N. Takayabu / Kevin E. Trenberth)
- **Cloud Processes in the Climate System**
  (*Stephen A. Klein* / Bjorn Stevens / Eric J. Jensen / Yi Ming)
- **Absorbing Aerosols and Asian Monsoon**
  (*Kuo-Nan Liou* / V. Ramanathan / W.K.M. Lau)
- **Recent Climate Change**
  (*John M. Wallace* / Cecilia M. Bitz / Steven C. Sherwood / Regine Hock)
- **Geo-Engineering**
  (*Brian Toon* / Alan Robock / Phil J. Rasch)

RED CELLS

Jun 28 - Jul 3, 2009
University of New England
Biddeford, ME
Chair: James J. Bieker
Vice Chair: Velia M. Fowler

- **Membrane Skeleton Organization and Dynamics**
  (*Velia Fowler* / Vann Bennett / Luanne Peters)
- **Transcriptional Control of Gene Expression**
  (*Gerd Blobel* / Stu Orkin / Masi Yamamoto / Mitch Weiss)
- **Membrane Biogenesis, Maturation, and Enucleation**
  (*David Anstee* / John Crispino / Michel Vidal)
- **Erythroid Epigenetics**
  (*Emery Bresnick* / Frank Grosveld / Ann Dean / Gordon Ginder)
- **Infected Red Cells**
  (*Pat Gallagher* / Athar Chishti / Kasturi Haldar / Tom Wellems / Elisabeth Winzeler)
- **Developmental Controls in Erythropoiesis**
  (*Doug Engel* / Kyunghee Choi / Don Wojchowski / Bob Paulson)
- **Membrane Proteins: Structures and Associations**
  (*Jon Morrow* / Lesley Bruce / Phil Low)
- **Environmental Cues in Erythroid Differentiation**
  (*Jim Palis* / Joel Chasis / Margaret Baron)
- **Red Cell Disorders**
  (*Len Zon* / Prem Ponka / Alan D'Andrea)

SOFT CONDENSED MATTER PHYSICS
Soft Meets Biology

Aug 9-14, 2009
Colby-Sawyer College
New London, NH
Chairs: David R. Nelson & David A. Weitz
Vice Chairs: Heinrich M. Jaeger & M. Christina Marchetti

- **Biophysics of Viruses**
  (Robijn Bruinsma / Jack Johnson)
- **Directed Assembly of Biopolymers**
  (Paul Rothemund / Fred MacKintosh)
- **Biologically Inspired Materials Science**
  (Joanna Aizenberg / Michael Cates)
- **Collective Effects in Soft Matter**
  (Paul Chaikin / L. Mahadevan / David Quere)
- **Cooperative Effects in Biological Systems**
  (Andreas Bausch / Ray Goldstein)
- **Genetic Regulation and Evolution**
  (Erez Braun / Terry Hwa)
- **Biophysics of Lipids and Polymers**
  (Sarah Keller / Erwin Frey)
- **Motors and Forces in Biology**
  (Dennis Discher / Frank Julicher / Joe Howard)
- **Self-Organization and Self-Assembly**
  (Greg Grason / Gerald Wong)

SOLID STATE CHEMISTRY
New Frontiers In Materials Synthesis And Characterization

Aug 30 - Sep 4, 2009
Magdalen College
Oxford, United Kingdom
Chair: Martin Jansen
Vice Chair: Mas Subramanian

- **Imaging Transient Structures with Ultrafast Diffraction**
  (N. Browning / A. Cavalleri)
- **Intermetallics: New Perspectives**
  (A. Guloy / F. Gascoin)
- **Chemical Bonding in Extended Solids**
  (C. Felser)
- **New HTSC's, Multiferroics and Magnetic Materials**
  (R. Cava / Y. Shimakawa)
- **Advanced Solid State Synthesis**
  (J. Shen)
- **High Spatial Temporal Resolution with Synchrotron, Neutron and Electron Diffraction**
  (G. Vaughan)
- **New Vistas in Heterogeneous Catalysis**
- **Solids with Nanoscopic and Mesoscopic Topologies**
  (U. Wiesner)
- **Electrochemical Synthesis of New Materials**
  (G. Tsirlina)
- **Solid State Chemistry of Main Group Elements**
  (B. Albert / M. Eremets)

STAPHYLOCOCCAL DISEASES

Aug 30 - Sep 4, 2009
Waterville Valley Resort
Waterville Valley, NH
Chairs: Barry N. Kreiswirth & Kenneth W. Bayles
Vice Chairs: Fritz Goetz & Jodi Lindsay

- **Keynote Presentation: Update on Antibiotic Resistance**
  (*Patrick Schlievert* / Alexander Tomasz)
- **Evolution**
  (*Herminia de Lencastre* / Martin McGavin / Ashley Robinson / Ralf Rosenstein)
- **Innate Immunity / Host Response to Staphylococcal Infection**
  (*Tammy Kielian* / Rachel McLoughlin / Barbara Broeker / Suzan Rooijakkers)
- **Regulatory Control Mechanisms**
  (*Tim Foster* / Michael Otto / Pascal Romby / Masayori Inouye)
- **Other Staphylococcal Species**
  (*Paul Fey* / Wilma Ziebuhr / Greg Somerville / Ross Fitzgerald)
- **Biofilm Formation and Metabolism**
  (*Mark Smeltzer* / Kelly Rice / Blaise Boles / Dietrich Mack)
- **Therapeutics and Vaccines**
  (*Liesa Anderson* / Paul Dunman / Nicolas Kartsonis / Mark Shirtliff)
- **Animal Models and Virulence**
  (*Jean Lee* / Julie Wardenburg / Knut Ohlsen / Javad Aman)
- **Controversies / Hot Topics**
  (*Brigitte Berger-Bachi*)

NEW! STEM CELLS & CANCER
Molecular Mechanisms Controlling Normal And Cancer Stem Cells

Sep 13-18, 2009
Les Diablerets Conference Center
Les Diablerets, Switzerland
Chair: Maarten Van Lohuizen
Vice Chair: Catriona Jamieson

- **Keynote Presentation: Hemapoietic Stem Cells and Stem Cell Hierarchy**
  (Irving L. Weissman)
- **Self-Renewal and Cancer**
  (Ronald DePinho / Michael F. Clarke / Roel Nusse)
- **Reprogramming and Induced Pluripotent Stem Cells**
  (Austin Smith / Tariq Enver)
- **Hemapoietic Stem Cells and Leukemia**
  (*Irving L. Weissman* / Tannishtha Reya / Gerald de Haan / Amy Wagers)
- **Solid Tissue Stem Cells and Cancer**
  (Jane Visvader / Hans Clevers)
- **Niche Signaling and Stem Cell Control**
  (Fiona Watt / Andreas Trumpp / Shahragim Tajbakhsh)
- **Mouse Models and Stem Cells**
  (Anton Berns / David Tuveson)
- **Stem Cell Profiling and (Epi)Genomics**
  (Howard Chang / Dirk Schübeler / Kristian Helin)
- **Therapeutics Against Cancer Stem Cells**
  (Peter Dirks / Dean Felsher)

STRESS PROTEINS IN GROWTH, DEVELOPMENT & DISEASE

Jun 28 - Jul 3, 2009
Proctor Academy
Andover, NH
Chair: Jeff Brodsky
Vice Chair: Lea Sistonen

- **Keynote Presentations: Cellular Adaptation to Misfolded Proteins and Heavy Metals** (*Jeffrey Brodsky* / Peter Walter / Dennis Thiele)
- **Cellular Stresses and Stress Responses** (*Rick Morimoto* / Jonathan Weissman / Bernd Bukau / Elizabeth Craig / Kazuhiro Nagata)
- **Chaperones and the Accumulation of Protein Aggregates** (*Jonathan Weissman* / Susan Lindquist / Rick Morimoto / Noboru Mizushima)
- **Protein Misfolding, Stress, and the Mechanisms of Disease Onset** (*Linda Hendershot* / William Balch / Ana Maria Cuervo / Ivor Benjamin / Judith Frydman)
- **Transcriptional Regulation of Stress Responses** (*Dennis Thiele* / Carol Gross / John Lis / Karen Adelman / Akira Nakai)
- **The Intersection Between Aging and Stress Pathways** (*Ana Maria Cuervo* / Lenny Guarante / Cynthia Kenyon / Dirk Bohmann / Andy Dillin)
- **Chaperone "Decisions" and Protein Quality Control** (*Ursual Jakob* / Linda Hendershot / Elke Deuerling / Kenji Kohno / Chris Nicchitta)
- **Pharmacological Correction of Protein Misfolding and Chaperone-Linked Disease** (*Ivor Benjamin* / Jeffery Kelly / Jason Gestwicki / Len Neckers / Luke Whitesell)
- **Signal Transduction Pathways and Cellular Stress** (*Andy Dillin* / David Ron / Elizabeth Vierling / Ursula Jakob / Valerie Mezger)

SUPERCONDUCTIVITY

Jun 7-12, 2009
Hong Kong University of Science and Technology
Hong Kong, China
Chair: Fuchun Zhang
Vice Chair: Ali Yazdani

- **Recent ARPES in Underdoped Cuprates** (*Zhi-Xun Shen* / Peter Johnson / Atsushi Fujimori)
- **Iron Pnictide Superconducting Materials** (*Zhong-Xian Zhao* / Xian-Hui Chen / C. W. Chu)
- **Normal State Properties of Iron Pnictide** (David Mandrus / Nan-Lin Wang / Suchitra Sebastian)
- **Transport in Cu-Oxides** (*Shin-ichi Uchida* / N. E. Hassey / Patrick A. Lee / Louis Taillefer / Greg Boebinger)
- **Miscellaneous Superconductivity** (*Hide Fukuyama* / Kazushi Kanoda)
- **Magnetism and Superconductivity** (*Joe Thompson* / Michel Kenzelmann / John Tranquada)
- **Quasi-Particles in Cuprates** (*Hidenori Takagi* / Seamus Davis / Tetsu Hanaguri / Abhay Pasupathy)
- **Pairing Symmetry in Iron Pnictide** (Hong Ding / Dung-Hai Lee)
- **Recent Advances in Superconductivity** (Naoto Nagaosa)

SUPRAMOLECULES & ASSEMBLIES, CHEMISTRY OF

Products And Processes Via Self-Assembly

Jun 28 - Jul 3, 2009
Colby College
Waterville, ME
Chair: Matthew Tirrell
Vice Chairs: Nicholas Kotov & Markus Antonietti

- **Dynamic Assembly** (*Matthew Tirrell* / E.W. "Bert" Meijer / Stuart Rowan)
- **Dynamic Assembly and Assemblies** (*Markus Antonietti* / Samuel Stupp / David Leigh / Sir J. Fraser Stoddart)
- **Synthesis of Supramolecular Assemblers** (*David Thompson* / Geoffrey Coates / Jonathan Nitschke)
- **Polyelectrolyte and Colloidal Assembly** (M.A. Cohen-Stuart / Glenn Fredrickson / Monica Olvera de la Cruz)
- **Responsive Assemblies** (Jonathan Sessler / Kristi Kiick)
- **Membrane Assemblies** (Paul Cremer / Arup Chakraborty / Nicholas A. Melosh / Tobias Baumgart)
- **Inorganic Assemblies** (Cassandra Fraser / Tianbo Liu)
- **Colloidal Assembly** (Katharina Landfester / Vinothan N. Manoharan / Sharon Glotzer / Harm-Anton Klok)
- **Macromolecular Assemblies** (*Nicholas Kotov* / Yunfeng Lu / Alexander Kros)

THIN FILM & CRYSTAL GROWTH MECHANISMS

Jul 12-17, 2009
Colby-Sawyer College
New London, NH
Chair: Jonah Erlebacher
Vice Chair: Christine Orme

- **Crystal Surface Morphology and Kinetics** (*Jonah Erlebacher* / Dieter Kolb / Peter Feibelman)
- **Crystal with Low Dimensionality** (*Jerry Tersoff* / Max Lagally / Kimberly Dick-Thelander / Joerg Weissmuller)
- **Fundamentals of Crystal Nucleation and Growth** (*Kristen Fichthorn* / David Srolovitz / Laszlo Granasy)
- **Large Biomolecule Crystallization** (*Naomi Chayen* / Alex Malkin / Richard Sear)
- **Biocrystallization and Biomineralization** (*Joanna Aizenberg* / Lara Estroff / Fiona Meldrum)
- **Organic Electronics** (Theo Siegrist / Zhenan Bao)
- **Advanced Imaging for Crystal Growth** (*Marcel Rost* / Ruud Tromp / Olaf Magnussen)
- **Structure / Function Relationships on Catalytic Crystal Surfaces** (*Karl Sieradzki* / Cyndy Friend / Stanko Brankovic / Annabella Selloni)
- **Hot Topics** (*Christine Orme*)

THREE DIMENSIONAL ELECTRON MICROSCOPY

Technical Advances And Recent Breakthroughs In 3DEM

Jun 28 - Jul 3, 2009
Colby-Sawyer College
New London, NH
Chairs: Andreas Hoenger & Stephen D. Fuller
Vice Chair: Holger Stark

- **Keynote Presentation: Reaching the Resolution Limits in 3D-EM** (*Stephen Fuller, Andy Hoenger* / Andreas Engel)
- **Keynote Presentation: Tomography of Large Cellular Structures** (*Stephen Fuller, Andy Hoenger* / J. Richard McIntosh)
- **Exciting News From the Single-Particle & Virus Structure** (*Trevor Sewell*)
- **Cryo-Tomography on Macromolecular Structures** (*Achilleas Frangakis* / Julia Cope)
- **Exciting News From the 2-D Crystal / Helical Community** (*Jenny Hinshaw*)
- **Presentations of Selected Posters** (*Holger Stark*)
- **Exciting News From the Hybrid Community (New Data & Software)** (*Dorit Hanein*)
- **Fancy Accessories to EMs: Phase Plates, Correctors, IFs, Cameras** (*Robert Glaser* / Radostin Danev / Max Haider)
- **Cryo-Tomography of Large Cellular Structures and Intact Small Cells** (*Grant Jensen*)

NEW! TIME-DEPENDENT DENSITY-FUNCTIONAL THEORY

Jul 5-10, 2009
Colby-Sawyer College
New London, NH
Chairs: Miguel A. L. Marques & Angel Rubio
Vice Chairs: Troy Van Voorhis & Fillipp Furche

- **Theoretical Foundations** (*Kieron Burke* / E.K.U. Gross / R.V. Leeuwen)
- **New Functionals** (*Stephan Kuemmel* / Kimihiko Hirao / Gustavo E. Scuseria / Francesc Illas)
- **Van der Waals Interactions** (*Troy Van Voorhis* / John Dobson / Georg Kresse)
- **Electronic Transport** (*Massimiliano di Ventra* / Harold Baranger / Kristian Thygessen / Mark Ratner)
- **Charge Transfer / Non Adiabatic Phenomena** (*Neepa Maitra* / Martin Head-Gordon / Todd Martinez / Lorenz Cederbaum)
- **Computational Challenges** (*Stefano Baroni* / Giulia Galli / Xavier Andrade / Nicola Marzari)
- **Non-Linear Phenomena** (*Carsten Ullrich* / Daniel Neuhauser / Thomas Brabec)
- **Biological Applications** (*Filipp Furche* / Paolo Carloni / Dage Sundholm)
- **Spectroscopy** (*Angel Rubio* / Claudia Ambrosch-Draxl / Alberto Castro / Elisa Molinari)

TISSUE REPAIR & REGENERATION
Jun 14-19, 2009
Colby-Sawyer College
New London, NH
Chair: Luisa A. DiPietro
Vice Chair: Michael Galko

- **Epithelium and Proliferation**
  (*Sabine Eming* / Raghu Kalluri / Marjana Tomic-Canic / Betty Fini)
- **Innovative Approaches**
  (*Luisa DiPietro* / Leroy Hood / Sam Stupp)
- **Bioengineering / Therapeutics**
  (*Damien Bates* / Molly Shoichet / Andrew Baird)
- **Inflammation**
  (*Joe Leibovich* / Manuela Martins-Green / Paul Martin / Anna Huttenlocher)
- **Regeneration**
  (*Derek Mann* / Sabine Werner / Elly Tanaka / Jeff Davidson)
- **Stressors of the Healing Response**
  (*Phil Marucha* / Rivkah Isseroff / Phil Stewart / Dana Graves)
- **Genetic Regulation**
  (Chandan Sen / Michael Galko / Enrique Martin-Blanco)
- **Fibrosis and Scarring**
  (*Liz Kovacs* / Jack Gauldie / Boris Hinz / Christine Theoret)
- **Stem Cells**
  (*Michael Galko* / Wei-Qiang Gao / Bridget Deasy / Rick Bucala)

TUBERCULOSIS DRUG DEVELOPMENT
Targets, Technologies And Trials
Aug 16-21, 2009
Magdalen College
Oxford, United Kingdom
Chairs: Eric J. Rubin & Bala Subramanian
Vice Chairs: Stewart Cole & Jose-Francisco Garcia-Bustos

- **What are the Requirements for a New Antibiotic?**
  (*Bala Subramanian* / Gary Maartens / Zarir Udwadia)
- **Potential New Targets for Treating Tuberculosis**
  (*Valerie Mizrahi* / Giovanna Riccardi / Chris Sassetti)
- **New Chemical Entities I**
  (*Jose Garcia-Bustos* / John Blanchard / Thomas Dick)
- **Screening for New Antibiotics**
  (*Jim Sacchettini* / Priscille Brodin / Deborah Hung / Derek Tan)
- **New Chemical Entities II**
  (*Véronique Dartois* / Vadim Makarov / David Barros)
- **Model Systems**
  (*Ken Duncan* / Tawanda Gumbo / Ajit Lalvani / Clif Barry)
- **Alternative Treatment Strategies**
  (*Stewart Cole* / Sjaak Neefjes / JoAnne Flynn)
- **Early Clinical Trials**
  (*Anne Ginsberg*)
- **How Should We Test New Drugs for TB?**
  (*Eric Rubin* / Chris Lipinski)

VIRUSES & CELLS
Jun 7-12, 2009
Il Ciocco Hotel and Resort
Lucca (Barga), Italy
Chair: Rozanne Sandri-Goldin
Vice Chair: Terence Dermody

- **Entry and Receptors**
  (*Gabriella Campadelli-Fiume, Roberto Cattaneo* / Yves Gaudin / Ari Helenius / Thilo Stehle / Steven Russell)
- **Assembly, Budding and Release**
  (*Anette Schneemann, Carol Carter* / Joel Baines / Thomas Wileman / Cristina Risco / Walther Mothes)
- **Dynamics of Cellular Trafficking**
  (*Peter Sarnow, Greg Smith* / Lynn Enquist / Julie Pfeiffer / Peter O'Hare / Thomas Hope)
- **Viral Replication and Gene Expression**
  (*Robert Kalejta, Sean Whelan* / Bert Semler / Paula Traktman / Peter Nagy / Juan Ortin)
- **Immune Response and Pathogenesis**
  (*Katherine Spindler / Edward Mocarski* / Sujan Shresta / Tatyana Golovkina / Sara Cherry / Hisashi Arase)
- **Cellular Inhibition of Virus Replication and Virus Countermeasures**
  (*Sandra Weller, Ellen Fanning* / Thomas Stamminger / Stacey Schultz-Cherry / Skip Virgin / Ellen Fanning)
- **Innate Immune Response and Virus Counter Response**
  (*Karen Mossman, Joanna Shisler* / Ganes Sen / Antonella Casola / Karla Kirkegaard / Edward Mocarski)
- **Exploiting Host Functions**
  (*Michael Gale, James Alwine* / Bernard Roizman / Thomas Shenk / Michael Katze / Peter Sarnow)
- **Epidemiology, Prevention and Therapy**
  (*Teresa Compton, Marianne Manchester* / Dianne Griffin / Nicolas Grassly / Marianne Manchester / Teresa Compton)

VISUALIZATION IN SCIENCE & EDUCATION
Revealing Nature, Generating Insight
Jul 26-31, 2009
Magdalen College
Oxford, United Kingdom
Chairs: Arthur J. Olson & Shaaron Ainsworth
Vice Chairs: Elizabeth M. Dorland & Ghislain Deslongchamps

- **Information, Uncertainty and Ambiguity**
  (*Ghislain desLongchamp* / Ben Schneiderman / Alex Pang)
- **Creativity and Discovery I**
  (*Lena Tibel* / Alyssa Goodman / Katy Borner)
- **Creativity and Discovery II**
  (*Michael Steiff* / Felice Frankel / David Gooding)
- **Dynamism and Interactivity**
  (*Peter Mahaffy* / Drew Berry / Colin Ware)
- **Results from Visionary Grants**
  (*Chris Watters*)
- **Complexity and Simplicity I**
  (*Pat Hanrahan* / Larry Gonick / Rob Goldstone)
- **Complexity and Simplicity II**
  (David Goodsell / Barbara Tversky / Brian White)
- **Diversity I: Engaging Learners through Visualization**
  (*Dave Geelan* / Tom Moher / Yvonne Rogers / Zafra Lerman)
- **Diversity II: Scientific Visualization for All**
  (*Elizabeth Dorland* / Nora Newcombe / Stephen Uzzo)

VITAMIN B_{12} & CORPHINS
Organometallic Magic Of Life On Earth: From Microorganisms To Humans
Aug 2-7, 2009
Magdalen College
Oxford, United Kingdom
Chair: Bernhard Kraeutler
Vice Chair: Catherine L. Drennan

- **B_{12}: New Developments in Medicine & Biology**
  (*Wilfred van der Donk* / Roy Gravel / Martin Warren)
- **B_{12}: Transport & Uptake in Humans**
  (*Ebba Nexø* / David Alpers / Søren Moestrup / Edward Quadros / Roger Schibli)
- **B_{12}-Uptake and Use in Bacteria**
  (*Charles Grissom / Helga Refsum* / Christof Holliger / Michael Wiener)
- **B_{12} in Medicine & Toxicology**
  (*Ralph Green* / Nicola Brasch / Frank Rutsch / Jacob Selhub / Lawrence Solomon)
- **B_{12}: Structures, Spectroscopy and Theory**
  (*Tetsuo Toraya* / Thomas Brunold / Sergey Fedosov / David Smith / Kazunari Yoshizawa)
- **Mechanisms of B_{12}-Enzymes I: Mutases**
  (*Neil Marsh* / Bernard T. Golding / Antonio Pierik / Naoki Shibata / Kurt Warncke)
- **Mechanisms of B_{12}-Enzymes II: Ribonucleotide Reductase**
  (*Kenneth Brown* / Catherine L. Drennan / Gary Gerfen / Derek Logan)
- **Corphins**
  (*Rudolf K. Thauer / Yoshio Hisaeda* / Bernhard Jaun / Stephen Ragsdale)
- **B_{12}: Perspectives and Prospects**
  (*Bernhard Kräutler* / Robert Doyle / Ruma Banerjee)

X-RAY SCIENCE
Aug 2-7, 2009
Colby College
Waterville, ME
Chair: Jun'Ichiro Mizuki
Vice Chair: G. Brian Stephenson

- **X-Ray Scattering/Spectroscopy Under Extreme Conditions**
  (*Yoichi Murakami* / Jean Pascal Rueff / Yasuhiro Matsuda)
- **Science Frontier Using New X-Ray Sources**
  (*Ian Robinson* / Alexander Foehlisch)
- **X-Rays in Environment and Nano Science**
  (*Eric Isaacs* / Helena van Swygenhoven)
- **Inelastic X-Ray Scattering**
  (*Alfred Baron* / Wei Ku / Kenji Ishii / Bridget Murphy)
- **New Techniques/Optics, Detectors and Others**
  (*Yuri Shvydko* / Kenji Tamasaku / Lothar Strueder)
- **Dynamics by Pump and Probe Technique**
  (*David Reis* / Shinichi Adachi / Paul Evans / Martin Meedom Nielsen)
- **X-Rays in Biology and Life Science**
  (Hyotcherl Ihee / Shuji Akiyama)

- **Use of Coherent X-Rays for Imaging and Studies of Dynamics**
  (*Simon Mochrie* / Sylvain Ravy / Ivan Vartaniants / Till Metzger)
- **Hot Topics**
  (Dino Jaroszynski)

www.grc.org

Check Out Our Newest Offerings:

New Conferences

Each year, GRC adds a number of new conferences to our portfolio. The 2009 Session II schedule contains ten new conferences, which are listed below. The preliminary programs for these meetings can be found in the previous pages of this listing.

- Amygdala In Health & Disease
- Antigen Cross-Presentation
- Cannabinoid Function In The CNS
- Cell-Cell Fusion
- Drinking Water Disinfection By-Products
- Hormone Action In Development & Cancer
- Inhibition In The CNS
- Plant Metabolic Engineering
- Stem Cells & Cancer
- Time-Dependent Density-Functional Theory

We welcome proposals for new Gordon Research Conferences from the scientific community. The Gordon Research Conferences have a long record of stimulating advanced research in industrial laboratories, colleges and universities, research institutes and government laboratories. To maintain discussions at the frontiers of knowledge, we invite proposals for new conferences in vital, emerging areas that will benefit from this type of interaction. Proposals for new Gordon Research Conferences may be submitted at any time throughout the year. Please visit our web site at **http://www.grc.org/proposals.aspx** for more information on proposing a new GRC.

Gordon Research Seminars

The Gordon Research Seminar Program (GRS) is a series of highly successful and unique opportunities for young researchers to share in the GRC experience. Each seminar is held in conjunction with a related GRC and begins the weekend immediately prior to the GRC. Graduate students, post docs, and other scientists with comparable levels of experience and education come together to discuss their current research and build informal networks with their peers that may lead to a lifetime of collaboration and scientific achievement. The 2-day Gordon Research Seminars are organized by young investigators with the support of leading scientists from the associated GRC. The majority, if not all, of the GRS participants are expected to participate in the following GRC.

The 2009 Session II schedule contains thirteen Gordon Research Seminars, which are listed below. The preliminary programs for these meetings can be found in the previous pages of this listing (in green text) underneath their associated Gordon Research Conference.

- Bones & Teeth (GRS)
- CAG Triplet Repeat Disorders (GRS)
- Catecholamines (GRS)
- Combinatorial Chemistry (GRS)
- Inorganic Chemistry (GRS)
- Magnetic Resonance (GRS)
- Nuclear Physics (GRS)
- Organometallic Chemistry (GRS)
- Phagocytes (GRS)
- Plant Cell Walls (GRS)
- Plant Metabolic Engineering (GRS)
- Polyamines (GRS)
- Polymers (GRS)

The Kenan Institute for Engineering, Technology & Science at North Carolina State University provides seed money to a limited number of new Gordon Research Seminars each year. Together with the Kenan Institute, GRC is very excited to invite young scientists to take part in this unique opportunity.